The Redox and Systems Biology of Ergothioneine Biosynthesis in *Aspergillus fumigatus*

Kevin Sheridan BSc

Maynooth University
National University of Ireland Maynooth

Thesis submitted to Maynooth University for the degree of Doctor of Philosophy

October 2016

Supervisor:
Prof. Sean Doyle,
Biotechnology Laboratory,
Department of Biology,
Maynooth University,
Maynooth,
Co. Kildare, Ireland.

Co-supervisor:
Dr. Gary Jones,
Yeast Genetics Laboratory,
Department of Biology,
Maynooth University,
Maynooth,
Co. Kildare, Ireland.

Head of Department:
Prof. Paul Moynagh

Table of contents

Chapter 3: Genetic Modification of *A. fumigatus*

Acknowledgements

Firstly, I would like to thank my supervisor, Professor Sean Doyle. I am very grateful for the opportunity to work on this project and for the help, advice and mentoring over the last 4 years to bring this PhD to fruition. My thanks are also extended to my co-supervisor Dr. Gary Jones, whose ideas and advice throughout this PhD were greatly appreciated. Thanks also to Dr. Özgür Bayram for his assistance in this project.

This PhD was funded by a Science Foundation Ireland Principal Investigator award to Professor Sean Doyle (PI/11/1188). Quantitative proteomic facilities were funded by a competitive award from Science Foundation Ireland (12/RI/2346 (3)). Quantitative PCR instrumentation was funded by Science Foundation Ireland (SFI/07/RFP/GEN/F571/ECO7). The image station for the visualization of Southern blots was funded by Science Foundation Ireland career development award 13/CDA/2142 to Dr Özgür Bayram.

I wish to thank Professor Hubertus Haas and Ms. Beatrix Lechner MSc. for providing the Δ*egtA*^{AfS77} strain and for their collaborative work on the Sheridan et al. (2016) paper. Thanks also to Professor Phil Dix, Dr. Peter Medgyesy and Dr. Éva Horvath for the kind gift of the *N. tabacum* L. cv. Petit Havana:*egtA*:*nfs1* strain. I would also like to thank Mr. Ge Wu MSc. for his assistance with fluorescence microscopy.

My thanks to everyone in the Biology department in Maynooth University for their help and support over the last four years. Thank you to all of the technical staff for their willing assistance whenever required. I would particularly like to thank Caroline for her help with all things mass spec related. Thanks also to Nick, for fixing the autoclave, eventually.

Thank you to everyone in the Biotechnology and Yeast Genetics labs for all the help and good times over the last four years. Thanks to Rebecca and Grainne for their training at the start of this project and for answering my many questions over the course of this PhD. To Darragh, Elizabeth, Eoin, Lara, Linan, Niamh, Nicola, Rose, Stephen D, Stephen H and Steven B, thank you for the help, the nights out, the tea breaks, the table tennis games and your friendship over the course of my PhD. This project would have been a lot less enjoyable without you all.

Thank you to my friends for their support throughout this project, for the well needed occasional pints and for understanding why my social appearances have diminished over the least six months. A special thank you to my girlfriend Louise, for her unwavering patience, support and love. I could not have gotten through this without you. Finally I would like to thank my family for their support and encouragement throughout my PhD, even if they never could quite grasp that it didn't involve mushrooms.

Declaration of Authorship

This thesis has not previously been submitted, in whole or in part, to this, or any other University, for any other degree. This thesis is the sole work of the author with the exception of: (i) Generation of the *A. fumigatus* Δ*egtA*^{AfS77} strain, which was generated by Professor Hubertus Haas and Ms. Beatrix Lechner MSc. (Innsbruck, Austria). (ii) Generation of the *N. tabacum* L. cv. Petit Havana:*egtA*:*nfs1* strain, which was performed by Professor Phil Dix, Dr. Peter Medgyesy and Dr. Éva Horvath (Maynooth University) (iii) Fluorescence microscopy, which was performed with the assistance of Mr. Ge Wu MSc. (Maynooth University).

_____

Kevin Sheridan BSc.

Publications and Presentations

Publications

Owens, R. A., Hammel, S., **Sheridan, K. J.**, Jones, G. W., & Doyle, S. (2014). A proteomic approach to investigating gene cluster expression and secondary metabolite functionality in Aspergillus fumigatus. *PloS One, 9*(9), e106942.

Owens, R. A., O'Keeffe, G., Smith, E. B., Dolan, S. K., Hammel, S., **Sheridan, K. J.**, Fitzpatrick, D.A., Keane, T.M., Jones, G.W. & Doyle S. (2015). Interplay between gliotoxin resistance, secretion, and the Methyl/Methionine cycle in Aspergillus fumigatus. *Eukaryotic Cell, 14*(9), 941-957.

Sheridan, K. J., Dolan, S. K., & Doyle, S. (2015). Endogenous cross-talk of fungal metabolites. *Frontiers in Microbiololgy, 5*(732), 1-11.

Sheridan, K. J.*, Lechner, B. E.*, O' Keeffe, G., Keller, M. A., Werner, E. R., Lindner, H., Jones, G.W., Haas, H. & Doyle, S. (2016). Ergothioneine biosynthesis and functionality in the opportunistic fungal pathogen, *Aspergillus fumigatus*. *Scientific Reports, 6*, 35306.

* Equal contribution

Oral Presentations

Sulphur Metabolism and Gliotoxin in *Aspergillus fumigatus*. Departmental Symposium, Maynooth University, September 2013.

Ergothioneine Biosynthesis and Function in *Aspergillus fumigatus.* Departmental Symposium, Maynooth University, December 2014.

Biosynthesis and Function of Ergothioneine in *Aspergillus fumigatus.* Alltech Seminar Series, Alltech, Co. Meath, April 2015.

Ergothioneine: A new antioxidant in *Aspergillus fumigatus*. Sixth FEBS Advanced Lecture Course:"Human Fungal Pathogens", La Colle sur Loup, France, May 2015.

Exploring the Role of Ergothioneine in *Aspergillus fumigatus.* Departmental Symposium, Maynooth University, September 2015.

Ergothioneine Biosynthesis and Function in *Aspergillus fumigatus*. 5th Annual Biology Research Day, Maynooth University, June 2016.

Poster Presentations

The Role of *metR* in Self-Protection Against Gliotoxin in *Aspergillus fumigatus.* 2nd Annual Maynooth University Biology Research Day, Maynooth University, June 2013.

The Role of *metR* in Self-Protection Against Gliotoxin in *Aspergillus fumigatus.* 3rd Annual Meeting of the Irish Fungal Society, Maynooth University, June 2013.

On the Biosynthesis and Function of the Antioxidant Ergothioneine in *Aspergillus fumigatus*. The Eleventh International Aspergillus Meeting (Asperfest11), Seville, Spain, March 2014.

On the Biosynthesis and Function of the Antioxidant Ergothioneine in *Aspergillus fumigatus*. 12th European Conference on Fungal Genetics (ECFG12). Seville, Spain, March 2014.

Insights into the Biosynthesis and Function of Ergothioneine in *Aspergillus fumigatus*. 4th Annual meeting of the Irish Fungal Society, NUI Galway, Galway, June 2014.

Insights into the Antioxidant Ergothioneine in *Aspergillus fumigatus*. Applications of Proteomics in Human Clinical and Infectious Disease, Dublin City University, Dublin, September 2014.

Insights into the Antioxidant Ergothioneine in *Aspergillus fumigatus*. 3rd Annual Maynooth University Biology Research Day, Maynooth University. September 2014. **Awarded Prize for Best Poster Presentation.**

Ergothioneine: A new antioxidant in *Aspergillus fumigatus*. Sixth FEBS Advanced Lecture Course:"Human Fungal Pathogens", La Colle sur Loup, France, May 2015.

Ergothioneine in *Aspergillus fumigatus*: Biosynthesis, Function and Interactions. 5th Annual Meeting of the Irish Fungal Society, Trinity College Dublin, Dublin, June 2015.

Ergothioneine in *Aspergillus fumigatus*: A New Antioxidant. 4th Annual Maynooth University Biology Research Day, Maynooth University, June 2015.

New insights into redox systems interactions in Aspergillus fumigatus. 6th Annual Meeting of the Irish Fungal Society, Grand Hotel, Malahide, Co. Dublin, March 2016.

Abbreviations

5'-IAF	5’-Iodoacetamidofluorescein
AMM	Aspergillus Minimal Media
AU	Absorbance Units
Bp	Base Pair
bZIP	Basic Leucine Zipper Domain
CBC	CCAAT-Binding Complex
CBL	Cystathionine β-Lyase
CBS	Cystathionine β-Synthase
CFW	Calcofluor White
CGL	Cystathionine γ-Lyase
CGS	Cystathionine γ-Synthase
CSPD	Chemiluminescent Substrate Phosphatase Detection
CWI	Cell Wall Integrity
DIG	Digoxigenin
DMSO	Dimethyl Sulphoxide
DNA	Deoxyribonucleic Acid
EDTA	Ethylenediaminetetraacetic acid
EGT	Ergothioneine
ETP	Epipolythiodioxopiperazine
FU	Fluorescence Units
GSH	Glutathione
GSSG	Glutathione Disulphide
H_2DCFDA	2',7'-Dichlorodihydrofluorescein Diacetate
HAL	Histidine Ammonia Lyase
IDV	Integrated Density Value
KEGG	Kyoto Encyclopedia of Genes and Genomes
LC-MS/MS	Liquid Chromotography – Mass Spectrometry/Mass Spectrometry
LFQ	Label-Free Quantitative
MAPK	Mitogen-Activated Protein Kinase
MEA	Malt Extract Agar

NADPH	Nicotinamide Adenine Dinucleotide Phosphate
NRPS	Non-Ribosomal Peptide Synthetase
OPA	*o*-Phthaldialdehyde
PAL	Phenylalanine Ammonia Lyase
PBS	Phosphate Buffered Saline
PBST	Phosphate Buffered Saline Tween
PCR	Polymerase Chain Reaction
PEG	Polyethylene Glycol
PKS	Polyketide Synthase
PLP	Pyridoxal Phosphate
qRT-PCR	Quantitative Reverse Transcription-Polymerase Chain Reaction
RNA	Ribonucleic Acid
ROS	Reactive Oxygen Species
RP-HPLC	Reverse Phase-High Performance Liquid Chromatography
RPM	Revolutions Per Minute
RT-PCR	Reverse Transcription-Polymerase Chain Reaction
SAH	*S*-Adenosylhomocysteine
SAM	*S*-Adenosylmethionine
SDS	Sodium Dodecyl Sulphate
SOD	Superoxide Dismutase
SSA	5'5-sulfosalicylic acid
SSC	Saline Sodium citrate
TAE	Tris:Acetate:EDTA
TCA	Trichloroacetic Acid
TFA	Trifluoroacetic Acid
UV	Ultraviolet
v/v	Volume per Volume
w/v	Weight per Volume

Summary

Ergothioneine (EGT) is a tri-*N*-methylated and sulphurised histidine derivative which exhibits antioxidant properties. EGT was first identified in *Aspergillus fumigatus*, in work pertaining to gliotoxin biosynthesis. Compared to wild-type, EGT levels were elevated in the absence of GliK, a gliotoxin biosynthetic enzyme. The work presented in this thesis demonstrates that deletion of *A. fumigatus egtA* (AFUA_2G15650), which encodes a trimodular enzyme, abrogated EGT biosynthesis in this opportunistic pathogen. A second EGT biosynthetic enzyme, *egtB* (AFUA_2G13295), was also identified. EgtB, a pyridoxal phosphate (PLP)-dependant cysteine desulphurase, contributed to, but was not essential for, EGT biosynthesis. EGT absence in *A. fumigatus* Δ*egtA* significantly reduced resistance to elevated concentrations of H_2O_2 and menadione, impaired gliotoxin production, increased glutathione biosynthesis, resulted in attenuated conidiation and affected cell wall integrity. EGT deficiency specifically decreased resistance to high H_2O_2 levels, which strongly infers functionality as an auxiliary, high-level, antioxidant. Quantitative proteomic analysis revealed significant proteomic remodelling in Δ*egtA* compared to wild-type under both basal and ROS conditions, whereby the abundance of 290 proteins was altered. Specifically, the reciprocal differential abundance of cystathionine γ-synthase and β-lyase, respectively, influenced cystathionine availability to affect EGT biosynthesis. Quantitative proteomic analysis also identified VipC (AFUA_8G01930), a putative methyltransferase which may be involved in the *A. fumigatus* response to EGT absence. A *vipC* deletion mutant was thus generated to further investigate VipC function in *A. fumigatus*. Δ*vipC* demonstrated significantly altered growth, development and metabolism compared to wild-type. Glutathione levels and abundance of related biosynthetic enzymes were significantly decreased in Δ*vipC*. Additionally, enzymes involved in the methionine cycle also had decreased abundance. These data indicate that VipC plays a significant role in coordinating the metabolic response to EGT absence in *A. fumigatus*. As a sulphur-containing metabolite, EGT therefore plays a key role in redox homeostasis and requires essential consideration in future oxidative stress studies in *A. fumigatus*.

Chapter 1

Introduction

1.1 Preamble

This Chapter will begin with a general introduction to *Aspergillus fumigatus* (Section 1.2), with particular focus on asexual development (Section 1.3) and the cell wall (Section 1.4). This will highlight important aspects of *A. fumiagtus* biology that are of interest in this study. Discussion of oxidative stress will follow (Section 1.5), which will cover sources of reactive oxygen species (ROS), ROS toxicity, oxidative stress defence and conclude with a section on the interactions between secondary metabolism and oxidative stress in fungi. This will set the scene for discussion of gliotoxin: a double thiolated, redox-active secondary metabolite produced by *A. fumigatus* (Section 1.6). The biosynthesis of gliotoxin and its toxicity in the cell will be reviewed, followed by focus on the gliotoxin null mutant Δ*gliK*, which provided the first identification of ergothioneine (EGT) in *A. fumigatus*. Subsequently, the importance of sulphur metabolism in *A. fumigatus* will be examined (Section 1.7), with emphasis on sulphur assimilation and biosynthesis of sulphurised metabolites. This section will conclude with discussion on *S*-adenosylmethionine (SAM), *S*-adenosylhomocysteine (SAH) and their role in methylation. This is followed by a detailed description of EGT, a sulphurised and tri-*N*-methylated histidine derivative with antioxidant properties and the main focus of this study (Section 1.8). Firstly, EGT function in animals and plants will be discussed briefly. Then the biosynthetic pathways of EGT in bacteria and fungi will be outlined, followed by a review of the current data on EGT functionality, highlighting areas where there are gaps in knowledge. This Chapter will then conclude with an outline of the rationale and objectives of this thesis (Section 1.9).

1.2 General Characteristics of *Aspergillus fumigatus*

Aspergillus fumigatus is an opportunistic human pathogen of the phylum Ascomycota (Dagenais and Keller, 2009). A saprophytic filamentous fungus, *A. fumigatus* plays an important ecological role in its natural habitat in the soil by recycling environmental carbon and nitrogen by feeding on decaying organic matter (Latgé, 1999). *A. fumigatus* grows optimally at 37 ^{o}C and can survive anywhere in the range of 12 ^{o}C – 65 ^{o}C (Kwon-Chung and Sugui, 2013), temperatures it encounters naturally in self-heating compost piles. In the laboratory, *A. fumigatus* can grow rapidly on minimal agar plates containing a carbon source (e.g. glucose), a nitrogen source (e.g. nitrate), and trace elements (Brakhage and Langfelder, 2002).

A. fumigatus predominantly reproduces asexually, producing small grey-green haploid spores called conidia (Rokas, 2013). These conidia are 2-3.5 µm in diameter and have a hydrophobic surface. Due to this hydrophobicity, *A. fumigatus* conidia are incredibly buoyant in the air and thus easily disperse in the environment (O'Gorman, 2011). As a result, *A. fumigatus* conidia are ubiquitous in the atmosphere and are estimated to be present at concentrations of 1 – 100 conidia per m^3 (Kwon-Chung and Sugui, 2013).

The life cycle of *A. fumigatus* can be summarised as follows: (i) conidia are produced from conidiophores and released into the atmosphere (ii) conidia germinate and form septate mycelia (iii) mycelia produce conidiophores and the cycle continues (Ward et al., 2005). *A. fumigatus* has also been demonstrated to reproduce sexually, however only under very specific conditions (O'Gorman et al., 2009).

As an opportunistic human pathogen, the primary route of *A. fumigatus* infection is inhalation via the lungs. Due to the ubiquitous nature of *A. fumigatus* conidia, humans are estimated to inhale several hundred of these spores every day (Latgé, 1999). The small size of the conidia enables them to penetrate into the pulmonary alveoli (Ben-Ami et al., 2010). In immunocompetent individuals, invading conidia are cleared rapidly from the lungs by mucociliary clearance and the innate immune system via alveolar macrophages and neutrophils (Dagenais and Keller, 2009). Conidia that escape clearance and germinate to form hyphae are targeted by neutrophils that release microbicidal molecules, reactive oxygen species (ROS) and neutrophil extracellular traps (McCormick et al., 2010; Hohl and Feldmesser, 2007; Bruns et al., 2010).

In immunocompromised individuals however, conidia can germinate and cause infection. Depending on the site of infection, four different categories of disease can occur: allergic bronchopulmonary aspergillosis, chronic necrotising *Aspergillus* pneumonia, aspergilloma and invasive aspergillosis (Pathak et al., 2011). Invasive aspergillosis is the most serious and most prevalent of these diseases and is characterised by germination of the conidia and rapid hyphal growth to colonise the surrounding tissue. This leads to thrombosis, haemorrhage and dissemination to other organs via the bloodstream (McCormick et al., 2010; Dagenais and Keller, 2009; Latge, 1999). Mortality of invasive aspergillosis ranges from 40% - 90% in high risk populations (Dagenais and Keller, 2009).

A. fumigatus produces a range of secondary metabolites, low molecular mass molecules produced separately to primary metabolism. While generally they are not essential for viability, secondary metabolites often have potent physiological activity that confer a competitive advantage on the producer (Keller et al., 2005; Macheleidt et al., 2016). *A. fumigatus* produces a range of secondary metabolites that can be separated into the following four categories: (i) non-ribosomal peptides (ii) alkaloids (iii) terpenes (iv) polyketides (Keller et al., 2005). Secondary metabolites are encoded in clusters that are dispersed throughout the genome, towards telomeric regions of chromosomes (Fedorova et al., 2008). Secondary metabolism in *Aspergilli* is regulated by the methyltransferase LaeA (Bok and Keller, 2004), with deletion of *laeA* associated with absence of secondary metabolite cluster expression. Many of the secondary metabolites produced by *A. fumigatus* contribute towards pathogenesis, as demonstrated by Bok et al. (2005) who demonstrated reduced virulence in Δ*laeA* in comparison to wild-type. Some of the secondary metabolites from *A. fumigatus* which are implicated in virulence include fumagillin, the fumitremorgins, fumitoxin and the fumigaclavines (Latgé, 1999). Siderophores, iron-chelating molecules that are used to sequester iron in the iron-starved environment of the host, have also been demonstrated to play an important role in virulence (Schrettl et al., 2007; Hissen et al., 2005; Schrettl et al., 2004). Gliotoxin has also been demonstrated to contribute towards virulence and will be described in more detail in Section 1.6.

1.3 Asexual Development in *A. fumigatus*

As discussed in the previous section, conidia are essential for the dispersal, infection, and proliferation of *A. fumigatus* (Latgé, 1999). Asexual development begins with the formation of aerial hyphae that grow away from the mycelia. The top of the aerial hyphae swell to form a multinucleated vesicle, containing elongated cells called phialides. The phialides undergo a series of mitotic divisions, resulting in a chain of haploid conidia. The overall structure is called a conidiophore (Adams et al., 1998; Mullins et al., 1976, 1984; Ni et al., 2010; Rhodes & Askew, 2010).

Conidiation in *A. fumigatus* is controlled by a central regulatory pathway consisting of BrlA, AbaA and WetA (Alkhayyat et al., 2015). BrlA is transcriptional activator with two C_2H_2 zinc finger motifs essential for conidiation. BrlA is essential for development of the multinucleated vesicles and deletion of *brlA* results in elongated aerial hyphae with no conidiophores (Adams et

al., 1988, 1998; Mah & Yu, 2006). AbaA is necessary for correct differentiation of the phialides and deletion of *abaA* results in conidiophores lacking chains of conidia. AbaA is predicted to be a transcriptional activator which induces transcription of genes involved in mid-to-late phases of conidiation (Adams et al., 1998; Andrianopoulos & Timberlake, 1994; Tao & Yu, 2011). WetA functions to complete conidial development and is important for conidial maturity, integrity and viability. Deletion of *wetA* results in development of colourless conidia with defective spore walls (Andrianopoulos & Timberlake, 1994; Tao & Yu, 2011).

Expression of *brlA* is required for activation of the asexual central regulatory pathway. Deletion of *brlA* results in abrogated expression of *abaA* and *wetA*. Additionally, expression of *abaA* is also required for *wetA* activation. This results in the expression cascade: expression of *brlA*, followed by *abaA*, followed by *wetA* (Figure 1.1). This ensures appropriate expression of genes depending on the developmental stage of the conidiophore. *wetA* deletion resulted in increased accumulation of *brlA* and *abaA* transcripts. This suggests negative feedback regulation involving *wetA* inhibition of *brlA* and *abaA* (Figure 1.1). *brlA* and *abaA* also regulate the expression of *rodA*. RodA forms part of the hydrophobic rodlet layer on the surface of the conidia, important for the aerial buoyancy of the conidia. *brlA* is essential for *rodA* expression, while deletion of *abaA* results in reduced expression of *rodA* (Figure 1.1) (Tao & Yu, 2011). .

Upstream regulation of conidiation is controlled by a variety of transcriptional regulators, including SomA, StuA, FluG, FlbB, FlbD and FlbE (Yu and Keller, 2005; Sheppard et al., 2005; Lin et al., 2015). These have been demonstrated to regulate expression of *brlA*, and thus activation of conidiation. The interactions between these proteins is outlined in Figure 1.1. Deletion mutants for these transcription factors result in a variety of defects to conidiation.

Asexual development is also regulated by the velvet family of proteins, which consists of VeA, VelB, VelC, and VosA. These proteins all contain a novel velvet DNA binding domain, which functions in their role as transcriptional regulators (Bayram and Braus, 2012). Deletion of *veA*, *velB* or *vosA* in *A. fumigatus* results in increased conidiation, elevated numbers of conidiophores, increased conidial germination and increased levels of *brlA* mRNA (Park et al., 2012a). VeA, VelB and VosA therefore appear to negatively regulate conidiation in *A. fumigatus* (Figure 1.1). VosA and VelB were demonstrated to play a role in conidial viability, with Δ*vosA* and Δ*velB* mutants associated with significant reduction in conidial viability compared to wild-type

(Fillinger et al., 2001; Park et al., 2012a, 2012b). AbaA has been demonstrated to regulate expression of VelB and VosA (Tao & Yu, 2011).

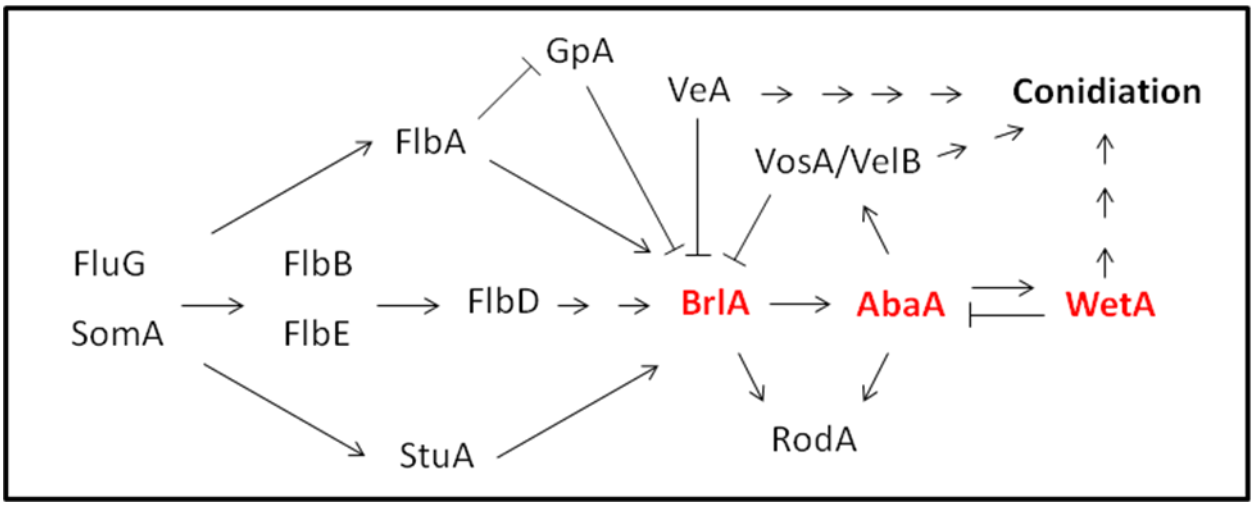

Figure 1.1. Schematic representing the regulation of asexual development in *A. fumigatus*. The central regulatory pathway is displayed in red. The central regulatory pathway is influence by a variety of upstream transcription factors, velvet proteins and G-proteins. Image adapted from Mah and Yu (2005), Sheppard et al. (2005) and Alkhayyat et al. (2015).

The heterotrimeric G-protein system has also been demonstrated to influence asexual development in *A. fumigatus*. Mah and Yu (2006) investigated two key components of the G-protein signaling system, GpaA and FlbA. Deletion of *flbA* or dominant activating GpaA mutations results in reduced conidiation with increased hyphal growth (Figure 1.1). The role of Gβγ heterodimer, SfaD (Gβ), and GpgA (Gγ), was analysed through deletion mutants for the two genes, *sfaD* and *gpgA*. Both mutants displayed impaired vegetative growth, conidial germination, and reduced conidial trehalose content (Shin et al., 2009).

1.4 The cell wall of *A. fumigatus*

The fungal cell wall provides structural integrity and protection to the cell and represents the first line of defence against external stresses. A dynamic structure, the cell wall is constantly undergoing modification in response to the growth environment (Bowman and Free, 2006). The cell wall is an important factor in considering the pathogenesis of *A. fumigatus*, as it plays an active role in infection and contains the majority of antigens detected by the host defence system

(Mouyna and Fontaine, 2009; Latgé, 1999). Due to its importance and because animal cells lack a cell wall, the cell wall of fungi represents a target for anti-fungal drug treatment. This is demonstrated by the echinocandins (e.g. caspofungin) which inhibit β(1,3)-glucan biosynthesis (Bowman et al., 2002).

The cell wall of *A. fumigatus* is comprised mainly of polysaccharides, interlaced and coated with glycoproteins. Of the polysaccharides present in the cell wall, the most abundant are: α(1,3)-glucans (35 – 46 %), β(1,3)-glucans (20 – 35 %), galactomannans (20 – 25 %), chitin (7 – 15 %) and β(1,6)-branched oligosaccharides (~4 %) (Fontaine et al., 2000). The fibrillar layer is composed of β(1,6)branched β(1,3) glucan linked to chitin, galactomannan and β(1,3;1,4)-glucan. The fibrillar layer is embedded in the amorphous layer, which consists mostly of α(1,3)-glucans and galactomannan. Glycoproteins are found embedded within the fibrillar layer and on the cell wall surface (Bernard and Latgé, 2001) (Figure 1.2). The polysaccharides of the cell wall are synthesised by membrane bound enzymes such as chitin synthases, β(1,3)-glucan synthases, mannosyltransferases and α(1,3)-glucan synthases. This is followed by transportation to the cell wall space where they undergo modification and crosslinking (Gastebois et al., 2009).

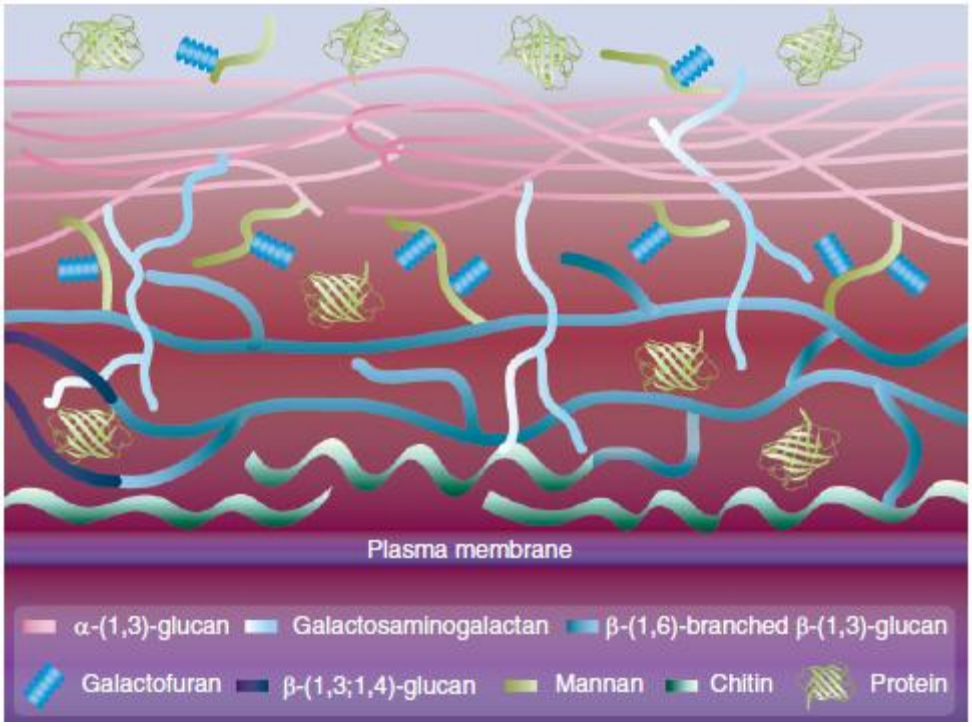

Figure 1.2. Organisation of the *A. fumigatus* cell wall. Image obtained from Gastebois et al. (2009).

Cell wall maintenance is regulated by the cell wall integrity (CWI) signalling pathway. The CWI pathway consists of three MAP kinases (MAPK): Bck1 (MAPK kinase kinase), Mkk2 (MAPK kinase), and MpkA (MAPK). These form a signal cascade which results in MpkA localising to the nucleus where it is predicted to activate transcriptional regulators (Valiente et al., 2015) (Figure 1.3). Gene deletion of any of these three MAPKs results in the failure of MpkA to localise to the nucleus and a block on the signalling cascade (Valiante et al., 2008, 2009).

Studies in *Saccharomyces cerevisiae* indicate that important upstream signals for the CWI pathway originate from WSC (CWI Stress Components) receptors, which are predicted to detect environmental stresses (Nanduri and Tartakoff, 2001; Dupres et al., 2009). These membrane bound proteins also contain a carbohydrate domain, leading to speculation they may act as a "bridge" between the cell wall and cytoplasmic membrane. *A. fumigatus* has four genes encoding WSC receptors: *wsc1*, *wsc2*, *wsc3*, and *midA*. Wsc1 is required for resistance to echinocandin antifungal drugs, while MidA was demonstrated to protect against elevated temperature and the cell wall perturbing agents congo red and calcofluor white. No function in the CWI pathway was demonstrated for Wsc2, and Wsc1, Wsc3 and MidA all displayed some redundancy in function (Dichtl et al., 2012). G protein coupled receptors are also predicted to partake in signalling upstream of the CWI in *A. fumigatus*. Deletion of *gprC* and *gprD* genes resulted in defects in cell wall related stress response (Gehrke et al., 2010). It has been demonstrated in *S. cerevisiae* that the WSC receptors are linked to the CWI pathway through different signalling elements (Figure 1.2). Two of these are conserved in *A. fumigatus*: Rho1 and PkcA (Rispail et al., 2009). PkcA, protein kinase A, has not been characterised in *A. fumigatus*, however Rho1 is known to localise to the hyphal tip and has been demonstrated to participate in CWI signalling (Ditchl et al., 2010).

While the CWI pathway is predicted to activate transcriptional regulators following localisation of MpkA to the nucleus, it has not been demonstrated which transcription factors are induced. Orthologs of transcription factors induced by the CWI pathway in *S. cerevisiae* have been identified in *A. fumigatus* (Rispail et al., 2009; Levin, 2011). Gene deletion studies for two of these genes, *dvrA* and *ace2*, demonstrated altered cell wall phenotypes (Ejzykowicz et al., 2009, 2010; Verwer et al., 2012). However, further study is required to elucidate the targets of the CWI pathway.

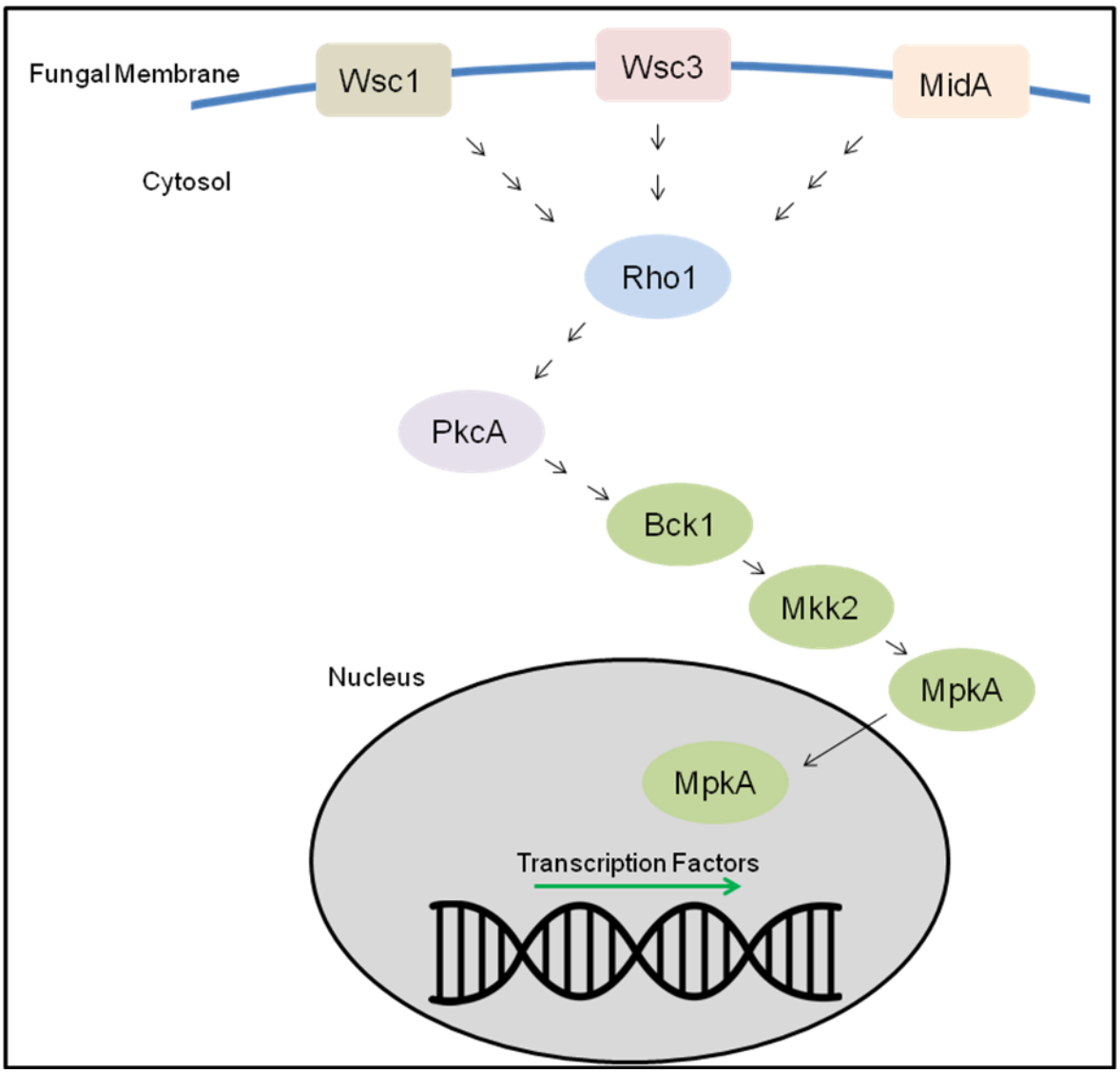

Figure 1.3. The CWI signalling pathway in *A. fumigatus*. Stress receptors (Wsc1, Wsc3, MidA) activate the MAPK cascade via Rho1 and PkcA. The phosphorylation of MpkA causes it to localise to the nucleus, resulting in the activation of specific transcription factors. Image adapted from Valiente et al. (2015).

1.5 Oxidative Stress

Oxidative stress occurs when levels of reactive oxygen species (ROS) in a cell rise above tolerable levels, leading to deleterious effects on cellular metabolism and signalling (Lushchak, 2011). ROS comprise of superoxide ($^{\bullet}O_2^-$), the hydroxyl radical ($^{\bullet}OH$) and hydrogen peroxide (H_2O_2) (Turrens et al., 2003). Oxidative stress is of particular concern for aerobic organisms, as

approximately 90 % of ROS is produced by the electron transport chain (Starkov, 2008). This is due to "leakage" of ROS from the mitochondria in the normal process of aerobic respiration (Ott et al., 2007). Intracellular ROS are also produced from other metabolic processes and enzymes such as NADPH oxidase, lipoxygenases, cyclooxygenases, and xanthine oxidase have been demonstrated to contribute to ROS levels in the cell (Puddu et al., 2008). Furthermore, ROS can be introduced from exogenous sources. For a human pathogen such as *A. fumigtaus*, this is perhaps most relevant in interactions with the host immune system. As an anti-microbial strategy, human neutrophils will produce ROS to damage pathogens in a process known as "respiratory burst". This is catalysed by an NADPH oxidase that generates superoxide ($^{\bullet}O_2^-$) and H_2O_2 (Dahlgren and Karlsson, 1999).

Elevated ROS can lead to damage to DNA, proteins and lipids. ROS can directly modify nucleotide bases in DNA; guanine in particular is vulnerable to modification by ROS, due to its low reduction potential. Modification of guanine by hydroxyl radicals can lead to the formation of 8-hydroxyguanosine. 8-hydroxyguanosine can pair with adenosine, leading to erroneous base pairing (Cooke et al., 2003). DNA damage also occurs in the form of single strand breakage, or less commonly, double strand breakage. This occurs when hydroxyl radicals interact with deoxyribose, resulting in the generation of peroxy radicals. These peroxy radicals can then nick the phosphodiester bonds in the backbone of the DNA strand, resulting in strand breakage (Dedon, 2008). Oxidative damage to proteins can result in fragmentation, formation of protein-protein cross-linkages and loss of function through oxidation of the protein backbone. Damage to proteins involved in intracellular signalling pathways and inhibition of correct proteolytic function can lead to severe disruption to cellular metabolism (Berlett and Stadtman, 1997). Protein thiol groups are particularly vulnerable to oxidative stress. Protein thiols can be modified by ROS to form sulfenic acid derivatives. While this modification is reversible, further oxidative attack can result in the formation of sulfinic acid or sulfonic acid derivatives. These modifications generally result in irreversible damage to the proteins, which then must be degraded by proteolytic enzymes (Biswas et al., 2006). Oxidative damage to lipids is best characterised by peroxidation of lipids in the cell membrane. This can result in loss of membrane fluidity and elasticity, impaired cellular functioning, and even cell rupture. Furthermore, lipid peroxidation results in the production of reactive aldehyde products, such as malondialdehyde

and 4-hydroxynonenal, which contribute towards DNA damage via formation of DNA adducts (Niki, 2009).

It is therefore important that the levels of cellular ROS are managed in order to avoid these toxic effects. The oxidative stress defence system metabolises ROS in order to ensure they do not rise above tolerable levels. A number of enzymes partake in oxidative stress defence; foremost amongst these are superoxide dismutase (SOD) and catalase. SODs are a family of antioxidant enzymes that catalyse the dismutation of superoxide into either water or H_2O_2 by adding or removing an electron from the superoxide molecule. SODs typically require either copper and zinc together or manganese as co-factors (Sheng et al., 2014). Lambou et al. (2010) characterised four SODs in *A. fumigatus*. Deletion mutants for the genes encoding each SOD revealed sensitivity to induced ROS stress via menadione, sensitivity to macrophages, sensitivity to heat, reduced conidial survival and delayed conidiation. Catalase is a tetrameric enzyme consisting of four identical subunits with a heme group and NADPH contained in the centre (Chelikani et al., 2004). Catalase converts two H_2O_2 molecules into water and O_2 via a two-stage reaction. Stage 1 involves the reaction of H_2O_2 with the heme group of catalase to form a high-valent iron intermediate. This high-valent iron intermediate then reacts rapidly with a second molecule of H_2O_2 to form O_2 and water (Alfonso-Prieto et al,. 2009). *A. fumigatus* produces three catalases, two produced in mycelia and one in conidia. Gene deletion studies demonstrated that these are required for protection from H_2O_2 (Paris et al., 2003b; Calera et al., 1997). Other enzymes which contribute to oxidative stress defence in *A. fumigatus* are glutathione peroxidases (Burns et al., 2005), thioredoxins (Kniemeyer et al., 2009) and peroxiredoxins (Hillmann et al., 2016).

The activity of these enzymes is complemented by small molecules which also contribute towards ROS detoxification. The most important of these is glutathione (GSH), a tripeptide of glutamate, cysteine and glycine (Lu, 2009). In cells, glutathione is found in a reduced (GSH) and oxidised (GSSG) form. In healthy cells, 90% of the total glutathione content is comprised of GSH and a decrease in the GSH/GSSG ratio is indicative of oxidative stress (Anderson et al., 1999; López-Mirabal and Winther, 2008). GSH is an efficient scavenger of free radicals and also functions to protect protein thiols from oxidative attack via glutathionylation (Galano and Alvarez-Idaboy, 2011; Dalle-Donne et al., 2009). Furthermore, GSH is required for the function of glutathione peroxidises (Brigelius-Flohé and Maiorino, 2013).

Regulation of the oxidative stress response occurs primarily at the genetic level. The transcription factor Yap1 is at the centre of the oxidative stress response in *A. fumigatus*. Lessing et al. (2007) demonstrated that under normal reduced conditions, Yap1 is located in the cytoplasm. However when stressed with ROS inducing agents, Yap1 localises to the nucleus to activate transcription of oxidative stress defence genes. Lessing et al. identified 29 proteins controlled directly or indirectly by Yap1, including catalase 2, thioredoxin peroxidase (AspF3) and cytochrome peroxidase. Deletion of *yap1* in *A. fumigatus* resulted in sensitivity to elevated ROS induced by H_2O_2 and mendione.

Another important aspect of the oxidative stress defence system is the CCAAT-binding complex (CBC). The CBC has been well characterised in *A. nidulans* and consists of three subunits: HapB, HapC and HapE. HapC senses the redox state of the cell through modifications of thiol groups within its histone fold motif (Thon et al., 2010). Under normal reduced conditions in the cell, HapC and HapE form a stable heterodimer, which is subsequently bound by HapB and transported to the nucleus. In the nucleus, the CBC prevents full expression of *napA* (*A. nidulans yap1* ortholog). When levels of intracellular ROS are elevated however, the thiol groups of HapC form disulphide bridges, preventing the formation of the heterodimer with HapE. Thus, the CBC does not localise to the nucleus and *napA* is expressed fully (Figure 1.4) (Thon et al., 2010).

It has been observed that much cross-talk occurs between oxidative stress and secondary metabolism in fungi (Sheridan et al., 2015). The expression of many secondary metabolites has been demonstrated to be induced by oxidative stress. Levels of type B trichothecenes, deoxynivalenol, and 15-acetyl-deoxynivalenol in *Fusarium graminearum* are increased and decreased in the presence of H_2O_2 and catalases respectively (Ponts et al., 2006, 2007). Similarly, levels of aflatoxin in *Aspergillus parisiticus* were demonstrated to be influenced by addition of H_2O_2 and antioxidants to culture media (Reverberi et al., 2005, 2008).

Several secondary metabolites function to induce oxidative stress. This is best studied in the epipolythiodioxopiperazine (ETP) class of metabolites. ETP metabolites are a class of fungal toxins characterised by a disulphide bridge. This disulphide bridge is essential for the activity of ETPs as it facilitates ROS generation by redox cycling and interaction with protein thiol groups (Gardiner et al., 2005). This can be seen in the mycotoxin sporidesmin A, which is known to cause to facial eczema and liver injury in livestock when produced by the saprophytic fungus

Pithomyces chartarum (Menna et al., 2009). Sporidesmin A has been demonstrated to induce injury via redox cycling to produce superoxide, hydroxyl radicals and H_2O_2 (Munday, 1982, 1984, 1987).

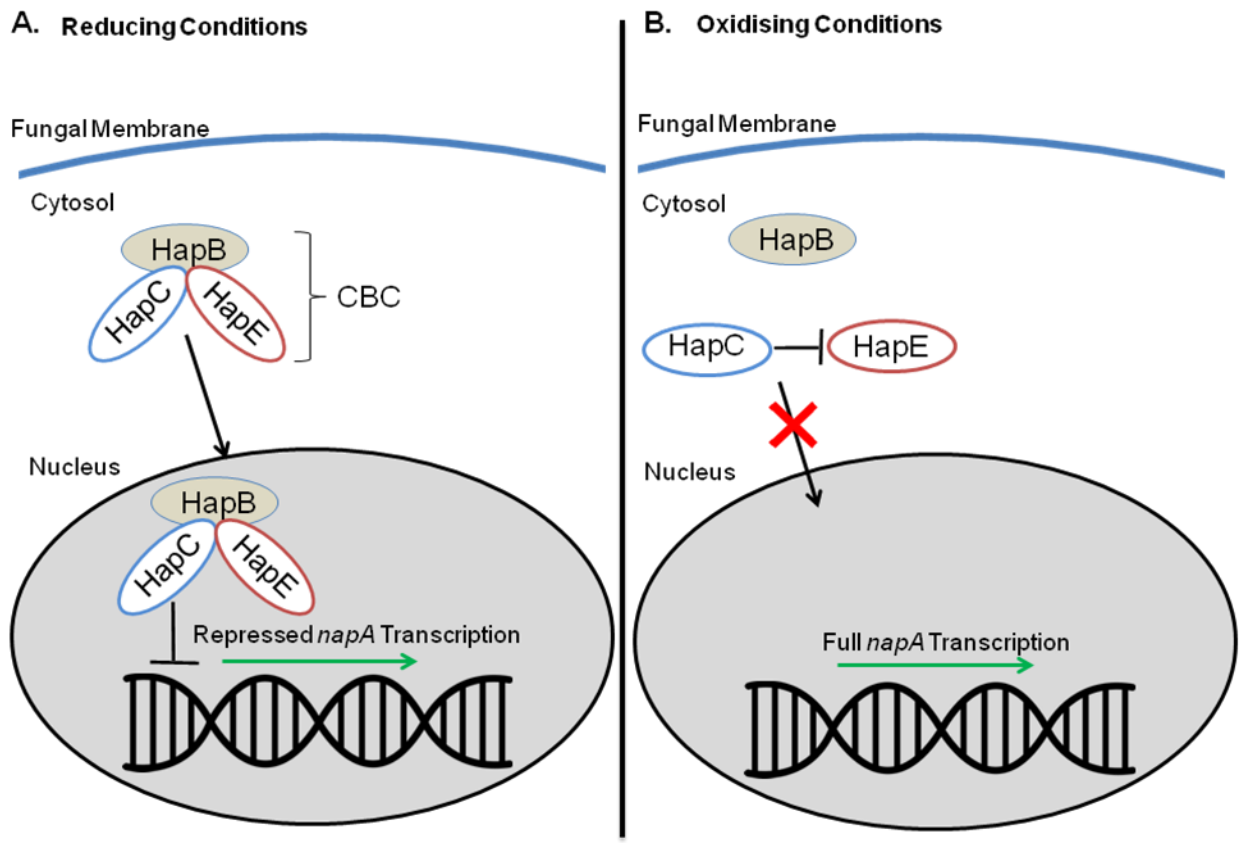

Figure 1.4. Coordination of the oxidative stress defence in *A. nidulans* via regulation of *napA* by the CBC. Image adapted from Thon et al. (2010). (A) Under reducing conditions, HapC forms a stable heterodimer with HapE, which is then subsequently bound by HapB to form the CBC. The CBC is then transported to the nucleus where it represses *napA* expression. (B) Under oxidising conditions, the thiol groups of HapC form disulphide bridges, preventing formation of the CBC and thus does not localise to the nucleus. *napA* is then expressed fully.

Gliotoxin is the best studied of the ETP metabolites and functions in a similar manner, which will be discussed further in Section 1.6. The naphthoquinones are another family of secondary metabolites that function through redox activity. Produced by a range of filamentous fungi, these metabolites have been demonstrated to interfere with the respiratory system of bacteria, yeast, fungi, and plant cells by accepting the reducing equivalents from redox enzymes and transferring

directly to oxygen, resulting in the respiratory chain being bypassed. Naphthoquinones have also been demonstrated to generate superoxide and interfere with glutathione reductase (Medentsev and Akimenko, 1998).

Secondary metabolites also function in management of ROS levels. Siderophores contribute to oxidative stress defence via management of iron homeostasis. Siderophores are non-ribosomal peptides that scavange iron, both intra- and extra-cellularly. Intracellular siderophores (e.g ferricrocin) function in iron storage, while extracellular siderophores (e.g. fusarinine C) function in iron uptake in iron starved environments (e.g. host infection)(Haas, 2012). Iron is an important element in oxidative stress defence, as heme groups are required for the function of many antioxidant enzymes (Conesa et al., 2002), however over abundance of iron can lead to oxidative stress through Fenton reaction (Papanikolaou and Pantopoulos, 2005). Siderophores therefore contribute to oxidative stress defence via regulation of iron homeostasis. This is underlined in *A. fumigatus* and *A. nidulans* by the demonstration that siderophore encoding genes are upregulated by exposure to ROS inducing agents, while deletion of siderophore encoding genes leads to sensitivity to ROS inducing agents (Eisendle et al., 2006; Schrettl et al., 2007)). Ergothioneine, a trimethylated and sulphurised histidine derivative also contributes to oxidative stress defence and will be discussed in Section 1.8.

1.6 Gliotoxin

Gliotoxin in a non-ribosomally synthesised ETP metabolite produced by many fungal species, including *A. fumigatus*. As with every other ETP toxin, the activity of gliotoxin comes from its disulphide bridge which facilitates redox cycling (Figure 1.5). Gliotoxin has many toxic effects in the cell, including generation of ROS through redox cycling, depletion of GSH levels and forming disulphide bridges with protein thiols (Gardiner et al., 2005). Through these toxic effects, gliotoxin acts as an anti-microbial agent, as well as contributing to *A. fumigatus* pathogenicity in humans (De Carvalho and Abraham, 2012; Sugui et al., 2007).

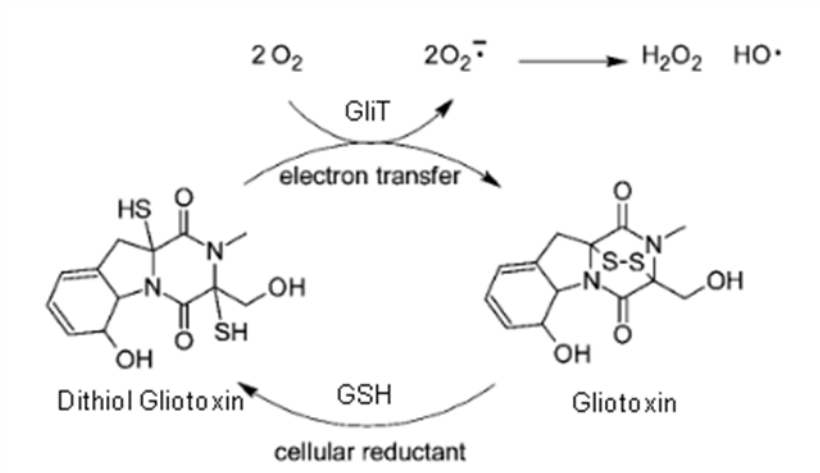

Figure 1.5. Gliotoxin redox cycling, between the reduced (Dithiol) and oxidised (Disulphide) forms. Image obtained from Gardiner et al. (2005).

1.6.1 Gliotoxin biosynthesis

Gliotoxin is biosynthesised by a series of enzymatic reactions (Figure 1.6). The genes encoding these enzymes are located in a 13 gene cluster known as the *gli* cluster (Gardiner and Howlett, 2005) (Figure 1.6). *gli* cluster activity is regulated by the transcription factor GliZ. Deletion of *gliZ* results in abrogation of the expression of key gliotoxin biosynthetic genes and gliotoxin biosynthesis (Bok et al., 2006). Gliotoxin biosynthesis is initiated by the non-ribosomal peptide synthetase GliP, which catalyses the conversion of serine and phenylalanine into cyclo-phenylalanyl-serine (Balibar and Walsh, 2006). The α-carbon of the phenylalanine in cyclo-phenylalanyl-serine is then hydroxylated by GliC to form an acyl imine intermediate (Chang et al., 2013). This acyl imine intermediate undergoes *bis*-glutathionylation, catalysed by GliG (Davis et al., 2011; Scharf et al., 2011), which introduces the thiol groups essential for gliotoxin activity. *Bis*-glutathionylation is followed by γ-glutamyl cyclotransferase activity, to remove both γ-glutamyl moieties. This is catalysed by GliK. (Gallagher et al., 2012; Scharf et al., 2013). GliJ then catalyses the removal of the two glycine fragments (Scharf et al., 2013), followed by processing by GliI, a pyridoxal phosphate (PLP)-dependant C-S lyase (Scharf et al., 2012). Methylation by GliN then follows to yield dithiol gliotoxin (Scharf et al., 2014).

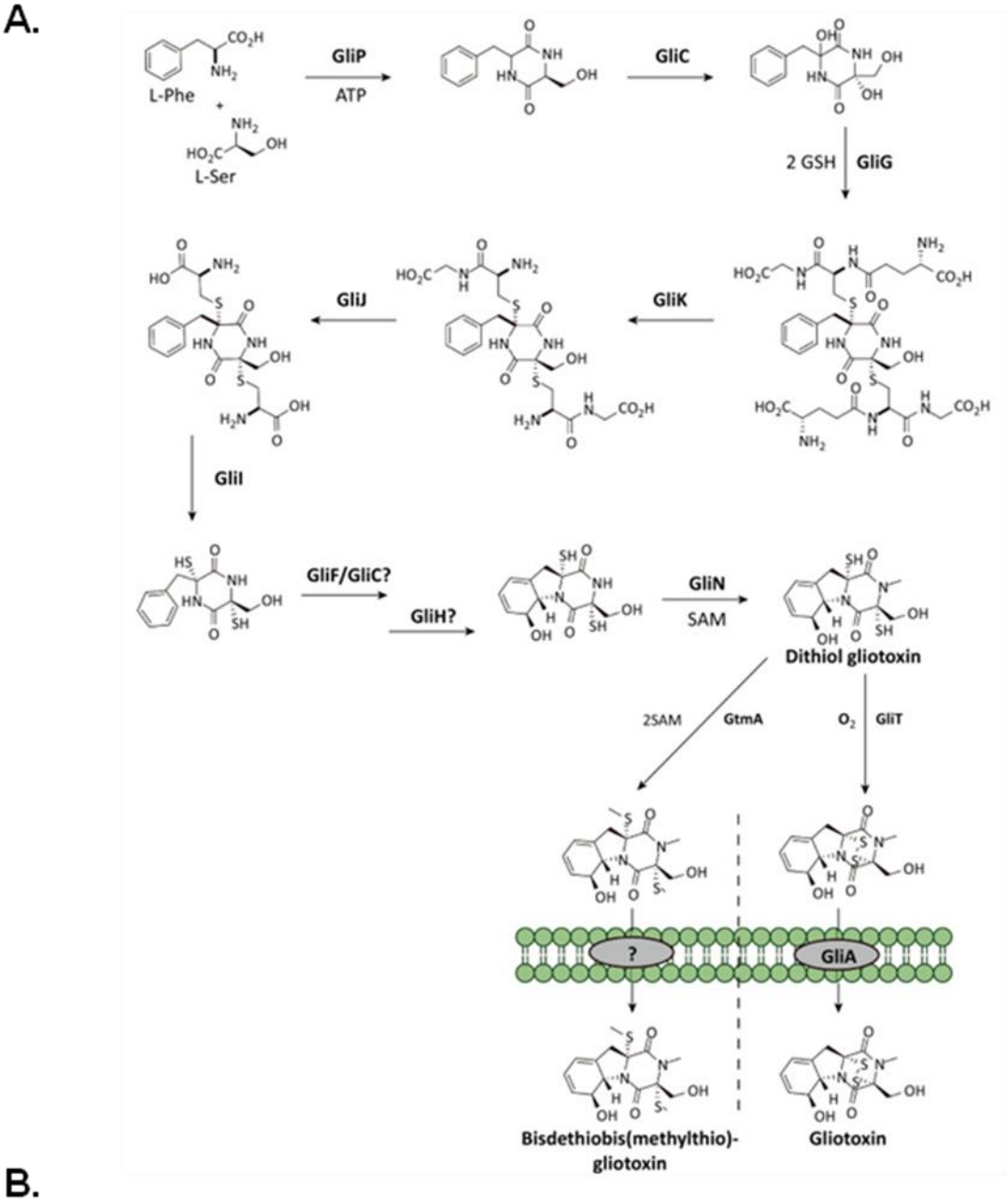

Figure 1.6. (A) Biosynthesis of gliotoxin and *bis*-methylgliotoxin and their subsequent secretion. (B) Gliotoxin biosynthetic gene (*gli*) cluster. Image obtained from Dolan et al. (2015).

GliT catalyses the final step in gliotoxin biosynthesis, closure of the disulphide bridge (Scharf et al., 2010, 2013; Schrettl et al., 2010). Gliotoxin is then secreted from the cell via the major facilitator superfamily (MFS) transporter GliA (Wang et al., 2014; Owens et al., 2015). Dithiol gliotoxin can also be processed by the *S*-adenosylmethionine (SAM)-dependant methyltransferase GtmA, which is not encoded in the *gli* cluster. GtmA catalyses the *S*-methylation of the gliotoxin thiol groups to form *bis*-methylgliotoxin. The method of secretion for *bis*-methylgliotoxin is unknown (Figure 1.6) (Dolan et al., 2014).

In addition to GliZ, gliotoxin biosyntheiss is regulated by many other factors (Dolan et al., 2015). LaeA, the master regulator of secondary metabolism, regulates gliotoxin biosynthesis. This was demonstrated in a Δ*laeA* muatant which had severely reduced levels of gliotoxin (Bok and Keller, 2004). Related to this, deletion of *veA*, which interacts with LaeA in the nucleus, also resulted in reduced gliotoxin production (Dhingra et al., 2012). LaeA and the velvet proteins are involved in asexual development as discussed previously, in addition to regulating secondary metabolism. The developmental regulators FlbB and FlbE, and the transcription factor StuA, which regulates *abaA* transcription, positively influence gliotoxin biosynthesis, further emphasising the link between asexual development and gliotoxin biosynthesis (Kim and Shin, 2013; Xiao et al., 2010; Kwon et al., 2010; Twumasi-Boateng et al., 2009). The MAP kinase MpkA, which also has a role in CWI signalling, positively regulates gliotoxin biosynthesis (Jain et al., 2011). The class 2 histone deacetylase HdaA and the histone methyltransferase CclA positively and negatively regulate gliotoxin biosynthesis respectively (Lee et al., 2009; Palmer et al., 2013). Gliotoxin is therefore regulated by a variety of factors and linked with metabolic processes such as asexual development.

Dolan et al. (2014) demonstrated that *bis*-methylated gliotoxin formation acts to attenuate gliotoxin biosynthesis. Dolan et al. identified GtmA, the SAM-dependent gliotoxin *bis*-thiomethyltransferase which is encoded outside the *gli* cluster, as responsible for gliotoxin *bis*-methylation. Deletion of *gtmA* resulted in abrogation of *bis*-methylgliotoxin production, increased gliotoxin production and a concurrent increased abundance of *gli* cluster proteins. GtmA acts to *bis*-methylate dithiol gliotoxin to form *bis*-methylgliotoxin, in place of GliT mediated disulphide bridge closure. In this way *bis*-methylgliotoxin is formed as an alternative to

gliotoxin (Figure 1.6). This novel post-biosynthetic regulation of nonribosomal peptide synthesis had never been observed previously.

1.6.2 Gliotoxin toxicity

One of the most important properties of ETP toxins is their ability to redox cycle to produce ROS. In the presence of an appropriate reducing agent (e.g. glutathione), gliotoxin can switch between a reduced and oxidised form, producing ROS (Figure 1.5). This leads to a decrease in intracellular reductants and an increase in ROS (Bernardo et al., 2003). Eichner et al. (1988) demonstrated DNA damage due to gliotoxin redox cycling, resulting in single and double stranded breaks in the DNA. Gliotoxin can also cause the formation of mixed disulphides by reacting with protein thiols. In this manner, gliotoxin can inhibit protein function, resulting in defective cellular metabolism. It has been demonstrated that gliotoxin can inhibit alcohol dehydrogenase, due to formation of a disulphide bridge in the co-factor binding region (Waring et al., 1995). It was however noticed, that gliotoxin could still inhibit alcohol dehydrogenase in the presence of a reductant, which prevented disulphide formation. This was due to generation of ROS by redox cycling of gliotoxin with the added reductant. Thus, gliotoxin inhibition of enzymes can occur through two mechanisms. Gliotoxin has also been noted to induce apoptosis in cells. This occurs through the activation of the pore-forming proapoptotic Bcl-2 family member Bak to elicit ROS generation, the mitochondrial release of apoptogenic factors, and caspase-3 activation (Hacker et al., 2013; Geissler et al., 2013).

Through these actions, gliotoxin can modulate the host immune system, making it an important factor in *A. fumigatus* pathogenesis. It has been demonstrated that gliotoxin can inhibit macrophage phagocytosis (Eichner et al., 1986), NADPH oxidase (Yoshida et al., 2000), mitogen-activated T-cell proliferation (Mullbacher and Eichner, 1984), mast cell activation (Niide et al., 2006) and cytotoxic T-cell responses (Yamada et al., 2000).

Because of these cytotoxic effects, it is important that *A. fumigatus* protects itself from the harmful actions of gliotoxin. It has been demonstrated that GliT is essential for self-protection against gliotoxin, with deletion of *gliT* resulting in severe sensitivity to exogenous gliotoxin compared to wild-type. Furthermore, strains of *A. nidulans* and *S. cerevisiae* transformed with *gliT* demonstrated increased resistance to exogenous gliotoxin compared to wild-type.

Relevantly, *gliT* was demonstrated to be regulated independently of *gliZ*, indicating gliotoxin self-protection can function autonomously of gliotoxin biosynthesis (Schrettl et al., 2010). GliA, the MFS transporter responsible for gliotoxin secretion, has also been demonstrated to contribute to gliotoxin self-protection, as the mutant Δ*gliA* had increased sensitivity to exogenous gliotoxin compared to wild-type. This indicates that efficient efflux of gliotoxin from the cell is required for gliotoxin self-protection in *A. fumigatus* (Wang et al., 2014; Owens et al., 2015).

1.6.3 *A. fumigatus* Δ*gliK*

Deletion mutants were utilised to study many of the genes in the *gli* cluster, including Δ*gliP*, Δ*gliT*, Δ*gliG*, Δ*gliZ* and Δ*gliA* (Kupfahl et al., 2006; Schrettl et al., 2010; Davis et al., 2011; Bok et al., 2006; Wang et al., 2014). This same strategy was used for investigating GliK function, using the Δ*gliK* mutant (Gallagher et al., 2012). GliK was demonstrated to be essential for gliotoxin biosynthesis, with gliotoxin production abrogated in Δ*gliK*. However, several other phenotypes were detected in addition to this. Δ*gliK* demonstrated sensitivity to exogenous gliotoxin and H_2O_2. It was observed that exogenous gliotoxin was exported from the cell at a reduced rate in Δ*gliK* compared to wild-type. RP-HPLC and LC-MS/MS analysis revealed increased levels of metabolites with a *m/z* between 394 and 396. These were later revealed to be members of the fumitremorgin family of secondary metabolites (Dr. Rebecca Owens and Professor Sean Doyle, personal communication). Additionally, Δ*gliK* led to the discovery of ergothioneine (EGT) in *A. fumigatus* and levels of the putative antioxidant were revealed to be significantly increased in Δ*gliK* compared to ATCC26933.

Absence of GliK in *A. fumigatus* therefore results in a number of phenotypes, for which the reasons have yet to be fully elucidated. Owens et al. (2015) demonstrated that Δ*gliK* has reduced GliT induction following exposure to exogenous gliotoxin, which would result in sensitivity to exogenous gliotoxin as observed. Oxidative stress sensitivity has been speculated to be caused by a "GSH sink" resulting from abrogation of gliotoxin biosynthesis directly following the glutathionylation step (Professor Sean Doyle, personal communication). Gallagher et al. (2012) speculated that gliotoxin reduction due to increased EGT levels may have led to inhibited gliotoxin efflux. Further study is required to elucidate the reasons behind the many phenotypes observed in Δ*gliK* and the implications they have for gliotoxin biosynthesis and self-protection in *A. fumigatus*.

1.7 Sulphur Metabolism

Sulphur is an essential element that is incorporated into various metabolic processes in *A. fumigatus*. This includes the proteinogenic amino acids cysteine and methionine, oxidative stress defence (GSH)(Lin, 2009), iron metabolism (Fe-S clusters)(Amich et al., 2013), ETP toxins (gliotoxin)(Davis et al., 2011) and methylation (*S*-adenosylmethionine)(Struck et al., 2012). *A. fumigatus* can acquire sulphur either through inorganic or organic sources (Amich et al., 2013). Sulphur availability is an important consideration in the pathogenesis of *A. fumigatus*, as it must source sulphur from the host environment to survive (Amich et al., 2016).

1.7.1 Assimilation of sulphur

Inorganic sources of sulphur that can be utilised by filamentous fungi include sulphate (SO_4^{2-}), sulphite (SO_3^{2-}) and sulphide (S^{2-}) (Paszewski et al., 1994). Sulphate is widespread in nature and its assimilation pathway has been well characterised in filamentous fungi. Sulphate is first transported into the cell by a sulphate permease (SB). Following transport into the cell, sulphate is reduced to adenosine 5'-phosphosulphate (APS) by an ATP sulphurylase (SC). APS is then phosphorylated by an APS kinase (SD) to form 3'-phosphoadenosine 5'-phosphosulphate (PAPS). Sulphite is then released from PAPS via the PAPS reductase SA. Sulphite is reduced to sulphide by a sulphite reductase (AFUA_6G08920, α-subunit; SF: β-subunit). Sulphide can then be incorporated into cysteine or homocysteine via cysteine synthase (CysB) and *O*-acetylserine or homocysteine synthase (CysD) and *O*-acetylhomoserine respectively (Figure 1.7) (Marzluf, 1997).

Amich et al. (2016) demonstrated that SB is essential for sulphate assimilation in *A. fumigatus*. Deletion of *sB* resulted in abrogation of growth on media containing sulphate as a sole sulphur source. This indicates that SB function in *A. fumigatus* as a sulphate permease is non-redundant. Δ*sB* also had reduced growth on sulphite and thiosulphite, indicating that SB contributes to the transport of other inorganic sulphur sources. Amich et al. (2016) also studied the sulphite reductase, responsible for converting sulphite into sulphide. The gene encoding the β subunit of sulphite reductase, *sF*, was deleted. Δ*sF* was incapable of growing on any inorganic sulphur source, with the exception of sulphide. Sulphite redudctase is therefore essential for assimilation of inorganic sulphur sources, apart for sulphide.

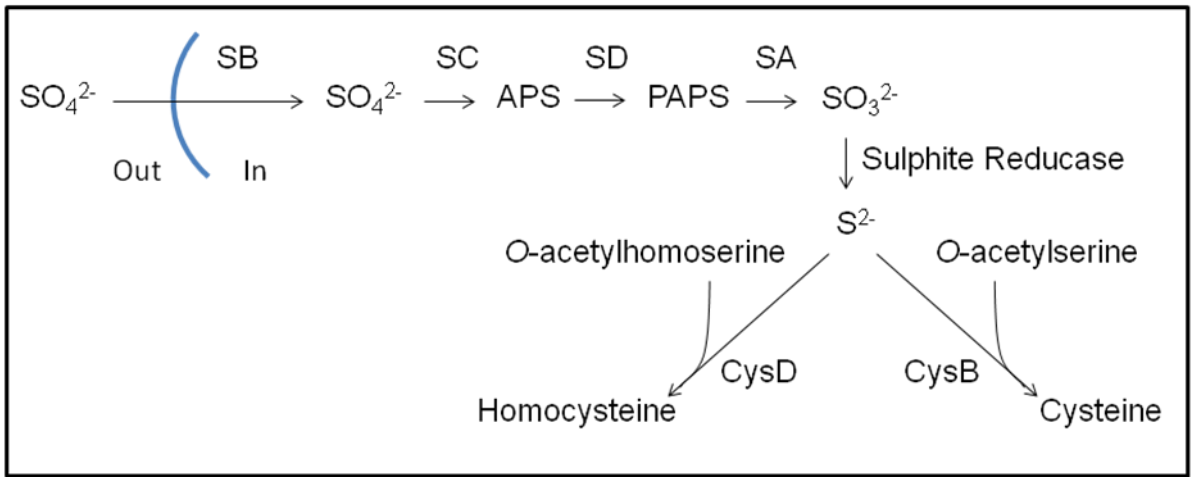

Figure 1.7. Assimilation of inorganic sulphur (sulphate) in filamentous fungi. Abbreviations: SB, sulphate permease; SC, ATP sulphurylase; SD, adenosine 5′-phosphosulphate (APS) kinase; SA, 3′-phosphoadenosine-5′-phosphosulphate (PAPS) reductase; CysB, cysteine synthase; CysD, homocysteine synthase (Amich et al., 2016).

The transcription factor MetR has been demonstrated to regulate inorganic sulphur assimilation in *A. fumigatus* (Amich et al., 2013). MetR is a leucine zipper (bZIP) transcription factor and orthlogs in *A. nidulans* (MetR) and *N. crassa* (CYS-3) have been demonstrated to regulate sulphur assimilation in their respective organisms (Natorff et al., 2003; Fu et al., 1989). Deletion of *metR* resulted in a complete absence of growth on media with inorganic sulphur as a sole sulphur source. Under sulphur rich conditions, MetR was demonstrated to be uniformly distributed throughout the cytoplasm, however under sulphur-depleted conditions, MetR localised strongly to the nucleus. MetR localisation to the nucleus was followed by upregulation of genes involved in the inorganic sulphur assimilation pathway: *sB, sC, sD, sA* and sulphite reductase. MetR was also demonstrated to bind to the promoter regions of *sB, sC* and *sD.* Deletion of *metR* resulted in decreased transcript of *sB, sC, sD, sA* and sulphite reductase relative to wild-type levels. MetR was therefore demonstrated to regulate inorganic sulphur assimilation.

A. fumigatus can also utilise organic sulphur sources such as methionine, cysteine, homocysteine and taurine (a cysteine derivative). Regulation of the assimilation of organic sources is independent of MetR, which is required for assimilation of inorganic sulphur sources. This is demonstrated by the Δ*metR* mutant, which matched wild-type growth on media with methionine or homocysteine as a sole sulphur source (Amich et al., 2013). Conversely, Δ*metR* had severely

reduced growth on media with cysteine as a sole sulphur source compared to wild-type and could not grow at all on media with glutathione or taurine as a sole sulphur source. However, it was noted that Δ*metR* could utilise GSH and cysteine as a sole sulphur source when simultaneously starved of nitrogen, indicating a link between sulphur and nitrogen utilisation. Taurine could not be utilised by Δ*metR* regardless of nitrogen availability. Amich et al. (2016) demonstrated that sulphite reductase, of the inorganic sulphur assimilation pathway, is also required for taurine assimilation. This is because taurine catabolism releases sulphite, which must then be reduced to sulphide via sulphite reductase. As sulphite reducase is under MetR regulation, it follows that taurine cannot be utilised as a sulphur source in Δ*metR*.

Analysis of genes involved in methionine uptake and catabolism revealed that their expression is mostly independent of MetR. Analysis of the genes encoding for the putative methionine uptake proteins *mupA* and *mupC* revealed that *mupC* expression was not altered by deletion of *metR*, while *mupA* expression was reduced in Δ*metR* compared to wild-type. The gene *metAT*, encoding for a methionine aminotransferase, had increased expression in Δ*metR* compared to wild-type under sulphur-limiting conditions. *metAT* is predicted to carry out catabolism of methionine, essential for utilisation of methionine as a sulphur source. Upregulation of *metAT* in Δ*metR* under sulphur limiting conditions indicates that not only is methionine utilisation independent of MetR, but can be increased in order to compensate for loss of inorganic sulphur utilisation. The question of cysteine utilisation could not be properly addressed as the mechanisms of cysteine catabolism have not been elucidated, However, *cynA*, encoding a putative cysteine permease, and *cysD* (cysteine synthase) appear to be regulated in a MetR dependant manner, indicating cystine uptake and assimilation may be regulated by MetR (Amich et al., 2013).

While MetR positively regulates sulphur assimilation, a set of 4 genes (*sconA, sconB, sconC and sconD*) act to negatively regulate sulphur assimilation. In *A. nidulans*, deletion of *scon* genes results in excessive accumulation of sulphur containing amino acids. Notably, exposure to Met had no affect on sulphate assimilation in *scon* deletion mutants, while in wild-type Met exposure almost eliminated inorganic sulphur assimilation (Natorff et al., 1993). *metR* transcript is increased in *scon* deletion mutants, particularly *sconB2*, indicating interaction between the positive and negative elements of sulphur regulation (Nartorff et al., 2003).

Amich et al. (2013, 2016) investigated the impact of sulphur utilisation in the pathogenesis of *A. fumigatus*. The importance of efficient sulphur utilisation in virulence was demonstrated by Δ*metR*, which had decreased virulence in *Galleria mellonella* compared to wild-type, indicating that sulphur assimilation can be a limiting factor in the pathogenesis of *A. fumigatus*. Deletion of *sB* and *sF* in *A. fumigatus* did not result in reduced virulence in a murine model, indicating inorganic sulphur sources nor taurine serve as an essential sulphur source during infection. Furthermore, a cysteine auxotroph mutant displayed reduced virulence in a murine model, indicating that cysteine levels in the murine lung are insufficient to act as a sulphur source during infection.

1.7.2 Biosynthesis of sulphur containing amino acids and metabolites

Cysteine (Cys) and methionine (Met) are sulphur-containing proteogenic amino acids. Cys can be formed directly from assimilated inorganic sulphur, as the enzyme cysteine synthase (CysB) converts sulphide and *O*-acetylserine into cysteine. Met can be converted from inorganic sulphur via homocysteine. Homocysteine synthase (CysD) catalyses the formation of homocysteine from sulphide and *O*-acetylhomoserine. A cobalamin-independent methionine synthase (MetH) then catalyses the transfer of a methyl group from methyltetrahydrofolate to homocysteine to form Met (Figure 1.8) (Brzywczy et al., 2007; Saint-Macary et al., 2015)

Cys and homocysteine can be interconverted through transsulphuration pathway, via the intermediate cystathionine. The forward transsulphuration pathway converts Cys into cystathionine by the enzyme cystathionine γ-synthase (CGS; MetB). Cystathionine is then converted into homocysteine by cystathionine β-lyase (CBL; MetG). The reverse transsulphuration pathway sees homocysteine converted into cystathionine by cystathionine β-synthase (CBS; MecA) and cystathionine converted into Cys by cystathionine γ-lyase (CGL; MecB). Through this pathway, the thiol group can be transferred between Cys and homocysteine (Figure 1.8) (Sieńko et al., 2009; Sohn et al., 2014).

Met and homocysteine are two components of the “Met cycle”, which also includes SAM and *S*-adenosylhomocysteine (SAH). Met is converted into SAM by the enzyme SAM synthetase (SasA). SAM is the universal methyl donor, as will be discussed in Section 1.7.3, and donation of the methyl group from SAM leads to the formation of SAH. SAH can then be converted into

homocysteine via a hydrolysis reaction catalysed by adenosylhomocysteinease (Sah1). As before, homocysteine is converted to Met by methionine synthase (MetH) to complete the cycle (Figure 1.8) (Saint-Macary et al., 2015; Owens et al., 2015).

Met can be also recovered from SAM via the Met salvage cycle. In the Met salvage pathway, SAM is decarboxylated to form decarboxylated SAM (dcSAM). In a reaction catalysed by spermidine synthase, dcSAM donates aminopropyl groups to putrescine to form spermidine and 5'-methylthioadenosine (MTA). MTA is then converted through a series of intermediates back to Met (Sauter et al., 2013). This pathway helps balance cellular Met and SAM levels (Figure 1.8).

To date, it is known that Cys provides the thiol group for two important redox active metabolites in *A. fumigatus*: GSH and gliotoxin. Cys is converted into GSH via a two step pathway. The first step is likely catalysed by glutamate–cysteine ligase (Gcs1), which catalyses the condensation of Cys and glutamate to form γ-glutamylcysteine. γ-glutamylcysteine is then converted to GSH by the addition of a glycine to the C-terminal of γ-glutamylcysteine by glutathione synthase (Gsh2) (Lin, 2009). In gliotoxin biosynthesis, the two thiol groups originate from the addition of two GSH molecules. This reaction is catalysed by the glutathione-S-transferase GliG (Figure 1.8) (Davis et al., 2011).

1.7.3 SAM, SAH and Methylation

Methylation is the process of transferring a methyl group (CH_3) to a substrate in place of a hydrogen atom. Methylation reactions are catalysed by methyltransferases, which can be categorised as *C*-, *N*-, *O*- or *S*-methyltransferases depending on their target. Targets of methylation include proteins, DNA, RNA and secondary metabolites. Functionally, methylation is involved in signal transduction, protein repair, chromatin regulation, gene silencing and secondary metabolite biosynthesis (Schubert et al., 2003; Liscombe et al., 2012).

SAM donates the methyl group for methylation in the majority of methylation reactions, across all branches of life. For this reason it is known as the universal methyl donor (Struck et al., 2012). Donation of the methyl group from SAM results in the formation of SAH, which can be hydrolysed to homocysteine as part of the Met cycle (Figure 1.8). SAH is a potent inhibitor of methylation (Caudill et al, 2001) and thus levels of SAH are an important factor in methylation

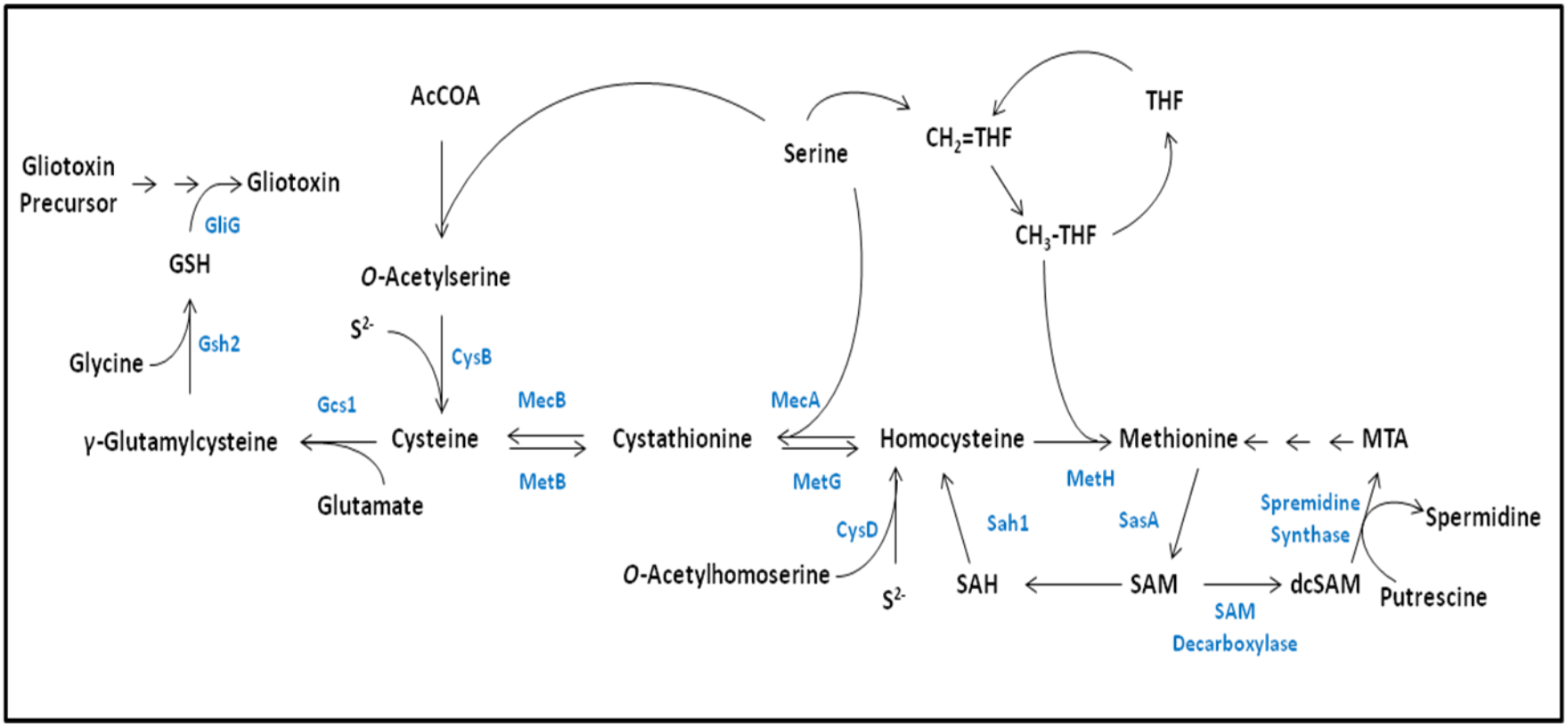

Figure 1.8. Sulphur metabolism in *A. fumigatus*, demonstrating the biosynthesis of sulphur containing amino acids and metabolites. Enzymes are shown in blue.

levels. For this reason the ratio of SAM/SAH is considered a useful indicator of cellular methylation potential.

The effects of perturbing SAM/SAH ratios have been studied through the disruption of adenosylhomocysteinase activity. As adenosylhomocysteinase catalyses the hydrolysis of SAH, any disruption to its activity would be expected to increase SAH levels, and reduce the SAM/SAH ratio. This would therefore be expected to inhibit methylation (Caudill et al., 2001). Fulneček et al. (2011) demonstrated that inhibition of adenosylhomocysteinase using 9-(S)-(2,3-dihydroxypropyl)-adenine (DHPA) in tobacco seeds resulted in global hypomethylation of DNA. Phenotypically this resulted in dosage dependant developmental defects, linked to increased expression of floral organ identity genes. The authors concluded that tobacco seeds were particularly sensitive to accurate SAM/SAH levels at critical developmental periods.

In fungi, Liao et al. (2012) investigated the effect of perturbed SAM/SAH ratios in *Cryphonectria parasitica*. Deletion of the gene encoding adenosylhomocysteinase resulted in a near 10-fold increase in SAH levels, and a 2-fold increase in SAM levels. This reduced the intraceullular SAM/SAH ratio from 2.63 to 0.53. Phenotypically, this resulted in reduced radial growth, decreased asexual development and loss of pigment. This was predicted to be due to a decrease in DNA methylation. Regulation of intracellular SAM/SAH levels are therefore important to regulate as disruption can result perturbation can effect tightly regulated gene expression.

As discussed previously, *bis*-thiomethylation of gliotoxin via the methytransferase GtmA is an important factor in negative regulation of gliotoxin biosynthesis in *A. fumigatus* (Dolan et al., 2014). While *bis*-methylation is not required for gliotoxin self-protection, disruption of the SAM/SAH ratio has been associated with gliotoxin sensitivity (Owens et al., 2015). Δ*gliT*, which demonstrates severe sensitivity to exogenous gliotoxin, had decreased levels of SAM and increased levels of SAH. Absence of GliT results in increased GtmA methyltransferase activity due to increased availability of dithiol gliotoxin. This leads to increased production of *bis*-methylgliotoxin and a concurrent shift in SAM/SAH ratio. Δ*gliK*, which is also sensitive to gliotoxin and has attenuated GliT induction following exogenous gliotoxin exposure, also displayed altered SAM/SAH ratio in a similar manner to Δ*gliT*. GliT therefore plays an important role in maintaining SAM/SAH homeostasis following exposure to exogenous gliotoxin

in *A. fumigatus* and absence of GliT leads to decreased SAM/SAH ratio, which contributes to gliotoxin toxicity in Δ*gliT* and Δ*gliK* (Owens et al., 2015).

1.8 Ergothioneine

Ergothioneine (2-mercaptohistidine trimethylbetaine; EGT) is a sulphurised and tri-*N*-methylated histidine derivative. In the cell, it exists in a tautomeric state between both the thione and thiol forms (Figure 1.9) and has demonstrable antioxidant properties. EGT exhibits a higher redox potential (E'0 = -0.06 V) than GSH (E'0 = -0.25 V), which means that EGT is less susceptible to auto-oxidation, and consequently more stable in an aerated aqueous solution (Hand et al., 2005; Hartman, 1990). EGT is produced by fungi (excepting members of the Saccharomycotina subphylum) and select bacteria, particularly members of Actinobacterial and Cyanobacterial phyla (Jones et al., 2014). While animals or plants cannot produce EGT, they can obtain it from dietary sources or from symbiotic microorganisms (Ey et al., 2007).

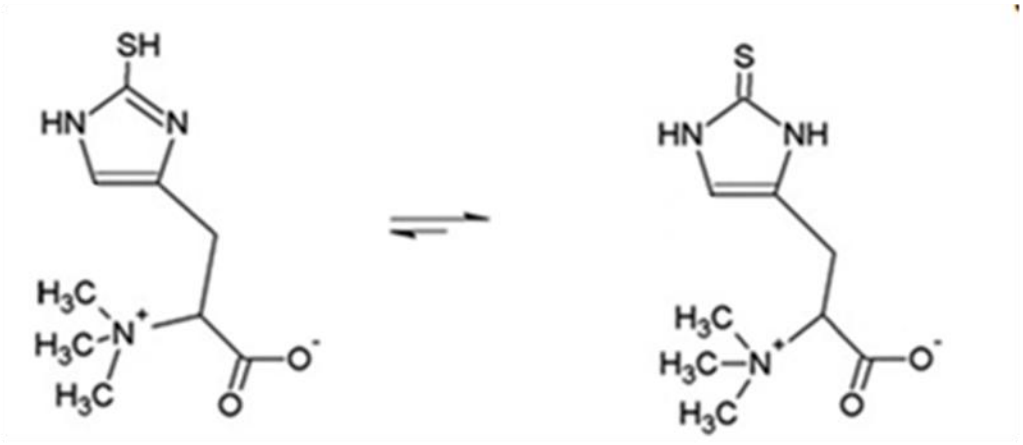

Figure 1.9. EGT structure in its thiol and thione form (Sheridan et al., 2016).

1.8.1 EGT in animals and plants

Humans acquire EGT from dietary sources. Rich sources of dietary EGT include mushrooms, oats, beans and red meat (Ey et al, 2007). Gründemann et al. (2005) identified a human EGT transporter, named OCTN1. OCTN1 is required for EGT transport into cells, as the plasma

membrane is otherwise impenetrable for EGT. Thus OCTN1 abundance correlates with cellular EGT content. Increased OCTN1 abundance has been demonstrated in erythrocyte progenitor cells, in fetal liver and bone marrow, ileum, trachea, kidney, cerebellum and lung, which have been associated with high intracellular EGT concentration. Thus, OCTN1 expression is a reliable indicator of EGT activity in human cells (Gründemann, 2012).

Various studies have been carried out on the antioxidant effects of EGT in animal cells. Aruoma et al. (1999) demonstrated that EGT protected against H_2O_2 induced cell death and peroxynitrite ($ONOO^-$) induced DNA damage in a human neuronal hybridoma cell line (N-18-RE-105). Deiana et al. (2004) reported that oral administration of EGT to rats protected against ferric-nitrilotriacetate induced peroxidation of fatty acids in the kidney and liver. Furthermore, administration of EGT conserved the concentrations of α-tocopherol and glutathione in the kidney and liver. Markova et al. (2009) demonstrated that skin cells are capable of internalising and accumulating EGT via the OCTN1 transporter. Cells with accumulated EGT had reduced levels ROS and resistance to UV mediated oxidative stress. Disruption of the OCTN1 transporter in a HeLa cell line resulted in increased mitochondrial DNA damage, protein oxidation and lipid peroxidation (Paul and Snyder, 2010). EGT has also been demonstrated to protect against the effects of cisplatin in neuronal cells (Song et al., 2010). EGT has therefore been demonstrated to be capable of protecting animal cells from oxidative damage.

EGT also has potential as a biomarker for human disease. Hatano et al. (2014) reported that levels of EGT are significantly decreased in the serum of patients with Parkinson's disease compared to healthy controls. Decreased EGT levels in blood are also associated with the onset of dementia (Cheah et al., 2016). Conversely, increased levels of EGT were detected in the brains of infants who died from sudden infant death syndrome (Graham et al., 2016).

EGT has been reported to be present in a variety of plants (Ey et al., 2007). EGT has been demonstrated to accumulate in plants from EGT producing symbiotic microorganisms. In *Gastrodia elata*, EGT concentrations were found to correlate with the levels of EGT biosynthesis in the symbiotic fungus *Armillaria mellea*. EGT levels in *G. elata* were increased in actively growing tissues, indicating EGT is actively transported within the plant to specific tissues where it is needed (Park et al., 2010). An unusual function for EGT was demonstrated in *G. elata* by

Guo et al. (2016). It was shown that the biosynthesis of the secondary metabolite gastrolatathioneine uses EGT as a precursor. Thus, symbiotic fungi produce EGT, where it is taken up by *G. elata* and modified into the final product, gastrolatathioneine. Gastrolatathioneine can therefore be said to be co-produced by plant and fungus and represents the first EGT derivative isolated from plant or animal.

1.8.2 EGT biosynthesis in bacteria

The first demonstration of EGT biosynthesis was made by Seebeck (2010), who identified a five gene cluster (*egtA-E*) which encoded genes for EGT production in *Mycobacteria smegmatis*. EGT biosynthesis in *M. smegmatis* is initiated by trimethylation of the NH_2 group of histidine by EgtD, a SAM-dependant histidine methyltransferase, to yield hercynine. Hercynine is then processed by EgtB, a sulphoxide synthase, which catalyses iron(II)-dependant oxidative sulphurisation to conjugate γ-glutamylcysteine to the imidazole side chain of hercynine. The product of this sulpurisation step, γ-glutamylhercynylcysteine sulphoxide, is processed by EgtC, a glutamine amindotransferase, which cleaves the γ-glutamyl residue to yield hercynylcysteine sulphoxide. Hercynylcysteine sulphoxide is then processed by a cysteine desulphurase (EgtE) to produce EGT (Figure 1.10). *egtA* encodes for a γ-glutamylcysteine synthase, which is predicted to provide the substrate for EgtB mediated sulphurisation.

The crystal structures of EgtD, EgtB and EgtC have all been elucidated (Vit et al., 2014, 2015; Goncharenko et al., 2015), furthering the understanding of the EGT biosynthetic process. EgtD catalyses the first step in EGT biosynthesis, the tri-*N*-methylation of histidine. While methyltransferases are a well characterised class of enzymes, methyltransferases like EgtD that catalyze the transfer of three methyl groups to the same substrate are less well understood. Diphthine synthases are an example of a well characterised methyltransferase which catalyse trimethylation (Kishishita et al., 2008). However diphthine synthases trimethylate proteins and have no discernible sequence homology with EgtD. Furthermore, diphthine synthases elute from size-exclusion chromatography as homodimers, while EgtB elutes as a monomer. The closest EgtD homologue with known function is EasF (24% sequence identity to EgtD), which catalyses the *N*(α)-methylation of dimethylallyl tryptophan in ergot alkaloid biosynthesis in *Claviceps* species. However, the crystal structure of EasF has not been determined. The closest homolog

(16 % sequence identity) to EgtD with a resolved crystal structure is human methyltransferase Ad-003, which catalyses the dimethylation of ribosomal proteins at N-terminal proline residues (Webb et al., 2010; Vit et al., 2014). EgtD therefore appears to be quite unique in structure, indicating the tri-*N*-methylation of histidine is a specialised enzymatic reaction.

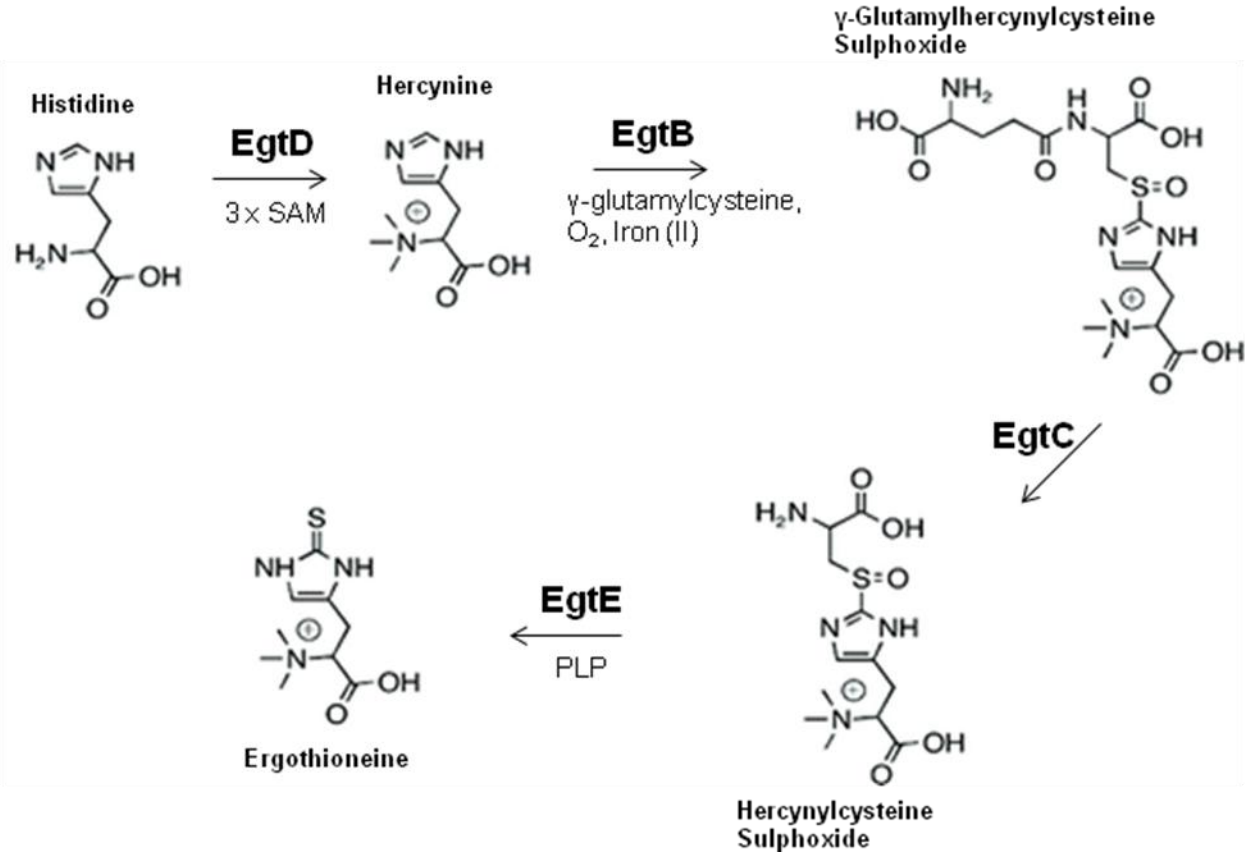

Figure 1.10. EGT biosynthesis in bacteria as elucidated from *M. smegmatis* (Seebeck, 2010).

EgtB catalyses O_2-dependent C-S bond formation between γ-glutamylcysteine and hercynine in EGT biosynthesis. The catalytic activity and the architecture of EgtB are distinct from known sulphur transferases or thiol dioxygenases. Together with OvoA, an enzyme involved in ovothiol biosynthesis (Song et al., 2014), EgtB represents a distinct class of C-S bond forming catalysts known as sulphoxide synthases. The crystal structure of EgtB in complex with γ-glutamyl cysteine and hercynine revealed that the two substrates and three histidine residues serve as ligands in an octahedral iron binding site. This active site geometry is consistent with a catalytic mechanism in which C-S bond formation is initiated by an iron(III)-complexed thiol radical attacking the imidazole ring of hercynine (Goncharenko et al., 2015).

EgtC catalyses the cleavage of the γ-glutamyl tail from γ-glutamyl hercynylcysteine sulphoxide. The set of active site residues that define substrate specificity in EgtC are highly conserved, even in homologs that are not involved in EGT production. This suggests that these homologs transform substrates with significant similarity to γ-glutamyl hercynylcysteine sulphoxide. This indicates that the common ancestor of EgtC may have developed for a purpose other than EGT production (Vit et al., 2015).

EgtE, a PLP-dependant cysteine desulphurase, catalyses the final step of EGT biosynthesis: conversion of hercynylcysteine sulphoxide in EGT. This reaction involves the cleavage of the hercynylcysteine sulphoxide cysteine residue at the sulphur atom. In the original *in vitro* reconstitution of EGT biosynthesis, Seebeck (2010) could not use EgtE to catalyse the final step due to solubility issues with the recombinant protein. As *egtA* was predicted to code for a PLP-dependant β-lyase, an unrelated β-lyase from *Erwinia tasmaniensis* was substituted for EgtE. This unrelated β-lyase was capable of completing EGT biosynthesis, indicating that the final step of EGT can be carried out by non-specific PLP-binding β-lyases. Song et al. (2015) confirmed that *M. smegmatis* EgtE could catalyse the final step of EGT biosynthesis.

egtA encodes for a γ-glutamylcysteine synthase and is predicted to contribute to EGT biosynthesis by biosynthesising the γ-glutamyl cysteine needed for iron(II)-dependant oxidative sulphurisation catalysed by EgtB. However, whether EgtA is necessary for EGT biosynthesis appears to vary between species. Deletion of *egtA* in *Mycobacterium tuberculosis* and *M. smegmatis* resulted in abrogation of EGT biosynthesis (Saini et al., 2016; Singh et al., 2016). However, a Δ*egtA* mutant in *Streptomyces coelicolor* A3(2) retained EGT production, albeit at a reduced level (Nakajima et al., 2015). Thus some bacterial species may be able to compensate for EgtA absence and complete EGT biosynthesis. This may be through an unrelated γ-glutamylcysteine synthase or through the use of cysteine as a sulphur donor.

In a study of the evolutionary history of EGT biosynthetic genes, Jones et al. (2014) reported that the 5 gene *egtA-E* cluster is specific for the Actinobacteria. However, EgtD and EgtB were found in a number of diverse phyla. Cyanobacteria are known producers of EGT (Pfeiffer et al., 2011), however they lack EgtA, EgtC and EgtE. This suggests that EgtD and EgtB are essential for EGT production in bacteria, while EgtA, EgtC and EgtE are dispensable. Presumably the activity of EgtA, EgtC and EgtE can be carried out by other enzymes, as demonstrated by the substitution of

an unrelated PLP-binding β-lyase for EgtE (Seebeck, 2010) and the observation that EGT biosynthesis proceeds in the absence in EgtA in *S. coelicolor* A3(2) (Nakajima et al., 2015). The importance of EgtD in bacterial EGT biosynthesis is underlined by the many studies which have targeted *egtD* for deletion or disruption in order to create an EGT null mutant (Saini et al. 2016; Nakajima et al., 2015; Alamgir et al., 2015; Sao Emani et al., 2013).

1.8.3 EGT biosynthesis in fungi

EGT biosynthesis in fungi has been studied by Bello et al. (2012) and Pluskal et al. (2014) in *Neurospora crassa* and *Schizosaccharomyces pombe*, respectively. Bello et al. (2012) identified the first fungal EGT biosynthetic enzyme in *N. crassa*. Through bioinformatic anaylsis, they determined the gene NCU04343 contain domains from both bacterial EgtB and EgtD. This was consistent with previous observations of a fusion gene in fungal homologs of EGT biosynthetic genes (Seebeck, 2010). To determine if this gene was responsible for EGT biosynthesis in *N. crassa*, a gene deletion mutant was obtained from the Fungal Genetics Stock Centre (Kansas City, USA). HPLC analysis determined that the *N. crassa* NCU04343 mutant was incapable of producing EGT. NCU04343 was thus determined to be the first biosynthetic gene in EGT biosynthesis and was renamed *egt-1*. Pluskal et al. (2014) demonstrated that deletion of the *egt-1* homolog in *S. pombe*, *egt1*, also abrogated EGT production. This was further confirmation of the importance of *egt-1* orthologs in fungal EGT biosynthesis.

Work by Ishikawa et al. (1974) demonstrated that cysteine is the sulphur donor for EGT biosynthesis in fungi, as opposed to γ-glutamylcysteine utilised by bacteria (Seebeck, 2010). It has been reported that fungi do not contain orthlogs of bacterial EgtA or EgtC (Jones et al., 2014). This would indicate that there is no γ-glutamylcysteine synthase to produce γ-glutamylcysteine, or a glutamate aminotransferase to cleave the γ-glutamyl residue. This supports the data from Ishikawa et al. (1974) and indicates that fungal production of hercynylcysteine sulphoxide is catalysed by *egt-1* using cysteine as a sulphur donor, without the need for the intermediate γ-glutamyl hercynylcysteine sulphoxide (Figure 1.11).

As *egt-1* catalyses the formation of hercynylcysteine sulphoxide, this indicated that only one other enzyme was required to complete EGT biosynthesis in fungi. Pluskal et al. (2014) investigated candidates for this second EGT biosynthetic enzyme by identifying genes encoding

PLP-dependant cysteine desulphurases. Four putative cysteine desulphurases were identified and deletion mutants for these were obtained from the Bioneer haploid deletion library (Kim et al., 2010). Only one of the four genes deletions, ΔSPBC660.12c, demonstrated a significant decrease in EGT levels. Concurrently, ΔSPBC660.12c displayed an increase in the intermediate hercynylcysteine sulphoxide. This demonstrated that SPBC660.12c catalyses the final step in EGT biosynthesis and was renamed *egt2*. Importantly, deletion of *egt2* did not abrogate EGT production; instead Δ*egt2* retained trace amounts of EGT. This demonstrates that, unlike *egt1*, *egt2* is not essential for EGT biosynthesis, which agrees with findings from Seebeck (2010) who demonstrated that EgtE activity could be substituted by a non-specific enzyme.

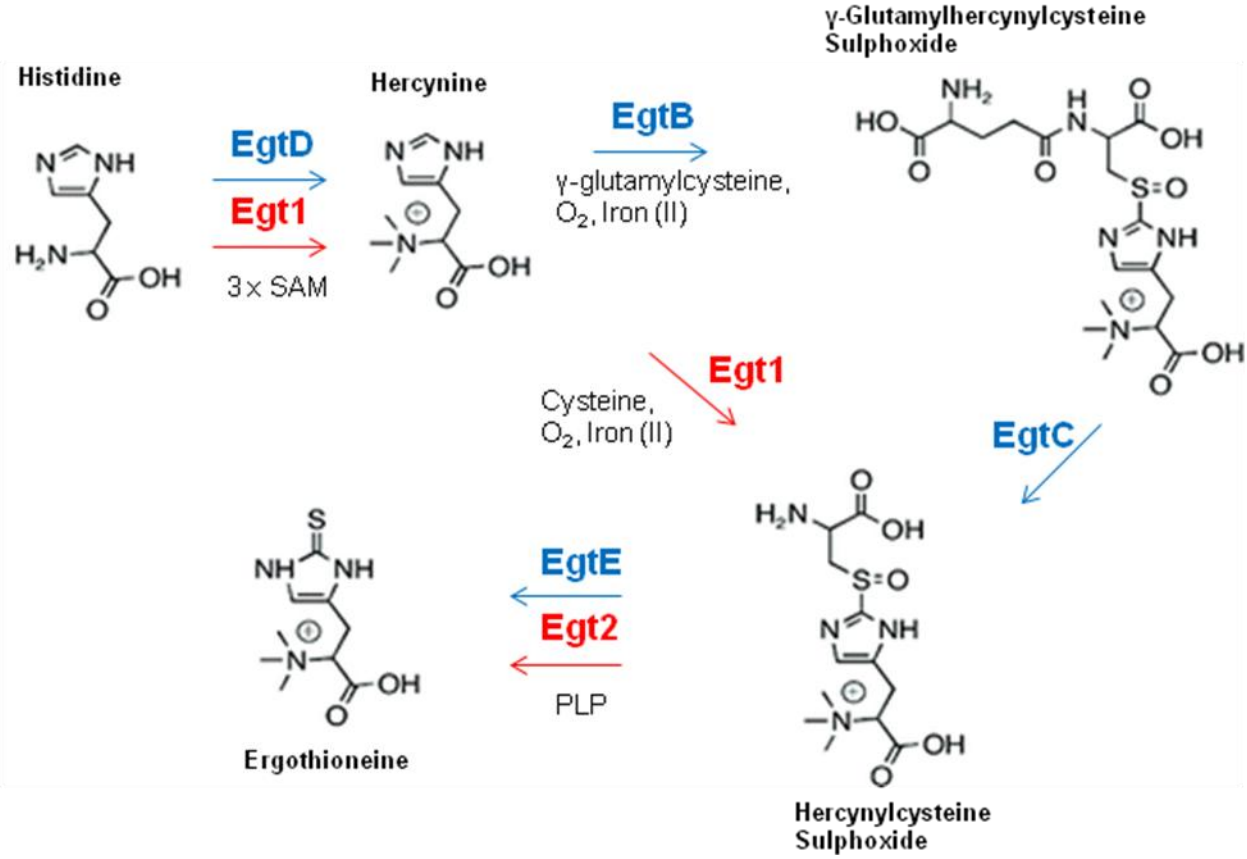

Figure 1.11. EGT biosynthesis in fungi and bacteria. Fungal enzymes are shown in red, bacterial enzymes are shown in blue. The fungal EGT pathway contains two enzymes, uses cysteine as a sulphur source and does not produce the intermediate γ-glutamyl hercynylcysteine sulphoxide.

Thus EGT bioynthesis in fungi was demonstrated to be carried out by 2 enzymes. The first, Egt-1, is a fusion protein of bacterial EgtB and EgtD and catalyses the tri-*N*-methylation of histidine to form hercynine, followed by iron(II)-dependant oxidative sulphurisation to conjugate cysteine to the imidazole side chain of hercynine. Egt-1 yields hercynylcysteine sulphoxide, which is then processed by the second enzyme, Egt2. Egt2 is a PLP-dependant cysteine desulphurase that catalyses the cleavage of the cysteine residue of hercynylcysteine sulphoxide at the sulphur atom to yield EGT (Figure 1.11).

Jones et al. (2014) investigated the evolutionary origins and distribution of EGT biosynthetic genes in fungi. Orthologs of *N. crassa* Egt-1 were identified in 73 fungal species. Egt-1 was absent in all members of *Saccharomycotina* analysed, indicating loss of Egt-1 occured before speciation occurred. Egt-1 was also absent in two members of the basidiomycetes: *Moniliophthora perniciosa* and *Malassezia globosa*. Due to the phylogenetic distance between *M. perniciosa* and *M. globosa* it is suggested that Egt-1 was lost independently in the two species. An Egt-1 ortholog was detected in all other members of the Basidiomycetes analysed, and in all members of the Ascomycetes, excepting members of *Saccharomycotina*.

All EgtB and EgtD domains in fungi were found in the form of the fusion protein Egt-1. However, Jones et al. (2014) reported that two independent fusions EgtB and EgtD have occurred in bacteria. Jones et al. were unable to determine if an interkingdom horizontal gene transfer event happened and thus were unable to unambiguously determine the evolutionary origins of EGT biosynthetic genes. Three possible scenarios for the origin of EGT biosynthesis were thus proposed. First, that EGT biosynthesis evolved in fungi originally and Egt-1 was transferred to bacteria, followed by gene fission to form EgtB and EgtD. Second, that EGT biosynthesis evolved in bacteria first and transferred to the last fungal ancestor in a gene fusion event to form Egt-1. Finally, EGT biosynthesis may have evolved independently in bacteria and fungi. This last option is considered unlikely however, given the similarity in the gene sequences and pathways involved in fungal and bacterial EGT biosynthesis.

1.8.4 EGT function in bacteria and fungi

EGT functionality in bacteria and fungi capable of producing it has been investigated by gene deletion or gene disruption studies. By targeting *egtD* in bacteria and *egt-1* fungi, EGT biosynthesis can be abolished and EGT function can be inferred from any phenotypes observed.

A *Streptomyces coelicolor* A3(2) Δ*egtD* mutant displayed abrogation of EGT production and was sensitive to the exogenous ROS inducers, H_2O_2 and cumene hydroperoxide. Abrogation of EGT in *S. coelicolor* A3(2) Δ*egtD* resulted in a concurrent increase in the levels of another low molecular mass thiol, mycothiol. Abrogation of mycothiol production had no effect on EGT production in *Streptomyces coelicolor* A3(2) (Nakajima et al., 2015). This indicates cross-talk between the two low molecular mass ROS scavengers. In *M. smegmatis*, *egtD* deletion also results in sensitivity to exogenous ROS. However, abrogation of EGT did not result in an increase in mycothiol (Sao Emani et al., 2013). Instead, a mycothiol deficient mutant demonstrated an increase in EGT (Ta et al., 2011). Once again cross-talk of low molecular mass thiols is demonstrated; however the priority appears to be reversed in *M. smegmatis*. Interestingly, Sao Emani et al. (2013) also reported that EGT is secreted into the culture medium in large quantities by *M. smegmatis*, indicating a possibly extracellular role for EGT. Saini et al. (2016) reported a similar EGT-mycothiol cross-talk in *Mycobacterium tuberculosis*, whereby EGT levels are increased in a mycothiol null mutant, but mycothiol is unaffected by absence of EGT. EGT protects *M. tuberculosis* against exogenous ROS inducing agents (H_2O_2, paraquat, menadione and cumene hydroperoxide) as observed elsewhere. EGT also contributed to antibacterial drug resistance in *M. tuberculosis*.

Richard-Greenblatt et al. (2015) demonstrated that EGT is important for *M. tuberculosis* viability during starvation. EGT levels were demonstrated to increase significantly in *M. tuberculosis* when grown under starvation conditions. An *M. tuberculosis* Δ*egtD* strain demonstrated decreased viability under starvation conditions compared to wild-type and complemented strains. EGT was also demonstrated to contribute to the virulence of *M. tuberculosis* (Richard-Greenblatt et al., 2015; Saini et al., 2016). In *Methylobacterium aquaticum*, abrogated EGT production resulted in sensitivity to heat shock, UV radiation and sunlight. Curiously, the *M. aquaticum* null mutant showed increased resistance to H_2O_2 compared to wild-type. Levels of GSH were demonstrated to be increased in the EGT null mutant compared to wild-type and it was

speculated that this may explain the observed increase in resistance (Alamgir et al., 2015). Zhao et al. (2015) demonstrated a particularly novel role for EGT in *Streptomyces lincolnensis*. EGT, in conjunction with mycothiol, was demonstrated to be involved with the biosynthesis of the antibiotic lincomycin A. EGT serves as a carrier, via *S*-glycosylation, for the lincomycin A precursor lincosamine and mediates its condensation with a *N* -methylated 4-propyl- L –proline moiety. Mycothiol then associates with this newly formed intermediate via a second *S*-glycosylation step to act as a sulphur donor. This represents the first biochemical evidence of EGT use in enzymatic reactions.

To date, EGT function in fungi has been best analysed in *N. crassa*. Bello et al. (2012, 2014) used a Δ*egt-1* mutant to investigate EGT functionality in *N. crassa*. Analysis of conidial germination and viability following exposure to cupric oxide, menadione and UV light (254 nm) showed no significant differences between the wild-type and Δ*egt-1* strains. EGT was also demonstrated to play no role in protecting mycelia from cupric oxide toxicity. However, Δ*egt-1* conidia showed a significant reduction in germination compared to wild-type when exposed to *tert*-butyl hydroperoxide. EGT was also demonstrated to contribute to *N. crassa* conidial longevity. Furthermore, the Δ*egt-1* mutant produced significantly less conidia compared to wild-type. EGT therefore appears to play an important role in conidiation and conidial health in *N. crassa*. However no role for EGT in the mycelia of *N. crassa* was detected.

Pluskal et al. (2014) generated an EGT null mutant (Δ*egt1*) and a strain producing trace amounts of EGT (Δ*egt2*) in *S. pombe*. Phenotypic analysis of these strains revealed no differences between the mutants and wild-type. EGT was demonstrated to play no role in protecting *S. pombe* from H_2O_2 and *tert*-butyl hydroperoxide. Metabolic analysis revealed no changes in the levels of metabolites in either strains, except for EGT itself and hercynylcysteine sulphoxide in Δ*egt2*. Thus, no role for EGT in *S. pombe* has been characterised.

The physiological function of EGT therefore appears to be both varied and ill-defined. There is strong evidence that EGT functions as an antioxidant, as many of the EGT null mutants display sensitivity to exogenous sources of ROS. However, as demonstrated in *S. pombe*, this is not always the case. Additionally, Bello et al. (2012, 2014) demonstrated that EGT only functions as an antioxidant in conidia, suggesting EGT function is required at specific stages of the *N. crassa* life cycle. EGT also demonstrated protection against antibacterial drugs, heat shock and UV light

(In *M. aquaticum*, but not *N. crassa*). EGT also appears to contribute to the virulence and starvation response of *M. tuberculosis*, while a novel role for EGT in contributing to lincomycin A biosynthesis in *S. lincolnensis* was also described. EGT function therefore appears to vary between species, while information of EGT function in filamentous fungi is limited to the studies from Bello et al. (2012, 2014).

1.9 Thesis rationale and objectives

EGT is a low molecular mass thiol produced by fungi and select bacteria that is utilised by plants and animals. EGT function has been investigated in bacteria and fungi and appears to play a variety of roles, oxidative stress defence the most prominent amongst them (Cheah and Halliwell, 2012). Two genes have been demonstrated to be responsible for EGT biosynthesis in fungi. The first, *egt-1* in *N. crassa*, encodes for a fusion protein with methylation and sulphoxide synthase domains (Bello et al., 2012). The second, *egt2* in *S. pombe*, encodes for a PLP-dependant cysteine desulphurase (Pluskal et al., 2014).

EGT was first identified in *A. fumigatus* by Gallagher et al. (2012) in the gliotoxin null mutant Δ*gliK* and its function in *A. fumigatus* has yet to be characterised. Δ*gliK*, in addition to abrogated gliotoxin biosynthesis demonstrated a range of phenotypes including: gliotoxin sensitivity, H_2O_2 sensitivity, decreased gliotoxin efflux, increased levels of fumitremorgins and increased levels of EGT. Owens et al. (2015) later added to this knowledge, demonstrating that Δ*gliK* had reduced induction of GliT and perturbed SAM/SAH levels following gliotoxin exposure.

The observed increase of EGT levels in Δ*gliK* was of considerable interest as EGT functionality in *A. fumigatus* was not characterised. Δ*gliK* demonstrated perturbations in oxidative stress defence, SAM/SAH levels and gliotoxin biosynthesis. Potentially, through SAM-dependant trimethylation and sulphurisation, EGT biosynthesis is linked metabolically with the same systems affected in Δ*gliK*. Additionally, the putative role of EGT as an antioxidant could be linked to H_2O_2 stress observed in Δ*gliK*. Thus EGT could be speculated to have a significant role in *A. fumigatus* adaption to *gliK* deletion. As such, further study of EGT function in *A. fumigatus* was required.

Therefore, the objectives of the work presented in this thesis were as follows:

(i) Identify and delete the genes responsible for EGT biosynthesis in *A. fumigatus*.

(ii) Characterise the function of EGT in *A. fumigatus* through the use of an EGT null mutant.

(iii) Investigate the global systems affected by EGT absence in *A. fumigatus* through phenotypic and metabolomic analysis of the EGT null mutant.

(iv) Investigate the impact of EGT absence on the *A. fumigatus* proteome through label-free quantitative proteomic analysis.

Chapter 2

Materials and Methods

2.1 Materials

All chemicals were purchased from Sigma-Aldrich Chemical Co. Ltd. (U.K.), unless otherwise stated.

2.1.1 *A. fumigatus* Agars and Media

2.1.1.1 *Aspergillus* Minimal Media

2.1.1.1.1 *Aspergillus* Trace Elements

$Na_2B_4O_7.10H_2O$ (0.04 g), $CuSO_4.5H_2O$ (0.4 g), $FeSO_4.7H_2O$ (0.8 g), $Na_2MoO_4.H_2O$ (0.8 g) and $ZnSO_4.7H_2$ (8 g) were dissolved in deionised H_2O (800 ml) in the order listed. The solution was made up to 1 L with deionised H_2O. The solution was filter sterilised into 50 ml aliquots and stored at -20 °C.

2.1.1.1.2 50 X *Aspergillus* Salt Solution

KCl (26 g), $MgSO_4.7H_2O$ (26 g) and KH_2PO_4 (76 g) were dissolved in 800 ml dH_2O. The solution was made up to 1 L with dH_2O and autoclaved at 121 °C for 15 min. The solution was then stored at room temperature.

2.1.1.1.3 100 X Ammonium Tartrate

Ammonium Tartrate (92 g) was dissolved in 1 L of dH_2O and autoclaved at 121 °C for 15 min. The solution was stored at room temperature.

2.1.1.1.4 *Aspergillus* Minimal Media (AMM) Liquid

100 X ammonium tartrate (10 ml) (Section 2.1.1.1.3), 50 X *Aspergillus* salt solution (20 ml) (Section 2.1.1.1.2), 1 ml *Aspergillus* Trace elements (Section 2.1.1.1.1) and glucose (10 g) were added to 800 ml dH_2O. The pH was adjusted to 6.8 and the solution was made up to 1 L with dH_2O. The solution was autoclaved at 105 °C for 30 min and stored at room temperature.

2.1.1.1.5 *Aspergillus* Minimal Media (AMM) Agar

100 X ammonium tartrate (10 ml) (Section 2.1.1.1.3), 50 X *Aspergillus* salt solution (20 ml) (Section 2.1.1.1.2), 1 ml *Aspergillus* Trace elements (Section 2.1.1.1.1) and glucose (10 g) were added to 800 ml dH_2O. The pH was adjusted to 6.8. Agar (18 g) (Fischer Scientific, UK) was added to the solution and made up to 1 L with dH_2O. The solution was autoclaved at 105 °C for 30 min and allowed to cool to ~50 °C before being poured into 90 mm petri dishes under sterile conditions. The plates were allowed to set and stored at 4 °C.

2.1.1.2 Malt Extract Agar (MEA)

Malt extract agar powder (50 g) (Oxoid Ltd, Hants., England) was dissolved in 1 L of dH_2O and autoclaved at 115 °C for 10 min and allowed to cool to ~50 °C before being poured into 90 mm petri dishes under sterile conditions. The plates were allowed to set and stored at 4 °C.

2.1.1.3 Sabouraud Dextrose Broth

Sabouraud Dextrose broth powder (35 g) (Oxoid Ltd, Hants., England) was dissolved in 1 L of dH_2O and autoclaved at 121 °C for 15 min. The media was stored at room temperature.

2.1.1.4 Czapek-Dox Broth

Czapek-Dox powder (35 g) (BD biosciences) was dissolved in 1 L of dH_2O and autoclaved at 121 °C for 15 min. The media was stored at room temperature.

2.1.1.5 Regeneration Agar

2.1.1.5.1 1.8 % (w/v) Regeneration Agar

100 X ammonium tartrate (10 ml) (Section 2.1.1.1.3), 50 X *Aspergillus* salt solution (20 ml) (Section 2.1.1.1.2), 1 ml *Aspergillus* Trace elements (Section 2.1.1.1.1), sucrose (342 g) and glucose (10 g) were added to 800 ml dH_2O. The pH was adjusted to 6.8. Agar (18 g) (Fischer Scientific, UK) was added to the solution and made up to 1 L with dH_2O. The solution was autoclaved at 105 °C for 30 min and allowed to cool to ~50 °C before being poured into 90 mm petri dishes under sterile conditions. The plates were allowed to set and stored at 4 °C.

2.1.1.5.2 0.7 % (w/v) Regeneration Agar

100 X ammonium tartrate (10 ml) (Section 2.1.1.1.3), 50 X *Aspergillus* salt solution (20 ml) (Section 2.1.1.1.2), 1 ml *Aspergillus* Trace elements (Section 2.1.1.1.1), sucrose (342 g) and glucose (10 g) were added to 800 ml dH_2O. The pH was adjusted to 6.8. Agar (7 g) (Fischer Scientific, UK) was added to the solution and made up to 1 L with dH_2O. The solution was autoclaved at 105 °C for 30 min and allowed to cool to ~50 °C before being poured into 90 mm petri dishes under sterile conditions. The plates were allowed to set and stored at 4 °C.

2.1.2 *Escherichia coli* Agars and Media

2.1.2.1 Luria-Bertani Broth (LB broth)

LB broth powder (25 g) (Difco, Maryland, USA) was dissolved in 1 L dH_2O and autoclaved at 121 °C for 15 min. The media was stored at room temperature.

2.1.2.2 Luria-Bertani Agar (LB agar)

LB broth powder (25 g) (Difco, Maryland, USA) was dissolved in 800 L dH_2O. 18 g agar (Fisher Scientific, UK) was dissolved in the solution and the volume made up to 1 L with dH_2O. The solution was autoclaved at 121 °C for 15 min and allowed to cool to ~50 °C before being poured into 90 mm petri dishes under sterile conditions. The plates were allowed to set and stored at 4 °C.

2.1.2.3 Super Optimal Catabolite repression (SOC) media

SOC media was supplied with the One Shot® TOP10 Chemically Competent *E. coli* kit (Invitrogen).

2.1.3 Solutions for pH Adjustment

2.1.3.1 5 M Hydrochloric Acid (HCl)

HCl (43.64 ml) was added to 56.36 ml dH_2O, the solution was then stored at room temperature.

2.1.3.2 5 M Sodium Hydroxide (NaOH)

NaOH pellets (20 g) were dissolved in 100 ml dH_2O, the solution was then stored at room temperature.

2.1.4 Phosphate Buffered Saline (PBS)

10 PBS tablets (Oxoid, Cambridge, UK) were dissolved in 1 L dH_2O. The solution was autoclaved at 121 ^oC for 15 min and stored at room temperature.

2.1.5 Phosphate Buffered Saline-Tween 20 (PBST)

Tween-20 (500 µl) was added to 1 L PBS (Section 2.1.4). The solution was autoclaved at 121 ^oC for 15 min and stored at room temperature.

2.1.6 Antibiotics and Supplements

All antibiotics and supplements were prepared as stock solutions in water or methanol and filter sterilised. All were stored at – 20 °C. Further information is provided in Table 2.1.

Table 2.1. Antibiotics and supplements used during this study.

Condition Tested	Reagent Used	Stock Concentration	Tested Concentration
Oxidative Stress	H_2O_2	1 M (in H_2O)	1 – 4 mM
Oxidative Stress	Menadione	1 mM (in MeOH)	20 – 80 µM
Oxidative Stress	Diamide	100 mM (in H_2O)	1.25 – 1.75 mM
Gliotoxin Sensitivity	Gliotoxin	1 mg/ml (in MeOH)	5 – 20 µg/ml
Cell Wall Stress	Congo Red	5 mg/ml (in H_2O)	10 – 50 µg/ml
Cell Wall Stress	Calcofluor White	1 mg/ml (in H_2O)	20 – 100 µg/ml
Histidine Sensitivity	Histidine	200 mM (in Molten AMM Agar)	200 mM
Phenylalanine Sensitivity	Phenylalanine	150 mM (in Molten AMM Agar)	150 mM
Pyrithiamine Resistance	Pyrithiamine hydrobromide	0.1 mg/ml (in H_2O)	0.1 µg/ml
Hygromycin Resistance	Hygromycin B	100 mg/ml (in H_2O)	100 µg/ml
Ampicillin Resistance	Ampicillin	100 mg/ml (in H_2O)	100 µg/ml

2.1.7 Molecular Biology Reagents

2.1.7.1 50 X Tris-Acetate Buffer (TAE)

Trizma base (242 g) and Ethylenediaminetetraacetic acid (EDTA) disodium salt dihydrate (18.61 g) was added to 57.1 ml glacial acetic acid. The volume was adjusted to 1 L with dH_2O. The solution was stored at room temperature.

2.1.7.2 1 X Tris-Acetate Buffer (TAE)

50 X TAE (20 ml) (Section 2.1.7.1) was added to dH_2O (980 ml). The solution was stored at room temperature.

2.1.7.3 Ethidium Bromide

Ethidium Bromide (Sigma-Aldrich) was supplied at 1 mg/ml of which 2.5 µl was used per 100 ml agarose gel.

2.1.7.4 6 X DNA Loading Dye

Loading dye (Promega, Southampton, UK) was used at the concentration supplied.

2.1.7.5 Agarose Gels

2.1.7.5.1 1 % (w/v) Agarose Gel

Agarose powder (1 g) was dissolved into 100 ml 1 X TAE (Section 2.1.7.2). This mixture was heated in a microwave oven until the agarose had dissolved and the mixture was molten. Ethidium Bromide solution (Section 2.1.7.3) was added after pouring the molten solution into a cast. The gel was left to set for at least 30 min.

2.1.7.5.2 0.7 % (w/v) Agarose Gel

Agarose powder (0.7 g) was dissolved into 100 ml 1 X TAE (Section 2.1.7.2). This mixture was heated in a microwave oven until the agarose had dissolved and the mixture was molten. Ethidium Bromide solution (Section 2.1.7.3) was added after pouring the molten solution into a cast. The gel was left to set for at least 30 min.

2.1.7.6 Molecular Weight Ladders for Agarose Gel Electrophoresis

Molecular weight ladders used in agarose gel electrophoresis are displayed in Figure 2.1.

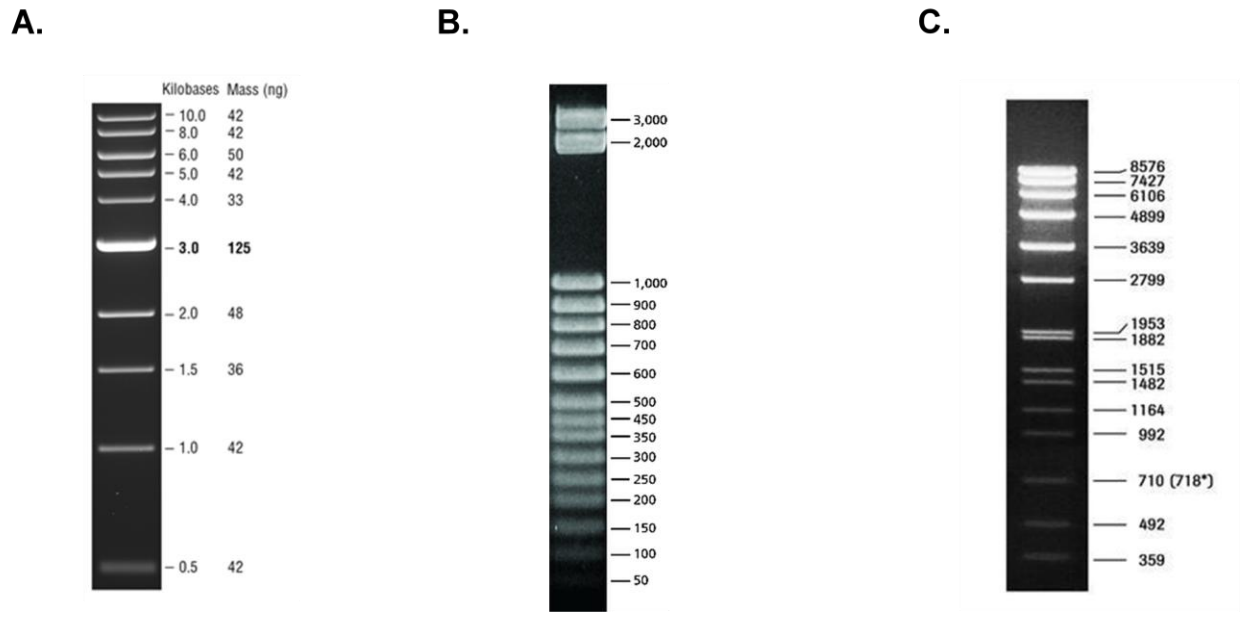

Figure 2.1. Molecular weight ladders used during this study. (A) New England Biolabs (NEB) 1 kb DNA ladder. (B) Sigma 50 bp DNA Step Ladder. (C) Roche Molecular Weight Ladder VII, Digoxigenin (DIG) labeled.

2.1.8 *Aspergillus* Transformation Reagents

2.1.8.1 0.7 M Potassium Chloride

KCl (13.05 g) was dissolved in 250 ml dH_2O. The solution was autoclaved at 121 ^oC for 15 min and stored at room temperature.

2.1.8.2 25 mM Potassium Phosphate Monobasic

KH_2PO_4 (1.7 g) was dissolved in 500 ml dH_2O.

2.1.8.3 25 mM Potassium Phosphate Dibasic

K_2HPO_4 (0.87 g) was dissolved in 200 ml dH_2O.

2.1.8.4 Lysis Buffer

KCl (26.1 g) was dissolved in 25 mM KH_2PO_4 (350 ml) (Section 2.1.8.2). The pH was adjusted to pH 5.8 with 25 mM K_2HPO_4 (Section 2.1.8.3). The solution was brought to 500 ml with dH_2O. The solution was autoclaved at 121 ^oC for 15 min and stored at room temperature.

2.1.8.5 Lytic Enzymes solution for protoplast generation

Lytic enzymes from *Trichoderma harzianum* (0.9 g) were added to 30 ml lysis buffer (Section 2.1.8.4) and filter sterilised with a 0.2 μm filter.

2.1.8.6 Buffer L6

Tris-HCl (0.484 g), sorbitol (72.88 g) and $CaCl_2.6H_2O$ (0.876 g) were dissolved in dH_2O. The pH was adjusted to pH 7.5 and the final volume adjusted to 400 ml with dH_2O. The solution was autoclaved at 121 ^oC for 15 min and stored at room temperature.

2.1.8.7 Buffer L7

Polyethylene glycol (PEG) 6,000 (60 g) was dissolved in dH_2O (40 ml) under gentle heat. Tris-HCl (0.157 g) and $CaCl_2.6H_2O$ (0.219 g) were then dissolved in the solution. The solution was removed from heat and pH adjusted to 7.5. The solution was autoclaved at 121 ^oC for 15 min and stored at room temperature.

2.1.9 Southern Blot Reagents

2.1.9.1 Southern Transfer Buffer

NaOH (16 g) and NaCl (35.07 g) were dissolved in 1 L of dH_2O.

2.1.9.2 20 x SSC

NaCl (175.3) and sodium citrate (88.2 g) were dissolved in dH_2O. The pH was adjusted to pH 7 and the final volume made up to 1 L.

2.1.9.3 2 x SSC

20 X SSC (100 ml) (Section 2.1.9.2) was added to 900 ml dH_2O and was stored at room temperature.

2.1.9.4 10 % (w/v) SDS

SDS (10 g) was dissolved in 1 L dH_2O. The solution was stored at room temperature.

2.1.9.5 0.1 % (w/v) SDS / 1 X SSC

20 X SSC (50 ml) (Section 2.1.9.2) and 10 % (w/v) SDS (10 ml) (Section 2.1.9.4) were dissolved in 1 L dH_2O. The solution was stored at room temperature.

2.1.9.6 Digoxigenin (DIG) Detection Buffers

2.1.9.6.1 10 % (w/v) Lauroylsarcosine

Lauroylsarcosine (1 g) was dissolved in 10 ml dH_2O.

2.1.9.6.2 Membrane Pre-hybridization Buffer

SDS (35 g), formamide (250 ml), blocking reagent (10 g) (Roche Applied Bioscience, Mannheim, Germany) and 10 % Lauroylsarcosine (w/v) (5 ml) (Section 2.1.9.6.1) were dissolved in 500 ml dH_2O and stored at 4 ^{o}C. The solution was pre-heated at 65 ^{o}C for 15 min before use.

2.1.9.6.3 DIG Buffer 1 (10 X)

Maleic Acid (58 g) and NaCl (43.75 g) were dissolved in 400 ml dH_2O. The pH was adjusted to pH 7.5 before the final volume was adjusted to 500 ml. The solution was autoclaved at 121 ^{o}C for 15 min and stored at room temperature.

2.1.9.6.4 DIG Buffer 1 (1 X)

100 ml 10 X DIG buffer 1 (Section 2.1.9.6.3) was added to 900 ml dH_2O and stored at room temperature.

2.1.9.6.5 DIG Buffer 2

Blocking reagent (0.4 g) (Roche Applied Bioscience, Mannheim, Germany) was dissolved in 40 ml 1 X DIG buffer 1 (Section 2.1.9.6.4) under gentle heat. The solution was prepared fresh on the day.

2.1.9.6.6 DIG Buffer 3

Tris-HCl (1.58 g), NaCl (0.58 g) and $MgCl_2.6H_2O$ (1.02 g) were dissolved in dH_2O. The pH was adjusted to pH 9.5 and the final volume adjusted 100 ml. The solution was filter sterilized through a 0.2 µm filter and stored at room temperature.

2.1.9.6.7 DIG Wash Buffer

Tween 20 (600 µl) was dissolved in 1X DIG buffer 1 (200 ml), filter sterilized through a 0.2 µm filter and stored at room temperature.

2.1.9.6.8 Anti-Digoxigenin-Alkaline Phosphatase (AP), Fab fragment conjugate

Anti-Digoxigenin-AP, Fab fragments (Roche, Mannheim, Germany) (2 µl) was added to 20 ml DIG buffer 2 (Section 2.1.9.6.5).

2.1.9.6.9 Chemiluminescent substrate phosphatase detection (CSPD) Substrate

CSPD (50 µl) (Roche, Mannheim, Germany) was added to 5 ml DIG Buffer 3 (Section 2.1.9.6.6).

2.1.9.6.10 DIG-labelled deoxynucleotide Triphosphates (dNTPs)

Pre-mixed DIG-labelled dNTPs were purchased from Roche and used according to the manufacturers guidelines for the generation of DIG-labelled probes for Southern detection probes.

2.1.9.6.11 Developer Solution

Developer (Kodak) was diluted 1/4 in dH_2O and stored in a tinfoil covered Duran in a dark room.

2.1.9.6.12 Fixer Solution

The fixer solution (Kodak) was diluted 1/5 in dH_2O and stored in a tinfoil covered Duran in a dark room.

2.1.10 Reverse-Phase High Performance Liquid Chromatography (RP-HPLC) Solvents

2.1.10.1 HPLC Grade Water with 0.1 % (v/v) Trifluoroacetic Acid (TFA)

TFA (1 ml) was added to 1 L HPLC Grade water.

2.1.10.2 HPLC Grade Acetonitrile with 0.1 % (v/v) Trifluoroacetic Acid (TFA)

TFA (1 ml) was added to 1 L HPLC Grade acetonitrile.

2.1.11 5' Iodoacetamidofluorescein (5'-IAF)

2.1.11.1 20 mg/ml 5' Iodoacetamidofluorescein (5'-IAF)

5'-IAF (25 mg) was dissolved in DMSO (1.25 ml). The solution was aliquoted into 200 µl tubes, wrapped in tinfoil and stored at -20 ^{o}C.

2.1.11.2 3 mg/ml 5' Iodoacetamidofluorescein (5'-IAF)

20 mg/ml 5'-IAF (15 µl) (Section 2.1.11.1) was added to DMSO (85 µl) in a 1.5 ml tube covered in tinfoil. The tube was kept in the dark at room temperature until needed.

2.1.12 Protein Analysis Reagents

2.1.12.1 Whole Protein Lysate Extraction Buffer

100 mM Tris-HCl (15.7 g), 50 mM NaCl (2.92 g), 20 mM EDTA (5.85 g), 10% (v/v) Glycerol (100 ml) was added to 800 ml dH_2O and brought into solution. The pH of the solution was adjusted to 7.5 and the volume made up to 1 L with dH_2O. The solution was autoclaved at 121 ^{o}C for 15 min and stored at 4 ^{o}C. PMSF (1 mM) (Section 2.1.12.3) and Pepstatin A (1 µg/ml) (Section 2.1.12.4) were added immediately before use.

2.1.12.2 *A. fumigatus* Phosphate Lysis Buffer

Sodium Phosphate monobasic (1.13 g), Sodium Phosphate dibasic (5.76 g), NaCl (2.92 g), EDTA (5.85 g), 10% (v/v) Glycerol (100 ml) was added to 800 ml dH_2O and brought into solution. The pH of the solution was adjusted to 7.5 and the volume made up to 1 L with dH_2O. The solution was autoclaved at 121 ^oC for 15 min and stored at 4 ^oC. PMSF (1 mM) (Section 2.1.12.3) and Pepstatin A (1 µg/ml) (Section 2.1.12.4) were added immediately before use.

2.1.12.3 100 mM Phenylmethylsulfonyl fluoride (PMSF)

PMSF (174 mg) was dissolved in 10 ml methanol. The solution was stored at -20 ^oC.

2.1.12.4 Pepstatin A (1 mg/ml)

Pepstatin A (5 mg) was brought to 5 ml with ethanol. The solution was stored at -20 ^oC.

2.1.12.5 Bradford Solution

Bradford Reagent (BioRad) was diluted 1/5 in PBS. This was stored at 4 ºC for up to one week.

2.1.13 Mass Spectrometry Reagents

2.1.13.1 100 % (w/v) Trichloroacetic acid (TCA)

Trichloroacetic acid (100 g) was added to 45.5 ml dH_2O and dissolved. The solution was stored in the dark at 4 ^oC.

2.1.13.2 50 mM Ammonium bicarbonate

Ammonium bicarbonate (395 mg) was dissolved in 100 ml of deionised H_2O. The solution was prepared fresh on day of use.

2.1.13.3 Protein Resuspension Buffer

Tris-HCl (1.21 g) was dissolved in 50 ml deionised H_2O. 36 g Urea (6 M) and 15.2 g Thiourea (2 M) were then dissolved. The pH was adjusted to 8.0 and the volume was brought to 100 ml with deionised H_2O. The solution was filtered with a 0.2 µm filter and stored at room temperature.

2.1.13.4 0.5 M Dithiontreitol (DTT)

DTT (77 mg) was dissolved in 100 mM ammonium bicarbonate (1 ml) (Section 2.1.13.2). The solution was prepared fresh on the day of use.

2.1.13.5 0.55 M Iodoacetamide

Iodoacetamide (IAA) (50.8 mg) was dissolved in 100 mM ammonium bicarbonate (0.5 ml) (Section 2.1.13.2). The solution was prepared fresh on the day of use.

2.1.13.6 Trypsin

Immediately before use a vial containing 20 µg sequence grade modified trypsin (Promega) was resuspended in 20 µl trypsin resuspension buffer (Promega). The vial was kept on ice before use. Remaining trypsin was snap frozen and stored at -20 ^{o}C.

2.1.13.7 0.1 % (v/v) Formic Acid

Formic acid (1 ml) was added to 1 L deionised H_2O.

2.1.13.8 ProteaseMax Sufactant Trypsin Enhancer

Immediately before use, a vial containing 1 mg ProteaseMax (Promega) was resuspended in 100 µl of 50 mM ammonium bicarbonate (Section 2.1.13.2). The vial was kept on ice until use. Remaining ProteaseMax was snap frozen and stored at -20 ^{o}C.

2.1.13.9 Q-Exactive Loading Buffer

TFA (1 ml) was added to 1 L deionised H_2O.

2.1.14 ZipTip ® Pipette Tip Solutions

2.1.14.1 Resuspension Buffer

TFA (5 µl) was added to 995 µl deionised H_2O in a 1.5 ml tube. Solution was made fresh on day of use.

2.1.14.2 Equilibration and Washing Solution

TFA (1 µl) was added to 999 µl deionised H_2O in a 1.5 ml tube. Solution was made fresh on day of use.

2.1.14.3 Wetting Solution

Acetonitrile (800 µl) and TFA (1 µl) was added to 199 µl deionised H_2O in a 1.5 ml tube. Solution was made fresh on day of use.

2.1.14.4 Elution Solution

Acetonitrile (600 µl) and TFA (1 µl) was added to 399 µl deionised H_2O in a 1.5 ml tube. Solution was made fresh on day of use.

2.1.15 Reagents for Measurement of Intracellular GSH and GSSG

2.1.15.1 125 mM Sodium Phosphate monobasic

Sodium Phosphate Monobasic (1.5 g) was dissolved in 100 ml dH_2O. It was stored at 4 °C until required for use.

2.1.15.2 125 mM Sodium Phosphate dibasic

Sodium Phosphate dibasic (1.77 g) was dissolved in 100 ml dH_2O. It was stored at 4 °C until required for use.

2.1.15.3 Assay Buffer

125 mM sodium phosphate monobasic (Section 2.1.15.1) was added, dropwise, to 125 mM sodium phosphate dibasic (Section 2.1.15.2), until the pH was adjusted to pH 7.5. EDTA (0.2345 g) was then dissolved in the solution. The solution was made up to 100 ml with dH_2O. The solution was stored at 4 °C.

2.1.15.4 5 % (w/v) 5'5-sulfosalicylic Acid (5 % (w/v) (SSA)

SSA (0.5 g) was dissolved in assay buffer (10 ml) (Section 2.1.15.3) and stored on ice.

2.1.15.5 50 % (v/v) Triethanolamine

Triethanolamine (250 µl) was added to assay buffer (250 µl) (Section 2.1.13.2).

2.1.15.6 20 % (v/v) 2-vinylpyridine

2-vinylpyridine (20 µl) was added to assay buffer (80 µl) (Section 2.1.13.2). This was carried out in the fumehood.

2.1.15.7 10 mM 5,5'-dithio-bis(2-nitrobenzoic acid) (DTNB)

DTNB (10.89 mg) was dissolved in assay buffer (3 ml) (Section 2.1.13.2). This was covered in tinfoil and stored on ice.

2.1.15.8 DTNB containing 1 U Glutathione Reductase

For every well to be assayed 1 U of glutathione reductase was added to 42 µl of 10 mM DTNB (Section 2.1.15.7).

2.1.15.9 β-nicotinamide adenine dinucleotide 2'-phosphate reduced tetrasodium salt hydrate (NADPH)

2.1.15.9.1 30 mM NADPH

NADPH (25 mg) was dissolved in assay buffer (1 ml) (Section 2.1.13.2). This was aliquoted into smaller volumes, covered in tinfoil and stored at -20 ^{o}C.

2.1.15.9.2 5 mM NADPH

1 volume of 30 mM NADPH (Section 2.1.15.9.1) was added to 5 volumes of assay buffer (Section 2.1.13.2). This was covered in tinfoil and stored on ice.

2.1.15.10 1 mg/ml Glutathione (GSH)

GSH (1 mg) was dissolved in assay buffer (1 ml) (Section 2.1.13.2). This was covered in tinfoil and stored on ice.

2.1.15.11 2 mg/ml Glutathione disulfide (GSSG)

GSSG (2 mg) was dissolved in assay buffer (1 ml) (Section 2.1.13.2). This was covered in tinfoil and stored on ice.

2.1.16 2',7'-dichlorodihydrofluorescein diacetate (H_2DCFDA)

H_2DCFDA dessicate (100 mg) (Invitrogen) was resuspended in 2 ml DMSO creating a 50 mg/ml stock which was stored at -20 ^{o}C.

2.2 Methods

2.2.1 Microbiological Methods – Strain Storage and Growth

Fungal and bacterial strains used in this study are listed in Table 2.2. Plasmids used in this study are listed in Table 2.3.

Table 2.2. Fungal and bacterial strains used in this study, including antibiotics used.

Species	Strain	Antibiotics	Reference
A. fumigatus	ATCC26933	N/A	http://www.atcc.org
A. fumigatus	AfS77	N/A	Hartmann et al., 2010
A. fumigatus	Δ*egtA*^{26933}	Pyrithiamine (100 ng/ml	This work
A. fumigatus	Δ*egtA*^{26933}::*egtA* (*egtA*^{C26933})	Hygromycin (200 µg/ml)	This work
A. fumigatus	Δ*egtA*^{AfS77}	Pyrithiamine (100 ng/ml)	Sheridan et al., 2016
A. fumigatus	Δ*vipC*^{26933}	Pyrithiamine (100 ng/ml)	This work
A. fumigatus	Δ*palA*^{26933}	Pyrithiamine (100 ng/ml)	This work
E. coli	TOP10	Ampicillin (100 µg/ml)	N/A

Table 2.3. List of Plasmids used in this study, including antibiotics used.

Plasmid	Encoded Antibiotic Resistance
pCR®2.1-TOPO	Ampicillin
pSK275	Pyrithiamine
pAN7.1	Hygromycin

2.2.1.1 *A. fumigatus* Growth, Maintenance and Storage

A. fumigatus strains were maintained on MEA (Section 2.1.1.2). A single inoculation loop of spores from a stock spore solution was streaked onto a plate and incubated at 37 ^{o}C in a static incubator for 5 days. Conidia were harvested from the plate by adding sterile PBST (10 ml) (Section 2.1.5) to the conidia and rubbing the surface with a sterile inoculation loop to dislodge the spores. The spore solution was centrifuged at 2000 x g for 5 min. The supernatant was removed and the spore pellet was resuspended in sterile PBS (5 ml) (Section 2.1.4). The spores were counted using a haemocytometer to determine the spore density (spores/ml). The spore solution was stored at 4 ^{o}C until required.

2.2.1.2 *E. coli* Growth, Maintenance and Storage

E. coli strains were grown on LB agar (Section 2.1.2.2) overnight at 37 ^{o}C or in LB broth (Section 2.1.2.1) overnight at 37 ^{o}C, shaking at 200 rpm. Where appropriate, media was supplemented with suitable antibiotics.

2.2.2 Plant Strains used in this study

Plant strains used in this study are listed in Table 2.4.

Table 2.4. Plant Strains used in this study.

Species	Strain
Nicotiana tabacum	L. cv. Petit Havana
Nicotiana tabacum	L. cv. Petit Havana:*egtA*:*nfs1*

2.2.3 Molecular Biology Methods

2.2.3.1 Isolation of Genomic DNA from *A. fumigatus*

A. fumigatus conidia were harvested as described in Section 2.2.1.1. 100 µl of these suspensions were used to inoculate 50 ml cultures of Sabouraud Dextrose broth (Section 2.1.1.3). These cultures were incubated at 37 ^{o}C overnight, rotating at 200 rpm. The cultures were then filtered through miracloth and the mycelia were collected, flash frozen in liquid N_2 and ground using a mortar and pestle. The DNA extractions were carried out using the ZR Fungal/Bacterial DNA kit

(Zymo Research, California, U.S.A.). DNA extraction was carried out according to the product protocol.

2.2.3.2 Polymerase Chain Reaction (PCR)

PCR was used to amplify fragments of DNA for cloning, transformation constructs, DIG-labelled probes and colony PCR. Reactions were carried out using Accu*Taq* LA polymerase. Annealing temperatures were estimated as *ca.* 4 ^{o}C below the melting temperature (T_m) of the primers used. Extension times were *ca*. 1 min/kb of DNA to be synthesised. Reactions were carried out using the G-storm PCR system (Roche). Primers used in this study are listed in Table 2.5.

The general reaction constituents for Accu*Taq* LA polymerase used were as follows:

10 X reaction buffer	2 µl
dNTP mix (10 mM)	2 µl
Forward Primer (l0 µM)	1 µl
Reverse Primer (10 µM)	1 µl
DMSO	0.8 µl
DNA template	10 – 100 ng
Accu*Taq*	0.2 µl
Molecular grade H_2O	to a total of 20 µl

The following reaction cycle was used unless otherwise stated:

95 ^{o}C (denaturing)	5 min	
95 ^{o}C (denaturing)	1 min	x 30 – 35 cycles
56 ^{o}C (annealing)	1.5 min	
68 ^{o}C (extending)	1 min	
68 ^{o}C (extending)	10 min	

Table 2.5. Oligonucleotide primers used in this study. Restriction sites are underlined

Primer Name	Sequence (5' – 3')
oAoPtrA1	GAGGACCTGGACAAGTAC
oAoPtrA2	CATCGTGACCAGTGGTAC
HYoptrA1	GCTCCATACAAGCCAACCAC
YGoptrA2	GTCCTGCGGGTAAATAGCTG
egtA1	GATCCACAAGATACGGGC
egtA2	GGTGGGCAATGATCTTGG
egtA3	CCGTCTTTGGACCTGTTC
egtA4	GATAGTCTCCGCCGAAAG
egtA5	TCATCCATCTCGCCTCTG
egtA6	CAGGGTACATCCAGGTAC
QPCR egtA F	CTATGATGATGCCCTTGCCT
QPCR egtA R	GCATTCGCATGTAATAGCCC
egtB1	ATCTACTAGTGAATCAGAGGGAATGGCA
egtB2	GGAGATTCAAGAGGCGGAGG
egtB3	GCCGAGCAGGAGCGTTTG
egtB4	CACCAAGCTTCCATCAAAGTATGTCTCG
egtB5	TGTCTCCCTCATTCATCTGTTCAA
egtB6	CCCTCTCCGACATCCGCTCT
QPCR egtB F	TTTGCCGTGTCTGGTAGTGA
QPCR egtB R	GCAAACACAGGCACAAAGGT
vipC1	AGCGGTGATGTGATTGACTAGTGGAG
vipC2	GAGATGAGACGCCAGTGT
vipC3	CAGGAGGAACTGGTGGAGAG
vipC4	GTGCGGGCATAACATAAAGCTTCGGT
vipC5	AGATGATGGCGAATACGATGT
vipC6	GGGATGCCACTGGATTACC
QPCR vipC F	CGTTAGTCGCCTCTCTGTCG
QPCR vipC R	TCCAGGCGGTCTTGTTCTTG

palA1	CCGTCTCAAGATGGGCACTAGTATTA
palA2	ACTTTGGGAGCAGTGGTAGAG
palA3	CCAACAACAGGTTCCATCG
palA4	CACTGGTACCTGGCAAACGGAAACTG
palA5	TTTGCCCAATCCATCACAC
palA6	GGACGGTAGGCTATGGCA
QPCR palA F	CGCATCAACTGGCTGTCCTA
QPCR palA R	GCGGAGATGAACGGATGGAA
egtA_HYG_1	GCAGTCGACTGGGCAATGATCTTGG
egtA_HYG_2	CCGTCTTTGGACCTGTGGATCCTGA
gliK_HYG_1	GCGCATGCGCTTTCCCCATGTTGCTTG
gliK_HYG_2	GCATACTGTAGTCGCGGTAGA
gliK_HYG_3	ACGCCTCTAACATGCCATAC
gliK_HYG_4	AGCGGATCCTGAAGATGCTGCGGC
gliK_HYG_5	GCATTGGAAGAAGAGGACG
gliK_HYG_6	GTAGTAGCCGATGATGCCG
NFS1.1	ATAGGCGGCCGCACAGCAAAGGAGGGAG
NFS1.2	GGCTTCGTATTCCTCGCA
NFS1.3	CAATGGTGTATGTGCTGGG
NFS1.4	CATTAAAGCTTCCCTTATTATCTGCCTCG
NFS1.5	ATTTTGGTAAACTCTGCTCCG
NFS1.6	AAGGCTTGAGAAACAACTGATT
QPCR calm F	CCGAGTACAAGGAAGCTTTCTC
QPCR calm R	GAATCATCTCGTCAACTTCGTCGTCAGT

2.2.3.3 Colony PCR

PCR screening of bacterial colonies were carried out by colony PCR. An isolated colony was aseptically removed using a sterile tip and placed into a 0.2 ml tube containing PCR mastermix (Section 2.2.3.2) and also streaked onto a reference plate. PCR was carried out as per Section 2.2.3.2 and genomic DNA and negative controls were included.

2.2.3.4 Restriction Enzyme Digest

Restriction enzymes, 10 X reaction buffers and bovine serum albumin (BSA) were obtained from Promega. Reactions were carried out according to the manufacturer's instructions as follows:

DNA	1- 5 µg
Enzyme	1 µl
10 X Buffer	2.5 µl
10 X BSA	2.5 µl
Sterile Molecular Grade H_2O	to a total of 25 µl

Restriction digests were carried out at 37 ^oC for 2 h.

2.2.3.5 Ligation of DNA Fragments

Ligation of DNA was used for the generation of gene disruption constructs and plasmids for gene complementation. Ligation was carried out using the Ligafast Rapid DNA Ligation System (Promega), as per the manufacturer's instructions. DNA fragments containing either a cohesive end (a single stranded overhang) or a blunt end (no overhang) were produced by restriction digest (Section 2.2.3.5). The preferred molecular ratio of insert to backbone for all ligations was 3:1, this was estimated based off the size of the DNA fragment using the following formula:

$$\frac{(\text{ng of vector}) * (\text{kb size of insert})}{\text{kb size of vector}} * \frac{3}{1} = \text{ng of insert}$$

Ligations were carried out using 50 – 200 ng of vector DNA, T4 DNA ligase (1 µl) and 2 X rapid ligation buffer.

2.2.3.6 TOPO TA Cloning

One step cloning of PCR products were carried out using the TOPO TA Cloning kit from Invitrogen, according to the manufacturer's instructions. Prior to cloning, TOP10 cells were thawed on ice and LB agar plates (Section 2.1.2.2) containing 100 µg/ml ampicillin (Section 2.1.6) were pre-warmed in a 37 ^oC incubator. Genomic DNA PCR product (4 µl), Salt solution (1 µl) and pCR®2.1-TOPO vector (1 µl) were added to a sterile 0.2 ml tube and left at room temperature for 30 min. A 2 µl aliquot of this reaction mixture was added to a vial of TOP10 *E.*

coli cells and placed on ice for 30 min. Cells were heat shocked at 42 ^{o}C for 30 s in a water bath and room temperature Super Optimal Catabolite repression (SOC) media (250 µl) (Section 2.1.2.3) was added to the vial. The vial was then incubated at 37 ^{o}C for 1 h, shaking at 200 rpm. During this incubation period, 32 µl of 5-bromo-4-chloro-3-indolyl-beta-D-galactopyranoside (X-gal) (Promega, UK) (40 mg/ml) was spread over the pre-warmed agar plates using a sterile spreader and the plates were returned to the incubator. A 50 µl aliquot of the cell suspension was spread on the selection plates using a sterile disposable spreader and the plates were incubated overnight at 37 °C. White colonies were selected and sub-cultured on to LB agar plates (Section 2.1.2.2) with ampicillin (100 µg/ml). Potential colonies were screen by colony PCR (Section 2.2.3.3) and restriction digestion (Section 2.2.3.4).

2.2.3.7 Plasmid Purification from *E. Coli*

Plasmid purification was carried out according to the Qiagen Plasmid purification manual using the QIA prep Mini-prep kit. All buffers and columns were supplied with the kit. An isolated colony was picked aseptically and used to inoculated 10 ml LB broth (Section 2.1.2.1) containing 100 µg/ml ampicillin. Cultures were grown overnight at 37 ^{o}C and the cells harvested by centrifugation at 13,000 x g for 10 min. Procedures were then carried out according to the manufacturers guidelines. Purified plasmids were subsequently analysed by restriction digestion (Section 2.2.3.4) followed by DNA gel electrophoresis (Section 2.2.3.8).

2.2.3.8 DNA Gel Electrophoresis

2.2.3.8.1 Preparation of Agarose Gel

Agarose gel electrophoresis was used to visualise restriction digests, to separate DNA for Southern analysis, to separate differently sized DNA fragments prior to purification, for ensuring accuracy of PCR reactions and for estimation of DNA yield. Agarose gels were cast and run using Bio-Rad electrophoresis equipment. Agarose gels between 0.7 – 1 % (w/v) (Section 2.1.7.5) were prepared in 1 X TAE buffer (Section 2.1.7.2) depending on the expected size of DNA to be examined. Powdered agarose was added to an appropriate volume of 1 X TAE buffer in a 500 ml Erlenmeyer flask. This was then heated in a microwave, with frequent mixing, until the agarose had fully dissolved. The gel was allowed to cool and poured into a sealed casting unit. A gel comb was inserted and the gel to cool to 40 – 50 ^{o}C. At this point, ethidium bromide

(Section 2.1.7.3) was added to the solution (2.5 µl ethidium bromide per 100 ml molten agarose). The gel was then allowed to set for 30 min. Once set, the gel comb was removed gently and the gel casting unit containing the agarose gel was placed into the gel tank, with the wells nearest the negative electrode. 1 X TAE buffer (Section 2.1.7.2) was then poured into the gel tank to fully submerge the gel.

2.2.3.8.2 Loading and Running Samples on an Agarose Gel

DNA samples were prepared for loading by adding 1 volume of 6 X loading dye (Section 2.1.7.4) to 5 volumes DNA sample. DNA fragment size was estimated by running molecular weight markers alongside the unknown samples. The different molecular weight markers used in this study are outlined in Section 2.1.7.6. Gels were electrophoresed at 90 – 120 volts for 60 – 90 min. Gels were visualised under UV light and images captured using a Syngene G:Box.

2.2.3.8.3 DNA Gel Extraction

DNA gel extraction was carried out using the QIA quick gel extraction kit (Qiagen, UK). All reagents and columns were supplied with the kit and the procedure was carried out according to the manufacturer's instructions. DNA was eluted in 50 µl of sterile molecular grade H_2O.

2.2.4 Generation of *A. fumigatus* Mutant strains

2.2.4.1 Generation of Constructs for *A. fumigatus* gene deletions

A bipartite gene disruption strategy was employed for the generation of *A. fumigatus* mutant strains in this study (Nielsen et al., 2006). This strategy involved the generation of two constructs which each contain a partial fragment of a pyrithiamine resistance gene (*ptrA*) from *A. oryzae*. (Kubodera et al., 2000) ligated to a 5' or 3' flanking region of the gene of interest. These two constructs overlap and upon homologous recombination reconstitute the deletion cassette *in vivo*. The *ptrA* gene was excised from a plasmid vector pSK275 (a kind gift from Prof. Sven Krappmann, Erlangen, Germany) using restriction enzymes. 5' and 3' flanking regions of the gene of interest were amplified from *A. fumigatus* genomic DNA via PCR (Section 2.2.3.2) using primers with restriction sites incorporated. Flanking regions of 1 – 1.5 kb were amplified and digested with the same restriction enzymes as *ptrA* to make the ends compatible for ligation (Section 2.2.3.5). The ligation products provided the template for a subsequent round of PCR

where nested primers amplified the flanking region and a partial fragment of *ptrA*. Schematic representation of the bipartite gene deletion strategy is illustrated in Figure 2.2. PCR products were extracted using a Qiagen gel extraction kit. Successful transformation of *A. fumigatus* protoplasts generated potential *A. fumigatus* transformants which had the ability to grow on pyrithiamine selection plates. This only occurred with the successful integration of a fully reconstituted *ptrA*. These transformants were then screened by Southern blot analysis (Section 2.2.5) where a single homologous integration of *ptrA* in place of the gene of interest was desired.

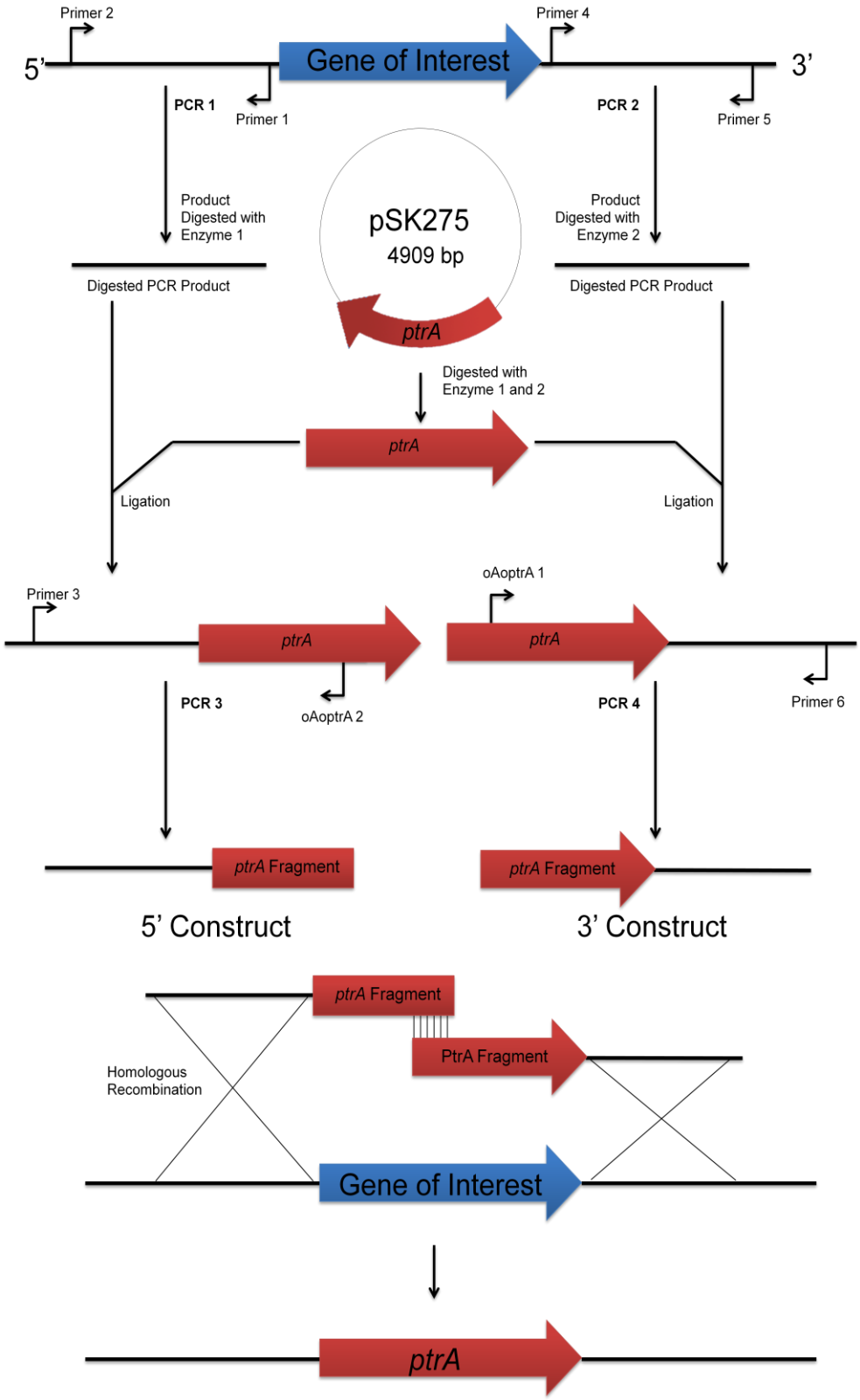

Figure 2.2. A schematic representation of the bipartite strategy for gene deletion in *A. fumigatus*, using *ptrA* as a selection marker.

2.2.4.2 Generation of Constructs for complementation of *egtA* in Δ*egtA*^{26933}

To restore *A. fumigatus egtA* back into the genome of *A. fumigatus* Δ*egtA*^{26933}, a construct containing the full *egtA* sequence with the respective 5'and 3' flanking regions was generated. The primers used for the complemented construct are listed in Table 2.5. The *egtA* coding sequence was PCR amplified from wild-type genomic DNA using the primers egtA5 and egtA6. The PCR products were cloned into the pCR®2.1-TOPO vector (Section 2.2.3.6) to create pegtA. This vector was then linearised using a restriction enzyme that had a unique site in the sequence, *Aat*II. For the selection marker, the hygromycin resistance plasmid, pAN7.1 was used, which contains the hygromycin resistance gene *hph*. The linearised pegtA was then transformed into protoplasts of *A. fumigatus* Δ*egtA* alongside pAN7.1 and grown on media containing hygromycin. Successful transformants were identified by the ability to grow on hygromycin due to the presence of the *hph* gene. Potential transformants were screened by Southern blot analysis (Section 2.2.5).

12.2.4.3 *A. fumigatus* Protoplast Preparation

Three 500 ml Erlenmeyer flasks containing 100 ml AMM (Section 2.1.1.1.4) were inoculated with 500 µl conidia each. These cultures were incubated overnight at 37 ^{o}C, shaking at 200 rpm. The mycelia were harvested by filtering through autoclaved miracloth and washed with autoclaved dH_2O. The mycelia were blotted gently on autoclaved paper towel in order to remove excess liquid. 1.5 g of mycelia was weighed out in duplicate and each was added to lysis buffer (15 ml) (Section 2.1.8.4). Both tubes were shaken vigorously in order to remove large mycelial clumps. The tubes were then incubated horizontally at 30 ^{o}C, shaking at 100 rpm for 30 min. Following this incubation, the mycelia were disrupted with vigorous pipetting using a P1000 micropipette set to 800 µl in order to break up all mycelial clumps. The tubes were then returned to incubation at 30 ^{o}C, shaking at 100 rpm for a further 2.5 h. The tubes were then placed in ice for 5 min, followed by centrifugation at 900 rpm for 18 min with the brake turned off. The supernatant was filtered through autoclaved miracloth into a new 50 ml tube and the volume brought up to 40 ml with 0.7 M KCl (Section 2.1.8.1). The tubes were centrifuged at 3300 rpm for 12 min with the brake turned off. The supernatant was discarded and the pellet resuspended in 0.7 M KCl (10 ml) (Section 2.1.8.1). The previous centrifugation step was then repeated. The supernatant was discarded and the tubes were inverted on autoclaved paper towels in order to

remove excess liquid. The pellet was resuspended in Buffer L6 (70 µl) (Section 2.1.8.6) by gentle pipetting. The tubes were centrifuged at 600 rpm for 1 min with the brake turned off and the solutions pooled together. The protoplasts were viewed on a haemocytometer using a microscope to ensure yield and viability were adequate. The protoplasts were stored on ice prior to use in the transformation protocol.

2.2.4.4 *A. fumigatus* Protoplast Transformation

Between 2 µg and 7 µg of 5' and 3' constructs were mixed together in a 50 ml tube for each transformation, with the final volume brought up to 50 µl with buffer L6 (Section 2.1.8.6). 150 µl of *A. fumigatus* protoplasts were added to the constructs. A negative control was prepared by adding 15 µl of *A. fumigatus* protoplasts to buffer L6 (185 µl) (Section 2.1.8.6). Buffer L7 (50 µl) (Section 2.1.8.7) was added to both DNA containing and negative control mixtures and mixed with gentle swirling. These were placed on ice for 20 min. Following this, buffer L7 (1 ml) (Section 2.1.8.7) was added to each mixture and left at room temperature for 5 min. Buffer L6 (5 ml) (Section 2.1.8.6) was added to each tube and stored on ice until plating.

2.2.4.5 Plating of *A. fumigatus* Transformation Protoplasts

1.8% (w/v) regeneration agar (25 ml) (Section 2.1.1.5.1) containing pyrithiamine (0.1 µg/ml) or hygromycin (100 µg/ml) (Section 2.1.6) was poured into 90 mm petri dishes. Plates were stored at room temperature until required. For each transformation, six plates containing the selection agent and two plates without were prepared. For the negative control, 1.25 ml of *A. fumigatus* protoplasts from the negative control transformation were added to a sterile tube and the volume made up to 6 ml with 0.7% (w/v) regeneration agar (Section 2.1.1.5.2). This was then poured onto a plate containing a selection agent. For the protoplast viability control, two tubes were prepared: containing 12.5 µl and 1.25 µl transformed *A. fumigatus* protoplasts respectively. The volume of both tubes was brought up to 6 ml with 0.7% (w/v) regeneration agar (Section 2.1.1.5.2). These tubes were then poured onto the two plates containing no selection agent. The remaining transformed *A. fumigatus* were brought up to a volume of 30 ml with 0.7% (w/v) regeneration agar (Section 2.1.1.5.2). 6 ml of this solution was then poured onto 5 plates containing selection agent. All plates were stored overnight at room temperature.

2.2.4.6 Overlaying of *A. fumigatus* Transformation Plates

0.7% (w/v) regeneration agar (36 ml) (Section 2.1.1.5.2) containing pyrithiaimine (0.1 µg/ml) or hygromycin (100 µg/ml) was prepared in a sterile tube. 6 ml of this was poured onto each of the 5 transformation plates as well as the negative control. All plates were the incubated at 37 ^{o}C for approximately 5-7 days or until colonies were observed on top of the overlay layer. The appearance of colonies on the proplast viability control plates confirms that viable protoplasts had been generated

2.2.4.7 Isolation of *A. fumigatus* Transformants following Transformation

Potential transformants exhibited the ability to grow on transformation plates containing the selective agent. Spores from each transformant were picked aseptically from the transformation plates and point inoculated onto fresh AMM agar (Section 2.1.1.1.5) plates containing the selection agent. The plates were then incubated at 37 ^{o}C in a static incubator until colonies were observed. The individual colonies were excised from the plates using the base of a P1000 tip. The plugs were transferred to sterile 1.5 ml tubes containing PBS (750 µl). The tubes were vortexed vigorously to release the conidia into solution and the solutions stored at 4 ^{o}C until needed. 500 µl of conidial suspension from each potential *A. fumigatus* transformant was pipetted into separate 50 ml Erlenmeyer flasks containing 20 ml Sabouraud Dextrose broth (Section 2.1.1.3). The cultures were incubated overnight at 37 ^{o}C with shaking at 200 rpm. The cultures were then harvested and DNA extraction (Section 2.2.3.1) was performed for Southern blot analysis (Section 2.2.5).

2.2.4.8 Single Spore Isolation of *A. fumigatus* Transformant Colonies

Following a first round of Southern blot analysis, transformants showing a correct signal were selected for single spore isolation. This was done to ensure that a transformant contained a homogenous single nucleus and that it was not a heterokaryon. Potential transformants were diluted by serial dilutions ranging from 10^{-2} to 10^{-6} in sterile PBS (Section 2.1.4). 50 µl of the each dilution was spread onto separate AMM plates containing a selective agent and incubated at 37 ^{o}C in a static incubator until colonies were observed. Conidia from individual colonies were isolated in sterile PBS (Section 2.1.4) and inoculated into Sabouraud Dextrose media (20 ml)

(Section 2.1.1.3) and incubated as per Section 2.2.4.7. Mycelia were then harvested and subjected to a second round of Southern blot analysis (Section 2.2.5).

2.2.5 Southern Blot Analysis

2.2.5.1 Synthesis of DIG-labelled Probes

The probes used in Southern analysis were generated by PCR (Section 2.2.3.2) with the incorporation of DIG-labelled dNTPs. PCR products were resolved on a 1 % agarose gel and the bands excised (Section 2.2.3.8.3). DNA was denatured by heating at 95 ^{o}C for 5 min on a heating block. 400 ng of the DNA was added to 15 ml membrane pre-hybridisation buffer (Section 2.1.9.6.2) which had been heated to 65 ^{o}C for 30 min. The probe was stored at – 20 ^{o}C and heated at 65 ^{o}C for 30 min before use in Southern analysis.

2.2.5.2 DNA Transfer

Genomic DNA was isolated from potential transformants (Section 2.2.3.1) and digested using a suitable restriction endonuclease (Section 2.2.3.4). The enzyme chosen would cut on either the 5' or 3' side of the gene of interest, once inside the wild-type loci and once inside the replacement gene for the mutant loci. This would generate different sized bands on the blot for the wild-type and mutants strains, allowing for identification of successfully generated mutants. The digested DNA was resolved on a 0.7 % (w/v) agarose gel (Section 2.2.3.8). After the DNA was resolved sufficiently, it was placed on a UV cross linking machine (Stratagene, La Jolla, CA) and pulsed at 800 KJ. Following this, the Southern tower was set up (Figure 2.3). The tower was constructed on a Bio-Rad electrophoresis tank with the two reservoirs on either side filled with Southern transfer buffer (Section 2.2.9.1). Two large sheets of filter paper were draped between the two reservoirs until they were soaked in the transfer buffer. The DNA gel was placed face down on top of these. Nylon membrane (H+ Bond Nylon Membrane, GE Electric) was placed on top of the gel, followed by 3 pieces of filter paper. 3 stacks of pocket-sized tissue paper were then placed on top of the filet paper. A glass plate was placed on top of the stack and a duran containing 400 ml H_2O was placed on top of this. The Southern blot tower was left overnight at room temperature.

2.2.5.3 Pre-hybridisation of the Nylon Membrane

Following overnight incubation the nylon membrane was washed for 20 min in 2 X SSC buffer (Section 2.1.9.3) followed by crosslinking in the UV crosslinking machine. The membrane was then placed in a Hybaid tube and pre-hybridisation buffer (20 ml) (Section 2.1.9.6.1) was placed inside. The tube was incubated at 42 ^{o}C in a hybaid oven whilst rotating for 5 – 6 h to block the membrane.

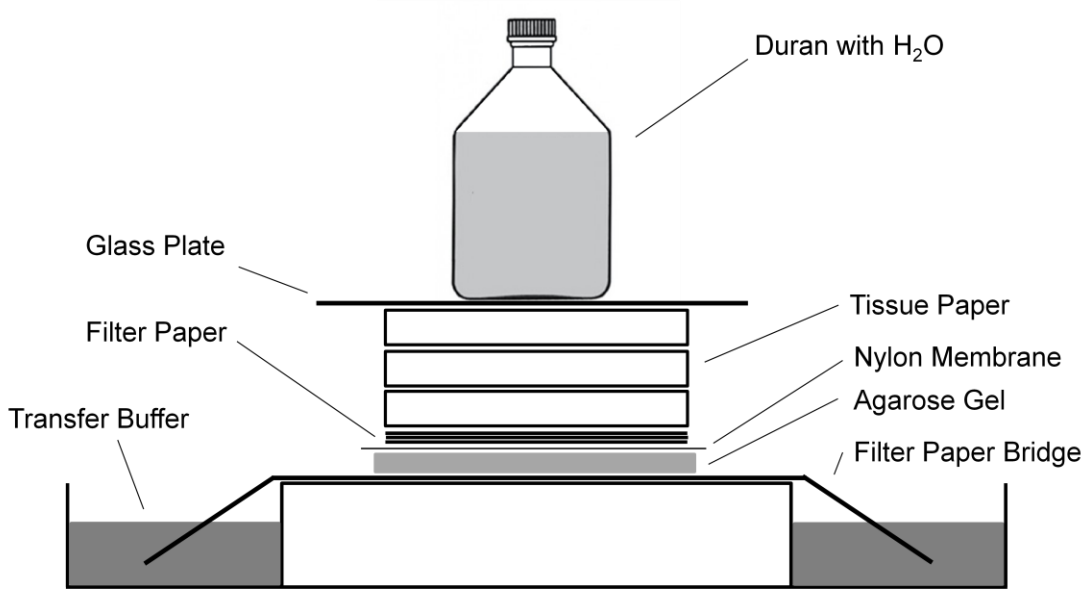

Figure 2.3. Schematic representation of the Southern transfer tower.

2.2.5.4 Addition of DIG-labelled probe to Southern Blot

Following pre-hybridisation of the Southern blot the pre-hybridisation buffer was removed. The DIG-labelled probe (Section 2.2.5.1) was pre-heated to 65 ^{o}C for 30 min and then added to the tube. The tube was then incubated overnight at 42 ^{o}C whilst rotating to allow the probe to hybridise to regions of homology on the membrane. Following the overnight incubation, the probe was removed and stored at – 20 ^{o}C.

2.2.5.5 DIG Detection

After probing, the membrane was removed from the Hybaid tube and was washed with 0.1 % (w/v) SDS / 1 X SCC buffer (Section 2.1.9.5) for 15 min. This wash was repeated once and then the membrane returned to the Hybaid tube. 0.1 % (w/v) SDS / 1 X SCC buffer (20 ml) (Section 2.1.9.5), which had been pre-heated to 65 ^{o}C, was added to the tube and it was rotated in the Hybaid oven at 65 ^{o}C for 15 min. This wash was repeated once and then the solution discarded. DIG wash buffer (10 ml) (Section 2.1.9.6.7) was added to the tube and the tube rotated at room temperature for 5 min. The buffer was then discarded and the membrane was blocked with DIG buffer 2 (15 ml) (Section 2.1.9.6.5) for 30 min whilst rotating at room temperature. Following the blocking step, Anti-Digoxigenin-AP conjugate (Section 2.1.9.6.8) (20 ml) was added and the tube rotated at room temperature for 30 min. The antibody solution was then discarded and DIG wash buffer (15 ml) (Section 2.1.9.6.7) was added to the tube and rotated at room temperature for 15 min. This wash step was repeated once. Following the wash steps, DIG buffer 3 (10 ml) (Section 2.1.9.6.6) was added and the tube rotated at room temperature for 5 min. The buffer was then poured off and CSPD substrate (5 ml) (Section 2.1.9.6.9) was added. This was rotated at room temperature for 5 min. The CSPD substrate was collected in a tube covered in tin foil and stored at 4 ^{o}C. The membrane was removed from the Hybaid tube, wrapped in a single layer of cling film and incubated at 37 ^{o}C for 15 min.

2.2.5.6 Developing the Southern blot membrane

The cling film wrapped membrane was taped into a photo developer cassette and an X-ray film was placed over the membrane. The X-ray film was allowed to expose for 2 – 3 h initially, followed by an overnight exposure. Following exposure, the X-ray film was removed and placed in developer solution (Section 2.1.9.6.11) until a signal was visible on the X-ray film. The X-ray film was then briefly washed with H_2O and then placed into fixer solution (Section 2.1.9.6.12). Alternatively, instead of using the X-ray film, a digital image of the blot was obtained by exposing the membrane in a Syngene Image Station for 1 h.

2.2.6 RNA Analysis

2.2.6.1 RNA Isolation

A. fumigatus liquid cultures, which were incubated at 37 ^{o}C for the required time, were filtered through autoclaved miracloth, washed with autoclaved H_2O and the mycelia collected. Mycelia were snap frozen in liquid N_2 and ground to a fine powder in liquid N_2. The RNA was isolated using the RNeasy Kit supplied by Qiagen, according to the manufacturer's instructions. β-mercaptoethanol (10 µl) was added to Buffer RLC (1 ml) before RNA extraction. For each sample, 100 mg of ground mycelia were placed in sterile 2 ml tubes. Buffer RLC (QIAshredder spin columns. The columns were centrifuged at 13,000 x g for 2 min. The flow through was transferred to new 1.5 ml tubes, avoiding the cell debris pellet. 0.5 volumes of molecular grade ethanol (100 %) was added to the lysates and mixed immediately. Samples were then transferred to RNeasy spin columns, which were placed in 2 ml collection tubes. Columns were centrifuged at 10,000 x g for 15 s. The flow through was discarded. Buffer RW1 (700 µl) was added to the columns and then centrifuged at 10,000 x g for 15 s. The flow through was discarded. Buffer RPE (500 µl) was added to the columns and centrifuged at 10,000 x g for 15 s. The flow through was discarded. Buffer RPE (500 µl) was added to the columns and centrifuged at 10,000 x g for 2 min. The spin columns were removed and placed in new collection tubes and centrifuged for 2 min at 13,000 x g, to remove residual buffer. The spin columns were placed in sterile 1.5 ml tubes. RNase-free water (50 µl) was added to the columns and the RNA was eluted by centrifuging at 10,000 x g for 1 min. The RNA samples were stored at –70 °C until required.

2.2.6.2 DNase Treatment of RNA samples

A DNase 1 kit from Sigma was used to DNase treat RNA samples. RNA samples (Section 2.2.6.1) (500 ng) were adjusted to a final volume of 8 µl in molecular grade H_2O. 10 X Reaction Buffer (1 µl) and DNase (1 µl) were added to the RNA samples and the mixture was left to incubate at room temperature for 15 min. Stop Solution (1 µl) was added to the reaction and they were then incubated at 70 ^{o}C for 10 min. The samples were chilled on ice and stored at – 70 ^{o}C if not for immediate use.

2.2.6.3 cDNA Synthesis

cDNA synthesis was carried out using qScript cDNA Supermix (Quanta BioSciences) using the reagents supplied in the kit and following the manufacturer's instructions.

2.2.6.4 Semi-quantitative RT-PCR

PCR was carried out on the cDNA samples (Section 2.2.6.3) as described in Section 2.2.3.2 using appropriate target gene primers (Table 2.5). The *A. fumigatus* calmodulin (*calm*) gene (AFUA_4g10050) was used as a housekeeping gene (Burns et al., 2005). The primers calmF and calmR (Table 2.5) span an intronic region in *calm*, resulting in an amplicon size of 617 bp from gDNA and an amplicon size of 314 bp from cDNA. This allows the detection of any contaminating gDNA in the cDNA samples. The RT-PCR amplicons were resolved on a 0.7 % (w/v) Agarose Gel (Section 2.2.3.8) and visualised using a Syngene G:Box.

2.2.6.5 Quantitative RT-PCR (qRT-PCR)

RNA samples to be analysed by qRT-PCR were extracted as described in Section 2.2.6.1, DNase treated (Section 2.2.6.2) and cDNA synthesised (Section 2.2.6.3). qRT-PCR was carried out using the LightCycler® 480 Real-Time PCR System (Roche) and LightCycler® 480 SYBR Green I Master (Roche). PCR reactions were carried out in 96-well plates in a reaction volume of 10 µl containing 1 µl of template cDNA. Relative quantification analysis of differences in gene expression between different growth conditions and/or *A. fumigatus* strains was carried out using the Relative Quantification module, allowing for differences in gene expression levels between samples to be calculated. Standard curves for the gene *calm* (internal control) and genes of interest were created to measure PCR efficiency. Standard curves were prepared for *calm* and each of the genes of interest by creating 5 orders of 4 fold serial dilutions of control cDNA in molecular grade H_2O using 5 experimental replicates for each dilution series and for each PCR reaction with their respective specific primer pairs. Standard curves were calculated using the Absolute Quantification Module which yielded a specific efficiency figure based on the reaction. An efficiency of 2 ± 0.2 meant the PCR was successful and was saved for reference during experiments using these same cycling requirements for subsequent qRT-PCR. For this cDNA was diluted 1:2 in order for it to fit within the standard curve, and was done in quintuplicate for each sample and for each gene of interest being amplified. All samples and standards were

cycled 45 times as per manufacturer's instructions. Relative expression was calculated using the 2-(Delta Delta C(T)) method (Livak & Schmittgen, 2001) on the LightCycler® software. Results were given as a bar chart and table depicting the mean values for all genes and the relative ratio of a particular gene of interest:*calm* expression. Negative controls containing 1 µl of molecular grade water were performed in triplicate on each 96-well plate, and T_m Calling Analysis was performed after each PCR reaction to check that only one PCR product was present in each well following the PCR run.

2.2.7 *A. fumigatus* Plate Assays

Conidial stocks from *A. fumigatus* wild-type and mutant strains (Table 2.2) were diluted to a concentration of 1 x 10^6 conidia/ml in PBS and 5 µl of each dilution was used to spot test plates. Plates were incubated at 37 ºC and growth was measured after 72 h by measuring the radial span of fungal colonies. Plate assays were performed independently three times, and radial growths (mm) of colonies were tested for significant differences by means of a one-way ANOVA. Strains were tested for growth on agar with a variety of supplements and these are summarized in Table 2.1. Plate assays to analyse *A. fumigatus* response to light took place in an incubator with an LED light. Control plates were grown in the dark by covering them in tinfoil.

2.2.8 Bradford Protein Assay

Bio-Rad protein assay dye was diluted 1/5 in PBS (Section 2.1.12.5) prior to use. The sample to be assayed was also diluted appropriately (1/5 – 1/20). 20 µl of sample was added to 980 µl of the diluted Bio-Rad protein assay dye and mixed thoroughly. The final sample (1 ml) was transferred to a 1 ml plastic cuvette and incubated for 5 min at room temperature. The A_{595} was read relative to a blank and the protein concentration was determined based on values obtained from a standard curve. All samples were prepared and analysed in duplicate.

2.2.9 *A. fumigatus* Protein Extraction

A. fumigatus liquid cultures were harvested using miracloth and dried using tissue paper to remove excess liquid. Harvested mycelia were then placed into a 50 ml tube, snap frozen in liquid N_2 and lyophilised overnight. 100 mg of lyophilised mycelia was weighed into a 1.5 ml tube and tungsten bead added. The sample was bead beaten for 5 min at 30 Hz. Whole protein

lysate extraction buffer (500 µl) (Section 2.1.12.1) containing 30 mM DTT was added to the sample and the bead beating repeated (samples to be analysed using *o*-Phthalaldehyde (Section 2.2.12.3), were lysed in *A. fumigatus* phosphate lysis buffer (Section 2.1.12.2) instead of the Tris based lysis buffer). The sample was then left on ice for 1 h. Following this incubation, the sample was centrifuged at 12,000 x g at 4 ^{o}C for 15 min. The supernatant was then transferred to a clean 1.5 ml tube. Protein lysates were stored at -20 ^{o}C.

2.2.10 Organic extraction of *A. fumigatus* Supernatants

20 ml of *A. fumigatus* culture supernatants were added to 20 ml chloroform in 50 ml falcon tubes in the fumehood. Samples were shaken vigorously by hand, with intermittent gas release followed by centrifugation for 5 min at 2000 x g. The lower organic layers were removed to new 50 ml falcon tubes and stored at -20^{o}C.

2.2.11 Rotary Evaporation of Organic Extraction Samples

Organic extracts (Section 2.2.10) were placed in an evaporation bulb and the bulb was evaporated under vacuum whilst sitting in a water bath set to 60 ^{o}C (Stuart RE300DB digital water bath). The chloroform evaporated leaving the dried organic extract in the bulb. The extracts were resuspended in HPLC grade methanol (250 µl) until all the dried material was fully resuspended. The resuspended extract was centrifuged at 13,000 x g for 5 min and the supernatant transferred to a new 1.5 ml tube and stored at -20 ^{o}C.

2.2.12 Metabolite Analysis

2.2.12.1 5'-Iodoacetamidofluorescein (5'-IAF) Labelling

30 µl of lysate from *A. fumigatus* (Section 2.2.9), *N. tabacum* (Section 2.2.14.2),EGT standard or GSH standard were placed in 1.5 ml tubes. PBS (105 µl) (Section 2.1.4) and methanol (15 µl) were added to the samples and the tubes vortexed. 50 µl of each sample solution was added to a new 1.5 ml tube. 3 mg/ml 5'-IAF (10 µl) (Section 2.1.11.2) was added to the solutions and the tubes vortexed briefly. The samples were then incubated at room temperature in the dark for 40 min. The tubes were then centrifuged at 13,000 x g for 5 min. The supernatants were then removed to a new 1.5 ml tube and the pellets discarded. Samples were stored on ice in the dark until needed.

2.2.12.2 TCA Precipitation of 5'-IAF Labelled Samples

5'-IAF labelled samples to be analysed by LC-MS/MS were TCA precipitated prior to analysis. 100 % (w/v) TCA (5 µl) (Section 2.1.13.1) was added to 45 µl of 5'-IAF labelled lysates or EGT standard (Section 2.2.12.1). The samples were incubated at 4 ^{o}C in the dark for 2 h. Following the incubation, the samples were centrifuged at 12,000 x g at 4 ^{o}C for 15 min. The supernatants were then removed to a new 1.5 ml tube and the pellets discarded. Samples were stored on ice in the dark until needed.

2.2.12.3 *o*-Phthalaldehyde (OPA) Labelling of *A. fumigatus* protein lysates

50 µl of room temperature OPA was added to 10 µl of *A. fumigatus* protein lysate extracted in phosphate lysis buffer (Section 2.2.9) or 10 µl 2 mM histidine standard in 50 mM phosphate, pH 7.6. Samples were allowed to sit for 90 s at room temperature and then centrifuged at 13,000 x g for 1 min. 50 µl of the solution was then placed in a HPLC vial and analysed via RP-HPLC (Section 2.2.12.6) immediately.

2.2.12.4 Filtration of *N. tabacum* lyates using an Amicon centrifuge filter

200 µl of *N. tabacum* lysates (Section 2.2.14.2) was placed in an Amicon 3 kDa centrifuge filter. The filter was centrifuged at 4,000 x g for 30 min and the filtrate was then transferred to a clean 1.5 ml tube using a micropipette

2.2.12.5 Determination of Ergothioneine reactivity with H_2O_2

Reactivity between EGT and H_2O_2 was analysed by incubating 3 mM EGT with either 3 mM H_2O_2 or an equivalent volume of dH_2O for 3 h at room temperature. Triplicate specimens were then analyzed by back-titration to detect remaining EGT by labeling the solutions with 5'-IAF (Section 2.2.12.1) followed by detection via RP-HPLC analysis (Section 2.2.12.6). Peak areas of residual EGT amounts were compared using unpaired t-test.

2.2.12.6 Metabolite Analysis Using RP-HPLC

Organic extracts from supernatants (Section 2.2.11), 5'-IAF labelled samples (Section 2.2.12.1) and OPA labelled samples (Section 2.2.12.3) were analysed by RP-HPLC (Agilent 1200 system or Shimadzu prominence HPLC system) using a C18 RP-HPLC column (Agilent Zorbax Eclipse

XDB-C18 Semi-preparative; 5 mm particle size; 4.6 x 250 mm) at a flow rate of 1 ml/min. A mobile phase of H_2O (Section 2.1.10.1) and acetonitrile (Section 2.1.10.2) with TFA, was used under various gradient conditions. Injection volume was 20 µl. Unlabelled metabolites were detected at 254 nm using the photodiode array detector, while 5'-IAF labelled samples were detected using the fluorescence detector, using an excitation wavelength of 494 nm, and an emission wavelength of 518 nm. OPA labelled samples were detected using the fluorescence detector, using an excitation wavelength of 340 nm, and an emission wavelength of 455 nm.

2.2.12.7 Metabolite Analysis using LC-MS/MS

Organic extracts from supernatants (Section 2.2.11) or TCA precipitated 5'-IAF labelled mycelial lysates (Section 2.2.12.2) were analysed by LC-MS/MS. All samples were filtered through 0.2 µm cellulose spin-filters (Costar) before transfer to polypropylene vials. Samples were loaded onto a Zorbax 300 SB C-18 Nano-HPLC chip (150 mm x 75 µm) at a flow rate of 4 µl/min. Metabolites were eluted using the appropriate gradient with a post run of 5 min. MSn was carried out on the 3 most abundant precursor ions at each timepoint, with n ranging from 2 to 5, depending on the analysis. Singly charged ions were not excluded from analysis, with the precursor range adjusted to include ions with *m/z* between 15 and 2200.

2.2.13 Measurement of Intracellular GSH and GSSG

This method measures levels of intracellular glutathione in *A. fumigatus*. Levels of total glutathione and levels of glutathione disulfide (GSSG) are measured directly. By subtracting the levels of GSSG from total glutathione, levels of reduced glutathione (GSH) can be determined. The assay involves the reduction of 5,5'-dithiobis-(2-nitrobenzoic acid) (DTNB) by GSH. Reduction of DTNB releases 5-thio-2-nitrobenzoic acid (TNB) as well as forming glutathione-TNB adducts (GS-TNB). Glutathione reductase (with NADPH as an electron donor) cleaves this adduct, releasing further free TNB, which can be detected at 412 nm. The released GSH is then free to react with DTNB again, repeating the cycle (Figure 2.4). As glutathione reductase converts GSSG to GSH, this method measures total glutathione. In order to measure GSSG levels, samples are treated with 2-vinylpyridine. 2-vinylpyridine covalently reacts with GSH, but not GSSH. Thus, when DTNB and glutathione reductase is added only the GSSG present in the sample reacts to release TNB for measurement at 412 nm. The rate of TNB formation is

proportional to the amount of GSH present in the sample. This method was developed from Thon et al. (2010) and Rahman et al. (2006) and has previously been used to measure glutathione levels in *A. fumigatus* (O'Keeffe et al., 2010). Care was taken throughout the protocol to avoid exposing samples to light. All tubes were covered in tinfoil and a lid was kept on the ice box.

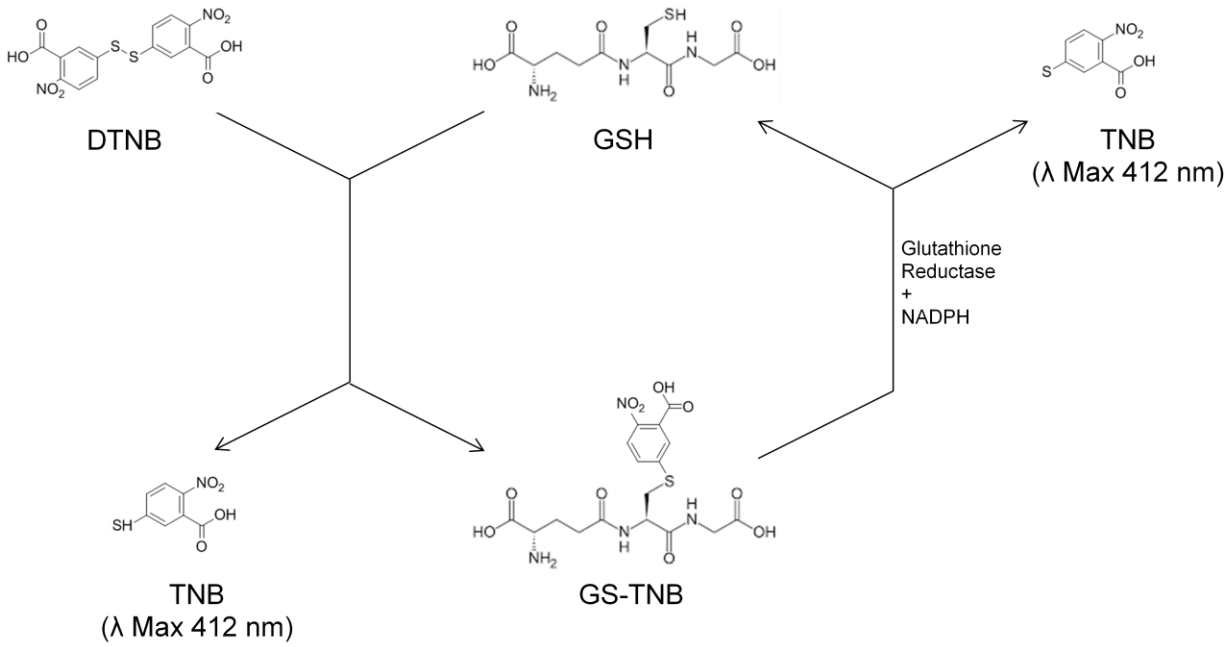

Figure 2.4. Overview of the glutathione assay**.** Reduction of DTNB by GSH produces TNB and GS-TNB. GS-TNB is then enzymatically reduced to GSH via glutathione reductase and NADPH, releasing free TNB. The GSH is then free to react with DTNB again, restarting the cycle. This recycling process releases free TNB, which can be measured at 412 nm and thus forms the basis of the glutathione assay.

2.2.13.1 Sample Preparation

A. fumigatus mycelia were harvested through miracloth and dried on tissue paper to remove excess liquid. Mycelia were then snap-frozen in liquid N_2 and crushed into a powder using a mortar and pestle. 200 mg of crushed mycelia were added to a 2 ml tube containing 5 % (w/v) SSA (250 µl) (Section 2.1.15.4). This was repeated for each sample into a tube containing whole protein lysate extraction buffer (Section 2.1.12.1). A tungsten bead was added to each sample and they were bead beaten at 30 Hz for 3 min, followed by centrifugation at 12,000 x g for 10 min at 4 ^{o}C. The supernatant from samples bead beaten in whole protein lysate extraction buffer

were used to perform a Bradford assay (Section 2.2.8). The supernatants from samples bead beaten in 5% (w/v) SSA were removed to tubes covered in tinfoil and neutralised using 50 % (v/v) triethanolamine (Section 2.1.15.5). The samples were diluted (1/10 – 1/30) in assay buffer (Section 2.1.15.3) and centrifuged at 12,000 x g for 10 min at 4 ^{o}C. The supernatants were removed to clean 1.5 ml tubes. Samples were stored at -70 ^{o}C if not assayed immediately.

2.2.13.2 GSH Standard Preparation

GSH (1 mg/ml) (Section 2.1.15.10) was diluted 1/100 in assay buffer (Section 2.1.15.3) to give a working solution of 10 µg/ml. A 26.4 nmol/ml stock was prepared by adding 800 µl of the working solution to 200 µl assay buffer (Section 2.1.15.3). A series of 1:1 dilutions were performed to obtain the following set of standards: 13.2, 6.6, 3.3, 1.65, 0.825 and 0.4125 nmol/ml.

2.2.13.3 GSSG Standard Prepartion

GSSG (2 mg/ml) (Section 2.1.15.11) was diluted 1/100 in assay buffer (Section 2.1.15.3) to give a working solution of 20 µg/ml. A 26.4 nmol/ml stock was prepared by adding 800 µl of the working solution to 200 µl assay buffer (Section 2.1.15.3). A series of 1:1 dilutions were performed to obtain the following set of standards: 13.2, 6.6, 3.3, 1.65, 0.825 and 0.4125 nmol/ml.

2.2.13.4 Pre-treatment of GSSG samples

GSSG standards and samples to be assayed for GSSG were pre-treated with 2-vinylpyridine. 2-vinylpyridine (2 µl) (Section 2.1.15.6) was added to 100 µl of GSSG standards (Section 2.2.13.3), samples to be assayed for GSSG (Section 2.2.13.1) and a blank sample (assay buffer (Section 2.1.15.3). This was carried out in the fume hood. The samples were incubated at room temperature for 1 h, before 50 % (v/v) triethanolamine (6 µl) (Section 2.1.15.5) was added to each sample to neutralise the 2-vinylpyridine. The samples were incubated for 10 min at room temperature before being assayed.

2.2.13.5 Glutathione Assay

All samples to be assayed for GSH or GSSG were assayed in the same manner. 20 µl each standard/sample/blank was added to a clear 96-well microtiter plate. To these, 10 mM DTNB and glutathione reductase (44.2 µl) (Section 2.1.15.8) was added and left for 30 s. 5 mM NADPH (Section 2.1.15.9.2) (42 µl), the electron donor for glutathione reductase, was then added to each well and the plate shaken gently to mix. The absorbance at 412 nm was measured after 90 s.

2.2.14 Q-Exactive Mass Spectrometry

2.2.14.1 Preparation of *A. fumigatus* samples for Q-Exactive Mass spectrometry

Harvested mycelia were snap frozen in liquid N_2 and crushed using a mortar and pestle in liquid N_2. 200 mg of mycelia powder was weighed into a 2 ml tube. Whole protein lysate extraction buffer (Section 2.1.12.1) (500 µl) was added to the tube. The suspension was sonicated using a Sonoplus HD 2200 sonicator and an MS72 sonication probe (Bandelin Electronic, Germany) at 10% power, cycle 6 for 10 s. This was repeated twice, with samples cooled on ice in between each sonication. The suspension was then sonicated using sonication probe MS73 (Bandelin Electronic, Germany) at 10% power, cycle 6 for 10 s. Lysates were then incubated on ice for 1 h, followed by centrifugation at 12,000 x g for 10 min at 4 ^{o}C. The supernatants were transferred to fresh 1.5 ml tubes and the centrifugation step was repeated to obtain clarified supernatants. A Bradford assay (Section 2.2.8) was carried out to determine the protein concentration in each sample. 100 % TCA (Section 2.1.13.1) was added to samples (1 mg total protein) to a final concentration of 15 % (v/v). The samples were vortexed briefly and incubated at 4 ^{o}C for 2 h. Samples were centrifuged at 12,000 x g for 10 min at 4 ^{o}C and the supernatant was discarded. Ice-cold acetone (500 µl) was added to each protein pellet, pipetted briefly and then incubated at -20 ^{o}C for 2 h. Samples were centrifuged at 12,000 x g for 10 min at 4 ^{o}C and the supernatant was discarded. The acetone wash was repeated twice (an overnight incubation, followed by another 2 h incubation). After the acetone was removed from the final washes, the pellets were allowed to dry for no more than 5 min. Each pellet was then resuspended in protein resuspension buffer (80 µl) (Section 2.1.13.3). A Bradford assay was carried out to determine the protein concentration of each sample.

2.2.14.2 Protein Extraction from *Nicotiana tabacum* leaves

Leaves from *N. tabacum* plant were removed from the stem, snap frozen in liquid N_2 and crushed using a mortar and pestle in liquid N_2. 400 mg of *N. tabacum* leaf powder was weighed into a 2 ml tube. Whole protein lysate extraction buffer (Section 2.1.12.1) (500 µl) was added to the tube. The suspension was sonicated using a Sonoplus HD 2200 sonicator and an MS72 sonication probe (Bandelin Electronic, Germany) at 10% power, cycle 6 for 10 s. This was repeated twice, with samples cooled on ice in between each sonication. The suspension was then sonicated using sonication probe MS73 (Bandelin Electronic, Germany) at 10% power, cycle 6 for 10 s. Lysates were then incubated on ice for 1 h, followed by centrifugation at 12,000 x g for 10 min at 4 ^{o}C. The supernatants were transferred to fresh 1.5 ml tubes and the centrifugation step was repeated to obtain clarified supernatants. The pH of the lysates was checked using a pH strip and adjusted to pH 7.5 using 2 M Trizma Base if necessary. A Bradford assay (Section 2.2.8) was carried out to determine the protein concentration in each sample.

2.2.14.3 Preparation of *Nicotiana tabacum* lysates for Trypsin digestion

100 % TCA (Section 2.1.13.1) was added to *N. tabacum* lysates (Section 2.2.14.2) (1 mg total protein) to a final concentration of 15 % (v/v). The samples were vortexed briefly and incubated at 4 ^{o}C for 2 h. Samples were centrifuged at 12,000 x g for 10 min at 4 ^{o}C and the supernatant was discarded. Ice-cold acetone (500 µl) was added to each protein pellet, pipetted briefly and then incubated at -20 ^{o}C for 2 h. Samples were centrifuged at 12,000 x g for 10 min at 4 ^{o}C and the supernatant was discarded. The acetone wash was repeated twice (an overnight incubation, followed by another 2 h incubation). After the acetone was removed from the final washes, the pellets were allowed to dry for no more than 5 min. Each pellet was then resuspended in protein resuspension buffer (80 µl) (Section 2.1.13.3). A Bradford assay was carried out to determine the protein concentration of each sample.

2.2.14.4 Protein Digestion for Q-Exactive Mass Spectometry

Samples (15 µl; 50 µg) in protein resuspension buffer (Section 2.1.13.1 or Section 2.1.13.3) were brought to room temperature for 10 min to ensure urea was in solution. 50 mM ammonium bicarbonate (78.5 µl) (Section 2.1.13.2) was added to each sample. DTT (1 µl) (Section 2.1.13.3) was added to each sample, followed by incubation at 56 ^{o}C for 20 min. Samples were allowed to

cool to room temperature before addition of IAA (2.7 µl) (Section 2.1.13.4). Samples were then incubated at room temperature in the dark for 15 min. ProteaseMax (1 µl) (Section 2.1.13.8) and trypsin (1.8 µl) (Section 2.1.13.6) was then added to each sample, followed by overnight incubation at 37 ^{o}C. The following day, samples were spun briefly to collect any condensate and acidified by adding TFA (1 µl). The samples were the vortexed and incubated at room temperature for 5 min. Samples were then centrifuged at 13,000 x g for 10 min at room temperature. Supernatants were then transferred to clean 1.5 ml tubes. Samples were then dried down using a speedy vac (DNA Speedy Vac Concentrator, Thermo Scientific) and the pellets stored at -20 ^{o}C.

2.2.14.5 ZipTip ® Pipette Tip Protocol

The sample pellets were resuspended in resuspension buffer (20 µl) (Section 2.1.14.1) and sonicated for 2 min in a sonication bath to aid pellet resuspension. The samples were then centrifuged briefly. The ZipTip was then wet by aspirating and dispensing wetting solution (10 µl) (Section 2.1.14.3) into the tip. This was repeated 5 times. The ZipTip was then equilibrated by aspirating and dispensing 10 µl equilibration solution (Section 2.1.14.2) into the tip. This was repeated 5 times. To bind the sample to the ZipTip, 10 µl of the resuspended sample was aspirated and dispensed ten times. The Ziptip was the washed by aspirating and dispensing 10 µl of the washing solution (Section 2.1.14.2) from the tip into a waste tube. This was repeated 5 times. The sample was then eluted from the Ziptip by aspirating and dispensing 10 µl elution solution (Section 2.1.14.4) into a new 1.5 ml tube 5 times. The eluted sample was then dried down using a speedy vac and resuspended in 15 µl Q-Exactive Loading Buffer (Section 2.1.13.9). The samples were stored at -4 ^{o}C until analysis.

2.2.14.6 Q-Exactive Mass Spectrometry Method

Peptide mixtures for label free quantitative (LFQ) proteomic analysis were run on a Thermo Fisher Q-Exactive mass spectrometer coupled to a Dionex RSLCnano. LC gradients ran from 4-35 % B over 2 h, and data was collected using a Top15 method for MS/MS scans. Comparative proteome abundance and data analysis was performed using MaxQuant software (Version 1.3.0.5) (Cox and Mann, 2008), with Andromeda used for database searching and Perseus used to organise the data (Version 1.4.1.3). Carbamidomethylation of cysteines was set as a fixed

modification, while oxidation of methionines and acetylation of N-termini were set as variable modifications. The maximum peptide/protein false discovery rates (FDR) were set to 1% based on comparison to a reverse database. The LFQ algorithm was used to generate normalised spectral intensities and calculate relative protein abundance. Proteins that matched to a contaminants database or the reverse database were removed and proteins were only retained in final analysis if detected in at least three replicates from at least one sample. Quantitative analysis was performed using a t-test to compare pairs of samples, and proteins with significant change in abundance (p value < 0.05; fold change ≥ 2) were included in the quantitative results. Qualitative analysis was also performed, to detect proteins that were found in at least 3 replicates of a particular condition, but undetectable in the other sample condition. MASCOT MS/MS Ion search, with interrogation of the NCBI (National Centre for Biotechnology Information, http://www.ncbi.nlm.nih.gov) database, was used for protein identification.

2.2.15 H_2DCFDA Superoxide Detection in *A. fumigatus*

A. fumigatus conidia (1×10^6 conidia/ml per well, in 6 well plates) were added to Sabouraud liquid media (4 ml/well) (Section 2.1.1.3) and incubated for 24 h at 37°C, static. Each well contained a sterile glass microscope slide. After removal of the top layer of mycelia, H_2O_2 (3 mM final concentration) or an equivalent volume (120 µl) of molecular grade H_2O were added to wells. Plates were re-incubated 37°C, static, for 30 min, culture supernatants removed and mycelial mats washed once with 4 ml PBS (Section 2.1.4) for 5 min. After PBS removal, Sabouraud medium (3 ml) containing 2′,7′-dichlorodihydrofluorescein diacetate (2.5 µg/ml) (Section 2.1.16) was added to each well followed by incubation 37°C for 40 min, static. After washing twice with PBS (2×20 min each) (Section 2.1.4), mycelia were visualised using a fluorescent microscope (GFP filter: Ex/Em: 492–495/517–527 nm). Fluorescence from duplicate samples was quantified by measuring Integrated Density Value (IDV) of selected areas from each image (n=5/treatment).

2.2.16 Conidial Quantification

A. fumigatus colonies were grown on AMM (Section 2.1.1.1.5) for 72 h at 37 ^{o}C. Plugs were taken from the centre of each colony and placed into PBS (1 ml) (Section 2.1.4) in 1.5 ml tubes. After vigorous vortexing, 20 µl of each solution was placed on a haemocytometer and quantified.

Mean conidial concentrations were computed from 3 independent colonies. Conidial concentrations were compared via unpaired t-test.

2.2.17 Statistical Analysis

All data was analysed using built-in GraphPad prism version 5.01 functions, as specified. The level of significance was set at $p < 0.05$ (*), $p < 0.001$ (**), and $p < 0.0001$ (***), unless otherwise stated. Post-hoc comparisons between groups were performed using the Bonferroni multiple comparisons test, unless otherwise stated.

2.2.18 Multiple Sequence Alignment

Amino acid sequences were obtained from the Ensembl genome browser (http://www.ensembl.org/) and were aligned using the Kalign program (http://www.ebi.ac.uk/Tools/msa/kalign/).

2.2.19 Software Graphing

All graphs were compiled using Graphpad Prism version 5.01, unless otherwise stated.

Chapter 3

Genetic Modification of *A. fumigatus*

3.1 Introduction

Ergothioneine (EGT) is low molecular mass thiol produced by non-yeast fungi and select bacteria. A tri-*N*-methylated and sulphurised histidine derivative, EGT has been demonstrated to have antioxidant properties, however it is yet to be characterised in *A. fumigatus* (Cheah and Halliwell, 2012; Jones et al., 2014). The first identification of EGT in *A. fumigatus* was made by Gallagher et al. (2012), where it was observed that deletion of *gliK* resulted in augmented levels of EGT. *A. fumigatus* Δ*gliK* exhibited a range of other phenotypes, including abrogated gliotoxin production, sensitivity to exogenous gliotoxin, sensitivity to H_2O_2 and perturbed levels of SAM and SAH upon gliotoxin exposure (Gallagher et al., 2012; Owens et al., 2015). As a putative antioxidant, elevated EGT may be linked to H_2O_2 stress observed in Δ*gliK*. Furthermore, as the EGT biosynthetic pathway involves SAM-dependant methylation and as the thiol group is likely sourced from cysteine, EGT biosynthesis is linked metabolically with the SAM/SAH cycle and gliotoxin biosynthesis; both of which are disrupted in Δ*gliK*. EGT may therefore play an important role in adapting to *gliK* deletion in *A. fumigatus*. However, in the absence of characterised EGT function in *A. fumigatus*, this can only be speculated. A gene deletion strategy was therefore implemented to investigate EGT function in *A. fumigatus*.

EGT biosynthesis in fungi has been demonstrated to require two enzymes. The first of these, which has been characterised in *N. crassa* (Egt-1) and *S. pombe* (Egt1), catalyses tri-*N*-methylation of histidine to form hercynine, followed by iron(II)-dependant oxidative sulphurisation to form hercynylcysteine sulphoxide (Figure 3.1) (Bello et al., 2012; Pluskal et al., 2014). Egt-1 is a fusion protein of bacterial EgtD and EgtB, which carry out the methylation and sulphurisation steps respectively (Seebeck, 2010). The second enzyme in fungal EGT biosynthesis is carried out by a pyridoxal phosphate (PLP)-dependant cysteine desulphurase. This enzyme catalyses the cleavage of the cysteine residue in hercynylcysteine sulphoxide at the sulphur atom to yield EGT (Figure 3.1). This enzyme has been characterised in *S. pombe* (Egt2) and is homologous to bacterial EgtE. It has been noted in both fungi and bacteria that the cysteine desulphurase step can be carried out non-specifically and that the cysteine desulphurase encoded within the EGT biosynthetic gene cluster is not essential for EGT biosynthesis (Seebeck, 2010; Pluskal et al., 2014).

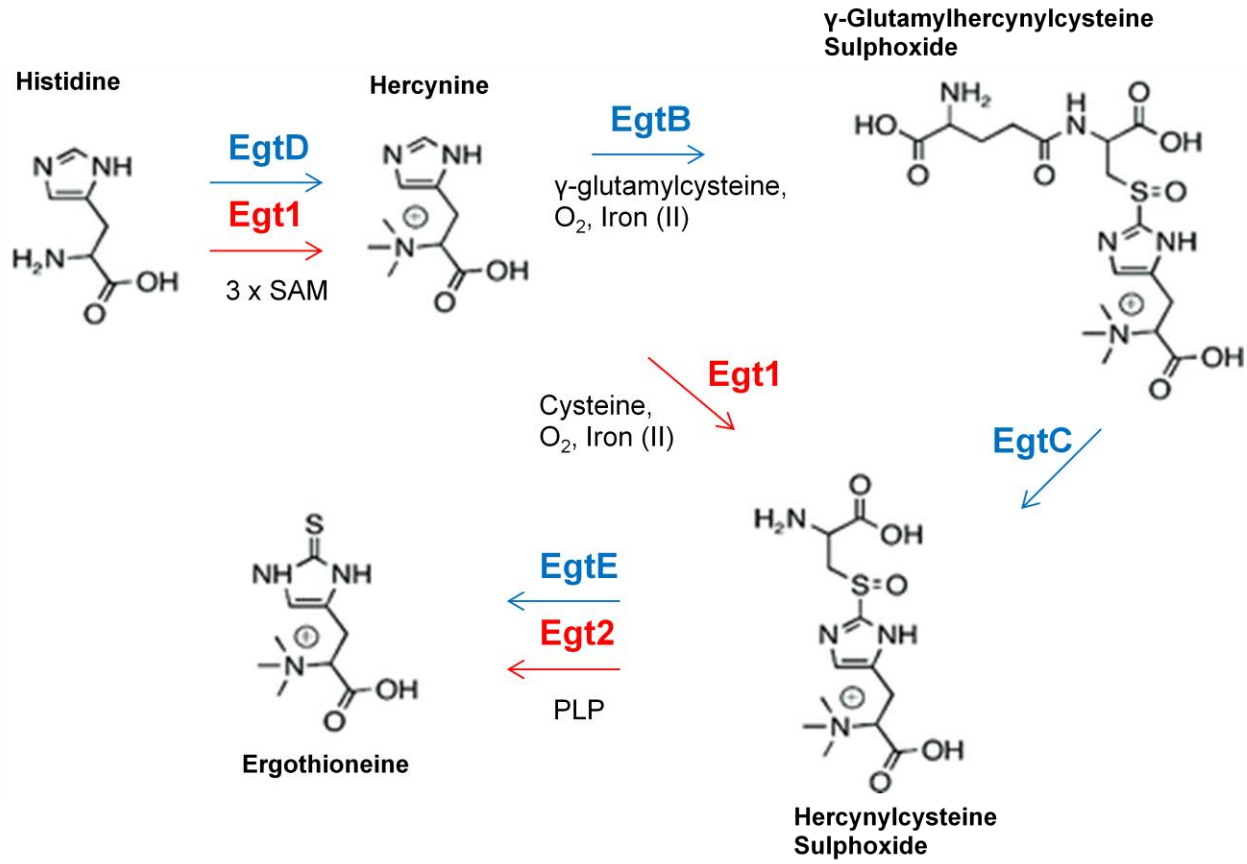

Figure 3.1. EGT biosynthesis in fungi and bacteria. The fungal pathway, outlined in red, involves two enzymes which catalyse a 3 step biosynthetic pathway. The bacterial pathway, outlined in blue, involves four enzymes which catalyse four biosynthetic reactions. Fungal EGT biosynthesis utilises cysteine instead of γ-glutamylcysteine and does not produce the intermediate γ-glutamylhercynylcysteine sulphoxide (Seebeck, 2010; Bello et al., 2012; Pluskal et al., 2014).

The genes encoding EGT biosynthetic enzymes in *A. fumigatus* have not yet been identified. Identification of the EGT biosynthetic genes in *A. fumigatus* would allow for targeted deletion in order to investigate EGT biosynthesis and function in *A. fumigatus*. Furthermore, creation of an EGT null mutant in a Δ*gliK* background would facilitate further investigation into the role of EGT in Δ*gliK* as discussed previously.

Two genes which may be of interest in the context of investigating EGT function in *A. fumigatus* are AFUA_2G09110 (*palA*) and AFUA_8G01930 (*vipC*). *palA* encodes for a phenylalanine ammonia lyase (PAL) which catalyses the breakdown of phenylalanine into ammonia and *trans*-

cinnamic acid (Camm and Towers, 1973). PAL is of much interest in plants due it its role in producing phenyl propanoid compounds, which function in a variety of cellular processes, most prominently in defence against pathogens (Zhang and Liu , 2015). However, PAL has not been characterised in fungi beyond catabolism of phenylalanine for carbon and nitrogen utilisation (Hyun et al., 2011). PAL is thus an intriguing enzyme in *A. fumigatus* in the context of investigating EGT, as PAL has been demonstrated to produce phenyl propanoid molecules in plants that have antioxidant properties (Korkina, 2007). PAL may therefore represent a novel facet of oxidative stress defence in fungi. Furthermore, Muramatsu et al. (2013) reported an ergothionase from *Burkholderia* sp. HME13 with 17 % similarity to PAL. PAL may therefore function in EGT catabolism, which has not been observed in fungi previously.

VipC is a SAM-dependant methyltransferase which has been demonstrated to regulate the switch between sexual and asexual reproduction in *A. nidulans*. VipC responds to environmental signals such as a light and interacts with the nuclear velvet complex to regulate the transcription of genes promoting sexual or asexual development (Sarikaya-Bayram et al., 2014). VipC function has not been elucidated in *A. fumigatus* and it is difficult to predict how it might function compared to its well characterised role in *A. nidulans* due to the differences in sexual development between the two *Aspergilli*. While sexual development is readily activated in *A. nidulans* when grown in the absence of light, *A. fumigatus* requires very specific conditions to activate sexual development (O'Gorman et al., 2009). VipC may still regulate asexual development in *A. fumigatus* however, as it is the dominate life cycle observed. EGT has been demonstrated to influence conidiation in *N. crassa*, with Δ*egt-1* exhibiting reduced conidiation and conidial survival (Bello et al., 2012, 2014) Furthermore, EGT is speculated to influence SAM/SAH levels. As a trimethylated metabolite, EGT biosynthesis interacts significantly with the SAM/SAH cycle as the biosynthesis of 1 mol of EGT requires 3 mol of SAM. Abrogation of EGT biosynthesis may therefore disrupt SAM/SAH ratios. As a SAM-dependant methyltransferase, VipC is likely sensitive to alterations in SAM/SAH levels. Thus, analysis of VipC in *A. fumigatus* may contribute to characterisation of EGT function.

In order to investigate these genes and their products, a strategy of gene deletion was implemented. Gene deletion is a valuable tool that has been used to study the functions of genes in filamentous fungi such as *A. fumigatus* (Wiemann and Keller, 2014). Through analysis of any

phenotypes that are observed in the absence of the gene, the function of the gene can be inferred. This reverse genetic analysis has been used several times in the past to elucidate gene function, for example with the regulator of secondary metabolism, *laeA* (Bok and Keller, 2004). Gene deletion strategies commonly involve replacing or disrupting the gene of interest with a selection marker. Auxotrophic markers can be used in background strains which have been engineered to have an autotrophy. An example of this is the *pyrG* gene (Weidner et al., 1998), which can be used as a selection marker in uracil/uradine auxotrophs. Alternatively, anti-fungal drug resistance genes such as *ptrA* and *hph* can be used as selection markers. The *ptrA* gene provides resistance to pyrithiamine, while *hph* endows resistance to hygromycin (Cullen et al., 1987; Kubodera et al., 2002).

A bipartite gene deletion strategy was employed in this study. The bipartite gene deletion method allows for targeted deletion or disruption of genes. This method involves two constructs, which consist of either the 5' or 3' flanking region of the gene of interest fused to a fragment of a selection marker. The two fragments of the selection marker on either construct overlap, which serves as a site for homologous recombination. These constructs are transformed into *A. fumigatus* protoplasts using polyethylene glycol (PEG) and $CaCl_2$. Upon transformation, homologous recombination of the constructs with the flanking regions of the gene of interest causes a third recombination event within the overlapping segment of the selection marker. This results in an intact selection marker gene, in place of the gene of interest (Figure 3.2).

As two targeted recombination events are required in order for integration of an intact selection marker into the target genome, the rate of false positives is reduced. Thus, this method is more efficient than single construct deletion strategies (Nielsen et al., 2006). Following gene deletion is important to complement the mutant by reinserting the gene. This ensures that any phenotypes observed can be attributed to the loss of the gene, and not the expression of the selection marker.

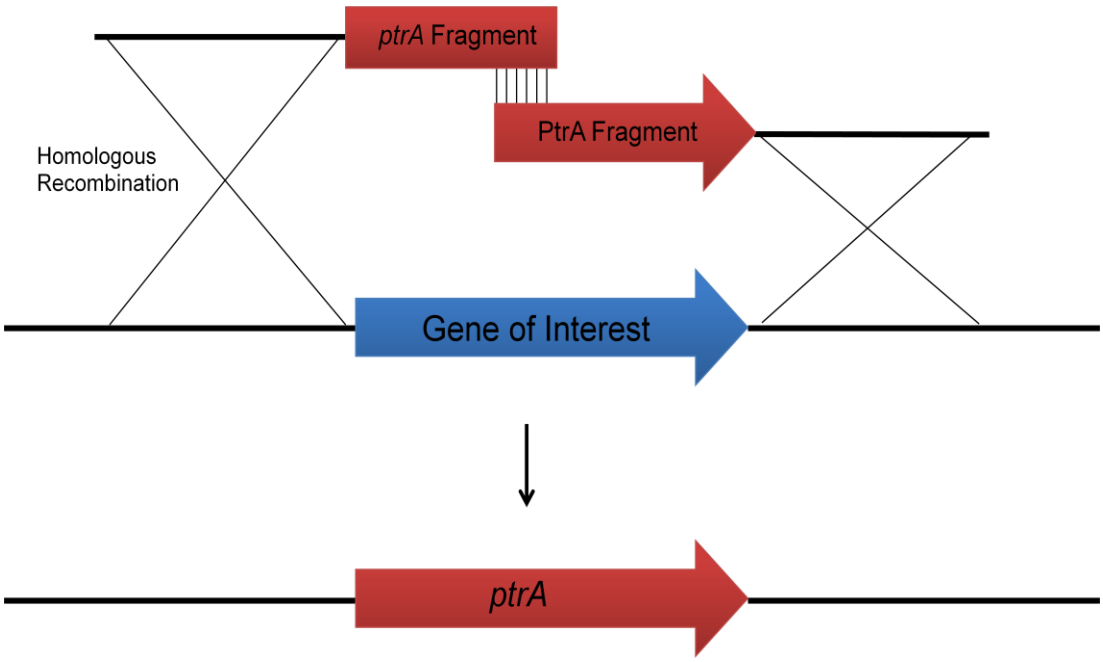

Figure 3.2. Schematic representation of the bipartite method of gene deletion used in this study. *ptrA* is used as an example of a selection marker.

The objectives of the work presented in this chapter were to:

(i) Identify EGT biosynthetic genes in *A. fumigatus* via bioinformatic analysis.

(ii) Generate gene deletion mutants and complemented strains in *A. fumigatus* ATCC26933 for the EGT biosynthetic genes identified in (i). Furthermore, generate deletion mutants for *vipC* and *palA* in *A. fumigatus* ATCC26933. Additionally it was hypothesised the generation of an EGT null mutant in a *gliK* background could yield useful information.

(iii) Confirm all gene deletions and completed strains by semi-quantitative RT-PCR.

3.2 Results

3.2.1 Bioinformatic identification of EGT biosynthetic genes in *A. fumigatus*

3.2.1.1 Identification of *A. fumigatus egtA*

BLAST searches (http://blast.ncbi.nlm.nih.gov/Blast.cgi) revealed AFUA_2G15650 to be a possible homologous enzyme to *M. smegmatis* EgtB and EgtD in *A. fumigatus*. AFUA_2G15650, annotated as DUF323, also had homology to NCU04343 (Egt-1) in *N. crassa*, and SPBC1604.01 (Egt1) in *S. pombe*. AFUA_2G15650 was therefore renamed EgtA. In *A. fumigatus*, EgtA comprises 844 amino acids, has domains of a histidine-specific SAM-dependent methyltransferase at the N-terminal end, a sulphatase-modifying factor enzyme 1 at the C-terminal end and an intervening 5-histidylcysteine sulphoxide synthase domain (Figure 3.3). EgtA shows 82 % similarity with *S. pombe* Egt1, 80 % similarity with *N. crassa* Egt-1, 38 % similarity with *M. smegmatis* EgtB and 28 % similarity with *M. smegmatis* EgtD (Figure 3.4). The *egtA* genomic sequence is 2890 bp long and contains six introns (http://www.aspergillusgenome.org/cgi-bin/locus.pl?locus=AFUA_2g15650&organism=A_fumigatus_Af293).

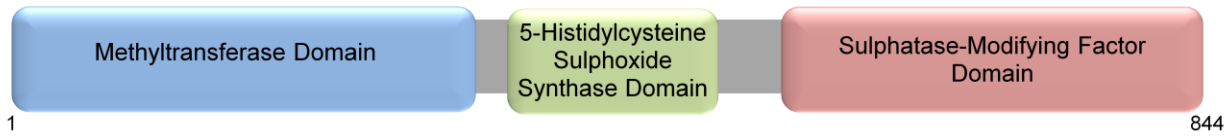

Figure 3.3. EgtA domain architecture, 844 amino acids in length. Domains include a methyltransferase domain at the N-terminal end, a sulphatase-modifying factor enzyme 1 at the C-terminal and an internal 5'-histidylcysteine sulphoxide synthase domain.

Figure 3.4. Alignment of *A. fumigatus* EgtA (AFUA_2G15650), *N.crassa* Egt-1 (NCU04343), *S. pombe* Egt1 (SPBC1604.01) and *M. smegmatis* EgtD (MSMEG_6247) and EgtB (MSMEG_6249).

3.2.1.2 Identification of *egtB* and *nfs1* as putative EGT biosynthetic genes in *A. fumigatus*

BLAST searches (http://blast.ncbi.nlm.nih.gov/Blast.cgi) revealed AFUA_2G13295 as a possible homologous enzyme to *M. smegmatis* EgtE (MSMEG_6246) and *S. pombe* Egt2 (SPBC660.12c). AFUA_2G13295, annotated as a putative aminotransferase, was therefore renamed EgtB. *A. fumigatus* EgtB is 453 amino acids in length and contains a cysteine desulphurase domain as well as a PLP-binding pocket. (Figure 3.5). EgtB shows 30 % similarity with *S. pombe* Egt2 and 27 % similarity with *M. smegmatis* EgtE (Figure 3.6). The *egtB* genomic sequence is 1510 bp long and contains two introns (http://www.aspergillusgenome.org/cgi-bin/locus.pl?dbid=ASPL0000362536).

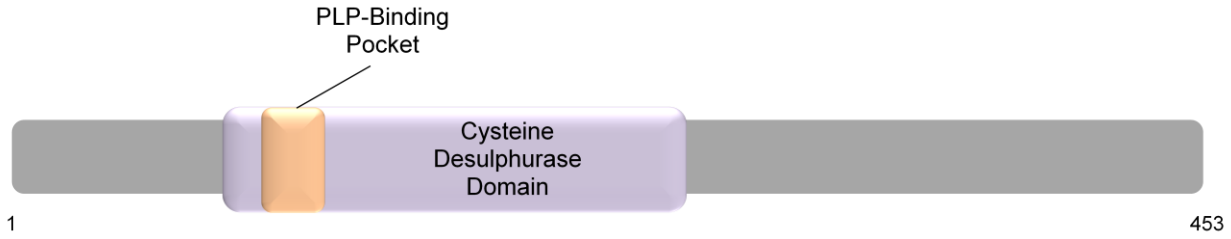

Figure 3.5. EgtB domain architecture, 453 amino acids in length. Domains include a cysteine desulphurase domain, which itself contains a PLP-binding pocket.

As is it has been demonstrated in both *M. smegmatis* and *S. pombe* that the cysteine desulphurase step in EGT biosynthesis can be carried out non-specifically, a second enzyme, Nfs1 (AFUA_3G14240), was identified as a possible alternative candidate for completing the final step of EGT biosynthesis. Nfs1 has 26 % similarity to *A. fumigatus* EgtB, 28 % similarity with *M. smegmatis* EgtE and 23 % similarity with *S. pombe* Egt2 (Figure 3.6), and like EgtB, contains cysteine desulphurase and PLP-binding domains (http://www.aspergillusgenome.org/cgi-bin/locus.pl?locus=AFUA_3G14240&organism=A_fumigatus_Af293).

Figure 3.6. Alignment of *A. fumigatus* EgtB (AFUA_2G13295), *S. pombe* Egt2 (SPBC660.12c). *A. fumigatus* Nfs1 (AFUA_3G14240), and *M. smegmatis* EgtE (MSMEG_6246).

3.2.2 Generation of *A. fumigatus egtA* deletion and complemented strains

3.2.2.1 Generation of deletion constructs for transformation of *egtA*

In order to investigate the function of *egtA* (AFUA_2G15650), a gene deletion strategy was employed (Figure 3.7). Protoplast transformations were performed using the background strain ATCC26933. This background was chosen due to the high amounts of gliotoxin it produces (Schrettl et al., 2010). ATCC26933 was transformed with two DNA constructs, each of which contained an incomplete fragment of the pyrithiamine resistance gene (*ptrA*) released from the plasmid pSK275 via restriction digest. These fragments were fused to 1090 bp and 1066 bp of 5' and 3' *egtA* flanking sequences respectively. The fragments shared an overlapping region of the *ptrA* gene spanning 561 bp, allowing for recombination of the complete cassette upon transformation. Homologous recombination of the flanking region in each fragment allowed for targeted disruption of the *egtA* gene with the intact *ptrA* gene. Due to the size of *egtA*, a small fragment of the 3' section of the gene remained following the deletion transformation (Figure 3.7).

To aid generation of the deletion constructs, an *egtA* deletion mutant in the AfS77 strain (A kind gift from Professor Hubertus Haas, Innsbruck, Austria) was used as a template for PCR. The AfS77 strain is a Δ*akuA::loxP* derivative of ATCC46645 (Hartmann et al., 2010), which produces low levels of gliotoxin. For this reason it was unsuitable for this study, however using it as a template for PCR allowed for the generation of deletion constructs with a single round of PCR (Figure 3.7) when two rounds are normally necessary (Section 2.2.4.1).

The 5' deletion construct was amplified by PCR, using primers egtA1 and oAoptrA1, for a product of 2022 bp (Figure 3.8). The 3' deletion construct was amplified similarly, using primers egtA4 and oAoptrA 2, for a product of 2476 bp (Figure 3.8). The products were gel purified (Section 2.2.3.8.3) to ensure no non-specific products were present.

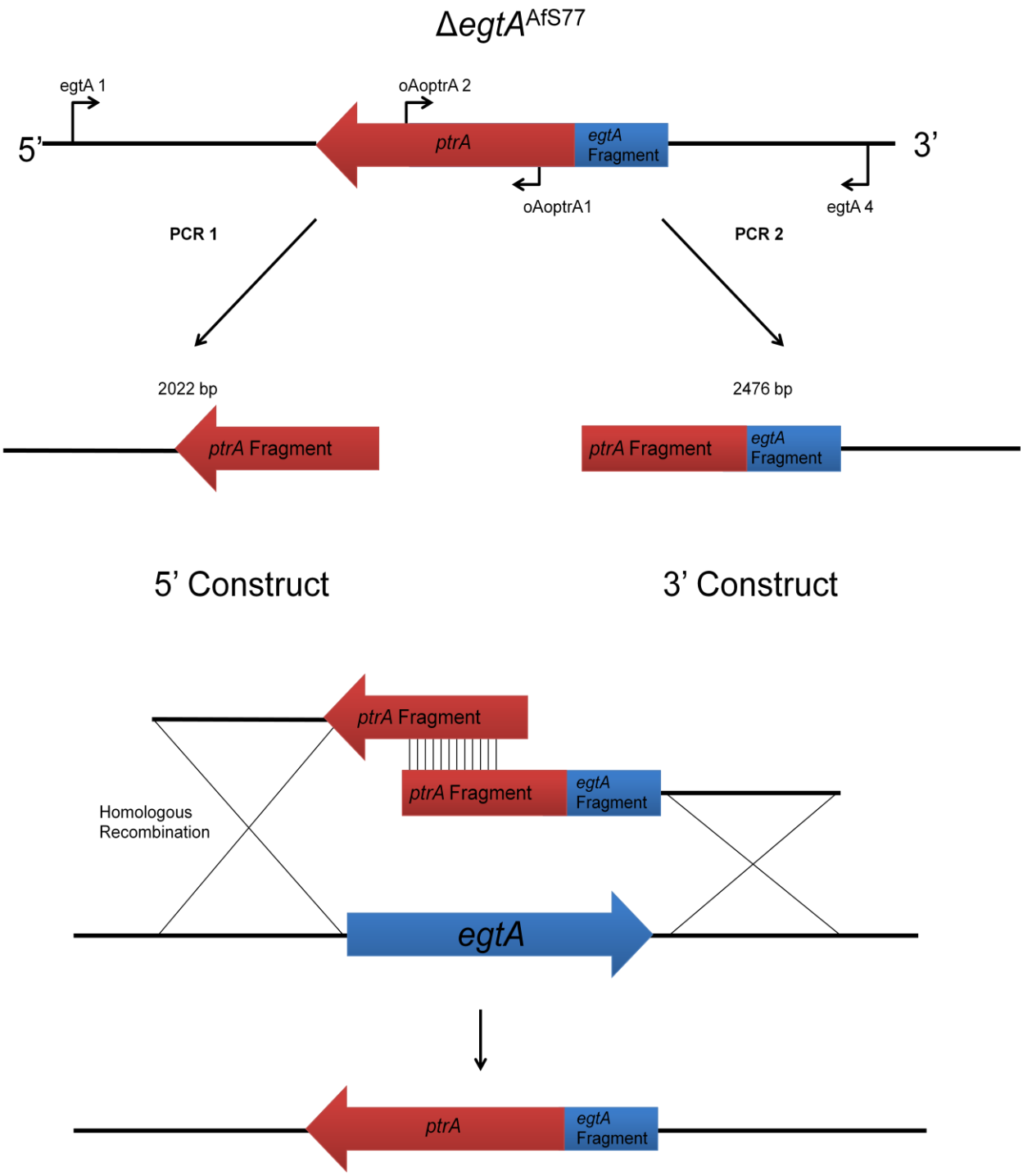

Figure 3.7. A schematic representation of the bipartite strategy for the deletion of *egtA* in *A. fumigatus* ATCC26933, using *ptrA* as a selection marker.

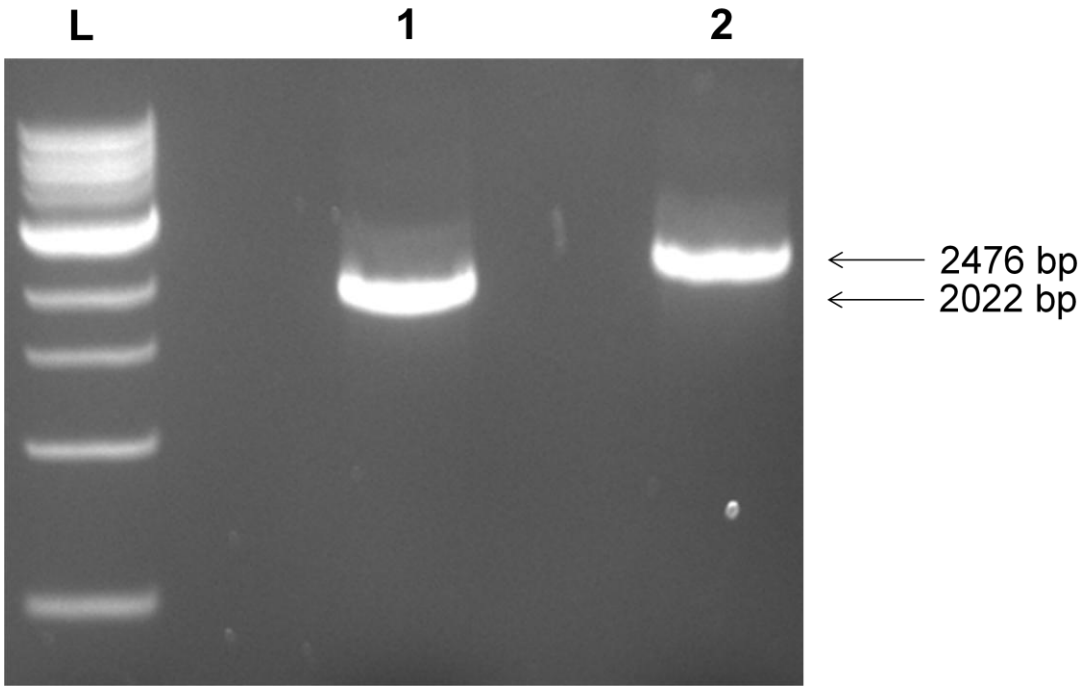

Figure 3.8. Final *egtA* gene deletion constructs. Lane L: NEB 1 kb DNA Ladder (Section 2.1.7.6). Lane 1: PCR 1 (2022 bp), the 5' flanking region of *egtA* fused to a partial fragment of the *ptrA* selection marker. Lane 2: PCR 2 (2427 bp), the 3' flanking region of of *egtA* fused to a partial fragment of the *ptrA* selection marker.

3.2.2.2 Generation of 5' DIG-labelled probe by PCR for Δ*egtA* transformant identification

A single 5' upstream probe was prepared by PCR amplification for use in Southern blot analysis. The probe was generated using DIG-labelled nucleotides, which allowed for detection during Southern blot analysis (Section 2.2.5.1). A 5' probe was made using primers egtA2 and egtA5 which amplified a 1090 bp region just upstream of *egtA* (Figure 3.9).

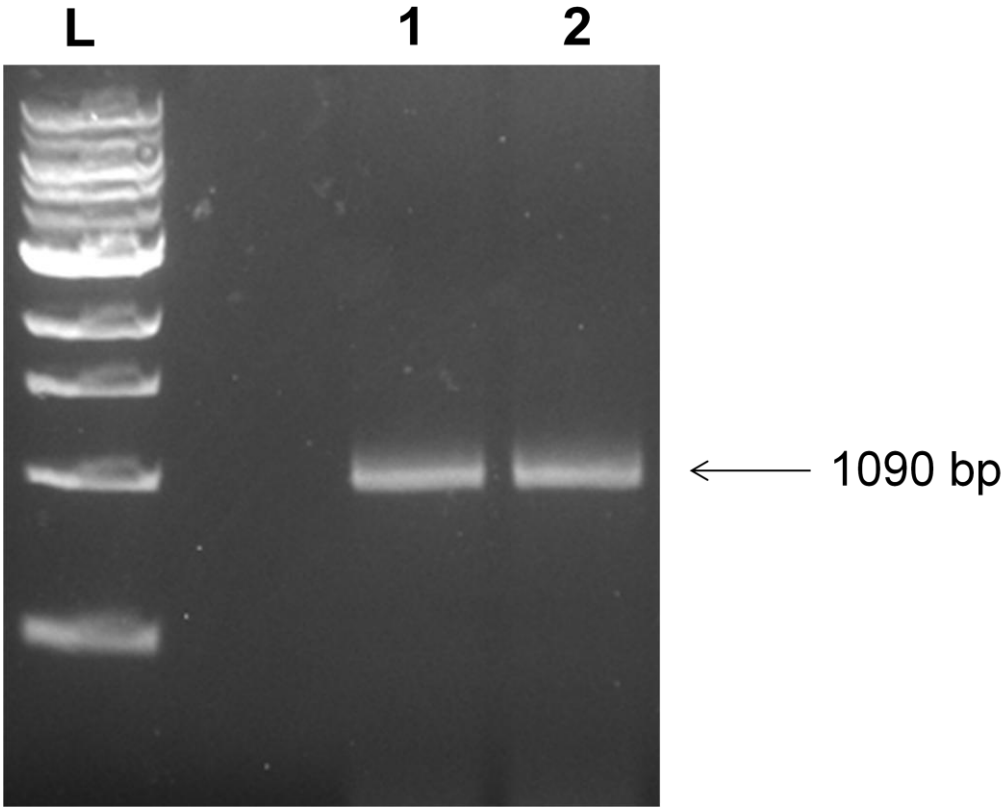

Figure 3.9. Generation of DIG-labelled nucleotide probe which facilitated Δ*egtA* detection with Southern blot analysis. Lane L: NEB 1 kb DNA Ladder (Section 2.1.7.6). Lane 1: *egtA* 5' DIG labelled nucleotide probe. Lane 2: positive control using standard dNTPs.

3.2.2.3 Deletion of *egtA* in *A. fumigatus* ATCC26933

The *egtA* deletion constructs from Section 3.2.2.1 were transformed into *A. fumigatus* ATCC26933 protoplasts, which were prepared as described in section 2.2.4.3. Approximately 3 µg total of 5' and 3' construct was used per transformation event. The transformation procedure was carried out as described in Section 2.2.4.4. Transformants were selected on agar plates containing pyrithiamine (100 ng/ml). Colonies with the ability to grow on these plates were predicted to have an intact *ptrA* gene incorporated into their genome, and thus considered potential Δ*egtA* transformants.

Following the transformation event, 23 colonies were observed on pyrithiamine selection plates. Genomic DNA from 10 of these colonies was digested using *Sph*I restriction endonuclease. These were screened by Southern analysis (section 2.2.5) using a 5' probe (Section 3.2.2.2). The Southern strategy used to confirm *egtA* deletion is outlined in Figure 3.10. The mutant band (2045 bp) was present in transformant 2 (Figure 3.11). This colony was selected for single spore isolation (Section 2.2.4.8). Eight single spore isolates of transformant 2 were digested with *Sph*I and a second round of Southern blot analysis using the 5' probe was performed. All eight isolates displayed the correct band for *egtA* deletion, confirming a single integration of the *ptrA* gene in place of *egtA* (Figure 3.12).

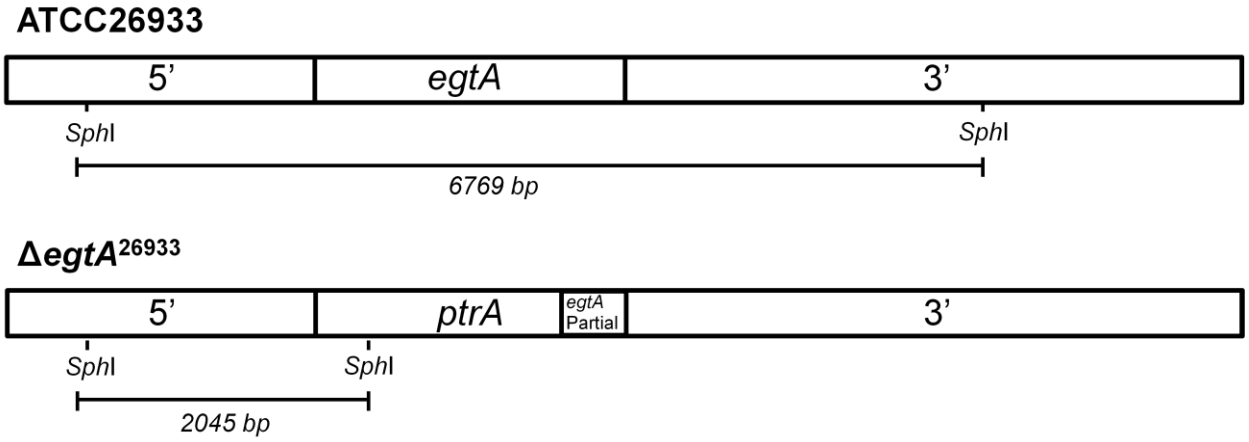

Figure 3.10. A schematic of the Southern blot strategy employed to detect the deletion of *egtA*. DNA was digested using *Sph*I restriction endonuclease. The digested DNA was screened using a 5' probe. A correct gene deletion event would result in a band of 2045 bp in length. Wild-type *Sph*I digested DNA would result in a band of 6769 bp in length.

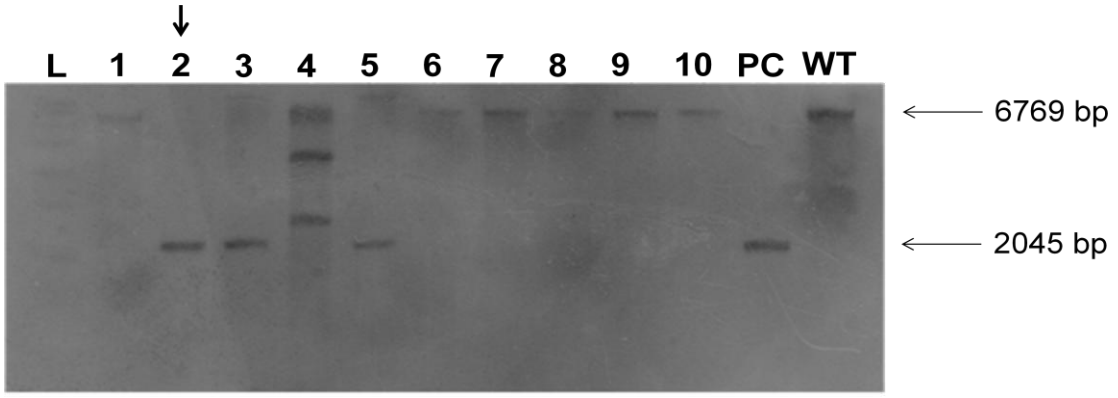

Figure 3.11. Southern Analysis of potential *egtA* deletion mutants in *A. fumigatus* strain ATCC26933 using a 5' probe. Successful deletion of *egtA* was indicated by the presence of a single 2045 bp band. Lane L: Roche Molecular Weight Ladder VII, DIG labelled (Section 2.1.7.6). Lanes 1-10: Potential Δ*egtA* transformants. Lane PC: Δ*egtA*^{AfS77} (2045 bp). Lane WT: ATCC26933 (6769 bp). Transformant 2 displays the correct band for the Δ*egtA* genotype.

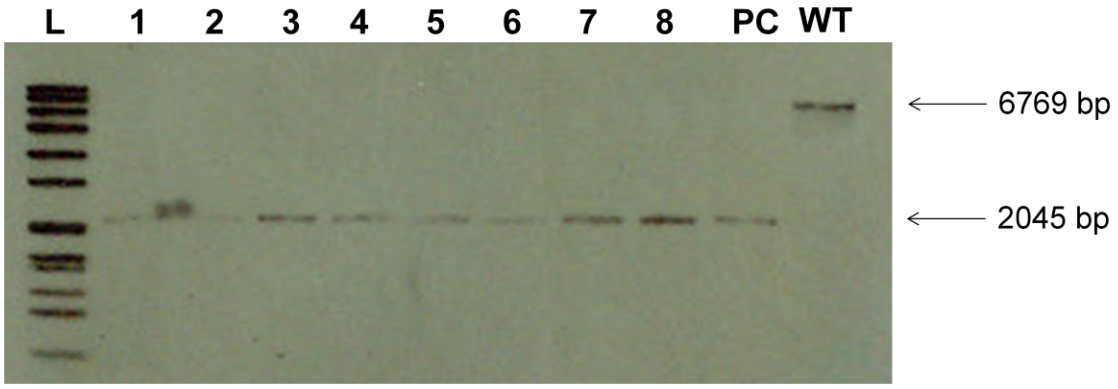

Figure 3.12. Southern Analysis of single spore isolates of a potential *egtA* deletion mutant using a 5' probe. Successful deletion of *egtA* was indicated by the presence of a single 2045 bp band. Lane L: Roche Molecular Weight Ladder VII, DIG labelled (Section 2.1.7.6). Lanes 1-8: Single spore isolates. Lane PC: Δ*egtA*^{AfS77} (2045 bp). Lane WT: ATCC26933 (6769 bp). All single spore isolates display the correct band for the Δ*egtA* genotype.

3.2.2.4 Generation of the *egtA* complementation construct

Once *egtA* had been successfully deleted it was necessary to reintroduce the gene into the genome of Δ*egtA*^{26933}. This ensured that any phenotypes observed could be solely attributed to the deletion of *egtA*. The *egtA* complementation strategy is outlined in Figure 3.13. To complement Δ*egtA*, a PCR fragment containing the *egtA* locus, including promoter and terminator, was amplified using primers egtA5 and egtA6 (Figure 3.14). This was then inserted into the pCR® 2.1-TOPO vector, to create pegtA. Insertion of *egtA* was confirmed by colony PCR (Figure 3.15) and restriction digest (Figure 3.116). The pegtA vector was linearised using *Aat*II and co-transformed into the Δ*egtA* mutant alongside pAN7.1, which contains the *hph* selection marker for hygromycin resistance.

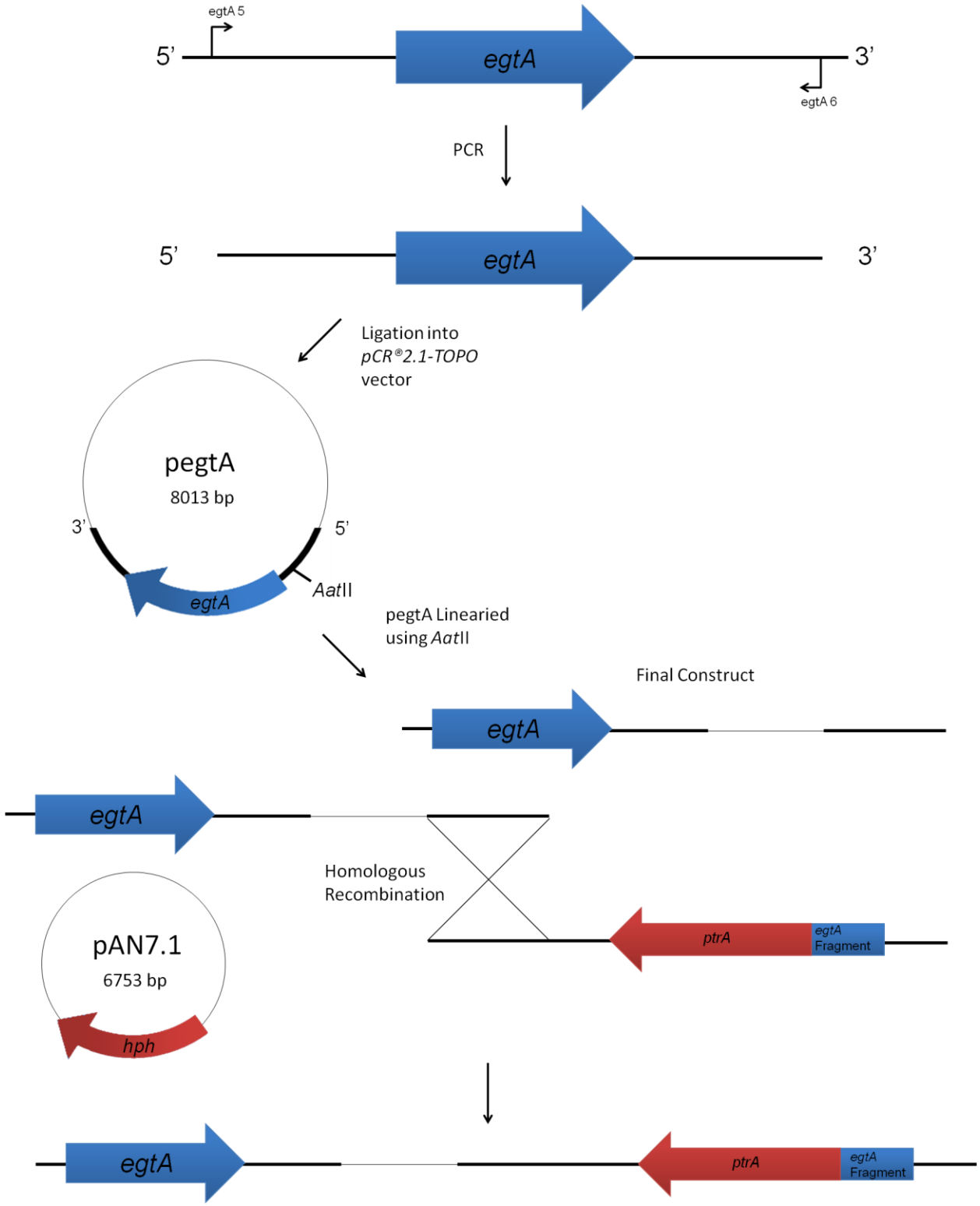

Figure 3.13. A schematic representation of the complementation strategy for the re-insertion of *egtA* in *A. fumigatus* Δ*egtA*[26933], using *hph* as a selection marker.

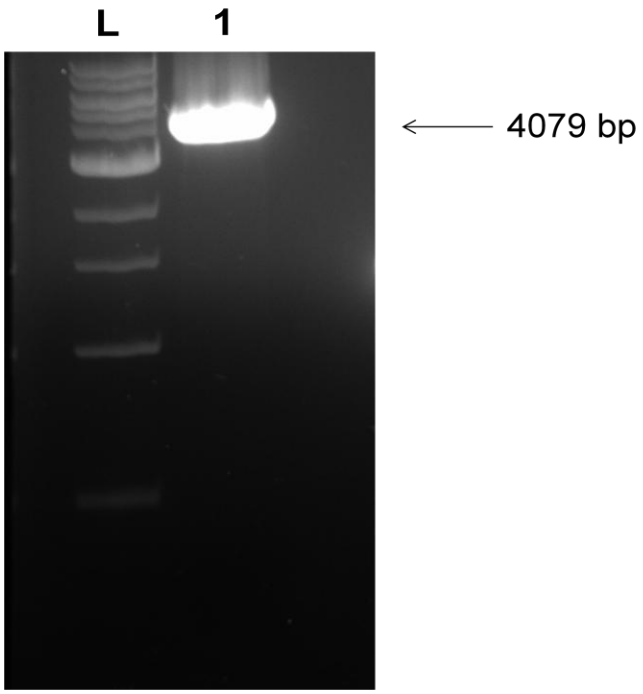

Figure 3.14. Amplification of *egtA*, including 5' and 3' flanking regions, for TOPO cloning. Lane L: NEB 1 kb DNA Ladder (Section 2.1.7.6). Lane 1: Amplified *egtA* gene and flanking regions (4079 bp).

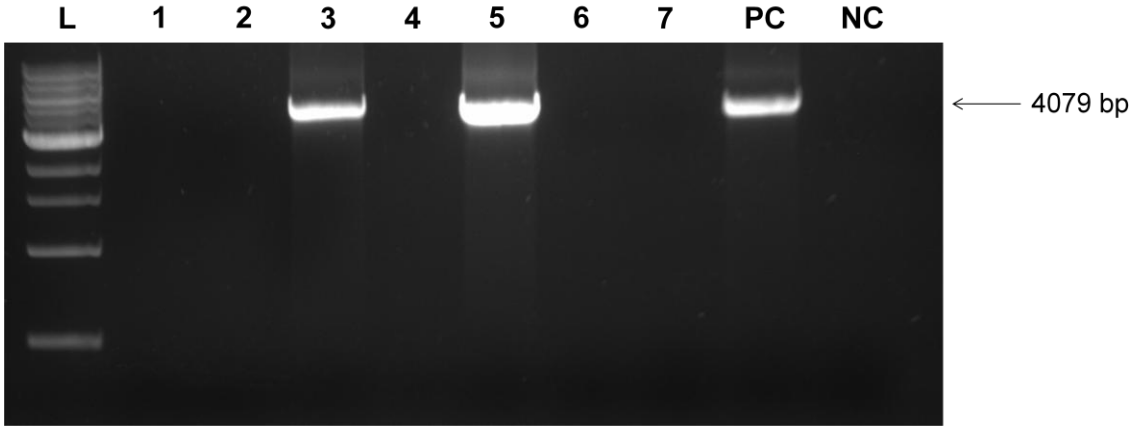

Figure 3.15. Colony PCR of transformed *E. coli* TOP10 cells to test for insertion of *egtA* and flanking regions into the *pCR®2.1-TOPO* vector. Lane L: NEB 1 kb DNA Ladder (Section 2.1.7.6). Lanes 1 – 7: Transformed colonies Lane PC: gDNA positive control. Lane NC: Negative control.

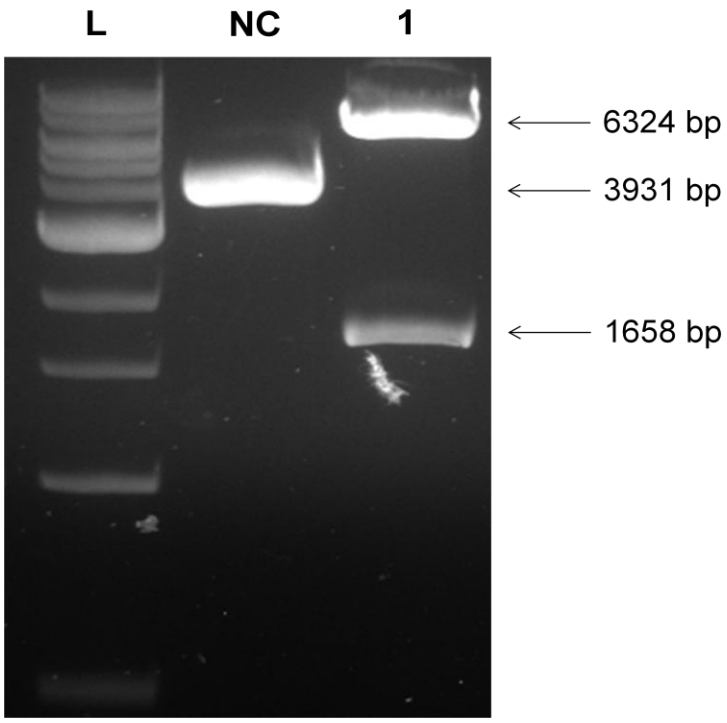

Figure 3.16. Restriction digest with *BssH*II to check the orientation of *egtA* and flanking region insert in the pegtA plasmid. A 5' – 3' insertion was indicated by two bands, 6324 bp and 1658 bp in length. Lane L: NEB 1 kb DNA Ladder (Section 2.1.7.6). Lane NC: empty pCR®2.1-TOPO vector digested with *BssH*II (3931 bp). Lane 1: pegtA digested with *BssH*II (6324 bp and 1658 bp).

3.2.2.5 Generation of 3' DIG-labelled probe by PCR for *egtA*^{C} transformant identification

The 5' probe used to detect Δ*egtA* (Section 3.2.2.2) was unsuitable for detecting *egtA*^{C} so it was necessary to generate a 3' probe. The probe was generated using DIG-labelled nucleotides as before and was made using primers egtA4 and egtA6 which amplified a 1066 bp region just downstream of *egtA* (Figure 3.17)

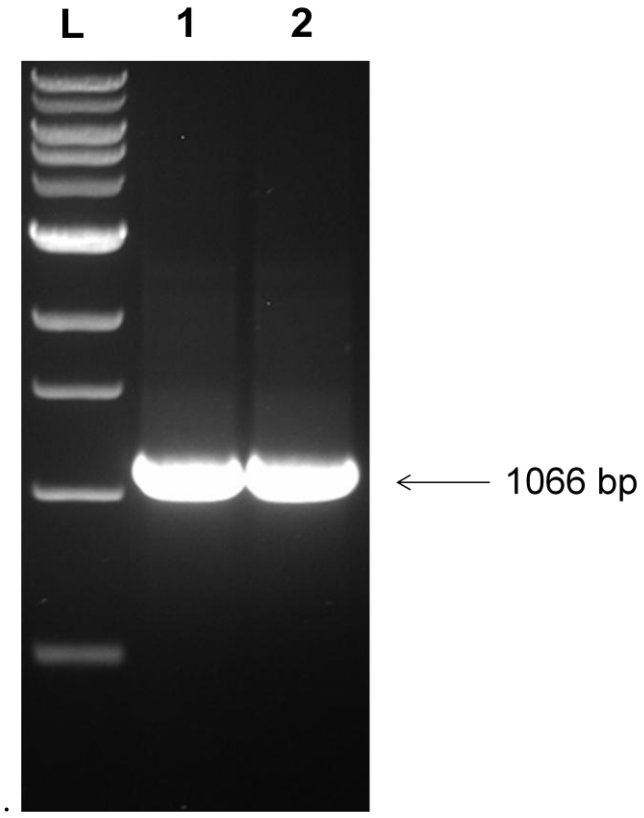

Figure 3.17. Generation of DIG-labelled nucleotide probe which facilitated Δ*egtA* and *egtA*^{C} detection with Southern blot analysis. Lane L: NEB 1 kb DNA Ladder (Section 2.1.7.6). Lane 1: *egtA* 3' DIG labelled nucleotide probe. Lane 2: positive control using standard dNTPs.

3.2.2.6 Southern blot analysis of transformants from *A. fumigatus egtA* complementation

Figure 3.18 illustrates the Southern strategy employed to confirm *egtA* complementation. 86 colonies were observed on the hygromycin plates. These were screened via Southern blot in groups of 20. Genomic DNA from these potential transformants was digested with *BamH*I and probed with the 3' probe (Section 3.2.2.5). Southern analysis (Section 2.2.5) identified one tranformant which showed the correct banding pattern (2087 bp & 6467 bp) for complementation of *egtA* (Figure 3.19).

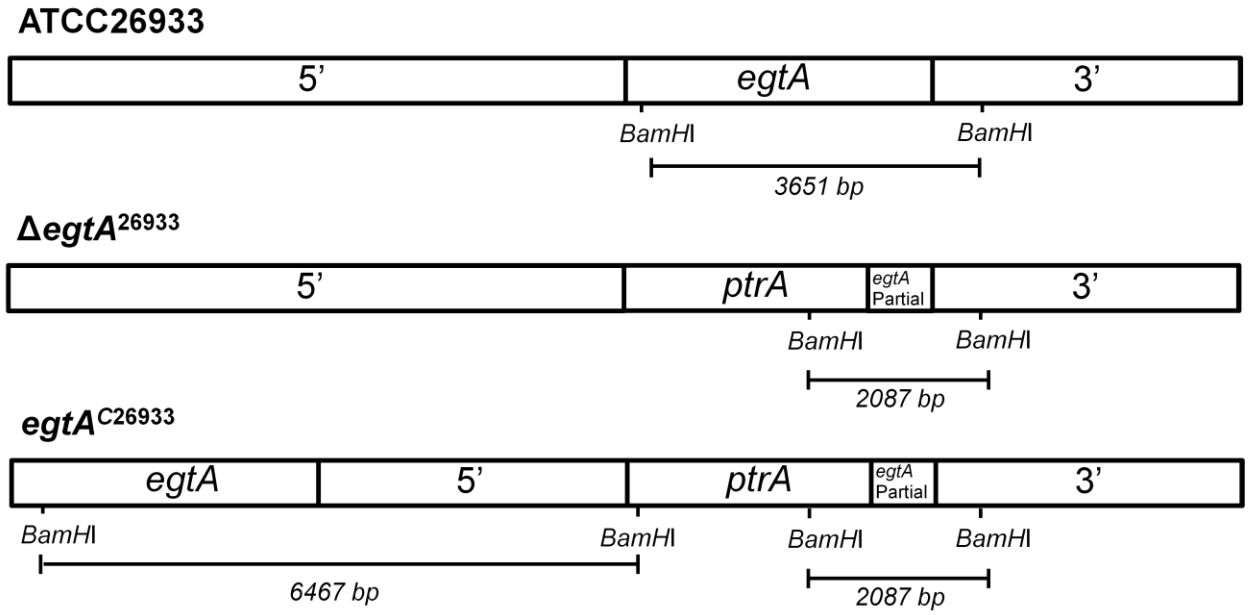

Figure 3.18. A schematic of the Southern blot strategy employed to detect re-insertion of *egtA* into Δ*egtA*^{26933}. DNA was digested using *BamH*I. The digested DNA was screened using a 3' probe. A correct gene insertion event would result in bands of 2087 bp and 6467 bp. Δ*egtA*^{26933} *BamH*I digested DNA would result in a band of 2087 bp. Wild-type *BamH*I digested DNA would result in a band of 3651 bp.

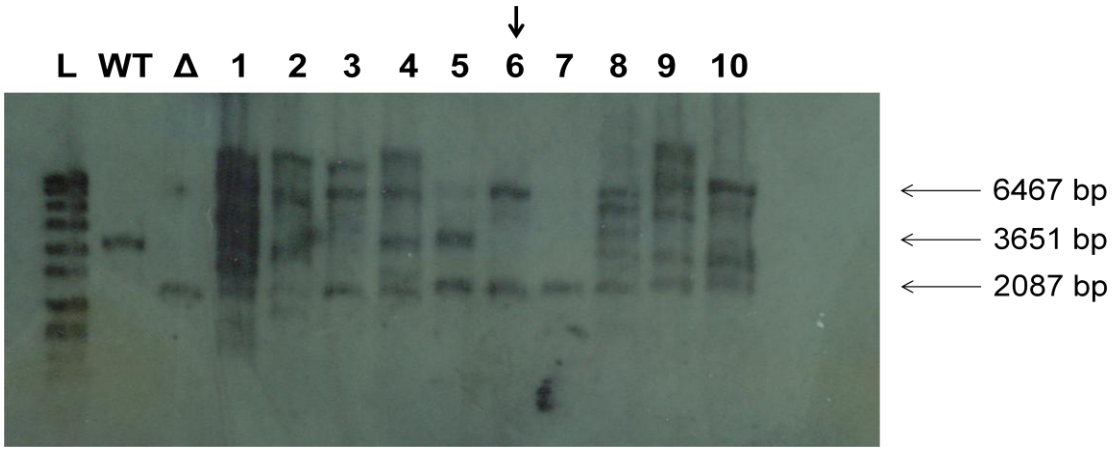

Figure 3.19. Southern Analysis of potential *egtA*^{C} transformants in *A. fumigatus* Δ*egtA*^{26933} using a 3' probe. Successful insertion of *egtA* was indicated by the presence of two bands, 2087 bp and 6467 bp. Lane L: Roche Molecular Weight Ladder VII, DIG labeled (Section 2.1.7.6). Lane WT: ATCC26933 (6467 bp). Lane Δ: Δ*egtA*^{26933} (2087 bp). Lanes 1-10: Potential *egtA*^{C} transformants. Transformant 6 displays the correct banding pattern for the *egtA*^{C} genotype.

3.2.2.7 Semi-quantitative RT-PCR Analysis of *egtA* expression in Δ*egtA*^{26933} and *egtA*^{C26933}

The deletion of *A. fumigatus egtA* from ATCC26933 and its subsequent complementation was confirmed by Southern analysis. Semi-quantitative RT-PCR (section 2.2.6.4) was employed to confirm that the deletion of *egtA* resulted in the cessation of *egtA* expression and that the restoration of *egtA* expression was evident in *egtA*^{C26933}. Both wild-type and mutant strains were cultured in Sabouraud Dextrose liquid broth and incubated at 37 °C for 24 h. Total RNA was extracted and subjected to cDNA synthesis (Section 2.2.6.4). RT-PCR was carried out using the primers QPCR egtA F and QPCR egtA R (Table 2.5). Expression of *egtA* was evident in *A. fumigatus* wild-type and *egtA*^{C26933} and absent from Δ*egtA*^{26933}. This confirmed that *egtA* expression was abrogated by *egtA* deletion and restored in the complemented strain (Figure 3.20).

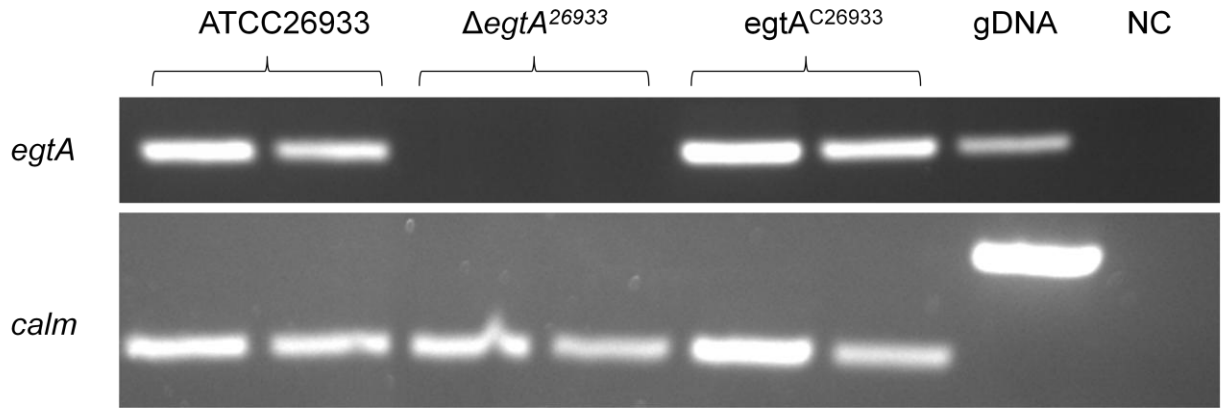

Figure 3.20. Confirmation of the absence of *egtA* expression in *A. fumigatus* Δ*egtA*^{26933} and its restoration in *egtA*^{C26933} by semi-quantitative RT-PCR (n = 2 biological replicates per condition). *calm* is used as cDNA control (Burns et al., 2005). gDNA was used as a positive control. NC: negative control; no cDNA or DNA present in amplification reactions.

3.2.3 Generation of an *egtB* deletion strain in *A. fumigatus* ATCC26933

3.2.3.1 Generation of deletion constructs for transformation of *egtB*

A gene deletion strategy was employed to investigate the function of *egtB* (AFUA_2G13295) (Figure 3.21). Protoplast transformations were performed using the background strain ATCC26933. As before, this is due to the high levels of gliotoxin produced. It would also allow for a comparison with Δ*egtA*^{26933}. As with the deletion of *egtA* (Section 3.2.2.1), ATCC26933 was transformed with two DNA constructs which comprised of either the 5' or 3' flanking sequence of *egtB* fused to an incomplete fragment of the *ptrA* gene. The 5' construct consisted of 1459 bp of upstream flanking region fused to 1527 bp of *ptrA* fragment. The 3' construct consisted of 1337 bp of downstream flanking region fused to 1083 bp of *ptrA* fragment. The two constructs shared 561 bp of overlap within the *ptrA* gene, which served as a site for homologous recombination.

The two fragments were generated using two round of PCR. The 5' and 3' flanking regions of *egtB* were amplified from ATCC26933 genomic DNA. The 5' flanking region was amplified using the primers egtB1 and egtB2 (1560 bp), while the 3' flanking region was amplified using the primers egtB4 and egtB5 (1509 bp) (Figure 3.22). The flanking regions were excised using gel purification (section 2.2.3.8.3) and digested using *Spe*I (5' region) and *Hind*III (3' region). The *ptrA* selection marker was released from plasmid pSK275 by digestion with *Spe*I and *Hind*III (Figure 3.23), and ligated with the two digested flanking regions. The final deletion constructs were amplified from the ligation product using primers egtB3 and PTRoptrA2 for the 5' construct (2989 bp) and primers egtB6 and PTRoptrA1 for the 3' construct (2420 bp) (Figure 3.24). The products were gel purified (Section 2.2.3.8.3) to ensure no non-specific products were present.

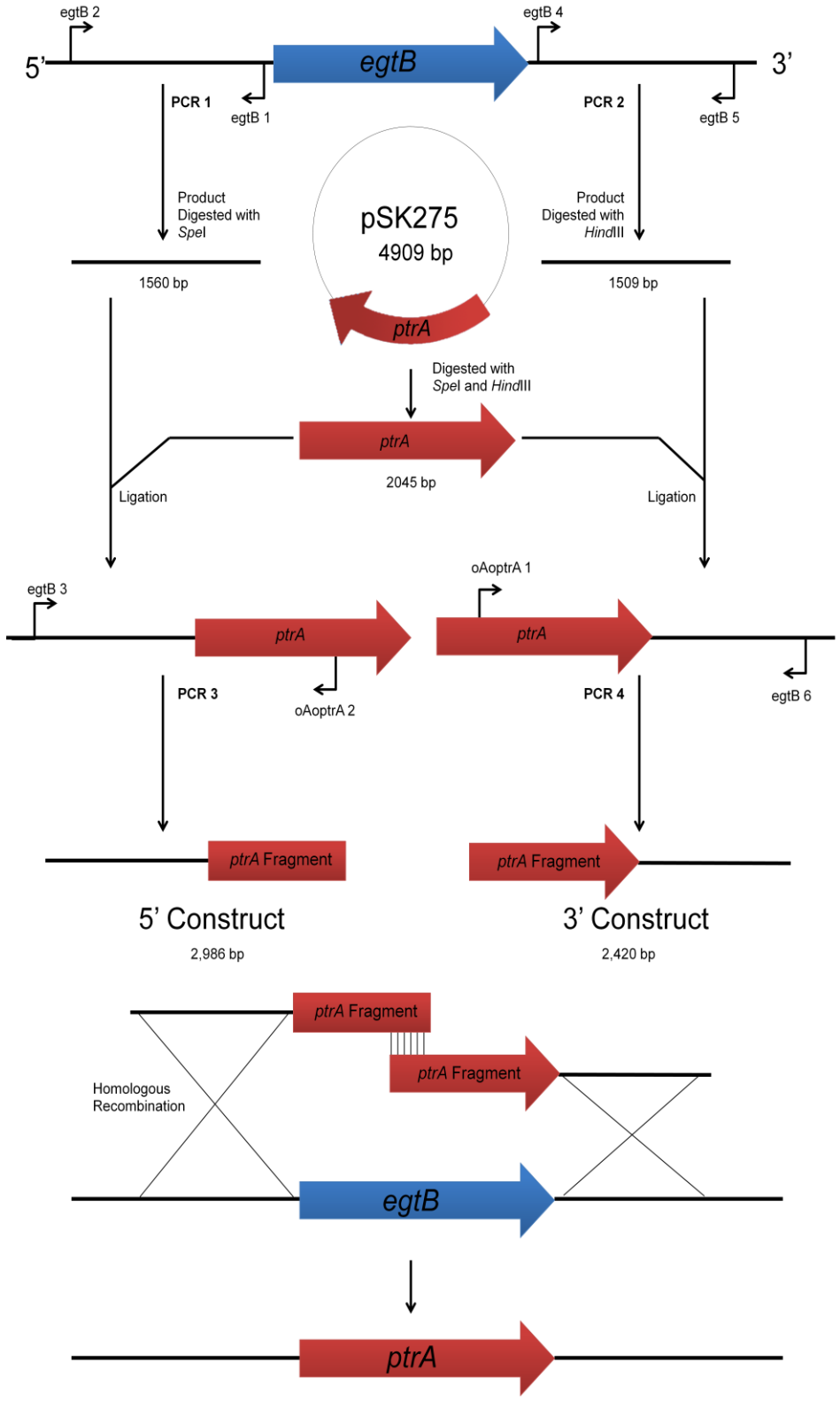

Figure 3.21. A schematic representation of the bipartite strategy for the deletion of *egtB* in *A. fumigatus* ATCC26933, using *ptrA* as a selection marker.

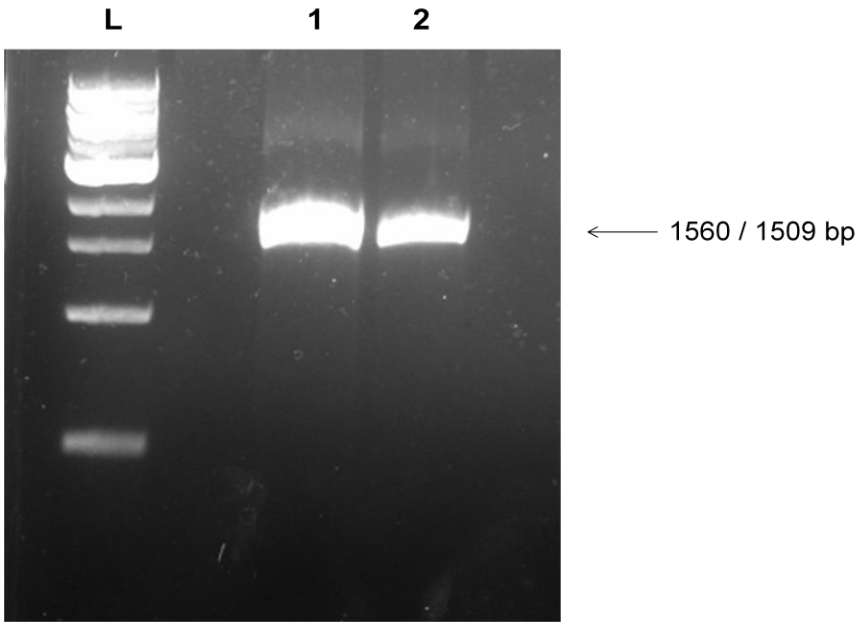

Figure 3.22. PCR products of the flanking regions of *egtB*. Lane L: NEB 1 kb DNA Ladder (Section 2.1.7.6). Lane 1: PCR 1 (1560 bp), the 5' flanking region of *egtB*. Lane 2: PCR 2 (1509 bp), the 3' flanking region of *egtB*.

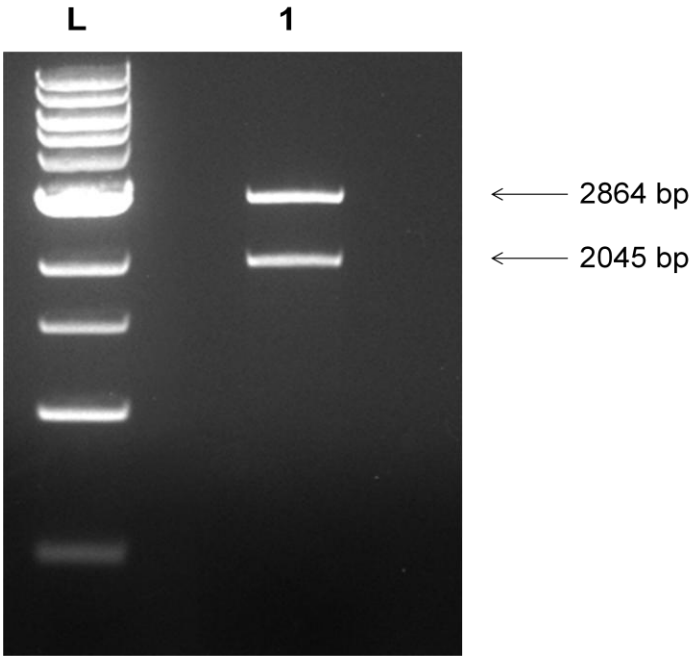

Figure 3.23. Restriction digest of the pSK275 plasmid with *Spe*I and *Hind*III to release *ptrA*. Lane L: NEB 1 kb DNA Ladder (Section 2.1.7.6). Lane 1: *pSK275* digested with *SpeI* and *HindIII* , releasing *ptrA* (2045 bp).

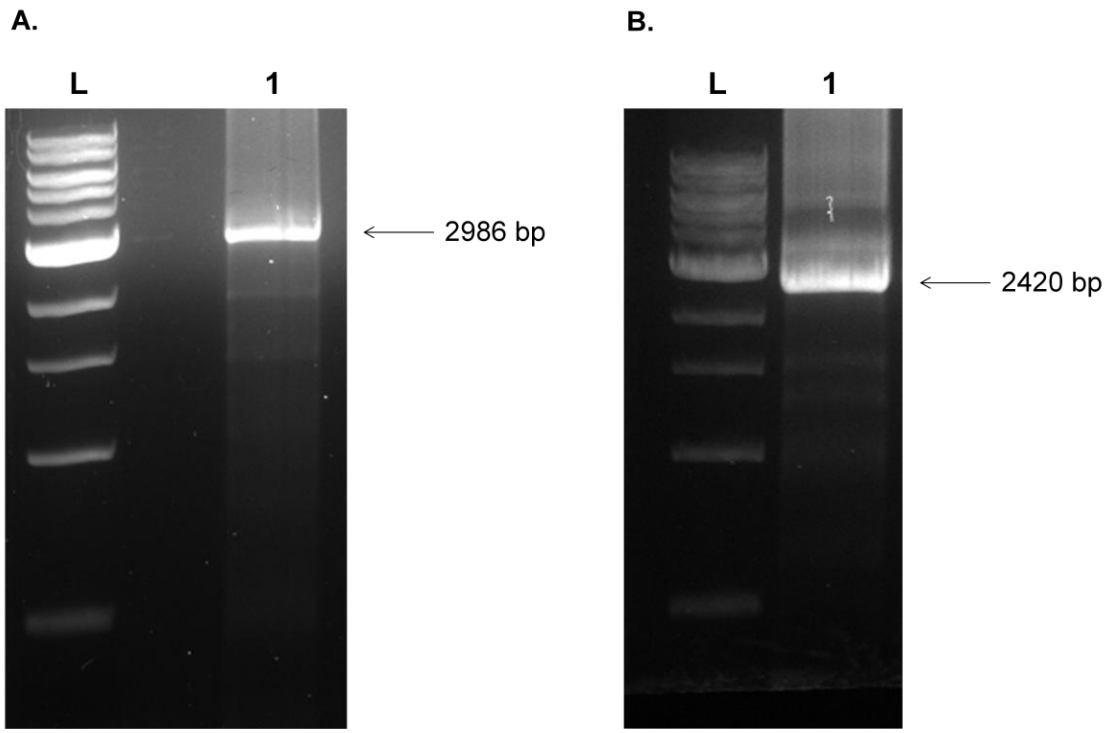

Figure 3.24. Final *egtB* gene deletion constructs. (A) Lane L: NEB 1 kb DNA Ladder (Section 2.1.7.6). Lane 1: PCR 3 (2986 bp), the 5' flanking region of *egtB* fused to a partial fragment of the *ptrA* selection marker. (B) Lane L: NEB 1 kb DNA Ladder (Section 2.1.7.6). Lane 1: PCR 4 (2420 bp), the 3' flanking region of *egtB* fused to a partial fragment of the *ptrA* selection marker.

3.2.3.2 Generation of 3' DIG-labelled probe by PCR for Δ*egtB* transformant identification

A single 3' downstream probe was prepared by PCR amplification for use in Southern blot analysis. The probe was generated using DIG-labelled nucleotides, which allowed for detection during Southern blot analysis (Section 2.2.5). A 3' probe was made using primers egtB4 and egtA6 which amplified a 1358 bp region just downstream of *egtB* (Figure 3.25).

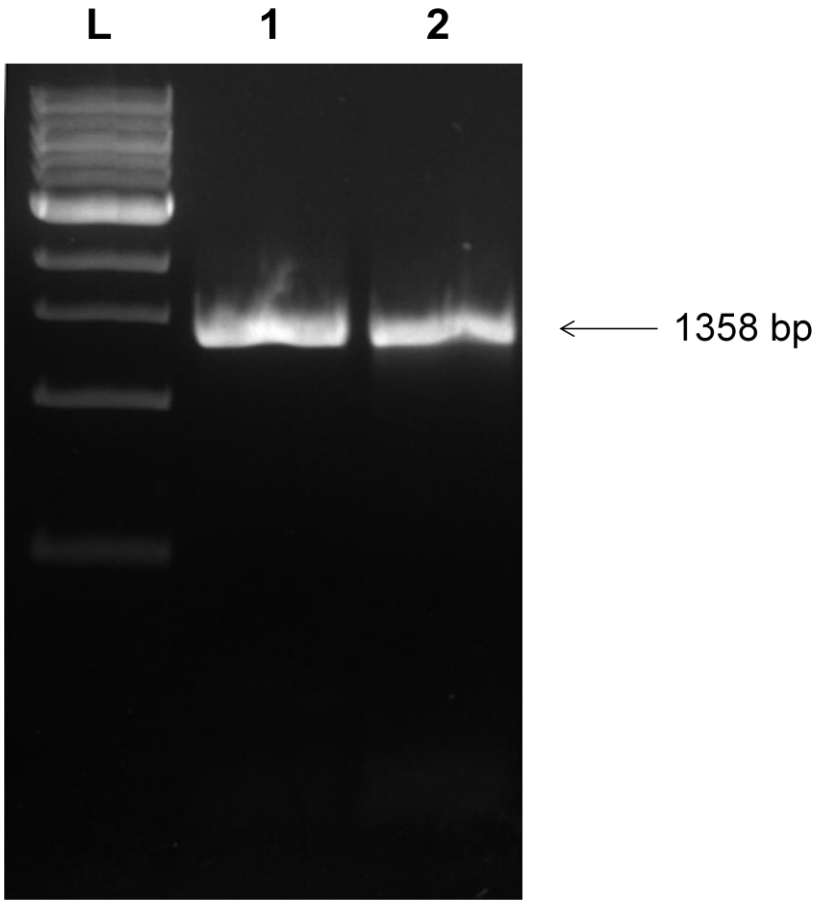

Figure 3.25. Generation of DIG-labelled nucleotide probe which facilitated Δ*egtB* detection with Southern blot analysis. Lane L: NEB 1 kb DNA Ladder (Section 2.1.7.6). Lane 1: *egtB* 3' DIG labelled nucleotide probe. Lane 2: positive control using standard dNTPs.

3.2.3.3 Deletion of *egtB* in *A. fumigatus* ATCC26933

The *egtB* deletion constructs from Section 3.2.3.1 were transformed into *A. fumigatus* ATCC26933 protoplasts, which were prepared as described in section 2.2.4.3. Approximately 3 μg total of 5' and 3' construct was used per transformation event. The transformation procedure was carried out as described in Section 2.2.4.4. Transformants were selected on agar plates containing pyrithiamine (100 ng/ml). Colonies with the ability to grow on these plates were predicted to have an intact *ptrA* gene incorporated into their genome, and thus considered potential Δ*egt*B transformants.

Following the transformation event, 11 colonies were observed on pyrithiamine selection plates. Genomic DNA from these colonies was digested using *pspOM*I. These were screened by Southern analysis (section 2.2.5) using a 3' probe (Section 3.2.3.3). The Southern strategy used to confirm *egtB* deletion is outlined in Figure 3.26. The mutant band (2288 bp) was present in transformants 3 and 11 (Figure 3.27), meaning these two transformants were potential Δ*egtB* mutants.

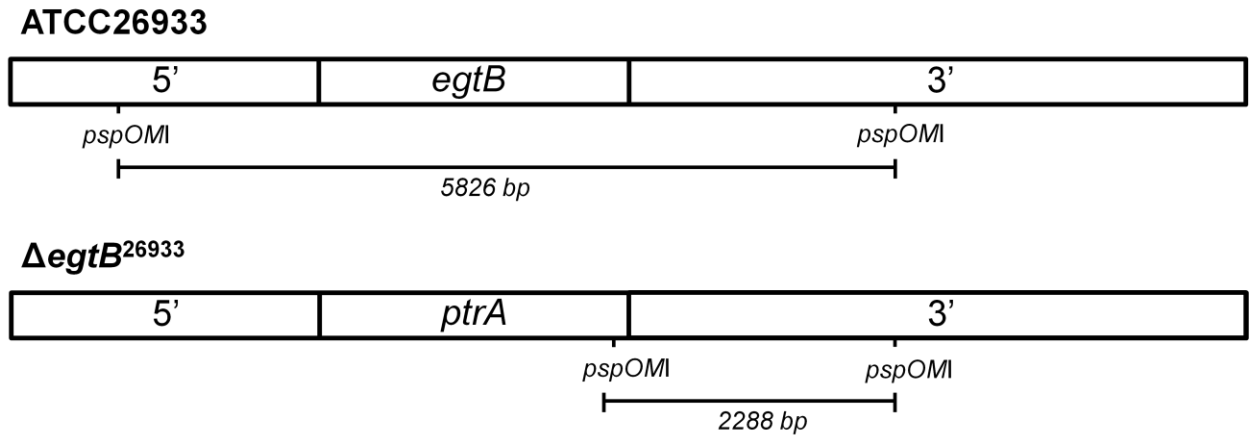

Figure 3.26. A schematic of the Southern blot strategy employed to detect the deletion of *egtB.* DNA was digested using *pspOM*I. The digested DNA was screened using a 3’ probe. A correct gene deletion event would result in a band of 2288 bp. Wild-type *pspOM*I digested DNA would result in a band of 5826 bp.

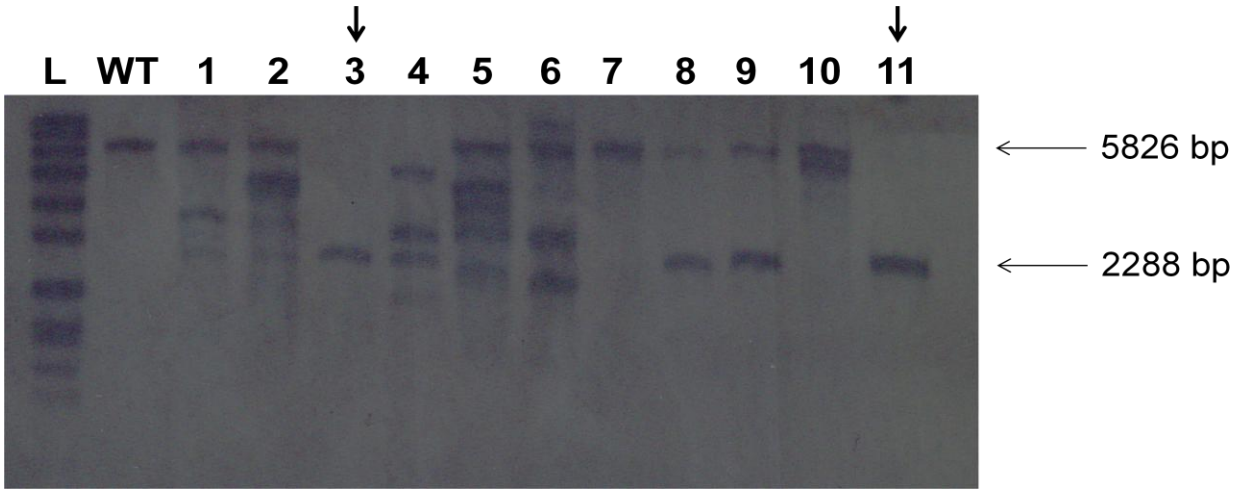

Figure 3.27. Southern Analysis of potential *egtB* deletion mutants in *A. fumigatus* strain ATCC26933 using a 3’ probe. Successful deletion of *egtB* was indicated by the presence of a single 2288 bp band. Lane L: Roche Molecular Weight Ladder VII, DIG labelled (Section 2.1.7.6). Lane WT: ATCC26933 (5826 bp). Lanes 1-11: Possible Δ*egtB* transformants. Transformants 3 and 11 display the correct band for the Δ*egtB* genotype.

3.2.3.4 Semi-quantitative RT-PCR Analysis of *egtB* expression in Δ*egtB* transformants

The deletion of *A. fumigatus egtB* from ATCC26933 was detected by Southern analysis in two transformants, 3 & 11. Semi-quantitative RT-PCR (section 2.2.6.5) was employed to confirm that the deletion of *egtB* resulted in the cessation of *egtB* expression in the two transformants. Both wild-type and mutant strains were cultured in Sabouraud Dextrose liquid broth and incubated at 37 °C for 24 h. Total RNA was extracted and subjected to cDNA synthesis (Section 2.2.6.3). RT-PCR was carried out using the primers QPCR egtB F and QPCR egtB R (Table 2.5). Expression of *egtB* was evident in *A. fumigatus* wild-type and *egtB* transformant 11 and absent from Δ*egtB* transformant 3 (Figure 3.28). This confirmed that *egtB* expression was abrogated by *egtB* deletion in transformant 3. Transformant 11 was discarded as it continued to express *egtB.*

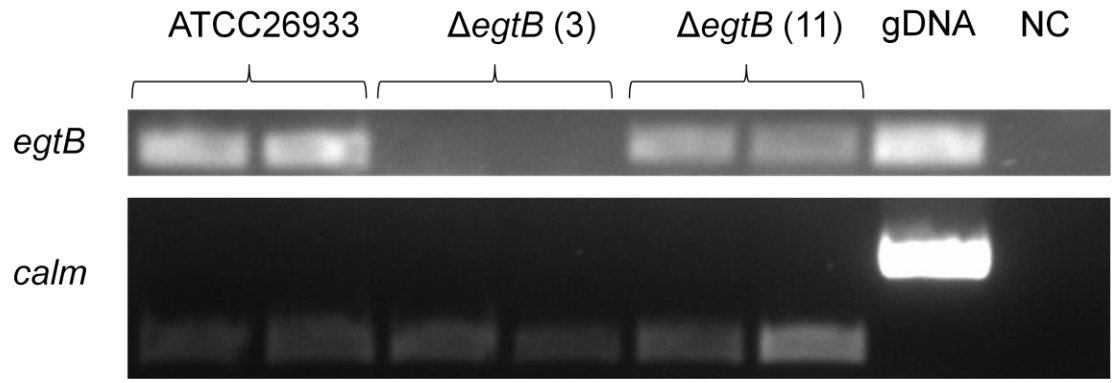

Figure 3.28. Confirmation of the absence of *egtB* expression in *A. fumigatus* Δ*egtB* transformant 3, but not transformant 11, by semi-quantitative RT-PCR (*n* = 2 biological replicates per condition). *calm* is used as cDNA control (Burns et al., 2005). gDNA was used as a positive control. NC: negative control; no cDNA or DNA present in amplification reactions.

3.2.4 Generation of a *vipC* deletion strain in *A. fumigatus* ATCC26933

3.2.4.1 Generation of deletion constructs for transformation of *vipC*

A gene deletion strategy was employed to investigate the function of *vipC* (AFUA_8G01930) (Figure 3.29). Protoplast transformations were performed using the background strain ATCC26933, as this allow for a comparison with Δ*egtA*^{26933} and Δ*egtB*^{26933}. Following the same strategy as the previous transformations, ATCC26933 was transformed with two DNA constructs which comprised of either the 5' or 3' flanking sequence of *vipC* fused to an incomplete fragment of the *ptrA* gene. The 5' construct consisted of 1301 bp of upstream flanking region fused to 1527 bp of *ptrA* fragment. The 3' construct consisted of 1031 bp of downstream flanking region fused to 1083 bp of *ptrA* fragment. The two constructs shared 561 bp of overlap within the *ptrA* gene, which would serve as a site for homologous recombination.

The two fragments were generated using two round of PCR. The 5' and 3' flanking regions of *vipC* were amplified from ATCC26933 genomic DNA. The 5' flanking region was amplified using the primers vipC1 and vipC2 (1617 bp), while the 3' flanking region was amplified using the primers vipC4 and vipC5 (1536 bp) (Figure 3.30). The flanking regions were excised using gel purification (section 2.2.3.8.3) and digested using *Spe*I (5' region) and *Hind*III (3' region). The *ptrA* selection marker was released from plasmid pSK275 by digestion with *Spe*I and *Hind*III (Figure 3.30), and ligated with the two digested flanking regions. The final deletion constructs were amplified from the ligation product using primers vipC3 and oAoptrA2 for the 5' construct (2828 bp) and primers vipC6 and oAoptrA1 for the 3' construct (2114 bp) (Figure 3.31). The products were gel purified (Section 2.2.3.8.3) to ensure no non-specific products were present.

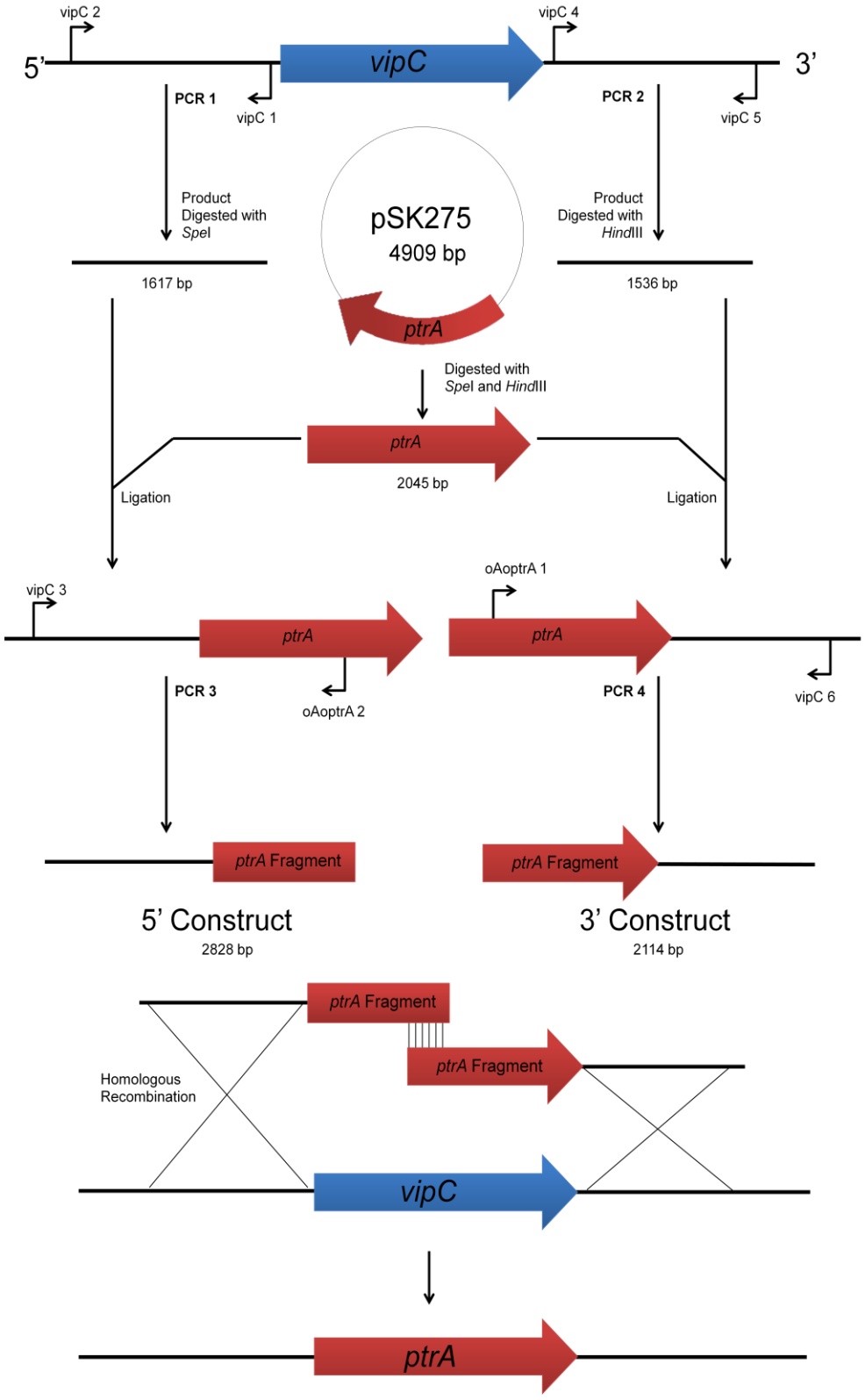

Figure 3.29. A schematic representation of the bipartite strategy for the deletion of *vipC* in *A. fumigatus* ATCC26933, using *ptrA* as a selection marker.

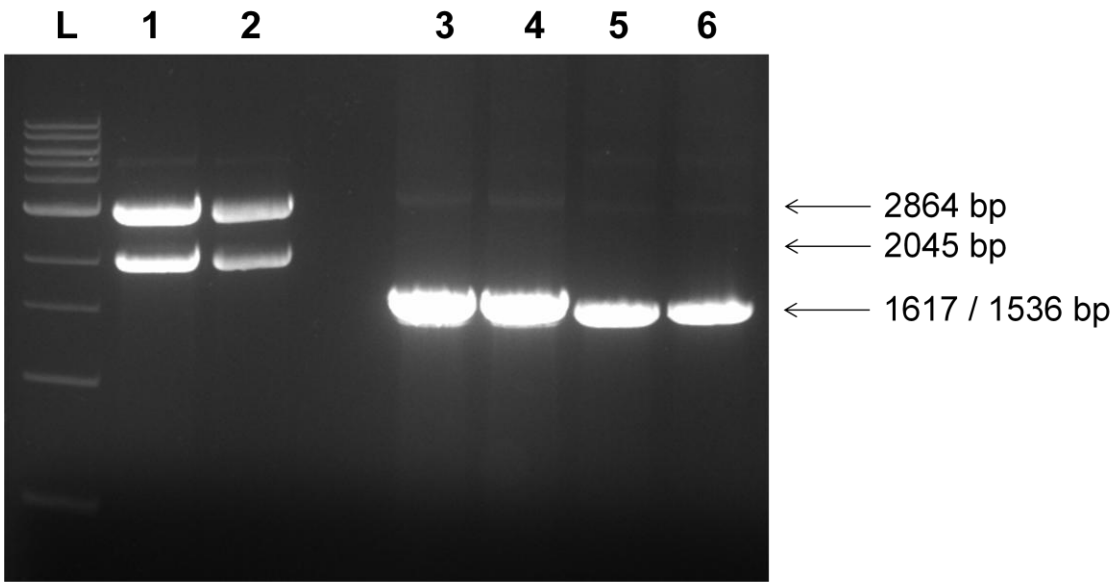

Figure 3.30. Restriction digest of the pSK275 plasmid with *Spe*I and *Hind*III to release the *ptrA* gene and PCR products of the flanking regions of *vipC*. Lane L: NEB 1 kb DNA Ladder (Section 2.1.7.6). Lanes 1 & 2: *pSK275* digested with *Spe*I and *Hind*III , releasing *ptrA* (2045 bp). Lanes 3 & 4: PCR 1 (1617 bp), the 5' flanking region of *vipC*. Lanes 5 & 6: PCR 2 (1536 bp), the 3' flanking region of *vipC*.

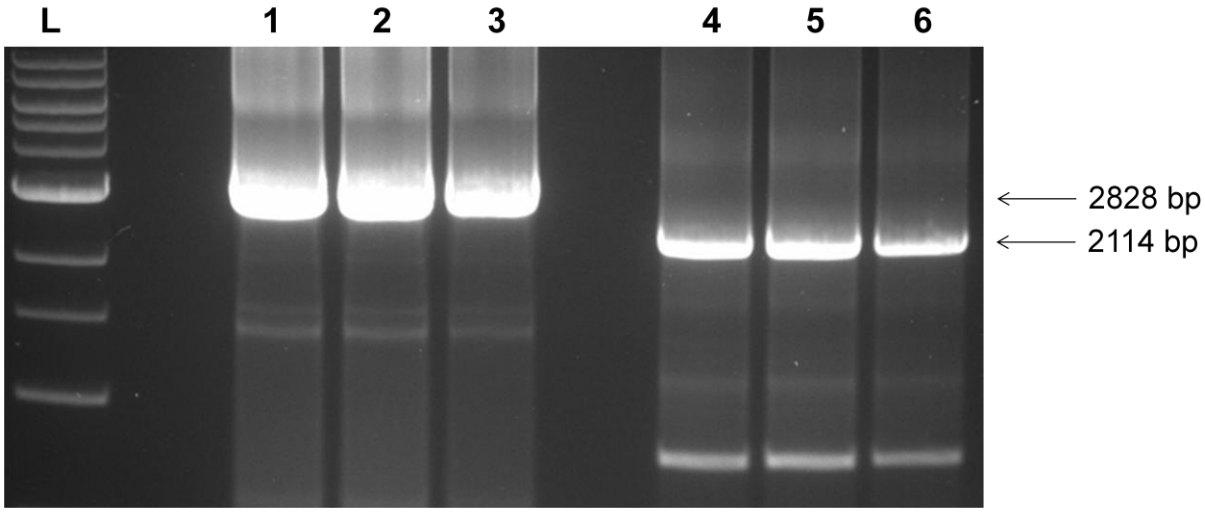

Figure 3.31. Final *vipC* gene deletion constructs. Lane L: NEB 1 kb DNA Ladder (Section 2.1.7.6). Lanes 1 - 3: PCR 3 (2828 bp), the 5' flanking region of *vipC* fused to a partial fragment of the *ptrA* selection marker. Lanes 4 - 6: PCR 4 (2114 bp), the 3' flanking region of *vipC* fused to a partial fragment of the *ptrA* selection marker.

3.2.4.2 Generation of 5' DIG-labelled probe by PCR for Δ*vipC* transformant identification

A single 3' downstream probe was prepared by PCR amplification for use in Southern blot analysis. The probe was generated using DIG-labelled nucleotides, which allowed for detection during Southern blot analysis (Section 2.2.5). A 3' probe was made using primers vipC1 and vipC3 which amplified a 1402 bp region just downstream of *egtB* (Figure 3.32).

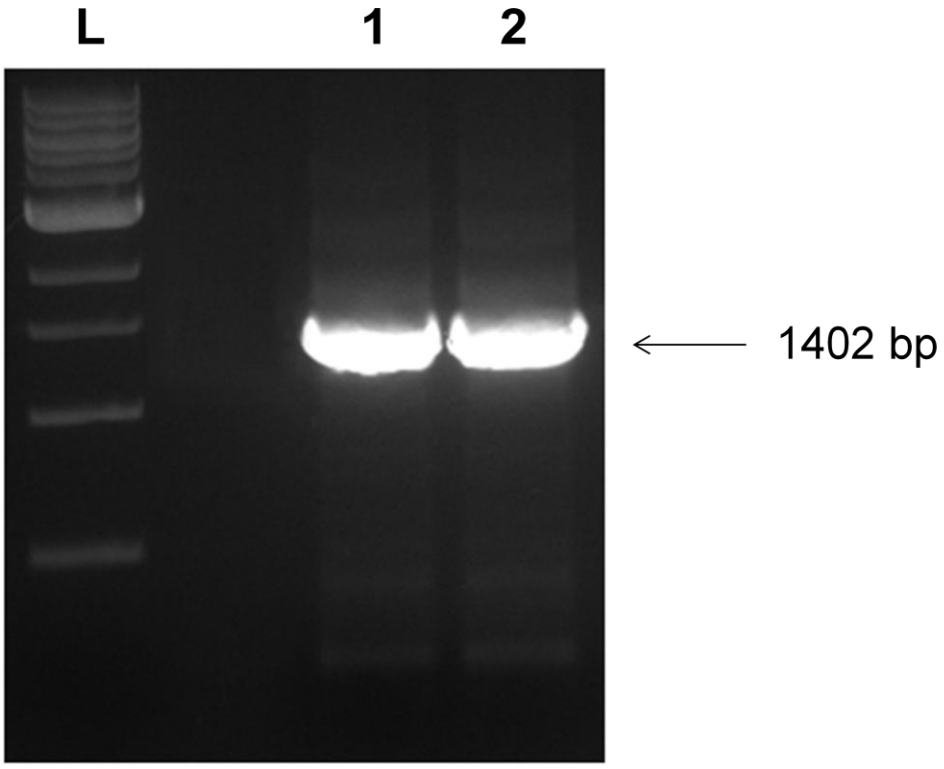

Figure 3.32. Generation of DIG-labelled nucleotide probe which facilitated Δ*vipC* detection with Southern blot analysis. Lane L: NEB 1 kb DNA Ladder (Section 2.1.7.6). Lane 1: *vipC* 5' DIG labelled nucleotide probe. Lane 2: positive control using standard dNTPs.

3.2.4.3 Deletion of *vipC* in *A. fumigatus* ATCC26933

The *vipC* deletion constructs from Section 3.2.4.1 were transformed into *A. fumigatus* ATCC26933 protoplasts, which were prepared as described in section 2.2.4.3. Approximately 3 µg total of 5' and 3' construct was used per transformation event. The transformation procedure was carried out as described in Section 2.2.4.4. Transformants were selected on agar plates containing pyrithiamine (100 ng/ml). Colonies with the ability to grow on these plates were predicted to have an intact *ptrA* gene incorporated into their genome, and thus considered potential Δ*vipC* transformants.

Following the transformation event, 29 colonies were observed on pyrithiamine selection plates. Genomic DNA from 10 of these colonies was digested using *EcoR*I. These were screened by Southern analysis (section 2.2.5) using a 5' probe (Section 3.2.4.2). The Southern strategy used to confirm *vipC* deletion is outlined in Figure 3.33. The mutant band (5880 bp) was present in transformant 9 (Figure 3.34), meaning this transformant is a potential Δ*vipC* mutant.

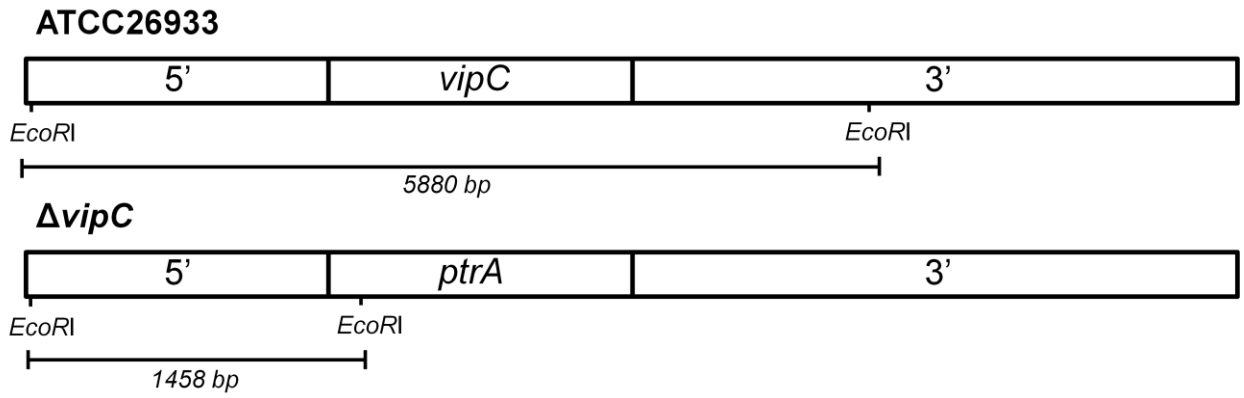

Figure 3.33. A schematic of the Southern blot strategy employed to detect the deletion of *vipC*. DNA was digested using *Eco*RI. The digested DNA was screened using a 5’ probe. A correct gene deletion event would result in a band of 1458 bp. Wild-type *EcoRI* digested DNA would result in a band of 5880 bp.

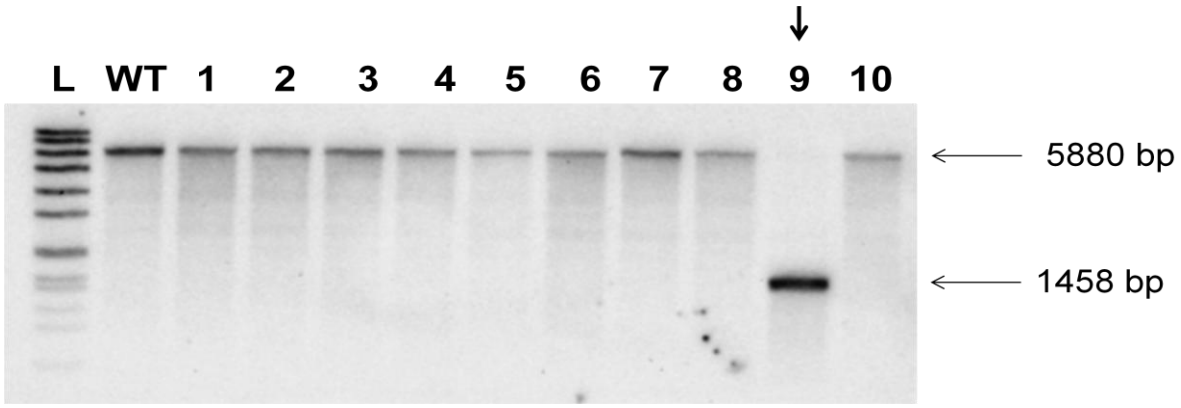

Figure 3.34. Southern Analysis of potential *vipC* deletion mutants in *A. fumigatus* strain ATCC26933 using a 5’ probe. Successful deletion of *vipC* was indicated by the presence of a single 1458 bp band. Lane L: Roche Molecular Weight Ladder VII, DIG labelled (Section 2.1.7.6). Lane WT: ATCC26933 (5880 bp). Lanes 1-10: Potential Δ*vipC* transformants. Transformant 9 displays the correct band for the *vipC* genotype.

3.2.4.4 Semi-quantitative RT-PCR Analysis of *vipC* expression in Δ*vipC*^{26933}

The deletion of *A. fumigatus vipC* from ATCC26933 was detected by Southern analysis in a single transformant. Semi-quantitative RT-PCR (section 2.2.6.4) was employed to confirm that the deletion of the *vipC* gene abrogated expression of *vipC.* Both wild-type and mutant strains were cultured in Sabouraud Dextrose liquid broth and incubated at 37 °C for 24 h. Total RNA was extracted and subjected to cDNA synthesis (Section 2.2.6.3). RT-PCR was carried out using the primers QPCR vipC F and QPCR vipC R (Table 2.5). Expression of *vipC* was present in *A. fumigatus* wild-type and absent from Δ*vipC* (Figure 3.35). This confirmed deletion of *vipC* in Δ*vipC*^{26933}.

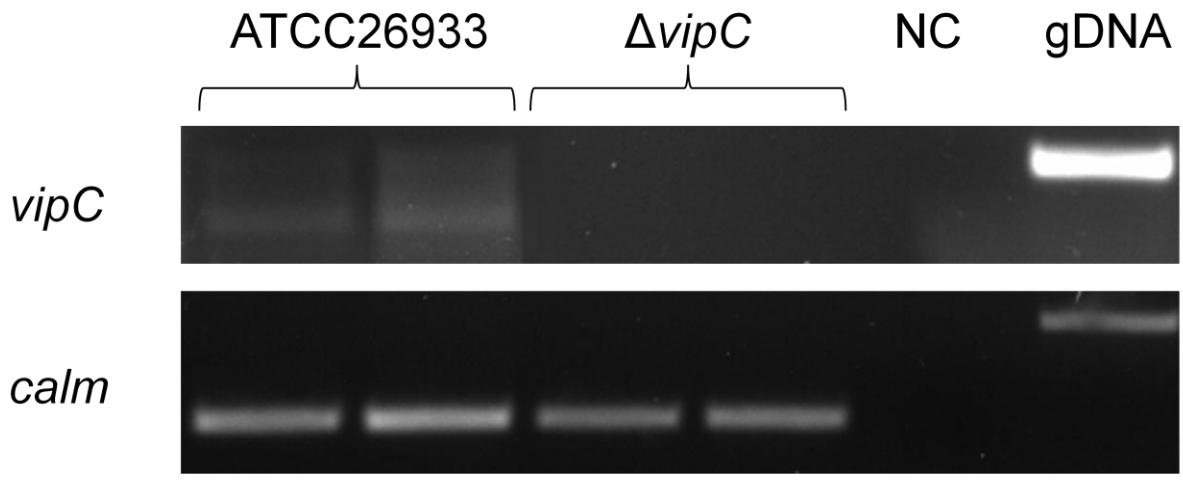

Figure 3.35. Confirmation of the absence of *vipC* expression in *A. fumigatus* Δ*vipC* by semi-quantitative RT-PCR (*n* = 2 biological replicates per condition). *calm* is used as cDNA control (Burns et al., 2005). gDNA was used as a positive control. NC: negative control; no cDNA or DNA present in amplification reactions.

3.2.5 Generation of a *palA* deletion strain in *A. fumigatus* ATCC26933

3.2.5.1 Generation of deletion constructs for transformation of *palA*

A gene deletion strategy was employed to investigate the function of *palA* (AFUA_2G09110) (Figure 3.36). Protoplast transformations were performed using the background strain ATCC26933, as this allow for a comparison with Δ*egtA*^{26933} and Δ*egtB*^{26933}. As before, ATCC26933 was transformed with two DNA constructs which comprised of either the 5' or 3' flanking sequence of *palA* fused to an incomplete fragment of the *ptrA* gene. The 5' construct consisted of 1292 bp of upstream flanking region fused to 1527 bp of *ptrA* fragment. The 3' construct consisted of 1098 bp of downstream flanking region fused to 1119 bp of *ptrA* fragment. The two constructs shared 561 bp of overlap within the *ptrA* gene, served as a site for homologous recombination.

The two fragments were generated using two round of PCR. The 5' and 3' flanking regions of *palA* were amplified from ATCC26933 genomic DNA. The 5' flanking region was amplified using the primers palA1 and palA2 (1489 bp), while the 3' flanking region was amplified using the primers palA4 and palA5 (1430 bp) (Figure 3.37). The flanking regions were excised using gel purification (section 2.2.3.8.3) and digested using *Spe*I (5' region) and *Kpn*I (3' region). The *ptrA* selection marker was released from plasmid pSK275 by digestion with *Spe*I and *Kpn*I (Figure 3.38), and ligated with the two digested flanking regions. The final deletion constructs were amplified from the ligation product using primers palA3 and oAoptrA2 for the 5' construct (2819 bp) and primers palA6 and oAoptrA1 for the 3' construct (2217 bp) (Figure 3.39). The products were gel purified (Section 2.2.3.8.3) to ensure no non-specific products were present.

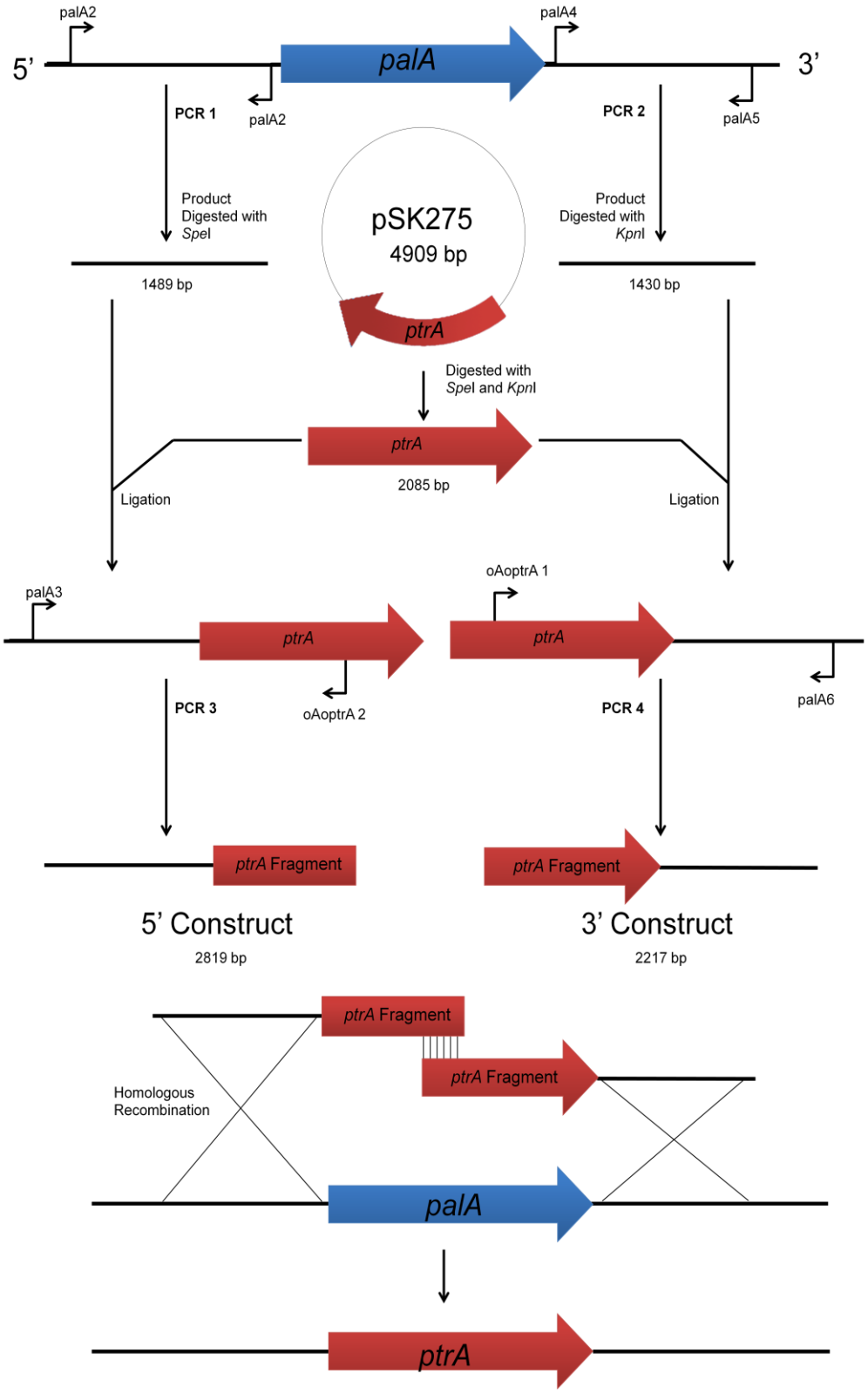

Figure 3.36. A schematic representation of the bipartite strategy for the deletion of *palA* in *A. fumigatus* ATCC26933, using *ptrA* as a selection marker.

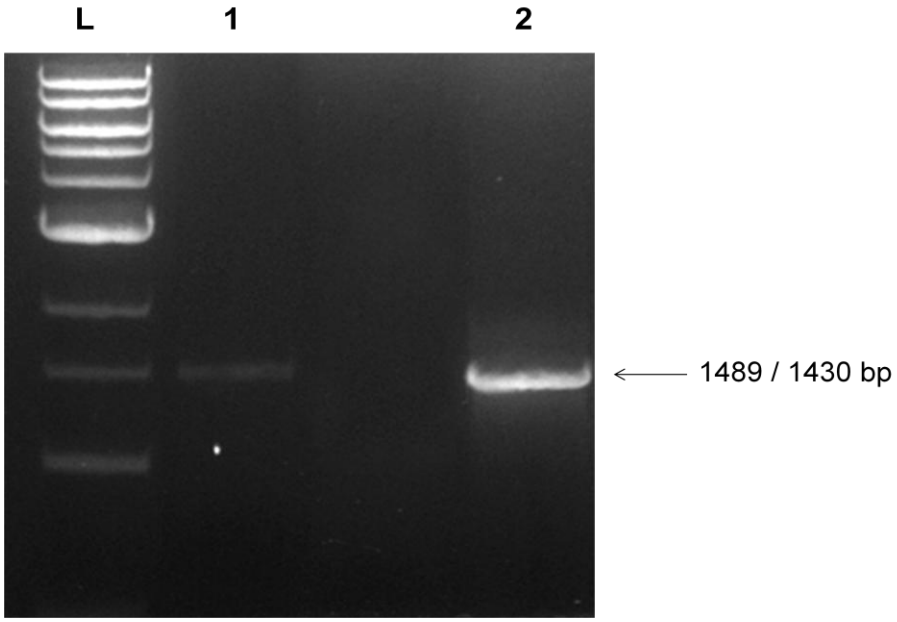

Figure 3.37. PCR products of the flanking regions of *palA.* Lane L: NEB 1 kb DNA Ladder (Section 2.1.7.6). Lane 1: PCR 1 (1489 bp), the 5' flanking region of *palA*. Lane 2: PCR 2 (1430 bp),the 3' flanking region of *palA.*

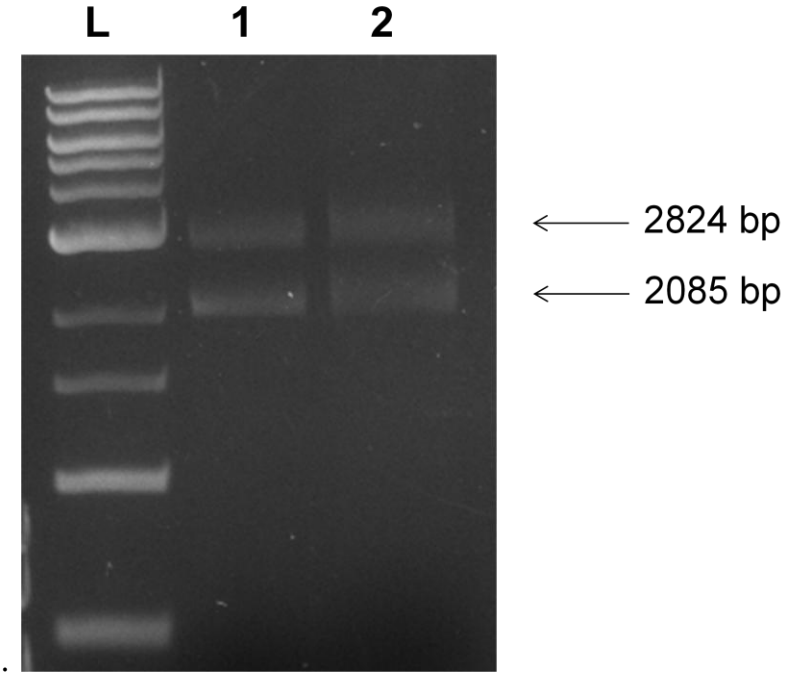

.

Figure 3.38. Restriction digest of the pSK275 plasmid with *Spe*I and *Kpn*I to release the *ptrA* gene. Lane L: NEB 1 kb DNA Ladder (Section 2.1.7.6). Lanes 1 & 2: pSK275 digested with *SpeI* and *HindIII* , releasing *ptrA* (2085 bp).

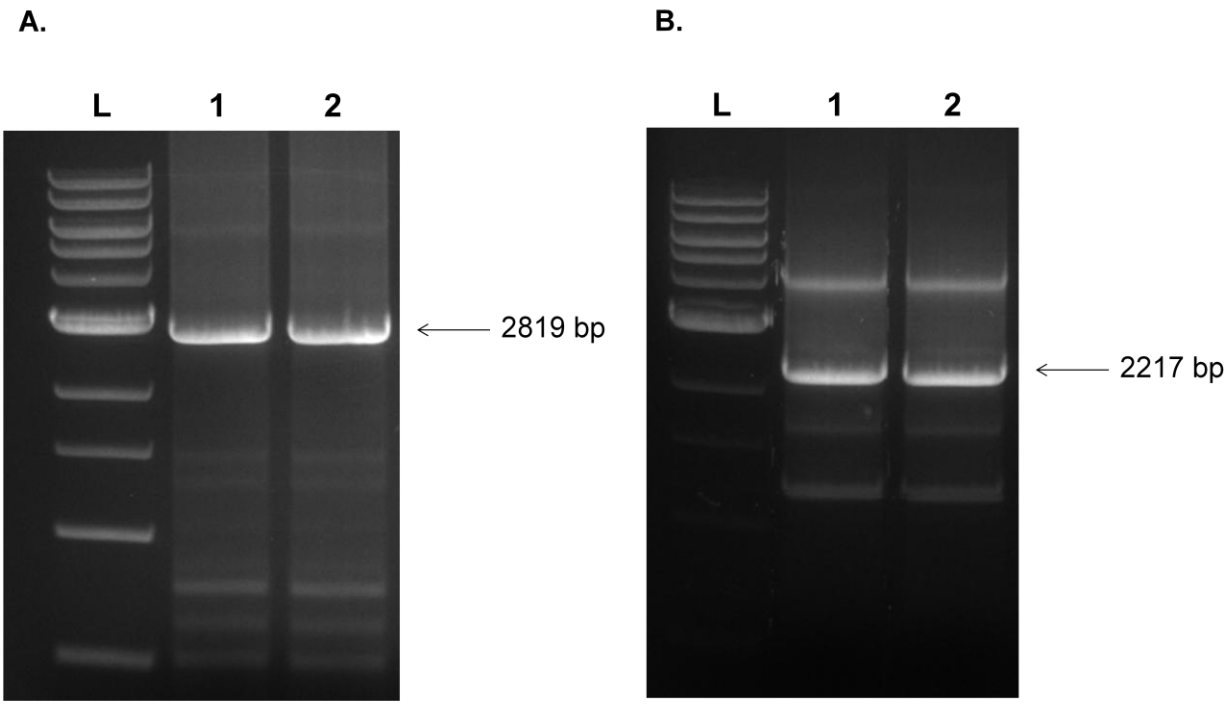

Figure 3.39. Final *palA* gene deletion constructs. (A) Lane L: NEB 1 kb DNA Ladder (Section 2.1.7.6). Lanes 1 & 2: PCR 3 (2819 bp), the 5' flanking region of *palA* fused to a partial fragment of the *ptrA* selection marker. (B) Lane L: NEB 1 kb DNA Ladder (Section 2.1.7.6). Lanes 1 & 2: PCR 4 (2217 bp), the 3' flanking region of *palA* fused to a partial fragment of the *ptrA* selection marker.

3.2.5.2 Generation of 3' DIG-labelled probe by PCR for Δ*palA* transformant identification

A single 3' downstream probe was prepared by PCR amplification for use in Southern blot analysis. The probe was generated using DIG-labelled nucleotides, which allowed for detection during Southern blot analysis (Section 2.2.5). A 3' probe was made using primers palA4 and palA6 which amplified a 1402 bp region just downstream of *palA* (Figure 3.40).

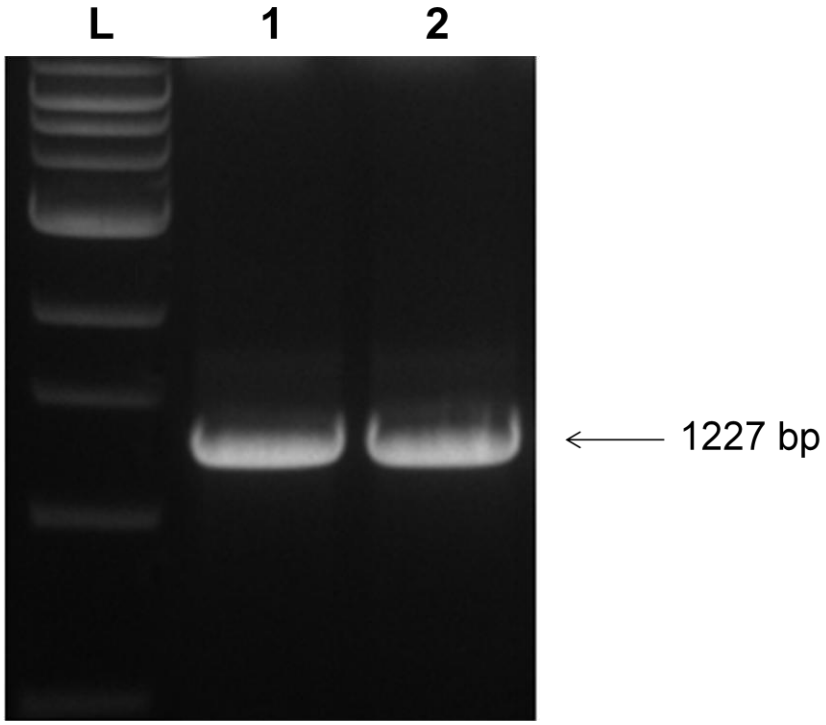

Figure 3.40. Generation of DIG-labelled nucleotide probe which facilitated Δ*palA* detection with Southern blot analysis. Lane L: NEB 1 kb DNA Ladder (Section 2.1.7.6). Lane 1: *palA* 3' DIG labelled nucleotide probe. Lane 2: positive control using standard dNTPs.

3.2.5.3 Deletion of *palA* in *A. fumigatus* ATCC26933

The *palA* deletion constructs from Section 3.2.5.1 were transformed into *A. fumigatus* ATCC26933 protoplasts, which were prepared as described in section 2.2.4.3. Approximately 3 µg total of 5' and 3' construct was used per transformation event. The transformation procedure was carried out as described in Section 2.2.4.4. Transformants were selected on agar plates containing pyrithiamine (100 ng/ml). Colonies with the ability to grow on these plates were predicted to have an intact *ptrA* gene incorporated into their genome, and thus considered potential Δ*palA* transformants.

Following the transformation event, 24 colonies were observed on pyrithiamine selection plates. Genomic DNA from 12 of these colonies was digested using *BamH*I. These were screened by Southern analysis (section 2.2.5) using a 3' probe (Section 3.2.5.2). The Southern strategy used to confirm *palA* deletion is outlined in Figure 3.41. The mutant band (5124 bp) was present in transformant 1 (Figure 3.42), meaning this transformant is a potential Δ*palA* mutant. However there was a faint wild-type band visible in transformant 1 so it was decided to create single spore isolates of the colony to ensure it was a clean deletion. DNA from five single spore isolates of transformant 1 were digested with *BamH*I and a second round of Southern blot analysis using the 3' probe was performed. Isolates 1, 3, 4 & 5 displayed the correct band for *palA* deletion, while transformant 2 contained the wild-type band and two etopic integrations (Figure 3.43). Isolate 5 was therefore chosen to create the stock of Δ*palA*.

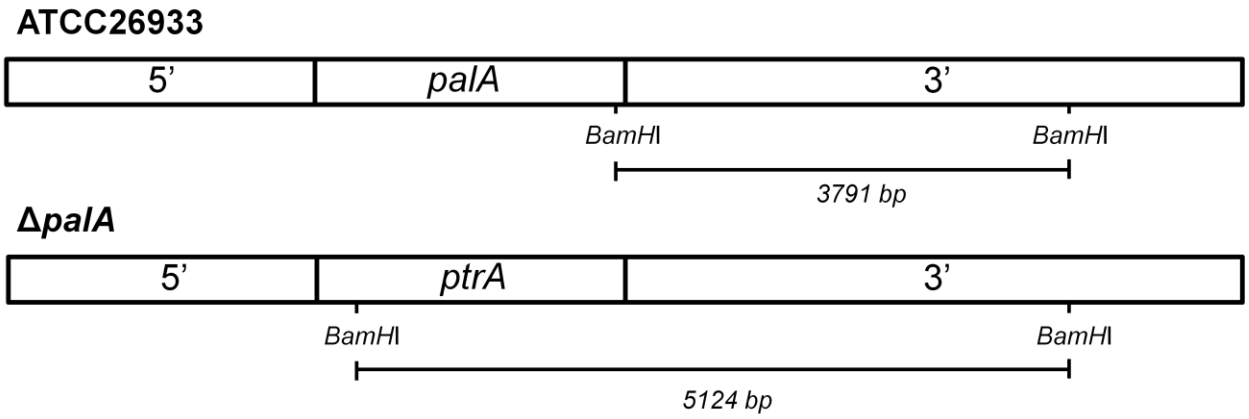

Figure 3.41. A schematic of the Southern blot strategy employed to detect the deletion of *palA*. DNA was digested using *BamH*I. The digested DNA was screened using a 3' probe. A correct gene deletion event would result in a band of 5124 bp. Wild-type *BamH*I digested DNA would result in a band of 3791 bp.

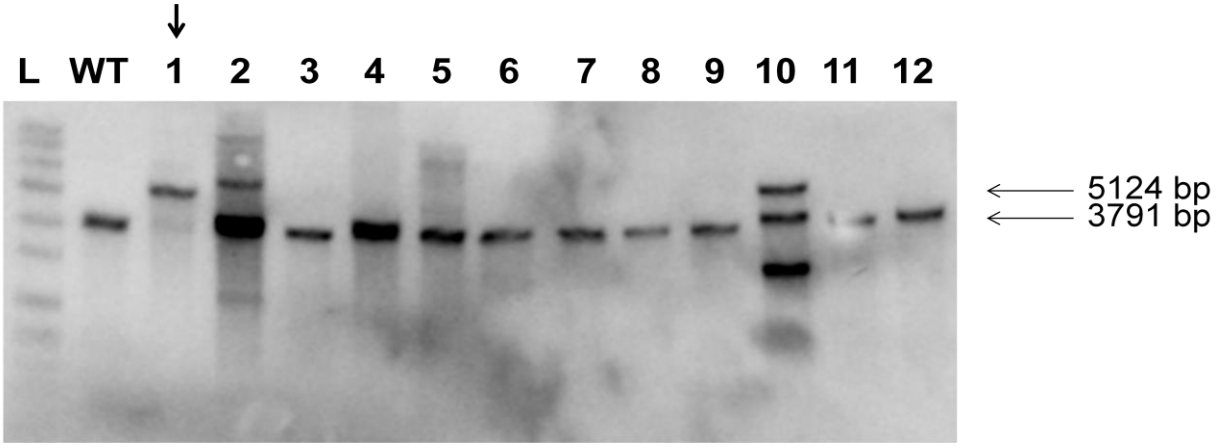

Figure 3.42. Southern Analysis of potential *palA* deletion mutants in *A. fumigatus* strain ATCC26933 using a 3' probe. Successful deletion of *palA* was indicated by the presence of a single 5124 bp band. Lane L: Roche Molecular Weight Ladder VII, DIG labelled (Section 2.1.7.6). Lane WT: ATCC26933 (5124 bp). Lanes 1-12: Potential Δ*palA* transformants. Transformant 1 displays the correct band for the Δ*palA* genotype.

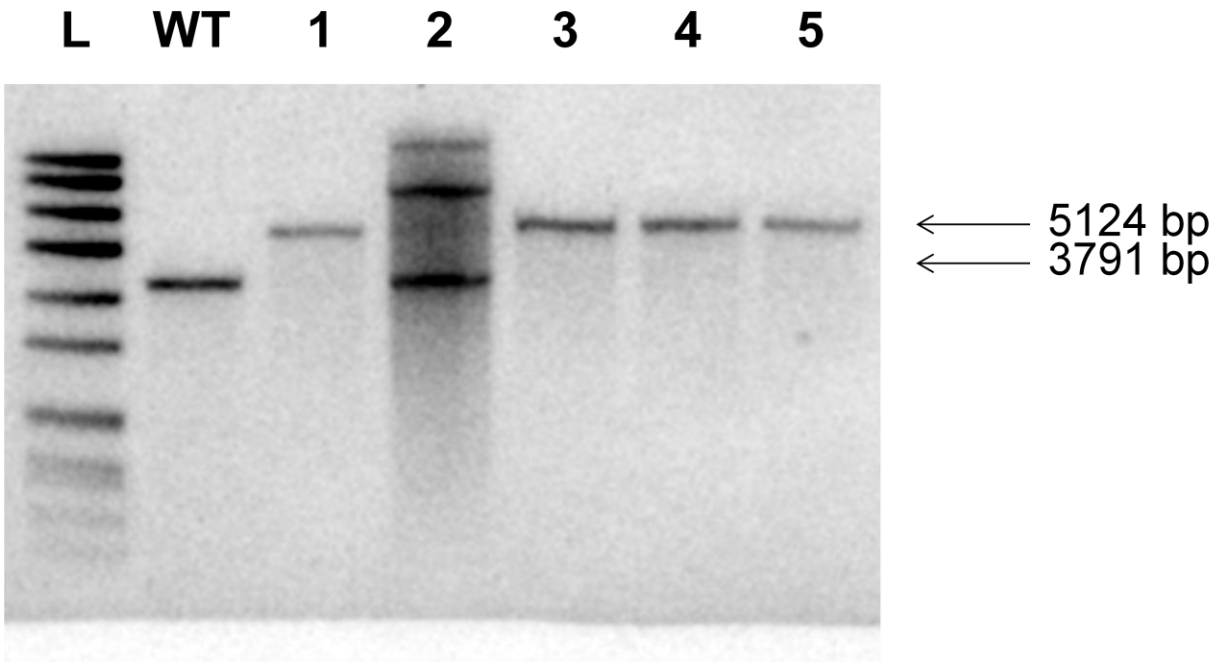

Figure 3.43. Southern Analysis of single spore isolates of a potential *palA* deletion mutant using a 3' probe. Successful deletion of *palA* was indicated by the presence of a single 5124 bp band. Lane L: Roche Molecular Weight Ladder VII, DIG labelled (Section 2.1.7.6), Lanes 1-5: Single spore isolates. Lane WT: ATCC26933 (3791 bp). Isolates 1, 3, 4 & 5 display the correct band for the Δ*palA* genotype.

3.2.5.4 Semi-quantitative RT-PCR Analysis of *palA* expression in Δ*palA*^{26933}

The deletion of *A. fumigatus palA* from ATCC26933 was detected by Southern analysis in a single transformant. Semi-quantitative RT-PCR (section 2.2.6.4) was employed to confirm that the deletion of the *palA* gene prevented expression of *palA.* Both wild-type and mutant strains were cultured in Sabouraud Dextrose liquid broth and incubated at 37 °C for 24 h. Total RNA was extracted and subjected to cDNA synthesis (Section 2.2.6.3). RT-PCR was carried out using the primers QPCR palA F and QPCR palA R (Table 2.5). Expression of *palA* was present in *A. fumigatus* wild-type and absent from Δ*palA* (Figure 3.44). This confirmed deletion of *palA* in Δ*palA*^{26933}.

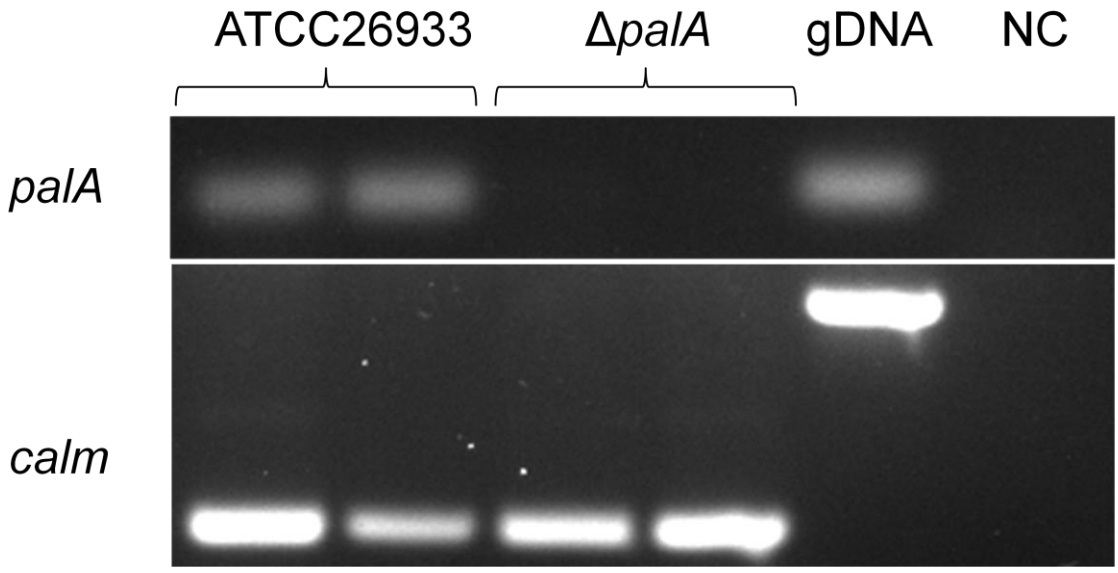

Figure 3.44. Confirmation of the absence of *palA* expression in *A. fumigatus* Δ*palA* by RT-PCR (*n* = 2 biological replicates per condition). *calm* is used as cDNA control (Burns et al., 2005). gDNA was used as a positive control. NC: negative control; no cDNA or DNA present in amplification reactions.

3.2.6 Attempted deletion of *nfs1* in ATCC26933

A gene deletion strategy was employed to investigate the function of *nfs1 (*AFUA_3G14240). Protoplast transformations were performed using the background strain ATCC26933, as this would allow for a comparison with Δ*egtB*^{26933}. As before, ATCC26933 was transformed with two DNA constructs which comprised of either the 5' or 3' flanking sequence of *nfs1* fused to an incomplete fragment of the *ptrA* gene.

nfs1 flanking regions were amplified using nfs1.1 and nfs1.2 (5' flanking) and nfs1.4 & nfs1.5 (3' flanking). These were digested with *Not*I and *Hind*III respectively and ligated to *ptrA*, which had been released from pSK275 using the same enzymes. The final constructs were generated by PCR; primers nfs1.3 and oAoptrA 2 used for the 5' construct and nfs1.6 and oAoptrA 1 used for the 3' construct.

The constructs were transformed into ATCC26933 as described (section 2.2.4.4). The transformation was attempted **six times**, varying the amount of total construct used from 2 – 5 µg, however no *nfs1* deletion mutant was generated. *nfs1* is essential in *Saccharomyces cerevisiae* (Li et al., 1999) and may be essential to *A. fumigatus* as well. This could explain why no deletion mutant was generated despite multiple attempts.

3.2.7 Attempted generation of a Δ*egtA*::Δ*gliK* double mutant

In order to investigate the apparent relationship between GliK activity and EGT biosynthesis (Gallagher et al., 2012) it was decided to generate a Δ*egtA::*Δ*gliK* double mutant. This was approached in two different ways: deleting *egtA* in a Δ*gliK* background, and deleting *gliK* in a Δ*egtA* background. In both cases the background strain already contained *ptrA* so it was necessary to use *hph*, the hygromycin resistance gene as a selection marker. In either strategy, the deletion constructs consisted of flanking regions of the target gene fused to overlapping fragments of the *hph* gene.

For deleting *egtA* in Δ*gliK*, the 5' flanking region was amplified using the primers egtA_HYG_1 and egtA1. The 3' flanking region was amplified using primers egtA_HYG_2 and egtA4. These were digested using *Sal*I and *BamH*I respectively. The constructs were then ligated to *hph*, which had been released from pAN7.1 using the same enzymes. The final constructs were generated by

PCR; primers egtA3 and HYoptrA1 used for the 5' construct and egtA6 and YGoptrA2 used for the 3' construct.

For deleting *gliK* in Δ*egtA*, the 5' flanking region was amplified using the primers gliK_HYG_1 and gliK_HYG_2. The 3' flanking region was amplified using primers gliK_HYG_4 and gliK_HYG_5. These were digested using *Sph*I and *BamH*I. The constructs were then ligated to *hph*, which had been released from pAN7.1 using the same enzymes. The final constructs were generated by PCR; primers gliK_HYG_3 and HYoptrA1 used for the 5' construct and gliK_HYG_6 and YGoptrA2 used for the 3' construct.

Transformation using either set of constructs was attempted **12 times** in total. Several supplements (Table 3.1) to aid protoplast regeneration were added to the regeneration media. Furthermore, the Δ*egtA*^{AfS77} mutant, with increased homologous recombination (Hartmann et al., 2010), was used as the background strain for *gliK* deletion. A summary of all transformation attempts can be seen in Table 3.1.

Despite these exhaustive efforts, no Δ*egtA::*Δ*gliK* double mutant was generated. This indicates that simultaneous absence of *egtA* and *gliK* may be fatal in *A. fumigatus*.

Table 3.1. Summary of all attempts at generating a Δ*egtA*Δ*gliK* mutant, including any supplements added to the media.

Transformation Attempts	**Target Gene**	**Background Strain**	**Supplement**
3	*egtA*	Δ*gliK*^{26933}	None
2	*gliK*	Δ*egtA*^{26933}	None
1	*gliK*	Δ*egtA*^{26933}	0.2 mM EGT
1	*gliK*	Δ*egtA*^{26933}	1 mM EGT
1	*gliK*	Δ*egtA*^{26933}	5 mM GSH
1	*gliK*	Δ*egtA*^{26933}	+ 50 % sucrose
1	*gliK*	Δ*egtA*^{26933}	- 50 % sucrose
2	*gliK*	Δ*egtA*^{AfS77}	None

3.3 Discussion

This chapter describes the work done to identify and delete the putative EGT biosynthetic genes in *A. fumigatus* ATCC26933: *egtA* and *egtB.* The generation of *vipC* and *palA* deletion mutants in ATCC26933 was also undertaken. Additionally the re-insertion of the *egtA* gene into Δ*egtA*^{26933} was presented. Absence of gene expression was confirmed via RT-PCR of all four gene deletion mutants, while restoration of *egtA* expression in *egtA*^{C26933} was also demonstrated. Furthermore, the attempted deletion of *nfs1* in ATCC26933 and generation of a Δ*egtA::*Δ*gliK* double mutant are also described.

EGT biosynthetic genes were identified via bioinformatic analysis. *A. fumigatus egtA* was identified through BLAST searches of *N. crassa egt-1, S. pombe egt1* and *M. smegmatis egtD* and *egtB*. *egtA* encodes for a proteins with 844 amino acids and contains a methyltransferase domain, a sulphatase-modifying factor domain and a 5'-histidylcysteine sulphoxide synthase domain. *A. fumigatus egtB* was identified through BLAST searches of *S. pombe egt2* and *M. smegmatis egtE*. *egtB* encodes for a protein 453 amino acids in length and contains cysteine desulphurase and PLP-binding domains. Additionally, Nfs1 was identified as an alternative candidate for performing the cysteine desuphurase step in EGT biosynthesis.

A bipartite method (Nielsen et al., 2006) was employed to delete the genes described. All genes were targeted using two constructs. These constructs consisted of ~1 – 1.5 kb of flanking region fused to a fraction of the *ptrA* gene. The constructs were then transformed into protoplasts of ATCC26933. Selection of potential transformants took place on pyrithiamine plates, with an intact *ptrA* cassette necessary for growth.

Deletion constructs for Δ*egtA*^{26933} were generated directly from Δ*egtA*^{AfS77}. It was decided to delete *egtA* in ATCC26933 due to the high amounts of gliotoxin it produces compared to AfS77. Gallagher et al. (2012) demonstrated that EGT levels increase significantly when *gliK* is deleted. Δ*gliK* is gliotoxin deficient and the subsequent rise in EGT provoked a question about the relationship between the two metabolites. Thus deletion of *egtA* in a high gliotoxin producing strain was deemed the optimal strategy for investigating this phenomenon. Additionally, this provided the opportunity to compare *egtA* deletion in strains producing different levels of gliotoxin.

The Δ*egtA* transformation produced 23 colonies. A screen of 10 colonies by Southern blot revealed one transformant which displayed the mutant band only (2045 bp). However, as the blot lacked clarity, it was decided to subject the colony to single spore isolation and a second round of Southern analysis to ensure a clean deletion had taken place. Southern analysis of 8 single spore isolates revealed all eight isolates displayed a single mutant band, and thus the transformation as considered a success.

The construct for complementation of Δ*egtA* was generated by cloning of the *egtA* gene and flanking regions into a pCR®2.1-TOPO vector, to create pegtA. Linearisation of this vector in the 5' flanking region allowed for the homologous recombination of the 5' flanking region and insertion of the *egtA* gene upstream of the original locus. The *hph* gene for hygromycin resistance was used as a selection marker for this transformation, with the pAN7.1 vector co-transformed alongside the complementation constructs. Optimally, the *hph* gene would have been included in the complementation vector so it could be transformed as a single construct. However, insertion of the *hph* gene into the *pegtA* vector would have rendered linearization within one of the *egtA* flanking regions impossible due to the limited number of unique restriction sites. Thus, it was necessary to transform *pegtA* and *pAN7.1* independently. This resulted in a large amount of false positives (86 colonies observed on the hygromycin plates following the transformation) because pAN.7.1 could be integrated into a target protoplast independent of the complementation construct. One transformant was observed that displayed the correct banding pattern for $egtA^{C}$ when analysed by Southern blot.

Semi-quantitative RT-PCR was employed to analyse gene expression following the deletion and complementation of *egtA*. Gene expression was absent in $\Delta egtA^{26933}$ and re-instated in $egtA^{C26933}$. This confirmed that the deletion of *egtA* in ATCC26933 and its complementation in $\Delta egtA^{26933}$.

Deletion constructs for *egtB, vipC* and *palA* were generated by the amplification of the respective gene's flanking regions from ATCC26933 genomic DNA. These flanking regions were digested via restriction endonucleases and ligated to *ptrA* which had been released from pSK275. A final round of PCR generated the final constructs, which consisted of a flanking region fused to a fragment of the *ptrA* gene. The transformation for the deletion of *egtB* produced 11 colonies, which were screened via Southern blotting and revealed 2 transformants with the correct Δ*egtB* band (2288 bp). The transformation for the deletion of *vipC* produced 29 colonies. Screening 10

of these revealed a single transformant which displayed the correct band for Δ*vipC* (1458 bp). The transformation for the deletion of *palA* produced 24 colonies. Screening 12 of these revealed a single transformant which displayed the correct band for Δ*palA* (5124 bp). However, there was a slight wild-type band (3791 bp) visible on the blot so it was decided to carry out single spore isolation of the transformant to ensure a clean deletion of *palA* was present. 5 single spore isolates were analysed, with 4 of them showing the correct banding pattern for *palA* deletion. Isolate 2 however displayed the wild-type band in addition to two etopic integrations. This genotype likely contributed to the faint wild-type band in the original colony and single spore isolation was necessary to obtain a clean Δ*palA* mutant. Due to time constraints, complementation of these genes was not carried out.

Semi-quantitative RT-PCR was employed to analyse gene expression of potential Δ*egtB*, Δ*vipC* and Δ*palA* mutants. Two potential Δ*egtB* mutants had been identified, so semi-quantitative RT-PCR analysis was carried out on both. This revealed that while no *egtB* expression was present in transformant 3, transformant 11 continued to express *egtB*. Therefore transformant 3 was considered a successful *egtB* deletion and transformant 11 was discarded. Semi-quantitative RT-PCR demonstrated the absence of expression of *vipC* and *palA* in Δ*vipC*^{26933} and Δ*palA*^{26933}, respectively.

In addition to the four genes successfully deleted, two deletion mutants were attempted which were unsuccessful: the deletion of *nfs1* in ATCC26933 and the generation of a Δ*egtA*Δ*gliK* double mutant. *nfs1* was targeted as it was identified as a potential enzyme for the cysteine desulfurase step in EGT biosynthesis. This transformation was attempted six times, with no transformants displaying the correct band for *nfs1* deletion from any of the attempts. While *nfs1* has been successfully deleted in *S. pombe* (Pluskal et al., 2014), it is an essential gene in *S. cerevisiae* (Li et al., 1999). It is therefore possible that *nfs1* is also essential in *A. fumigatus* and any deletion of *nfs1* would be lethal.

Double deletion of *egtA* and *gliK* was proposed and attempted due to the increased levels of EGT observed in the gliotoxin null mutant Δ*gliK* (Gallagher et al., 2012). A double mutant would have aided in elucidating the mechanism behind this increase in EGT and help with analysing any relationship between gliotoxin and EGT. Availability of this mutant was sought in two different ways, deletion of *egtA* in Δ*gliK* and deletion of *gliK* in Δ*egtA*. In addition to this,

several supplements and alterations to the regeneration media were made in an attempt to recover transformed protoplasts (Table 3.1). EGT (0.2 mM and 1mM) and GSH (5 mM) were added to the media in case the loss of EGT was leading to a lethal rise in ROS or depletion of antioxidants. Sucrose levels were altered ± 50% in case osmotic stress. Furthermore, the deletion of *gliK* was attempted in the Δ*egtA*^{AfS77} background. AfS77 contains a deletion of the *akuA* gene, which encodes for the Ku70 component of the non-homologous end joining pathway. Absence of Ku70 results in an increased frequency of homologous recombination, which aids gene deletion (Krappmann et al., 2006, Hartmann et al., 2010).

Overall and disappointingly, generation of a Δ*egtA*::ΔgliK double mutant was attempted 12 times with no success. The observed rise of EGT in Δ*gliK* (Gallagher et al., 2012) suggests that the antioxidant plays an important role in the absence of *gliK*; indeed Δ*gliK* shows sensitivity to H_2O_2 compared to wild-type, suggesting a disruption of redox homeostasis (Gallagher et al., 2012; Sheridan et al., 2015). This data suggests that EGT may well be essential in Δ*gliK*.

All new strains generated were used to explore the mechanism and functionality of EGT biosynthesis in *A. fumigatus*; as outlined in subsequent chapters.

Chapter 4

Characterisation of Ergothioneine

Biosynthesis and Functionality in *A. fumigatus*

4.1 Introduction

The availability of an *A. fumigatus egtA* deletion strain as detailed in Chapter 3 presented the opportunity to perform phenotypic analysis in order to elucidate gene function, which will aid in determining if *egtA* contributes to EGT biosynthesis in *A. fumigatus*. This would also allow for the first functional characterisation of EGT in *A. fumigatus*, an opportunistic human pathogen.

Functional characterisation of EGT in fungi is lacking, with the work of Bello et al. (2012, 2014) providing the only significant data. Bello et al. demonstrated that EGT protects *N. crassa* conidia against *tert*-butyl hydroperoxide and contributes to conidial health and conidiogenesis. No role for EGT in *S. pombe* was demonstrated, despite the generation of an *egt1* deletion mutant (Pluskal et al., 2014). The augmented EGT levels in *A. fumigatus* Δ*gliK* observed by Gallagher et al. (2012) offered insight into potential EGT function in *A. fumigatus*. Δ*gliK* exhibited a variety of phenotypes in addition to increased EGT levels, including abrogated gliotoxin, production, sensitivity to exogenous gliotoxin, sensitivity to H_2O_2 and perturbed levels of SAM and SAH (Gallagher et al., 2012; Owens et al., 2015). The putative role for EGT as an antioxidant may be related to H_2O_2 sensitivity in Δ*gliK* and as a sulphurised and trimethylated metabolite, EGT biosynthesis may be linked with both gliotoxin biosynthesis and SAM/SAH metabolism, both of which are disrupted in Δ*gliK*. Further characterisation of EGT is therefore needed to elucidate the metabolic and redox alterations taking place in Δ*gliK*.

The work by Gallagher et al. (2012) also presented a novel strategy for detecting EGT via alkylation with 5'-iodoacetamidofluorescein (5'-IAF) in combination with either RP-HPLC or LC-MS/MS. 5'-IAF reacts with thiol groups to form a stable thioester bond at physiological pH. Alkylation with 5'-IAF decreases the polarity of EGT, resulting in increased retention time in RP-HPLC and LC-MS/MS. This leads to improved separation during chromatography, aiding identification. Additionally, 5'-IAF can be detected via fluorescence detector (Ex/Em: 494/518 nm), increasing the confidence of identification via RP-HPLC. 5'-IAF can also be used in the detection of GSH in the same manner (Gallagher et al., 2012). This method has been subsequently and independently utilised for the identification of EGT in human serum (Sotgia et al., 2013, 2014).

Oxidative stress occurs as a result of elevated levels of reactive oxygen species (ROS). ROS are produced via various metabolic pathways, particularly aerobic respiration (Takemoto et al., 2007; Starkov, 2008) and comprise of superoxide ($^{\bullet}O_2^-$), the hydroxyl radical ($^{\bullet}OH$) and hydrogen peroxide (H_2O_2) (Turrens et al., 2003). Excess ROS can lead to modification of cellular components, which can interfere with both metabolism and regulatory pathways. Therefore, management of ROS is an essential part of cellular homeostasis (Lushchak, 2011). Excess ROS is managed by various enzymes, such as superoxide dismutase, peroxidases and catalases. Additionally, low molecular mass molecules such as glutathione (GSH) also contribute to oxidative stress defence (Halliwell and Gutteridge, 2007). The ratio of reduced (GSH) to oxidised (GSSG) glutathione is carefully maintained and changes to the GSH/GSSG ratio is indicative of a change in the redox state of the cell. GSH/GSSG ratio can be measured through the reduction of DTNB, utilising glutathione reductase, as described in Section 2.2.13 (Thon et al., 2010; Rahman et al., 2006). EGT has been characterised as an antioxidant in *N. crassa* and several bacterial species (Bello et al., 2012, 2014; Sao Emani et al., 2013; Saini et al., 2015) and thus may contribute to oxidative stress defence in *A. fumigatus*.

Oxidative stress sensitivity is commonly investigated through the use of reagents that induce elevated levels of ROS. H_2O_2, menadione and diamide were employed for this purpose in this study. H_2O_2 acts to induce ROS in organisms by increasing the intracellular peroxide and superoxide levels, and leads to the formation of $^{\bullet}OH$ radicals (Lessing et al., 2007). As a result, oxidation products such as sulfinic-acid, sulfenic-acid, sulfonic-acid and methionine sulfoxide are formed (Thon et al., 2010). Menadione is an organic molecule which can induce the formation of superoxides, H_2O_2 and $^{\bullet}OH$ radicals. It has also been observed that menadione can chemically modify cell components via arylation and enhance membrane fluidity (Pusztahelyi et al., 2010). Diamide induces oxidative stress in a different manner to H_2O_2 and menadione. Instead of inducing the formation of radicals, diamide oxidizes the GSH thiol to form disulphide groups. Without a free thiol group, GSH cannot scavenge free radicals and as such cannot contribute to oxidative stress defence (López-Mirabal and Winther, 2008). By depleting GSH levels in such a way, diamide induces oxidative stress.

In conjunction with the above reagents, ROS levels in *A. fumigatus* were investigated by fluorescent microscopy using 2',7'-dichlorodihydrofluorescein diacetate (H_2DCFDA; Figure 4.1),

a reduced form of fluorescein. H_2DCFDA is a cell permeable indicator of ROS. Fluorescence of this probe is activated upon oxidative cleavage of the acetate group, converting H_2DCFDA into 2',7'-dichlorofluorescein. 2',7'-dichlorofluorescein is then detectable via fluorescence (Ex/Em: 492–495/517–527 nm), which can be measured to give an indication of ROS levels in mycelia. This method has been previously employed in *A. fumigatus* to investigate gliotoxin and H_2O_2 interaction (Owens et al., 2014).

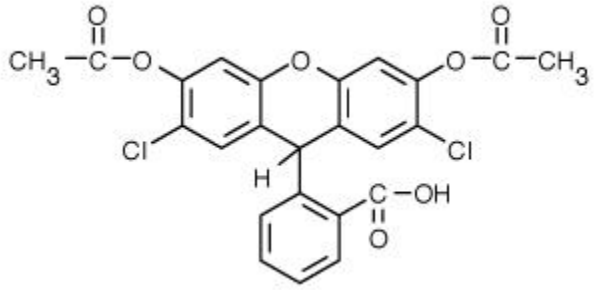

Figure 4.1. Structure of 2',7'-dichlorodihydrofluorescein diacetate (H_2DCFDA)

EGT function in organisms that cannot biosynthesise it naturally, such as plants and mammals, is a topic of much interest (Spicer et al., 1951; Aruoma et al., 1999; Deiana et al., 2004; Ey et al., 2007; Markova et al., 2009; Song et al. 2010). It has been demonstrated that plants can obtain EGT from symbiotic microorganisms (Park et al., 2010); however its role in plants is as yet unclear. In order to develop a better understanding of EGT function in plants, a *Nicotiana tabacum* strain was transformed with *A. fumigatus egtA* and *nfs1* (performed by Professor Phil Dix, Dr. Peter Medgyesy and Dr. Éva Horvath, Maynooth University). The *egtA* and *nfs1* genes were cloned individually into pZ1S-197 plasmids for transformation into *N. tabacum*. The pZS-197 plasmid facilitates integration of a gene of interest into the *N. tabacum* chloroplast genome and confers resistance to spectinomycin (Svab and Maliga, 1993). The *N. tabacum* transformation for *egtA* and *nfs1* was carried out as per Figure 4.2. Gene insertion was confirmed via PCR.

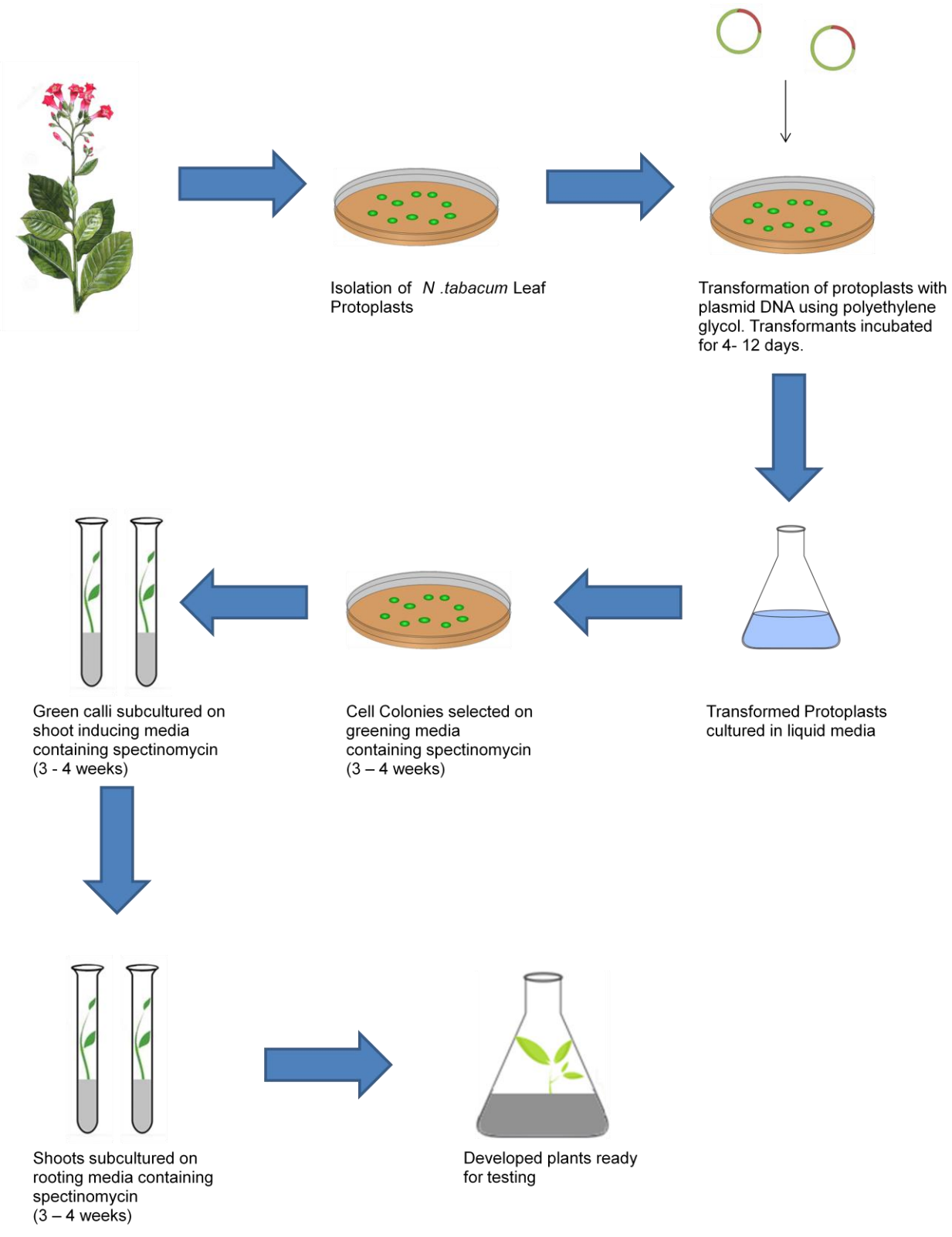

Figure 4.2. Schematic outline of the *N. tabacum* transformation process.

The aim of the work presented in this chapter was to:

(i) Determine if *egtA* is essential for EGT biosynthesis in *A. fumigatus*.

(ii) Investigate the phenotypic effect of EGT loss in *A. fumigatus* following exposure to ROS inducing agents, cell wall perturbing agents and gliotoxin.

(iii) Investigate EGT interplay with H_2O_2 in *A. fumigatus*.

(iv) Analyse the effect of EGT loss on total glutathione and GSH/GSSG ratio

(v) Determine if EGT influences gliotoxin biosynthesis and gliotoxin self-protection.

(vi) Determine if EGT loss affects conidiation in *A. fumigatus*.

(vii) Determine if EgtA and Nfs1 are present in *N. tabacum* L. cv. Petit Havana:*egtA*:*nfs1* and investigate if this strain can biosynthesise EGT.

4.2 Results

4.2.1 Analysis of EGT production in ATCC26933, Δ*egtA*^{26933} and *egtA*^{C26933}

4.2.1.1 Detection of EGT via RP-HPLC

5'-IAF alkylation allowed for the detection of EGT via RP-HPLC. The retention time of EGT was determined by comparing chromatograms from 5'-IAF labelled EGT standard and 5'-IAF only control to identify the derivatized EGT peak. EGT was determined to elute at 12.4 min (Figure 4.3).

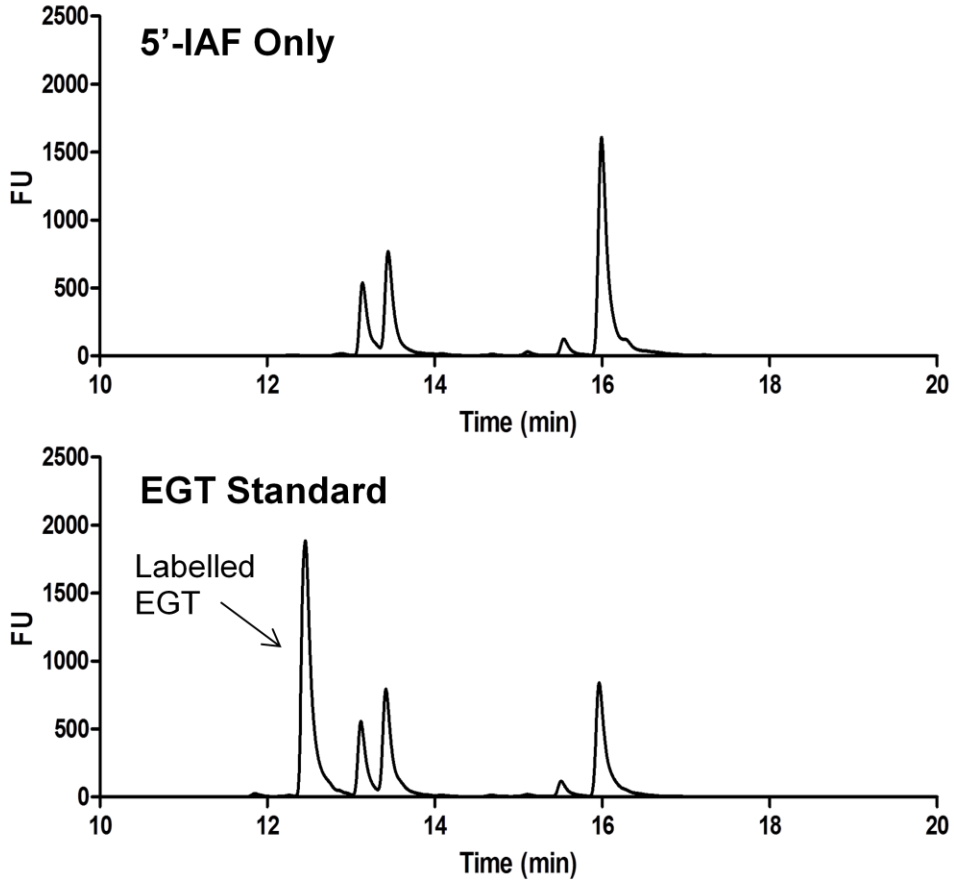

Figure 4.3. Detection of EGT by RP-HPLC. EGT is demonstrated to elute at 12.4 min.

4.2.1.2 Analysis of EGT production in ATCC26933, Δ*egtA*^{26933} and *egtA*^{C26933} via RP-HPLC

Mycelia from 72 h cultures of ATCC26933, Δ*egtA*^{26933} and *egtA*^{C26933} in Czapek-Dox broth were harvested and mycelial lysates obtained as per Section 2.2.9. Mycelial lysates were alkylated using 5'-IAF as described in Section 2.2.12.1 and analysed via RP-HPLC (Section 2.2.12.6) using the fluorescence detector and an Ex/Em of 494/518 nm. EGT was detected in ATCC26933 and *egtA*^{C26933}, but was absent in Δ*egtA*^{26933} (Figure 4.4). This demonstrates that *egtA* is essential for EGT production in *A. fumigatus*, confirming it functions as an EGT biosynthetic gene. EGT levels were demonstrated to be elevated approximately fivefold in *egtA*^{C26933} compared to ATCC26933 ($P = 0.0007$).

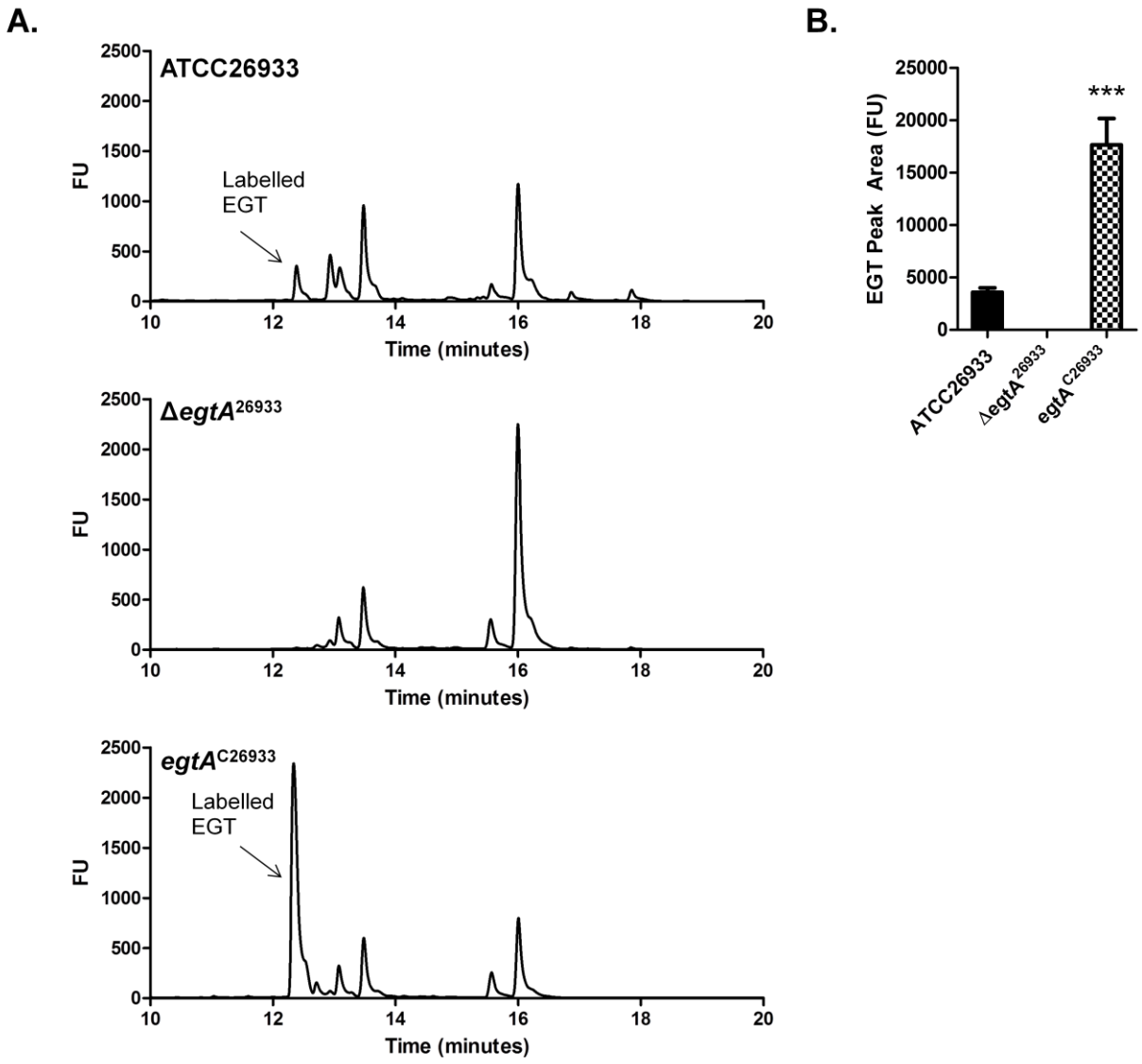

Figure 4.4. Detection and measurement of 5'-IAF alkylated EGT via RP-HPLC in ATCC26933, Δ*egtA*^{26933} and *egtA*^{C26933}. (A) Detection of 5'-IAF alkylated EGT in ATCC26933 and *egtA*^{C26933} at a retention time of 12.4 min. No EGT was detected in Δegt*A*^{26933} (B) Comparison of EGT levels in ATCC26933, Δegt*A*^{26933} and *egtA*^{C26933}. EGT is absent in Δ*egtA*^{26933}. EGT levels were significantly (P = 0.0007) elevated in *egtA*^{C26933} compared to ATCC26933.

4.2.1.3 Detection of EGT via LC-MS/MS

5'-IAF alkylation also facilitated EGT detection via LC-MS/MS. Alkylated EGT was identified using its known fragmentation pattern (Figure 4.5) (Gallagher et al., 2012). 5'-IAF alkylated EGT has been identified as having a single charged *m/z* of 617 $(M + H)^+$ and a *m/z* of 309 $(M + H)^{2+}$ when double protonated. The daughter ions *m/z* 573 and *m/z* 514 have also been detected using tandem mass spectrometry as well as their double protonated versions *m/z* 287 and *m/z* 257 respectively (Figure 4.5)(Gallagher et al., 2012). EGT eluted at 5.3 min (Figure 4.5).

4.2.1.4 Analysis of EGT production in Δ*egtA*^{26933} via LC-MS/MS

Mycelia from 72 h cultures of ATCC26933, Δ*egtA*^{26933} and *egtA*^{C26933} in Czapek-Dox broth were harvested and mycelial lyastes obtained as per Section 2.2.9. Mycelial lysates were alkylated using 5'-IAF (Section 2.2.12.1), TCA precipitated (Section 2.2.12.2) and analysed via LC-MS/MS (Section 2.2.12.7). In addition, an EGT standard was alkylated and TCA precipitated as before was analysed in the same manner. Extracted ion chromatograms (*m/z*: 617) for ATCC26933, Δ*egtA*^{26933} and *egtA*^{C26933} revealed the presence of EGT in the wild-type and complemented strains, while no EGT was detected for Δ*egtA*^{26933} (Figure 4.6). This unambiguously confirmed the absence of EGT in Δ*egtA*^{26933} and its restoration in *egtA*^{C26933}. EGT levels are elevated approximately threefold in *egtA*^{C26933} compared to ATCC26933.

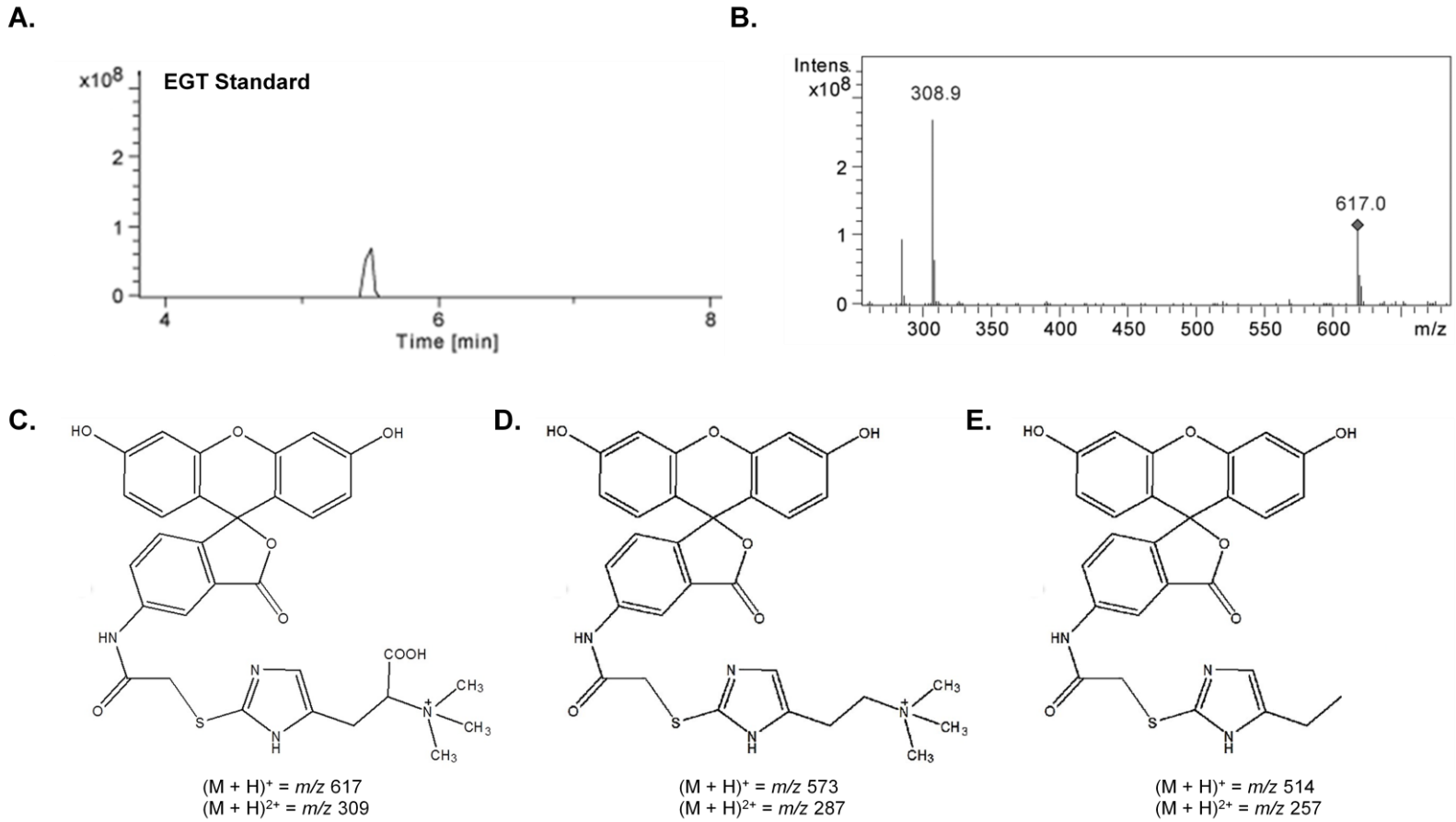

Figure 4.5. 5'-IAF alkylated EGT detection via LC-MS/MS. (A) Extracted ion chromatogram (*m/z*: 617) for alkylated EGT standard. EGT elutes at 5.3 min. (B) Signature ion breakdown for 5'-IAF alkylated EGT. (C) 5'-IAF-EGT molecular ion: $(M + H)^{+}$ = *m/z* 617 and $(M + H)^{2+}$ = *m/z* 309 (double protonated). (D) 5'IAF-EGT daughter ion, with a neutral loss of 44 from the loss of COO- from the molecular ion: $(M + H)^{+}$ = *m/z* 573 and $(M + H)^{2+}$ = *m/z* 287 (double protonated). (E) 5'IAF-EGT, with a neutral loss of 103 from with the loss of COO- and N(CH3)3+ from the molecular ion: (M + H)+ = *m/z* 514 and (M + H)2+ = *m/z* 257 (double protonated) (Gallagher et al., 2012).

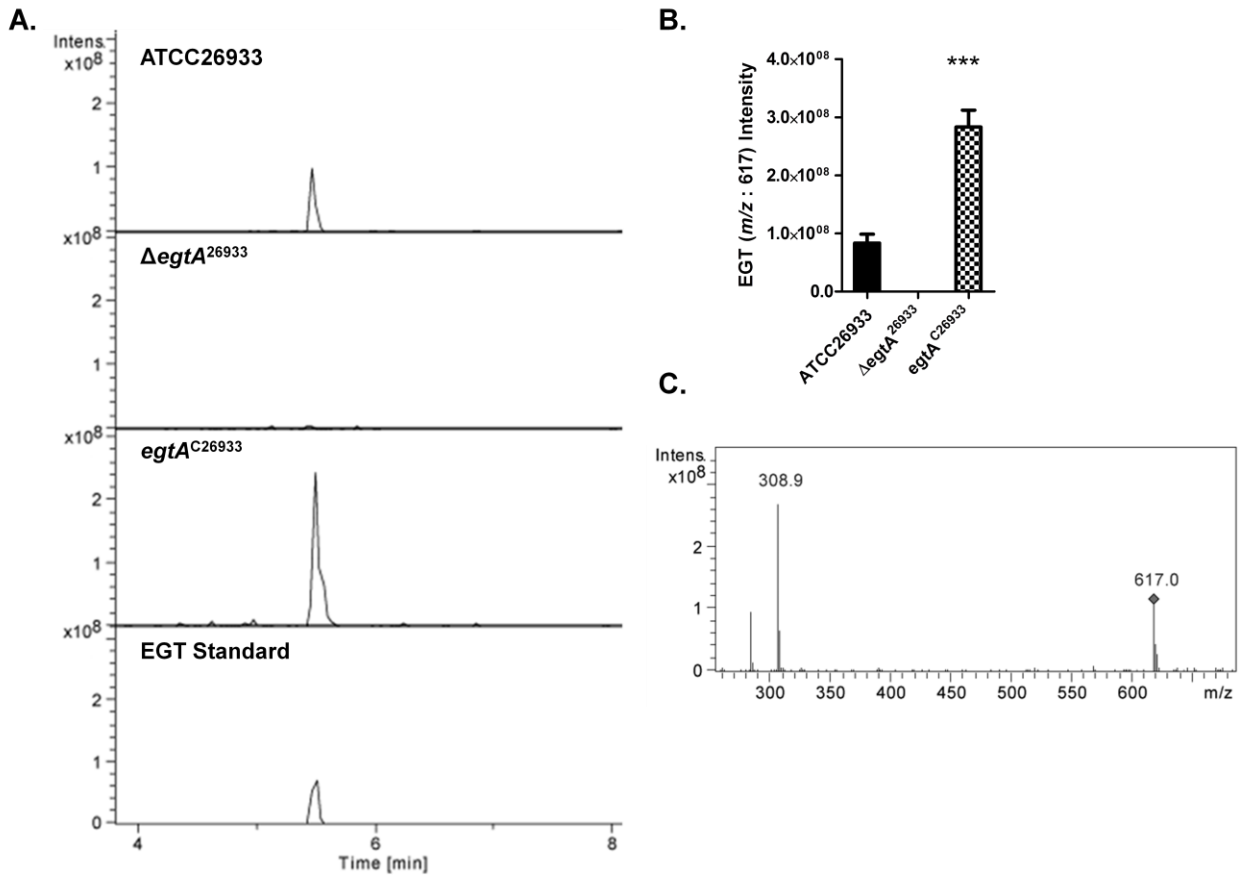

Figure 4.6. Detection of 5'-IAF labelled EGT via LC-MS/MS (A) Extracted Ion Chromatographs (*m/z*: 617) from ATCC26933, Δ*egtA*^{26933} and *egtA*^{C26933}, in addition to an EGT standard. A peak at 5.3 min was confirmed to be EGT. This peak was absent from Δ*egtA*^{26933}, confirming the absence of EGT from the mutant. (B) Comparison of EGT (*m/z*: 617) peak intensity. EGT is absent in Δ*egtA*^{26933}. Levels of EGT are significantly (P = 0.0004) increased in *egtA*^{C26933} compared to ATCC26933. (C) Signature Ion breakdown corresponding to 5'-IAF labelled EGT.

4.2.2 Phenotypic analysis of Δ*egtA*^{26933} in response to ROS inducing agents

4.2.2.1 Phenotypic analysis of ATCC26933, Δ*egtA*^{26933} and *egtA*^{C26933} in response to H_2O_2

Sensitivity to H_2O_2 was tested at a range of 0 – 4 mM as per Section 2.2.7. Comparison of the radial growth of ATCC26933, Δ*egtA*^{26933} and *egtA*^{C26933} colonies revealed no significant difference between the two strains at 1mM and 2 mM H_2O_2. However, radial growth of Δ*egtA*^{26933} at 3mM H_2O_2 was significantly reduced compared to ATCC26933and *egtA*^{C26933} (P = 0.0081) (Figure 4.7). No growth was observed for any of the strains at 4mM H_2O_2. Loss of *egtA* therefore results in sensitivity to high levels of H_2O_2. This demonstrates that EGT functions as an antioxidant and protects against high levels of ROS in *A. fumigatus*.

4.2.2.2 Phenotypic analysis of ATCC26933, Δ*egtA*^{26933} and *egtA*^{C26933} in response to menadione

Sensitivity to menadione was tested at a range of 0 – 60 µM as per Section 2.2.7. Significant reduction in the radial growth of Δ*egtA*^{26933} colonies compared to ATCC26933 and *egtA*^{C26933} colonies was observed at 40 µM (P = 0.0043) and 60 µM (P = 0.0013) menadione (Figure 4.8). However no significant difference in radial growth at 20 µM menadione was observed for any of the three strains. Deletion of *egtA* therefore results in sensitivity to high concentrations of menadione. EGT therefore protects against high levels of menadione induced ROS further emphasising the role of EGT as an antioxidant in *A. fumigatus*.

4.2.2.3 Phenotypic analysis of ATCC26933, Δ*egtA*^{26933} and *egtA*^{C26933} in response to diamide

Diamide sensitivity was tested at a range of 0 – 1.75 mM as per Section 2.2.7. No significant differences in the radial growth of ATCC26933, Δ*egtA*^{26933} and *egtA*^{C26933} colonies were observed at any concentration of diamide tested (Figure 4.9). *egtA* deletion, and the consequent absence of EGT, therefore has no effect on defence against diamide induced oxidative stress in *A. fumigatus*. Therefore, it can be concluded that EGT is not involved in conferring protection against diamide induced oxidative stress.

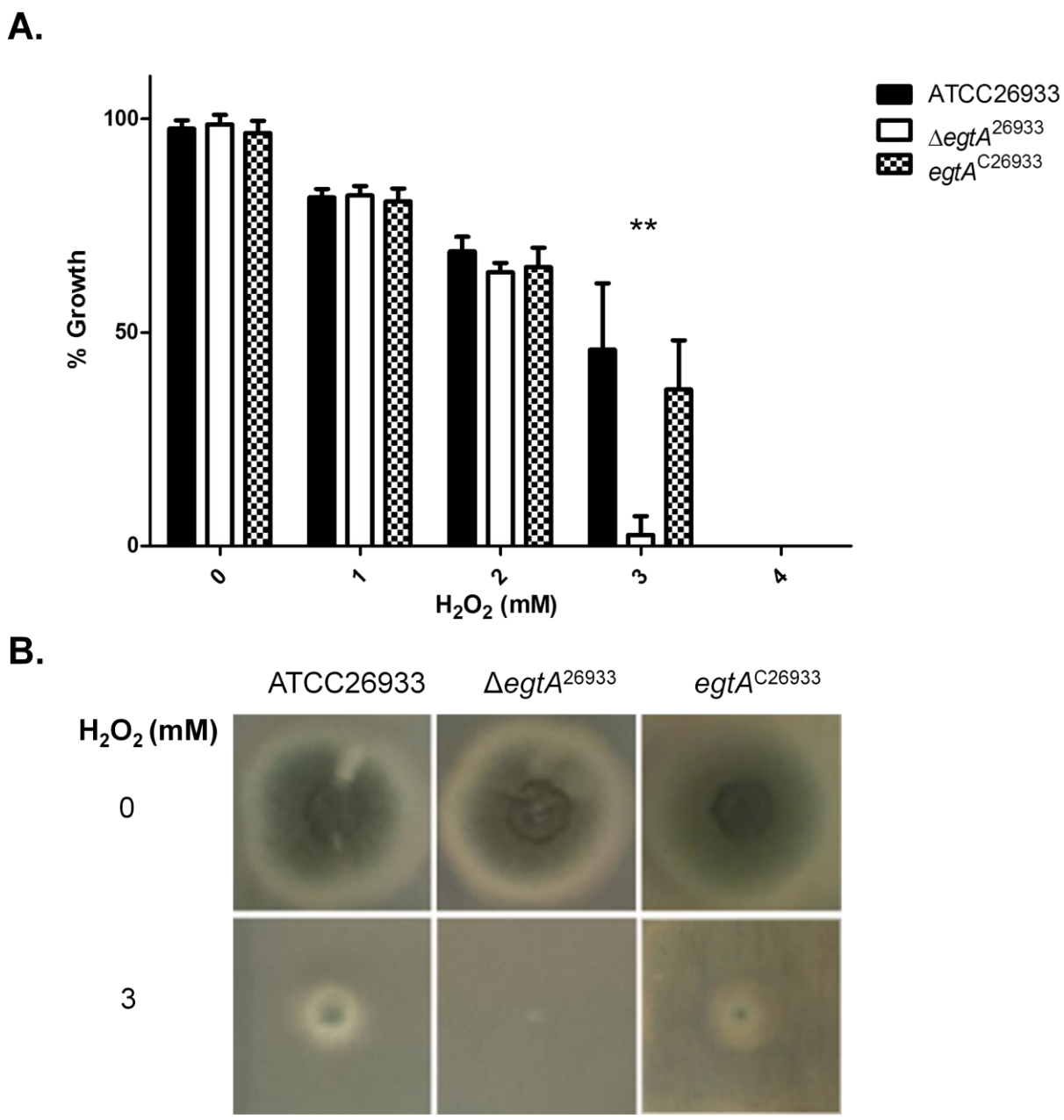

Figure 4.7. H_2O_2 sensitivity assay performed on AMM agar. (A) Comparison of radial growth of ATCC26933, Δ*egtA*^{26933} and *egtA*^{C26933} on AMM agar plates containing 0 to 4 mM H_2O_2. Δ*egtA*^{26933} shows a significant (P = 0.0081) reduction in growth compared to ATCC26933 and *egtA*^{C26933} at 3 mM H_2O_2. No growth was detected for any of the three strains at 4 mM H_2O_2. (B) Images of ATCC26933, Δ*egtA*^{26933} and *egtA*^{C26933} colonies on AMM plates containing 0 and 3 mM H_2O_2. A visible decrease in the size of the Δ*egtA*^{26933} colony can be observed compared to the ATCC26933 and *egtA*^{C26933} colonies at 3 mM H_2O_2.

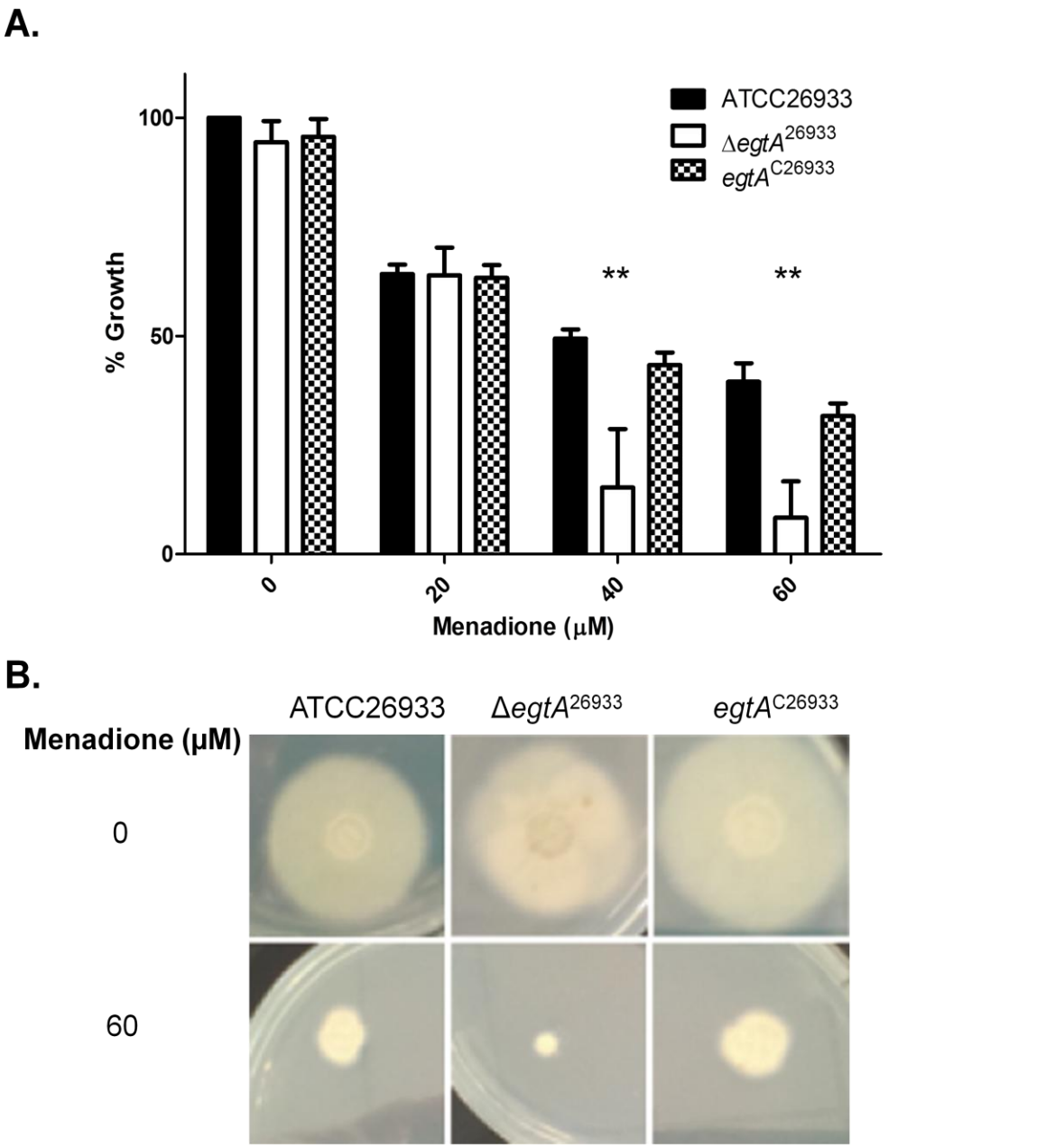

Figure 4.8. Menadione sensitivity assay performed on AMM agar. (A) Comparison of radial growth ATCC26933, Δ*egtA*^{26933} and *egtA*^{C26933} on AMM agar plates containing 0 to 60 µM menadione. Δ*egtA*^{26933} shows a significant reduction in growth compared to ATCC26933 and *egtA*^{C26933} at 40 µM (P = 0.0043) and 60 µM (P = 0.0013) menadione. (B) Images of ATCC26933, Δ*egtA*^{26933} and *egtA*^{C26933} colonies on AMM plates containing 0 and 60 µM menadione. A visible decrease in the size of the Δ*egtA*^{26933} colony can be observed compared to the ATCC26933 and *egtA*^{C26933} colonies at 60 µM menadione.

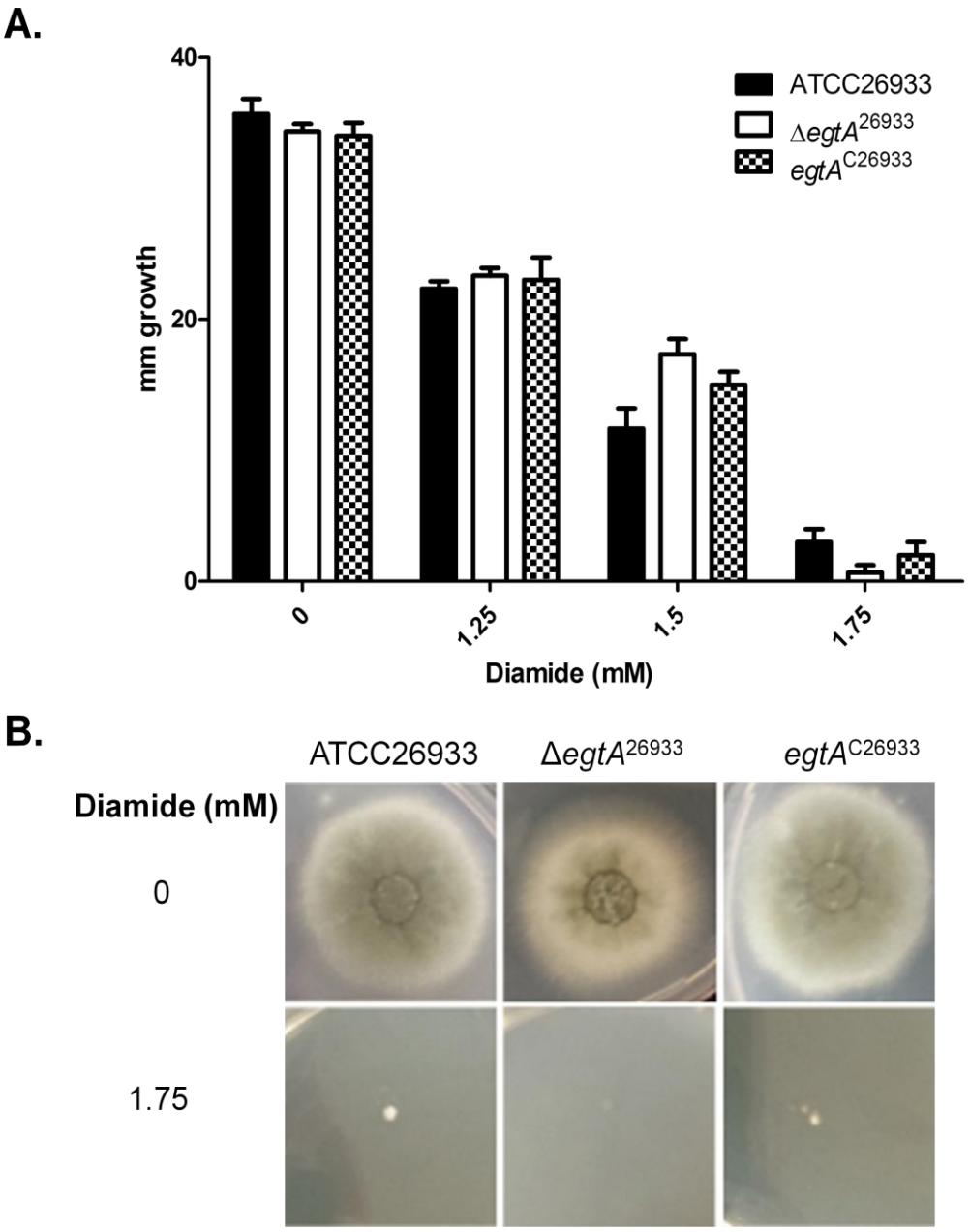

Figure 4.9. Diamide sensitivity assay performed on AMM agar. (A) Comparison of radial growth of ATCC26933, Δ*egtA*^{26933} and *egtA*^{C26933} on AMM agar plates containing 0 to 1.75 mM diamide. Δ*egtA*^{26933} shows no significant difference in radial growth compared to ATCC26933 and *egtA*^{C26933} at any concentration of diamide tested. (B) Images of ATCC26933, Δ*egtA*^{26933} and *egtA*^{C26933} colonies on AMM plates containing 0 and 1.75 mM diamide. A slight decrease in the size of the Δ*egtA*^{26933} colony can be observed compared to the ATCC26933 colonies at 1.75 mM diamide, however it is too small to be significant.

4.2.3 Measurement of ROS levels in Δ*egtA*^{26933} following H_2O_2 exposure

ROS levels in ATCC26933 and Δ*egtA*^{26933} with and without 3 mM H_2O_2 were analysed via fluorescence microscopy as described in Section 2.2.15. Under basal conditions, ROS levels in Δ*egtA*^{26933} were significantly (P = 0.0089) lower than ATCC26933 (Figure 4.10). This suggests that Δ*egtA*^{26933} is compensating for the absence of EGT under basal conditions. Addition of 3 mM H_2O_2 resulted in significantly (P = 0.038) elevated ROS in Δ*egtA*^{26933} compared to ATCC26933 (Figure 4.10). This demonstrates that absence of EGT leads to reduced antioxidant potential, resulting in elevated ROS when challenged with H_2O_2. This supports previous data demonstrating that EGT is important for detoxifying high levels of H_2O_2 in *A. fumigatus*.

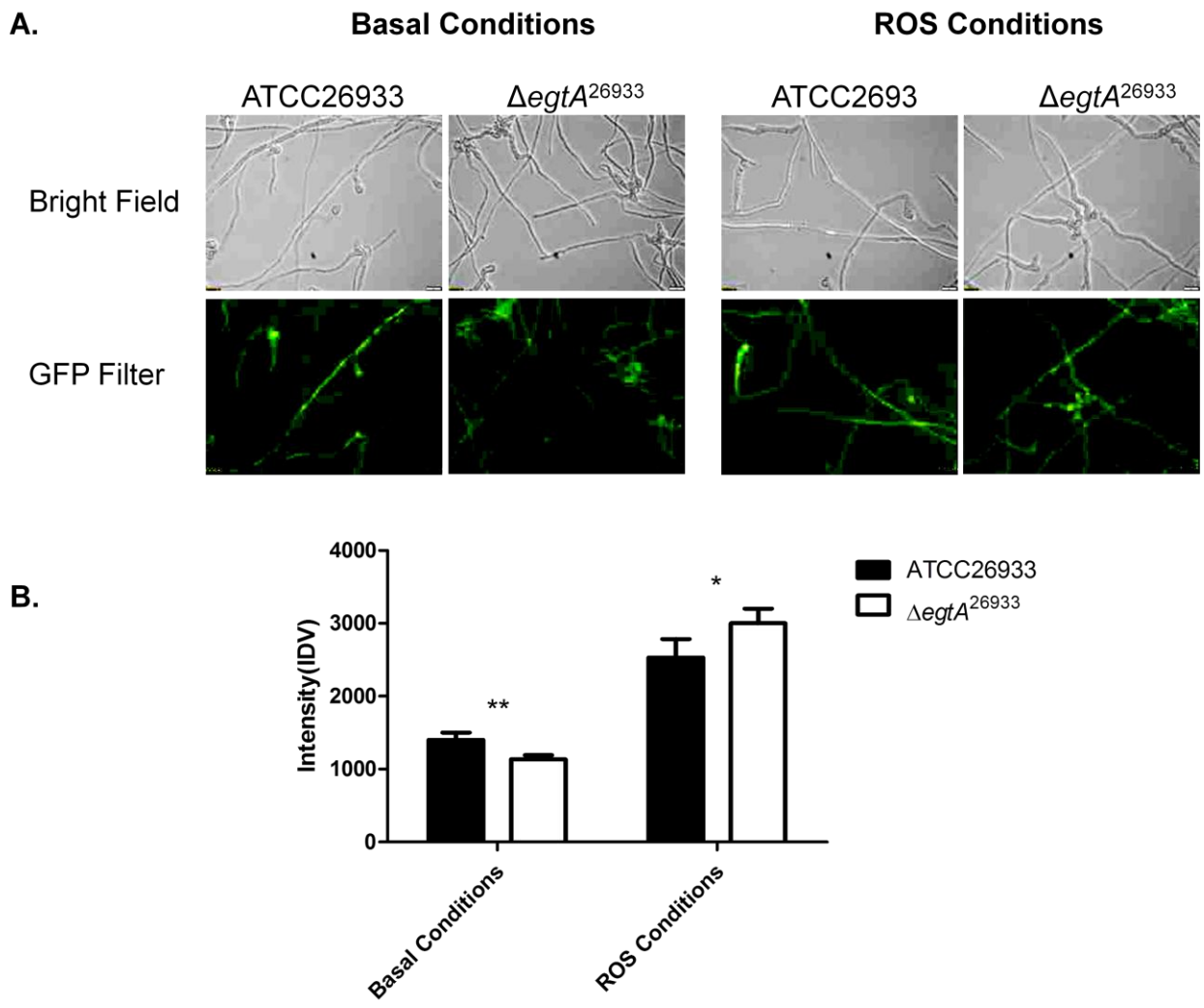

Figure 4.10. Analysis of ROS levels via fluorescent microscopy using H_2DCFDA in ATCC26933 and Δ*egtA*^{26933} with and without H_2O_2. (A) Microscopy images, showing both the bright field and GFP filter for each image. (B) Comparison of integrated density values obtained for each strain and condition. Under basal conditions, ATCC26933 shows higher levels of ROS compared to Δ*egtA*^{26933} (P = 0.0089). Δ*egtA*^{26933} demonstrates higher levels of ROS compared to ATCC26933 when exposed to 3 mM H_2O_2 (P = 0.038).

4.2.4 qRT- PCR Analysis of *egtA* expression following H_2O_2 Exposure

As results from plate assays (Section 4.2.2) and fluorescent microscopy (Section 4.2.3) indicated EGT is involved in oxidative stress defence, analysis of *egtA* expression in response to H_2O_2 was undertaken. Quadruplicate cultures of ATCC26933 were grown in Sabouraud Dextrose broth for 23 h at 37 ^{o}C, 200 rpm shaking. Following 23 h incubation, H_2O_2 was added in duplicate to a final concentration of 3 mM. As a control, an equivalent volume of sterile H_2O was added in duplicate. The cultures were then incubated as before for 1 h. Following this incubation, the mycelia were harvested from each culture. RNA isolation (Section 2.2.6.1), DNase treatment (Section 2.2.6.2) and cDNA synthesis (Section 2.2.6.3) then followed. qRT-PCR was then undertaken as described in Section 2.2.6.5. qRT-PCR analysis revealed relative *egtA* expression increased significantly (P = 0.0002) when exposed to 3 mM H_2O_2 for 1 h (Figure 4.11). This threefold increase in *egtA* expression in response to ROS further elaborates that EGT has a protective role against oxidative stress in *A. fumigatus.*

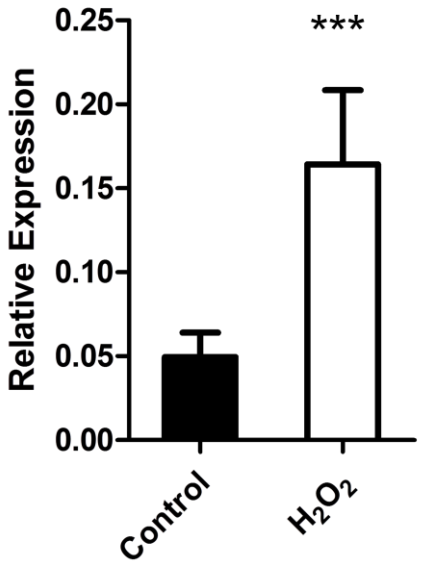

Figure 4.11. Quantitative RT-PCR data showing the relative expression of *egtA* in ATCC26933 following exposure to 3 mM H_2O_2. *egtA* expression was significantly (P = 0.0002) increased in ATCC26933 when exposed to H_2O_2 compared to control levels.

4.2.5 RP-HPLC analysis of EGT levels following H_2O_2 exposure

As it was demonstrated that *egtA* expression increased in response to H_2O_2 (Section 4.2.4), it was necessary to analyse EGT levels following a similar treatment to see if a corresponding rise in EGT levels was observed. Quadruplicate cultures of ATCC26933 were grown in Czapek-Dox broth for 71 h at 37 ^{o}C, 200 rpm shaking. Following this incubation, H_2O_2 was added in duplicate to a final concentration of 3 mM. As a control, an equivalent volume of sterile H_2O was added in duplicate. The cultures were then incubated as before for 1 h. Following this incubation, the mycelia were harvested from each culture. Mycelial lyastes were then obtained as per Section 2.2.9. Mycelial lysates were labelled using 5'-IAF as described in Section 2.2.12.1 and analysed via RP-HPLC (Section 2.2.12.6) using fluorescence detection with an Ex/Em of 494/518 nm. Unexpectedly, RP-HPLC analysis revealed a non-significant reduction in EGT levels in ATCC26933 following 3 mM H_2O_2 exposure (Figure 4.12). This presents a contradictory situation, whereby the biosynthetic gene, *egtA*, shows an increase in expression following H_2O_2 exposure, but the cognate metabolite shows a small decrease.

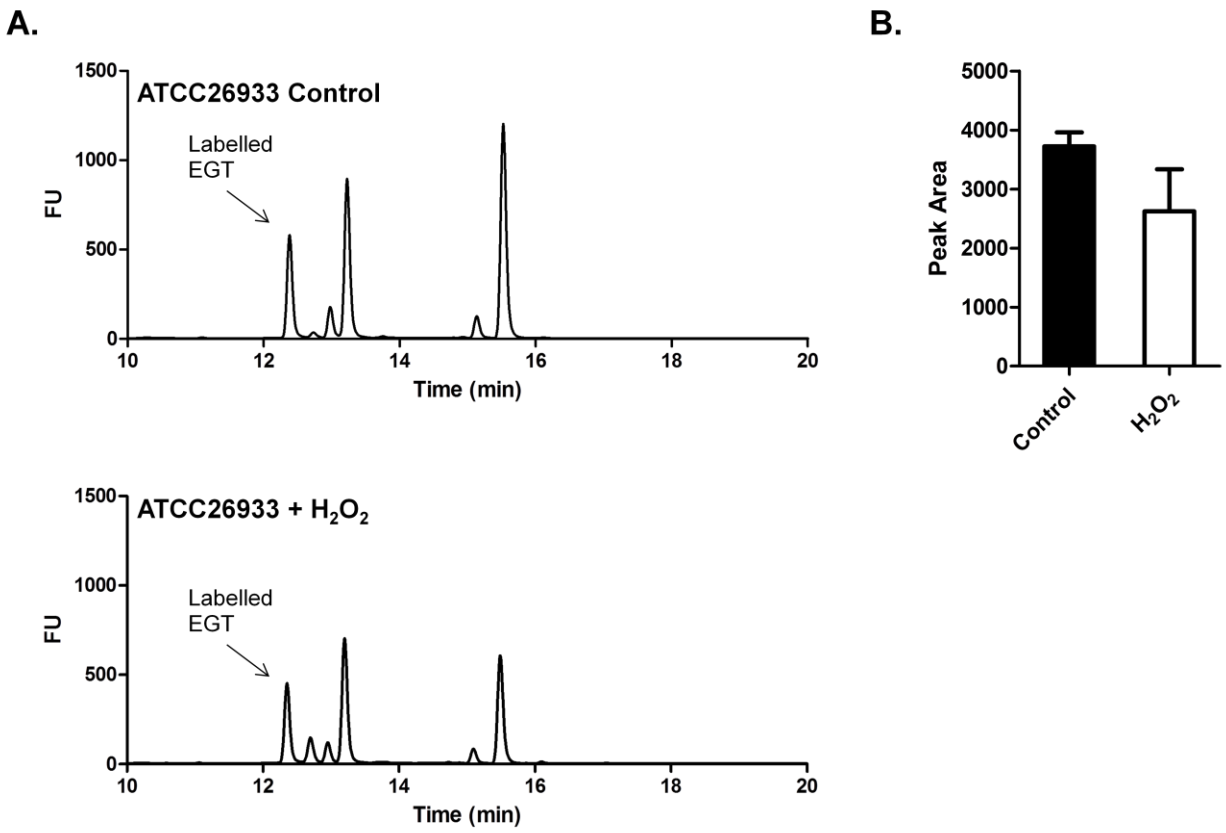

Figure 4.12. Analysis of EGT levels in ATCC26933 following incubation with 3 mM H_2O_2. (A) RP-HPLC chromatograms showing the detection of alkylated EGT in ATCC26933 with and without the addition of 3 mM H_2O_2. (B) Comparison of alkylated EGT peak areas from RP-HPLC analysis. Addition of H_2O_2 resulted in a non-significant reduction in EGT levels compared to the control.

4.2.6 Analysis of EGT reactivity with H_2O_2

The apparent contradictory data between *egtA* expression and EGT levels prompted an investigation into the interplay between EGT and H_2O_2. EGT was incubated with H_2O_2 for 3 h, followed by back-titration, alkylation and RP-HPLC analysis (Section 2.2.12.5) in order to determine if EGT levels are altered by H_2O_2 exposure. RP-HPLC analyses revealed that the residual EGT levels were significantly decreased (P = 0.029) in the samples exposed to H_2O_2 compared to the control samples (Figure 4.13). This data suggests that EGT is dissipated in the process of detoxifying H_2O_2, which is consistent with data from Servillo et al. (2015).

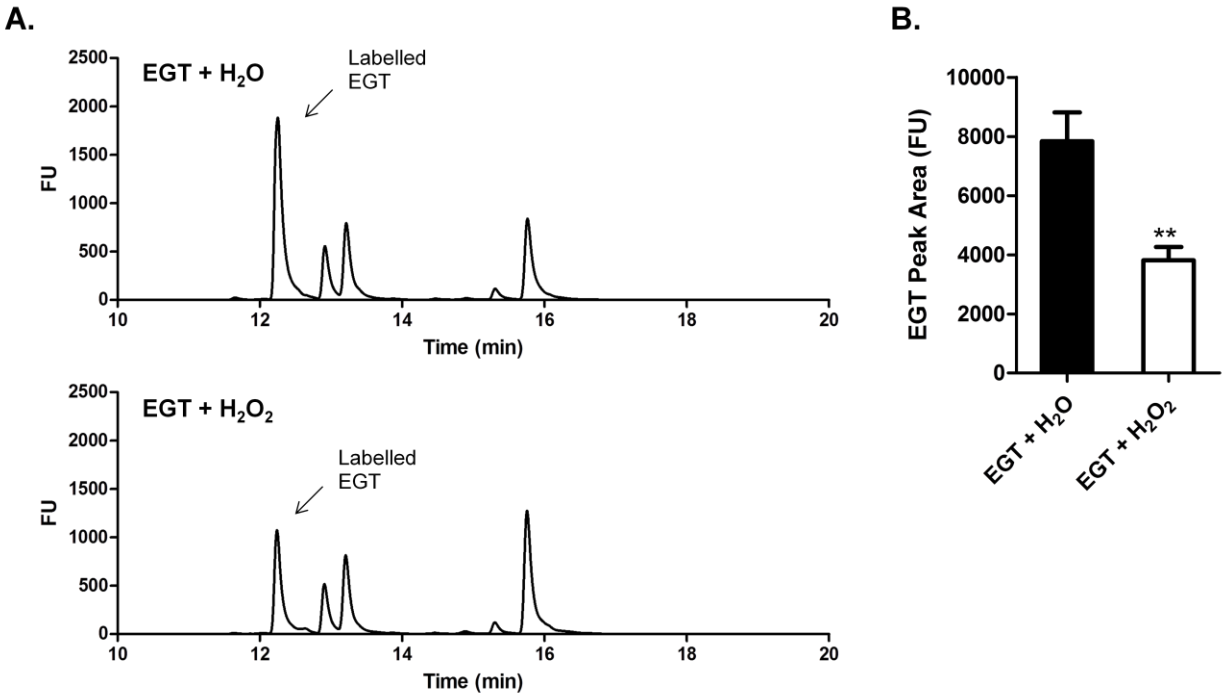

Figure 4.13. Analysis of EGT reavtivity with H_2O_2. (A) RP-HPLC chromatograms showing the detection of alkylated EGT with and without the addition of 3 mM H_2O_2. (B) Comparison of alkylated EGT peak area following RP-HPLC analysis. Addition of H_2O_2 resulted in a significant (P = 0.029) decrease in EGT levels compared to the control.

4.2.7 Glutathione analysis in ATCC26933, Δ*egtA*^{26933} and *egtA*^{C26933}

4.2.7.1 Total glutathione measurement via LC-MS/MS

Mycelia from triplicate 72 h cultures of ATCC26933, Δ*egtA*^{26933} and *egtA*^{C26933} in Czapek-Dox broth were harvested and cell lysate supernatants obtained as per Section 2.2.9. The presence of DTT in the lysis buffer reduces GSSG to GSH, allowing for total glutathione measurement. Mycelial lysates were alkylated using 5'-IAF (Section 2.2.12.1), TCA precipitated (Section 2.2.12.2) and analysed via LC-MS/MS (Section 2.2.12.7). In addition, a GSH standard, alkylated with 5'-IAF and TCA precipitated as before, was analysed in the same manner. Alkylated GSH was demonstrated to elute at 5.9 min, with an *m/z* of 695 (Gallagher et al., 2012). Extracted ion chromatograms (*m/z*: 695) for the samples show GSH present in all 3 strains. However Δ*egtA*^{26933} shows significantly (P = 0.0016) elevated levels of GSH compared to ATCC26933 and *egtA*^{C26933} (Figure 4.14). This suggests that loss of EGT in *A. fumigatus* results in an increase in total intracellular GSH, which is likely to compensate for the drop in antioxidant potential.

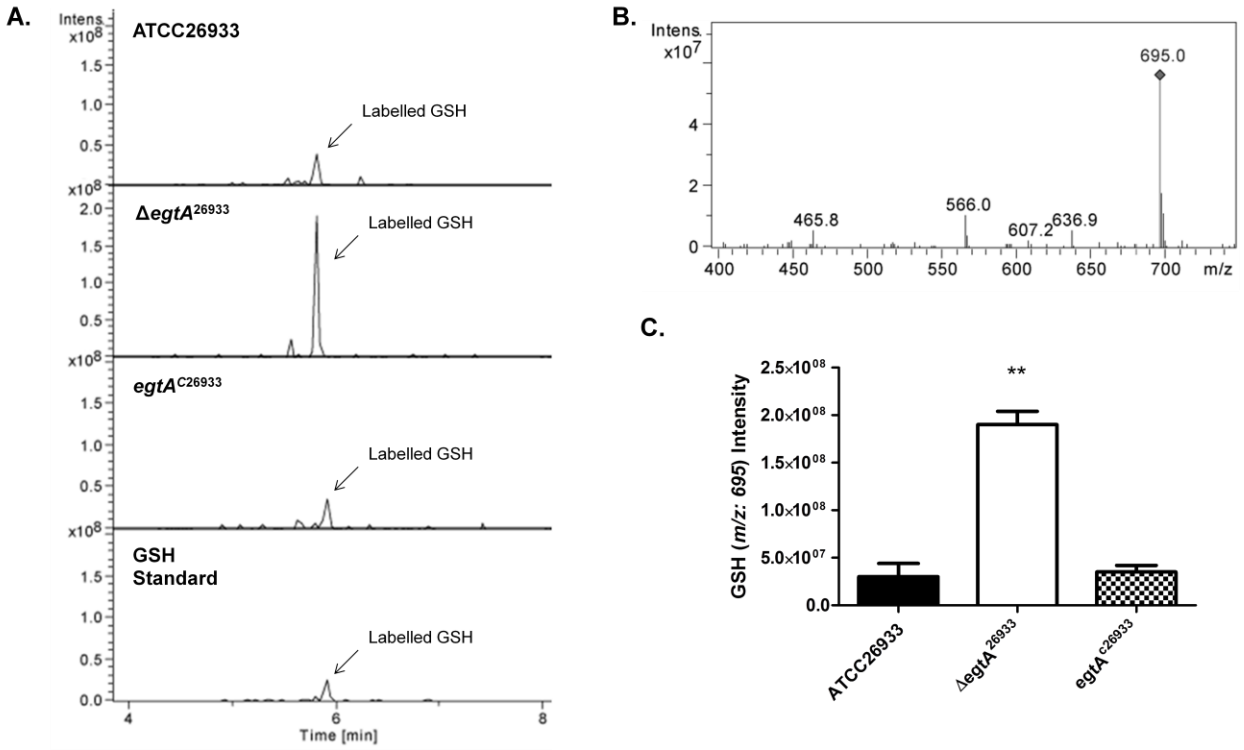

Figure 4.14. Total glutathione detection via LC-MS/MS in ATCC26933, Δ*egtA*^{26933} and *egtA*^{C26933}. (A) Extracted Ion Chromatographs (*m/z*: 695) following LC-MS/MS analysis of TCA precipitated alkylated mycelial extracts. A peak at 5.9 min was confirmed to be GSH. (B) Signature ion breakdown corresponding to alkylated GSH. (C) Comparison of peak height data from LC-MS analysis. GSH levels are significantly (P = 0.0016) increased in Δ*egtA*^{26933} compared to the wild-type and complemented strains.

4.2.7.2 Measurement of GSH/GSSG ratio in ATCC26933, Δ*egtA*^{26933} and *egtA*^{C26933}

4.2.7.2.1 GSH and GSSG standard curve determination

In order to measure the intracellular levels of total GSH and GSSG, standard curves for GSH and GSSG were constructed as described in Sections 2.2.13.2 and 2.2.13.3 respectively. The standards were prepared at a concentration range of 26.4 – 0.4125 nmol/ml and assayed as described in Section 2.2.13.5. A linear relationship occurs between the concentration of glutathione and the absorbance. The standard curves (Figure 4.15) were used in subsequent assays to calculate the amount of intracellular GSH and GSSG in mycelial extracts (O'Keeffe et al., 2013).

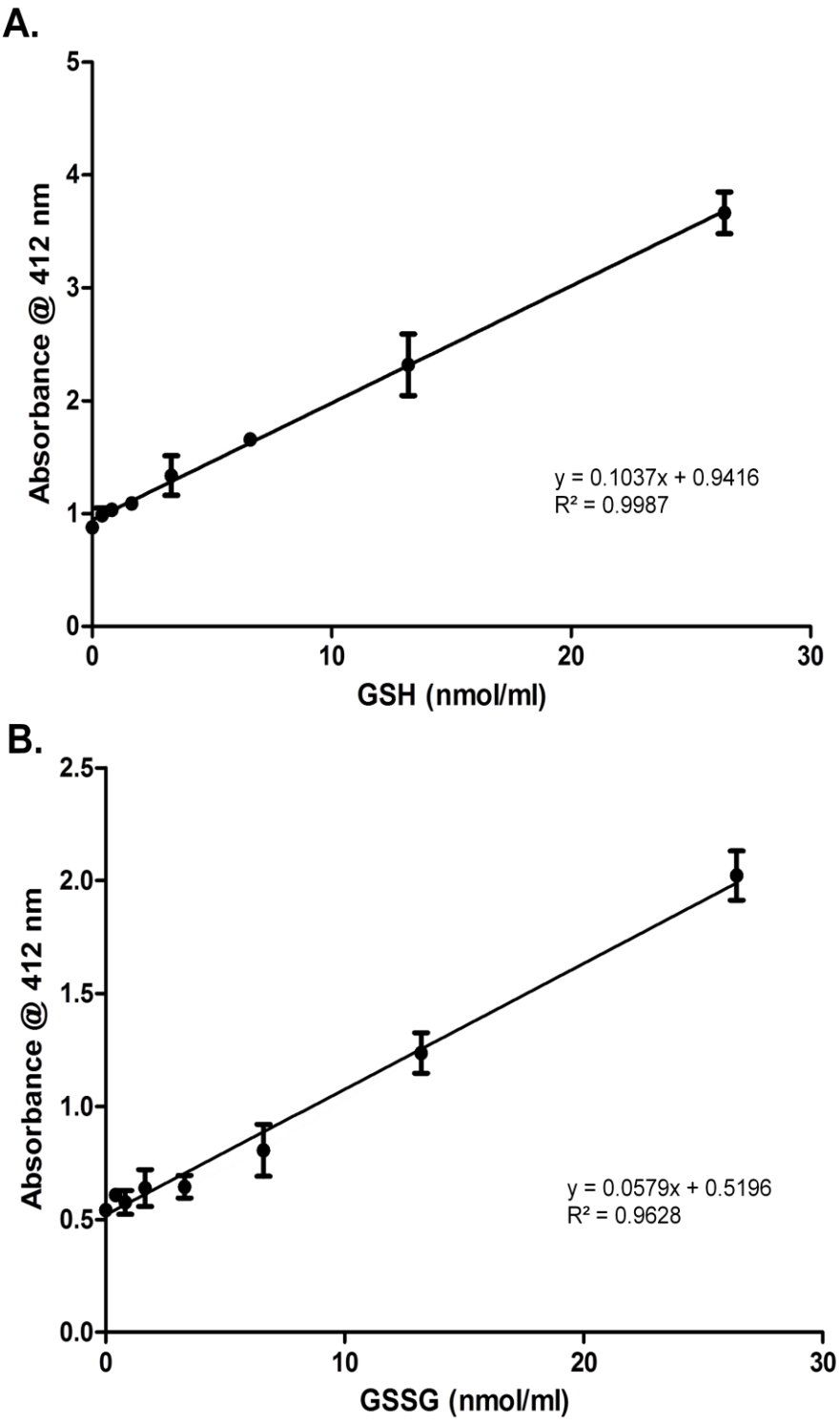

Figure 4.15. Standard curves for the measurement of GSH and GSSG. (A) Standard curve for the measurement of GSH (B) Standard curve for the measurement of GSSG.

4.2.7.2.2 Analysis of GSH/GSSG ratios in ATCC26933, Δ*egtA*^{26933} and *egtA*^{C26933}

Duplicate cultures of ATCC26933, Δ*egtA*^{26933} and *egtA*^{C26933} were grown in Czapek-Dox broth for 72 h. Mycelia were harvested, lysed and the GSH/GSSG assay carried out as per Section 2.2.13, using the standard curves generated in Section 4.2.7.2.1 for quantitation of GSH and GSSG. The GSH/GSSG ratio increased from 2.7 in ATCC26933 to 3.16 in Δ*egtA*^{26933} and decreased to 1.52 in *egtA*^{C26933} (Table 4.1). It appears that loss of EGT leads to an increase in GSH/GSSG ratio, which indicates Δ*egtA*^{26933} is under less oxidative stress than wild-type. This may be due to the increase in total GSH seen before (Section 4.2.7.1). With the exception of GSSG levels in Δ*egtA*^{26933} and *egtA*^{C26933} (P = 0.0301), none of the differences in GSH and GSSG levels were deemed significant (Figure 4.16).

Table 4.1. GSH/GSSG ratios in ATCC26933, Δ*egtA*^{26933} and *egtA*^{C26933}.

Strain	GSH/GSSG Ratio
ATCC26933	2.7
Δ*egtA*^{26933}	3.16
egtA^{C26933}	1.52

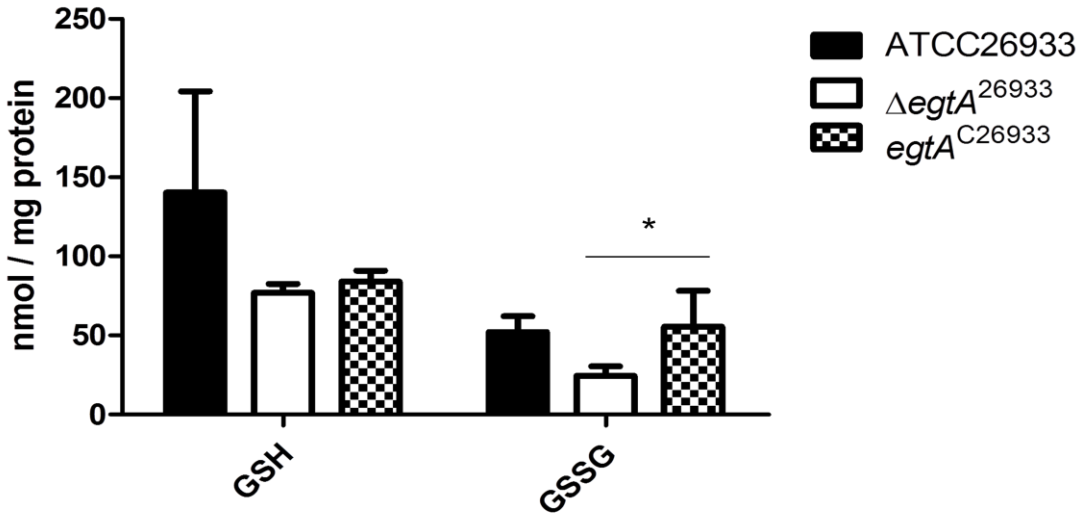

Figure 4.16. Measurement of GSH and GSSG levels in ATCC26933, Δ*egtA*^{26933} and *egtA*^{C26933}. All differences were non-significant, with the exception of GSSG levels in Δ*egtA*^{26933} and *egtA*^{C26933} (P = 0.0301).

4.2.8 Comparison of glutathione in Δ*egtA*^{26933} and Δ*egtA*^{AfS77}

4.2.8.1 Total glutathione measurement via LC-MS/MS

Mycelia from triplicate 72 h cultures of ATCC26933, Δ*egtA*^{26933}, AfS77 and Δ*egtA*^{AfS77} in Czapek-Dox broth were harvested and cell lysate supernatants obtained as per Section 2.2.9. The presence of DTT in the lysis buffer reduced GSSG to GSH, allowing for total glutathione measurement. Mycelial lysates were alkylated (Section 2.2.12.1), TCA precipitated (Section 2.2.12.2) and analysed via LC-MS/MS (section 2.2.12.7). In addition, a GSH standard labelled with 5'-IAF and TCA precipitated as before was analysed in the same manner. 5'-IAF alkylated GSH was demonstrated to elute at 6.2 min, with an *m/z* of 695. Extracted ion chromatograms (*m/z*: 695) for the samples show GSH present in all 4 strains (Figure 4.17). While deletion of *egtA* in ATCC26933 resulted in an increase in total GSH (as demonstrated previously in Section 4.2.7.1), the same deletion in AfS77 had no effect on GSH levels. It appears the levels of total GSH in ATCC26933 are significantly ($P = 0.0083$) lower than those in AfS77. This difference in total GSH in the background strains may explain the difference in GSH response to *egtA* deletion.

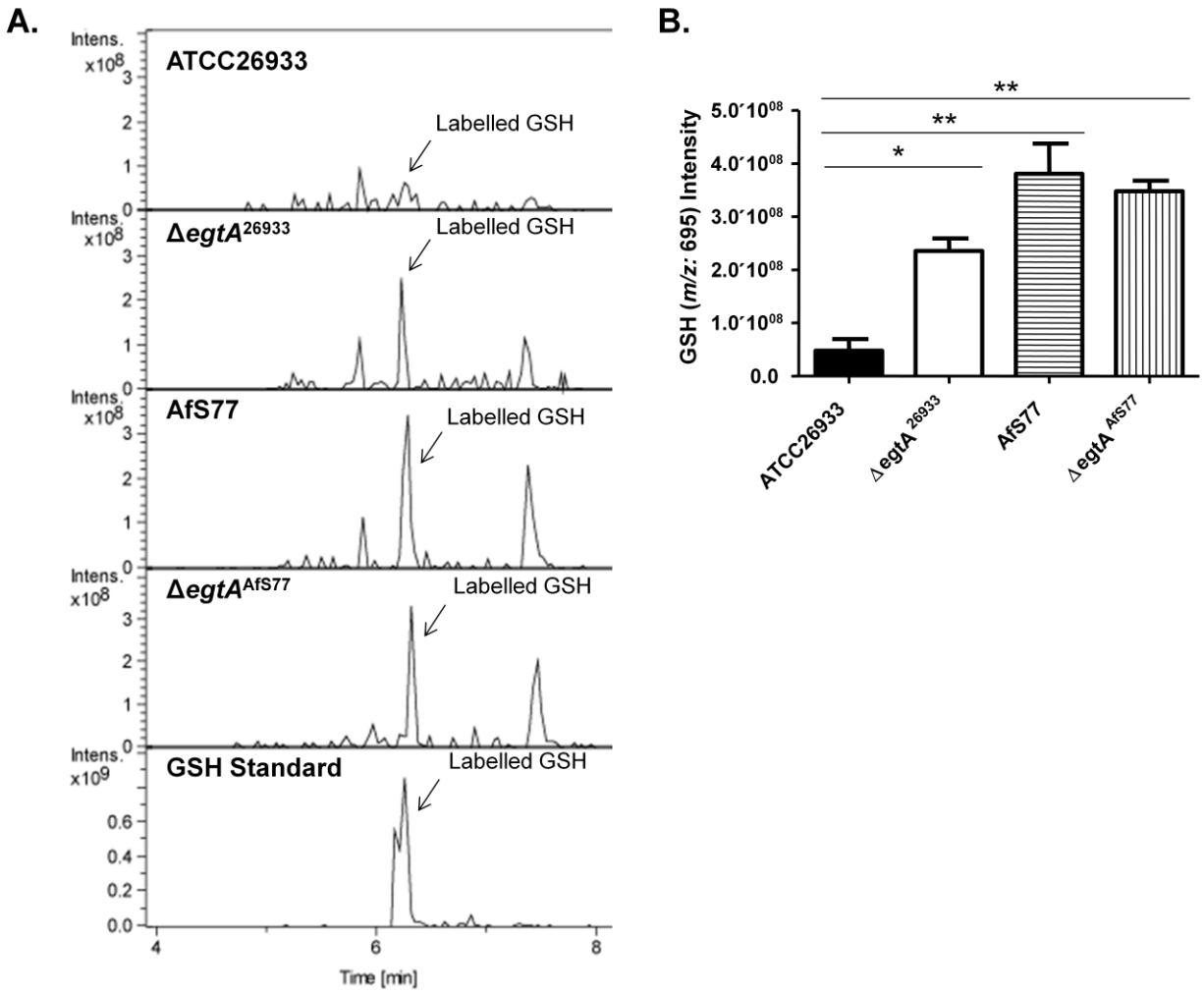

Figure 4.17. Comparison of GSH levels in ATCC26933, AfS77 and their respective Δ*egtA* mutants. (A) Extracted Ion Chromatographs (*m/z*: 695) following LC-MS/MS analysis of TCA precipitated alkylated extracts from ATCC26933, Δ*egtA*^{26933}, AfS77 and Δ*egtA*^{AfS77} , in addition to a GSH standard. (B) Comparison of peak height data from LC-MS analysis. Levels of GSH in ATCC26933 were significantly lower than those of Δ*egtA*^{26933} (P = 0.0144), AfS77 (P = 0.0083) and Δ*egtA*^{AfS77} (P = 0.0049).

4.2.8.2 Ananlysis of GSH/GSSG ratios in AfS77, Δ*egtA*^{AfS77} and Δ*egtA*^{CAfS77}

Duplicate cultures of AfS77, Δ*egtA*^{AfS77} and *egtA*^{CAfS77} were grown in Czapek-Dox broth for 72 h. Mycelia were harvested, lysed and the GSH/GSSG assay carried out as per Section 2.2.13, using the standard curves generated in Section 4.2.7.2.1 for quantitation of GSH and GSSG. The GSH/GSSG ratio increases from 1.4 in AfS77 to 3.74 in Δ*egtA*^{AfS77} and decreased to 0.64 in *egtA*^{CAfS77} (Table 4.2). This follows the same trend seen in the ATCC26933 background, whereby *egtA* deletion causes the GSH/GSSG ratio to rise, and then fall again in the complemented strain. With the exception of GSH levels in Δ*egtA*^{AfS77} and *egtA*^{CAfS77} (P = 0.0011), none of the differences in GSH and GSSG levels were deemed significant (Figure 4.18).

Table 4.2. GSH/GSSG ratios in AfS77, Δ*egtA*^{AfS77} and *egtA*^{CAfS77}.

Strain	GSH/GSSG Ratio
AfS77	1.4
Δ*egtA*^{AfS77}	3.74
egtA^{CAfS77}	0.64

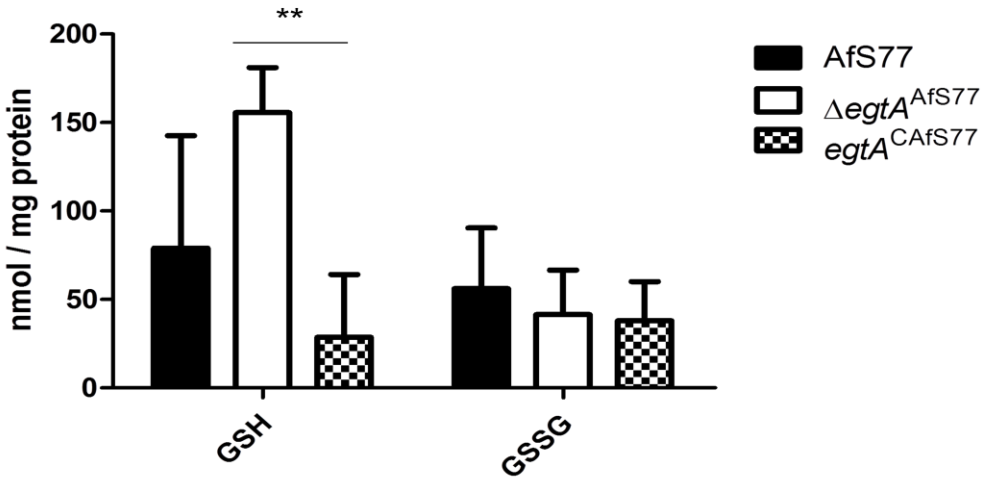

Figure 4.18. Measurement of GSH and GSSG levels in AfS77, Δ*egtA*^{AfS77} and *egtA*^{CAfS77}. All differences were non-significant, with the exception of GSH levels in Δ*egtA*^{AfS77} and *egtA*^{CAfS77} (P = 0.0011).

4.2.9 Analysis of gliotoxin production in ATCC26933 and Δ*egtA*^{26933}

4.2.9.1 Analysis of gliotoxin production in ATCC26933 and Δ*egtA*^{26933} via RP-HPLC

Supernatants from triplicate 72 h cultures of ATCC26933 and Δ*egtA*^{26933} in Czapek-Dox broth were collected and organic extraction carried out as per Section 2.2.10. The organic extracts were then analysed via RP-HPLC (Section 2.2.12.6). In addition, a gliotoxin control was analysed in the same manner. Gliotoxin was detected at 14.9 min and was observed to be present in both ATCC26933 and Δ*egtA*^{26933} (Figure 4.19). However a comparison between ATCC26933 and Δ*egtA*^{26933} of gliotoxin peak areas revealed Δ*egtA*^{26933} produced significantly less gliotoxin ($P = 0.0003$). Therefore it appears that the inability to biosynthesise EGT impacts negatively upon gliotoxin production.

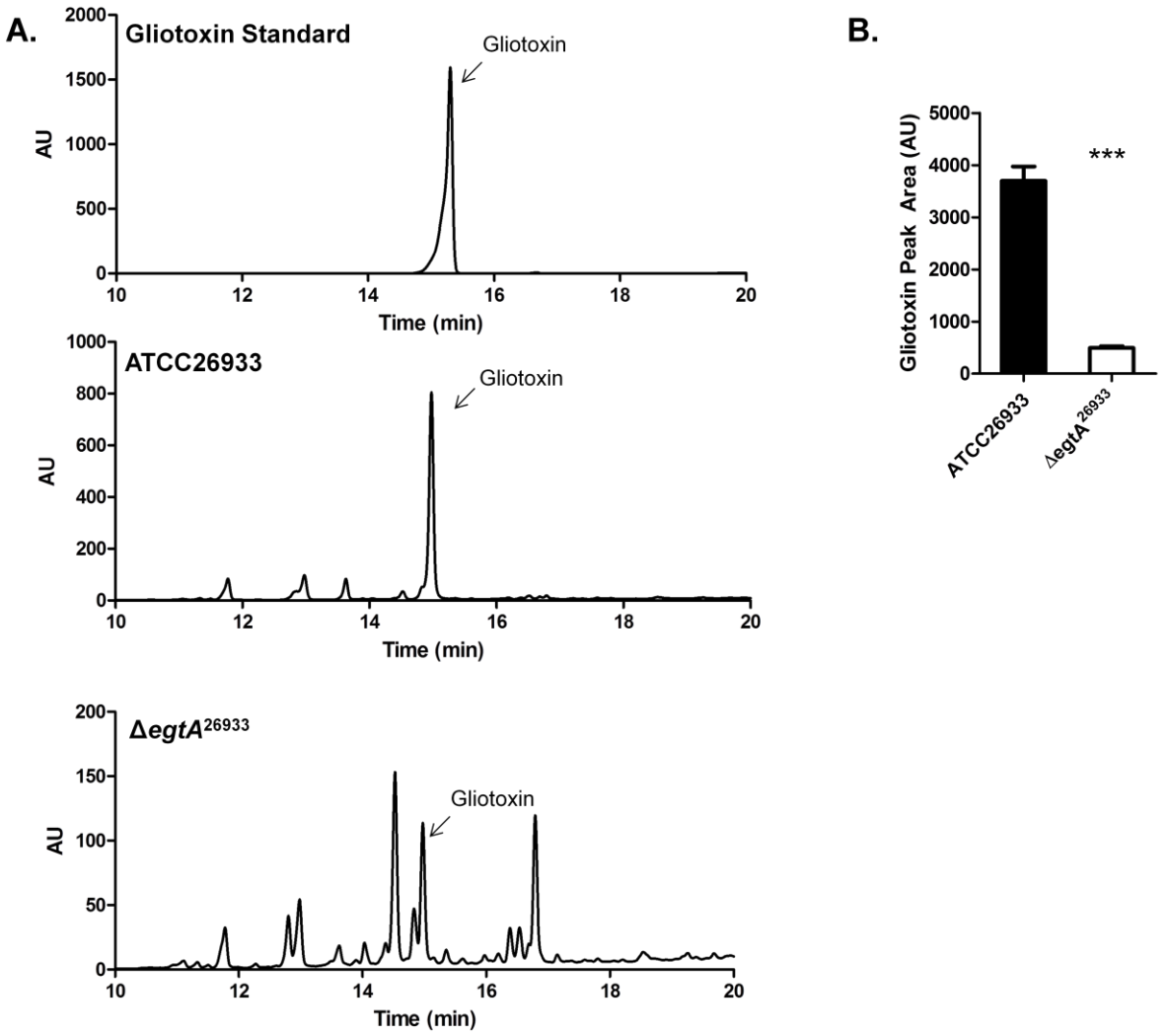

Figure 4.19. Gliotoxin detection via RP-HPLC in ATCC26933 and Δ*egtA*^{26933}. (A) RP-HPLC analysis of organic extracts from the supernatants of 72 h cultures (n = 3) of ATCC26933 and Δ*egtA*^{26933}. Gliotoxin is present in both chromatograms at 14.9 min. (B) Comparison of gliotoxin peak area from RP-HPLC analysis for ATCC26933 and Δ*egtA*^{26933} performed in triplicate. Gliotoxin levels were found to be significantly (P = 0.0003) lowered in Δ*egtA*^{26933} compared to ATCC26933.

4.2.9.2 Analysis of gliotoxin production in ATCC26933 and Δ*egtA*^{26933} via LC-MS/MS

Supernatants from triplicate 72 h cultures of ATCC26933 and Δ*egtA*^{26933} in Czapek-Dox broth were collected and organic extraction carried out as per Section 2.2.10. The organic extracts were then analysed via LC-MS/MS (Section 2.2.12.7). In addition a gliotoxin standard was analysed in the same manner. Gliotoxin was determined to elute at 6.3 min, with a *m/z* of 327. Extracted ion chromatograms (*m/z*: 327) for ATCC26933 and Δ*egtA*^{26933} confirmed the presence of gliotoxin in both strains (Figure 4.20). Comparison of gliotoxin peak intensity revealed that gliotoxin levels in Δ*egtA*^{26933} are significantly (P = 0.0002) decreased compared to ATCC26933. This is in agreement with data from RP-HPLC.

4.2.9.3 Analysis of *bis*-methylgliotoxin production in ATCC26933 and Δ*egtA*^{26933} via LC-MS/MS

Supernatants from triplicate 72 h cultures of ATCC26933 and Δ*egtA*^{26933} in Czapek-Dox broth were collected and organic extraction carried out as per Section 2.2.10. The organic extracts were then analysed via LC-MS/MS (Section 2.2.12.7). *Bis*-methylgliotoxin (BmGT) was determined to elute at 6.7 min, with a *m/z* of 357 (Domingo et al., 2012; Dolan et al., 2014). Extracted ion chromatograms (*m/z*: 357) for ATCC26933 and Δ*egtA*^{26933} confirmed the presence of BmGT in both strains (Figure 4.21). Comparison of BmGT peak intensity revealed that BmGT production in Δ*egtA*^{26933} is significantly (P = 0.0371) decreased compared to ATCC26933.

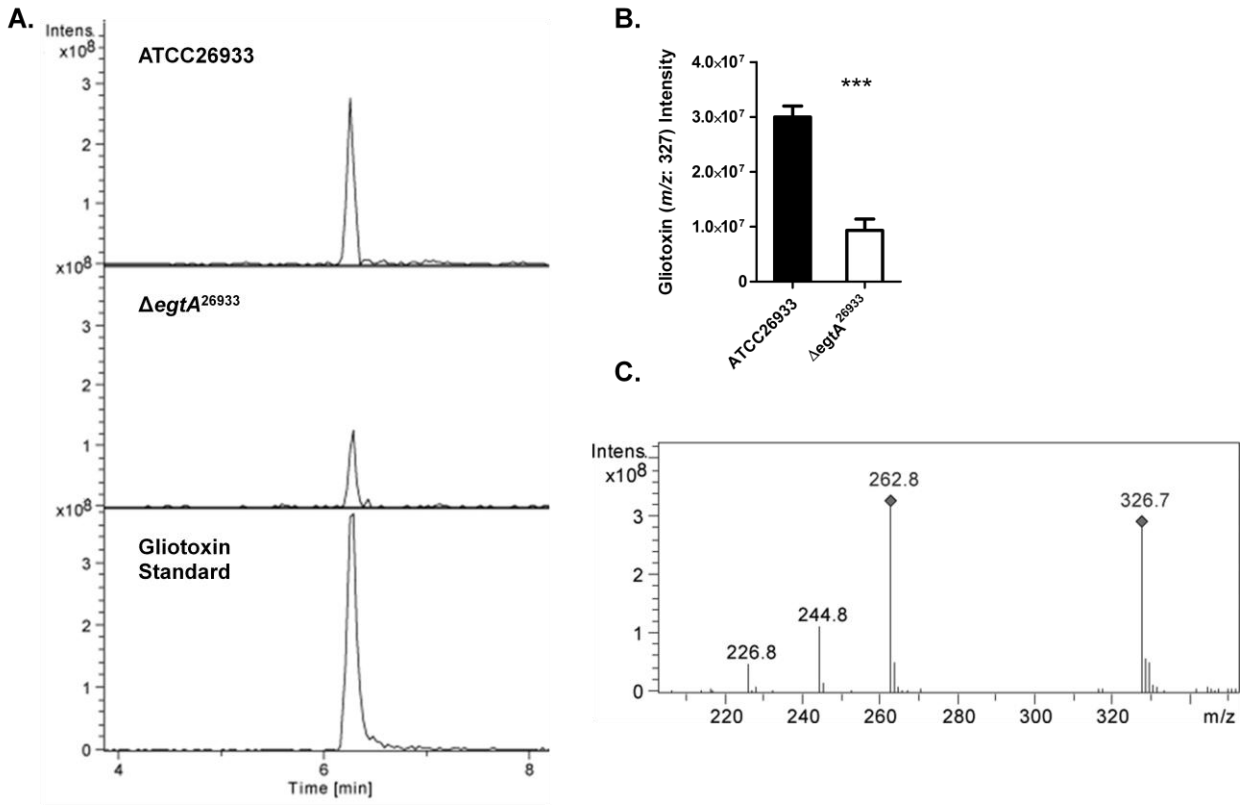

Figure 4.20. Gliotoxin detection via LC-MS/MS in ATCC26933 and Δ*egtA*^{26933}. (A) Extracted Ion Chromatographs (*m/z*: 327) following LC-MS/MS analysis of organic extracts of supernatants from ATCC26933 and Δ*egtA*^{26933}, in addition to a gliotoxin standard. A peak at 6.3 min was confirmed to be gliotoxin. (B) Comparison of gliotoxin peak intensity. Gliotoxin levels are significantly (P = 0.0002) reduced in Δ*egtA*^{26933} compared to ATCC26933. (C) Signature ion breakdown corresponding to gliotoxin.

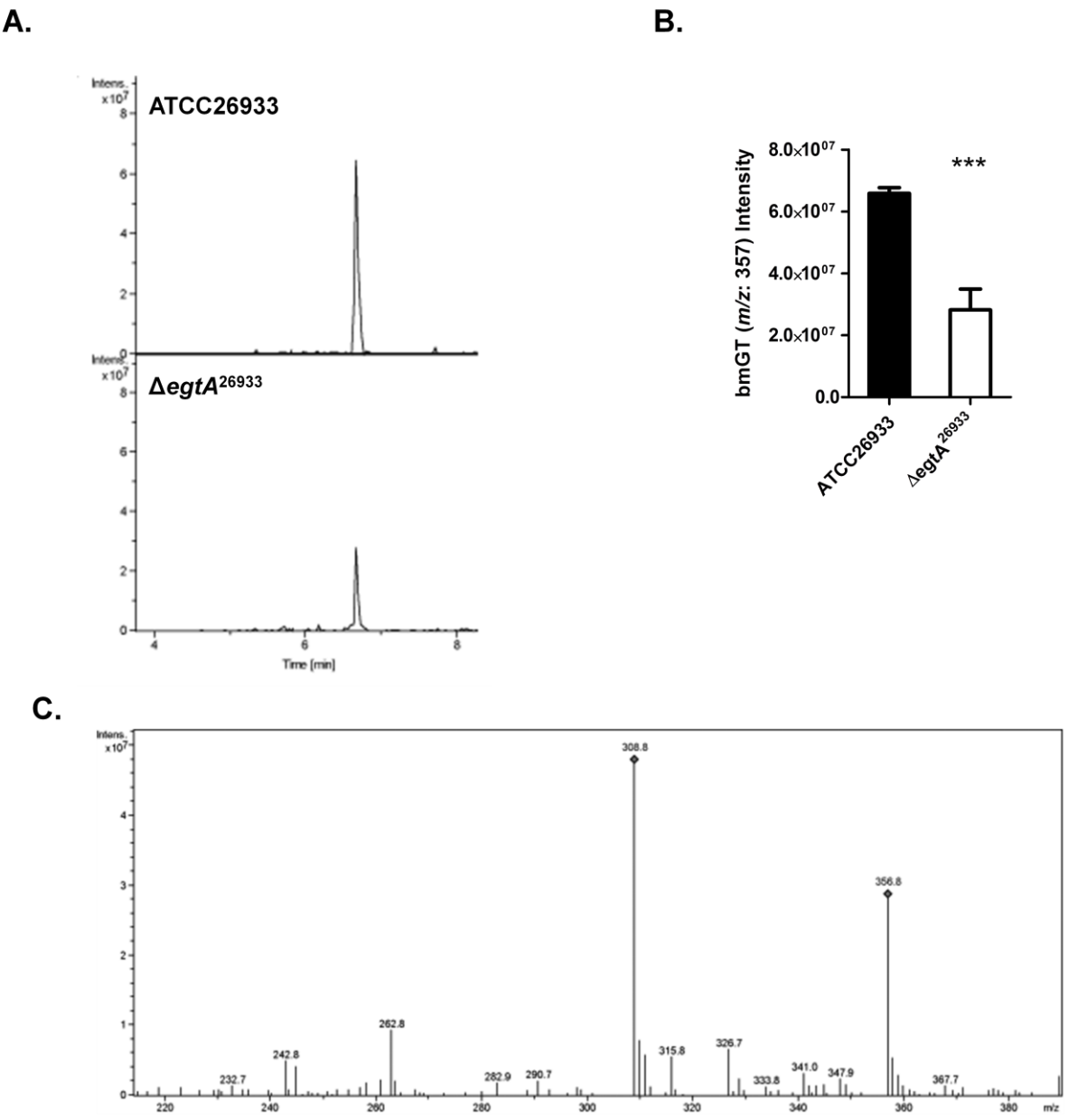

Figure 4.21. BmGT detection via LC-MS/MS in ATCC26933 and Δ*egtA*^{26933}. (A) Extracted Ion Chromatographs (*m/z*: 357) following LC-MS/MS analysis of organic extracts of supernatants from ATCC26933 and Δ*egtA*^{26933} A peak at 6.7 min was confirmed to be BmGT. (B) Comparison of BmGT (*m/z*:357) peak intensity. Levels of BmGT are significantly (P = 0.0371) reduced in Δ*egtA*^{26933} compared to ATCC26933. (C) Signature ion breakdown corresponding to BmGT (Domingo et al., 2012; Dolan et al., 2014).

4.2.10 Analysis of gliotoxin self-protection in ATCC26933 and Δ*egtA*^{26933}

4.2.10.1 Phenotypic analysis of ATCC26933 and Δ*egtA*^{26933} in response to gliotoxin

Continuing the investigation into the relationship between gliotoxin and EGT, gliotoxin sensitivity assays (Section 2.2.7) were performed in order to ascertain if EGT conferred any protection against gliotoxin. Sensitivity to gliotoxin was tested at a range of 0 – 20 µg/ml. Following 72 h growth, no significant difference in radial growth between ATCC26933 and Δ*egtA*^{26933} was observed at any concentration of gliotoxin (Figure 4.22). As Δ*egtA*^{26933} did not show any sensitivity towards gliotoxin, it was concluded that EGT has no role in gliotoxin self-protection in *A. fumigatus.*

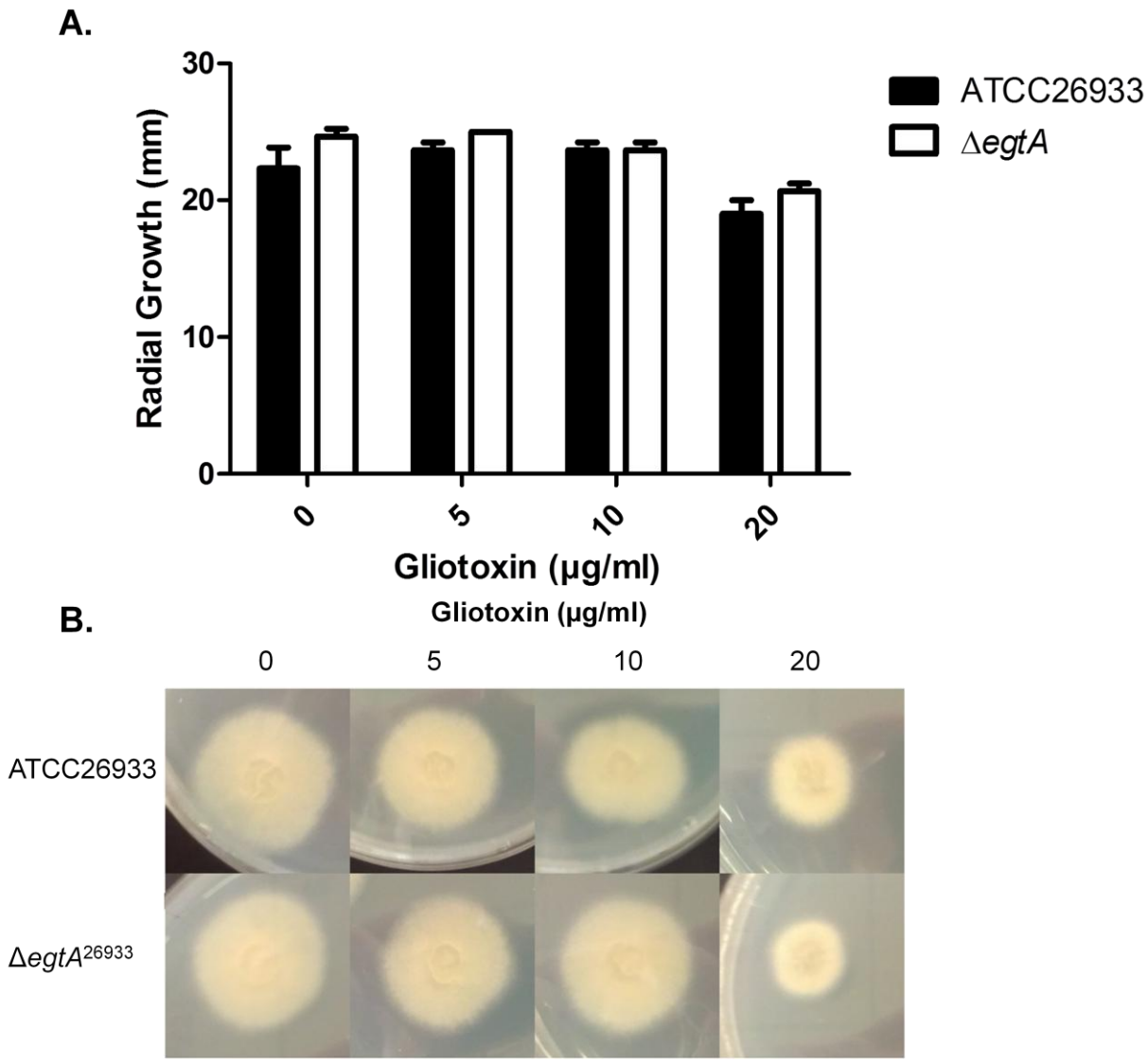

Figure 4.22. Gliotoxin sensitivity assay performed on AMM agar for 72 h to test for sensitivity to gliotoxin. (A) Comparison of the radial growth of ATCC26933 and Δ*egtA*26933 on AMM plates containing gliotoxin ranging from 0 to 20 μg/ml. No significant change in radial growth is observed for either strain at any concentration of gliotoxin (B) Images of ATCC26933 and Δ*egtA*^{26933} colonies on AMM plates containing 0 to 20 μg/ml gliotoxin. No visible differences in growth between the two strains can be observed at any concentration of gliotoxin tested.

4.2.10.2 Label-Free Quantitative Proteomic analysis demonstrates GliT induction in Δ*egtA*^{26933} following gliotoxin exposure

Label-free quantitative (LFQ) proteomic analysis was employed to investigate GliT induction following gliotoxin exposure in Δ*egtA*^{26933}. Quadruplicate Δ*egtA*^{26933} cultures in AMM were incubated for 69 h at 37 ^{o}C, 200 rpm shaking. Gliotoxin was added in duplicate to a final concentration of 5 µg/ml. An equivalent volume of methanol was added in duplicate. The cultures were then incubated as before for a further 3 h. Following this incubation, the mycelia were harvested from each culture and processed for Q-Exactive Mass Spectrometry analysis as per Section 2.2.14.1. Samples were then digested using sequencing grade trypsin (Section 2.2.14.4), purified, normalised and desalted using ZipTips ® (Section 2.2.14.5) and analysed on a Q-Exactive mass spectrometer (Section 2.2.14.6). 19 peptides for GliT were detected, with sequence coverage of 77.2 % (Figure 4.23). GliT underwent a $\log_2$ 1.14 fold increase in abundance in Δ*egtA*^{26933} exposed to gliotoxin compared to Δ*egtA*^{26933} exposed to methanol (P = 0.043). GliT is therefore induced by gliotoxin exposure in Δ*egtA*^{26933}.

MSIGKLLSNGALLVDVLIIGAGPAGLSTATGLARQLHTAVVFDSGVYRNAKTQHMHN
VLGWDHRNPAELRAAGRADLTTRYSTIQFQNSTIEAIRQVETNQLFEARDNEGHSWY
GRKVVLATGVRDIPLDIEGYSECWANGIYHCLFCDGYEERGQETVGVLALGPIANPA
RALHLARMALRLSESVTIYTNGNEQLAKEIQQAAEESPVGASGLKFEARPIRRFEKG
DVAKTVIVHLGESESKTEGFLVYNPQTEVNGPFAKQLALNMTEGGDILTTPPFYETS
VPGVFAVGDCATPLKAVTPAVSMGSLAAGGLVAQLQAQALPEFRLDQEL

Figure 4.23. The amino acid sequence for GliT, with detected peptides highlighted in red (19 peptides, 77.2 % coverage).

4.2.11 Analysis of conidiation in ATCC26933 and Δ*egtA*^{26933}

Colonies from Δ*egtA*^{26933} grown on AMM for 72 h exhibited visibly paler conidia compared to those of ATCC26933 (Figure 4.24A). Levels of conidiation in ATCC26933 and Δ*egtA*^{26933} were then measured via haemocytometry (Section 2.2.16). Conidiation levels in Δ*egtA*^{26933} were significantly lower (P = 0.0426) than those of ATCC26933 (Figure 4.24B). EGT absence appears to cause a reduction in conidiation levels in *A. fumigatus*, suggesting EGT may be involved in conidiation

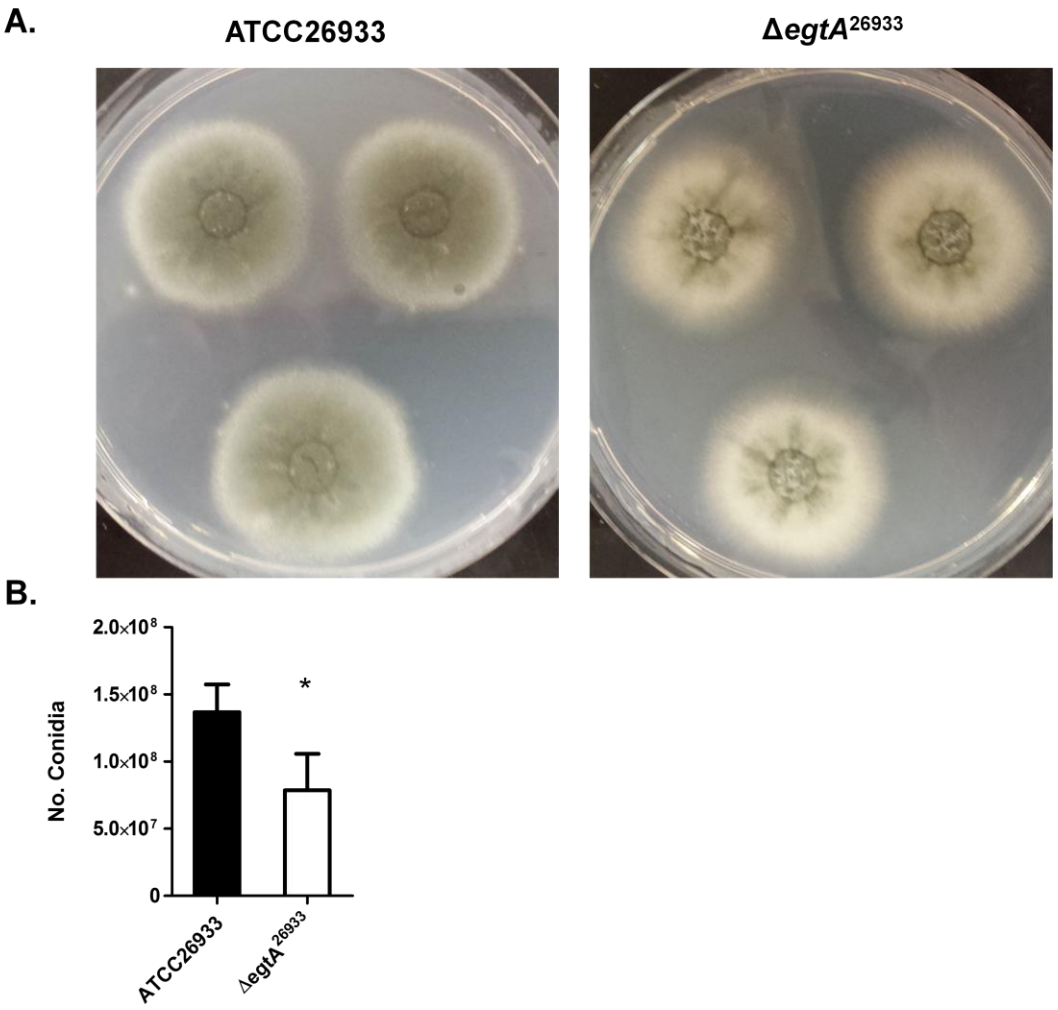

Figure 4.24. Conidiation in ATCC26933 and Δ*egtA*^{26933}. (A) Comparison of conidial colour and appearance in colonies reveal colonies from *egtA*^{26933} appear to produce paler conidia than the colonies of ATCC26933. (B) Comparison of conidiation levels from ATCC26933 and *egtA*^{26933}. Levels of conidiation are significantly (P = 0.0426) lower in *egtA*^{26933} compared to ATCC26933.

4.2.12 Phenotypic analysis of ATCC26933, Δ*egtA*^{26933} and *egtA*^{C26933} in response to cell wall perturbing agents

4.2.12.1 Phenotypic analysis of ATCC26933, Δ*egtA*^{26933} and *egtA*^{C26933} in response to congo red

Sensitivity to congo red was tested at a range of 0 – 50 µg/ml as per Section 2.2.7. Δ*egtA*^{26933} demonstrated a significant decrease in radial growth compared to ATCC26933 and *egtA*^{C26933} at 30 µg/ml (P = 0.0132), 40 µg/ml (P = 0.0014) and 50 µg/ml (P = 0.0046) congo red. Yet, no significant difference radial growth was observed at 0 – 20 µg/ml congo red (Figure 4.25). Absence of EGT therefore results in sensitivity to congo red. This indicates that *egtA* deletion may cause alterations to the composition of the fungal cell wall.

4.2.12.2 Phenotypic analysis of ATCC26933, Δ*egtA*^{26933} and *egtA*^{C26933} in response to calcofluor white

Sensitivity to calcofluor white (CFW) was tested at a range of 0 – 100 µg/ml as per Section 2.2.7. Δ*egtA*^{26933} demonstrated a significant decrease in radial growth compared to ATCC26933 and *egtA*^{C26933} at 60 µg/ml (P = 0.0155), 80 µg/ml (P = 0.0249) and 100 µg/ml (P = 0.0001) CFW. No significant difference in radial growth was observed at 0 – 40 µg/ml CFW (Figure 4.26). Absence of EGT therefore results in sensitivity to CFW. This further indicates that *egtA* deletion may cause significant changes to the cell wall in *A. fumigatus*.

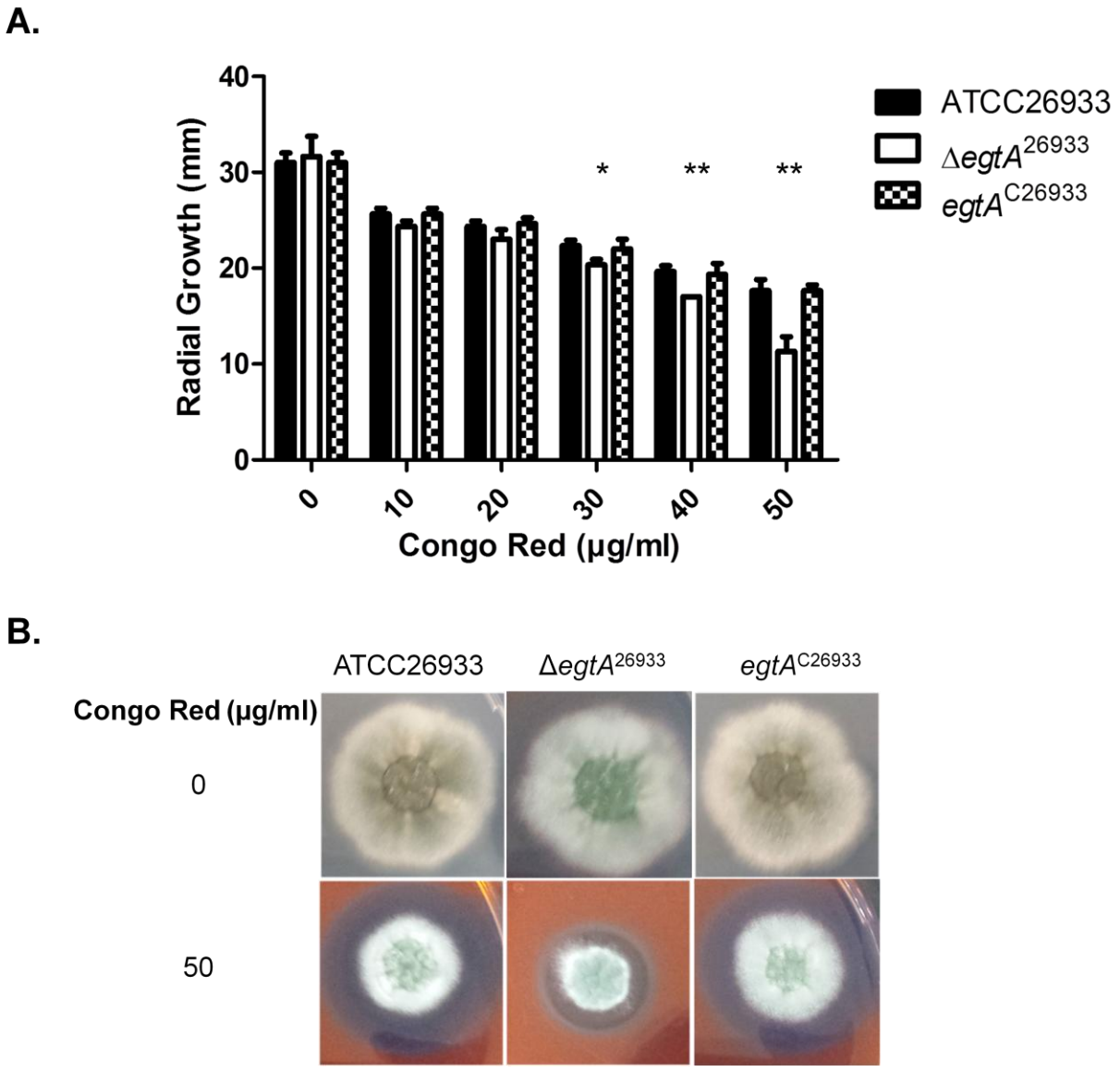

Figure 4.25. Congo red sensitivity assay performed on AMM for 72 h. (A) Comparison of radial growth of ATCC26933, Δ*egtA*^{26933} and *egtA*^{C26933} on AMM agar plates containing 0 - 50 µg/ml congo red. Δ*egtA*^{26933} shows a significant decrease in radial growth compared to ATCC26933 and *egtA*^{C26933} when grown at 30 µg/ml (P = 0.0132), 40 µg/ml (P = 0.0014) and 50 µg/ml (P = 0.0046) congo red. (B) Images of ATCC26933, Δ*egtA*^{26933} and *egtA*^{C26933} colonies on 0 and 50 µg/ml congo red. A visible decrease in the size of the Δ*egtA*^{26933} colony can be observed compared to the ATCC26933 and *egtA*^{C26933} colonies at 50 µg/ml congo red.

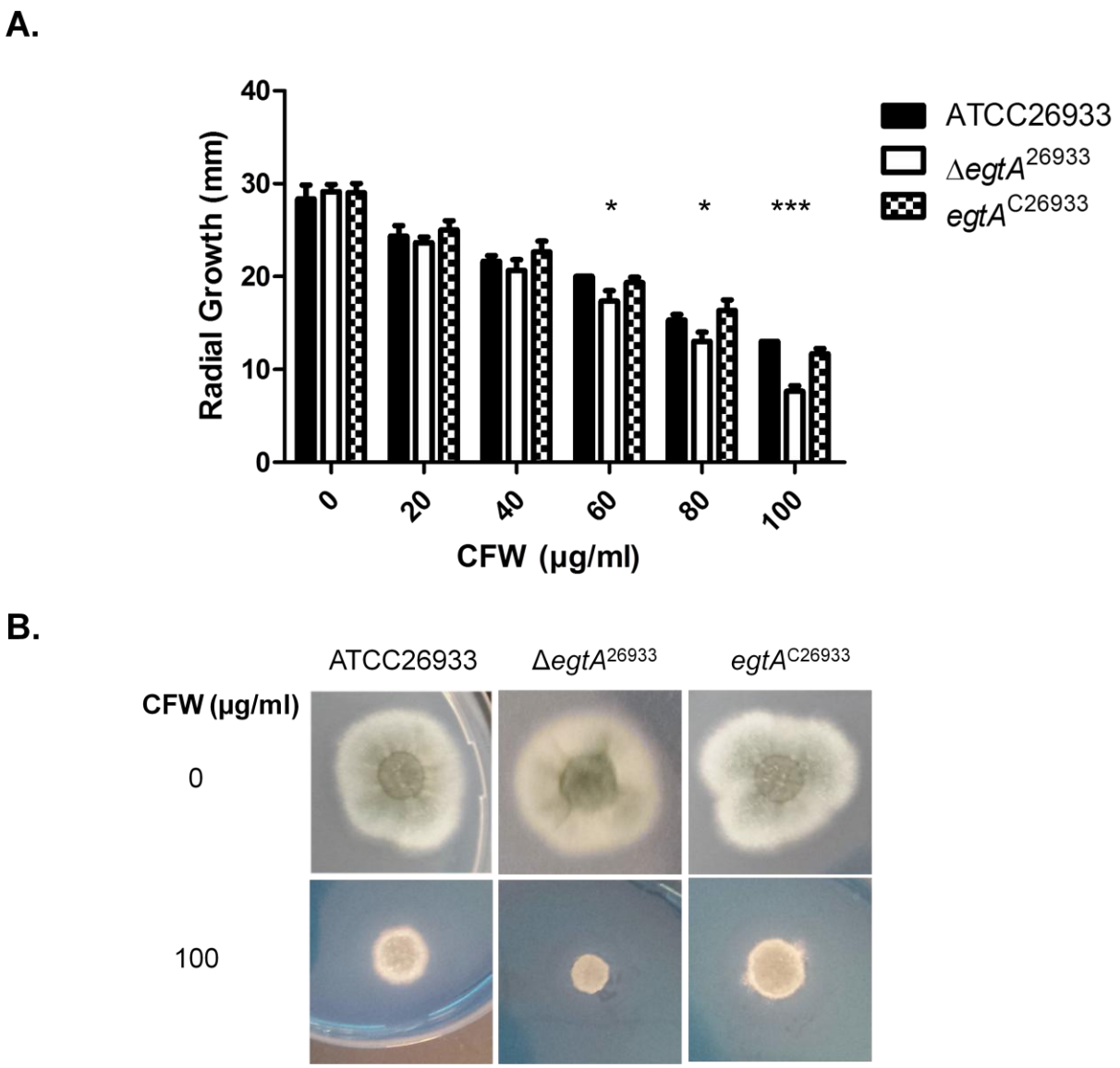

Figure 4.26. CFW sensitivity assay performed on AMM for 72 h. (A) Comparison of radial growth of ATCC26933, Δ*egtA*^{26933} and *egtA*^{C26933} on AMM agar plates containing 0 - 100 µg/ml CFW. Δ*egtA*^{26933} shows a significant decrease in radial growth compared to ATCC26933 and *egtA*^{C26933} when grown at 60 µg/ml (P = 0.0155), 80 µg/ml (P = 0.0249) and 100 µg/ml (P = 0.0001) CFW. (B) Images of ATCC26933, Δ*egtA*^{26933} and *egtA*^{C26933} colonies on 0 and 100 µg/ml CFW. A visible decrease in the size of the Δ*egtA*^{26933} colony can be observed compared to the ATCC26933 and *egtA*^{C26933} colonies at 100 µg/ml CFW.

4.2.13 Analysis of *N. tabacum* L. cv. Petit Havana:*egtA*:*nfs1*

EGT is taken up by plants from symbiotic microorganisms (Park et al., 2010), however little data is available on the function of EGT in plants. In order to address this, an *N. tabacum* strain transformed with *A. fumigatus egtA* and *nfs1* was generated by Prof. Phil Dix, Dr. Peter Medgyesy and Dr. Éva Horvath (Maynooth University). By generating a *N. tabacum* strain capable of biosynthesising EGT, EGT function in plants could be characterised. It was thus necessary to verify the presence of EgtA and Nfs1 proteins in *N. tabacum* leaf lysates via Q-Exactive mass spectrometry. Furthermore, LC-MS/MS analysis was undertaken to investigate if EGT biosynthesis had occurred in the transformed *N. tabacum* strain.

4.2.13.1 Proteomic Analysis of *N. tabacum* L. cv. Petit Havana:*egtA*:*nfs1*

Cell lysates from leaves of wild-type L. cv. Petit Havana and L. cv. Petit Havana:*egtA*:*nfs1* were obtained as per Section 2.2.14.2. Lysates were then concentrated, washed, reduced and alkylated as per Section 2.2.14.3. Samples were then trypsin digested (Section 2.2.14.4), purified, normalised and desalted using ZipTips ® (2.2.14.5) and analysed by Q-Exactive mass spectrometry (Section 2.2.14.6). Q-Exactive analysis failed to identify EgtA or Nfs1 peptides in either sample. This suggests that the EgtA and Nfs1 proteins are absent or are below the levels of detection in L. cv. Petit Havana:*egtA*:*nfs1*.

4.2.13.2 EGT analysis in *N. tabacum* L. cv. Petit Havana:*egtA*:*nfs1*

Lysate supernatants from leaves of wild-type L. cv. Petit Havana and L. cv. Petit Havana:*egtA*:*nfs1* were obtained as per Section 2.2.14.2. Lysate supernatants were then filtered through an Amicon 3 kDa centrifuge filter (Section 2.2.12.4) and the filtrate collected. Lysate filtrates were then alkylated (Section 2.2.12.1), TCA precipitated (Section 2.2.12.2) and analysed via LC-MS/MS (Section 2.2.12.7). In addition, an EGT standard alkylated with 5'-IAF and TCA precipitated as before was analysed in the same manner. 5'-IAF alkylated EGT eluted at 7.5 min, with an *m/z* of 617. Extracted ion chromatograms (*m/z*: 617) for wild-type L. cv. Petit Havana and L. cv. Petit Havana:*egtA*:*nfs1* demonstrate that EGT is absent in the wild-type strain and present in the transformed strain (Figure 4.27). Transformation of *N. tabacum* with *egtA* and *nfs1* therefore confers the ability to biosynthesise EGT.

A.

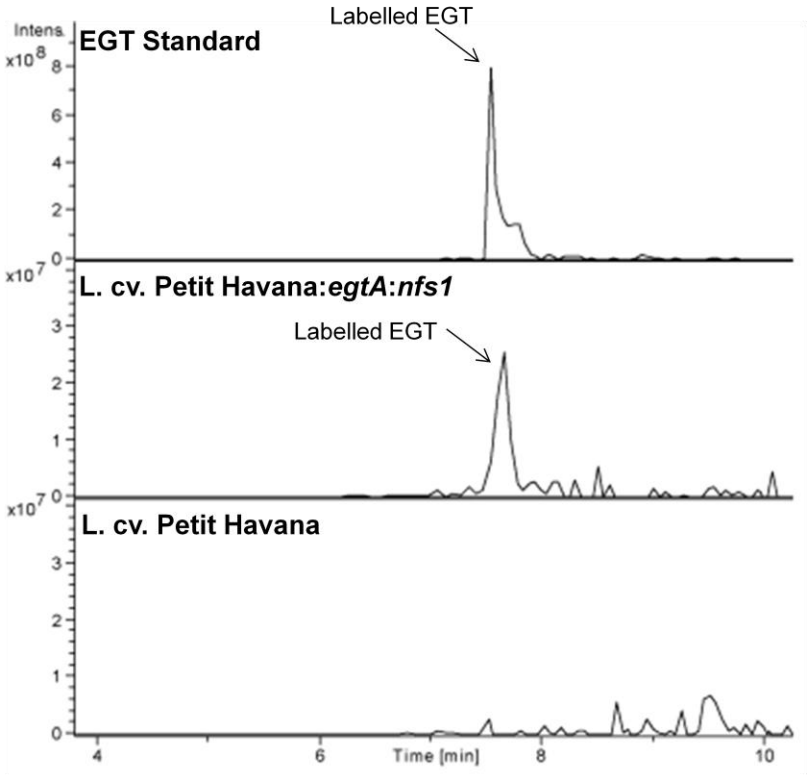

B.

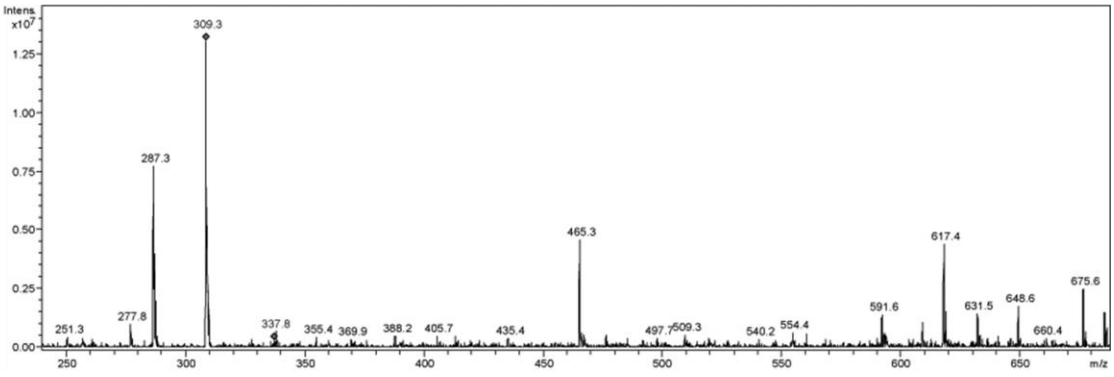

Figure 4.27. Detection of alkylated EGT in L. cv. Petit Havana:*egtA*:*nfs1*. (A) Extracted Ion Chromatographs (*m/z*: 617) for wild-type L. cv. Petit Havana and L. cv. Petit Havana:*egtA*:*nfs1*, in addition to an EGT standard. A peak at 7.5 min in the transformed strain was confirmed to be EGT. This peak was absent from the wild-type strain. (B) Signature Ion breakdown corresponding to 5'-IAF alkylated EGT (Gallagher et al., 2012) in L. cv. Petit Havana:*egtA*:*nfs1*.

4.3 Discussion

This chapter presents the work done to investigate the function of *A. fumigatus egtA*, as well as the role of EGT in *A. fumigatus* ATCC26933. *egtA* was demonstrated to be essential for EGT biosynthesis, facilitating investigation into the role of the metabolite in *A. fumigatus*. EGT absence resulted in sensitivity to high concentrations of H_2O_2 and menadione, confirming a role for EGT as an antioxidant in *A. fumigatus*. GSH levels in the ATCC26933 background increased following EGT deletion, but the same effect was not observed in the AfS77 background. However GSH/GSSG ratios were similarly altered in both backgrounds. EGT loss also had an impact on apparently unrelated systems, with gliotoxin levels significantly reduced, levels of conidiation attenuated and sensitivity to cell wall perturbing agents observed in Δ*egtA*^{26933}.

RP-HPLC and LC-MS/MS analysis was employed to investigate the effect of *egtA* deletion and complementation on EGT production in *A. fumigatus* ATCC26933. No EGT was in *egtA*^{26933}, while reinsertion of the gene restored EGT production in *egtA*^{C26933}. Thus *egtA* was shown to be essential for EGT production in *A. fumigatus*. Interestingly, EGT production in *egtA*^{C26933} was elevated compared to ATCC26933. This may be due to differences in gene regulation due to *egtA* reinsertion outside of its natural locus in *egtA*^{C26933}. This data demonstrates unambiguously that *egtA* is essential for EGT biosynthesis and represents the first targeted deletion of an EGT biosynthetic gene in fungi as previous work from Bello et al. (2012) and Pluskal et al. (2014) utilised mutants obtained from deletion libraries. Furthermore, *A. fumigatus* Δ*egtA* represents the first EGT null mutant in the *Aspergillus* spp. and the first EGT deletion mutant in a fungal pathogen of humans.

Δ*egtA*^{26933}, alongside ATCC26933 and *egtA*^{C26933}, was subjected to oxidative stress via H_2O_2, menadione and diamide assay for sensitivity to elevated ROS. The role of EGT as antioxidant in fungi is unclear. *egt-1* deletion in *N. crassa* caused no sensitivity to Cu^{2+} or menadione, however *N. crassa* conidia showed sensitivity to 2 mM *tert*-butyl hydroperoxide (Bello et al., 2012). In *S. pombe*, an *egt1* deletion mutant showed no deleterious effects when exposed to hydrogen peroxide (0 – 2 mM) and *tert* -butyl hydroperoxide (0 – 0.5 mM) (Pluskal et al., 2014). Plate assays for H_2O_2 with ATCC26933, Δ*egtA*^{26933} and *egtA*^{C26933} revealed Δ*egtA*^{26933} was sensitive to H_2O_2 compared to the wild-type and complemented strains at a concentration of 3 mM only. At 1 mM and 2 mM H_2O_2, no difference between the three strains was observed, however at 3 mM,

radial growth of Δ*egtA*^{26933} was reduced dramatically. None of the three strains were capable of growth at 4 mM, suggesting 3 mM H_2O_2 is approaching the limit of H_2O_2 that wild-type *A. fumigatus* can tolerate. Thus it appears that EGT absence is deleterious only at very high levels of H_2O_2. In testing menadione sensitivity, it was found that Δ*egtA*^{26933} was significantly sensitive compared to ATCC26933 and *egtA*^{C26933} at concentrations of 40 µM and 60 µM. At 20 µM, no difference between the 3 strains was observed. This suggests EGT has an important role in protection from superoxide radicals in *A. fumigatus*, however it may not be the primary mechanism of defence. No significant differences were observed in any of the strains following diamide exposure. This indicates that EGT does not confer protection against diamide-mediated GSH depletion, which may be due to the elevated levels of GSH observed.

The role of EGT in oxidative stress defence was further illustrated by fluorescence analysis using H_2DCFDA. H_2DCFDA is used as an indicator of ROS levels via fluorescence, allowing for the measurement of ROS levels in *A. fumigatus* mycelia. Upon exposure to 3 mM H_2O_2, ROS levels in Δ*egtA*^{26933} were found to be significantly elevated compared to ATCC26933. This demonstrates that EGT functions to dissipate ROS in *A. fumigatus* and its absence in Δ*egtA*^{26933} leads to elevated ROS and impaired growth as observed in the H_2O_2 plate assay. Interestingly, under basal conditions, Δ*egtA*^{26933} displayed lower levels of ROS than ATCC26933. This suggests compensatory mechanisms may be in place consequent to EGT loss. The results of the oxidative stress testing, combined with fluorescent microscopy using H_2DCFDA, show that EGT functions as an antioxidant in *A. fumigatus*. However, high levels of induced stress, particularly with H_2O_2, were necessary to show the effects of EGT loss. This indicates that EGT is important for detoxifying high levels of ROS in *A. fumigatus*. This could be due to the physical properties of EGT, which confer increased stability compared to other low molecular mass thiols such as GSH (Cheah and Halliwell, 2012). It may be that EGT is not essential for detoxifying low levels of ROS as it can be effectively dissipated by other facets of the oxidative stress defence system. At high levels of ROS, when these other components of the oxidative stress defence system have been exhausted, EGT is then available to dissipate the remaining ROS. Thus EGT may be an "antioxidant of last resort".

The elucidation of EGT function as an antioxidant in *A. fumigatus* may help explain in part the rise in intracellular EGT observed by Gallagher et al. (2012) in Δ*gliK*. *A. fumigatus* Δ*gliK*

displayed sensitivity to H_2O_2, suggesting *gliK* deletion leaves *A. fumigatus* vulnerable to elevated levels of ROS. The increase in EGT observed may be a counter-measure to try and combat this sensitivity. If this is the case, it could explain the inability to generate a Δ*egtA::*Δ*gliK* double mutant. EGT may be essential for maintaining redox homeostasis following the deletion of *gliK*, which would explain the observed rise of intracellular EGT in Δ*gliK*. If this is the case, concurrent absence of EgtA and GliK would not be viable. This would further underline the importance of EGT as an antioxidant in *A. fumigatus*.

egtA response to H_2O_2 was demonstrated via qRT-PCR. *A. fumigatus* ATCC26933 exposed to 3 mM H_2O_2 showed elevated *egtA* expression in comparison to control conditions. Relevantly, Northern blot analysis has demonstrated that *egtA* expression is increased following exposure to 1 mM H_2O_2, signifying that low levels of ROS are capable of inducing *egtA* expression (Sheridan et al., 2016). This would suggest that EGT levels are increased in response to elevated ROS, which might be expected given that EGT has been demonstrated to function as an antioxidant in *A. fumigatus*. However this was not the case, as RP-HPLC analysis demonstrated that EGT levels showed a non-significant drop following H_2O_2 exposure. While this result was unexpected, analysis of EGT-H_2O_2 interaction provided an explanation. Co-incubation of EGT and H_2O_2 resulted in decreased EGT levels when measured by RP-HPLC, which suggests that EGT reactivity with ROS dissipates the antioxidant. This is consistent with data from Servillo et al. (2015) who demonstrated EGT degradation into hercynine and sulphurous acid upon oxidation (Figure 4.28). Thus it appears that *egtA* expression rises in response to H_2O_2 in order to maintain EGT levels, as they are dissipated by elevated ROS. Note that different media was used for the qRT-PCR and EGT analyses. Sabouraud Dextrose broth was used for the qRT-PCR analysis in order to facilitate hyphal growth. Czapeck-Dox broth was used for EGT analysis to facilitate optimal EGT production.

Analysis of total GSH levels and GSH/GSSG ratio in ATCC26933, Δ*egtA*^{26933} and *egtA*^{C26933} was carried out to investigate if *egtA* deletion affected GSH biosynthesis or cellular redox status. GSH and EGT are linked metabolically as cysteine provides the thiol group in both metabolites. Furthermore, EGT and GSH are redox active molecules that form part of the oxidative stress defence system. Thus EGT absence may result in alterations to GSH metabolism and redox state.

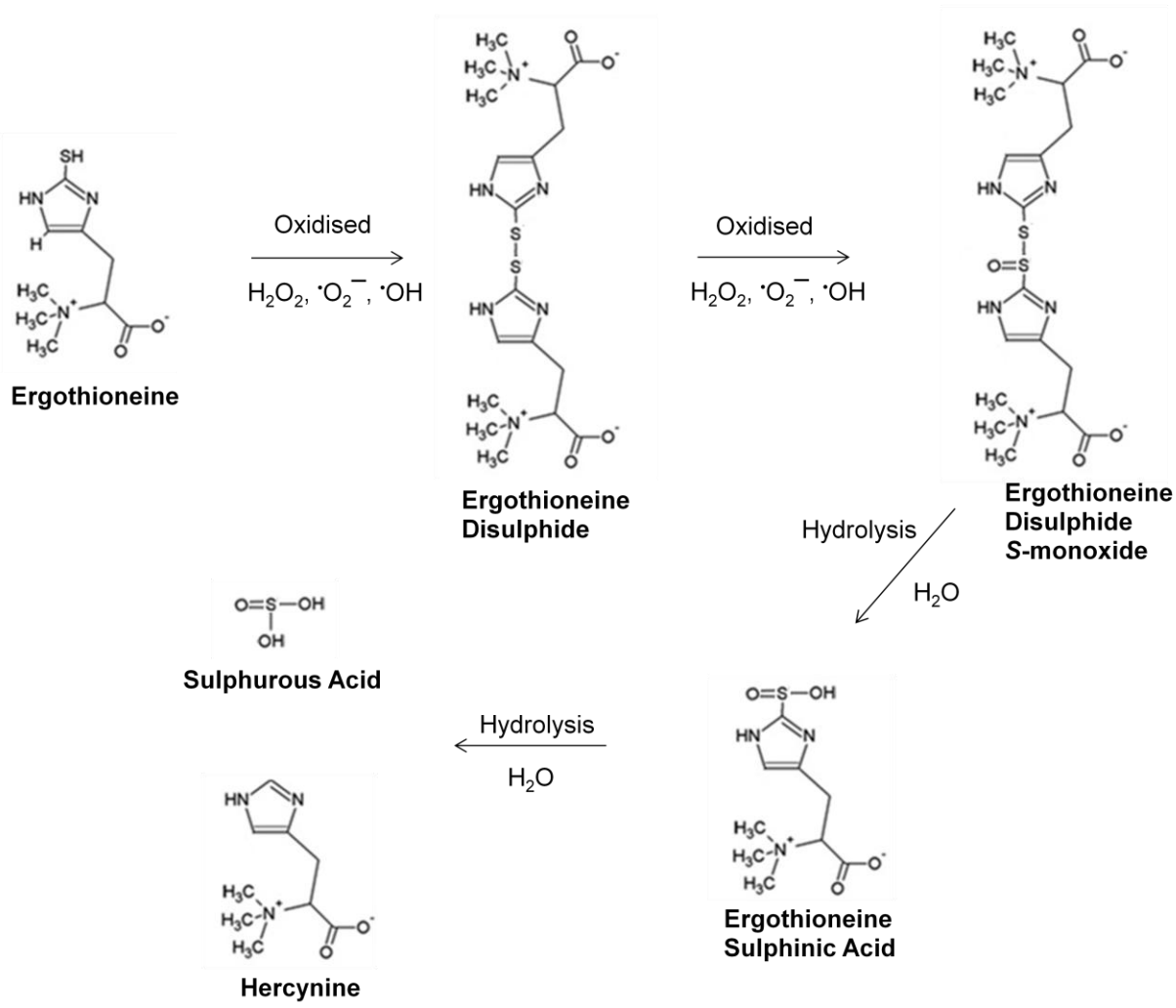

Figure 4.28. The oxidative degradation pathway of EGT. Upon oxidation, EGT forms EGT disulphide, which undergoes further oxidation to form EGT disulphide *S*-monoxide. EGT disulphide *S*-monoxide is then hydrolysed to form the unstable intermediate EGT sulphinic acid. EGT sulphinic acid is degraded rapidly to yield hercynine and sulphurous acid (Servillo et al., 2015).

Measurement of total GSH by LC-MS/MS revealed total GSH levels were significantly elevated in Δ*egtA*^{26933} and returned to wild-type levels in *egtA*^{C26933}. EGT loss therefore appears to lead to an increase in total GSH. This is likely to compensate for the loss antioxidant potential resulting from EGT absence. Measuring the GSH/GSSG ratios of ATCC26933, Δ*egtA*^{26933} and *egtA*^{C26933} revealed a rise in the GSH/GSSG ratio in Δ*egtA*^{26933}. This suggests that Δ*egtA*^{26933} is under less oxidative stress than the wild-type or complemented strain. This may be due to the increase in total GSH observed and would explain the lower levels of ROS observed in Δ*egtA*^{26933} through

fluorescent microscopy under basal conditions. Alternatively, EGT absence may leads to increased oxidative stress, prompting the increase in total GSH observed, resulting in an increase in GSH/GSSG ratio.

Comparison of total glutathione levels in Δ*egtA*^{26933} and Δ*egtA*^{AfS77} and their respective background strains revealed an intriguing difference between the strains. While *egtA* deletion in ATCC26933 led to a significant elevation in total glutathione, the same effect was not observed in Δ*egtA*^{AfS77}, where no significant change in total GSH was observed. Interestingly, the basal levels of total GSH in the two wild-type strains were significantly different. Total glutathione levels in ATCC26933 were observed to be significantly lower than those of AfS77. This may explain the need to increase total glutathione following *egtA* deletion in ATCC26933, but not in AfS77. Analysis of GSH/GSSG ratios in the AfS77 background strains revealed a similar pattern in ratio change to ATCC26933. Like ATCC26933, *egtA* deletion led to an increase in GSH/GSSG ratio, while complementation lowered GSH/GSSG ratio. This suggests that loss of EGT has a similar effect on GSH redox state across the two background strains, even though total GSH levels differ.

EGT was observed to be elevated in *A. fumigatus* Δ*gliK* (Gallagher et al., 2012), the first identification of EGT in *A. fumigatus*. GliK catalyses a *bis*-glutamyl elimination step in gliotoxin biosynthesis, following double thiolation with GSH. GliK is essential for gliotoxin biosynthesis and *gliK* deletion results in abrogation of gliotoxin production (Gallagher et al., 2012; Scharf et al., 2013). Furthermore, Δ*gliK* exhibited sensitivity to exogenous gliotoxin. The reason for this sensitivity remains to be fully elucidated, however it has been demonstrated that GliT induction following exogenous gliotoxin exposure is decreased in Δ*gliK* compared to wild-type (Gallagher et al., 2012; Owens et al., 2015). GliT is important for gliotoxin self-protection and induction of GliT following exogenous gliotoxin exposure forms part of the self-protection mechanism (Schrettl et al., 2010; Scharf et al., 2010). In order to investigate if increased levels of EGT in Δ*gliK* were linked to concurrent abrogated gliotoxin biosynthesis and sensitivity to exogenous gliotoxin, gliotxin biosynthesis and self-protection were analysed in Δ*egtA*^{26933}. Gliotoxin analysis was carried out via RP-HPLC and LC-MS/MS on organic extracts from ATCC26933 and Δ*egtA*^{26933}. Δ*egtA*^{26933} was still capable of producing gliotoxin, however levels of gliotoxin were significantly lower than wild-type. Furthermore, LC-MS/MS analysis revealed BmGT was

also reduced in Δ*egtA*^{26933} compared to ATCC26933. This suggests that EGT loss is deleterious to gliotoxin production. Another explanation is that gliotoxin production could be curtailed in order to increase total GSH. GSH is essential for gliotoxin biosynthesis (Davis et al., 2011; Scharf et al., 2011), and in order to increase total GSH as observed in Δ*egtA*^{26933}, GSH may be diverted from gliotoxin biosynthesis. No sensitivity to gliotoxin was observed in Δ*egtA*^{26933} compared to ATCC26933. Furthermore, GliT was demonstrated to be induced by exogenous gliotoxin in Δ*egtA*^{26933}. This indicates that the gliotoxin self-protection mechanism remains intact in the absence of EGT. Therefore EGT appears to have no role in self-protection against gliotoxin.

Absence of EGT in *A. fumigatus* was demonstrated to result in alterations to conidia. Δ*egtA*^{26933} colonies exhibited paler conidia in comparison to ATCC26933. Furthermore, levels of conidiation in Δ*egtA*^{26933} were reduced compared to ATCC26933. EGT therefore appears to function in promoting conidiation and conidial health in *A. fumigatus*. This may occur through the management of ROS levels. ROS is well known to function as a signaling agent and it has been demonstrated influence cellular differentiation, virulence and hyphal growth in fungi (Breitenbach et al, 2015). Relevantly, ROS has been linked with conidiation in *Epichloë festucae* (Kayano et al, 2013). Thus, perturbations in ROS levels due to EGT absence may result in altered conidiation as observed. EGT has also been demonstrated to function in conidial protection and conidiogenesis in *N. crassa* (Bello et al., 2012, 2014).

EGT absence in *A. fumigatus* was demonstrated to result in sensitivity to cell wall perturbing agents. Δ*egtA*^{26933} was significantly sensitive to congo red compared to ATCC26933 and *egtA*^{C26933} at concentrations of 30, 40 and 50 µg/ml. Δ*egtA*^{26933} was also significantly sensitive to CFW compared to ATCC26933 and *egtA*^{C26933} at concentrations of 60, 80 and 100 µg/ml. Both congo red and CFW disrupt cell wall biosynthesis by inhibiting chitin and β(1,3)-glucan biosynthesis (Roncero and Duran, 1985). This indicates that *egtA* deletion causes alterations to cell wall biosynthesis in *A. fumigatus*, resulting in the observed sensitivity to congo red and CFW. As with conidiation, this may be due to changes in ROS signalling, as ROS has been demonstrated to regulate cell wall biosynthesis in plants (Kärkönen and Kuchitsu, 2015).

Analysis of a *N. tabacum* L. cv. Petit Havana strain transformed with *A. fumigatus egtA* and *nfs1* was undertaken in order to investigate EGT biosynthesis in an organism than cannot synthesise

EGT naturally. Proteomic analysis failed to detect the presence of either EgtA or Nfs1 proteins. Despite this, EGT was still detected in L. cv. Petit Havana:*egtA*:*nfs1* lysate filtrates at low levels and demonstrated to be absent in wild-type *N. tabacum*. Thus, EGT was demonstrated to be biosynthesised in *N. tabancum* L. cv. Petit Havana:*egtA*:*nfs1*. This was unexpected given that EgtA and Nfs1 were not detected via proteomic analysis, and this suggests that the abundance of EgtA and Nfs1 in L. cv. Petit Havana:*egtA*:*nfs1* is below the threshold of detection. This demonstrates that detectable levels of EGT can still be catalysed by enzymes at very low abundance. Moreover, this data emphasises the role of *egtA* in EGT biosynthesis and supports the hypothesis that *nfs1* also may contribute to EGT biosynthesis. Furthermore, confirmation of EGT expression in *N. tabacum* L. cv. Petit Havana:*egtA*:*nfs1* represents an important step in the generation of a system for studying EGT function in organisms that ordinarily acquire EGT from the environment.

To summarise, *egtA* was confirmed as an essential gene for EGT biosynthesis. EGT provides a protective role against high levels of H_2O_2- and menadione-induced oxidative stress. *egtA* levels increase in response to 3 mM H_2O_2 in order to maintain EGT levels as it is dissipated in detoxifying H_2O_2. Total GSH levels are significantly increased following *egtA* deletion in ATCC26933, but not AfS77. This may be due to the differences in the basal levels of total GSH between the two background strains. Loss of EGT leads to reduced gliotoxin production, but gliotoxin self-protection functions at the same level as wild-type. EGT absence also leads to changes in conidiation and cell wall biosynthesis. Expression of *egtA* and *nfs1* in *N. tabacum* led to the detection of EGT in plant lysate filtrates, even though presence of the two proteins was too low to detect.

This data presents the first characterisation of EGT biosynthesis and function in *A. fumigatus*. In addition to contributing to oxidative stress defence, EGT influences gliotoxin biosynthesis, GSH biosynthesis, conidiation and cell wall integrity. In order to further assess the global systems impact of EGT absence, ATCC26933 and $\Delta egtA^{26933}$ were investigated via label-free quantitative (LFQ) proteomic analysis, as presented in Chapter 5.

Chapter 5

Comparative LFQ Proteomic Analysis

of *A. fumigatus* ATCC26933 and Δ*egtA*^{26933}

5.1 Introduction

Chapter 4 demonstrated the importance of *A. fumigatus* Δ*egtA*^{26933} as a system for investigating EGT functionality in *A. fumigatus*. In the absence of *egtA*, EGT production was abrogated and led to the observation of phenotypes such as oxidative stress sensitivity, increased GSH production, decreased gliotoxin biosynthesis, reduced levels of conidiation and alterations to cell wall biosynthesis. In this chapter, Δ*egtA*^{26933} is further analysed via comparative label-free quantitative (LFQ) proteomics. A comparison of the ATCC26933 proteome to that of the Δ*egtA*^{26933} proteome would elucidate the effect of EGT loss the *A. fumigatus* proteome. As well as analysing the two strains under basal conditions, both strains were analysed under ROS inducing conditions. 3 mM H_2O_2 was used to induce ROS as it has been demonstrated to result in reduced radial growth in Δ*egtA*^{26933} compared to ATCC26933. Furthermore, *egtA* expression was induced by exposure to 3 mM H_2O_2 in ATCC26933. For these reasons, comparative LFQ proteomics was undertaken on ATCC26933 and Δ*egtA*^{26933} cultures exposed to 3 mM H_2O_2 to gain a greater insight into how *A. fumigatus* responds to high levels of ROS in the absence of EGT.

Comparative proteomics aims to investigate changes at a proteome level in different strains (e.g. wild-type and mutant) or strains grown in different conditions (e.g. ± oxidative stress, hypoxia, antibiotic presence, etc (Lessing et al., 2007; Gautam et al., 2008; Vodisch et al., 2011). By identifying proteins with differential abundance or that are present/absent in one sample compared to the other, the effect of a mutation or growth condition on an organism can be inferred. The "classic" proteomic strategy involved the separation of proteins by 2D-polyacrylamide gel electrophoresis (2D-PAGE) followed by identification of spots by mass spectrometry (Carberry and Doyle, 2007). However advances in high resolution mass spectrometry have led to the use of LFQ proteomics (Zhu et al., 2009). This involves analysis of trypsin-digested whole cell protein lysates using a high resolution mass spectrometer, such as Thermo-Fisher's Q-Exactive Hybrid-Quadrupole Orbitrap (Scheltema et al., 2014), which was used in this study. One advantage of the LFQ proteomic strategy over the classic 2D-PAGE strategy is the increase in sensitivity; LFQ proteomic analysis has a three- to four-fold increase in protein dynamic range compared to 2D-PAGE strategies (Wang et al., 2008). Therefore, LFQ proteomics, using high resolution mass spectrometry, allows for the detection of low abundance

proteins that would not be detected via 2D-PAGE. Furthermore, detection of proteins that are very hydrophobic, contain transmembrane regions, have a larger molecular mass or have an extreme p*I* can be limited by 2D-PAGE (Bantscheff et al., 2007). For these reasons, LFQ proteomics allows for greater depth of analysis compared to 2D-PAGE combined with mass spectrometry.

Comparative proteomics has been utilised in the study of *A. fumigatus* numerous times to investigate proteomic response to a range of conditions. Investigation of *A. fumigatus* under different growth conditions such as oxidative stress (Lessing et al., 2007), hypoxia (Vodisch et al., 2011), heat shock (Albrecht et al., 2010) and gliotoxin exposure (Schrettl et al., 2010) has revealed essential processes in response to their respective conditions. Owens et al. (2014) utilised comparative proteomics to investigate *A. fumigatus* response to co-incubation with H_2O_2 and gliotoxin. Proteomic analysis has also been employed to investigate *A. fumigatus* response to antifungal drugs, including amphotericin B (Gautam et al., 2008), coumarin (Singh et al., 2012) and caspofungin (Cagas et al., 2011) with the aim of elucidating the molecular mechanisms of the drugs and identifying novel target pathways. Proteomic analysis can be used to investigate specific cellular components, such as the cell wall, secretome and conidia (Bruneau et al., 2001; Singh et al., 2010; Teutschbein et al., 2010). Moloney et al. (2016) investigated the microsomal proteome of *A. fumigatus* in response to iron-deplete conditions. Additionally, comparative proteomics has been used to characterise deletion mutants in *A. fumigatus*. Owens et al. (2015) demonstrated proteomic analysis of several gliotoxin cluster mutants, including Δ*gliK*, Δ*gliG* and Δ*gliA*. Relevantly, Lessing et al. (2007) investigated the oxidative stress sensitive mutant, Δ*yap1*, via 2D-PAGE combined with LC-MS/MS. This was used to identify targets of *yap1*, a transcription factor key to oxidative stress defence. O'Keeffe et al. (2013) studied the proteomic response of Δ*elfA*, another mutant sensitive to elevated ROS, to oxidative stress conditions.

Comparative proteomics has therefore been established as a robust method of analysis for *A. fumigatus*. The work presented in this chapter represents the first large scale proteomic investigation into EGT function performed in any organism and as such represents an important study for *A. fumigatus* and for studies into EGT functionality as a whole.

The aim of the work presented in this chapter was to carry out comparative LFQ proteomics on ATCC26933 and Δ*egtA*^{26933} under basal conditions and following addition of 3 mM H_2O_2.

5.2 Results

5.2.1 LFQ Proteomic Analysis of ATCC26933 and Δ*egtA*^{26933} under basal conditions and following H_2O_2 exposure

ATCC26933 and Δ*egtA*^{26933} (n = 4 biological replicates each) were cultured in Sabouraud-Dextrose media for 23 h at 37^{o}C, 200 rpm. This was followed by H_2O_2 addition (3 mM final) or equivalent volume of H_2O for 1 h. These incubation times and conditions were chosen in order to mirror qRT-PCR analysis which demonstrated increased *egtA* expression following H_2O_2 exposure (Section 4.2.4). Following 1 h incubation, mycelia were harvested from each culture and processed for Q-Exactive Mass Spectrometry analysis as per Section 2.2.14.1. Samples were then digested using sequencing grade trypsin (Section 2.2.14.4), purified, normalised and desalted using ZipTips ® (Section 2.2.14.5) and analysed on the Q-Exactive mass spectrometer (Section 2.2.14.6). Data was analysed via Max Quant in the following manner:

(i) Comparison of ATCC26933 and Δ*egtA*^{26933} under basal conditions.
(ii) Comparison of ATCC26933 and Δ*egtA*^{26933} under ROS conditions.
(iii) Comparison of Δ*egtA*^{26933} under basal and ROS conditions.
(iv) Comparison of ATCC26933 under basal and ROS conditions.

Significantly enriched functional categories of proteins were identified using the web based application FungiFun 2 (Priebe et al., 2015; https://elbe.hki-jena.de/fungifun/fungifun.php)

5.2.1.1 LFQ Proteomic Comparison of ATCC26933 and Δ*egtA*^{26933} under basal conditions

A proteomic comparison of ATCC26933 and Δ*egtA*^{26933} under basal conditions was undertaken to investigate the effect of EGT loss in *A. fumigatus* in the absence of external oxidative stressors. Proteomic comparisons revealed that 26 proteins showed increased abundance or were unique in Δ*egtA*^{26933} compared to ATCC26933, while 121 proteins showed decreased abundance or were absent in Δ*egtA*^{26933} compared to ATCC26933. This is a total of 147 proteins that showed differential abundance due to the loss of EGT, which suggests that even without any induced stress, EGT loss causes significant proteomic remodelling in *A. fumigatus*. Figure 5.1 summarises the most significantly enriched functional categories of the proteins showing

differential abundance. The full list of proteins showing differential abundance can be seen in Appendix 1.

A number of proteins with differential abundance were reductases, oxidases, stress response proteins and enzymes with oxidising products (Table 5.1). This suggests at a shift in redox homeostasis, which is reflected by the changes in these redox sensitive proteins. Of particular interest is HapC (AFUA_1G03840), the redox sensitive subunit of the CCAAT-Binding Complex (CBC), which is absent in Δ*egtA*^{26933} compared to ATCC26933. Thon et al. (2010) demonstrated in *Aspergillus nidulans* that the CBC is essential for oxidative stress defence. HapC function in the CBC is to sense the redox status of the cell. This is achieved via oxidative modification of thiol groups within its histone fold motif. HapC was demonstrated to be essential for correct CBC function, with impaired oxidative stress response demonstrated upon HapC deletion. The absence of HapC in Δ*egtA*^{26933} would therefore indicate a defective oxidative stress response in this mutant.

The gliotoxin oxidoreductase, GliT (AFUA_6G09740), was also observed to be absent in Δ*egtA*^{26933} compared to ATCC26933 (Table 5.1). The absence of this protein was of interest due to the observed drop in gliotoxin production following *egtA* deletion in ATCC26933 (Section 4.2.9). GliT is involved in disulphide bridge closure in gliotoxin biosynthesis and gliotoxin production is abrogated in its absence (Schrettl et al., 2010). Thus, GliT is essential for gliotoxin biosynthesis and the decrease in abundance following *egtA* deletion may well be responsible for the observed reduction in gliotoxin levels.

Proteins involved in the biosynthesis of other secondary metabolites also demonstrated differential abundance in Δ*egtA*^{26933}. A SirN-like methyltransferase (AFUA_8G00550), predicted to be involved in pseurotin A biosynthesis (Vödisch et al., 2011) showed a $\log_2$ 1.28 fold increase in abundance. OrdA (AFUA_8G00510), a cytochrome P450 enzyme encoded within the fumagillin cluster (Lin et al., 2013), was demonstrated to be absent in Δ*egtA*^{26933} (Table 5.1).

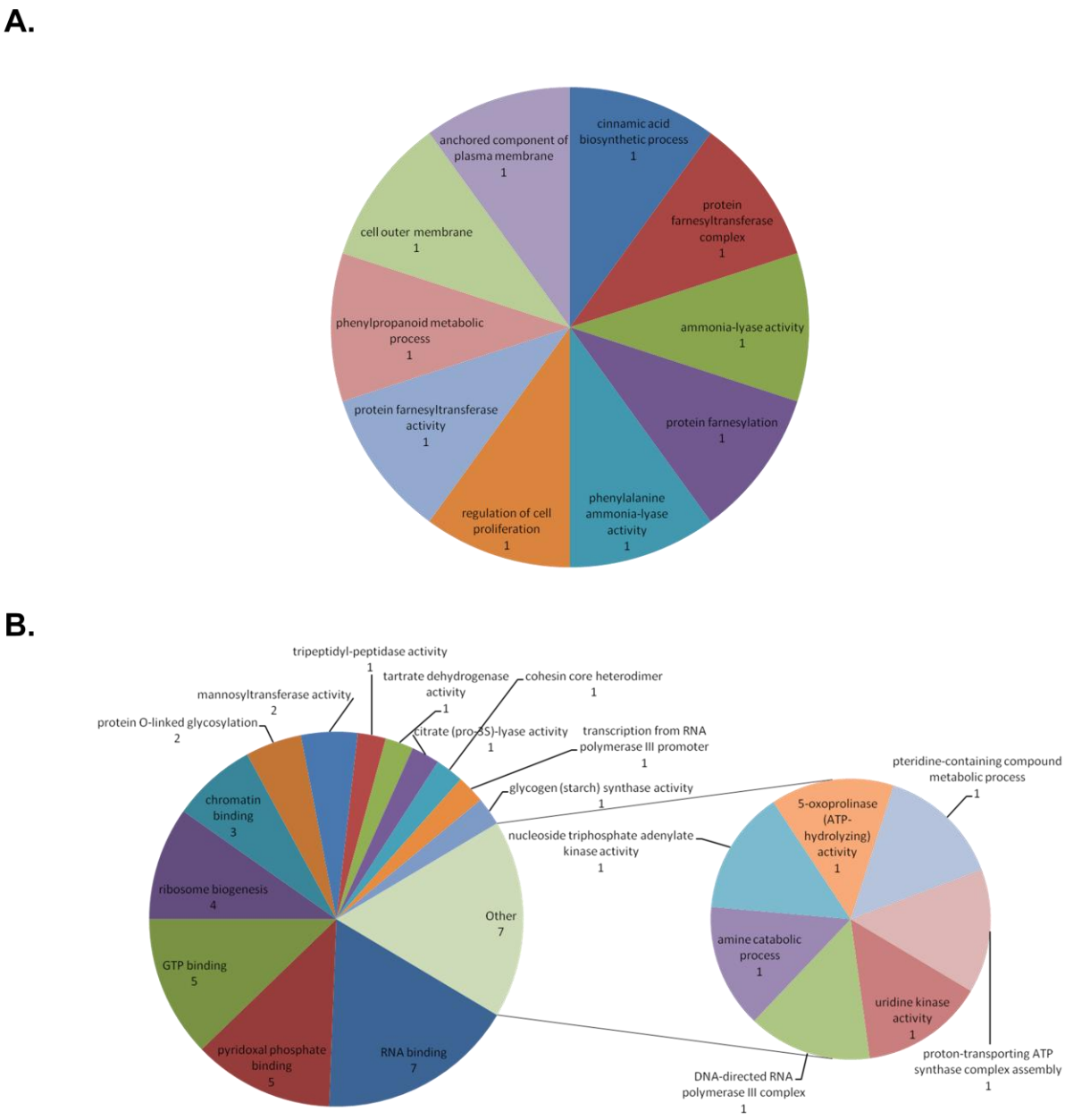

Figure 5.1. Significantly enriched functional categories of proteins showing differential abundance in Δ*egtA*^{26933} compared to ATCC26933 under basal conditions. The number under each category represents the number of proteins detected within that category. (A) Significantly enriched functional categories from proteins showing increased abundance, whereby all 26 proteins in the data set were annotated. (B) Significantly enriched functional categories from proteins showing decreased abundance, whereby 119 out of 121 proteins in the data set were annotated.

Another protein of interest from this data set was cystathionine γ-synthase (CGS; AFUA_7G01590), which was observed to be absent in Δ*egtA*^{26933} compared to ATCC26933 (Table 5.1). CGS catalyses the formation of cystathionine from homoserine and cysteine (Ravanel, 1997) and its absence in Δ*egtA*^{26933} suggests that cystathionine production is attenuated when EGT biosynthesis is abrogated. The absence of CGS may be related to the rise in total glutathione observed in Δ*egtA*^{26933} (Section 4.2.7.1). Cysteine is essential for glutathione biosynthesis (Lu, 2009), in addition to being a substrate of CGS in cystathionine biosynthesis. Therefore, it is feasible that CGS may be decreased in abundance in order to preserve cysteine for the production of glutathione (Figure 5.2).

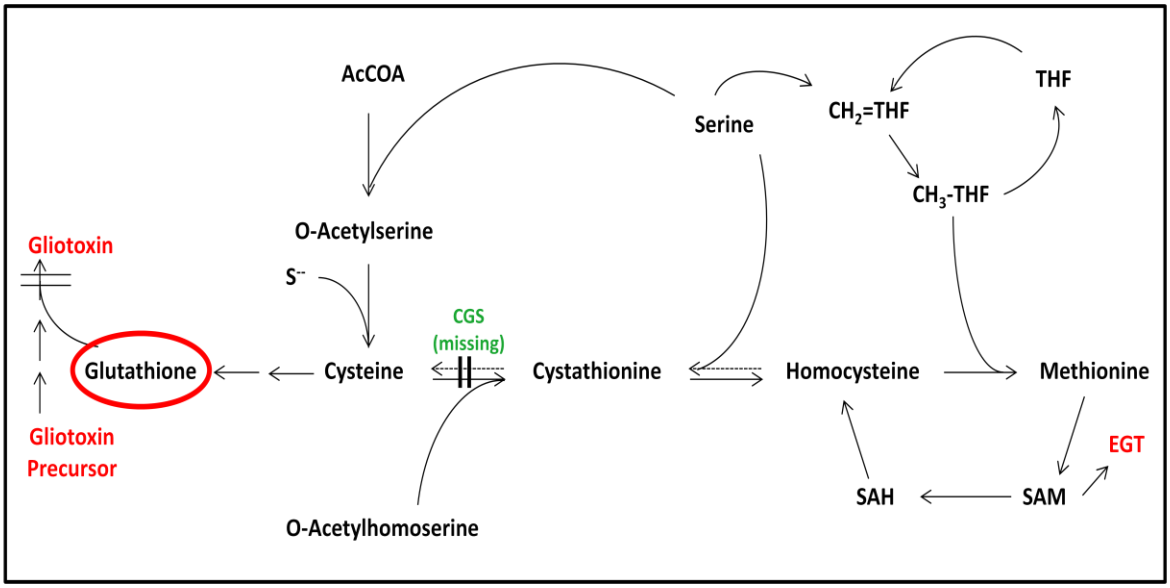

Figure 5.2. Comparison of Δ*egtA*^{26933} and ATCC26933 under basal conditions showing an absence of cystathionine γ-synthase (CGS), which converts cysteine to cystathionine. This could be facilitating the switch towards increased glutathione production.

Conidial health and conidiation was of interest as Δ*egtA*^{26933} displayed paler conidia compared to wild-type as well as lower levels of conidiation (Section 4.2.10), evidence of a role for EGT in conidial protection and conidiation in *A. fumigatus*. Bello et al. (2012, 2014) also reported conidial sensitivity to peroxide and lower levels of conidiogenesis in *N. crassa*. In this context, the absence of several conidial proteins was of interest (Table 5.1). These include mannosyltransferases PMT2 (AFUA_1G07690)(Fang et al., 2010) and PMT4 (AFUA_8G04500)(Mouyna et al., 2010), conidial hydrophobin RodB (AFUA_1G17250)(Paris

et al, 2003a), developmental regulator FlbA (AFUA_2G11180)(Yu et al., 1996) and extracellular developmental signal biosynthesis protein FluG (AFUA_3G07140)(Mah and Yu, 2006). The unavailability of these proteins due to EGT absence is further evidence of the role of EGT in conidiation and conidial health in *A. fumigatus*.

Potentially related to this is the increase (log_2 1.23 fold) in the methyltransferase VipC (AFUA_8G01930) in Δ*egtA*^{26933} compared to ATCC26933 under basal conditions. In *A. nidulans*, VipC interacts with the velvet complex and has been shown to play a role in controlling the switch between sexual and asexual reproduction. Relevantly, a VipC overexpression mutant demonstrated reduced asexual reproduction (Sarikaya-Bayram et al., 2014). VipC has yet to be characterised in *A. fumigatus*, however the evidence from *A. nidulans* suggests that the differential abundance of VipC observed could be linked to the abnormal conidiation demonstrated in Δ*egtA*^{26933}.

The protein showing the largest increase in abundance in Δ*egtA*^{26933} compared to ATCC26933 under basal conditions was phenylalanine ammonia lyase (PAL; AFUA_2G09110)(Table 5.1). PAL showed a log_2 2.71 fold increase in Δ*egtA*^{26933} compared to ATCC26933. PAL is involved in the breakdown of phenylalanine, converting it into ammonia and *trans*-cinnamic acid (Camm and Towers, 1973). PAL is associated with defence from pathogens in plants (Shadle et al., 2003; Kim and Hwang, 2014; Tonnessen et al., 2015), and has also been implicated in oxidative stress defence (Desikan et al., 1998; Lee et al., 2003). Thus, this observed increase in abundance may be part of an alternative oxidative stress defence in the absence of EGT.

Five proteins related to *A fumigatus* cell wall biosynthesis were noted to show differential abundance in Δ*egtA*^{26933} compared to ATCC26933 (Table 5.1). This was of interest because Δ*egtA*^{26933} exhibited decreased radial growth in comparison to ATCC26933 and *egtA*^{C26933} when exposed to the cell wall perturbing agents congo red and CFW. 1,3-beta-glucanosyltransferase (GEL5; AFUA_8G02130) showed a log_2 1.18 fold increase, while chitin synthase activator Chs3 (AFUA_3G05580), a putative cell wall protein (AFUA_3G081110), a putative MAP kinase kinase (Mkk2;AFUA_1G05800)(Valiante et al., 2009) and a putative cell wall glucanase (AFUA_3G09250) were absent. In addition, the mannosyltransferases PMT2 and PMT4, which are both absent in Δ*egtA*^{26933} compared to ATCC26933 and discussed previously in relation to conidial health, also function in cell wall biosynthesis in *A. fumigatus* (Mouyna et al., 2010; Fang

et al., 2010). The differential abundance of these proteins supports previous data that suggested EGT absence leads to cell wall alterations.

Table 5.1. Selected proteins with significant log_2 fold change or absent in *A. fumigatus* Δ*egtA*^{26933} compared to ATCC26933 under basal conditions. Data sorted by fold change, in descending order.

Protein Description	Present/log_2 (Fold Change)	p value	Peptides	Sequence coverage [%]	Protein IDs
phenylalanine ammonia-lyase	2.70643	0.000688551	26	52.8	AFUA_2G09110
1,3-beta-glucanosyltransferase (GEL5)	1.17592	0.00673139	4	8.8	AFUA_8G02130
2-dehydropantoate 2-reductase	1.48361	0.018129	5	16.7	AFUA_4G13960
Methyltransferase SirN-like, putative	1.28453	0.0206547	19	76	AFUA_8G00550
Methyltransferase LaeA-like, putative (VipC)	1.22923	0.0152246	6	13.8	AFUA_8G01930
Sulfhydryl oxidase	1.22122	0.008832	7	37.3	AFUA_3G08850
Oxidoreductase, 2OG-Fe(II) oxygenase family	1.10977	0.018011	16	58.7	AFUA_1G01000
Oxidoreductase, short chain dehydrogenase/reductase family	-1.0044	0.00741	13	86.4	AFUA_5G14000
Cytochrome P450 monooxygenase, putative	-1.01068	0.030958	15	34.7	AFUA_6G02210
5-oxo-L-prolinase, putative	-1.08559	0.000788	65	63.9	AFUA_6G14330
Isoflavone reductase family protein (Oxidoreductase activty)	-1.09131	0.021158	13	57	AFUA_1G12510
Mitochondrial enoyl reductase, putative	-1.23179	0.001484	17	61.8	AFUA_3G03330
Oxidoreductase, zinc-binding dehydrogenase family, putative	-2.01615	0.02697	12	61	AFUA_1G15610
CCAAT-binding factor complex subunit HapC	Absent	n/a	3	23.8	AFUA_1G03840
Cystathionine gamma-synthase	Absent	n/a	7	30.6	AFUA_7G01590

Protein Description	**Present/log_2 (Fold Change)**	**p-value**	**Peptides**	**Sequence coverage [%]**	**Protein IDs**
Cytochrome c oxidase assembly protein (Pet191), putative	Absent	n/a	2	26.5	AFUA_5G08965
MAP kinase kinase (Mkk2), putative	Absent	n/a	2	5.8	AFUA_1G05800
Protein O-mannosyl transferase (PMT2)	Absent	n/a	3	4.1	AFUA_1G07690
Conidial hydrophobin RodB	Absent	n/a	5	67.9	AFUA_1G17250
Chitin synthase activator (Chs3), putative	Absent	n/a	7	16.1	AFUA_3G05580
Extracellular developmental signal biosynthesis protein FluG	Absent	n/a	8	15.8	AFUA_3G07140
Cell wall protein, putative	Absent	n/a	2	2.9	AFUA_3G08110
Cell wall glucanase, putative	Absent	n/a	3	8	AFUA_3G09250
Gliotoxin oxidoreductase GliT	Absent	n/a	9	43.4	AFUA_6G09740
Cytochrome P450 oxidoreductase OrdA-like, putative	Absent	n/a	5	11.9	AFUA_8G00510
Mannosyltransferase PMT4	Absent	n/a	3	5.4	AFUA_8G04500

5.2.1.2 LFQ Proteomic Comparison of ATCC26933 and Δ*egtA*^{26933} under ROS conditions

A proteomic comparison of ATCC26933 and Δ*egtA*^{26933} following the addition of 3 mM H_2O_2 was undertaken in investigate the effect of EGT loss on the ability of *A. fumigatus* to respond to high levels of H_2O_2-induced stress. Proteomic comparisons revealed 250 proteins showed increased abundance or were unique in Δ*egtA*^{26933} compared to ATCC26933 under ROS conditions, while 40 proteins showed decreased abundance or were absent in Δ*egtA*^{26933} compared to ATCC26933 under ROS conditions. This represents a total of 290 proteins which showed differential abundance under oxidative stress conditions due to EGT deficiency in *A. fumigatus*. This is an increase on the 147 proteins showing differential abundance in Δ*egtA*^{26933} compared to ATCC6933 under basal conditions and indicates that addition of 3 mM H_2O_2 induces an even greater proteomic remodelling in Δ*egtA*^{26933} compared to ATCC269333. Figure 5.3 summarises the most significantly enriched functional categories of the proteins showing differential abundance. The full list of proteins showing differential abundance can be seen in Appendix 2.

As with Δ*egtA*^{26933} compared to ATCC26933 under basal conditions (Section 5.2.1.1), a number of proteins with differential abundance were reductases, oxidases, stress response proteins and enzymes with oxidising products (Table 5.2). With the addition of H_2O_2, even more of these proteins show differential abundance. This is indicative of a severe change in redox homeostasis, likely due to EGT absence and concurrent cellular inability to dissipate high levels of H_2O_2-induced ROS, as demonstrated at the phenotypic level in the data presented in Chapter 4.

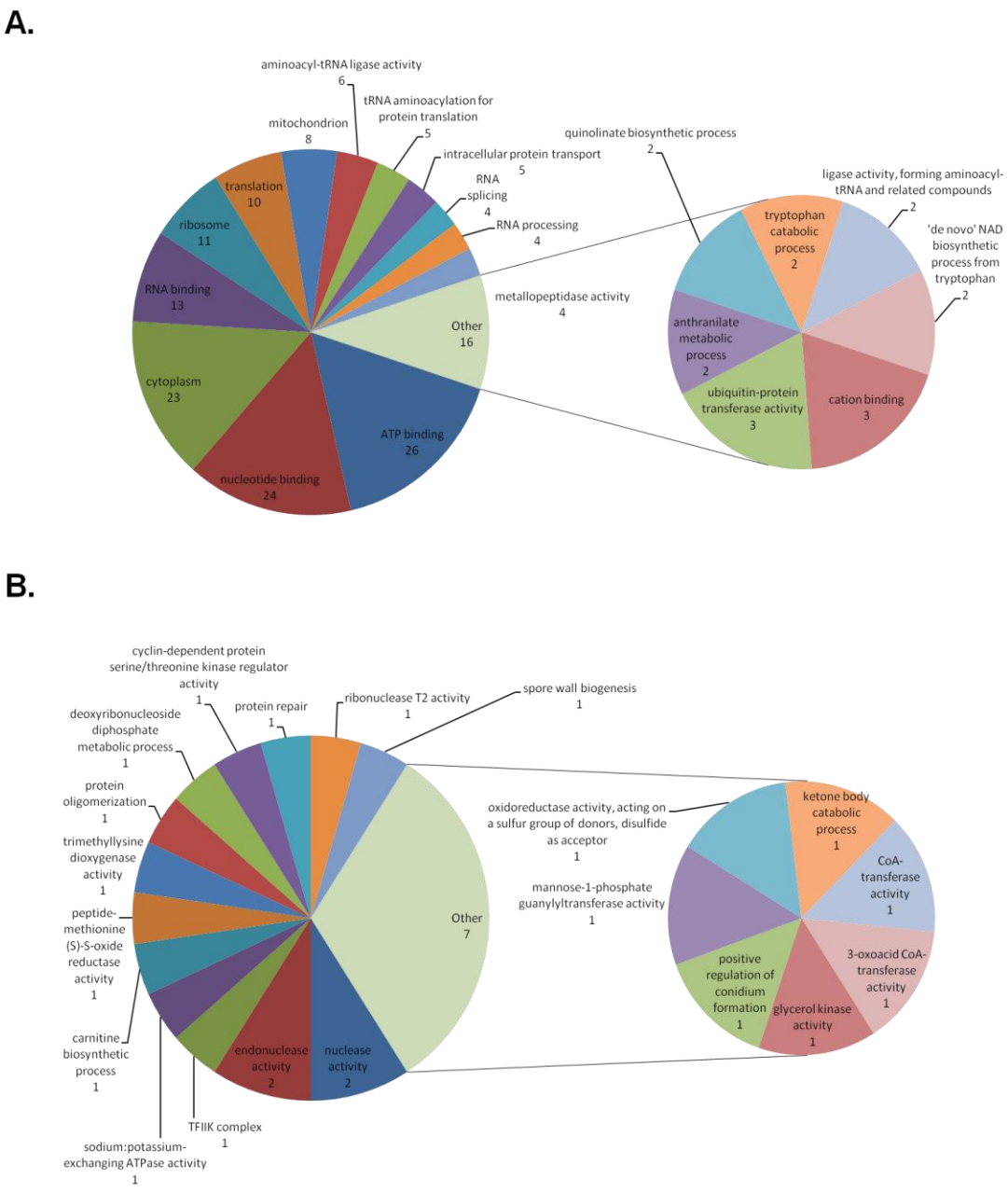

Figure 5.3. Significantly enriched functional categories of proteins showing differential abundance in Δ*egtA*^{26933} compared to ATCC26933 under ROS conditions. The number under each category represents the number of proteins detected within that category. (A) Significantly enriched functional categories from proteins showing increased abundance, whereby 237 out of 250 proteins in the data set were annotated. (B) Significantly enriched functional categories from proteins showing decreased abundance, whereby 37 out of 40 proteins in the data set were annotated.

Following the absence of CGS in Δ*egtA*^{26933} under basal conditions, the differential abundance of another cystathionine related enzyme upon addition of H_2O_2 was of much interest. Cystathionine β-lyase (CBL; AFUA_4G03950) showed a $\log_2$ 3.1 fold increase in abundance in Δ*egtA*^{26933} compared to ATCC26933 under ROS conditions (Table 5.2). CBL catalyses the conversion of cystathionine to homocysteine, ammonia and pyruvate. Homocysteine is part of the methionine cycle, which involves *S*-adenosylmethionine (SAM), the universal methyl donor (Ravanel, 1997)(Figure 5.4). SAM is essential for EGT biosynthesis, as it is a key substrate for the tri-methylation of histidine to form hercynine. Significantly, 3 mol of SAM are required to produce 1 mol of EGT, meaning EGT biosynthesis utilises SAM intensively. The observed rise in CBL may be part of a shift towards attempted EGT biosynthesis due to increased levels of ROS, even though the necessary enzyme, EgtA, is absent.

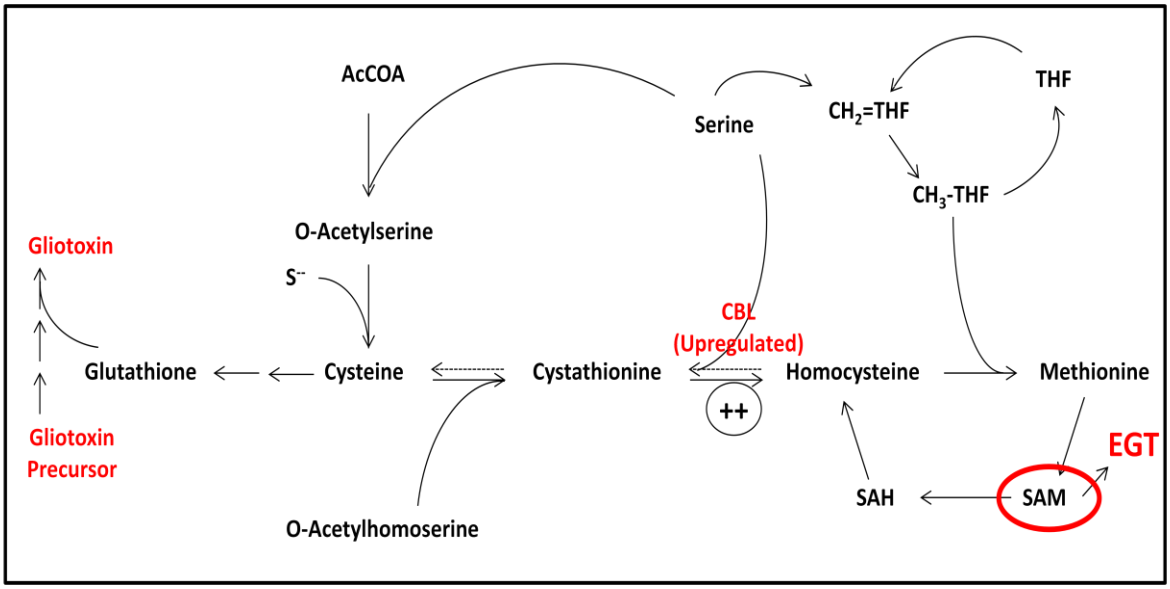

Figure 5.4. Comparison of Δ*egtA*^{26933} and ATCC26933 upon addition of 3 mM H_2O_2 shows an increased abundance of cystathionine β-lyase, which converts cystathionine to homocysteine. This could result in increased production of SAM, which is essential for EGT biosynthesis.

Related to this, HisF (AFUA_2G06230), an imidzole glycerol phosphate synthase subunit, showed a $\log_2$ 1.11 fold increase in Δ*egtA*^{26933} compared to ATCC26933 following the addition of H_2O_2 (Table 5.2). HisF is essential for histidine biosynthesis, as it catalyses the closure of the imidazole ring (Rieder et al., 1994). This suggests that Δ*egtA*^{26933} attempts to increase levels of histidine production. Histidine is a key precursor for EGT biosynthesis and an increase in

histidine levels would be necessary in order to increase EGT production. Relevantly, attenuated histidine levels have been associated with heavy metal toxicity in *A. fumigatus*, indicating that histidine availability is an important factor in cellular defence (Dietl et al., 2016). Furthermore, a $\log_2$ 2.22-fold increase in a putative sulphite reductase (AFUA_2G15590) likely indicates an increased need for sulphur in Δ*egtA*^{26933}, which could reflect attempted EGT production, or an increase in GSH biosynthesis (Table 5.2).

Several proteins related to secondary metabolism were shown to have increased abundance in Δ*egtA*^{26933} compared to ATCC26933 under ROS conditions (Table 5.2). These were an aflatoxin B1-aldehyde reductase (AFUA_1G13370), a hybrid NRPS/PKS (PsoA; AFUA_8G00540), an aldehyde reductase (GliO; AFUA_5G02020), a putative NRPS-like enzyme (AFUA_5G10120) and a SirN-like methyltransferase (AFUA_8G00550). This aligns with the differential abundance of two proteins related to secondary metabolism under basal conditions, which suggests an increase in secondary metabolism in response to H_2O_2 in the absence of EGT.

Two proteins with increased abundance in Δ*egtA*^{26933} compared to ATCC26933 under basal conditions were VipC and PAL (Table 5.1). Upon addition of 3 mM H_2O_2, both of these proteins showed an even larger increase in abundance in Δ*egtA*^{26933} compared to ATCC26933 under ROS conditions (Table 5.2). VipC showed a $\log_2$ 1.23 fold increase under basal conditions, while it showed a $\log_2$ 2.5 fold increase in abundance under ROS conditions. PAL showed a $\log_2$ 2.71 fold increase in Δ*egtA*^{26933} compared to ATCC26933 under basal conditions, while it showed a $\log_2$ 3.73 fold increase under ROS conditions. This suggests that the cause of the increased abundance these proteins in Δ*egtA*^{26933} under basal conditions is exacerbated by an increase in ROS.

Following the observation of five cell wall related proteins with differential abundance in Δ*egtA*^{26933} compared to ATCC26933 under basal conditions, two additional cell wall related proteins also showed differential abundance in Δ*egtA*^{26933} compared to ATCC26933 under elevated ROS conditions. A putative class V chitinase (AFUA_3G11280) showed a $\log_2$ 2.05 fold increase and a putative cell wall integrity signalling protein (AFUA_6G07520) showed a $\log_2$ 1.63 fold increase. This is further evidence of changes in cell wall biosynthesis due to EGT loss, following the differential abundance of several cell wall proteins in Δ*egtA*^{26933} compared to ATCC26933 under basal conditions.

Table 5.2. Selected proteins with significant $\log_2$ fold change or unique/absent in *A. fumigatus* Δ*egtA*^{26933} compared to ATCC26933 under ROS conditions. Data sorted by fold change, in descending order.

Protein Description	Present/$\log_2$ (Fold Change)	p-value	Peptides	Sequence coverage [%]	Protein IDs
Flavin containing amine oxidase, putative	Unique	n/a	3	9.3	AFUA_3G12150
Cytochrome P450, putative	Unique	n/a	1	4	AFUA_5G01360
Autophagy protein Atg20, putative	Unique	n/a	3	7.5	AFUA_2G14160
Epoxide hydrolase, putative	Unique	n/a	4	19	AFUA_2G16900
Protein kinase Yak1, putative	Unique	n/a	4	5.5	AFUA_4G03850
Zinc-binding oxidoreductase CipB	Unique	n/a	6	28.8	AFUA_4G00700
NADPH-dependent FMN reductase Lot6, putative	4.40163	0.00432	8	69.2	AFUA_7G06600
Phenylalanine ammonia-lyase	3.72865	0.0202547	26	55.8	AFUA_2G09110
Pyridoxal kinase, putative	3.61996	0.007665	7	34.6	AFUA_1G02900
NmrA-like family protein	3.19014	0.010049	8	44.7	AFUA_6G00280
Cystathionine beta-lyase MetG	3.09553	0.0355343	8	32.5	AFUA_4G03950
Oxidoreductase, 2OG-Fe(II) oxygenase family	2.88667	0.002938	18	60	AFUA_1G01000
Short chain dehydrogenase family protein	2.87187	0.011169	6	23	AFUA_1G16630
CsgA-like short chain dehydrogenase/reductase, putative	2.86184	0.046537	6	62.8	AFUB_075540
NifU-related protein	2.62307	0.048628	7	44.8	AFUA_1G04680
Flavin-binding monooxygenase-like protein	2.56424	0.027902	8	21.2	AFUA_6G01900
Ortholog(s) have cytochrome-c oxidase activity	2.50787	0.028945	5	21.3	AFUA_Mt00120
Methyltransferase LaeA-like, putative (VipC)	2.49862	0.0001273	9	21.5	AFUA_8G01930

Protein Description	Present/log_2 (Fold Change)	p-value	Peptides	Sequence coverage [%]	Protein IDs
Short-chain dehydrogenase, putative	2.45341	0.019904	7	29.3	AFUA_8G00280
Sulfite reductase, putative	2.22575	0.003046	35	31.2	AFUA_2G15590
NADH-ubiquinone oxidoreductase subunit GRIM-19, putative	2.20179	0.038593	4	34.6	AFUA_3G08770
Class V chitinase, putative	2.04796	0.025086	14	56.8	AFUA_3G11280
Aflatoxin B1-aldehyde reductase GliO-like, putative	2.01845	0.049263	13	48.3	AFUA_1G13370
DUF255 domain protein	1.88685	0.041084	12	20.8	AFUA_1G12370
2-dehydropantoate 2-reductase	1.80192	0.041835	4	16.1	AFUA_3G00740
Cell wall integrity signaling protein Lsp1/Pil1, putative	1.63067	0.0084455	10	41.5	AFUA_6G07520
2-oxo acid dehydrogenases acyltransferase, putative	1.62889	0.037992	17	46.3	AFUA_4G12010
Hybrid NRPS/PKS enzyme, putative (PsoA)	1.54538	0.0288011	45	16.2	AFUA_8G00540
NADH-ubiquinone oxidoreductase 304 kDa subunit	1.50531	0.043681	16	52.1	AFUA_6G08810
Methyltransferase SirN-like, putative	1.47973	0.0227853	21	78.2	AFUA_8G00550
AhpC/TSA family protein	1.44847	0.014711	11	54.1	AFUA_6G12500
NADH-dependent flavin oxidoreductase, putative	1.43235	0.030737	33	76.1	AFUA_7G06420
Pyridoxal reductase (AKR8), putative	1.42837	0.01439	11	38.6	AFUA_1G10270
Aldehyde reductase (GliO), putative	1.40263	0.0179692	28	84.1	AFUA_5G02020
Glycerol dehydrogenase (GldB), putative	1.37995	0.019009	30	85.5	AFUA_4G11730
NRPS-like enzyme, putative	1.33723	0.0410764	41	44.1	AFUA_5G10120
Arsenate reductase (Arc2), putative	1.27464	0.027714	9	63.3	AFUA_6G13400

Protein Description	Present/log_2 (Fold Change)	p-value	Peptides	Sequence coverage [%]	Protein IDs
2-methylcitrate dehydratase, putative	1.23478	0.009205	38	65.2	AFUA_6G03730
DNA damage-inducible protein 1	1.21829	0.034152	24	73.8	AFUA_7G06050
Short chain dehydrogenase/reductase family protein	1.17302	0.024341	13	80.5	AFUA_1G00990
Imidazole glycerol phosphate synthase subunit hisF	1.10807	0.024405	32	74.4	AFUA_2G06230
Pyridoxamine phosphate oxidase, putative	1.13607	0.038128	17	52.4	AFUA_5G10650
Aldehyde dehydrogenase, putative	-1.07759	0.046538	24	53.7	AFUA_2G00720
Cytochrome B	-1.13698	0.017889	2	4.9	AFUA_Mt00001
Trimethyllysine dioxygenase TmlH, putative	-1.27237	0.027847	6	25.2	AFUA_1G06180
Glycerol kinase, putative	-1.99179	0.048473	7	20.7	AFUA_4G11540
Ferrooxidoreductase Fet3, putative	Absent	n/a	2	5.6	AFUA_5G03790
Oxidoreductase CipA-like, putative	Absent	n/a	3	13.4	AFUA_1G12460

5.2.1.3 LFQ Proteomic Comparison of Δ*egtA*^{26933} under ROS and basal conditions

A proteomic comparison of Δ*egtA*^{26933} with and without 3 mM H_2O_2 was undertaken to assess the impact of high levels of oxidative stress on Δ*egtA*^{26933}. A total of 132 proteins showed differential abundance in Δ*egtA*^{26933} when exposed to 3 mM H_2O_2 compared to Δ*egtA*^{26933} under basal conditions. Of these, 113 showed an increase in abundance, while 19 proteins showed a decrease in abundance. Figure 5.5 summarises the most significantly enriched functional categories of the proteins showing differential abundance. The full list of proteins showing differential abundance can be seen in Appendix 3.

One protein of interest showing differential abundance is a putative superoxide dismutase copper chaperone, Lys7 (AFUA_2G09700), which shows a $\log_2$ -1.12 fold decrease in abundance. Copper is an essential co-factor for many superoxide dismutases (Miyayama et al., 2011) and superoxide dismutase copper chaperones are responsible for delivery of copper to superoxide dismutase. Decreased abundance of Lys7 in Δ*egtA*^{26933} following exposure to 3 mM H_2O_2 may indicate defective superoxide dismutase behaviour. Alternatively, it may point towards a shift in copper homeostasis.

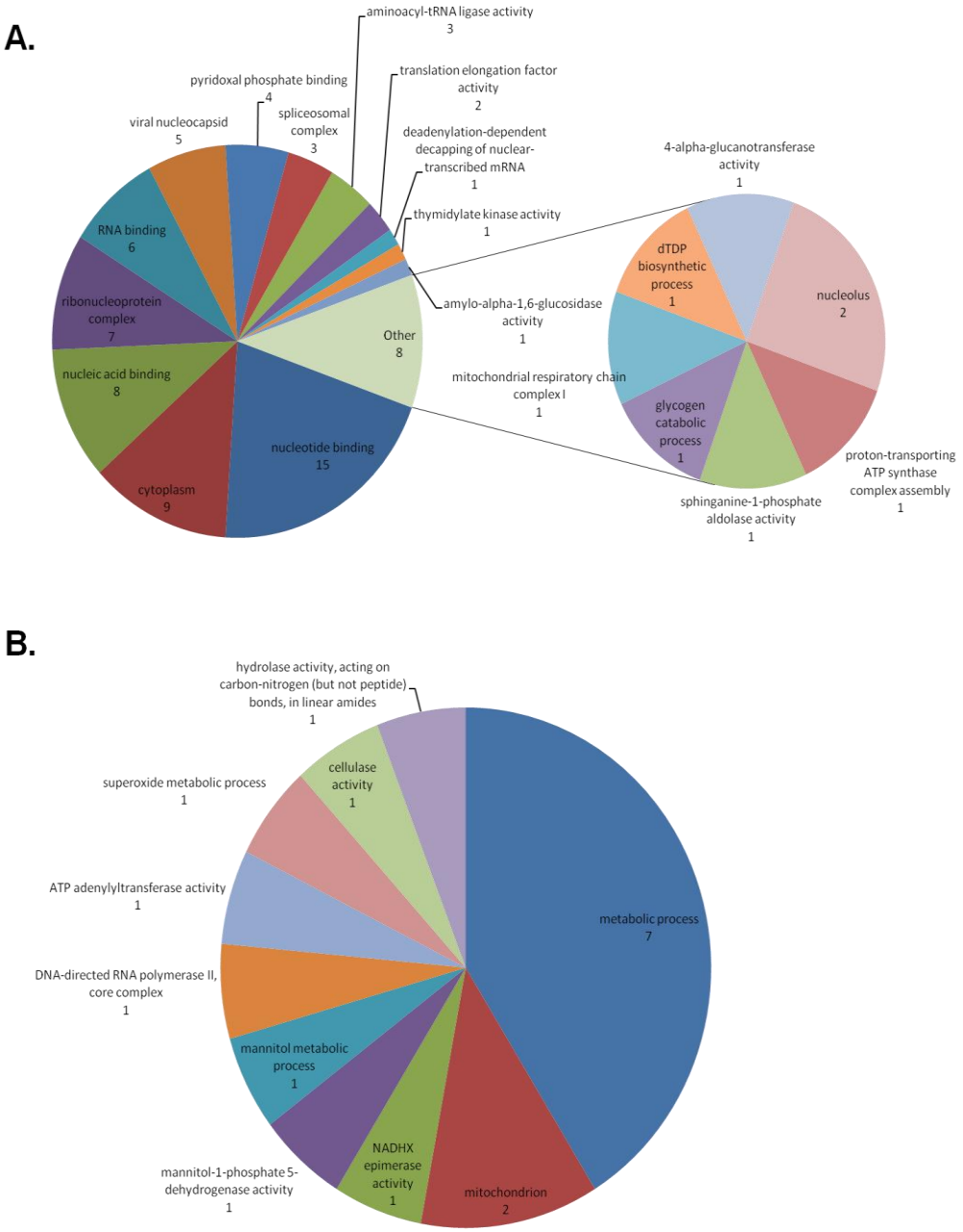

Figure 5.5. Significantly enriched functional categories of proteins showing differential abundance in Δ*egtA*^{26933} under ROS conditions compared to Δ*egtA*^{26933} under basal conditions. The number under each category represents the number of proteins detected within that category. (A) Significantly enriched functional categories from proteins showing increased abundance, whereby 109 out of 113 proteins in the data set were annotated. (B) Significantly enriched functional categories from proteins showing decreased abundance, whereby 18 out of 19 proteins in the data set were annotated.

5.2.1.4 LFQ Proteomic Comparison of ATCC26933 under ROS and basal conditions

A proteomic comparison of ATCC26933 with and without 3 mM H_2O_2 was undertaken to assess the impact of high levels of oxidative stress on ATCC26933. This would allow for a comparison with Δ*egtA*^{26933} with and without 3 mM H_2O_2 (Section 5.2.1.3). A total of 71 proteins showed differential abundance in ATCC26933 following exposure to 3 mM H_2O_2. Of these, 28 proteins showed increased abundance, while 43 proteins showed decreased abundance. Figure 5.6 summarises the most significantly enriched functional categories of the proteins showing differential abundance. The full list of proteins showing differential abundance can be seen in Appendix 4.

One protein of interest showing differential abundance is HapC (AFUA_1G03840), the redox sensitive subunit of the CBC. HapC is absent in ATCC26933 upon addition of 3 mM H_2O_2. This is of interest because HapC is absent in Δ*egtA*^{26933} compared to ATCC26933 under basal conditions (Section 5.2.1.1). The observation that HapC is absent upon addition of H_2O_2 in ATCC26933 suggests that this is a result of dealing with high levels of ROS. An increase in ROS due to loss of EGT may explain the absence of HapC in Δ*egtA*^{26933} compared to ATCC26933 under basal conditions

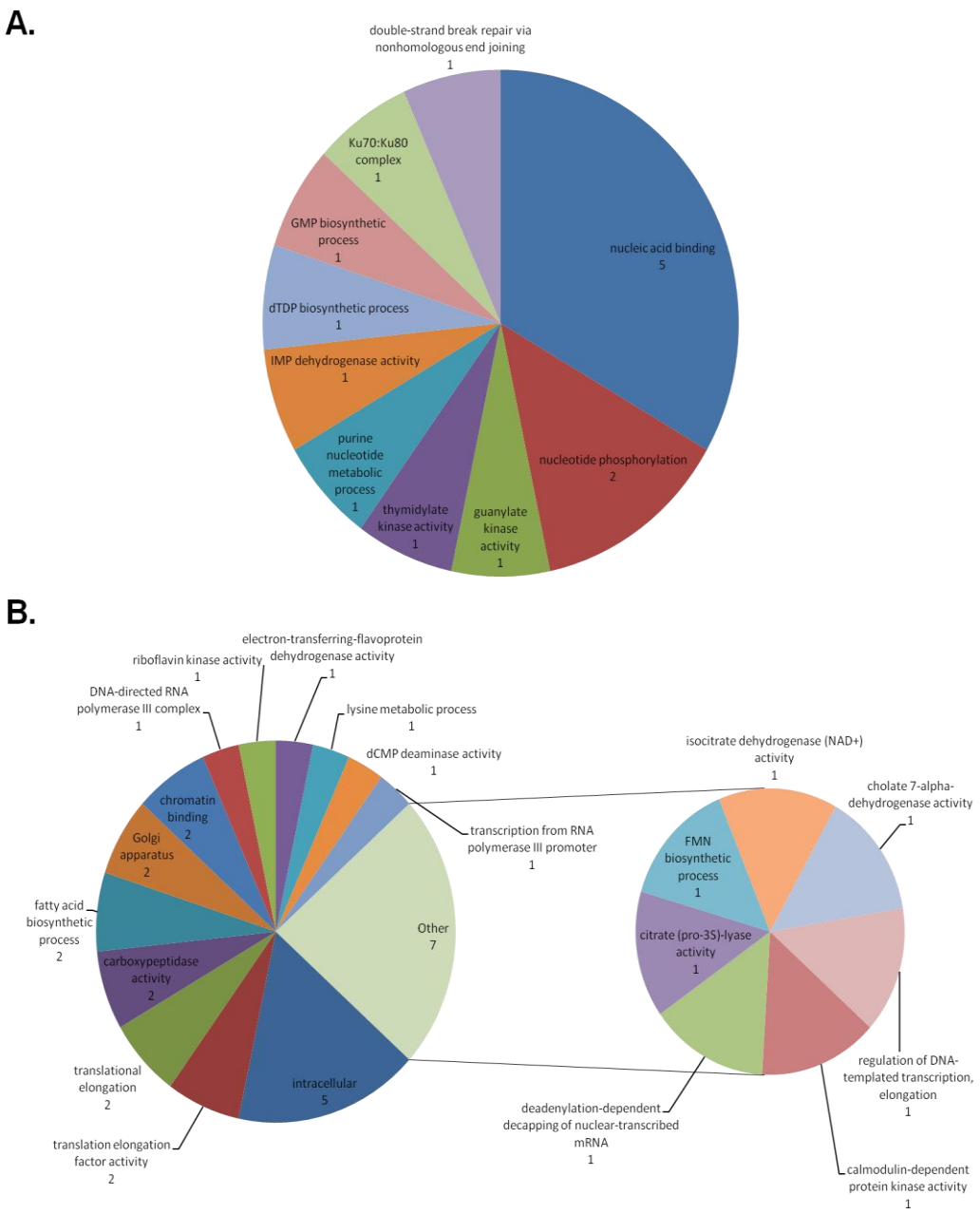

Figure 5.6. Significantly enriched functional categories of proteins showing differential abundance in ATCC26933 under ROS conditions compared to ATCC26933 under basal conditions. The number under each category represents the number of proteins detected within that category. (A) Significantly enriched functional categories from proteins showing increased abundance, whereby 27 out of 28 proteins in the data set were annotated. (B) Significantly enriched functional categories from proteins showing decreased abundance, whereby 41 out of 43 proteins in the data set were annotated.

5.3 Discussion

LFQ proteomics provided powerful insight into the systems affected by abrogation of EGT biosynthesis in *A. fumigatus*. Comparing Δ*egtA*^{26933} to ATCC26933 under both basal and ROS conditions revealed significant proteomic remodelling due to *egtA* deletion. Under basal conditions, 147 proteins were observed to have differential abundance in Δ*egtA*^{26933} compared to ATCC26933. Upon addition of 3 mM H_2O_2, the number of proteins with differential abundance in Δ*egtA*^{26933} compared to ATCC26933 increased to 290. This suggests that induction of oxidative stress has a significant impact on *A. fumigatus* when EGT is absent, and is underlined by the number of proteins showing differential abundance in each strain when challenged with H_2O_2. Comparison of ATCC26933 under basal and ROS conditions reveals that 71 proteins show differential abundance. Comparing Δ*egtA*^{26933} under basal and ROS conditions reveals 132 proteins with differential abundance, an increase of 85.9 % compared to ATCC26933. This further underlines the effect of EGT loss on *A. fumigatus*

Many proteins with differential abundance in Δ*egtA*^{26933} compared to ATCC26933 under both basal and ROS conditions were reductases, oxidases, stress response proteins and enzymes with oxidising products (Tables 5.1 & 5.2). This strongly suggests a disruption of redox homeostasis and oxidative stress defence in the Δ*egtA*^{26933} mutant, compared to ATCC26933, particularly when exposed to 3 mM H_2O_2, and implicates a role for EGT in oxidative stress defence and regulating redox homeostasis.

Of particular importance was HapC, the redox sensitive subunit of the CBC (Thon et al., 2010). The CBC is essential for sensing changes in the redox status of the cell and for mounting an effective response to oxidative stress (Thon et al., 2010). HapC was absent in ATCC26933 under ROS conditions compared to ATCC26933 under basal conditions (Appendix 4). The absence of HapC in the wild-type strain following addition of 3 mM H_2O_2 indicates that absence of HapC is a result of dealing with ROS. HapC was also absent in Δ*egtA*^{26933} compared to ATCC26933 under basal conditions. As HapC absence is associated with elevated ROS, this would indicate that Δ*egtA*^{26933} is undergoing oxidative stress under basal conditions. This is further evidence of the role of EGT in maintaining redox homeostasis.

Differential abundance of two cystathionine related proteins in Δ*egtA*^{26933} under either basal or ROS conditions, respectively, indicates that the inability to biosynthesise EGT reveals the molecular wiring necessary to integrate EGT biosynthesis into *A. fumigatus* cellular systems. Cystathionine is a sulphur-containing metabolite involved in cysteine and methionine metabolism (Ravanel, 1997). Cystathionine γ-synthase (CGS; AFUA_7G01590), was absent in Δ*egtA*^{26933} compared to ATCC26933 under basal conditions (Table 5.1), while cystathionine β-lyase (CBL; AFUA_4G03950) showed a $\log_2$ 3.1 fold increase in abundance in Δ*egtA*^{26933} compared to ATCC26933 under ROS conditions (Table 5.2). CGS catalyses the formation of cystathionine from homoserine and cysteine. CBL catalyses the conversion of cystathionine to homocysteine, ammonia and pyruvate (Ravanel, 1997). This indicates that under basal conditions, due to CGS absence, Δ*egtA*^{26933} undergoes a metabolic shift from producing cystathionine to conserving cysteine (Figure 5.7). Under ROS conditions, Δ*egtA*^{26933} undergoes a metabolic shift to convert cystathionine to homocysteine. The move towards cysteine conservation under basal conditions may be to facilitate increased glutathione biosynthesis, while the move towards homocysteine may be to provide the SAM necessary for EGT biosynthesis (Figure 5.4). This latter observation is supported by the $\log_2$ 1.11 fold increase in HisF, essential for histidine biosynthesis, while a $\log_2$ 2.22 fold increase in abundance of a putative sulphite reductase indicated an increased need for sulphur, which could be linked to abortive attempts to biosynthesise EGT. Cystathionine is at the centre of both metabolic pathways involved, which indicates a "cystathionine switch" is a novel molecular mechanism at the heart of sulphur metabolism in *A. fumigatus*.

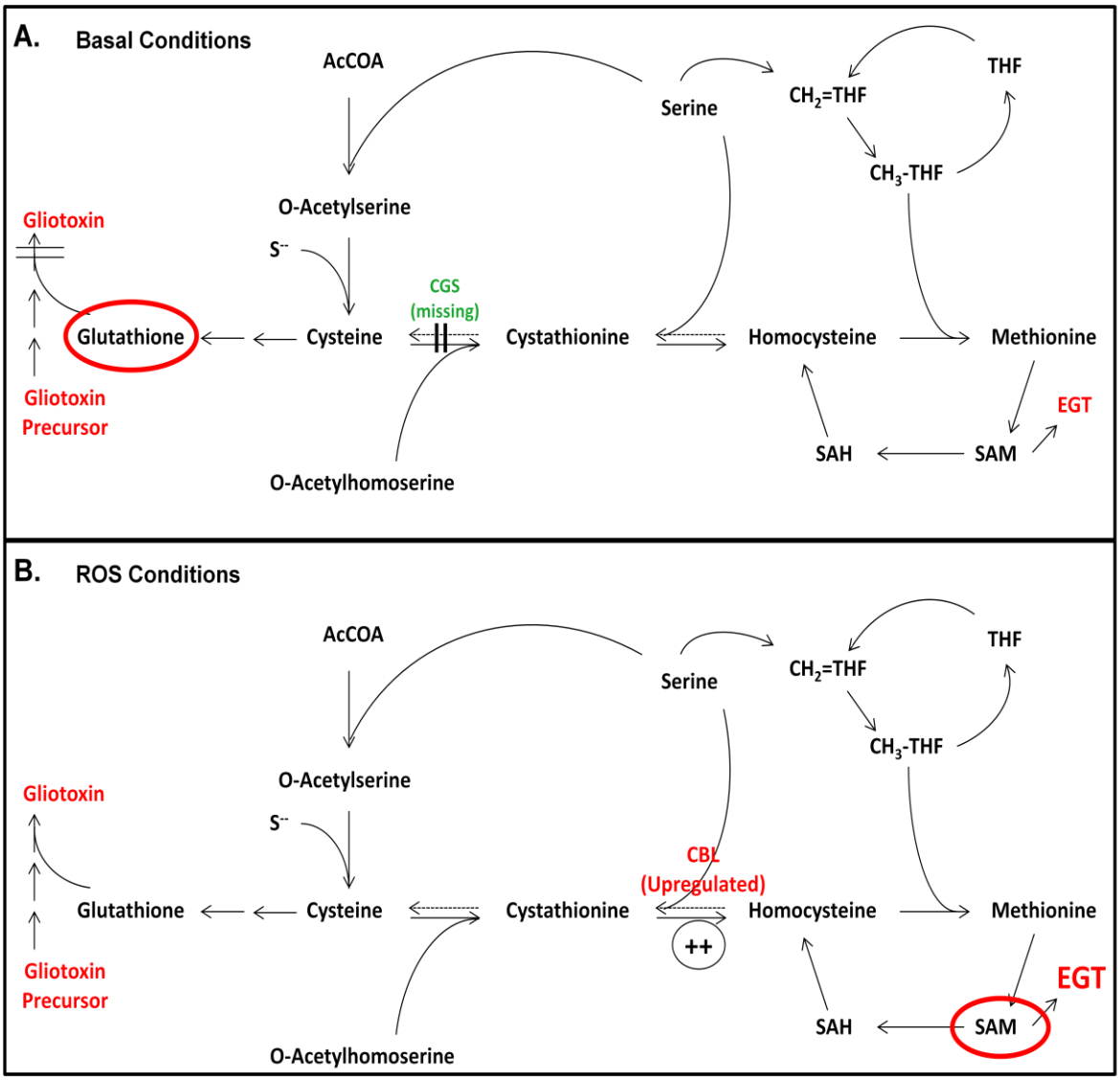

Figure 5.7. The "cystathionine switch" in *A. fumigatus*. (A) Comparison of Δ*egtA*^{26933} and ATCC26933 under basal conditions showing an absence of cystathionine γ-synthase, which converts cysteine to cystathionine. This may facilitate a switch towards increased glutathione production. (B) Comparison of Δ*egtA*^{26933} and ATCC26933 upon addition of 3 mM H_2O_2 shows an increased abundance of cystathionine β-lyase, which converts cystathionine to homocysteine. This is predicted to result in increased production of SAM, which is essential for EGT biosynthesis.

It was observed in the gliotoxin null mutant Δ*gliK* that EGT levels were increased. This led to a hypothesis that EGT and gliotoxin biosynthesis is linked (Gallagher et al., 2012). It was demonstrated that levels of gliotoxin were reduced in Δ*egtA*^{26933} (Section 4.2.9), which was further evidence of cross-talk between EGT and gliotoxin biosynthesis (Sheridan et al., 2015). The gliotoxin oxidoreductase GliT was observed to be absent in Δ*egtA*^{26933} compared to ATCC26933 under basal conditions. GliT is essential for gliotoxin production, catalyzing the closure of the disulphide bridge, as was demonstrated in *A. fumigatus* Δ*gliT*, which is unable to produce gliotoxin (Schrettl et al., 2010). Absence of GliT in Δ*egtA*^{26933} is likely to be the cause of the observed drop in gliotoxin production. As GliT is an oxidoreductase, it may be affected by a shift in redox homeostasis, as it was observed that many other redox active enzymes showed differential abundance (Table 5.1). Indeed, gliotoxin itself has redox activity (Gardiner et al., 2005) and the reduced levels observed may be in response to the altered redox state in Δ*egtA*^{26933}.

A key phenotype of Δ*gliT* was severe sensitivity to exogenous gliotoxin (Schrettl et al., 2010; Scharf et al., 2010). However gliotoxin sensitivity was not observed in Δ*egtA*^{26933} (Section 4.2.10.1), despite the absence of GliT under basal conditions. This can be explained by the induction of GliT in Δ*egtA*^{26933} as demonstrated in Section 4.2.10.2. Thus it appears that GliT is absent under basal conditions, which could diminish gliotoxin production, but GliT is still induced by gliotoxin exposure for the purpose of self-protection (Schrettl et al., 2010; Scharf et al., 2010). Induction of GliT by exogenous gliotoxin has been previously observed in wild-type *A. fumigatus* and is considered part of the self-protection strategy (Schrettl et al., 2010; Scharf et al., 2010). Relevantly, GliT is regulated independently of the rest of the *gli* cluster, meaning gliotoxin self-protection and gliotoxin biosynthesis can function autonomously (Schrettl et al., 2010).

It appears that gliotoxin is not the only secondary metabolite affected by the loss of EGT. Several proteins involved in the biosynthesis of secondary metabolites were observed to exhibit differential abundance under both basal and ROS conditions. OrdA (AFUA_8G00510), a cytochrome P450 enzyme encoded within the fumagillin cluster (Vödisch et al., 2011), was demonstrated to be absent in Δ*egtA*^{26933} compared to ATCC26933 under basal conditions. Two proteins associated with pseurotin A biosynthesis were observed to show increased abundance in

Δ*egtA*^{26933} compared to ATCC26933. Abundance of PsoA (AFUA_8G00540), a hybrid NRPS/PKS, was increased by $\log_2$ 1.28 fold in *egtA*^{26933} compared to ATCC26933 under ROS conditions and it has been demonstrated that deletion or overexpression of *psoA* leads to absence or increased abundance of pseurotin A, respectively (Maiya et al., 2007). A putative SirN-like methyltransferase (AFUA_8G00550) had increased abundance in Δ*egtA*^{26933} compared to ATCC26933 under both basal ($\log_2$ 1.28 fold) and ROS ($\log_2$ 1.48 fold) conditions. Alcazar-Fuoli et al. (2014) demonstrated that deletion of the AFUA_8G00550 gene resulted in a near total absence of pseurotin A, indicating this enzyme plays an important role in pseurotin A biosynthesis. This data suggests a potential increase in pseurotin A biosynthesis in Δ*egtA*^{26933}, particularly when it is challenged with H_2O_2. Pseurotin A has been known to be induced by hypoxic conditions (Vödisch et al., 2011), so it may form part of the stress response, particularly in the absence of EGT.

Other proteins with differential abundance in Δ*egtA*^{26933} compared to ATCC26933, not associated with a specific metabolite but predicted to be involved in secondary metabolism, were an aflatoxin B1-aldehyde reductase (AFUA_1G13370), an aldehyde reductase (GliO; AFUA_5G02020) and a putative NRPS-like enzyme (AFUA_5G10120) (Khaldi et al., 2010). All three showed increased abundance in Δ*egtA*^{26933} compared to ATCC26933 under ROS conditions. This further emphasises the alterations which occur in secondary metabolism in *A. fumigatus* in the absence of EGT. This is indicative of a "cross-talk" between secondary metabolite systems, which is a well observed phenomenon (Sheridan et al., 2015).

A role for EGT in conidial health and conidiation in *A. fumigatus* was apparent following the observation that *A. fumigatus* Δ*egtA*^{26933} colonies appeared paler and produced lower levels of conidia than ATCC26933. EGT also appeared to be involved in conidial protection and conidiogenesis in *N. crassa* (Bello et al., 2012, 2014). Therefore the absence of several conidial related proteins in Δ*egtA*^{26933} compared to ATCC26933 was of particular interest. These were: PMT2, PMT4, FluG, FlbA and RodB. The mannosyltransferases PMT2 (AFUA_1G07690) and PMT4 (AFUA_8G04500) have both been demonstrated to play an important role in conidiation. Deletion of PMT4 led to highly reduced conidiation (Mouyna et al., 2010), while reduced expression of *pmt2* was associated with reduced conidiation and lagged germination times (Fang et al., 2010). FluG (AFUA_3G07140) and FlbA (AFUA_2G1118) are signalling proteins

associated with conidial development in *A. fumigatus* (Mah and Yu, 2006; Park and Yu, 2016). Deletion mutants for both proteins were associated with reduced conidiation and delayed expression of BrlA (Figure 5.8), which is essential for conidiation in *A. fumigatus*. Conidial hydrophobin RodB (AFUA_1G17250) is one of two proteins (Along with RodA) that form part of the rodlet layer on the cell wall of *A. fumigatus* conidia (Paris et al., 2003a). The rodlet layer forms a hydrophobic layer around the conidial cell wall, which favours aerial buoyancy and thus aids dispersal of conidia through the air. While RodA may have a role in protecting conidia from macrophages, the role of RodB appears to be entirely structural (Paris et al., 2003a).

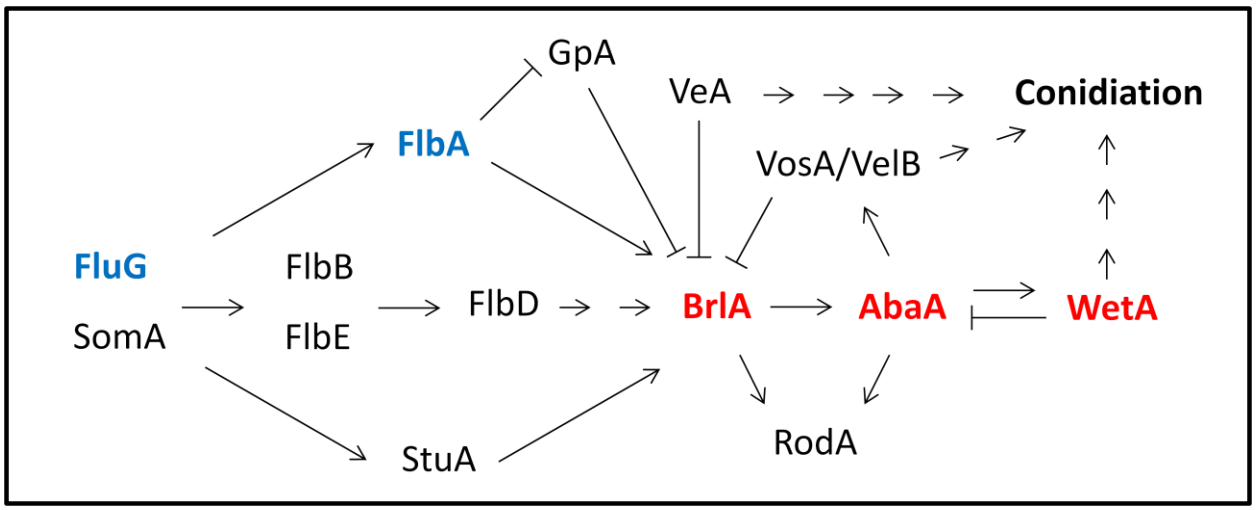

Figure 5.8. Schematic representing the regulation of asexual development in *A. fumigatus*. FluG and FlbA (outlined in blue), absent in Δ*egtA*^{26933} compared to ATCC26933, are upstream regulators of the asexual development central regulatory pathway (outlined in red). Image redrawn from Mah and Yu. (2005), Sheppard et al. (2005) and Alkhayyat et al. (2015).

My data demonstrates that EGT loss leads to an absence of a range of proteins associated with *A. fumigatus* conidia, with two mannosyltransferases, two signaling proteins and one structural protein affected. This indicates that EGT plays a significant role in conidiation in *A. fumigatus*, potentially through the management of ROS levels. ROS is known to function as signalling molecules in fungi and has been demonstrated to regulate cellular differentiation, virulence and hyphal growth (Breitenbach et al., 2015). Kayano et al. (2013) have reported that conidiation, in addition to polarised growth and hyphal fusion, is regulated by ROS in *Epichloë festucae*. Thus, the defects in conidiation observed in Δ*egtA*^{26933} may be due to altered cellular redox state.

Phenotypic characterisation of Δ*egtA*^{26933} in Chapter 4 demonstrated that Δ*egtA*^{26933} is significantly sensitive to cell wall perturbing agents compared to ATCC26933 (Section 4.2.12). This indicated that EGT absence resulted in alterations to *A. fumigatus* cell wall composition. This was supported by proteomic data which demonstrated several proteins related to cell wall biosynthesis were found to have differential abundance in Δ*egtA*^{26933} compared to ATCC26933 under basal conditions. A 1,3-beta-glucanosyltransferase (GEL5; AFUA_8G02130) showed a $\log_2$ 1.18 fold increase in abundance. This is a glycosylphosphatidylinositol (GPI)-anchored protein involved in the elongation of the β(1-3) glucans in the cell wall (Gastebois et al., 2010). The putative chitin synthase activator Chs3 (AFUA_3G05580) was shown to be absent in Δ*egtA*^{26933} compared to ATCC26933. Chitin synthase activators play a role in the activity and localization of chitin synthases. Loss of a chitin synthase activator causes decreased abundance of chitin in the cell wall (Reyes et al., 2007). A putative cell wall glucanase CRH3 (AFUA_3G09250) was also demonstrated to be absent in Δ*egtA*^{26933} compared to ATCC26933. CRH3 is an ortholog of *S. cerevisiae* CRH1, a chitin transglycosylase, which functions to transfer chitin to β(1-6) and β(1-3) glucans in the cell wall (Cabib, 2009; Mouya et al., 2013). The mannosyltransferases PMT2 (AFUA_1G07690) and PMT4 (AFUA_8G04500) were described previously due to their role in conidiation and were both absent in Δ*egtA*^{26933} compared to ATCC26933 under basal conditions. However both proteins have been demonstrated to participate in cell wall biosynthesis as well. Decreased expression of *pmt2* resulted in sensitivity to cell wall-perturbing agents and alterations to cell wall contents (Fang et al., 2010). Electron microscopy analysis of a PMT4 deletion mutant revealed an electron-dense layer at the surface of the cell wall that was not observed in the wild-type. This suggests that an increase in secreted proteins to the cell wall is observed following PMT4 deletion (Mouyna et al., 2010). AFUA_3G08110, described as a putative cell wall protein, was also absent in Δ*egtA*^{26933}. Little information is available about the function or role of this protein in the cell wall of *A. fumigatus*, though downregulation of gene transcript has been associated with exposure to amphotericin B, calcium and human platelets (Soriani et al., 2008; Gautam et al., 2008; Perkhofer et al., 2015). This suggest that downregulation of the AFUA_3G08110 gene is associated with stress. The putative MAP kinase kinase Mkk2 (AFUA_1G05800) has been demonstrated to form part of the cell wall integrity (CWI) signalling pathway and deletion of *mkk2* resulted in a significant drop in radial growth and sensitivity to cell wall-perturbing agents

(Valiante et al., 2009). Given its role in CWI signalling, the absence of Mkk2 is likely responsible for the differential abundance of the other cell wall proteins observed.

Under ROS conditions, two cell wall biosynthesis proteins had differential abundance in Δ*egtA*^{26933} compared to ATCC26933. A putative class V chitinase (AFUA_3G11280) showed a $\log_2$ 2.05 fold increase in abundance. Chitinases catalyse the hydrolytic breakdown of glycan bonds in chitin and play a role in reshaping the cell wall (Adams, 2004). A putative cell wall integrity signalling protein (Lsp1/Pil1; AFUA_6G07520) showed a $\log_2$ 1.63 fold increase in abundance in Δ*egtA*^{26933} compared to ATCC26933 under ROS conditions.

As demonstrated, loss of EGT leads to differential regulation of a variety of cell wall related proteins, particularly under basal conditions. The absence of the MAP kinase kinase Mkk2 is of particular significance as it is it part of the CWI signalling pathway and its absence could be expected to have a knock-on effect on other proteins due to its role in regulating transcription (Valiante et al., 2009). This proteomic data, in concurrence with the phenotypic data that demonstrated Δ*egtA*^{26933} is sensitive to cell wall perturbing agents, demonstrates that EGT absence results in alterations to cell wall biosynthesis in *A. fumigatus*. As with conidiation, this may linked with perturbations in ROS signalling. It has been observed in plants that ROS signalling regulates the cell wall (Kärkönen and Kuchitsu, 2015). However to my knowledge, this has not been observed in fungi before.

The methyltransferase VipC was demonstrated to have increased abundance in Δ*egtA*^{26933} compared to ATCC26933 under basal conditions ($\log_2$ 1.23 fold) and shows a larger increase in abundance under ROS conditions ($\log_2$ 2.5 fold). VipC was characterised in *A. nidulans* by Sarikaya-Bayram et al. (2014), where it was demonstrated that VipC, in conjunction with a second methyltransferase, VapB, interacts with the velvet complex (VelB-VeA-LaeA) to regulate activation of sexual development. Elgabbar and Han (2015) attempted to investigate VipC function in *A. fumigatus* through the generation of a deletion mutant. However no phenotype was observed and thus VipC function in *A. fumigatus* remains to be elucidated. VipC function, as described in *A. nidulans,* may not carry over to *A. fumigatus* due to the differences in sexual development between *A. nidulans* and *A. fumigatus*. While *A. nidulans* readily switches between sexual and asexual development depending on light exposure, with VipC playing a key role in differentiation, asexual development dominates in *A. fumigatus*. Indeed, identification of a

sexual cycle in *A. fumigatus* was only confirmed within the last decade, with specific conditions required for the formation of sexual fruiting bodies (6 months incubation at 30 ^{o}C on parafilm-sealed Oatmeal agar in darkness)(O'Gorman et al., 2009). Thus it appears that sexual development only occurs in *A. fumigatus* under very specific circumstances, in contrast to *A. nidulans* where sexual development occurs readily (Sarikaya-Bayram et al., 2014). Due to the significant differences in environmental triggers necessary for sexual development between these two *Aspergilli*, it cannot be assumed that VipC function is identical in *A. fumigatus*. Given the dominance of the asexual cycle *A. fumigatus*, the paler conidia and reduced conidiation phenotypes observed in Δ*egtA*^{26933}, the subsequent proteomic data describing the absence of five conidial related proteins Δ*egtA*^{26933} and concurrent proteomic data demonstrating increased abundance of VipC in Δ*egtA*^{26933}, a role for VipC in regulating asexual development in *A. fumigatus* is a distinct possibility.

VipC had increased abundance in Δ*egtA*^{26933} compared to ATCC26933 under basal conditions ($\log_2$ 1.23 fold). This increase in abundance is larger under ROS conditions ($\log_2$ 2.5 fold), where it shows more than twice an increase in Δ*egtA*^{26933} compared to ATCC26933 upon addition of H_2O_2. As a SAM-dependant methyltransferase, VipC may be regulated by availability of intracellular SAM. It has been demonstrated that addition of H_2O_2 increased the abundance of CBL, which was predicted to increase levels of intracellular SAM. Thus, the larger increase in abundance of VipC in Δ*egtA*^{26933} compared to ATCC26933 under ROS conditions may be due to increased availability of SAM.

An increase in abundance of phenylalanine ammonia lyase (PAL; AFUA_2G09110) was observed in Δ*egtA*^{26933} compared to ATCC26933 under basal conditions ($\log_2$ 2.71 fold), where it was the protein with the largest increase in abundance in the data set (Appendix 1). Under ROS conditions, PAL showed an even greater increase in abundance in Δ*egtA*^{26933} compared to ATCC26933 ($\log_2$ 3.73 fold). This indicates that PAL is of particular significance in Δ*egtA*^{26933} and addition of H_2O_2 increases the demand for PAL. PAL is involved in the breakdown of phenylalanine, converting it into ammonia and *trans*-cinnamic acid (Camm and Towers, 1973). This reaction is carried out in fungi in order to release carbon and nitrogen from phenylalanine, in a catabolic reaction (Fritz et al., 1976). In plants however, PAL is involved in defence through the generation of phenyl compounds. While this strategy has been well documented in response

to infection (Shadle et al., 2003; Kim and Hwang, 2014; Tonnessen et al., 2015), genes encoding for PAL have been noted to be induced through oxidative stress (Desikan et al., 1998; Lee et al., 2003). Furthermore, Gao et al. (2008) demonstrated a rise in PAL in the leaves and roots of *Jatropha curcas* L. seedlings in response to copper induced stress. While this has not been observed in fungi previously, this rise in PAL in response to EGT loss could be compensating for the loss of an oxidative stress defence mechanism in EGT by providing an alternative means of dissipating ROS.

There are, however, alternative hypotheses for the increased abundance of PAL. PAL has been noted to have a high similarity to histidine ammonia lyase (HAL)(Schwede et al., 1999), an enzyme which catalyses the breakdown of histidine in a similar manner to PAL. In the absence of EGT biosynthesis, histidine levels may elevated as it is not being used for EGT production. In this instance, histidine may need to be catabolised, requiring the use of a HAL. If PAL was misannotated, or otherwise have HAL activity, increased abundance of the protein would be required to dissipate elevated histidine levels.

Another potential reason for increased abundance of PAL involves ergothioneine degradation. Muramatsu et al. (2013) noted in *Burkholderia* sp. HME13 that an enzyme with ergothionase degradation activity showed 17 % similarity to PAL. This raises the possibility that the PAL observed is actually an ergothionase, indeed a fungal ergothionase would be a particularly novel discovery. Thus the increased abundance of PAL in Δ*egtA*^{26933} raises several intriguing questions, which warrant future investigation.

The work presented in this chapter demonstrates that loss of EGT in *A. fumigatus* affects a range of systems including redox homeostasis, sulphur metabolism, secondary metabolism, conidiation & conidial health and the cell wall. This data has greatly aided in elucidation of phenotypes observed in Δ*egtA*^{26933} in Chapter 4, including the identification of key proteins which may play crucial roles in particular phenotypes, such as HapC in oxidative stress sensitivity, GliT in reduced gliotoxin production and VipC in reduced conidiation. The observation of a "cystathionine switch" was another significant find from this data, a novel switch in sulphur metabolism centred on cystathionine. The increased abundance of a PAL in Δ*egtA*^{26933} compared to ATCC26933 under basal conditions, and furthermore under ROS conditions, raised several

questions as its role in *A. fumigatus*. For this reason, PAL, alongside VipC which was also discussed in this chapter, were investigated further in Chapter 6.

Chapter 6

Phenotypic Characterisation of *A. fumigatus* Δ*palA*^{26933}, Δ*egtB*^{26933} and Δ*vipC*^{26933}

6.1 Introduction

The work presented in Chapters 4 and 5 characterised EGT functionality in *A. fumigatus*. Through analysis of the Δ*egtA*^{26933} mutant, EGT was demonstrated to function as an antioxidant that plays a key role in protection against high levels of ROS. Furthermore, EGT absence altered conidiation, cell wall integrity signalling and secondary metabolism. Three proteins were identified for further study with the aim of further understanding EGT biosynthesis and function in *A. fumigatus*, and the systems with which it interacts. These were phenylalanine ammonia lyase (PAL; AFUA_2G09110), EgtB (AFUA_2G13295) and VipC (AFUA_8G01930). Deletion mutants for the corresponding gene for each protein were created described as Chapter 3.

PAL catalyzes the conversion of phenylalanine into ammonia and *trans*-cinnamic acid (Camm and Towers, 1973). It was observed to have increased abundance in Δ*egtA*^{26933} compared to ATCC26933 under both basal and ROS conditions. Under basal conditions, PAL had a $\log_2$ 2.71 fold increase in abundance in Δ*egtA*^{26933}, the largest increase in abundance of any proteins in that data set. Under ROS conditions, PAL had a $\log_2$ 3.73 fold increase in abundance. Thus, PAL was identified as a protein which may play a key role in *A. fumigatus* adaptation to *egtA* deletion.

PAL activity has been detected in a diverse range of plants, select fungi and two prokaryotes: *Streptomyces verticillatu* and *Streptomyces maritimus* (Hyun et al., 2011; Xiang and Moore, 2005). PAL function has been extensively studied in plants, where it is of much interest due to involvement in the first and committed step of the phenyl propanoid pathway (Zhang and Liu, 2015). By converting phenylalanine into *trans*-cinnamic acid, phenylalanine can be diverted from primary to secondary metabolism. *Trans*-cinnamic acid is then converted into a range of metabolites with important physiological functions. The best characterised function of these phenyl propanoid compounds is in defence against pathogens (Shadle et al., 2003; Kim and Hwang, 2014; Tonnessen et al., 2015). However, they also function in mechanical support (Davin and Lewis, 1992), stress defence (Dixon and Paiva, 1995), pigments (Holton and Cornish, 1995), and signalling (Xie et al., 1995). PAL is proposed to act as a regulator of the biosynthesis of these compounds, as gene expression is induced by environmental factors such as pathogenic attacks, tissue wounding, UV irradiation, exposure to heavy metals, low temperatures, and low levels of nitrogen, phosphate, or ions (Dixon and Paiva, 1995; Weisshaar

and Jenkins, 1998). PAL, through the production of these phenyl propanoid compounds, has also been demonstrated to play a role in plant development (Jones, 1984).

In contrast to plants, PAL function in fungi has not been studied nearly as extensively. PAL activity has been demonstrated in several basidiomycetes such as *Rhodotorula* (Ogata et al., 1967), *Ustilago hordei* (Kim et al., 1996), *Schizophyllum commune* (Moore and Towers, 1967), and *Sporobolomyces roseus* (Camm and Towers, 1969). Additionally, it has been reported in deuteromycetes such as *Alternaria* sp. (Pridham and Woodhead, 1974), *Rhizoctonia solani* (Kalghatgi et al., 1974) and *Penicillium brevicompactum* (Campbell et al., 1987). PAL function has been demonstrated in a single ascomycete, *Nectria cinnabarina* (Swimburne and Brown, 1975). No role beyond catabolism of phenylalanine has been demonstrated in fungi, where it has been shown that PAL can catabolise phenylalanine for use as a carbon or nitrogen source in *Rhodotorula glutinis (*Marusich et al., 1981). *Lentinus lepideus* produces phenylpropanoid compounds from cinnamic acid derived from phenylalanine via PAL. These include *p*-coumaric acid, caffeic acid, isoferulic acid, phloretic acid, and *p*-methoxycinnamic acid (Power et al., 1965). No physiological role for these compounds has been determined however. The production of benzoic acid derivatives from *trans*-cinnamic acid has also been demonstrated (Nambudiri et al., 1970; Campbell et al., 1987).

Thus, no clear function for fungal PAL has been determined beyond phenylalanine catabolism. The observed increased abundance of PAL in Δ*egtA*^{26933} under both basal and ROS conditions is therefore intriguing. Several phenylpropanoid compounds are known to have antioxidant activity (Korkina, 2007) and PAL gene expression has been demonstrated to be induced in plants by exposure to oxidative stress (Desikan et al., 1998; Lee et al., 2003). Increased PAL abundance may therefore be an oxidative stress response in the absence of EGT. Alternatively, this may be a misannotation of a closely related histidine ammonia lyase (HAL) (Schwede et al., 1999), which may have increased abundance to catabolise increased levels of histidine resulting from loss of EGT biosynthesis. Finally, Muramatsu et al. (2013) reported an ergothionase from *Burkholderia* sp. HME13 with 17 % similarity to PAL. Suggesting PAL may have ergothioneine degradation activity.

EgtB is predicted to catalyse the final step of EGT biosynthesis, which is the conversion of hycynylcysteine sulphoxide into EGT via cleavage of the cysteine residue at the sulphur atom

(Figure 6.1). *egtB* was identified as an ortholog of *S. pombe egt2* (Pluskal et al., 2014). Deletion of *egt2* in *S. pombe* resulted in a 74.5 % reduction in EGT levels compared to wild-type. As residual levels of EGT remained, *egt2* was determined to be non-essential for EGT production in *S. pombe.* Pluskal et al. speculated that the final reaction may be catalysed non-specifically by other PLP-binding enzymes. This is supported by data from Seebeck (2010), who demonstrated that EGT could be produced *in vitro* using an unrelated PLP-binding β-lyase from *Erwinia tasmaniensis*, which cannot biosynthesise EGT. By using the Δ*egtB*^{26933} mutant, it can be determined whether *egtB* contributes to EGT biosynthesis in *A. fumigatus*, and if it is essential for EGT biosynthesis if that is the case.

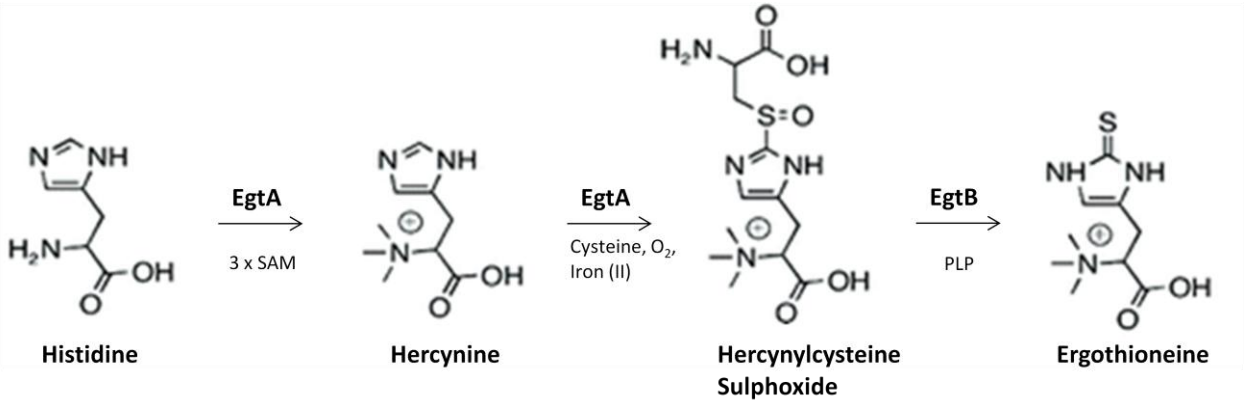

Figure 6.1. Proposed EGT biosynthetic pathway for *A. fumigatus*. EgtA catalyses the first two steps, converting histidine into hercynine and hercynine into hercynalcysteine sulphoxide. EgtB catalyses the final step, converting hercynylcysteine sulphoxide into ergothioneine.

VipC is a methyltransferase that has been demonstrated to regulate sexual and asexual development in response to the presence or absence of light in *A. nidulans* (Sarikaya-Bayram et al., 2014). In *A. nidulans*, VipC functions in conjunction with a second methyltransferase, VapB. In the absence of appropriate environmental signal (i.e. light), the VipC-VapB complex is tethered to the membrane bound VapA. While VipC-VapB is bound, the nuclear complex VelB-VeA-LaeA activates transcription for sexual development. When exposed to light, VipC-VapB is released from VapA and localises to the nucleus. In the nucleus, VipC-VapB interacts with VeA, reducing the nuclear import and protein stability of the VelB-VeA-LaeA complex, and thus repressing sexual development. Simultaneously, VapB decreases histone 3 lysine 9 trimethylation, which activates *brlA* and *abaA* transcription, resulting in asexual development (Figure 6.2). Deletion of VipC in *A. nidulans* resulted in decreased asexual development and

increased sexual development when grown in light, compared to wild-type. No changes were observed when grown in darkness, demonstrating that VipC functions to regulate development in response to light.

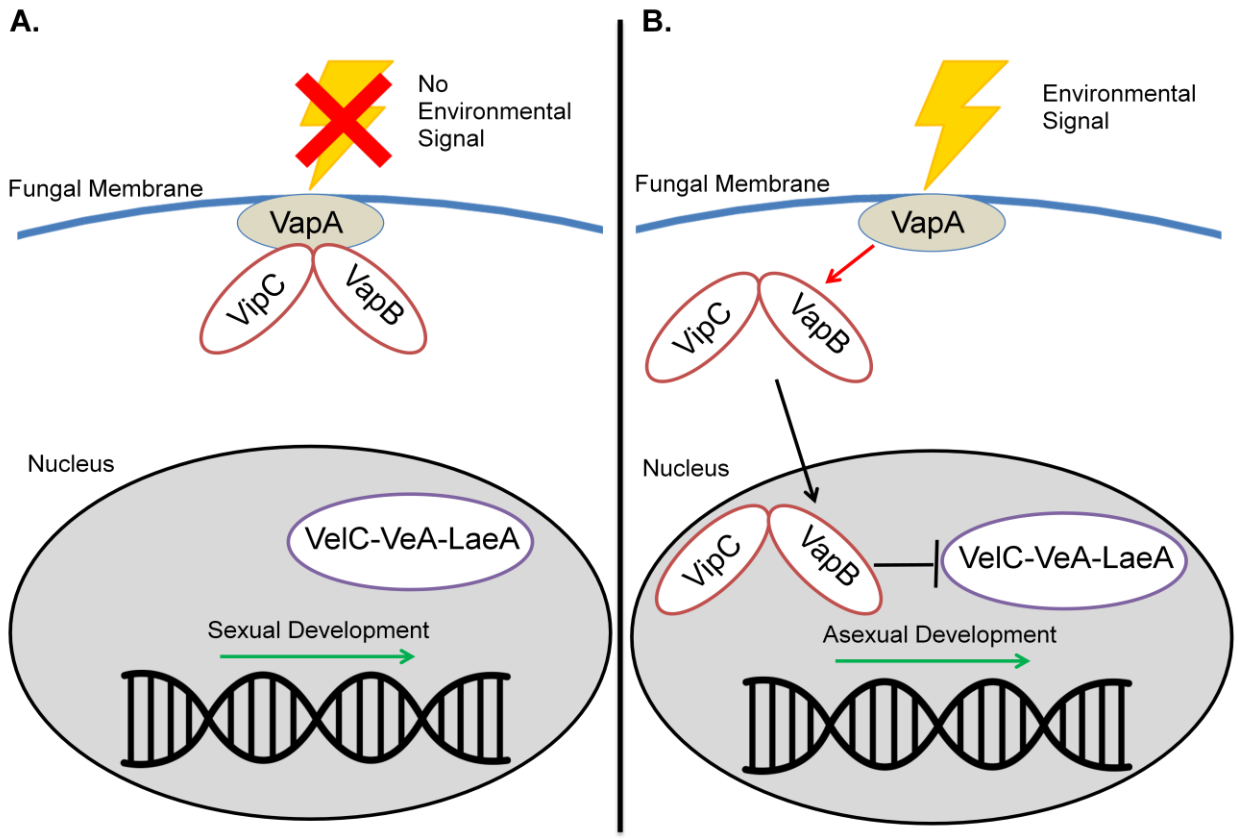

Figure 6.2. Regulation of sexual and asexual development in response to light in *A. nidulans*. (A) VipC-VapB remains tethered to membrane bound VapA in the absence of light. VelC-VeA-LaeA complex is localized to the nucleus and induces sexual development. (B) VipC-VapB is released from VapA and localizes to the nucleus when exposed to light. VipC-VapB reduces VelC-VeA-LaeA stability and nuclear import. Increased levels of nuclear VapB induce asexual development. Image adapted from Sarikaya-Bayram et al. (2014).

Unexpectedly, VipC was found to have increased abundance in *A. fumigatus* Δ*egtA*^{26933} under basal conditions ($\log_2$ 1.23 fold; Table 5.1), which further increased under ROS conditions ($\log_2$ 2.5 fold; Table 5.2). Δ*egtA*^{26933} had reduced levels of conidiation compared to ATCC26933 and the increased abundance of VipC was hypothesised to be involved in this phenotype due to its role in regulating asexual development in *A. nidulans*. However, it cannot be assumed that VipC

functions identically in *A. fumigatus* as sexual development is significantly different in *A. fumigatus* compared to *A. nidulans*. While *A. nidulans* readily forms sexual fruiting bodies when grown in the absence of light, *A. fumigatus* requires very specific conditions to activate sexual development (O'Gorman et al., 2009). Given the role of VipC in regulating development in response to environmental conditions in *A. nidulans*, and the differences in environmental conditions required to activate sexual development in these two species, VipC could be speculated to function differently in *A. fumigatus*. Elgabbar and Han (2015) attempted to investigate VipC function in *A. fumigatus* by generating a Δ*vipC* mutant. However they did not report any phenotypes and concluded that due to redundancy, no role for VipC in *A. fumigatus* could be established. However as a consequence of LFQ proteomic data demonstrating increased VipC abundance in Δ*egtA*^{26933}, Δ*vipC*^{26933} was employed to investigate VipC function in *A. fumgatus*, and also to elucidate the link between VipC and *egtA* deletion.

The aim of the work presented in this chapter was to:

(i) Investigate the phenotypic effect of *palA* deletion in *A. fumigatus* following exposure to ROS inducing agents, gliotoxin and high concentrations of His and Phe.

(ii) Investigate the effect of *palA* deletion on gliotoxin production and levels of intracellular EGT and His in *A. fumigatus*.

(iii) Determine if *egtB* contributes to EGT biosynthesis in *A. fumigatus*.

(iv) Investigate the effect of *egtB* deletion in *A. fumigatus* following exposure to ROS inducing agents and gliotoxin.

(v) Investigate the effect of *egtB* deletion on gliotoxin and glutathione production in *A. fumigatus*.

(vi) Determine if *vipC* deletion affects growth and/or development in *A. fumigatus*.

(vii) Investigate the effect of light exposure on Δ*vipC* growth and development

(viii) Investigate the effect of *vipC* deletion on EGT, gliotoxin and glutathione biosynthesis in *A. fumigatus*.

(ix) Investigate the effect of *vipC* deletion in *A. fumigatus* following exposure to ROS inducing agents and gliotoxin.

(x) Investigate the effect of *vipC* deletion on the *A. fumigatus* proteome using LFQ proteomic analysis.

6.2 Results

6.2.1 Phenotypic characterisation of Δ*palA*^{26933}

6.2.1.1 Analysis of EGT production in ATCC26933 and Δ*palA*^{26933} via RP-HPLC

Mycelia from 72 h cultures of ATCC26933 and Δ*palA*^{26933} in Czapek-Dox broth were harvested and cell lysate supernatants obtained as per Section 2.2.9. Lysate supernatants were alkylated using 5'-IAF as described in Section 2.2.12.1 and analysed via RP-HPLC (Section 2.2.12.6) using fluorescence detection at Ex/Em of 494/518 nm. EGT was detected in both ATCC26933 and Δ*palA*^{26933} at a retention time of 12.4 min (Figure 6.3). Comparing EGT levels by measuring the peak area of 5'-IAF alkylated EGT revealed no significant difference in EGT levels in ATCC26933 and Δ*palA*^{26933}. Deletion of *palA* therefore had no effect on EGT production, suggesting PAL does not influence EGT biosynthesis in *A. fumigatus*.

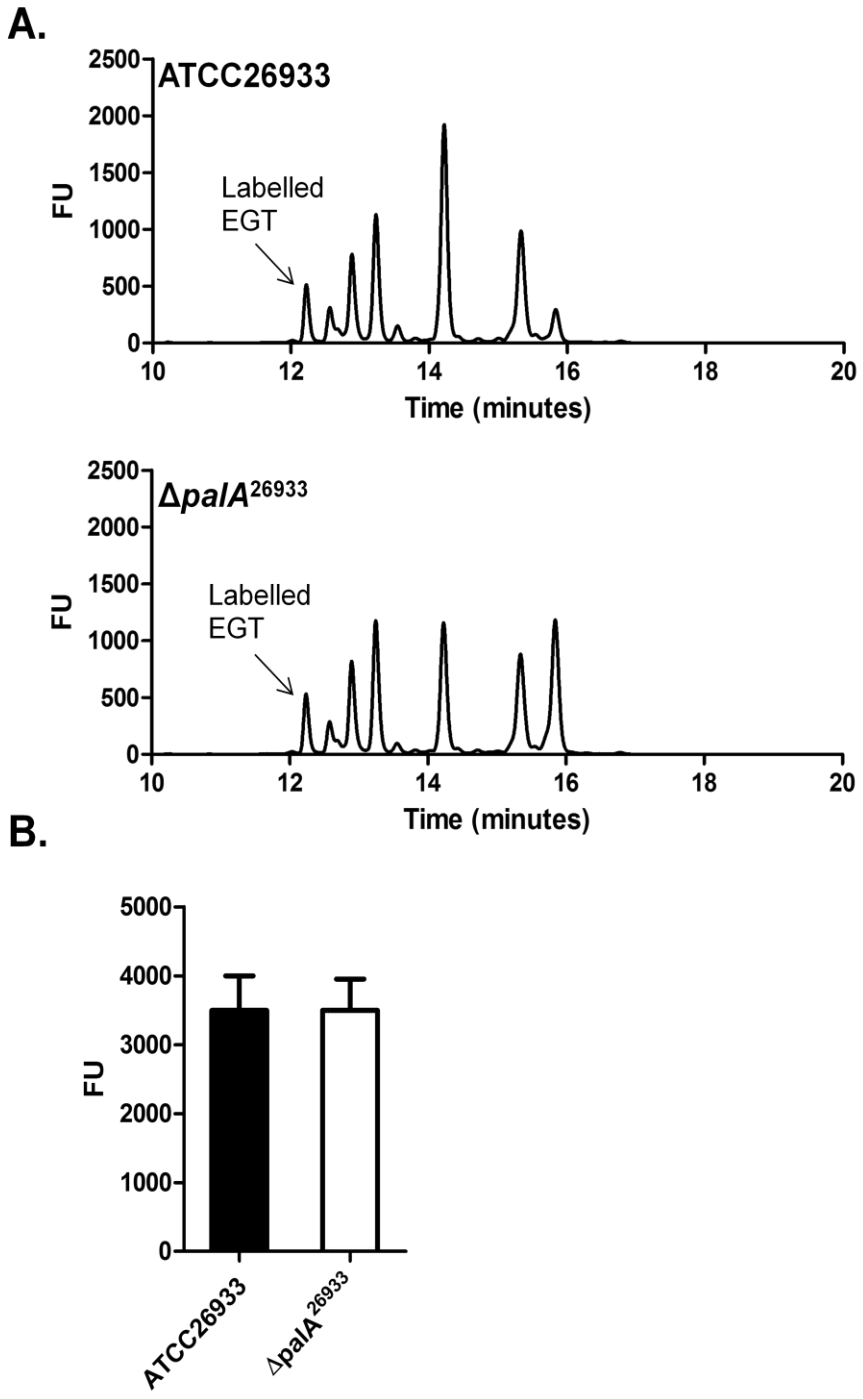

Figure 6.3. Detection and measurement of 5'-IAF alkylated EGT via RP-HPLC. (A) Detection of 5'-IAF alkylated EGT in ATCC26933 and Δ*palA*^{26933} at a retention time of 12.4 min. (B) Comparison of EGT levels in ATCC26933 and Δ*palA*^{26933}. No significant difference in the levels of EGT was observed in ATCC26933 and Δ*palA*^{26933}.

6.2.1.2 Phenotypic analysis of ATCC26933 and Δ*palA*^{26933} in response to ROS inducing agents

6.2.1.2.1 Phenotypic analysis of ATCC26933 and Δ*palA*^{26933} in response to H_2O_2

Sensitivity to H_2O_2 was tested at a range of 0 – 3 mM as per Section 2.2.7. Comparison of radial growth of ATCC26933 and Δ*palA*^{26933} colonies revealed no significant difference between the two strains at any concentration of H_2O_2 tested (Figure 6.4). Deletion of *palA* therefore does not lead to sensitivity to H_2O_2 induced stress.

6.2.1.2.2 Phenotypic analysis of ATCC26933 and Δ*palA*^{26933} in response to menadione

Sensitivity to menadione was tested at a range of 0 – 60 µM (Section 2.2.7). Comparison of radial growth of ATCC26933 and Δ*palA*^{26933} colonies revealed no significant difference between the two strains at any concentration of menadione tested (Figure 6.5). Deletion of *palA* therefore does not lead to sensitivity to menadione induced stress.

6.2.1.2.3 Phenotypic analysis of ATCC26933 and Δ*palA*^{26933} in response to diamide

Sensitivity to diamide was tested at a range of 0 – 1.75 mM (Section 2.2.7). No significant differences in the radial growth of Δ*palA*^{26933} colonies compared to ATCC26933 colonies were observed at any concentration of diamide tested (Figure 6.6). Deletion of *palA* therefore does not lead to sensitivity to diamide induced stress.

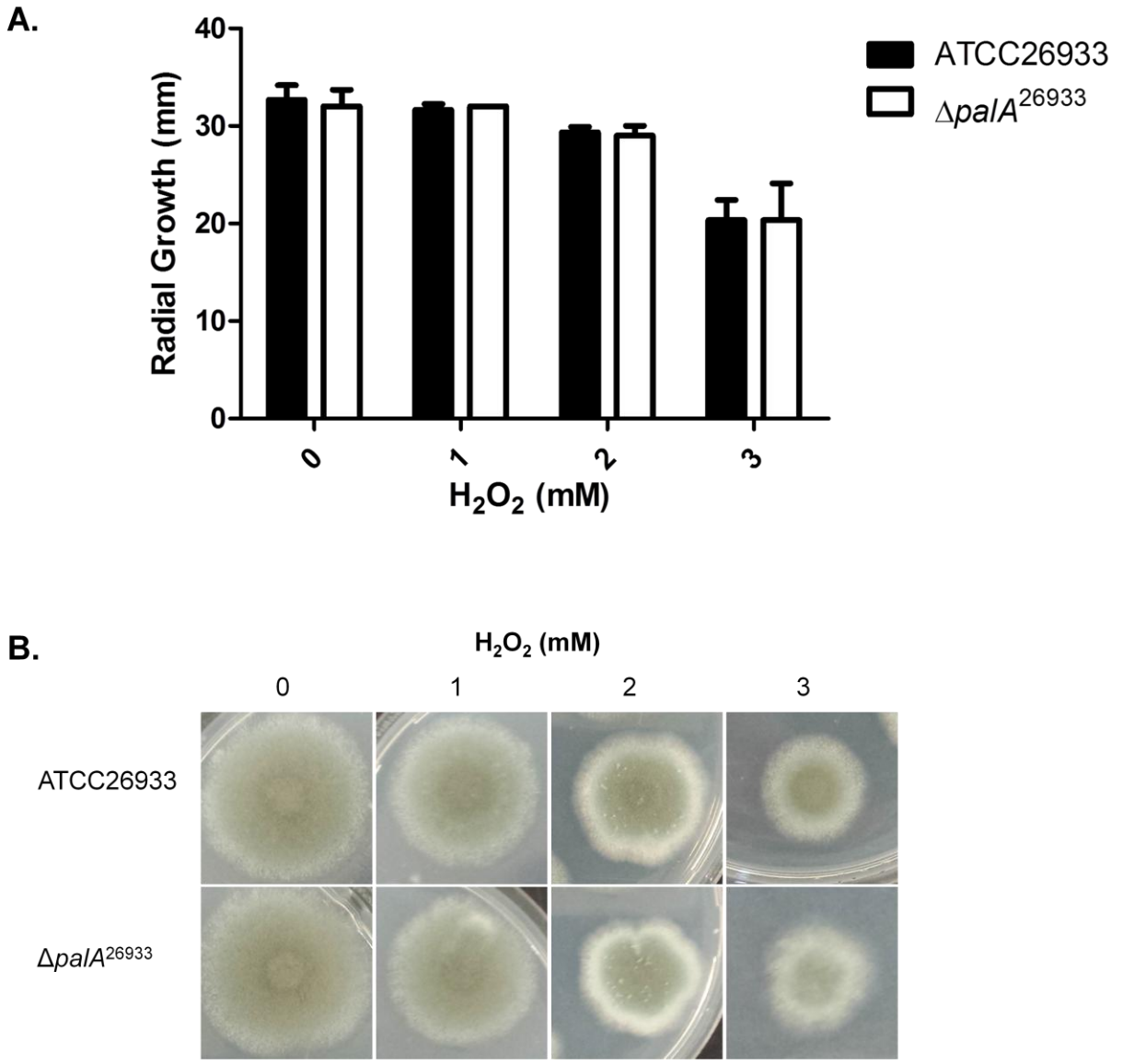

Figure 6.4. H_2O_2 sensitivity assay performed on AMM agar for 72 h. (A) Comparison of radial growth of ATCC26933 and Δ*palA*^{26933} on AMM agar plates containing 0 to 3 mM H_2O_2. Δ*palA*^{26933} shows no significant difference in radial growth compared to ATCC26933 at any concentration of H_2O_2 tested. (B) Images of ATCC26933 and Δ*palA*^{26933} colonies on AMM plates containing 0 to 3 mM H_2O_2. No visible decrease in the size of the Δ*palA*^{26933} colonies can be observed compared to the ATCC26933 colonies at any concentration of H_2O_2 tested.

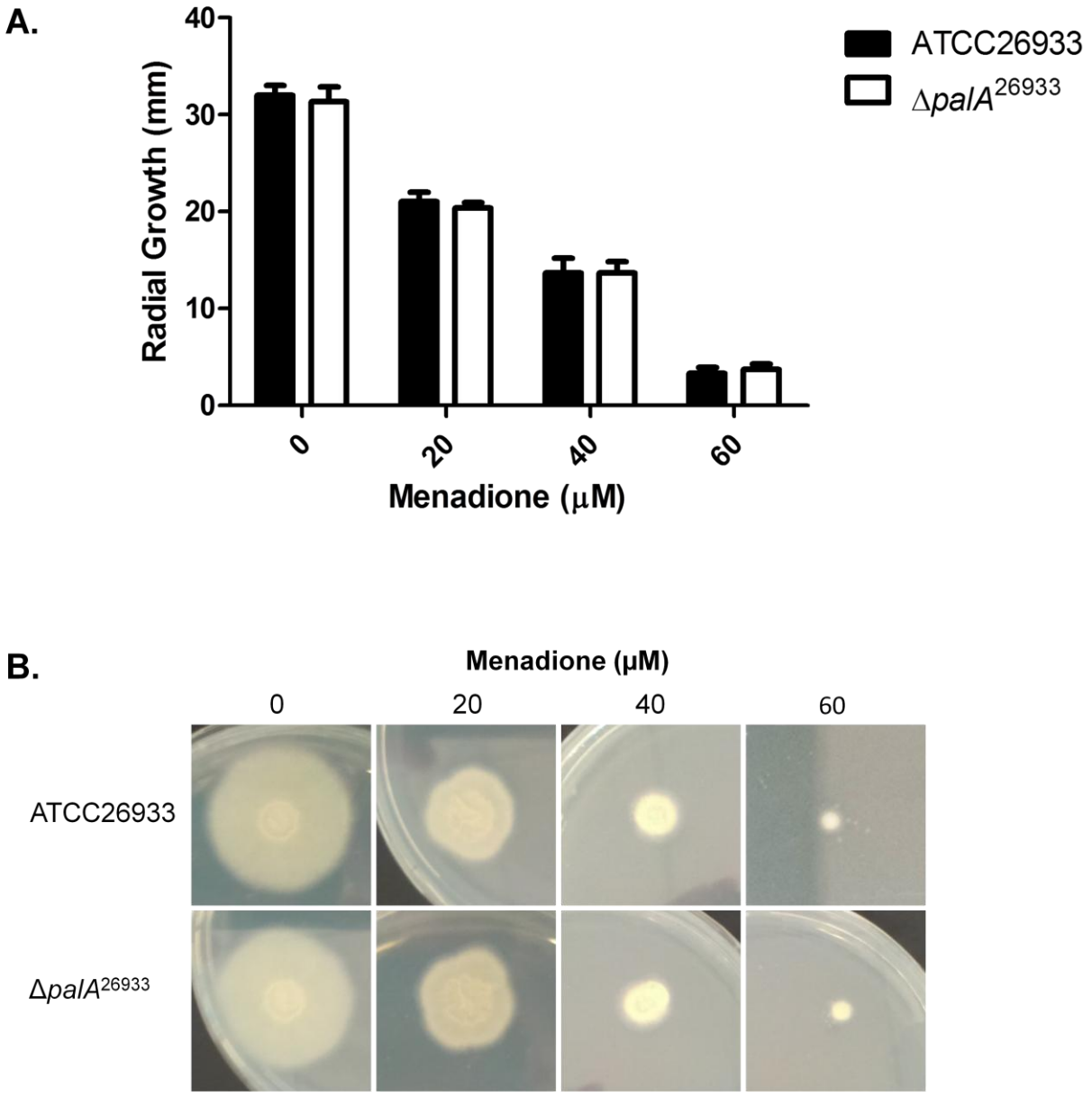

Figure 6.5. Menadione sensitivity assay performed on AMM agar for 72 h. (A) Comparison of radial growth of ATCC26933 and Δ*palA*^{26933} on AMM agar plates containing 0 to 60 µM menadione. Δ*palA*^{26933} shows no significant difference in radial growth compared to ATCC26933 at any concentration of menadione tested. (B) Images of ATCC26933 and Δ*palA*^{26933} colonies on AMM plates containing 0 to 60 µM menadione. No visible decrease in the size of the Δ*palA*^{26933} colonies can be observed compared to the ATCC26933 colonies at any concentration of menadione tested.

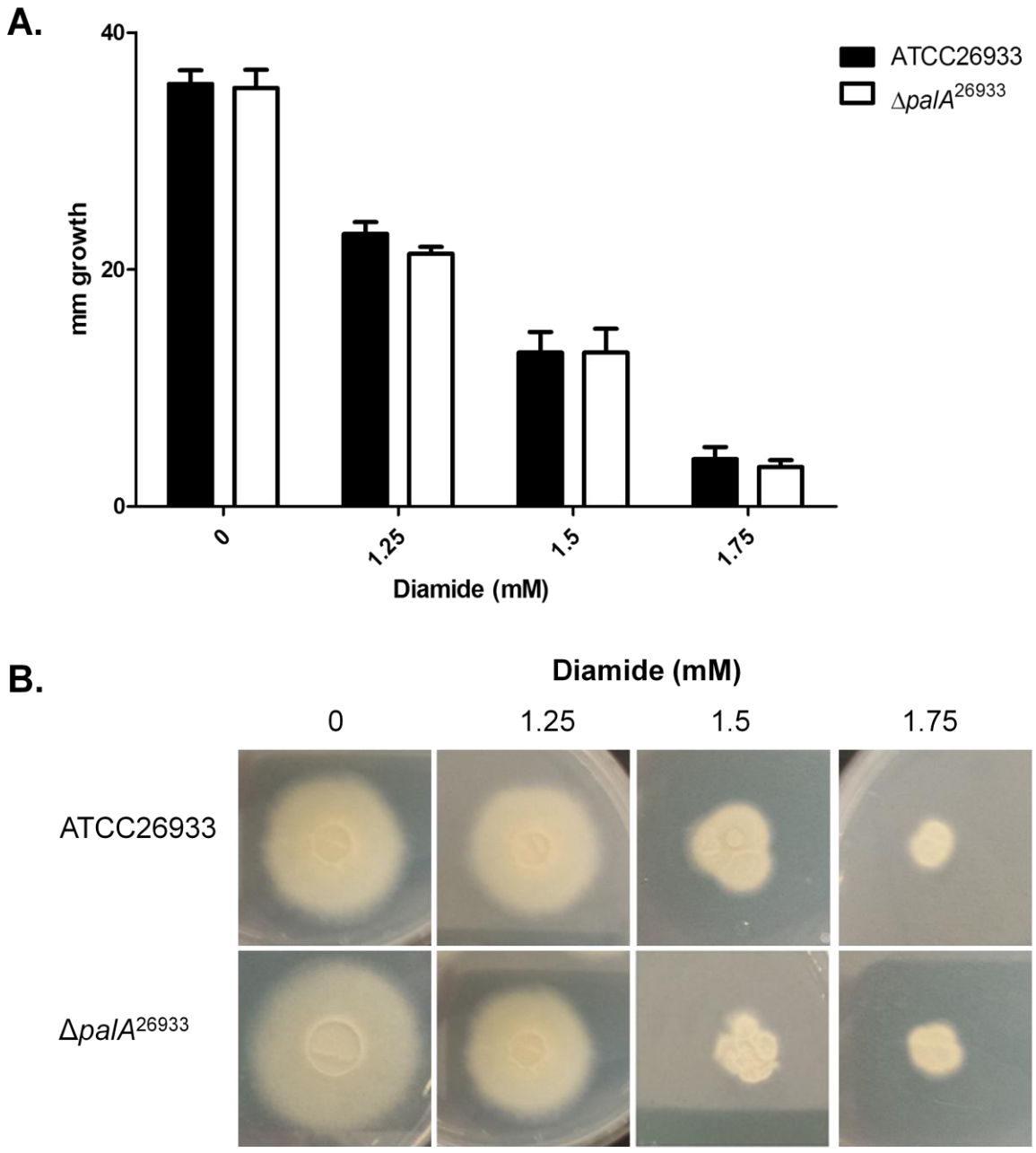

Figure 6.6. Diamide sensitivity assay performed on AMM agar for 72 h. (A) Comparison of radial growth of ATCC26933 and Δ*palA*^{26933} on AMM agar plates containing 0 to 1.75 mM diamide. Δ*palA*^{26933} shows no significant difference in radial growth compared to ATCC26933 at any concentration of diamide tested. (B) Images of ATCC26933 and Δ*palA*^{26933} colonies on AMM plates containing 0 to 1.75 mM diamide. No visible decrease in the size of the Δ*palA*^{26933} colonies can be observed compared to the ATCC26933 colonies at any concentration of diamide tested.

6.2.1.3 Analysis of histidine levels in ATCC26933 and Δ*palA*^{26933} via RP-HPLC

Mycelia from 72 h cultures of ATCC26933 and Δ*palA*^{26933} in Czapek-Dox broth were harvested and cell lysate supernatants obtained as per Section 2.2.9 using *A. fumigatus* phosphate lysis buffer (Section 2.1.12.2). Lysate supernatants and a His standard were labelled using OPA as described in Section 2.2.12.3 and analysed via RP-HPLC (Section 2.2.12.6) using fluorescence detection at an Ex/Em 340/455 nm. His was detected a retention time of 13.4 min and was present in both ATCC26933 and Δ*palA*^{26933} (Figure 6.7). Comparison of His peak height intensities revealed there was no significant difference in His levels in ATCC26933 and Δ*palA*^{26933}. His levels are therefore unaffected by deletion of *palA* in *A. fumigatus*. A peak at 12.5 min appears to be increased in Δ*palA* compared to ATCC26933. This could be due to alterations in the levels of another amino acid.

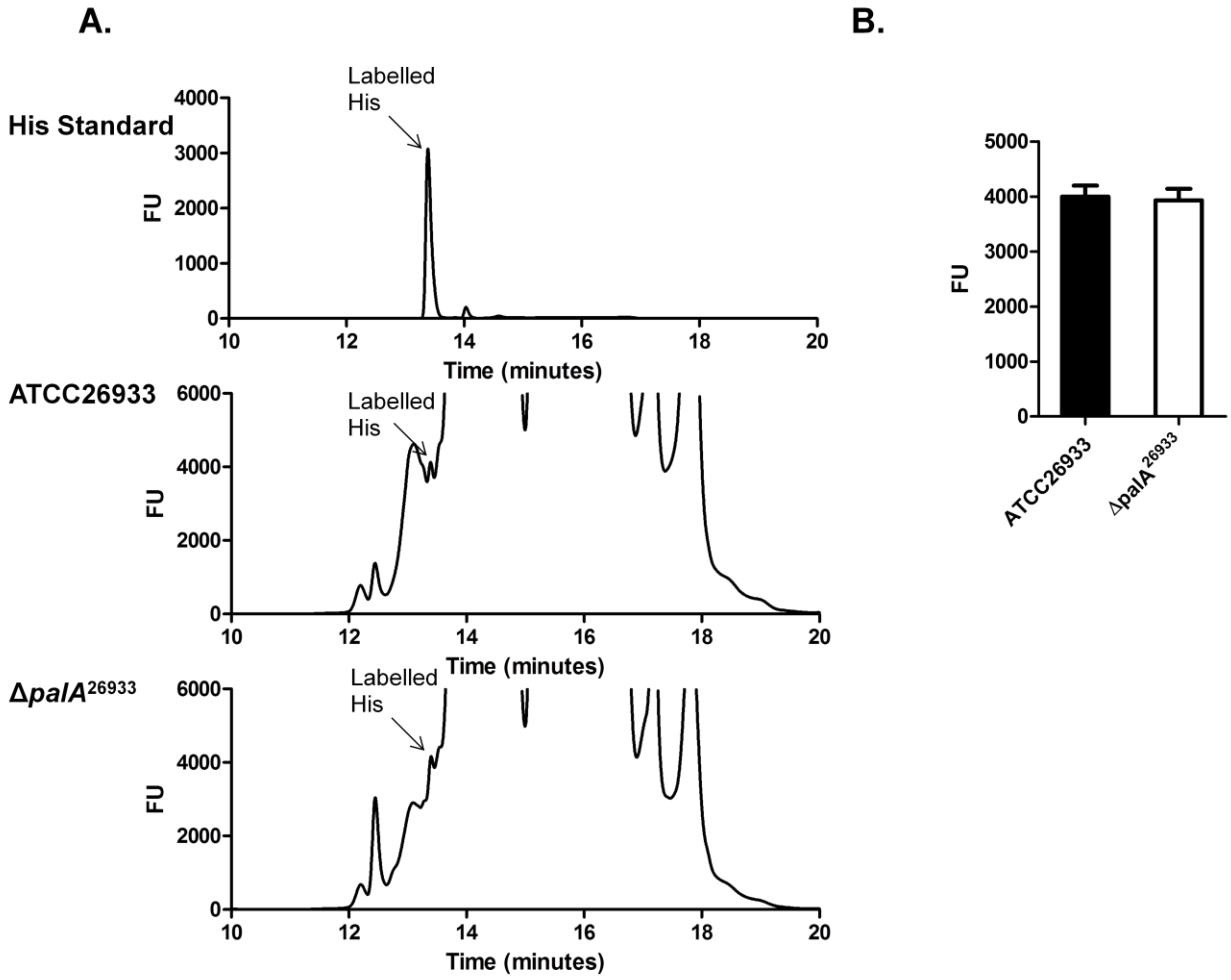

Figure 6.7. Detection and measurement of OPA labelled His via RP-HPLC. (A) Detection of OPA labelled His in a His standard, ATCC26933 and Δ*palA*^{26933}. His is detected at 13.4 min and was detected in both ATCC26933 and Δ*palA*^{26933}. (B) Comparison of His peak heights ATCC26933 and Δ*palA*^{26933}. No significant difference in the levels of His was observed in ATCC26933 and Δ*palA*^{26933}.

6.2.1.4 Phenotypic analysis of ATCC26933 and Δ*palA*^{26933} in response to phenylalanine and histidine

Sensitivity assays for Phe and His were performed in order to determine if *palA* deletion resulted in sensitivity to high levels of either amino acid. Sensitivity to Phe was tested at a concentration of 150 mM, while sensitivity to His was tested at a concentration of 200 mM (Section 2.2.7). Comparison of radial growth of ATCC26933 and Δ*palA*^{26933} colonies revealed no significant difference between the two strains when grown on 150 mM Phe or 200 mM His (Figure 6.8). Loss of *palA* therefore does not result in sensitivity to Phe or His.

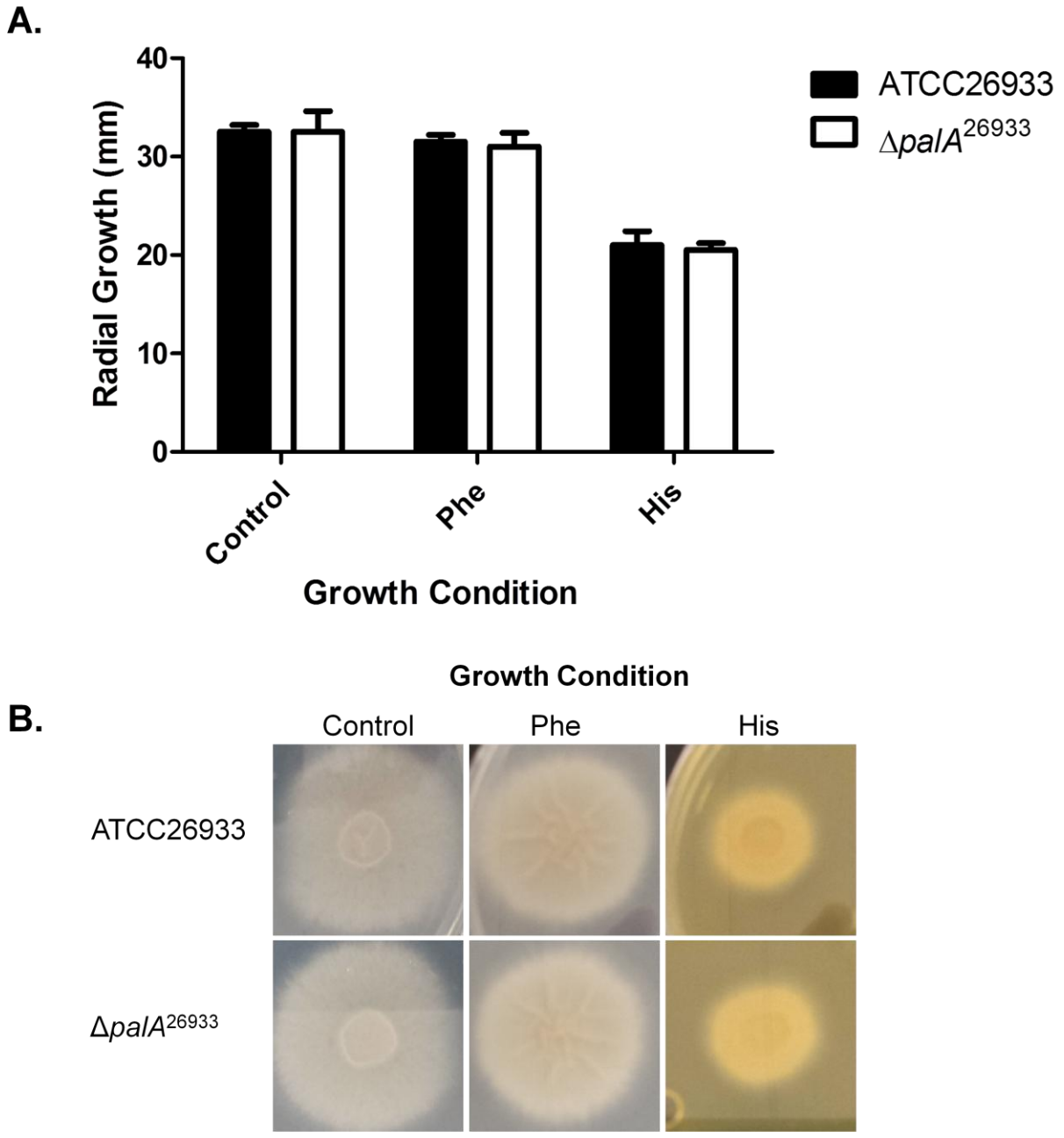

Figure 6.8. Sensitivity assay for Phe and His performed on AMM agar for 72 h. (A) Comparison of radial growth of ATCC26933 and Δ*palA*^{26933} on AMM agar plates containing no additive, 150 mM Phe or 200 mM His. No significant difference in the radial growth of the Δ*palA*^{26933} colonies compared to ATCC26933 was observed under any of the conditions tested. (B) Images of ATCC26933 and Δ*palA*^{26933} colonies on AMM plates containing no additive, 150 mM Phe or 200 mM His. No visible difference in the size of the Δ*palA*^{26933} colonies can be observed compared to the ATCC26933 colony in any of the conditions tested.

6.2.1.5 Analysis of gliotoxin production in ATCC26933 and Δ*palA*^{26933} via RP-HPLC

Supernatants from triplicate 72 h cultures of ATCC26933 and Δ*palA*^{26933} in Czapek-Dox broth were collected and organic extraction carried out as per Section 2.2.10. The organic extracts were then analysed via RP-HPLC (Section 2.2.12.6). In addition, a gliotoxin standard was analysed in the same manner. Gliotoxin was detected at 14.9 min and was observed to be present in both ATCC26933 and Δ*palA*^{26933} (Figure 6.9). A comparison of ATCC26933 and Δ*palA*^{26933} gliotoxin peak areas shows no significant difference in gliotoxin levels in Δ*palA*^{26933} compared to ATCC26933. Deletion of *palA* therefore has no impact on gliotoxin biosynthesis.

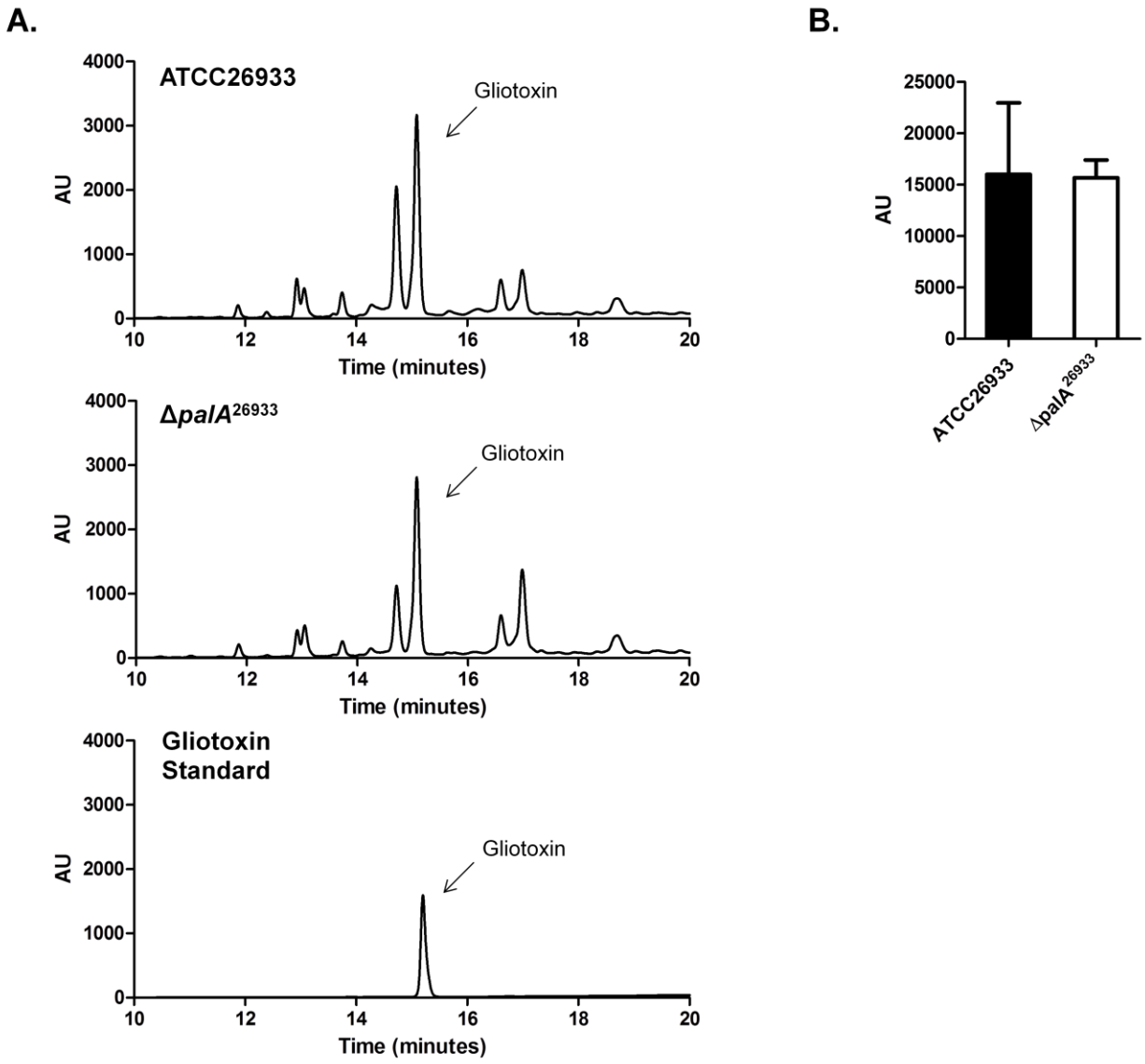

Figure 6.9. Gliotoxin detection via RP-HPLC in ATCC26933 and Δ*palA*^{26933}. (A) RP-HPLC analysis of organic extracts from the supernatants of 72 h cultures of ATCC26933 and Δ*palA*^{26933} (n = 3). Gliotoxin is present in both chromatograms at 14.9 min. (B) Comparison of gliotoxin peak area from RP-HPLC analysis for ATCC26933 and Δ*palA*^{26933} performed in triplicate. No significant difference in gliotoxin levels were observed in Δ*palA*^{26933} compared to ATCC26933.

6.2.1.6 Phenotypic analysis of ATCC26933 and Δ*palA*^{26933} in response to gliotoxin

Sensitivity to gliotoxin was tested at a range of 0 – 20 µg/ml as per (Section 2.2.7). No significant differences in the radial growth of Δ*palA*^{26933} colonies compared to ATCC26933 colonies were observed at any concentration of gliotoxin tested (Figure 6.10). Loss of *palA* therefore has no effect on gliotoxin sensitivity, it can therefore be concluded that *palA* is not involved in gliotoxin self-protection in *A. fumigatus*.

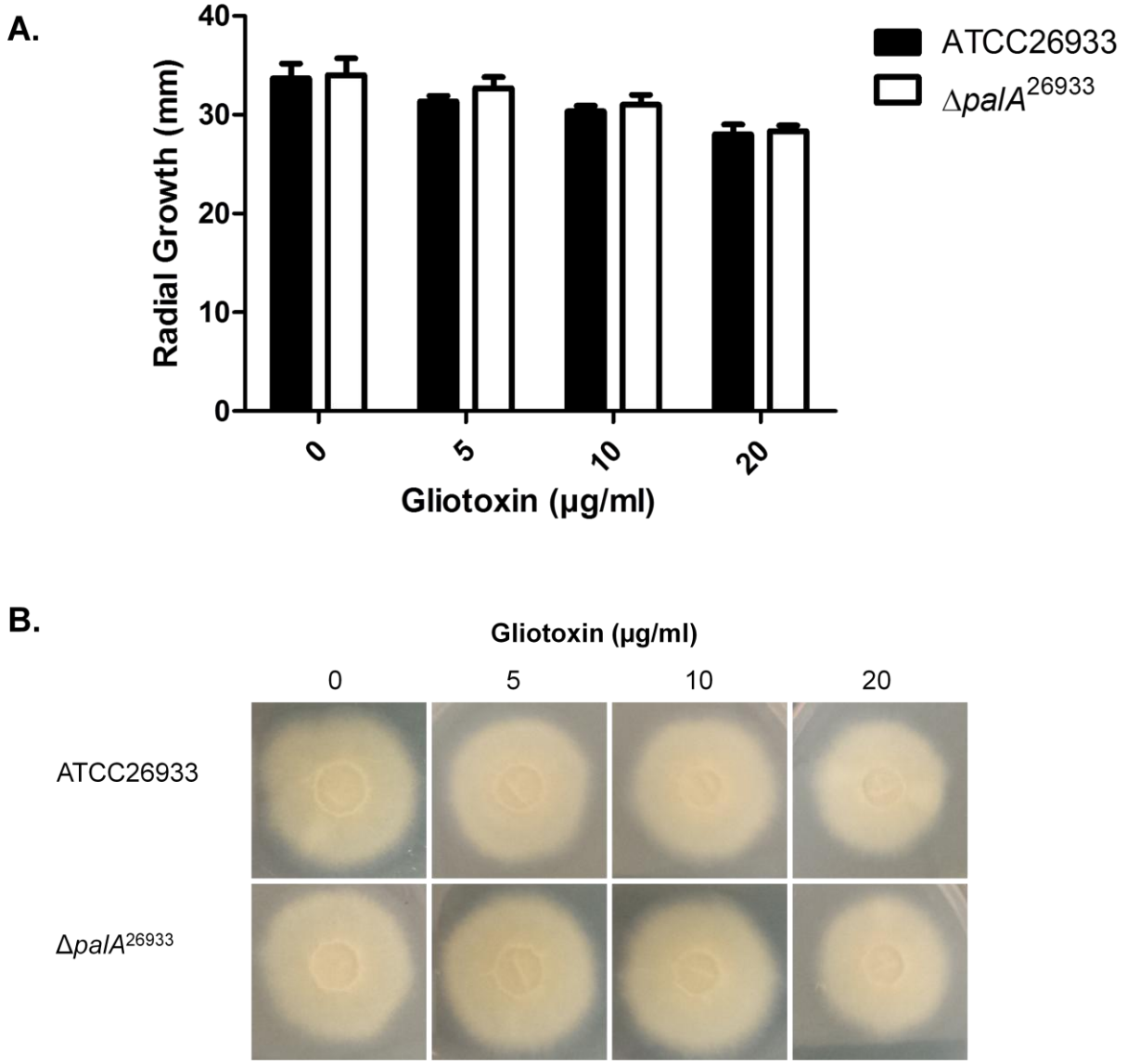

Figure 6.10. Gliotoxin sensitivity assay performed on AMM agar for 72 h. (A) Comparison of radial growth of ATCC26933 and Δ*palA*^{26933} on AMM agar plates containing 0 to 20 µg/ml gliotoxin. Δ*palA*^{26933} shows no significant difference in radial growth compared to ATCC26933 at any concentration of gliotoxin tested. (B) Images of ATCC26933 and Δ*palA*^{26933} colonies on AMM plates containing 0 to 20 µg/ml gliotoxin. No visible decrease in the size of the Δ*palA*^{26933} colonies can be observed compared to ATCC26933 colonies at any concentration gliotoxin tested.

6.2.2 Phenotypic charactarisation of Δ*egtB*^{26933}

6.2.2.1 Analysis of EGT production in ATCC26933 and Δ*egtB*^{26933}

6.2.2.1.1 Analysis of EGT production in ATCC26933 and Δ*egtB*^{26933} via RP-HPLC

Mycelia from 72 h cultures of ATCC26933 and Δ*egtB*^{26933} in Czapek-Dox broth were harvested and cell lysate supernatants obtained as per Section 2.2.9. Normalised lysate supernatants were labelled using 5'-IAF as described in Section 2.2.12.1 and analysed via RP-HPLC (Section 2.2.12.6) using fluorescence detection at Ex/Em of 494/518 nm. EGT was detected in both ATCC26933 and Δ*egtB*^{26933} at a retention time of 12.4 min (Figure 6.11A). Comparing EGT levels by measuring the peak area of 5'-IAF alkylated EGT revealed Δ*egtB*^{26933} produced significantly (P = 0.0465) lower levels of EGT compared to ATCC26933 (Figure 6.11B). EGT levels in Δ*egtB*^{26933} were 72 % of ATCC26933 EGT levels. From this data, it can be concluded that *egtB* contributes to EGT biosynthesis, but is not essential for its production.

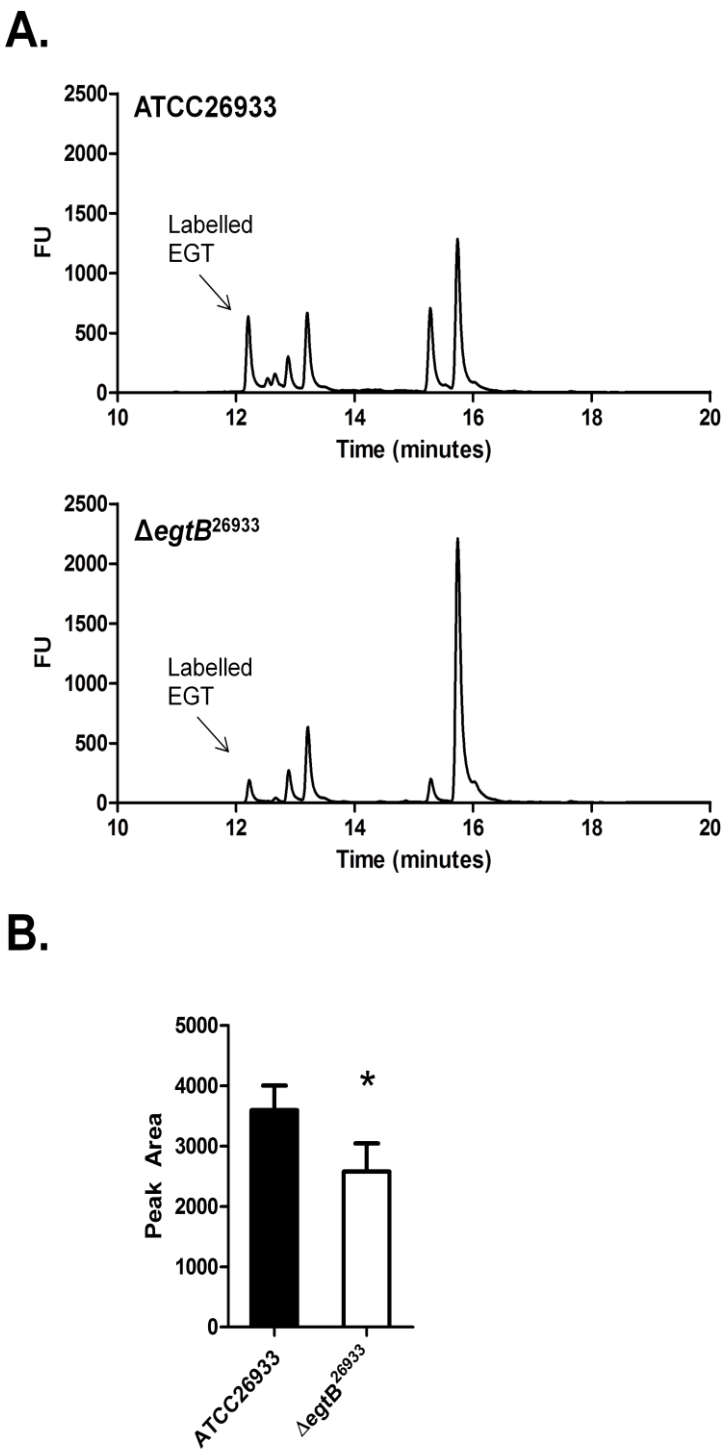

Figure 6.11. Detection and measurement of 5'-IAF alkylated EGT. (A) Detection of 5'-IAF alkylated EGT in ATCC26933 and Δ*egtB*^{26933} at a retention time of 12.4 min. (B) Comparison of EGT levels in ATCC26933 and Δ*egtB*^{26933}. EGT levels are significantly lower in Δ*egtB*^{26933} compared to ATCC26933 (P = 0.0465).

6.2.2.1.2 Analysis of EGT production in ATCC26933 and Δ*egtB*^{26933} via LC-MS/MS

Mycelia from 72 h cultures of ATCC26933 and Δ*egtB*^{26933} and in Czapek-Dox broth were harvested and cell lysate supernatants obtained as per Section 2.2.9. Lysate supernatants were alkylated using 5'-IAF (Section 2.2.12.1), TCA precipitated (Section 2.2.12.2) and analysed via LC-MS/MS (Section 2.2.12.7). In addition, an alkylated and TCA precipitated EGT standard was analysed in the same manner. 5'-IAF alkylated EGT eluted at 5.3 min, with an *m/z* of 617 (Gallagher et al., 2012). Extracted ion chromatograms (*m/z*: 617) for ATCC26933 and Δ*egtB*^{26933} demonstrated the presence of EGT in ATCC26933 and Δ*egtB*^{26933} (Figure 6.12). Comparison of EGT peak intensity confirmed Δ*egtB*^{26933} produced significantly ($P = 0.0432$) reduced levels of EGT compared to ATCC26933. This data is in agreement with the data from RP-HPLC (Section 6.2.2.1.1) and confirms *egtB* is not essential for, but does contribute to, EGT biosynthesis.

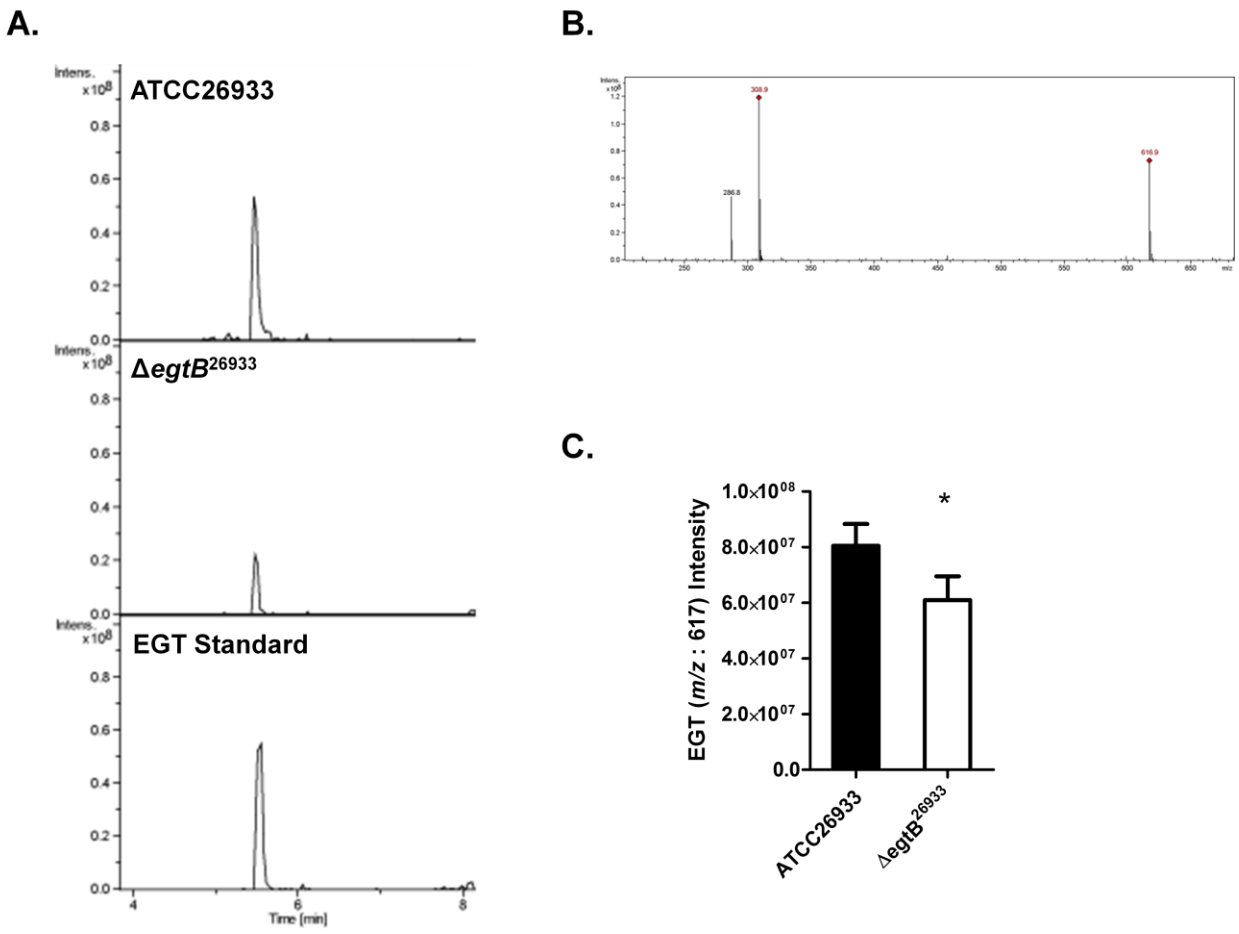

Figure 6.12. Detection of alkylated EGT via LC-MS/MS. (A) Extracted Ion Chromatographs (*m/z*: 617) from ATCC26933, Δ*egtB*^{26933} and an EGT standard. A peak at 5.3 min was confirmed to be EGT. EGT was demonstrated to be present in both ATCC26933 and Δ*egtB*^{26933}. (B) Signature ion breakdown corresponding to alkylated EGT (Gallagher et al., 2012). (C) Comparison of EGT (*m/z*: 617) peak intensity. Levels of EGT are significantly (P = 0.0432) reduced in Δ*egtB*^{26933} compared to ATCC26933.

6.2.2.2 Phenotypic analysis of ATCC26933 and Δ*egtB*^{26933} in response to ROS inducing agents

6.2.2.2.1 Phenotypic analysis of ATCC26933 and Δ*egtB*^{26933} in response to H_2O_2

Sensitivity to H_2O_2 was tested at a range of 0 – 3 mM as per Section 2.2.7. Comparison of radial growth of ATCC26933 and Δ*egtB*^{26933} colonies revealed no significant difference between the two strains at 1mM and 2 mM H_2O_2. At 3mM H_2O_2, radial growth of Δ*egtB*^{26933} was significantly (P = 0.0434) reduced compared to ATCC26933 (Figure 6.13). Loss of *egtB* therefore leads to sensitivity to high levels of H_2O_2. This demonstrates that a reduction of EGT levels may contribute to sensitivity to high levels of H_2O_2 induced ROS.

6.2.2.2.2 Phenotypic analysis of ATCC26933 and Δ*egtB*^{26933} in response to menadione

Sensitivity to menadione was tested at a range of 0 – 60 µM as per Section 2.2.7. Significant reduction in the radial growth of Δ*egtB*^{26933} colonies compared to ATCC26933 colonies was observed at 20 µM (P = 0.0132), 40 µM (P = 0.0013) and 60 µM (P = 0.0003) menadione (Figure 6.14). Loss of *egtB* therefore leads to sensitivity to menadione at all concentrations tested. Partial loss of EGT due to *egtB* deletion therefore appears to result in severe sensitivity to menadione.

6.2.2.2.3 Phenotypic analysis of ATCC26933 and Δ*egtB*^{26933} in response to diamide

Sensitivity to diamide was tested at a range of 0 – 1.75 mM as per Section 2.2.7. No significant differences in the radial growth of Δ*egtB*^{26933} colonies compared to ATCC26933 colonies were observed at any concentration of diamide tested (Figure 6.15). Loss of *egtB*, and the consequent reduction in EGT levels, therefore has no effect on defence against diamide induced oxidative stress in *A. fumigatus*.

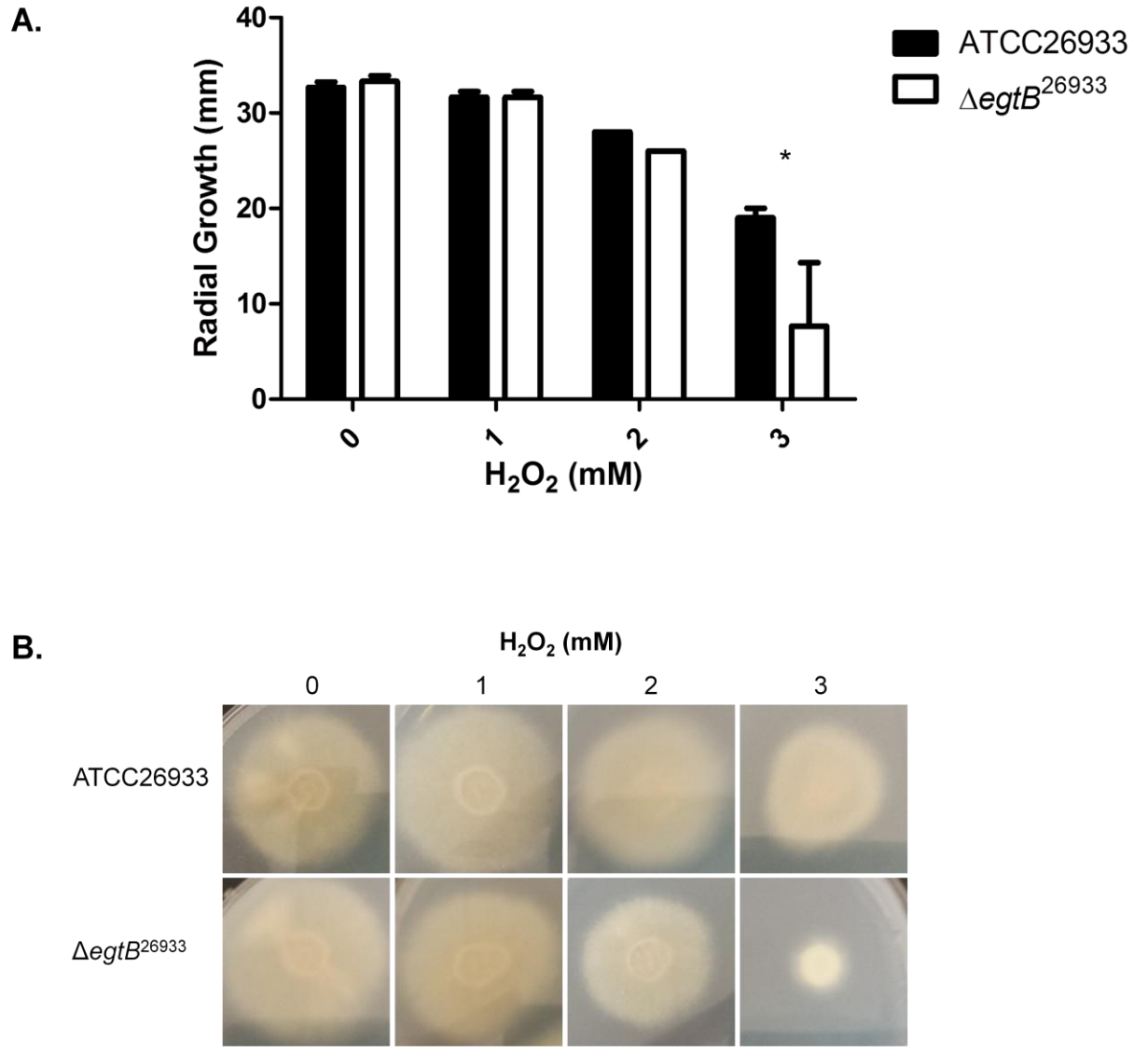

Figure 6.13. H_2O_2 sensitivity assay performed on AMM agar. (A) Comparison of radial growth of ATCC26933 and Δ*egtB*^{26933} on AMM agar plates containing 0 to 3 mM H_2O_2. Δ*egtB*^{26933} shows a significant (P = 0.0434) reduction in growth compared to ATCC26933 at 3 mM H_2O_2. (B) Images of ATCC26933 and Δ*egtB*^{26933} colonies on AMM plates containing 0 to 3 mM H_2O_2. A visible decrease in the size of the Δ*egtB*^{26933} colony can be observed compared to the ATCC26933 colony at 3 mM H_2O_2.

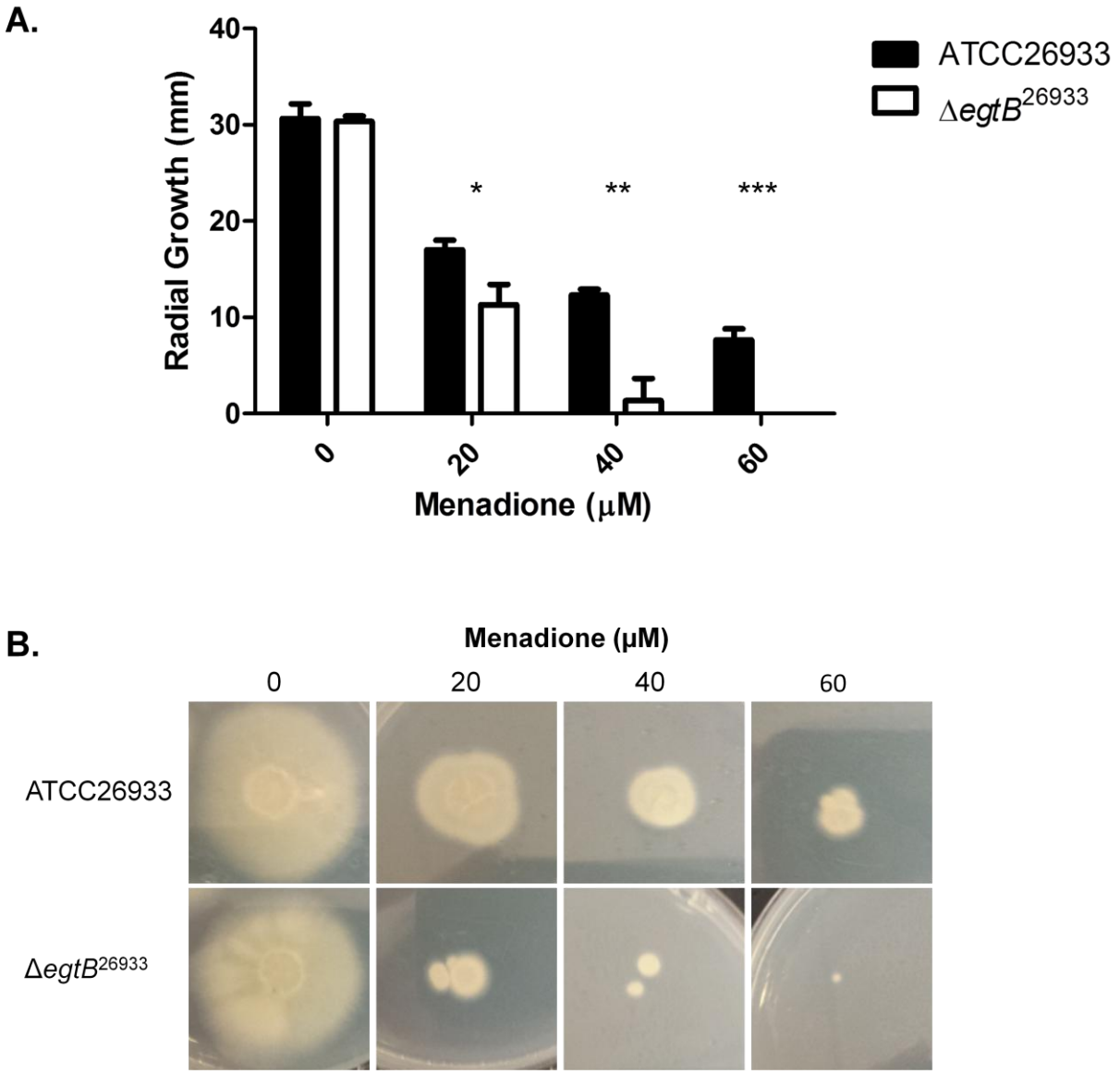

Figure 6.14. Menadione sensitivity assay performed on AMM agar. (A) Comparison of radial growth of ATCC26933 and Δ*egtB*^{26933} on AMM agar plates containing 0 to 60 µM menadione. Δ*egtB*^{26933} shows a significant reduction in growth compared to ATCC26933 at 20 µM (P = 0.0132), 40 µM (P = 0.0013) and 60 µM (P = 0.0003) menadione. (B) Images of ATCC26933 and Δ*egtB*^{26933} colonies on AMM plates containing 0 to 60 µM menadione. A visible decrease in the size of the Δ*egtB*^{26933} colonies can be observed compared to the ATCC26933 colonies at all concentrations of menadione tested.

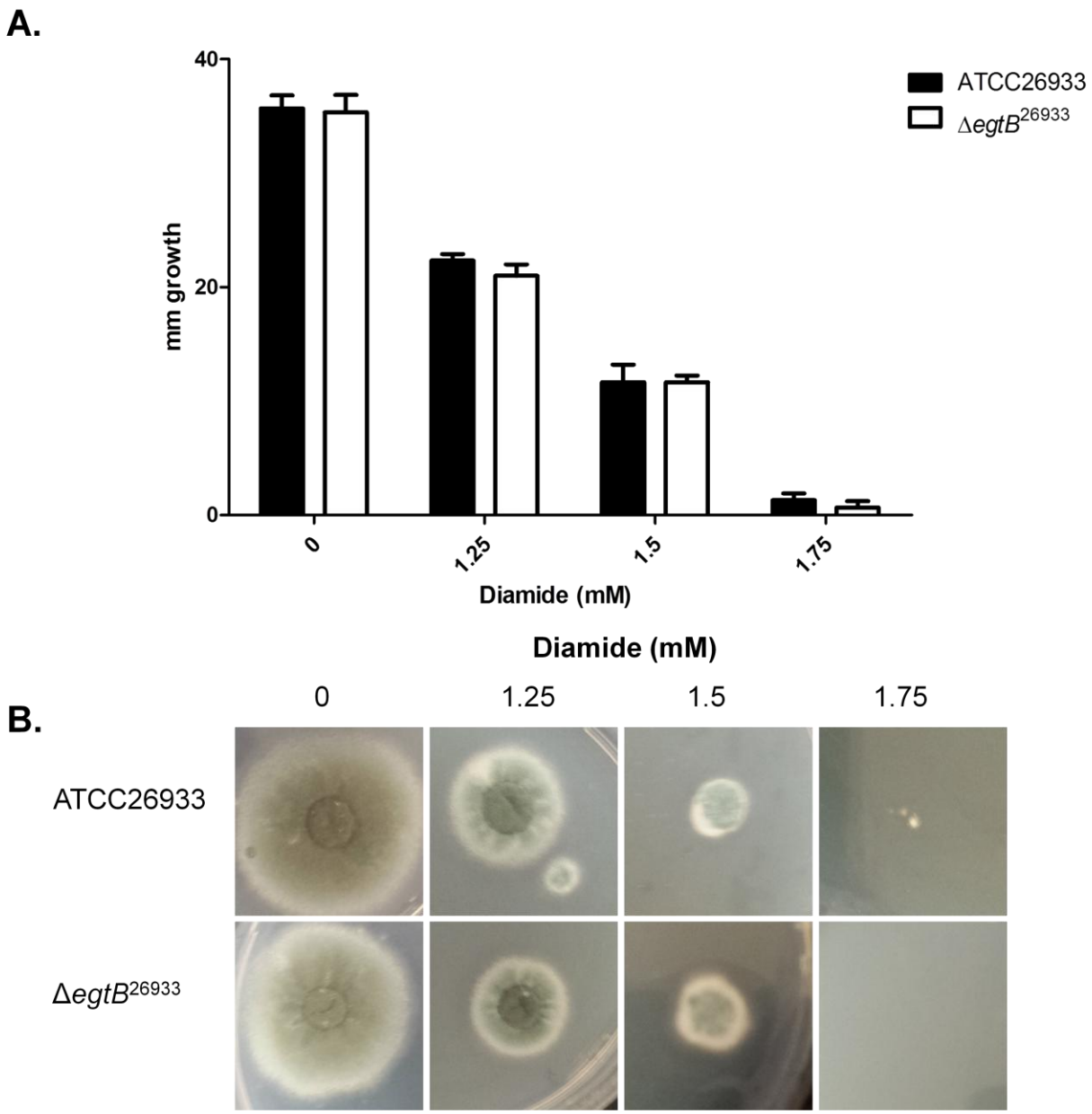

Figure 6.15. Diamide sensitivity assay performed on AMM agar. (A) Comparison of radial growth of ATCC26933 and Δ*egtB*^{26933} on AMM agar plates containing 0 to 1.75 mM diamide. Δ*egtB*^{26933} shows no significant difference in radial growth compared to ATCC26933 at any concentration of diamide tested. (B) Images of ATCC26933 and Δ*egtB*^{26933} colonies on AMM plates containing 0 to 1.75 mM diamide. No visible differences in the size of the Δ*egtB*^{26933} colonies can be observed compared to the ATCC26933 colonies at all concentrations of diamide tested.

6.2.2.3 Total Glutathione measurement in ATCC26933 and Δ*egtB*^{26933} via LC-MS/MS

Mycelia from triplicate 72 h cultures of ATCC26933 and Δ*egtB*^{26933} in Czapek-Dox broth were harvested and cell lysate supernatants obtained as per Section 2.2.9. The presence of DTT in the lysis buffer reduces GSSG to GSH, allowing for total glutathione measurement. Lysate supernatants were alkylated using 5'-IAF (Section 2.2.12.1), TCA precipitated (Section 2.2.12.2) and analysed via LC-MS/MS (Section 2.2.12.7). In addition, a GSH standard alkylated with 5'-IAF and TCA precipitated as before was analysed in the same manner. Alkylated GSH was demonstrated to elute at 5.9 min, with an *m/z* of 695 (Gallagher et al., 2012). Extracted ion chromatograms (*m/z*: 695) for the samples show GSH present in both strains (Figure 6.16). Comparison of GSH levels reveal a slight decrease in Δ*egtB*^{26933} compared to ATCC26933, however this was not significant. Partial loss of EGT in Δ*egtB*^{26933} therefore does not result in differential levels of GSH. This is in contrast to Δ*egtA*^{26933}, where complete loss of EGT resulted in increased levels of GSH (Section 4.2.8.1).

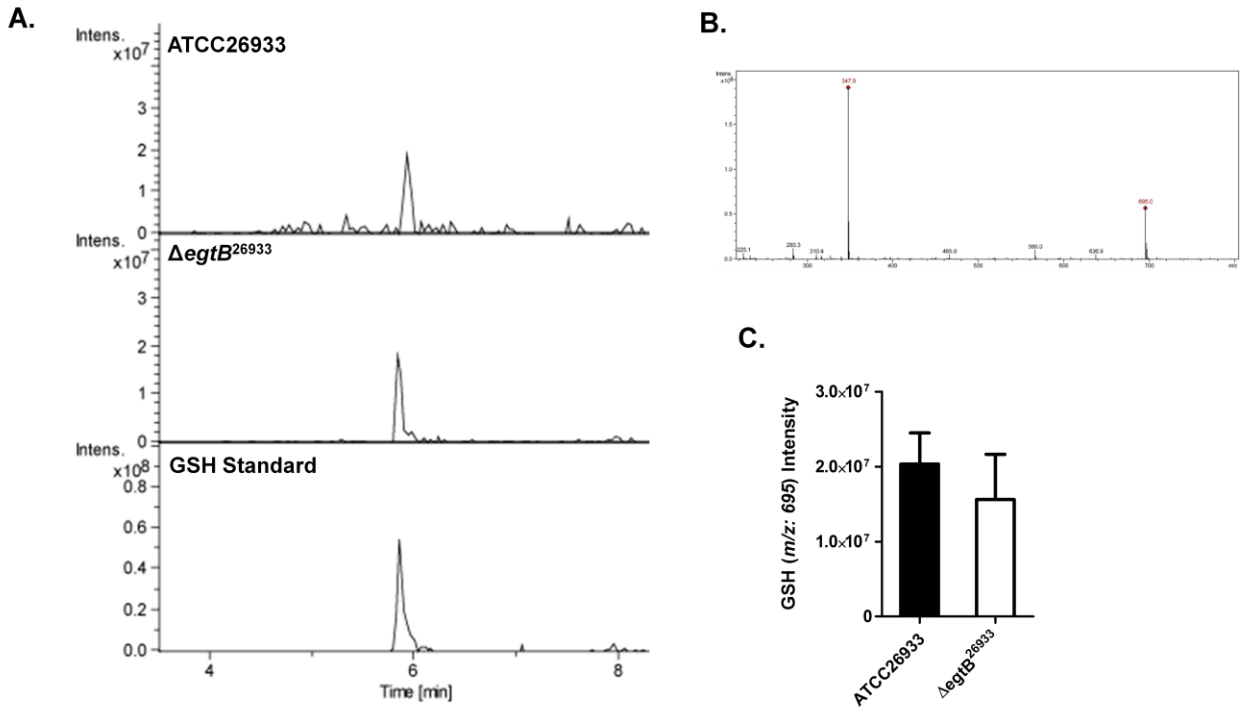

Figure 6.16. Total glutathione detection via LC-MS in ATCC26933 and Δ*egtB*^{26933} (A) Extracted Ion Chromatographs (*m/z*: 695) following LC-MS/MS analysis of TCA precipitated alkylated mycelial extracts from ATCC26933 and Δ*egtB*^{26933}, in addition to a GSH standard. A peak at 5.9 min was confirmed to be GSH. (B) Signature ion breakdown corresponding to alkylated GSH (Gallagher et al., 2012). (C) Comparison of GSH levels in ATCC26933 and Δ*egtB*^{26933}. No significant difference in GSH levels are observed in Δ*egtB*^{26933} compared to wild-type.

6.2.2.4 Analysis of gliotoxin production in ATCC26933 and Δ*egtB*^{26933} via RP-HPLC

Supernatants from triplicate 72 h cultures of ATCC26933 and Δ*egtB*^{26933} in Czapek-Dox broth were collected and organic extraction carried out as per Section 2.2.10. The organic extracts were then analysed via RP-HPLC (Section 2.2.12.6). In addition, a gliotoxin standard was analysed in the same manner. Gliotoxin was detected at 14.9 min and was observed to be present in both ATCC26933 and Δ*egtB*^{26933} (Figure 6.17). A comparison of ATCC26933 and Δ*egtB*^{26933} gliotoxin peak areas shows no significant difference in the levels of gliotoxin produced. Deletion of *egtB* therefore has no impact on gliotoxin biosynthesis.

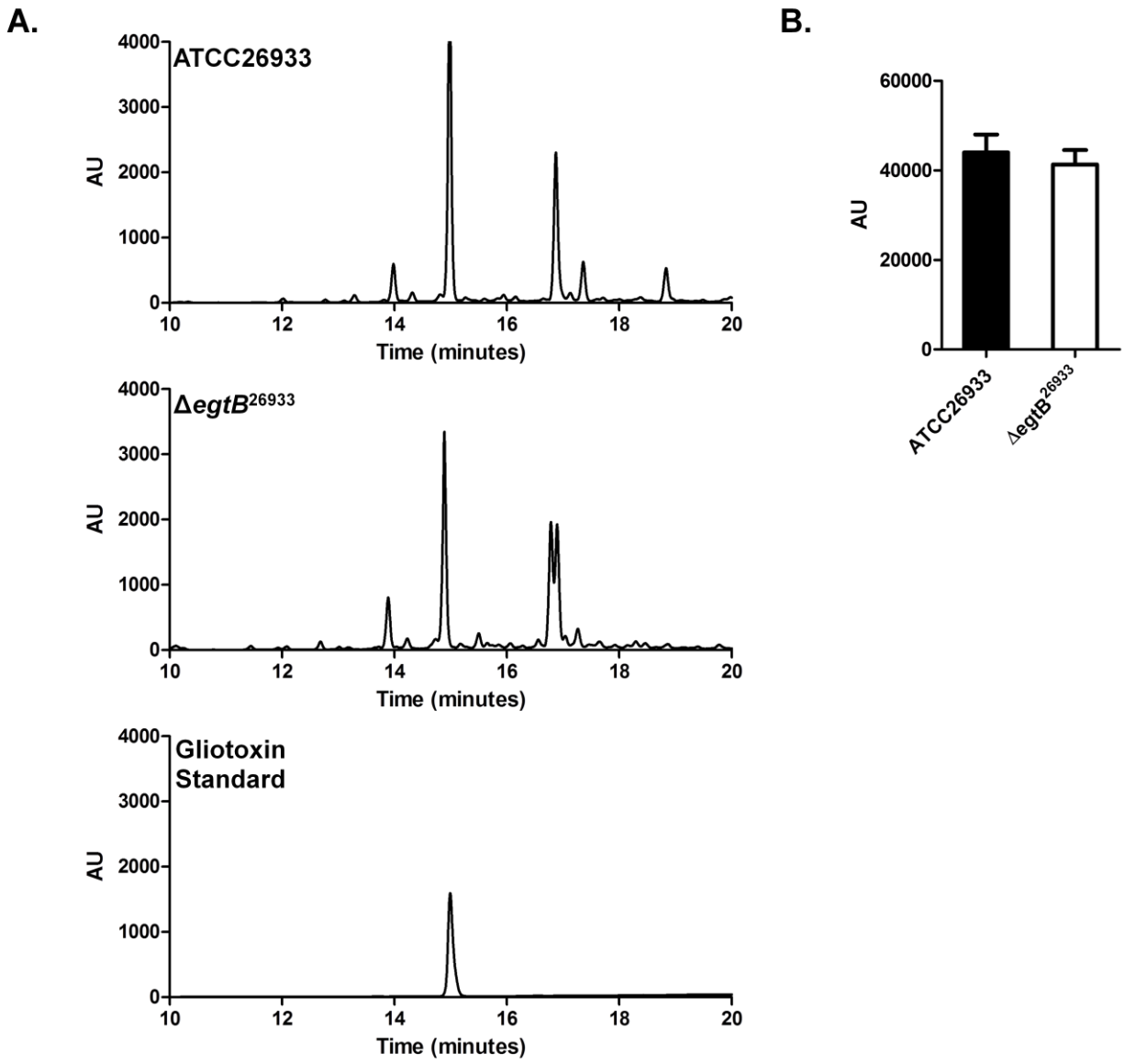

Figure 6.17. Gliotoxin detection via RP-HPLC in ATCC26933 and Δ*egtB*^{26933}. (A) RP-HPLC analysis of organic extracts from the supernatants of 72 h cultures of ATCC26933 and Δ*egtB*^{26933} (n = 3). Gliotoxin is present in both chromatograms at 14.9 min. (B) Comparison of gliotoxin peak area from RP-HPLC analysis for ATCC26933 and Δ*egtB*^{26933} performed in triplicate. No significant difference in gliotoxin levels were observed in Δ*egtB*^{26933} compared to ATCC26933.

6.2.2.5 Phenotypic analysis of ATCC26933 and Δ*egtB*^{26933} in response to gliotoxin

Sensitivity to gliotoxin was tested at a range of 0 – 20 µg/ml as per Section 2.2.7. No significant differences in the radial growth of Δ*egtB*^{26933} colonies compared to ATCC26933 colonies were observed at any concentration of gliotoxin tested (Figure 6.18). Deletion of *egtB*, and the consequent reduction in EGT levels, therefore has no effect on self-protection from gliotoxin in *A. fumigatus*.

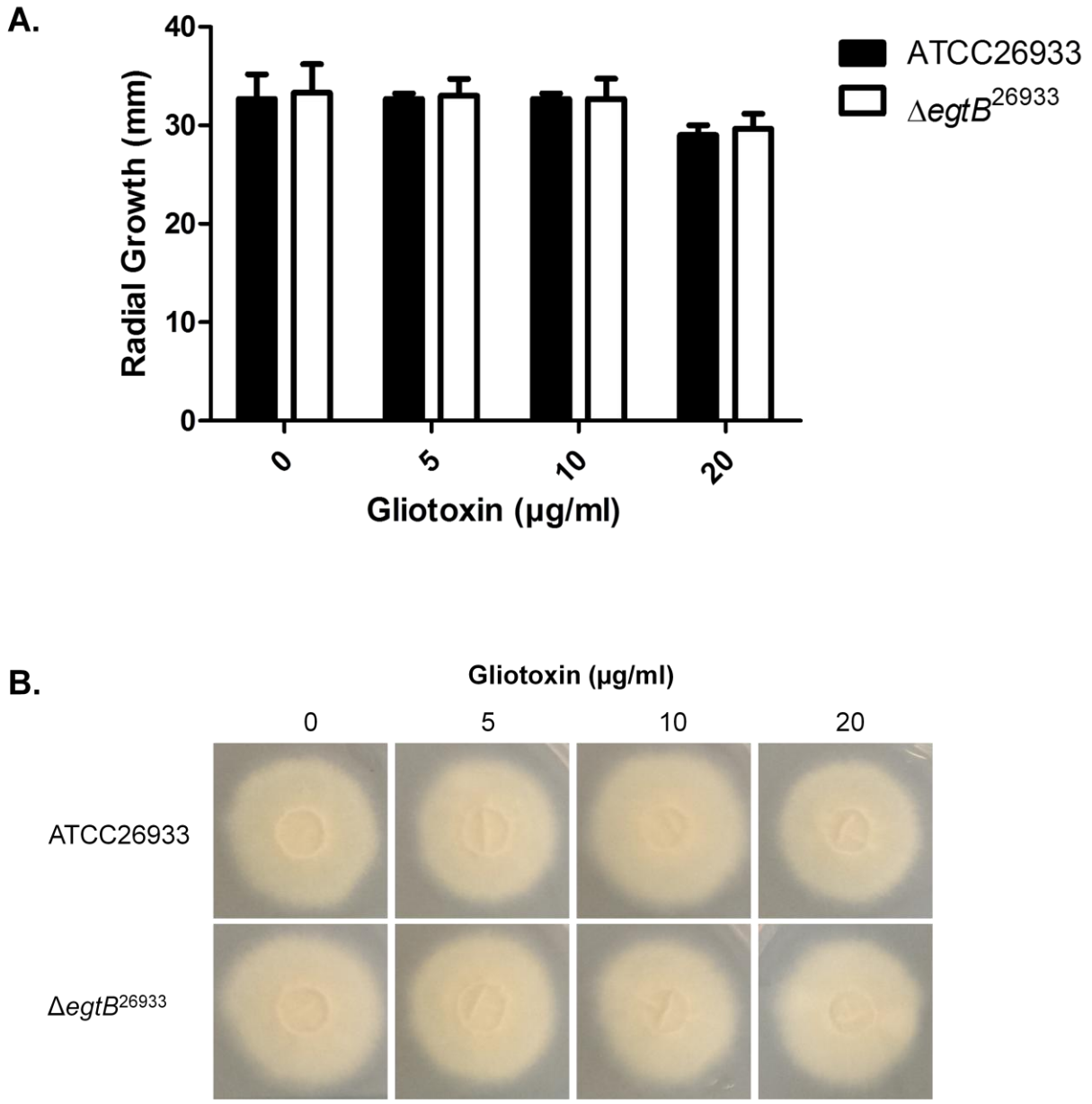

Figure 6.18. Gliotoxin sensitivity assay performed on AMM agar for 72 h. (A) Comparison of radial growth of ATCC26933 and Δ*egtB*^{26933} on AMM agar plates containing 0 to 20 µg/ml gliotoxin. No significant reduction in growth was observed in Δ*egtB*^{26933} compared to ATCC26933 at any concentration of gliotoxin tested. (B) Images of ATCC26933 and Δ*egtB*^{26933} colonies on AMM plates containing 0 to 20 µg/ml gliotoxin. No visible decrease in the size of the Δ*egtB*^{26933} colonies can be observed compared to the ATCC26933 colonies at any concentration of gliotoxin tested.

6.2.3 Phenotypic characterisation of Δ*vipC*^{26933}

6.2.3.1 Analysis of growth and development in Δ*vipC*^{26933}compared to ATCC26933

6.2.3.1.1 Analysis of growth and development in Δ*vipC*^{26933}compared to ATCC26933 on solid Media

Conidia from ATCC26933 and Δ*vipC*^{26933} were point inoculated onto AMM agar in triplicate as per Section 2.2.7 and incubated at 37 ^{o}C for 72 h. Comparison of the radial growth of resulting ATCC26933 and Δ*vipC*^{26933} colonies revealed Δ*vipC*^{26933} colonies show a significant (P = 0.0036) increase in radial growth compared to ATCC26933 (Figure 6.19A). Additionally, an abundance of aerial hyphae are visible at the centre of the Δ*vipC*^{26933} colonies that are not present on ATCC26933 colonies (Figure 6.19C and 6.19D). Deletion of *vipC* in ATCC26933 results in differential growth, with increased radial growth and the presence of aerial hyphae. This is evidence that VipC is involved in growth and development in *A. fumigatus*.

6.2.3.1.2 Analysis of growth in Δ*vipC*^{26933}compared to ATCC26933 in Liquid Media

Cultures (n = 5) of ATCC26933 and Δ*vipC*^{26933} in AMM were incubated for 72 h at 37 ^{o}C, 200 rpm shaking. Cultures were then harvested through miracloth, snap frozen and lyophilised overnight. Comparison of the dry weight of mycelia reveals a significant increase (P = 0.0012) in the dry weight of Δ*vipC*^{26933} mycelia, compared to ATCC26933 mycelia (Figure 6.19B). This is further evidence that VipC plays a role in the growth of *A. fumigatus*.

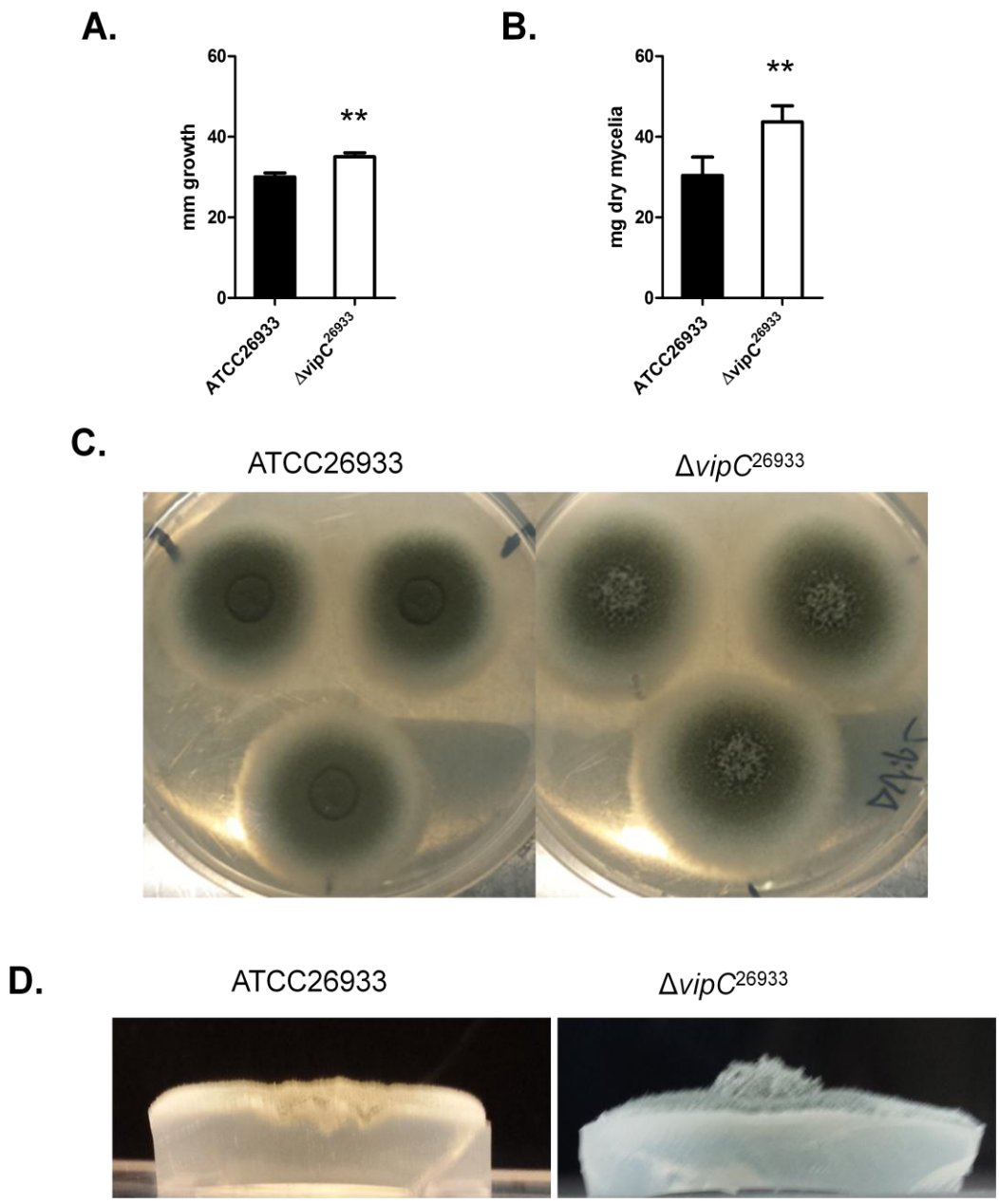

Figure 6.19. Analysis of differential growth in Δ*vipC*^{26933} compared to ATCC26933 (A) Comparison of ATCC26933 and Δ*vipC*^{26933} radial growth. Radial growth is significantly increased in Δ*vipC*^{26933} (P = 0.0036) compared to ATCC26933. (B) Comparison of dry weight of mycelia from liquid culture from ATCC26933 and Δ*vipC*^{26933}. Mycelial dry weight was significantly increased in Δ*vipC*^{26933} (P = 0.0012) compared to ATCC26933. (C) Images of ATCC26933 and Δ*vipC*^{26933} colonies demonstrating increased radial growth and presence of aerial hyphae in Δ*vipC*^{26933}. (D) Images of ATCC26933 and Δ*vipC*^{26933} colonies demonstrating the presence of aerial hyphae on the Δ*vipC*^{26933} colony.

6.2.3.1.3 Analysis of growth and development in Δ*vipC*^{26933} compared to ATCC26933 on solid media in response to light

Conidia from ATCC26933 and Δ*vipC*^{26933} were point inoculated onto AMM agar in triplicate as per (Section 2.2.7). Inoculated plates were incubated for 72 h in either darkness or light. Significantly decreased radial growth was demonstrated in both ATCC26933 and Δ*vipC*^{26933} in light compared to radial growth in darkness (P = 0.0161 for both strains) (Figure 6.20A). Δ*vipC*^{26933} had significantly increased radial growth compared to ATCC26933 when grown in both light and darkness (P = 0.0002 for both conditions) (Figure 6.20A). The increased radial growth phenotype in Δ*vipC*^{26933} therefore was not affected by the presence or absence of light. This was not the case with the aerial hyphae phenotype, however. Aerial hyphae were observed on Δ*vipC*^{26933} colonies grown in darkness. This was not observed on Δ*vipC*^{26933} grown in light or for ATCC26933 colonies grown in darkness or light (Figure 6.20B and 6.20C). The presence of aerial hyphae on Δ*vipC*^{26933} therefore only occurs when grown in the dark. This indicates that VipC has a role in suppressing aerial hyphae formation in *A. fumigatus* when grown in darkness, but not light. VipC function in *A. fumigatus* may be at least partially regulated by environmental signals.

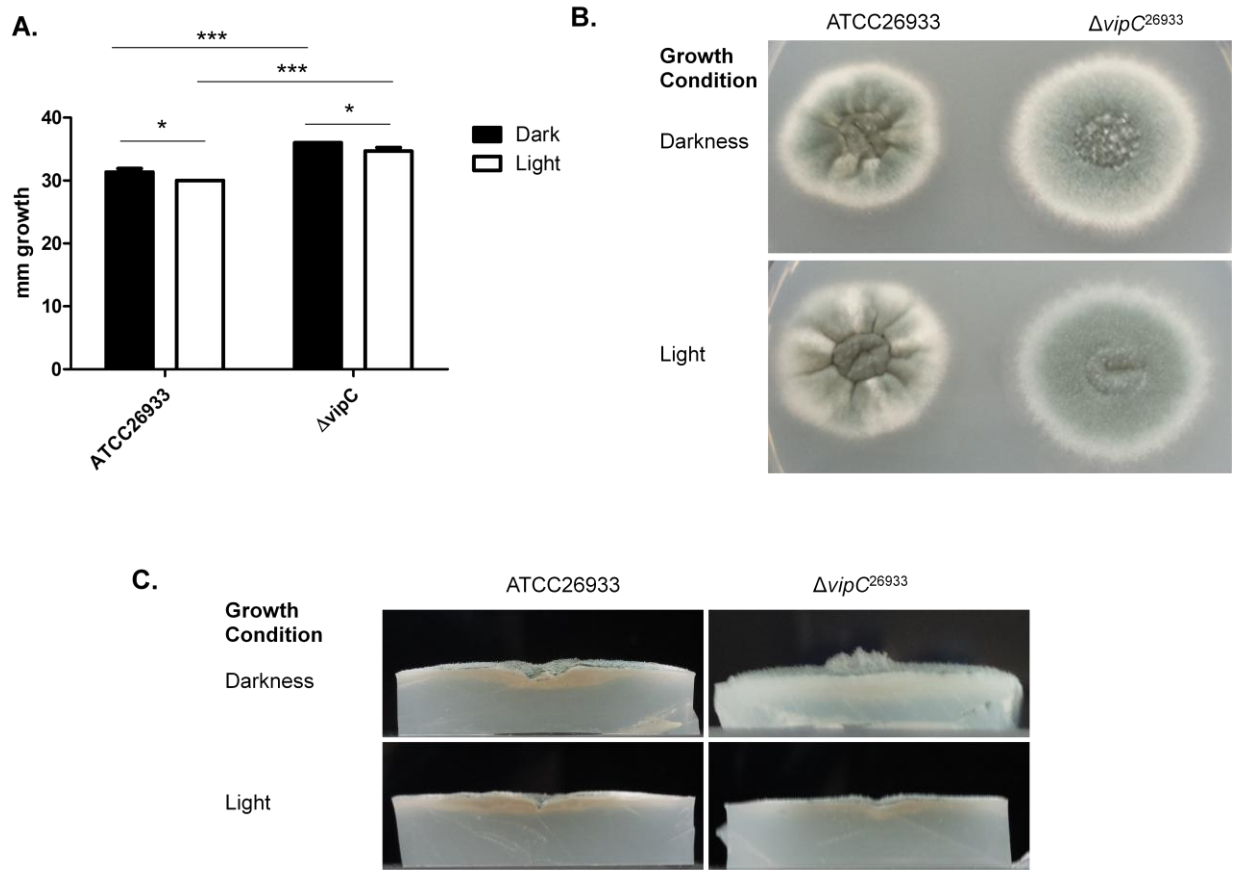

Figure 6.20. Comparison of ATCC26933 and Δ*vipC*^{26933} colonies grown in darkness and in light. (A) Comparison of radial growth of ATCC26933 and Δ*vipC*^{26933} colonies grown in darkness and in light. Radial growth was increased in both strains grown in darkness compared to light (P = 0.0161 for both strains). Δ*vipC*^{26933} demonstrated increased growth compared to ATCC26933 in both darkness and in light (P = 0.0002 for both conditions). (B) Photographs of ATCC26933 and Δ*vipC*^{26933} colonies, demonstrating increased radial growth of Δ*vipC*^{26933} colonies when grown in both darkness and light. Aerial hyphae are only visible on Δ*vipC*^{26933} colonies grown in dark. (C) Side-view photographs of ATCC26933 and Δ*vipC*^{26933} colonies, demonstrating aerial hyphae growth on Δ*vipC*^{26933} colonies grown in darkness.

6.2.3.2 Analysis of EGT production in ATCC26933 and Δ*vipC*^{26933} via RP-HPLC

Mycelia from 72 h cultures of ATCC26933 and Δ*vipC*^{26933} in Czapek-Dox broth were harvested and cell lysate supernatants obtained as per Section 2.2.9. Lysate supernatants were alkylated using 5'-IAF as described in Section 2.2.12.1 and analysed via RP-HPLC (Section 2.2.12.6) using fluorescence detection at Ex/Em of 494/518 nm. EGT was detected in both ATCC26933 and Δ*vipC*^{26933} at a retention time of 12.4 min (Figure 6.21). Comparing EGT levels by measuring the peak area of 5'-IAF alkylated EGT revealed no significant difference in EGT levels in ATCC26933 and Δ*vipC*^{26933}. Deletion of VipC therefore had no effect on EGT production, suggesting VipC does not influence EGT biosynthesis in *A. fumigatus*.

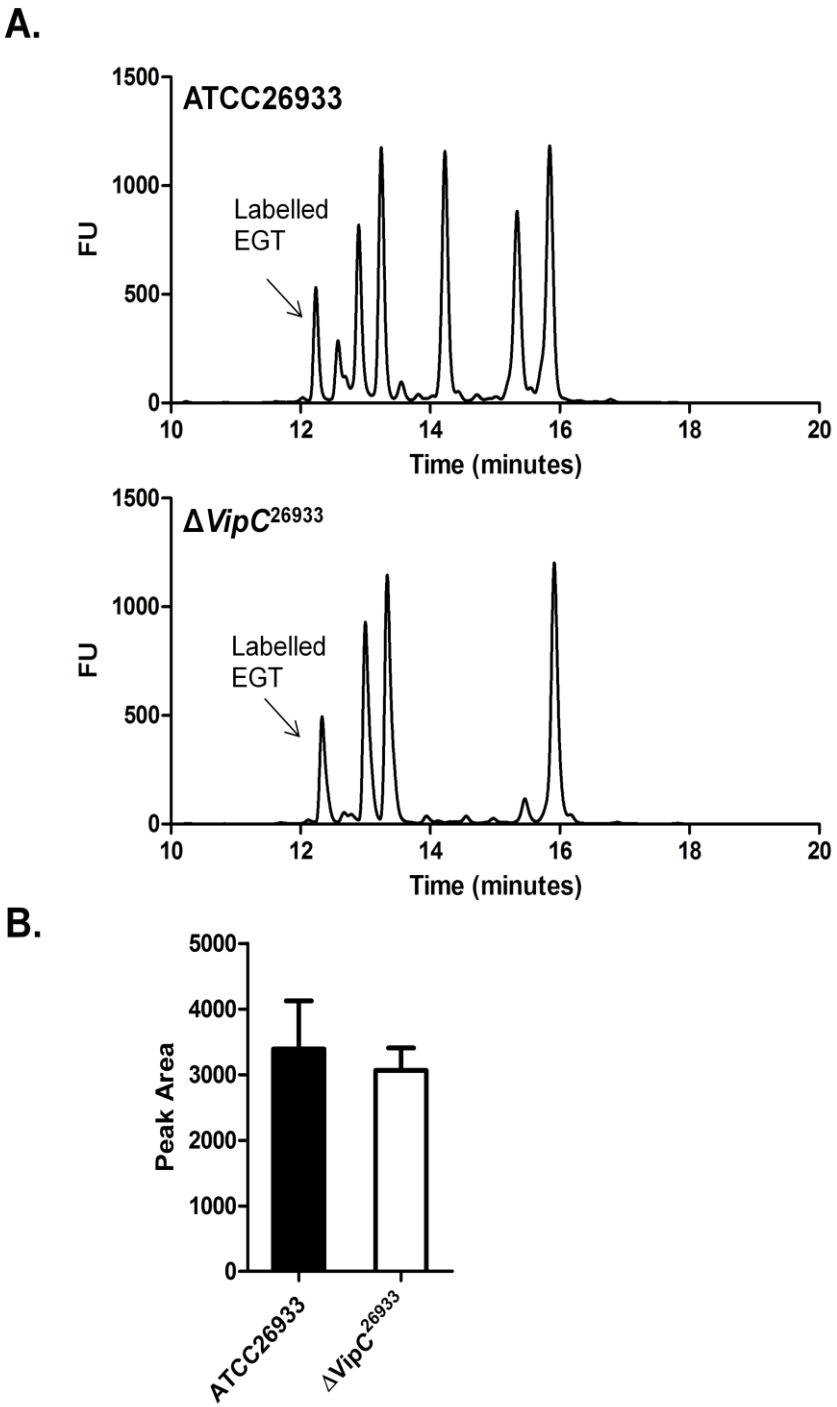

Figure 6.21. Detection and measurement of alkylated EGT via RP-HPLC. (A) Detection of alkylated EGT in ATCC26933 and Δ*vipC*^{26933} at a retention time of 12.4 min. (B) Comparison of EGT levels in ATCC26933 and Δ*vipC*^{26933}. No significant difference in the levels of EGT was observed in ATCC26933 and Δ*vipC*^{26933}.

6.2.3.3 Phenotypic analysis of ATCC26933 and Δ*vipC*^{26933} in response to ROS inducing agents

6.2.3.3.1 Phenotypic analysis of ATCC26933 and Δ*vipC*^{26933} in response to H_2O_2

Sensitivity to H_2O_2 was tested at a range of 0 – 3 mM as per Section 2.2.7. Comparison of radial growth of ATCC26933 and Δ*vipC*^{26933} colonies revealed no significant difference between the two strains at any concentration of H_2O_2 tested (Figure 6.22). Loss of *vipC* therefore does not lead to sensitivity to H_2O_2 induced stress.

6.2.3.3.2 Phenotypic analysis of ATCC26933 and Δ*vipC*^{26933} in response to menadione

Sensitivity to menadione was tested at a range of 0 – 60 µM as per Section 2.2.7. Comparison of radial growth of ATCC26933 and Δ*vipC*^{26933} colonies revealed no significant difference between the two strains at any concentration of menadione tested (Figure 6.23). Loss of *vipC* therefore does not lead to sensitivity to menadione induced stress.

6.2.3.3.3 Phenotypic analysis of ATCC26933 and Δ*vipC*^{26933} in response to diamide

Sensitivity to diamide was tested at a range of 0 – 1.75 mM as per Section 2.2.7. No significant differences in the radial growth of Δ*vipC*^{26933} colonies compared to ATCC26933 colonies were observed at any concentration of diamide tested (Figure 6.24). Loss of *vipC* therefore does not lead to sensitivity to diamide induced stress.

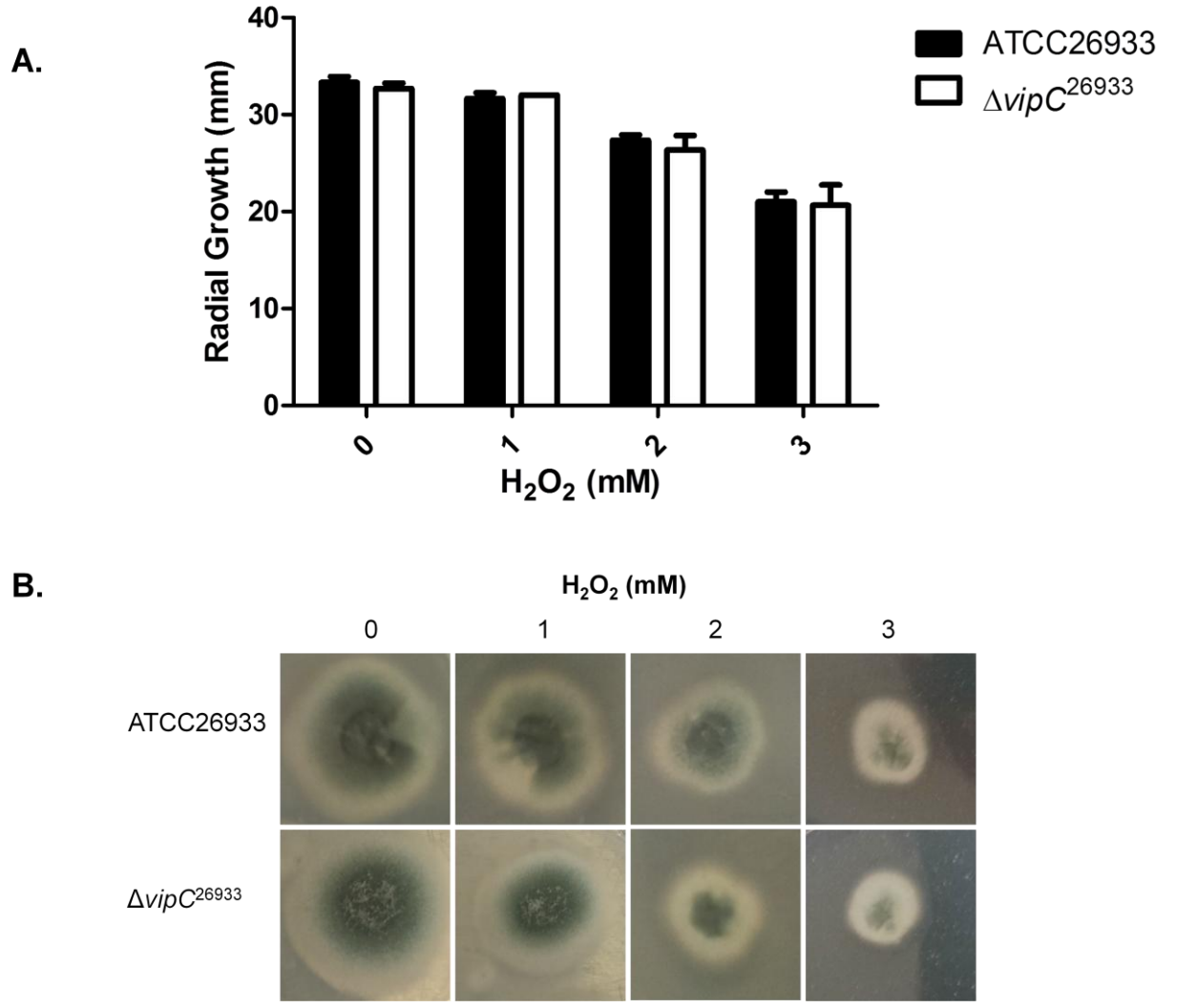

Figure 6.22. H_2O_2 sensitivity assay performed on AMM agar for 72 h. (A) Comparison of radial growth of ATCC26933 and Δ*vipC*^{26933} on AMM agar plates containing 0 to 3 mM H_2O_2. Δ*vipC*^{26933} shows no significant difference in radial growth compared to ATCC26933 at any concentration of H_2O_2 tested. (B) Images of ATCC26933 and Δ*vipC*^{26933} colonies on AMM plates containing 0 to 3 mM H_2O_2. No visible decrease in the size of the Δ*vipC*^{26933} colonies was observed compared to the ATCC26933 colonies at any concentration of H_2O_2 tested.

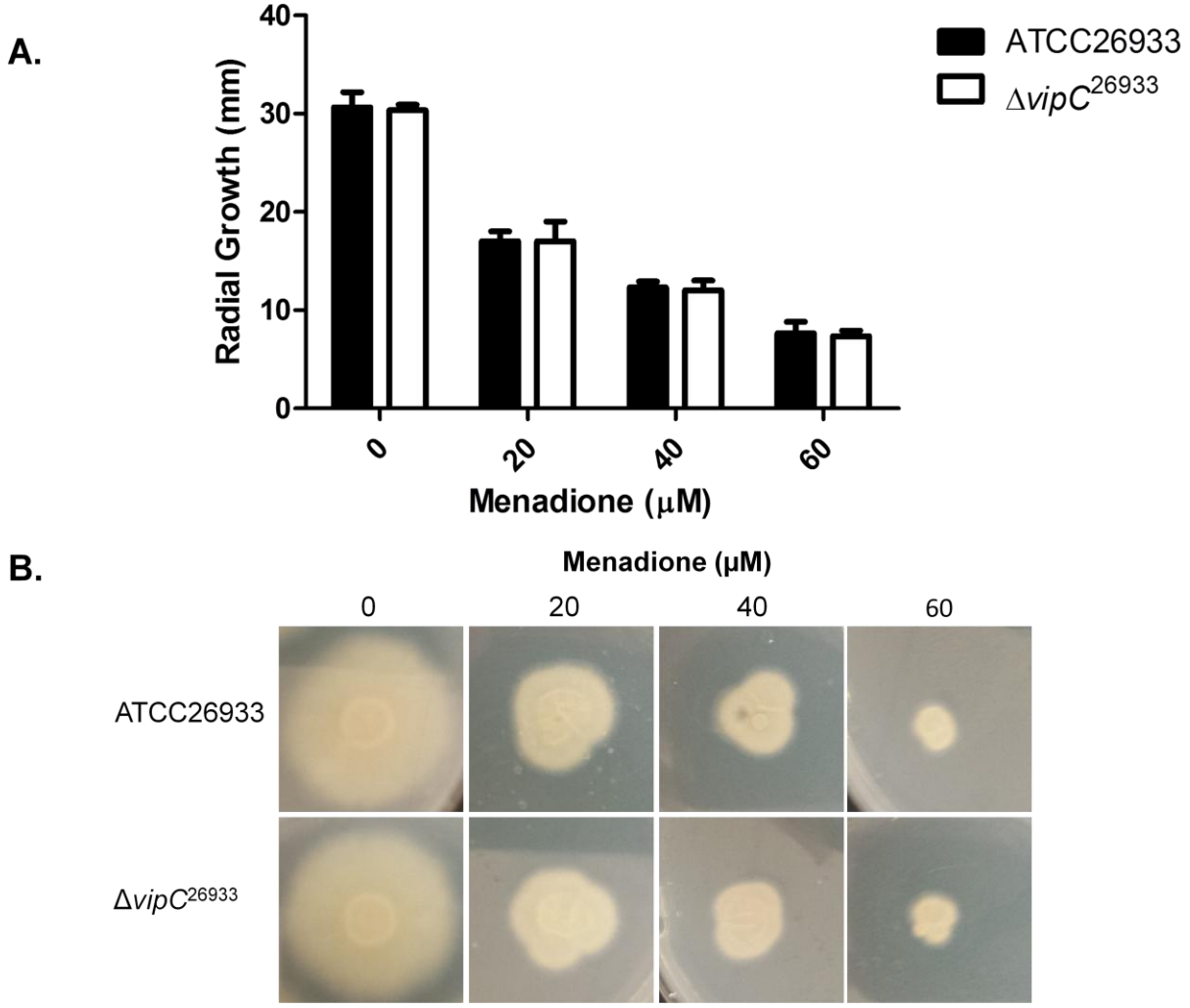

Figure 6.23. Menadione sensitivity assay performed on AMM agar for 72 h. (A) Comparison of radial growth of ATCC26933 and Δ*vipC*^{26933} on AMM agar plates containing 0 to 60 µM menadione. Δ*vipC*^{26933} shows no significant difference in radial growth compared to ATCC26933 at any concentration of menadione tested. (B) Images of ATCC26933 and Δ*vipC*^{26933} colonies on AMM plates containing 0 to 60 µM menadione. No visible decrease in the size of the Δ*vipC*^{26933} colonies was observed compared to the ATCC26933 colonies at any concentration of menadione tested.

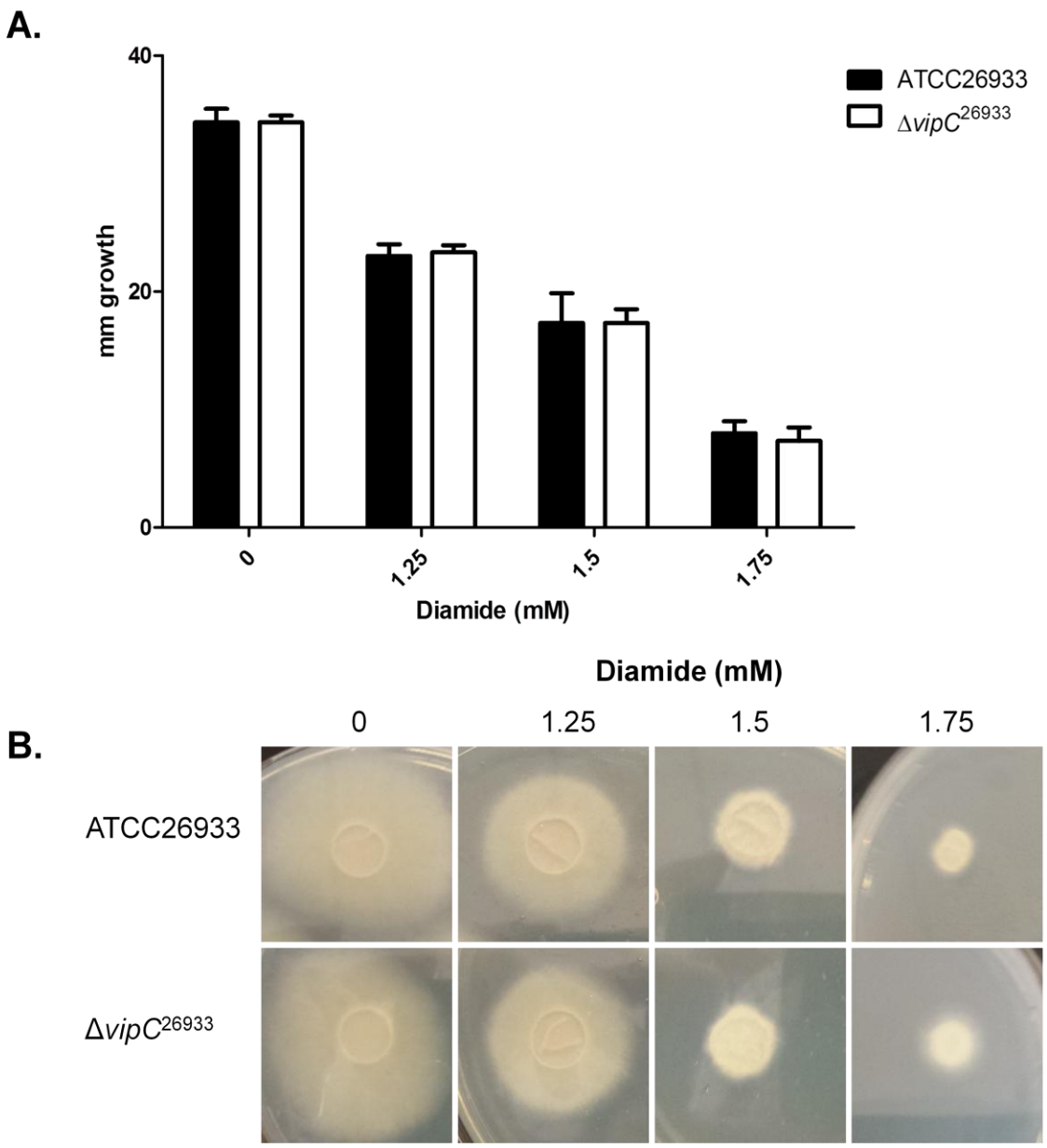

Figure 6.24. Diamide sensitivity assay performed on AMM agar for 72 h. (A) Comparison of radial growth of ATCC26933 and Δ*vipC*^{26933} on AMM agar plates containing 0 to 1.75 mM menadione. Δ*vipC*^{26933} shows no significant difference in radial growth compared to ATCC26933 at any concentration of diamide tested. (B) Images of ATCC26933 and Δ*vipC*^{26933} colonies on AMM plates containing 0 to 1.75 mM diamide. No visible decrease in the size of the Δ*vipC*^{26933} colonies was observed compared to the ATCC26933 colonies at any concentration of diamide tested.

6.2.3.4 Total glutathione measurement in ATCC26933 and Δ*vipC*^{26933} via LC-MS/MS

Mycelia from triplicate 72 h cultures of ATCC26933 and Δ*vipC*^{26933} in AMM were harvested and cell lysate supernatants obtained as per Section 2.2.9. The presence of DTT in the lysis buffer reduces GSSG to GSH, allowing for total glutathione measurement. Lysate supernatants were alkylated using 5'-IAF (Section 2.2.12.1), TCA precipitated (Section 2.2.12.2) and analysed via Thermo Q-Exactive LC-MS/MS (Section 2.2.12.7). In addition, a GSH standard labelled with 5'-IAF and TCA precipitated as before was analysed in the same manner. 5'-IAF alkylated GSH was demonstrated to elute at 46 min, with an *m/z* of 695 (Gallagher et al, 2012). Extracted ion chromatograms (*m/z*: 695) for the samples show GSH present in both ATCC26933 and Δ*vipC*^{26933}. Δ*vipC*^{26933} shows significantly (P = 0.0352) reduced levels of GSH compared to ATCC26933 (Figure 6.25). Therefore, *vipC* deletion resulted in a significant decrease (90 %) in total intracellular glutathione, indicating a novel interaction between VipC functionality and GSH biosynthesis.

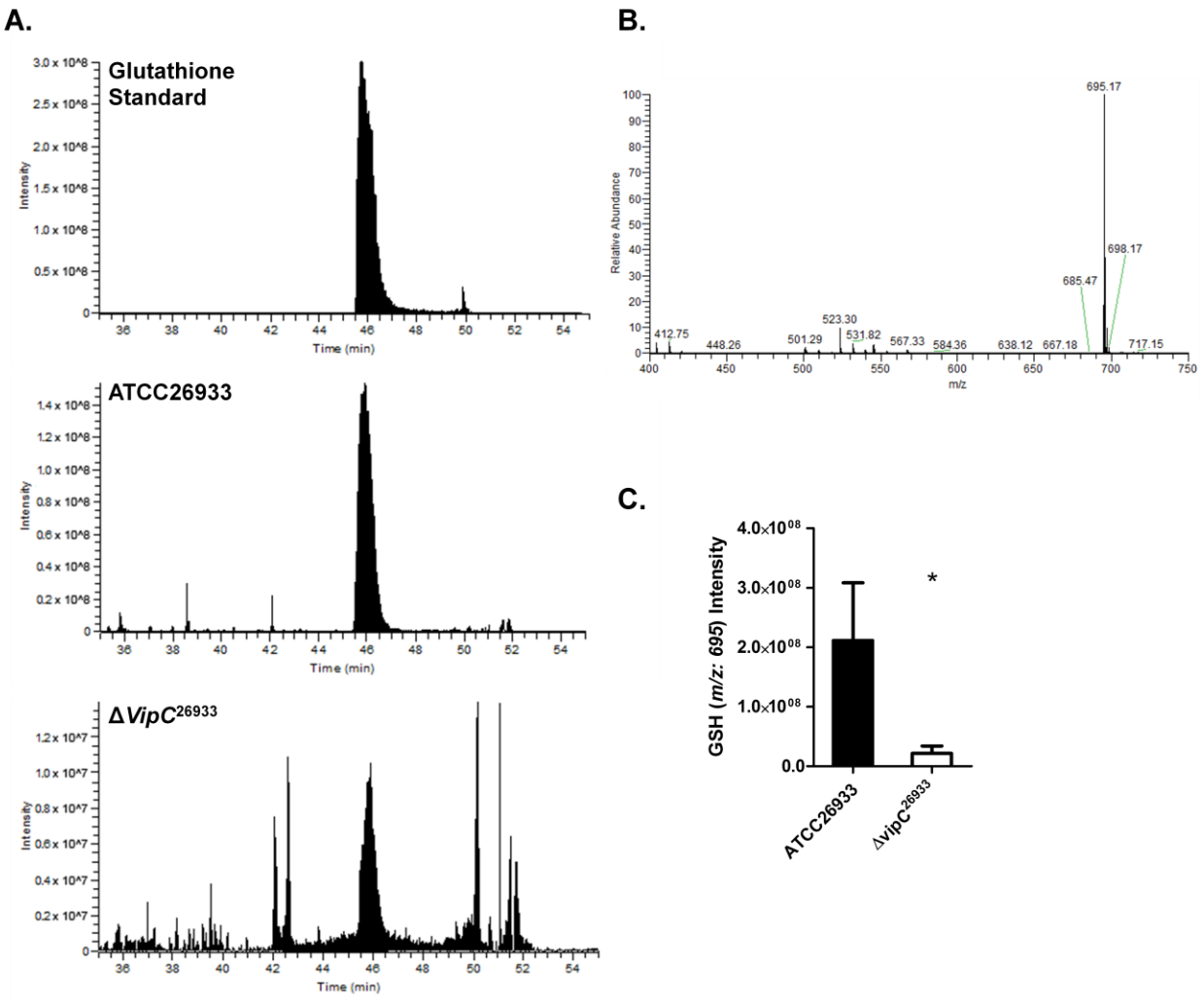

Figure 6.25. Total glutathione detection via LC-MS in ATCC26933 and Δ*vipC*^{26933} (A) Extracted ion chromatographs (*m/z*: 695) following LC-MS/MS analysis of TCA precipitated alkylated mycelial extracts from ATCC26933 and Δ*vipC*^{26933}, in addition to a GSH standard. A peak at 46 min was confirmed to be GSH. Note that Y-axis differ by 10-fold for ATCC26933 and Δ*vipC*^{26933} chromatograms. (B) Signature ion breakdown corresponding to alkylated GSH (Gallagher et al., 2012). (C) Comparison of GSH levels in ATCC26933 and Δ*vipC*^{26933}. GSH levels in Δ*vipC*^{26933} were significantly (P = 0.0352) reduced compared to ATCC26933.

6.2.3.5 Analysis of Conidiation in ATCC26933 and Δ*vipC*^{26933}

Triplicate colonies of ATCC26933 and Δ*vipC*^{26933} were grown on AMM for 72 h and levels of conidiation were measured via haemocytometry (Section 2.2.16). A non-significant reduction in conidiation in Δ*vipC*^{26933} compared to ATCC26933 was observed (Figure 6.26). Deletion of *vipC* therefore does not affect levels of conidiation in *A. fumigatus*.

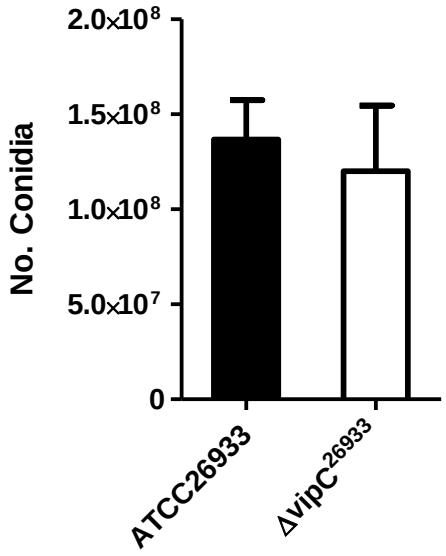

Figure 6.26. Comparison of conidiation levels from ATCC26933 and Δ*vipC*^{26933}. Levels of conidiation are lower in Δ*vipC* compared to ATCC26933, however the difference is not significant.

6.2.3.6 Analysis of gliotoxin production in ATCC26933 and Δ*vipC*^{26933} via RP-HPLC

Supernatants from triplicate 72 h cultures of ATCC26933 and Δ*vipC*^{26933} in Czapek-Dox broth were collected and organic extraction carried out as per Section 2.2.10. The organic extracts were then analysed via RP-HPLC (Section 2.2.12.6). In addition, a gliotoxin standard was analysed in the same manner. Gliotoxin was detected at 14.9 min and was observed to be present in both ATCC26933 and Δ*vipC*^{26933} (Figure 6.27). A comparison of ATCC26933 and Δ*vipC*^{26933} gliotoxin peak areas shows a non-significant increase in gliotoxin levels in Δ*vipC*^{26933} compared to ATCC26933. Deletion of *vipC* therefore has no impact on gliotoxin biosynthesis.

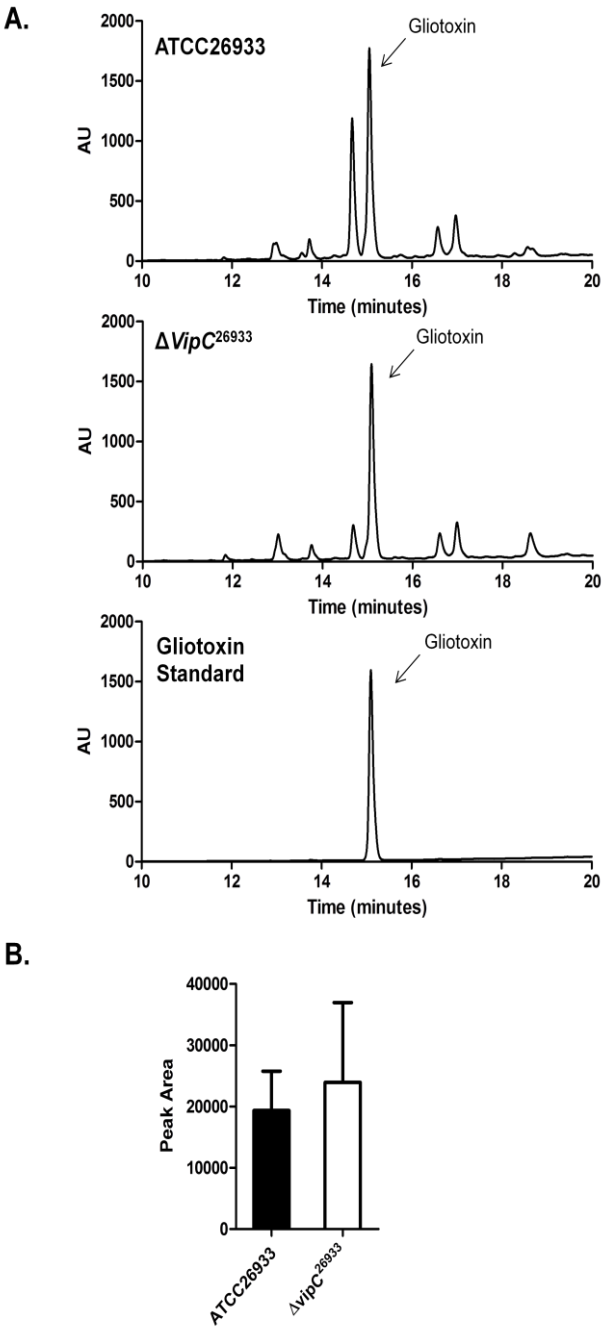

Figure 6.27. Gliotoxin detection via RP-HPLC in ATCC26933 and Δ*vipC*^{26933}. (A) RP-HPLC analysis of organic extracts from the supernatants of 72 h cultures of ATCC26933 and Δ*vipC*^{26933} (n = 3). Gliotoxin is present in both chromatograms at 14.9 min. (B) Comparison of gliotoxin peak area from RP-HPLC analysis for ATCC26933 and Δ*vipC*^{26933} performed in triplicate. A non-significant increase in gliotoxin levels is observed in Δ*vipC*^{26933} compared to ATCC26933.

6.2.3.7 Phenotypic analysis of ATCC26933 and Δ*vipC*^{26933} in response to gliotoxin

Sensitivity to gliotoxin was tested at a range of 0 – 20 µg/ml as per Section 2.2.7. No significant differences in the radial growth of Δ*vipC*^{26933} colonies compared to ATCC26933 colonies were observed at any concentration of gliotoxin tested (Figure 6.28). Deletion of *vipC* therefore has no effect on gliotoxin sensitivity, it can therefore be concluded that VipC is not involved in gliotoxin self-protection in *A. fumigatus*.

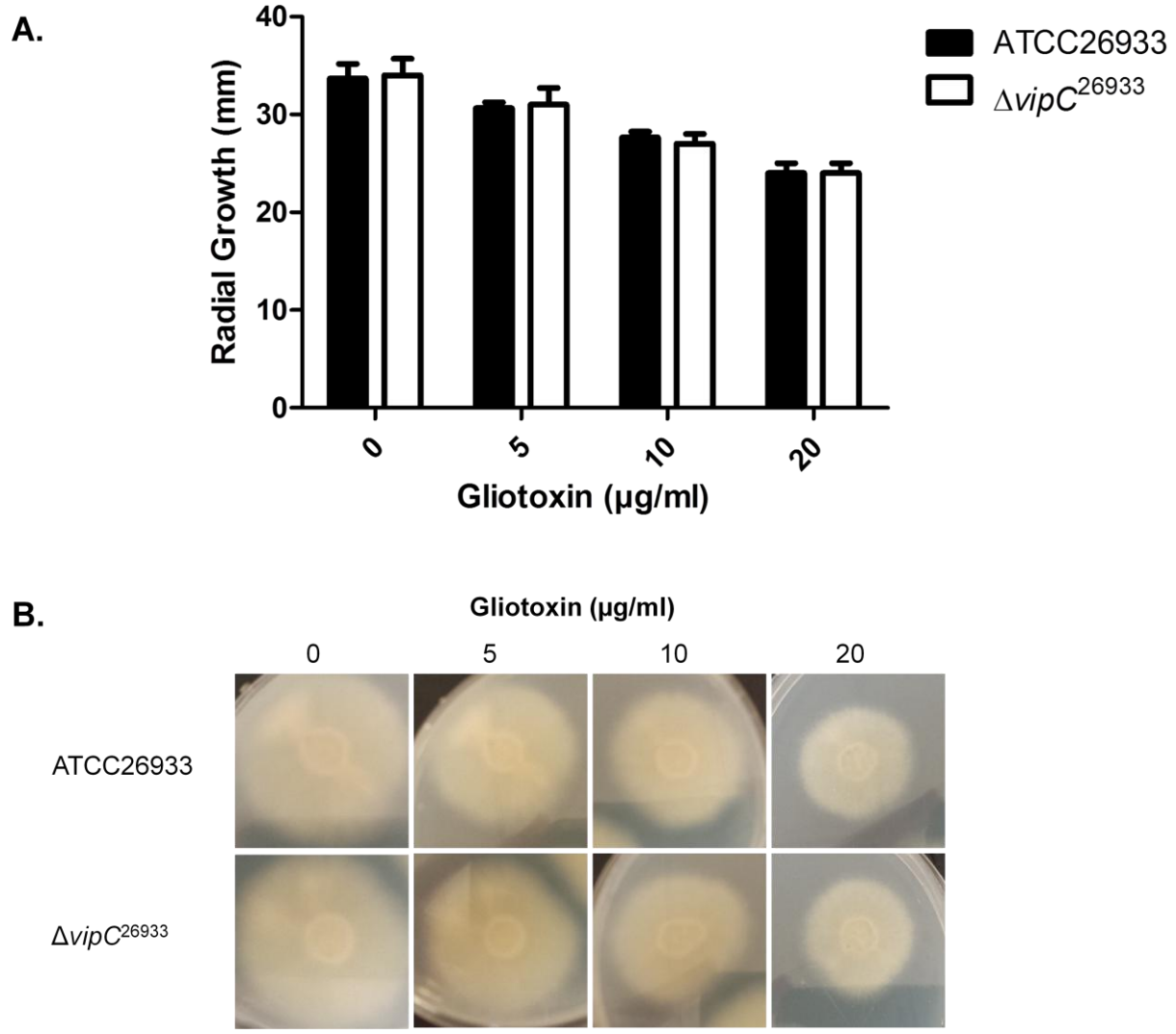

Figure 6.28. Gliotoxin sensitivity assay performed on AMM agar for 72 h. (A) Comparison of radial growth of ATCC26933 and Δ*vipC*^{26933} on AMM agar plates containing 0 to 20 µg/ml gliotoxin. Δ*vipC*^{26933} shows no significant difference in radial growth compared to ATCC26933 at any concentration of gliotoxin tested. (B) Images of ATCC26933 and Δ*vipC*^{26933} colonies on AMM plates containing 0 to 20 µg/ml gliotoxin. No visible decrease in the size of the Δ*vipC*^{26933} colonies can be observed compared to the ATCC26933 colonies at any concentration gliotoxin tested.

6.2.3.8 LFQ Proteomic Analysis of ATCC26933 and Δ*vipC*^{26933} under basal conditions

ATCC26933 and Δ*vipC*^{26933} (*n* = 3 biological replicates each) were cultured in AMM media for 72 h at 37 ^{o}C, 200 rpm shaking. This media and incubation conditions was chosen in order to mirror that of Section 6.2.3.1.2, which demonstrated increased dry weight of mycelia in Δ*vipC*^{26933} compared to ATCC26933. Following this incubation, the mycelia were harvested from each culture and processed for Q-Exactive Mass Spectrometry analysis as per Section 2.2.14.1. Samples were then digested using sequencing grade trypsin (Section 2.2.14.4), purified, normalised and desalted using ZipTips ® (Section 2.2.14.5) and analysed on a Q-Exactive mass spectrometer (Section 2.2.14.6). Data was analysed via Max Quant, comparing Δ*vipC*^{26933} to ATCC26933. Significantly enriched functional categories of proteins were identified using the web based application FungiFun 2 (Priebe et al., 2015; https://elbe.hki-jena.de/fungifun/fungifun.php)

Surprisingly. a total of 474 proteins had altered abundance in Δ*vipC*^{26933} compared to ATCC26933. Of these, 132 proteins had increased abundance, while 342 proteins had decreased abundance. Loss of *vipC* therefore induced significant proteomic remodelling in *A. fumigatus*. A full list of proteins with differential abundance can be seen in Appendix 5. Figure 6.29 summarises the most significantly enriched functional categories of the proteins showing differential abundance.

Δ*vipC*^{26933} displayed differential growth compared to ATCC26933, with increased radial growth and the presence of aerial hyphae indicative of altered growth regulation. Several proteins with increased abundance in Δ*vipC*^{26933} compared to ATCC26933 were identified with key roles in the regulation of fungal growth. These were Rho GTPase Rho1 (AFUA_6G06900; $\log_2$ 1.19 fold), Rho GTPase Rho3 (AFUA_3G06690; Unique) and transcriptional activator SomA (AFUA_7G02260; Unique) (Table 6.1). The Rho GTPases have been demonstrated to regulate the actin cytoskeleton arrangement in *A. fumigatus* (Dichtl et al., 2010), while SomA deletion resulted in slow growth and impaired asexual development (Lin et al., 2015). Increased abundance of these proteins as a result of *vipC* deletion provides a mechanism for the growth phenotypes observed in Δ*vipC*^{26933}. The increased growth is also reflected in significantly

enriched protein categories, with membrane proteins (*n* = 17), hyphal tip proteins (*n* = 2) and proteins involved in chromosome organisation (*n* = 2) indicative of cell growth (Figure 6.29A).

Conidial hydrophobin RodB (AFUA_1G17250) exhibited a $\log_2$ -5.22 fold decrease in abundance in Δ*vipC*^{26933}. Although *vipC* deletion did not affect conidiation levels, decreased abundance of this protein suggests that *vipC* may still influence the conidial proteome. However, hydrophobins have also been demonstrated to play an important role in aerial hyphae formation. In *Schizophyllum commune*, the Sc3p class I hydrophobin is secreted at the surface of the cell wall of aerial hyphal elements. This forms a rodlet layer at the interface between the cell wall and air (Wösten et al., 1994). Decrease abundance of RodB may therefore be linked to altered aerial hyphae growth observed in Δ*vipC*^{26933}.

Oxidoreducase activity (*n* = 67) and oxidation-reduction process (*n* = 69) were significantly enriched categories of proteins showing decreased abundance in Δ*vipC* compared to ATCC26933 (Figure 6.29B). This is indicative of a shift in the redox state of Δ*vipC*^{26933} compared to ATCC26933. Related to this, catalase B (AFUA_3G02270; $\log_2$ -1.8 fold) and superoxide dismutase (AFUA_5G09240; $\log_2$ -2.82 fold) had decreased abundance in Δ*vipC*^{26933} (Table 6.1). These are important enzymes in oxidative stress defence (Imlay, 2002). Furthermore, two components of the CCAAT-binding factor complex (CBC) show increased abundance in Δ*vipC*^{26933} compared to ATCC26933. HapC (AFUA_1G03840) is unique in Δ*vipC* compared to ATCC26933, while HapE (AFUA_6G05300) shows an increase in abundance of $\log_2$ 1.1 fold. As discussed previously, the CBC is essential for mounting an effective oxidative stress response (Thon et al., 2010). This is further indication of changes to the oxidative stress defense in Δ*vipC*^{26933}.

EgtB (AFUA_2G13295), predicted to catalyse the final step in EGT biosynthesis (Pluskal et al., 2014), showed a $\log_2$ -1.35 fold decrease in abundance in Δ*vipC* compared to wild-type. This would appear to indicate a change in EGT biosynthesis, however measurement of EGT levels in Δ*vipC*^{26933} (Section 6.2.3.2) revealed no difference in EGT levels compared to ATCC26933. This is likely due to redundancy in catalysing the final step of EGT biosynthesis.

Table 6.1. Selected proteins with significant log_2 fold change or unique/absent in *A. fumigatus* Δ*vipC*^{26933} compared to ATCC26933 under basal conditions. Data sorted by fold change, in descending order.

Protein Description	Present/log_2 (Fold Change)	p-value	Peptides	Sequence coverage [%]	Protein IDs
CCAAT-binding factor complex subunit HapC	Unique	n/a	3	23.8	AFUA_1G03840
Rho GTPase Rho3	Unique	n/a	3	21.8	AFUA_3G06690
Transcriptional activator SomA	Unique	n/a	2	4.5	AFUA_7G02260
Aflatoxin B1-aldehyde reductase GliO-like, putative	1.2167	0.001131	8	36.9	AFUA_1G13370
Rho GTPase Rho1	1.19404	0.031796	10	64	AFUA_6G06900
CCAAT-binding factor complex subunit HapE	1.09962	0.020565	5	25.1	AFUA_6G05300
Methyltransferase SirN-like, putative	-1.17769	0.014002	29	89.7	AFUA_8G00550
Aminotransferase family protein, putative (EgtB)	-1.34821	0.000589	21	74.6	AFUA_2G13295
Catalase B (Antigenic catalase) (Slow catalase)	-1.80239	0.007799	18	38.6	AFUA_3G02270
Superoxide dismutase [Cu-Zn]	-2.82331	0.010068	13	82.9	AFUA_5G09240
Conidial hydrophobin RodB	-5.21637	0.001205	4	61.4	AFUA_1G17250
12-alpha,13-alpha-dihydroxyfumitremorgin C prenyltransferase Fumitremorgin biosynthesis protein H	Absent	n/a	9	36.3	AFUA_8G00250
Verruculogen synthase (Fumitremorgin biosynthesis protein F)	Absent	n/a	6	26.5	AFUA_8G00230

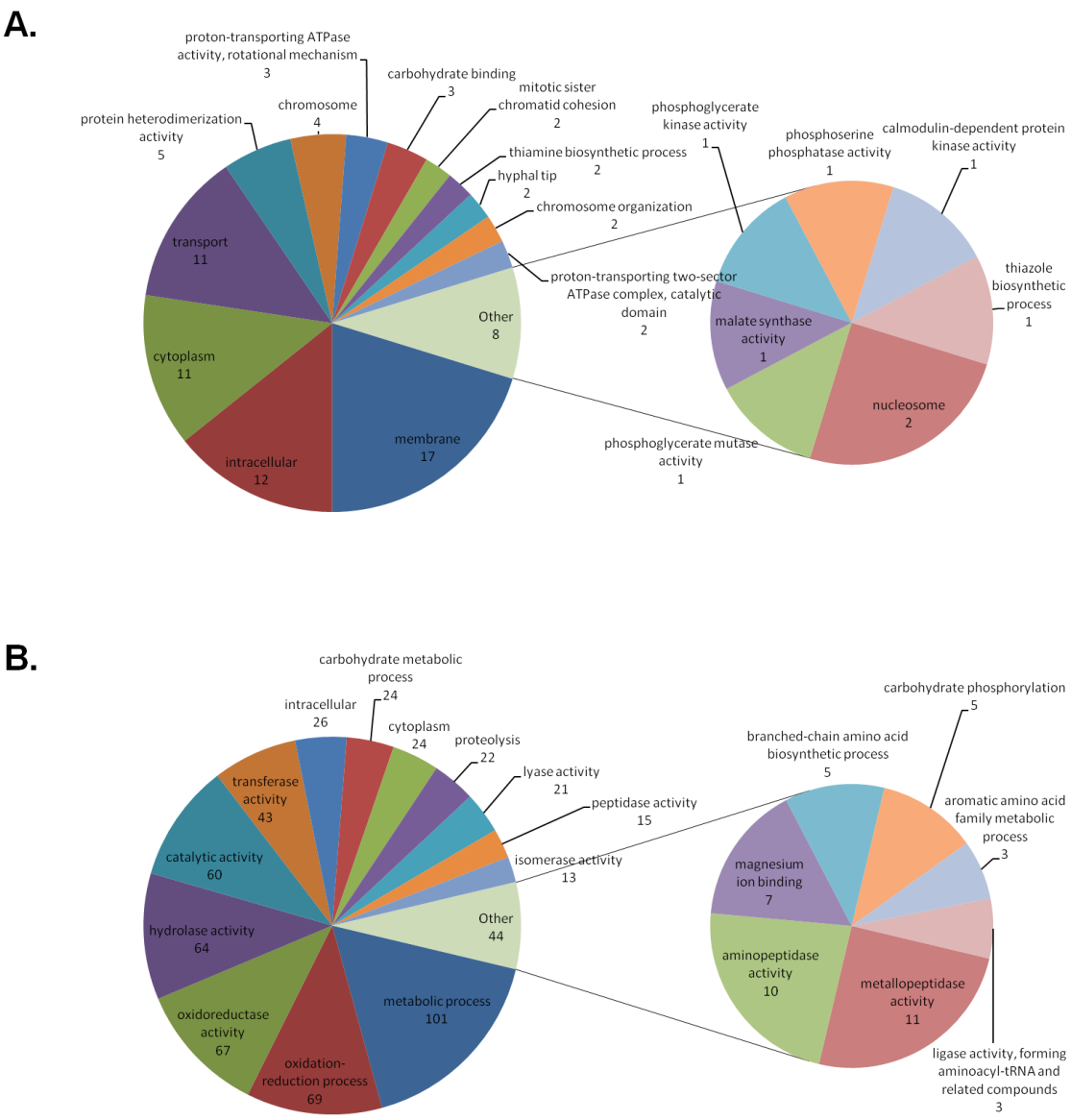

Figure 6.29. Significantly enriched functional categories of proteins showing differential abundance in Δ*vipC*^{26933} compared to ATCC26933 under basal conditions. The number under each category represents the number of proteins detected within that category. (A) Significantly enriched functional categories from proteins showing increased abundance, whereby 127 out of 132 proteins in the data set were annotated. (B) Significantly enriched functional categories from proteins showing decreased abundance, whereby 332 out of 342 proteins in the data set were annotated.

Dramatically, an array of proteins involved in glutathione and methionine metabolism underwent decreased abundance in Δ*vipC*^{26933} compared to ATCC26933 (Table 6.2). Enzymes which function primarily in the metabolism of glutathione showed decreased abundance in Δ*vipC*^{26933} compared to ATCC26933, these include γ-glutamylcysteine synthetase regulatory subunit (AFUA_3G14280; $\log_2$ -1.16 fold), glutathione-specific γ-glutamylcyclotransferase (AFUA_3G08560; $\log_2$ -1.5 fold), glutathione oxidoreductase (AFUA_1G15960; $\log_2$ -1.91 fold) and glutathione synthetase (AFUA_5G06610; $\log_2$ -1.98 fold). Furthermore, enzymes which biosynthesise the precursors of glutathione, cysteine and glutamate (Lu, 2009), also had decreased abundance. These include cysteine synthase (AFUA_5G02180; $\log_2$ -1.55 fold), glutamate carboxypeptidase (AFUA_3G10650; $\log_2$ -1.94 fold), cystathionine γ-lyase (AFUA_8G04340; $\log_2$ -2.03 fold) and two glutaminases (AFUA_3G10310; $\log_2$ -2.75 fold and AFUA_6G09910; absent) (Figure 6.30). This data unambiguously demonstrates how glutathione biosynthesis is downregulated in Δ*vipC*^{26933}, resulting in lower levels of glutathione, as observed (Figure 6.25).

In addition to this, 2 proteins associated with the glyoxalase system show decreased abundance in Δ*vipC* compared to ATCC26933. The glyoxalase system involves detoxifying hemithioacetal groups which form due to reactions between glutathione and aldehyde groups (Thornalley, 1990). The proteins were lactoylglutathione lyases: AFUA_6G07940 ($\log_2$ -1.98 fold) and AFUA_2G13550 (Absent). Lactoylglutathione lyase (also known as glyoxalase I) catalyses the isomerisation of hemithioacetal adducts. A second enzyme (glyoxalase II) then catalyses the hydrolysis of the hemithioacetal adduct into glutathione and lactate. Decreased abundance of the lactoglutathione lyases may be due to decreased occurrence of hemithioacetal groups resulting from diminished levels of glutathione.

The proteins involved in methionine metabolism were methionine synthase (AFUA_4G07360; $\log_2$ -1.25 fold) and adenosylhomocysteinase (AFUA_1G10130; $\log_2$ -1.8 fold). Methionine synthase catalyses the biosynthesis of methionine from homocysteine, while adenosylhomocysteinase cleaves *S*-adenosylhomocysteine (SAH) into homocysteine and adenosine (Figure 6.30). The decreased abundance of adenosylhomocysteinase is of particular interest as SAH is a potent inhibitor of methylation (Mandaviya et al., 2014). Increased levels of SAH caused by decreased abundance of adenosylhomocysteinase would lead to a decrease in

methylation. As a methyltransferase, VipC activity is directly linked to SAM and SAH levels. These alterations in the abundances of methionine cycle proteins indicates VipC could play a role in regulating methylation levels.

A number of proteins which function in the biosynthesis of secondary metabolism had differential abundance in Δ*vipC*^{26933} compared to ATCC26933 (Table 6.1). These include fumitremorgin biosynthesis protein F (AFUA_8G00230) and protein H (AFUA_8G00250) which were both absent in Δ*vipC*^{26933} compared to ATCC26933. A SirN-like methyltransferase, involved in pseurotin A biosynthesis (Alcazar-Fuoli et al., 2014) had a $\log_2$ -1.18 fold decrease in abundance. A putative Aflatoxin B1-aldehyde reductase (AFUA_1G13370) showed a $\log_2$ 1.22 fold increase in abundance in Δ*vipC* compared to ATCC26933. This indicates changes in secondary metabolism in *A. fumigatus* caused by *vipC* deletion.

Table 6.2. Proteins associated with glutathione and methionine metabolism with significant log_2 fold decrease or absent in *A. fumigatus* Δ*vipC*^{26933} compared to ATCC26933 under basal conditions. Data sorted by fold change, in descending order.

Protein Description	Present/log_2 (Fold Change)	p-value	Peptides	Sequence coverage [%]	Protein IDs
Gamma-cysteine synthetase regulatory subunit, putative	-1.16194	0.029487	8	46.3	AFUA_3G14280
Cobalamin-independent methionine synthase MetH/D	-1.25468	0.003155	67	73.8	AFUA_4G07360
Glutathione-specific gamma-glutamylcyclotransferase	-1.50449	0.000284	8	40.3	AFUA_3G08560
Cysteine synthase (O-acetylserine (Thiol)-lyase) (Csase)	-1.54878	0.002011	10	42	AFUA_5G02180
Adenosylhomocysteinase	-1.79604	0.001039	36	74.2	AFUA_1G10130
Glutamine synthetase, putative	-1.90463	0.016527	16	45.1	AFUA_6G03530
Glutathione oxidoreductase Glr1, putative	-1.91151	0.009301	25	67.4	AFUA_1G15960
Glutamate carboxypeptidase Tre2, putative	-1.93664	0.033893	15	27.5	AFUA_3G10650
Glutathione synthetase (GSH-S)	-1.97585	0.005413	21	63.8	AFUA_5G06610
Lactoylglutathione lyase (Glyoxalase I)	-1.98281	0.009525	26	85.5	AFUA_6G07940
Cystathionine gamma-lyase	-2.03402	0.007625	12	56.8	AFUA_8G04340
Glutaminase, putative	-2.74585	0.029525	18	33.6	AFUA_3G10910
Lactoylglutathione lyase (Glo1), putative	Absent	n/a	5	37.3	AFUA_2G13550
Glutaminase, putative	Absent	n/a	17	28.7	AFUA_6G09910

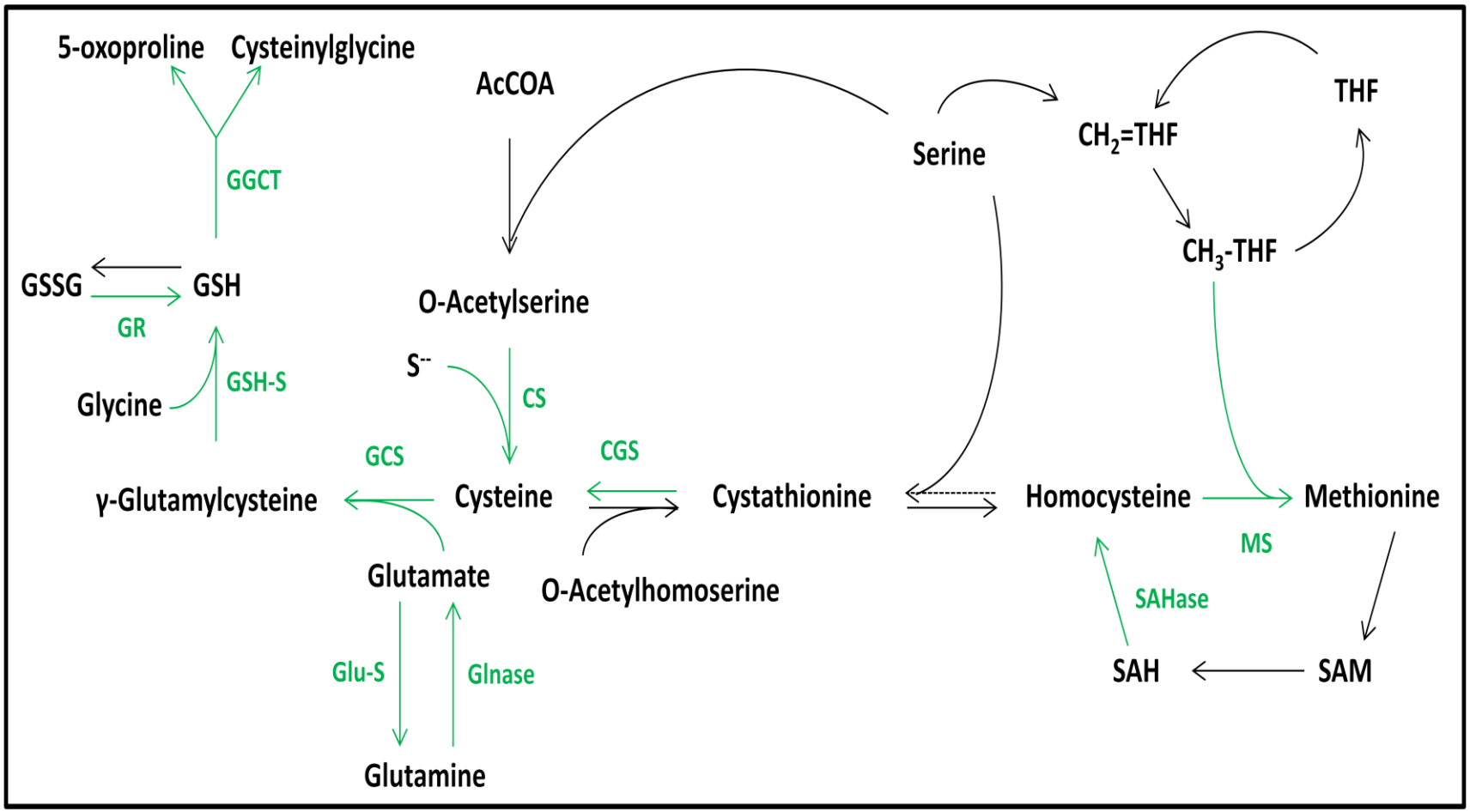

Figure 6.30. Proteins associated with glutathione and methionine metabolism which show decreased abundance in Δ*vipC*^{26933} compared to ATCC26933. Proteins with decreased abundance are shown in green. Abbreviations: GCS, Gamma-Glutamylcysteine Synthetase Regulatory Subunit; MS Methionine Synthase; GGCT, Glutathione-Specific Gamma-Glutamylcyclotransferase; CS, Cysteine Synthase; SAHase, Adenosylhomocysteinase; Glu-S, Glutamine Synthetase; GR, Glutathione Oxidoreductase; GSH-S, glutathione Synthase; CGL, Cystathionine γ-Lyase; Glnase, Glutaminase.

6.3 Discussion

This chapter presents the work done to characterise *A. fumigatus* Δ*palA*^{26933}, Δ*egtB*^{26933} and Δ*vipC*^{26933}. No phenotype was observed in Δ*palA*^{26933}. Analysis of EGT, His and gliotoxin levels in Δ*palA*^{26933} revealed no significant difference compared to ATCC26933. Similarly, analysis of sensitivity to H_2O_2, menadione, diamide, His, Phe and gliotoxin showed no significant differences between Δ*palA*^{26933} and ATCC26933. Δ*egtB*^{26933} had attenuated levels of EGT, confirming that EgtB forms part of the EGT biosynthetic pathway. EGT production was not completely abrogated in Δ*egtB*^{26933}, as was observed in Δ*egtA*^{26933}, meaning EgtB is not essential for EGT biosynthesis. Attenuated EGT levels in Δ*egtB*^{26933} resulted in sensitivity to H_2O_2 and menadione, further underlining the importance of EGT as an antioxidant in *A. fumigatus*. Δ*vipC*^{26933} had differential growth compared to ATCC26933, with increased growth in both solid and liquid media and the presence of aerial hyphae when grown on solid media. Δ*vipC*^{26933} also had reduced levels of GSH and decreased abundance of superoxide dismutase and catalase B in comparison to ATCC26933. LFQ proteomic analysis revealed Δ*vipC*^{26933} had decreased abundance of proteins associated with metabolic process, with prominent proteins involved in GSH, cysteine, glutamate and methionine metabolism identified.

Phenylalanine ammonia lyase (PAL) has been demonstrated to function in stress response in plants through the production of phenyl propanoid compounds (Dixon and Paiva, 1995). Additionally, it has also been implicated in oxidative stress defence (Desikan et al., 1998; Lee et al., 2003; Gao et al., 2008). PAL (AFUA_2G09110) had increased abundance in Δ*egtA*^{26933} compared to ATCC26933 under basal ($\log_2$ 2.71 fold) and ROS ($\log_2$ 3.73 fold) conditions. Thus, it was hypothesised that increased abundance of PAL may be part of an oxidative stress response in the absence of EGT. This would explain why PAL had a larger increase in abundance under ROS conditions compared to basal conditions. Assays for oxidative stress sensitivity using H_2O_2, menadione and diamide revealed no significant difference between Δ*palA*^{26933} and ATCC26933. Deletion of *palA* therefore had no deleterious effect on oxidative stress defence in *A. fumigatus*. PAL therefore appears to play no role in protecting *A. fumigatus* from elevated ROS levels. However it may be that PAL function in oxidative stress defence is only necessary when the oxidative stress defence system has been compromised (e.g. EGT absence).

PAL is known to have high similarity to histidine ammonia lyase (HAL)(Schwede et al., 1999), which breaks down histidine in manner similar to phenylalanine catabolism by PAL. It was speculated that if PAL was misannotated and had HAL activity, the observed increase in abundance in Δ*egtA*^{26933} may be due to increased histidine levels caused by absence of EGT biosynthesis, in which histidine is essential. In order to test this hypothesis, His levels in Δ*palA*^{26933} and ATCC26933 were measured via RP-HPLC and sensitivity to 200 mM His was analysed. RP-HPLC analysis revealed no significant difference in His levels in ATCC26933 and Δ*pal*^{26933}. Furthermore no sensitivity to exogenous His was observed in Δ*palA*^{26933} compared ATCC26933. Deletion of *palA* in *A. fumigatus* therefore caused no changes in His levels nor impacted on detoxifying high concentrations of His. Thus no role for PAL in metabolising His could be identified.

Another hypothesis for the increased abundance of PAL in Δ*egtA*^{26933} under both basal and ROS conditions was that it could be acting as an ergothionase. Muramatsu et al. (2013) reported an enzyme with ergothioneine degradation activity showed 17 % similarity to PAL in *Burkholderia* sp. HME13. If this was the case, EGT levels would be predicted to rise in Δ*palA*^{26933} as EGT would not be broken down. However measurement of EGT levels in Δ*palA*^{26933} and ATCC26933 revealed no significant differences, meaning no role for PAL in ergothioneine degradation could be identified.

Phe sensitivity analysis also revealed no significant differences between the radial growth of ATCC26933 and Δ*palA*^{26933} when grown on 150 mM Phe. *palA* deletion therefore does not result in a deleterious accumulation of Phe following exposure to 150 mM Phe. This is likely due to other enzymes, such as phenylalanine hydroxylase (Flatmark and Stevens, 1999), affecting phenylalanine catabolism in the absence of PAL.

Δ*palA*^{26933} gliotoxin production was analysed via RP-HPLC, which revealed no significant difference in gliotoxin levels in comparison to ATCC26933. Furthermore, Δ*palA*^{26933} displayed no sensitivity to gliotoxin in comparison to ATCC26933. *palA* deletion therefore has no impact on gliotoxin biosynthesis or self-protection from gliotoxin.

Thus no role for PAL in *A. fumigatus* could be established. It may be that there is redundancy, resulting in no observable phenotype following *palA*^{26933} deletion. Additionally, it may be that

PAL function only became necessary following *egtA* deletion, hence the observed rise in abundance. Further investigation is required to elucidate the function of this protein in *A. fumigatus*.

RP-HPLC and LC-MS/MS analysis of EGT levels in ATCC26933 and Δ*egtB*^{26933} demonstrated that Δ*egtB*^{26933} was capable of producing EGT, but at significantly reduced levels compared to ATCC26933. This demonstrates that EgtB participates in EGT biosynthesis. However, unlike Δ*egtA*^{26933}, EGT production was not abrogated entirely. Thus *egtB* is not essential for EGT biosynthesis in *A. fumigatus*. This indicates that there is redundancy in the final step of EGT biosynthesis in *A. fumigatus*. Seebeck (2010) demonstrated that conversion of hercynylcysteine sulfoxide to EGT does not require a specific enzyme. A PLP-binding β-lyase (ETA_14770) from *Erwinia tasmaniensis*, which does not biosynthesise EGT, was capable of producing EGT *in vitro* from hercynylcysteine sulfoxide. Indeed, Seebeck also reported that prolonged incubation (10 h) of hercynylcysteine sulfoxide with PLP was found to produce significant amounts of EGT. Thus conversion of hercynylcysteine sulfoxide to EGT may happen spontaneously in the presence of PLP. As it has been demonstrated that this final step of EGT biosynthesis does not require a specific enzyme, it likely that in the absence of *egtB*, EGT biosynthesis is completed non-specifically in Δ*egtB*^{26933} by unrelated PLP-binding enzyme.

Deletion of *Schizosaccharomyces pombe egt2*, an *egtB* ortholog, resulted in reduced EGT levels compared to wild-type (Pluskal et al., 2014). However *S. pombe* Δ*egt2* had a much greater reduction in EGT levels compared to *A. fumigatus* Δ*egtB*^{26933}. *egt2* deletion in *S pombe* reduced EGT levels to 25.5 % of wild-type EGT levels, while *A. fumigatus* Δ*egtB*^{26933} EGT levels were 72 % of ATCC26933 EGT levels. Thus *egtB* deletion in *A. fumigatus* results in smaller relative reduction in EGT levels compared to *egt2* deletion in *S. pombe*. This suggests a key difference in EGT biosynthesis between the two organisms, with greater redundancy measures in *A. fumigatus* for *egtB* activity compared to *egt2* in *S. pombe*. This could be due to relative importance of EGT in each organism. It has been demonstrated in Chapters 4 & 5 of this thesis that EGT loss in Δ*egtA*^{26933} affects redox homeostasis, oxidative stress defence, conidiation, cell wall integrity, glutathione metabolism and gliotoxin metabolism. In contrast to this, no phenotypes were observed in the EGT null *S. pombe* Δ*egt1*. Thus EGT appears to play a much more prominent

role in *A. fumigtaus* compared to *S. pombe*. This may explain the need for increased redundancy for *A. fumigatus egtB* compared to *S. pombe egt2*.

Sensitivity assays for H_2O_2, menadione and diamide revealed Δ*egtB*^{26933} is sensitive to H_2O_2 and menadione compared to ATCC26933, while no significant sensitivity to diamide was observed. Δ*egtB*^{26933} was sensitive to H_2O_2 compared to ATCC26933 at a concentration of 3 mM. However, no significant difference in radial growth between Δ*egtB*^{26933} and ATCC26933 was detected at 1 mM and 2 mM H_2O_2. Δ*egtB*^{26933} was sensitive to menadione compared to ATCC26933 at all concentrations of menadione tested (20 – 60 µM). *egtB* deletion in *A. fumigatus* therefore results in sensitivity to high levels of H_2O_2 induced ROS and to menadione induced superoxide radicals in particular. Diamide induced ROS however had no significant effect on Δ*egtB*^{26933} radial growth in comparison to ATCC26933.

The results for ROS sensitivity in Δ*egtB*^{26933} are similar to those obtained for Δ*egtA*^{26933} (Section 4.2.2). Both Δ*egtA*^{26933} and Δ*egtB*^{26933} were not sensitive to 1 mM and 2 mM H_2O_2 compared to ATCC26933, but displayed sensitivity to 3 mM H_2O_2 compared to ATCC26933. Δ*egtA*^{26933} and Δ*egtB*^{26933} were both significantly sensitive to menadione compared to ATCC26933 at concentrations of 40 µM and 60 µM. However, while Δ*egtA*^{26933} was not sensitive to 20 µM menadione in comparison to ATCC26933, Δ*egtB*^{26933} did display sensitivity at 20 µM menadione. Neither Δ*egtA*^{26933} nor Δ*egtB*^{26933} were sensitive to diamide compared to ATCC26933. Thus, Δ*egtB* displayed a similar phenotype to Δ*egtA*^{26933} in response to 3 mM H_2O_2 and was more sensitive to menadione in comparison to ATCC26933 than Δ*egtA*^{26933}.

That Δ*egtB*^{26933} matches and exceeds Δ*egtA*^{26933} sensitivity to H_2O_2 and menadione respectively was somewhat of a surprise given that Δ*egtB*^{26933} retains 71.1 % EGT production compared to ATCC26933, while EGT is abrogated in Δ*egtA*^{26933} entirely. This may be explained by differences in GSH levels in Δ*egtA*^{26933} and Δ*egtB*^{26933}. GSH levels were significantly increased in Δ*egtA*^{26933} compared to ATCC26933, which is hypothesised to compensate for EGT absence. However, there were no significant differences in GSH levels in Δ*egtB*^{26933} compared to ATCC26933. This suggests that *egtB* deletion is not compensated for in the same manner as *egtA* deletion. This would explain why a partial loss of EGT in Δ*egtB*^{26933} resulted in similar sensitivity to ROS as complete loss of EGT in Δ*egtA*^{26933}. That a partial loss of EGT can cause sensitivity further underlines the importance of EGT as an antioxidant in *A. fumigatus*.

Like GSH, gliotoxin levels were not significantly altered in Δ*egtB*^{26933} compared to ATCC26933. GSH and gliotoxin levels were increased and decreased respectively in Δ*egtA*^{26933} in comparison to ATCC26933. This is a significant metabolic adjustment in response to abrogation of EGT biosynthesis. This does not occur in Δ*egtB*^{26933}, which suggests that a partial reduction of EGT does not perturb *A. fumigatus* metabolism and/or cell redox state in the same manner as abrogated EGT biosynthesis.

LFQ proteomic analysis of Δ*vipC*^{26933} and ATCC26933 revealed that 474 proteins had differential abundance in Δ*vipC*^{26933} compared to ATCC26933. 132 proteins had increased abundance, while 342 proteins had decreased abundance. This is a significant proteomic remodelling. Of note, "metabolic process" was a significantly enriched protein category amongst proteins with decreased abundance (Figure 6.29B). 101 proteins in the dataset were in this category, indicating a significantly altered metabolism due to *vipC* loss.

Deletion of *vipC* in *A. fumigatus* resulted in altered growth phenotypes, with Δ*vipC*^{26933} exhibiting increased radial growth on solid media and increased mycelial dry weight in liquid media compared to ATCC26933. Furthermore, Δ*vipC*^{26933} colonies had distinct aerial hyphae that were not present on ATCC26933. *vipC* deletion therefore resulted in differential growth and development in *A. fumigatus*.

LFQ proteomics provided further insight into these phenotypes. SomA (AFUA_7G02260), a transcription factor that regulates growth and development in *A. fumigatus*, was unique in Δ*vipC*^{26933} compared to ATCC26933. Lin et al. (2015) demonstrated that deletion of *somA* in *A. fumigatus* resulted in attenuated radial growth and asexual development. SomA was demonstrated to regulate a number of developmental genes such as *brlA*, *medA*, *stuA* and *flbA*. Furthermore, Rho GTPases Rho1 (AFUA_6G06900; $\log_2$ 1.2 fold) and Rho3 (AFUA_3G06690; unique) showed increased abundance in Δ*vipC*^{26933} compared to ATCC26933. Rho GTPases are small signaling proteins which play a central role in regulation of the actin cytoskeleton (Etienne-Manneville and Hall, 2002). Rho1 is essential in *A. fumigatus* and conditional downregulation of *rho1* resulted in decreased radial growth, hyphal leakage and reduced conidiation (Dichtl et al., 2012). Rho1 is also a key regulator of CWI signalling and predominantly localizes to the hyphal tip (Dichtl et al., 2010). Rho3 also localises

predominantly to the hyphal tip and is predicted to regulate hyphal polarity and CWI signalling in conjunction with Rho1 (Dichtl et al., 2010).

It can therefore be postulated that in wild-type *A. fumigatus*, VipC represses SomA, Rho1 and Rho3 as a method of regulating growth and development. In Δ*vipC*^{26933}, SomA, Rho1 and Rho3 are then increased in abundance, resulting in increased radial growth and the presence of aerial hyphae.

That proteins associated with metabolic process have decreased abundance in Δ*vipC*^{26933} compared to ATCC26933, while radial growth is increased, suggests that metabolic processes are sacrificed in order to focus on increased growth. This may be a "starvation response", whereby radial growth rate is increased to search for and reach nutrients. *vipC* may control a metabolic switch between increased growth and metabolic processes and when deleted in Δ*vipC*^{26933}, this response cannot be turned off.

Aerial hyphae are linked with asexual development, as condiophores develop from the tips of aerial hyphae (Mah and Yu, 2006). Thus altered aerial hyphae growth could be linked to changes to asexual development following *vipC* deletion. Indeed, *vipC* deletion in *A. nidulans* resulted in a 70 – 75 % drop in asexual sporulation compared to wild-type when grown in light (Sarikaya-Bayram et al., 2014). However, no significant difference in the levels of conidiation was observed in Δ*vipC*^{26933} compared to ATCC26933. Thus conidiation levels are regulated independently of *vipC* in *A. fumigatus*. This represents a significant deviation in the role of *vipC* in *A. fumigatus* compared to *A. nidulans*. Interestingly, conidial hydrophobin RodB (AFUA_1G17250) had a $\log_2$ -5.22 fold decrease in abundance in Δ*vipC*^{26933} compared to ATCC26933. RodB, in conjunction with RodA, comprise the hydrophobic rodlet layer on the surface of conidia (Paris et al., 2003a). The rodlet layer contributes to conidial buoyancy in the air, essential for conidial dispersion. *vipC* therefore may play a role in development of conidia, if not levels of conidiation. Additionally, hydrophobins have been demonstrated to be present in aerial hyphae and form rodlets that are part of an extracellular matrix that holds aerial hyphae together (Beauvais et al., 2007). Decrease in RodB abundance may therefore be linked to the alterations in aerial hyphae observed.

Curiously, these phenotypes observed in Δ*vipC*^{26933} are very similar to phenotypes observed in a Δ*brlA* mutant. *brlA* is a central regulator of asexual development in *A. fumigatus* and its deletion resulted in increased hyphal mass and elongated aerial hyphae (Mah and Yu, 2006). However, unlike Δ*vipC*^{26933}, Δ*brlA* had a complete absence of asexual development. Relevantly, *brlA* is regulated by SomA (Figure 6.31), which had increased abundance in Δ*vipC*^{26933} compared to ATCC26933. Conditional downregulation of *somA* resulted in abolition of *brlA* expression (Lin et al., 2015). However, LFQ proteomic analysis did not show BrlA to have differential abundance. Whether BrlA is linked to the phenotypes observed in Δ*vipC*^{26933} can only be speculated from the data available, however the similarity in the phenotypes suggests that perturbations in asexual development regulation may be taking place, which could be linked in differential expression of SomA.

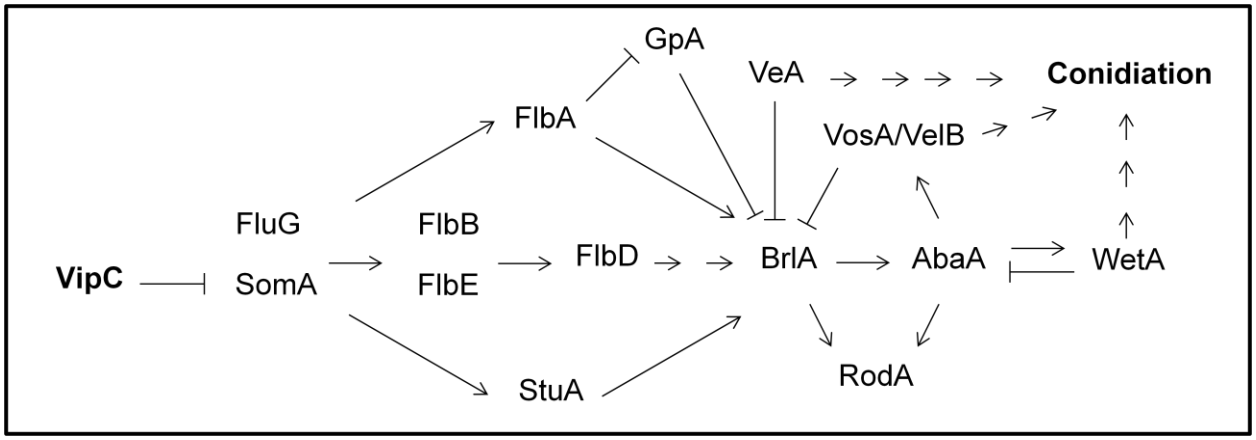

Figure 6.31. Schematic representing the regulation of asexual development in *A. fumigatus*. SomA is an upstream regulator of BrlA, the first protein in the asexual development central regulatory pathway (BrlA, AbaA and WetA). VipC may contribute to regulation of conidia through repression of SomA. Image modified from Mah and Yu (2005), Sheppard et al. (2005) and Alkhayyat et al. (2015).

VipC was demonstrated to regulate sexual and asexual development in response to light in *A. nidulans* (Sarikaya-Bayram et al., 2014). Therefore ATCC26933 and Δ*vipC*^{26933} were incubated in the presence or absence of light in order to investigate if VipC activity changes in response to light in *A. fumigatus*. Both ATCC26933 and Δ*vipC*^{26933} had significantly decreased radial growth when grown in light compared to darkness. Δ*vipC*^{26933} had increased radial growth compared to ATCC26933 in both darkness and light, indicating that VipC regulates growth independently of

exposure to light. However the aerial hyphae present on Δ*vipC*^{26933} in the dark did not develop on Δ*vipC*^{26933} when grown in light. Aerial hyphae were not present on ATCC26933 when grown in darkness or light. Thus the presence of elongated aerial hyphae only occurs on Δ*vipC*^{26933} when grown in darkness. This suggests that VipC suppresses development of aerial hyphae in darkness, but is regulated separately when grown in the light. VipC therefore does appear to regulate development in response to light, suggesting its role in *A. fumigatus* is not completely removed from the one it plays in *A. nidulans*.

LFQ proteomics indicated a shift in the redox state of Δ*vipC*^{26933} in comparison to ATCC26933. Proteins involved with oxidoreducase activity (n = 67) and/or involved with oxidation-reduction process (n = 69) were significantly enriched protein categories amongst proteins with decreased abundance. Two components of the CCAAT-binding factor complex (CBC) showed increased abundance in Δ*vipC*^{26933} compared to ATCC26933. HapC (AFUA_1G03840) is unique in Δ*vipC*^{26933} compared to ATCC26933, while HapE (AFUA_6G05300) had a $\log_2$ 1.1 fold increase in abundance. As discussed previously, the CBC is essential for co-coordinating the oxidative stress defence in eukaryotes (Thon et al., 2010). In Chapter 5, HapC was demonstrated to be absent in ATCC26933 under ROS conditions, suggesting that HapC absence is associated with increased ROS. HapC absence in ATCC26933 compared to Δ*vipC*^{26933} therefore indicates that Δ*vipC*^{26933} is experiencing less oxidative stress compared to ATCC26933.

Indeed, two key oxidative stress defence proteins, catalase B (AFUA_3G02270; $\log_2$ -1.8 fold) and superoxide dismutase (AFUA_5G09240; $\log_2$ -2.82 fold), were decreased in abundance in Δ*vipC*^{26933}. Catalases convert hydrogen peroxide in water and oxygen (Chelikani et al., 2004), while superoxide dismutase converts superoxide radicals into either water or hydrogen peroxide (McCord and Fridovich, 1969). In addition to this, total intracellular glutathione was reduced in Δ*vipC*^{26933} compared to ATCC26933. LFQ proteomics reveal decreased abundance of the glutathione biosynthetic enzymes γ-glutamylcysteine synthetase regulatory subunit (AFUA_3G14280; $\log_2$ -1.16 fold) and glutathione synthetase (AFUA_5G06610; $\log_2$ -1.98 fold). Biosynthetic proteins of cysteine and glutamate, essential precursors of glutathione (Lu, 2009), also had decreased abundance (Figure 6.32). Interestingly, EgtB (AFUA_2G13295), which catalyses the final step of EGT biosynthesis, also had decreased abundance. However, no significant difference in EGT levels in ATCC26933 and Δ*vipC*^{26933} was detected.

Despite the decreased abundance of oxidative stress defence proteins catalase B and superoxide dismutase, in addition to reduced levels of GSH, Δ*vipC*^{26933} displayed no sensitivity when challenged with ROS inducing agents. Δ*vipC*^{26933} was not sensitive to any concentration of H_2O_2, menadione or diamide tested compared to ATCC26933. This suggests that Δ*vipC*^{26933} can still mount an effective oxidative stress defence and that the observed reduction of oxidative stress defence mechanisms only occurs under basal conditions. It may be the case that levels of intracellular ROS are reduced in *vipC*^{26933} compared to ATCC26933. This can be explained by the observation that metabolic process is a significantly enriched category of proteins with decreased abundance (Figure 6.29B). ROS is a normal product of aerobic metabolism (Davies, 1995); therefore reduced metabolic process could lead to reduced levels of ROS under basal conditions. If basal ROS is reduced, abundance of catalase B and superoxide dismutase, in addition to GSH levels, can be decreased without adversely affecting the cell.

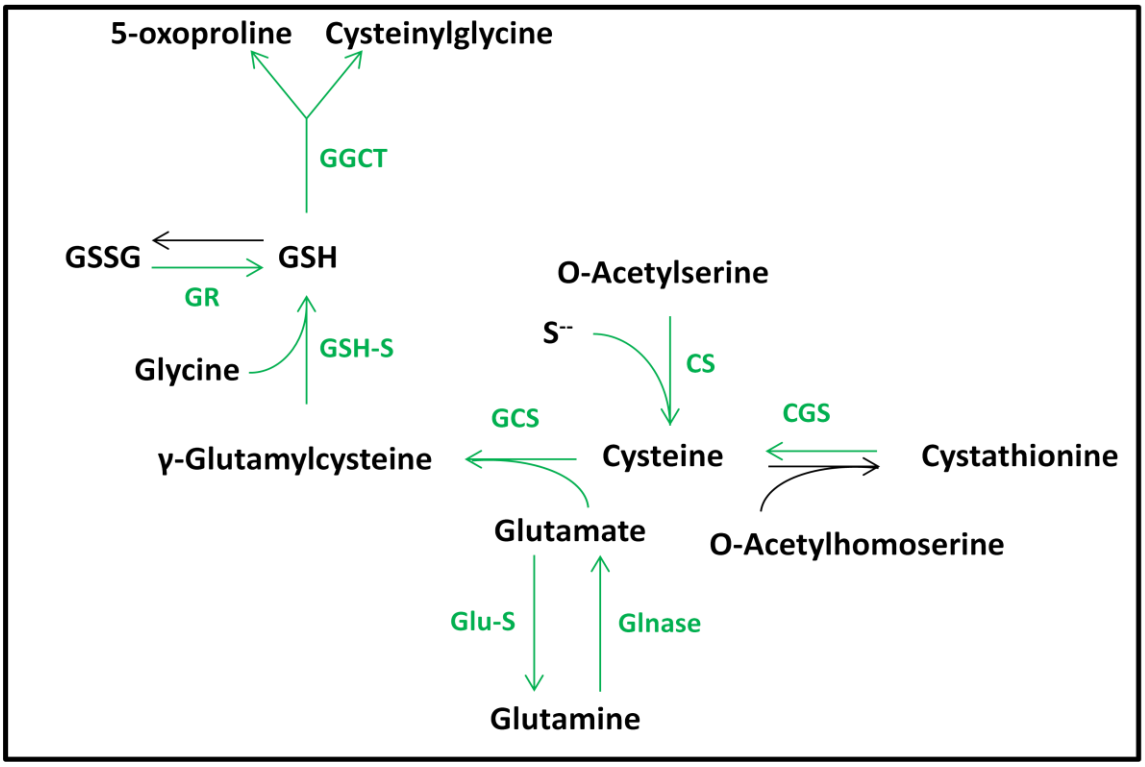

Figure 6.32. Proteins involved in the metabolism of glutathione, cysteine and glutamate have decreased abundance in Δ*vipC*^{26933}. Abbreviations: GCS, Gamma-Glutamylcysteine Synthetase Regulatory Subunit; GGCT, Glutathione-Specific Gamma-Glutamylcyclotransferase; CS, Cysteine Synthase; Glu-S, Glutamine Synthetase; GR, Glutathione Oxidoreductase; GSH-S, glutathione Synthase; CGL, Cystathionine γ-Lyase; Glnase, Glutaminase.

The decreased abundance of methionine cycle enzymes, methionine synthase (AFUA_4G07360; $\log_2$ -1.25 fold) and adenosylhomocysteinase (AFUA_1G10130; $\log_2$ -1.8 fold) had potential implications for SAM and SAH levels. As VipC is a SAM-dependant methyltransferase, this was of particular interest. Methionine synthase catalyzes the formation of methionine from homocysteine. As methionine is the precursor of SAM, the universal methyl donor (Lieber and Packer, 2002), this would be expected to reduce SAM levels (Figure 6.33). *vipC* deletion may result in decreased utilisation of SAM, due to the absence of VipC SAM-dependant methyltransferase activity. This would result in increased levels of intracellular SAM and decreased levels of SAH. In this case, adenosylhomocysteinase abundance may be reduced due to the decreased levels of its substrate, SAH. Methionine synthase may undergo decreased abundance to attenuate SAM biosynthesis as SAM levels are already elevated.

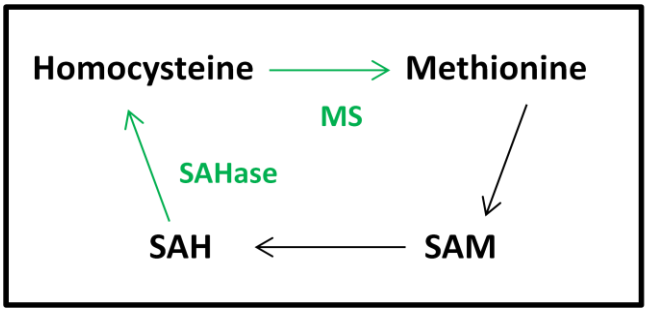

Figure 6.33. The components of the methionine cycle. Methionine synthase (MS) and adenosylhomocysteinease (SAHase) have decreased abundance in Δ*vipC*^{26933} compared to ATCC26933.

LFQ proteomics indicated that Δ*vipC*^{26933} had altered secondary metabolism compared to ATCC26933. Fumitremorgin biosynthesis protein F (FtmF; AFUA_8G00230) and protein H (FtmH; AFUA_8G00250) which were both absent in Δ*vipC*^{26933} compared to ATCC26933. FtmH catalyses the final step in fumitremorgin B biosynthesis (Grundmann et al., 2008), while FtmF converts fumitremorgin B into verruculogen (Kato et al., 2011), a tremorgenic mycotoxin. Decreased abundance of these proteins indicates a shift in fumitremorgin biosynthesis away from verruculogen due to *vipC*^{26933} absence. A SirN-like methyltransferase (AFUA_8G00550) demonstrated to be important in pseurotin A biosynthesis, had a $\log_2$ -1.18 fold decrease in abundance (Alcazar-Fuoli et al., 2014). This indicates a likely reduction in pseurotin A levels in Δ*vipC*^{26933} in comparison to ATCC26933. A putative Aflatoxin B1-aldehyde reductase

(AFUA_1G13370), predicted to be involved in secondary metabolite biosynthesis (Khaldi et al., 2010), showed a $\log_2$ 1.22 fold increase in abundance in Δ*vipC*^{26933} compared to ATCC26933. Gliotoxin biosynthesis was unaffected by *vipC* deletion however. RP-HPLC analysis showed no significant difference in gliotoxin levels in Δ*vipC*^{26933} and ATCC26933.

The data presented in this chapter demonstrates *vipC* functions in regulating growth, development and metabolism in *A. fumigatus*. This is a completely novel role for *vipC*, as previously the only function for *vipC* described was for controlling sexual and asexual development in *A. nidulans*. Elgabbar and Han (2015) attempted to characterise *vipC* in *A. fumigatus* through the creation of a Δ*vipC* mutant, but did not report any phenotypes and concluded that its role is redundant under normal culture conditions. That they did not observe the same growth phenotypes seen in Δ*vipC*^{26933} from this study may be due to differences in strain type or media. Furthermore, they lacked the insight from *A. fumigatus* Δ*egtA* data that we had and did not perform LFQ proteomic analysis.

The work presented in this chapter represents the first study of *palA* and *egtB* function in *A. fumigatus* and provides the first characterisation of *vipC* function in *A. fumigatus*. While no function for *palA* was elucidated, *egtB* was demonstrated to contribute to EGT biosynthesis. Δ*egtB* further emphasised the importance of EGT as an antioxidant, by demonstrating that a partial loss of EGT leads to ROS sensitivity. A novel role for *vipC* as a regulator of growth, development and metabolism was demonstrated, which had not been described in previous studies. This provides further insight into the metabolic changes observed in Δ*egtA*^{26933}, where VipC had increased abundance compared to ATCC26933.

Chapter 7

Discussion

7.1 Introduction

Many advances have been made in the study of ergothioneine in recent years. Seebeck (2010) presented the first elucidation of EGT biosynthesis in his seminal work using recombinant proteins cloned from *Mycobacterium smegmatis*. Following this, Bello et al. (2012) identified an enzyme required for EGT biosynthesis, *egt1*, in *Neurospora crassa*. This represented the first identification of an EGT biosynthetic gene in fungi. The second fungal EGT biosynthetic enzyme, *egt2*, was later identified by Pluskal et al. (2014) in *Schizosaccharomyces pombe*. The crystal structures of bacterial EgtB, EgtC and EgtD have been recently determined, furthering the understanding of EGT biosynthesis (Vit et al., 2014, 2015; Goncharenko et al., 2015). Studies into EGT functionality in fungi and bacteria have indicated a physiological role for EGT as an antioxidant (Bello et al., 2012, 2014; Sao Emani et al., 2013; Saini et al., 2015). EGT has also been associated with protection from heat (Alamgir et al., 2015), starvation response (Richard-Greenblatt et al., 2015) and antibiotic resistance (Saini et al., 2015). EGT was demonstrated to protect against UV radiation in *Methylobacterium* (Alamgir et al, 2015), but not in *N. crassa* (Bello et al., 2014). No physiological role for EGT was determined in *S. pombe* from their study using the EGT null Δ*egt1* mutant (Pluskal et al., 2014). The role of EGT, if any, therefore appears to vary between species and the antioxidant function as elucidated in *N. crassa* by Bello et al. (2012, 2014) has been the only physiological role described for EGT in a fungus.

Prior to this work, EGT biosynthesis and function had not been characterised in *Aspergillus fumigatus*, or any other human fungal pathogen. The first identification of EGT in *A. fumigatus* was made by Gallagher et al. (2012), who noted increased levels of EGT in the gliotoxin null mutant Δ*gliK*. Δ*gliK* exhibited many additional phenotypes, including abrogated gliotoxin production and sensitivity to H_2O_2 and exogenous gliotoxin. Whether increased levels of EGT were related to these phenotypes was a matter of speculation.

This discussion will describe the identification and deletion of two EGT biosynthetic genes: *egtA* and *egtB*. Data from *egtA* and *egtB* gene deletion mutants facilitated the analysis of EGT functionality in *A. fumigatus* through phenotypic and LFQ proteomic analysis. Of particular interest is the role of EGT in oxidative stress defence, the metabolic and redox systems interactions between EGT, GSH and gliotoxin, and EGT function in regulating conidiation and cell wall integrity. PAL and VipC were identified for further study through LFQ proteomic

analysis of Δ*egtA*^{26933}, which was facilitated by the generation of Δ*palA* and Δ*vipC* mutants. While PAL function in *A. fumigatus* remains unclear, VipC was characterised, for the first time, to influence growth, development and metabolism. Finally, the function of VipC in *A. fumigatus* adaption to EGT absence will be discussed.

7.2 Identification EGT biosynthetic genes in *A. fumigatus*

egtA (AFUA_2G15650) was identified to encode a potential EGT biosynthetic enzyme in *A. fumigatus* via bioinformatic analysis of *M. smegmatis egtB* and *egtD*, *N. crassa egt1* and *S. pombe egt1*. Chapter 3 detailed the generation of an *egtA* deletion mutant in *A. fumigatus* ATCC26933 using a bipartite gene deletion strategy. The *egtA* gene was then reinserted to generate the complemented strain, *egtA*^{C26933}. RT-PCR was utilized to confirm absence of gene expression in Δ*egtA*^{26933} and reinstatement of gene expression in *egtA*^{C26933}. In Chapter 4, RP-HPLC and LC-MS/MS demonstrated complete absence of EGT production in Δ*egtA*^{26933} and restoration of EGT production in *egtA*^{C26933}. This unambiguously proved EgtA to be an essential EGT biosynthetic enzyme, predicted to catalyse the first two steps of EGT biosynthesis (Figure 7.1).

Following the successful identification of *egtA* as an EGT biosynthetic gene, the question of a second EGT biosynthetic gene in *A. fumigatus* arose. *egtB* (AFUA_2G13295) was identified as a potential target, as it is a homolog of *S. pombe egt2* (Pluskal et al., 2014). In Chapter 3, it was described how *egtB* was deleted and absence of *egtB* expression demonstrated via RT-PCR. EGT production in ATCC26933 and Δ*egtB*^{26933} was analysed as described in Chapter 6 and it was demonstrated that Δ*egtB*^{26933} produced significantly less EGT compared to ATCC26933. It was concluded that EgtB does contribute to EGT production but is not essential for its biosynthesis. This data is in agreement with work from Seebeck (2010) and Pluskal et al. (2012), who demonstrated that the conversion of hercynylcysteine sulphoxide to EGT can be completed non-specifically, or even spontaneously, in the presence of the co-factor pyridoxal phosphate (PLP). EgtB was thus predicted to catalyse the final step of EGT biosynthesis (Figure 7.1), however this remains to be demonstrated biochemically.

During investigation of the redundancy of EgtB, Nfs1 (AFUA_3G14240) was also identified as a possible candidate for catalyzing the final step of EGT biosynthesis. Like EgtB, Nfs1 is a PLP-

dependant cysteine desulphurase that has been shown to provide inorganic sulphur for iron-sulphur cluster proteins in *Saccharomyces cerevisiae*. However, multiple attempts at deleting *Nfs1* in *A. fumigatus* proved unsuccessful, thus Nfs1 may be essential in *A. fumigatus*, as is the case in *S. cerevisiae* (Li et al., 1999). This would render generation of a deletion mutant impossible. Future studies into potential Nfs1 function in EGT biosynthesis could be undertaken through the generation of an *A. fumigatus* mutant with *Nfs1* under the control of a conditional inducible promoter, such as the tet-on system (Helmschrott et al., 2013).

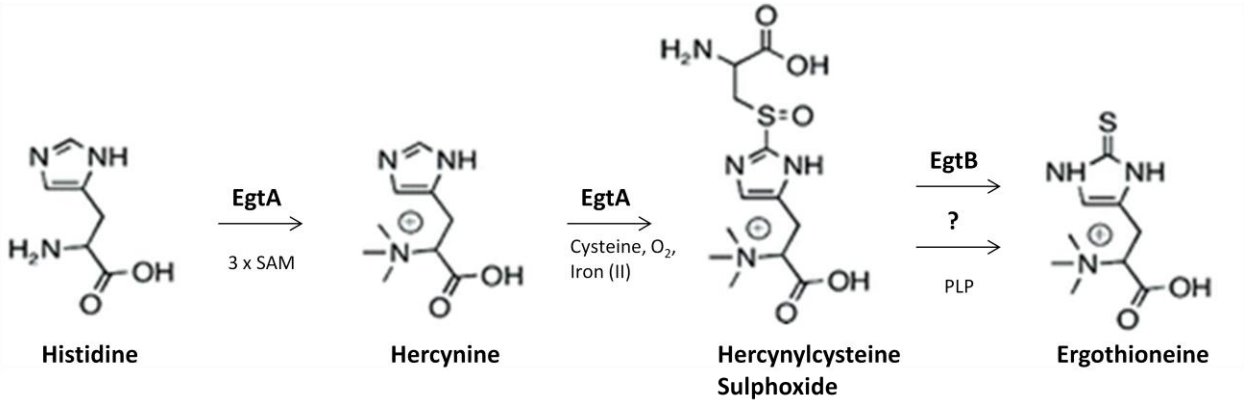

Figure 7.1. EGT biosynthetic pathway for *A. fumigatus* as elucidated from Δ*egtA*^{26933} and Δ*egtB*^{26933}. EgtA catalyses the first two steps, converting histidine into hercynine and hercynine into hercynylcysteine sulphoxide. EgtB may catalyse the final step, converting hercynylcysteine sulphoxide into ergothioneine. Conversion of hercynylcysteine to ergothioneine may take place by alternative mechanisms to EgtB.

Another protein which could be contributing to EgtB redundancy is cystathionine β-lyase (CBL; AFUA_4G03950). Seebeck (2010) demonstrated that a PLP-binding β-lyase (ETA_14770) from *Erwinia tasmaniensis* could catalyse the final step of EGT biosynthesis *in vitro*. ETA_14770 is annotated as a cystathionine β-lyase by KEGG, suggesting that *A. fumigatus* CBL, which is also a PLP-binding enzyme (Ravanel, 1997), could also catalyse the conversion of hercynylcysteine sulphoxide to EGT. Relevantly, CBL had increased abundance in Δ*egtA*^{26933} compared to ATCC26933 under ROS conditions. This is considered to be part of a metabolic shift towards SAM production in order to facilitate abortive EGT biosynthesis. Thus, CBL contribution to EGT biosynthesis may actually be twofold, and it may also catalyze the formation EGT from hercynylcysteine sulphoxide as hypothesised.

This work represents the first identification of an EGT biosynthetic pathway in *A. fumigatus* and in turn the first identification of an EGT biosynthetic pathway in a human fungal pathogen. This is only the second time the possible final step in EGT biosynthesis has been identified in a eukaryote, which is of particular importance because *S. pombe* does not display any phenotype following the loss of EGT biosynthesis. EGT biosynthesis was also demonstrated in a *Nicotiana tabacum* strain transformed with genes cloned from *A. fumigatus*. LC-MS/MS analysis demonstrated that an *N. tabacum* strain transformed with *A. fumigatus egtA* and *Nfs1* was able to produce EGT. That *egtA* is capable of catalysing EGT production in a plant is an important demonstration of its role in EGT biosynthesis. Whether Nfs1 contributed to EGT biosynthesis in *N. tabacum* is yet to be determined and will require analysis of *N. tabacum* strain transformed with *egtA* only.

7.3 The role of EGT in *A. fumigatus* oxidative stress defence and redox homeostasis

The availability of *A. fumigatus* strains with abrogated and reduced EGT production in the form of Δ*egtA*^{26933} and Δ*egtB*^{26933}, respectively, allowed for functional analysis of EGT in *A. fumigatus* as outlined in Chapters 4 and 6. Sensitivity assays using ROS inducing agents with ATCC26933, Δ*egtA*^{26933} and *egtA*^{C26933} demonstrated that absence of EGT led to sensitivity to 3 mM H_2O_2, but not at 1 mM or 2 mM. Similarly, absence of EGT led to sensitivity to 40 µM and 60 µM menadione, but not 20 µM. Sensitivity assays with ATCC26933 and Δ*egtB*^{26933} demonstrated similar results. Partial loss of EGT in Δ*egtB*^{26933} led to sensitivity to 3 mM H_2O_2 and 20 – 60 µM menadione. The role of EGT for dissipating ROS was further underlined by fluorescent microscopy, which demonstrated that Δ*egtA*^{26933} possessed higher levels of ROS than ATCC26933 when exposed to 3 mM H_2O_2. Thus EGT was demonstrated to function as an antioxidant in *A. fumigatus* and to form an important component of the oxidative stress defence system in *A. fumigatus*. This was further emphasised by the demonstration that *egtA* was induced by 3mM H_2O_2. However, it was observed that instead of resulting in increased intracellular EGT levels, it instead replenished EGT as it was dissipated in the process of detoxifying H_2O_2, consistent with data from Servillo et al. (2015).

In Chapter 5, LFQ proteomics demonstrated differential abundance of a multitude of reductases, oxidases, stress response proteins and enzymes with oxidising products in Δ*egtA*^{26933} compared

to ATCC26933 under both basal and ROS conditions. This is indicative of a shift in redox state due to EGT absence, particularly following exposure to 3 mM H_2O_2. Of particular importance was HapC, the redox sensitive subunit of the CCAAT-Binding Complex (CBC). The CBC senses changes in the redox state of the cell through modification of thiol groups within the histone fold motif of HapC. It then regulates Yap1 expression to coordinate oxidative stress response (Thon et al., 2010). HapC was demonstrated to be absent in ATCC26933 under ROS conditions compared to ATCC26933 under basal conditions, indicating HapC absence is a result of elevated ROS. HapC was also absent in Δ*egtA*^{26933} compared to ATCC26966 under basal conditions, which suggests that Δ*egtA*^{26933} is undergoing oxidative stress, even in the absence of a ROS inducing agent. This demonstrates that EGT absence leads to a significant shift in the redox state of the cell.

EGT therefore appears to play an important role in detoxifying high levels of ROS, making it an "antioxidant of last resort". This may be due to the properties of EGT that increase its stability. EGT exists in a thione state (Figure 1.8) at physiological pH and has a redox potential of - 0.06 V, in contrast to other typical thiols, such as GSH, which typically range between -0.2 and -0.32 V (Cheah and Halliwell, 2012). These factors combine to give EGT increased stability compared to other simple thiols. It can be speculated that these factors may allow EGT to avoid dissipation at low levels of ROS, when ROS can be effectively detoxified by other facets of the oxidative stress defence system such as superoxide dismutases, catalases and GSH. At high levels of ROS, when these other components of the oxidative stress defence system have been exhausted or overwhelmed, EGT is then available to dissipate the remaining ROS. To my knowledge, this represents a new concept in control of fungal redox homeostasis.

The characterisation of EGT as an antioxidant in *A. fumigatus* offered insight into the observed rise in EGT levels in Δ*gliK* (Gallagher et al., 2012). In addition to increased levels of EGT, Δ*gliK* was demonstrated to have significant sensitivity to H_2O_2 compared to wild-type. The cause of this sensitivity has yet to be elucidated, however it is speculated that it may be due to interruption of the gliotoxin biosynthetic pathway following the incorporation of GSH, as GliK catalyses the enzymatic step directly following GliG (Figure 7.2) (Davis et al., 2011). Thus, *gliK* deletion may result in a "GSH sink", as GSH is committed to the defective gliotoxin biosynthetic

pathway, resulting in compromised intracellular GSH content. EGT levels may therefore be increased in order to compensate for this possibility.

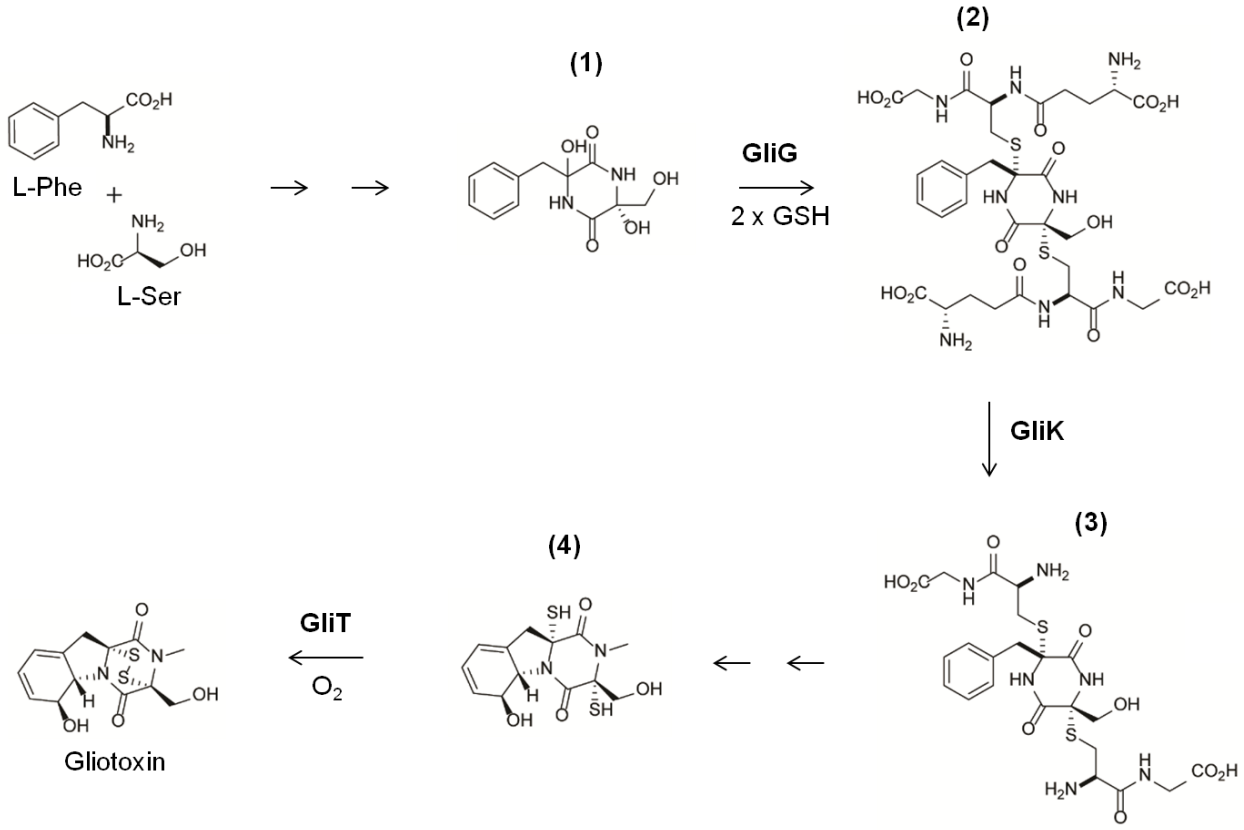

Figure 7.2. An abridged schematic of the gliotoxin biosynthetic pathway, demonstrating GliG, GliK and GliT activity. Phenylalanine and serine are processed by GliP and GliC to form intermediate **(1)**. **(1)** is then doubly thiolated using 2 GSH molecules by GliG, to form a sulphurised intermediate **(2)**. **(2)** then undergoes bisglutamyl elimination, catalysed by GliK, to yield **(3)**. **(3)** then undergoes several more enzymatic reactions to yield **(4)**. The final product, gliotoxin, is then formed from **(4)** by the closure of the disulphide bridge via GliT (Schrettl et al., 2010; Gallagher et al, 2012; Scharf et al., 2013).

Increased levels of EGT to compensate for attenuated GSH levels in Δ*gliK* would indicate a key role for maintaining redox homeostasis following *gliK* deletion. This was underlined by the attempts at generating a Δ*egtA*::Δ*gliK* mutant as described in Chapter 3. Despite attempting the generation of the mutant multiple times, in a variety of conditions, no successful Δ*egtA*::Δ*gliK* mutant was generated. This indicated that the simultaneous absence of EgtA and GliK is not viable in *A. fumigatus*. Given the observed rise in EGT levels in Δ*gliK*, it is predicted that EGT is

essential to maintain redox homeostasis when *gliK* is deleted and thus a Δ*egtA*::Δ*gliK* mutant would not be viable. This amounts to experimental verification.

7.4 Metabolic and redox interactions between EGT, GSH and gliotoxin

In Chapter 4, it was also detailed how LC-MS/MS analysis of ATCC26933, Δ*egtA*^{26933} and *egtA*^{C26933} revealed a significant increase in total glutathione in Δ*egtA*^{26933} compared to ATCC26933 and *egtA*^{C26933}. It was speculated that this may be a compensatory measure to deal with the absence of EGT. LFQ proteomics detailed in Chapter 5 described the absence of cystathionine γ-synthase (CGS; AFUA_7G01590) in Δ*egtA*^{26933} compared to ATCC26933 under basal conditions. CGS catalyses the conversion of cysteine into cystathionine, thus its absence would be expected to increase cysteine levels. This was speculated to be a measure to increase cysteine availability for GSH biosynthesis.

Concurrently, RP-HPLC and LC-MS/MS analysis revealed a significant reduction in gliotoxin levels in Δ*egtA*^{26933} compared to ATCC26933. Related to this, LFQ proteomic analysis revealed that the gliotoxin oxidoreductase, GliT (AFUA_6G09740) (Schrettl et al., 2010; Scharf et al., 2010), was absent in Δ*egtA*^{26933} compared to ATCC26933 under basal conditions. GliT catalyses disulphide bridge closure in *A. fumigatus* and has been demonstrated to be essential for gliotoxin biosynthesis (Figure 7.2) (Schrettl et al., 2010; Scharf et al., 2010). Thus, decreased gliotoxin levels in Δ*egtA*^{26933} may be caused by absence of GliT. GliT has also been demonstrated to play a key role in self-protection from gliotoxin (Schrettl et al., 2010) and its absence in Δ*egtA*^{26933} might be expected to result in sensitivity to gliotoxin. However, sensitivity assays for gliotoxin revealed no significant sensitivity in Δ*egtA*^{26933} compared to ATCC26933. This was explained by the observation that GliT expression was induced by gliotoxin exposure, a response that been demonstrated previously in wild-type and considered part of the self-protection strategy in *A. fumigatus*. Relevantly, *gliT* is regulated independently of the rest of the *gli* cluster, which allows gliotoxin biosynthesis and self-protection to function autonomously (Schrettl et al., 2010).

Gliotoxin and GSH metabolism is intrinsically linked because GSH is essential for gliotoxin biosynthesis. Davis et al. (2011) showed that GSH is incorporated into the gliotoxin biosynthetic pathway via the glutathione transferase GliG. Glutathione is the thiol source for gliotoxin, which is essential for its function, and deletion of *gliG* results in the complete abrogation of gliotoxin

biosynthesis (Figure 7.2). Thus the observed increase in GSH levels and concurrent decrease in gliotoxin levels in Δ*egtA*^{26933} could be related. Gliotoxin biosynthesis may be curtailed in order to diminish GSH incorporation into the gliotoxin biosynthetic pathway, thereby allowing for an increase in intracellular GSH. EGT therefore appears to be an important factor in gliotoxin production, as it compensates for reduced levels of intracellular GSH which is required for gliotoxin biosynthesis. In the absence of the antioxidant potential of EGT, GSH must be diverted from gliotoxin biosynthesis, resulting in reduced levels of gliotoxin. It may therefore be the case that EGT is required to maintain the optimal cellular redox state for high levels of gliotoxin production.

This was further emphasised by results for total GSH measurement in AfS77 and Δ*egtA*^{AfS77}. In contrast to ATCC26933, deletion of *egtA* in the AfS77 background resulted in no significant changes in GSH levels. However, it was particularly interesting that GSH levels in AfS77 were significantly increased compared to ATCC26933. AfS77 is derived from ATCC46645 (Hartmann et al., 2010), which has been demonstrated to produce low levels of gliotoxin compared to ATCC26933 (Schrettl et al., 2010). Thus, in ATCC26933, decreased levels of GSH compared to AfS77 may be a result of increased gliotoxin biosynthesis, relative to AfS77. In ATCC26933, EGT is required for high levels of gliotoxin production, due to the necessary utilisation of GSH. When *egtA* is deleted and no EGT is present, a metabolic adjustment occurs whereby gliotoxin biosynthesis is decreased in order to increase GSH levels (Figure 7.3). Notably, the levels of GSH in Δ*egtA*^{26933} were similar to those of AfS77 and Δ*egtA*^{AfS77} (i.e. there was no significant differences in the levels of GSH in Δ*egtA*^{26933}, AfS77 and Δ*egtA*^{AfS77}). This same increase in GSH levels was not observed in Δ*egtA*^{AfS77} compared to AfS77, because low levels of gliotoxin production in AfS77 results in higher basal levels of GSH compared to ATCC26933. This meant that a metabolic adjustment was not required in the absence of EGT as GSH levels were already sufficient.

The interplay between gliotoxin, GSH and EGT biosynthesis was also evident in Δ*gliK*. Deletion of *gliK* resulted in abrogated gliotoxin biosynthesis and increased levels of EGT (Gallagher et al., 2012). As discussed previously, this was speculated to be caused by the interruption of the gliotoxin biosynthetic pathway directly following the incorporation of GSH, resulting in a "GSH

sink". Thus, we see gliotoxin and EGT biosynthesis as interlinked, with a possible involvement of GSH.

It has therefore been demonstrated that *A. fumigatus* must carefully balance production of gliotoxin, GSH and EGT. As a result, disruption of one biosynthetic pathway may result in alterations in the other two. All three metabolites are redox-active molecules and, as such, the levels of each may be adjusted to maintain the redox homeostasis of the cell. As demonstrated in Δ*egtA*^{26933}, abrogation of EGT resulted in a shift in the redox state of the cell, which required the alteration of gliotoxin and GSH biosynthesis to compensate (Figure 7.3). The biosynthetic pathways of gliotoxin, GSH are EGT are also linked metabolically, as cysteine provides the thiol group for all three; directly in the case of EGT and GSH and via GSH in the case of gliotoxin (Figure 7.3). Additionally, the biosynthesis of both gliotoxin and EGT contains methyltransferase steps, requiring SAM as a co-factor. Thus, availability of cysteine (and therefore sulphur) will impact biosynthesis of all three, while levels of SAM will affect EGT and gliotoxin biosynthesis. Production of these metabolites must therefore be balanced against the availability of cysteine and SAM. SAM levels are of particular interest in EGT biosynthesis as 3 moles of SAM are required for every 1 mol of EGT produced.

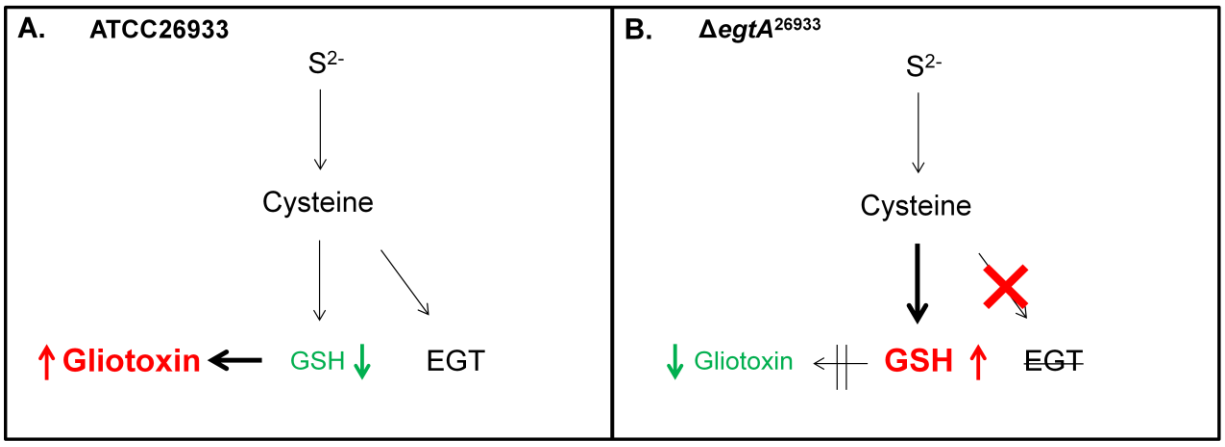

Figure 7.3. Interactions between EGT, GSH and gliotoxin in *A. fumigatus*. (A) In ATCC26933, high levels of gliotoxin biosynthesis result in reduced levels of intracellular GSH due to the double glutathiolation step in gliotoxin biosynthesis. This is facilitated by EGT which compensates for decreased levels of GSH. (B) In Δ*egtA*^{26933}, absence of EGT results in a reduction in antioxidant potential, necessitating increased levels of GSH to compensate. GSH is thus diverted from gliotoxin biosynthesis, resulting in decreased levels of gliotoxin.

The importance of cysteine and SAM availability for these metabolic adjustments was emphasised by the observation of a "cystathionine switch", as demonstrated in Δ*egtA*^{26933}. Under basal conditions, cystathionine γ-synthase (CGS; AFUA_7G01590) was absent in Δ*egtA*^{26933} compared to ATCC26933, while cystathionine β-lyase (CBL; AFUA_4G03950) had a $\log_2$ 3.1 fold increase in abundance in Δ*egtA*^{26933} compared to ATCC26933 under ROS conditions (Figure 7.4). In this manner, Δ*egtA*^{26933} can switch from directing cysteine towards GSH biosynthesis under basal conditions, to producing SAM to effect trimethylation of histidine for EGT biosynthesis under ROS conditions. Cystathionine therefore appears to be at the nexus of the metabolic response to EGT absence and this suggests a prominent role for cystathionine in directing the metabolic thiol flux of the cell.

7.5 The role of EGT in conidiation and cell wall integrity in *A. fumigatus*

Chapter 4 detailed alterations to conidiation and the cell wall of Δ*egtA*^{26933} compared to ATCC26933. Δ*egtA*^{26933} was observed to produce paler conidia compared to ATCC26933 and measurement of conidiation revealed a significant decrease in conidiation levels in Δ*egtA*^{26933} compared to ATCC26933. In addition to this, the cell wall integrity of Δ*egtA*^{26933} appeared to be altered compared to ATCC26933. This was demonstrated by sensitivity assays for congo red and calcofluor white, which showed Δ*egtA*^{26933} was sensitive to both dyes compared to ATCC26933. Both congo red and calcofluor white disrupt cell wall biosynthesis by inhibiting chitin and β(1,3)-glucan biosynthesis (Roncero and Duran, 1985). The sensitivity observed therefore indicated that chitin and β(1,3)-glucan content may be altered in the Δ*egtA*^{26933} cell wall compared to ATCC26933.

Chapter 5 discussed LFQ proteomic analyses which provided further insight into the conidiation and cell wall phenotypes observed in Δ*egtA*^{26933}. A number of proteins associated with conidiation were absent in Δ*egtA*^{26933} compared to ATCC26933 under basal conditions: mannosyltransferase PMT2 (AFUA_1G07690), mannosyltransferase PMT4 (AFUA_8G04500), conidial hydrophobin RodB (AFUA_1G17250), developmental regulator FlbA (AFUA_2G11180) and extracellular developmental signal biosynthesis protein FluG (AFUA_3G07140). FlbA and FluG were of particular interest as they have been demonstrated to play an important role in upstream regulation of sexual development (Mah and Yu, 2006).

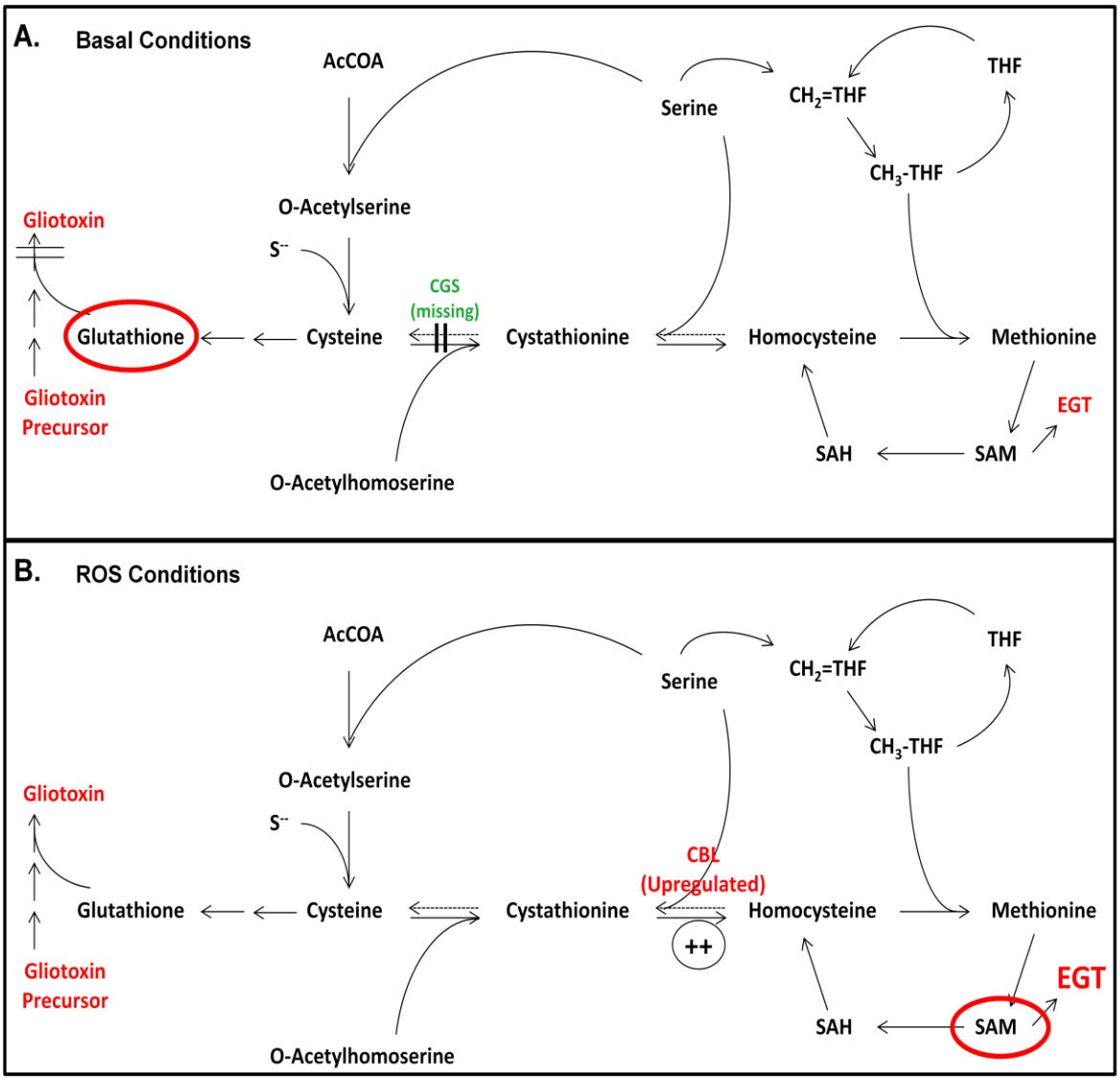

Figure 7.4. The "cystathionine switch" in *A. fumigatus*. (A) Comparison of Δ*egtA*^{26933} and ATCC26933 under basal conditions showing an absence of cystathionine γ-synthase, which normally converts cysteine to cystathionine. This may facilitate a switch towards increased glutathione production. (B) Comparison of Δ*egtA*^{26933} and ATCC26933 upon addition of 3 mM H_2O_2 shows an increased abundance of cystathionine β-lyase, which converts cystathionine to homocysteine. This is predicted to result in increased production of SAM, which is essential for EGT biosynthesis.

The mannosyltransferases PMT2 and PMT4, absent in Δ*egtA*^{269332} compared to ATCC26933 under basal conditions, have also been demonstrated to play a role in cell wall biosynthesis (Fang et al., 2010; Mouyna et al., 2010). Furthermore, chitin synthase activator Chs3 (AFUA_3G05580), a putative cell wall protein (AFUA_3G081110), a putative MAP kinase kinase (Mkk2; AFUA_1G05800) and a putative cell wall glucanase (AFUA_3G09250) were absent in Δ*egtA*^{26933} compared to ATCC26933 under basal conditions. GEL5, a 1,3-beta-glucanosyltransferase (AFUA_8G02130), showed a $\log_2$ 1.18 fold increase in Δ*egtA*^{26933} compared to ATCC26933 under basal conditions. Under ROS conditions, two proteins related to the *A. fumigatus* cell wall had differential abundance in Δ*egtA*^{26933} compared to ATCC26933: a putative class V chitinase (AFUA_3G11280; $\log_2$ 2.05 fold) and a putative cell wall integrity signalling protein (AFUA_6G07520; $\log_2$ 1.63 fold). The MAP kinase kinase Mkk2 is a key protein in the context of cell wall alterations in Δ*egtA*^{26933} as it functions as a signalling molecule in the cell wall integrity (CWI) pathway and thus regulates cell wall biosynthesis (Valiente et al., 2009). Chs3 (AFUA_3G05580), the cell wall glucanase (AFUA_3G09250), GEL5 (AFUA_8G02130) and the class V chitinase (AFUA_3G11280) all function in the biosynthesis or arrangement of chitin and/or β(1,3)-glucans in the cell wall of *A. fumigatus*. This is relevant to the sensitivity to congo red and calcofluor white observed in Δ*egtA*^{26933} compared to ATCC26933, as both of these dyes inhibit chitin and β(1,3)-glucan biosynthesis (Roncero and Duran, 1985). Differential abundance of these proteins indicate altered chitin and β(1,3)-glucan levels, as predicted from the congo red and calcofluor white sensitivity assays.

Thus, both conidiation and cell wall biosynthesis are altered in Δ*egtA*^{26933} compared to ATCC26933, indicating that absence of EGT leads to disruption of both processes. ROS has been demonstrated to function in signal transduction in fungi, with roles in cellular differentiation, virulence and hyphal growth previously demonstrated (Breitenbach et al., 2015). Relevantly, management of ROS has been linked with conidiation in *Epichloë festucae* (Kayano et al., 2013). To my knowledge, ROS signalling has not been associated with the cell wall of fungi before, however, ROS signalling has been well documented to play an important role in the cell wall of plants, regulating growth and development processes (Kärkönen and Kuchitsu, 2015). It could therefore be speculated that EGT regulates conidiation and cell wall biosynthesis indirectly through the management of ROS levels. Thus, the redox shift resulting from EGT

absence in Δ*egtA*^{26933} would disrupt conidiation and cell wall biosynthesis as observed. Future work will further capture the molecular basis of these alterations in Δ*egtA*^{26933}.

Of interest, Δ*gliK* demonstrated a similar perturbation in cell wall related enzymes upon exposure to gliotoxin (Dr. Rebecca Owens and Professor Sean Doyle, personal communication). Δ*gliK* is sensitive to exogenous gliotoxin, though the reason for this sensitivity has not been elucidated (Gallagher et al., 2012). The reason behind this gliotoxin-induced disruption of the cell wall is unclear, but it could be linked to changes in the cellular redox state as indicated by the increased levels of EGT and H_2O_2 sensitivity observed in Δ*gliK*. Increased EGT levels may, therefore, be part of an attempt to maintain cell wall integrity.

7.6 Investigations into PAL and VipC function in *A. fumigatus*

LFQ proteomic analysis of Δ*egtA*^{26933} and ATCC26933 under basal and ROS conditions identified two proteins that had increased abundance in Δ*egtA*^{26933} compared ATCC26933 under basal conditions, and a larger increase in abundance under ROS conditions. These were phenylalanine ammonia lyase (PAL; AFUA_2G09110) and VipC (AFUA_8G01930) which were identified as proteins with a potentially important role in *A. fumigatus* adaption to EGT absence. Thus, deletion mutants for *palA* and *vipC* were generated as described in Chapter 3 to facilitate characterisation of PAL and VipC.

PAL showed a $\log_2$ 2.71 fold increase in Δ*egtA*^{26933} compared to ATCC26933 under basal conditions and a $\log_2$ 3.73 fold increase in Δ*egtA*^{26933} compared to ATCC26933 under ROS conditions. A number of hypotheses were proposed for PAL function in *A. fumigatus*, including the generation of phenyl propanoid compounds as part of an oxidative stress defence strategy, catabolism of excess His due to abolition of EGT biosynthesis and a role as an ergothionase. However no phenotype was detected in Δ*palA*^{26933} when compared to ATCC26933, despite a variety of analyses to test the above hypotheses. It may be that PAL function is not as prominent when all other systems are intact and the importance of PAL only comes to the fore when other systems are disrupted, such as in Δ*egtA*^{26933}. As such, a double Δ*egtA*::Δ*palA* mutant could greatly aid future study into PAL in *A. fumigatus*.

VipC underwent a $\log_2$ 1.23 fold abundance increase in Δ*egtA*^{26933} compared to ATCC26933 under basal conditions and a $\log_2$ 2.5 fold increase in abundance in Δ*egtA*^{26933} compared to

ATCC26933 under ROS conditions. VipC has been demonstrated to regulate sexual and asexual development is response to light in *A. nidulans* (Sarikaya-Bayram et al., 2014), however it was speculated that VipC function may differ in *A. fumigatus* due to significant differences in sexual development between the two *Aspergilli* (O'Gorman et al., 2009). Phenotypic characterisation of Δ*vipC*^{26933}, as detailed in Chapter 6, revealed VipC absence caused unexpected alterations in growth in *A. fumigatus*. Δ*vipC*^{26933} displayed increased growth on solid media and in liquid culture. Additionally, Δ*vipC*^{26933} colonies had distinct aerial hyphae that were not visible on ATCC26933 colonies. LFQ proteomic analysis provided further insight into these phenotypes, revealing increased abundance of SomA and Rho GTPases Rho1 and Rho 3 in Δ*vipC*^{26933} compared to ATCC26933. SomA, Rho1 and Rho3 have been demonstrated to play key roles in the regulation of growth and development in *A. fumigatus* and the observed increase in abundance, in part at least, explains the observed growth phenotypes in Δ*vipC*^{26933} (Ditchl et al., 2010, 2012; Lin et al., 2015). VipC therefore was demonstrated to influence growth and development in *A. fumigatus*. Interestingly, the aerial hyphae present on Δ*vipC*^{26933} colonies were not present on Δ*vipC*^{26933} colonies grown in light. This suggests a role for VipC in controlling development in response to environmental stimuli such as light.

LFQ proteomics revealed altered abundance to key oxidative stress proteins in Δ*vipC*^{26933}. HapC (AFUA_1G03840; unique) and HapE (AFUA_6G05300; $\log_2$ 1.1 fold) had increased abundance in Δ*vipC*^{26933} compared to ATCC26933, while catalase B (AFUA_3G02270; $\log_2$ -1.8 fold) and superoxide dismutase (AFUA_5G09240; $\log_2$ -2.82 fold) had decreased abundance in Δ*vipC*^{26933} compared to ATCC26933. Furthermore, LC-MS/MS analysis revealed that total GSH levels were significantly reduced in Δ*vipC*^{26933} compared to ATCC26933. HapC and HapE are components of the CBC, essential for mounting an effective oxidative stress response (Thon et al., 2010). As discussed previously, HapC absence was associated with increased levels of ROS. This suggests that Δ*vipC*^{26933} has decreased levels of ROS compared to ATCC26933. This is supported by the observation that despite decreased abundance of catalase B and superoxide dismutase, in addition to decreased levels of GSH, no sensitivity to ROS inducing agents was observed in Δ*vipC*^{26933} compared to ATCC26933. This suggests that *vipC*^{26933} has lower levels of basal ROS compared to ATCC26933 and this was speculated to be linked to the decreased abundance of proteins involved in metabolic processes.

This decrease in proteins associated with metabolic processes was especially evident for GSH metabolism. As discussed previously, GSH levels were reduced in Δ*vipC*^{26933} compared to ATCC26933. LFQ proteomic analysis revealed a decrease in abundance of a myriad of proteins associated with GSH biosynthesis (Figure 7.5) including proteins directly involved in metabolising GSH, and those which biosynthesise cysteine and glutamate, the precursors of GSH. This demonstrates a concerted move towards reduced GSH biosynthesis in Δ*vipC*^{26933}.

Related to this, 2 proteins associated with methionine metabolism had decreased abundance in Δ*vipC*^{26933} compared to ATCC26933. Methionine synthase (AFUA_4G07360) had a $\log_2$ -1.25 fold decrease in abundance and adenosylhomocysteinase (AFUA_1G10130) had a $\log_2$ -1.8 fold decrease in abundance (Figure 7.5). These proteins are part of the methionine cycle and as such would be speculated to perturb cellular SAM/SAH levels. This in turn may be linked to the depressed metabolic processed observed as a proteomic level. Further study is definitely required to elucidate the exact effect these proteins have on SAM/SAH levels in Δ*vipC*^{26933}.

VipC was thus demonstrated to influence growth, development and metabolism in *A. fumigatus*. This was a completely novel role for a protein that had previously only been characterised as regulating sexual and asexual development in *A. nidulans* (Sarikaya-Bayram et al., 2014). While Elgabbar and Han (2015) attempted to investigate VipC function in *A. fumigatus* through the creation of a Δ*vipC* mutant, they did not observe any phenotypes. This data therefore represents the first characterisation of VipC in *A. fumigatus*.

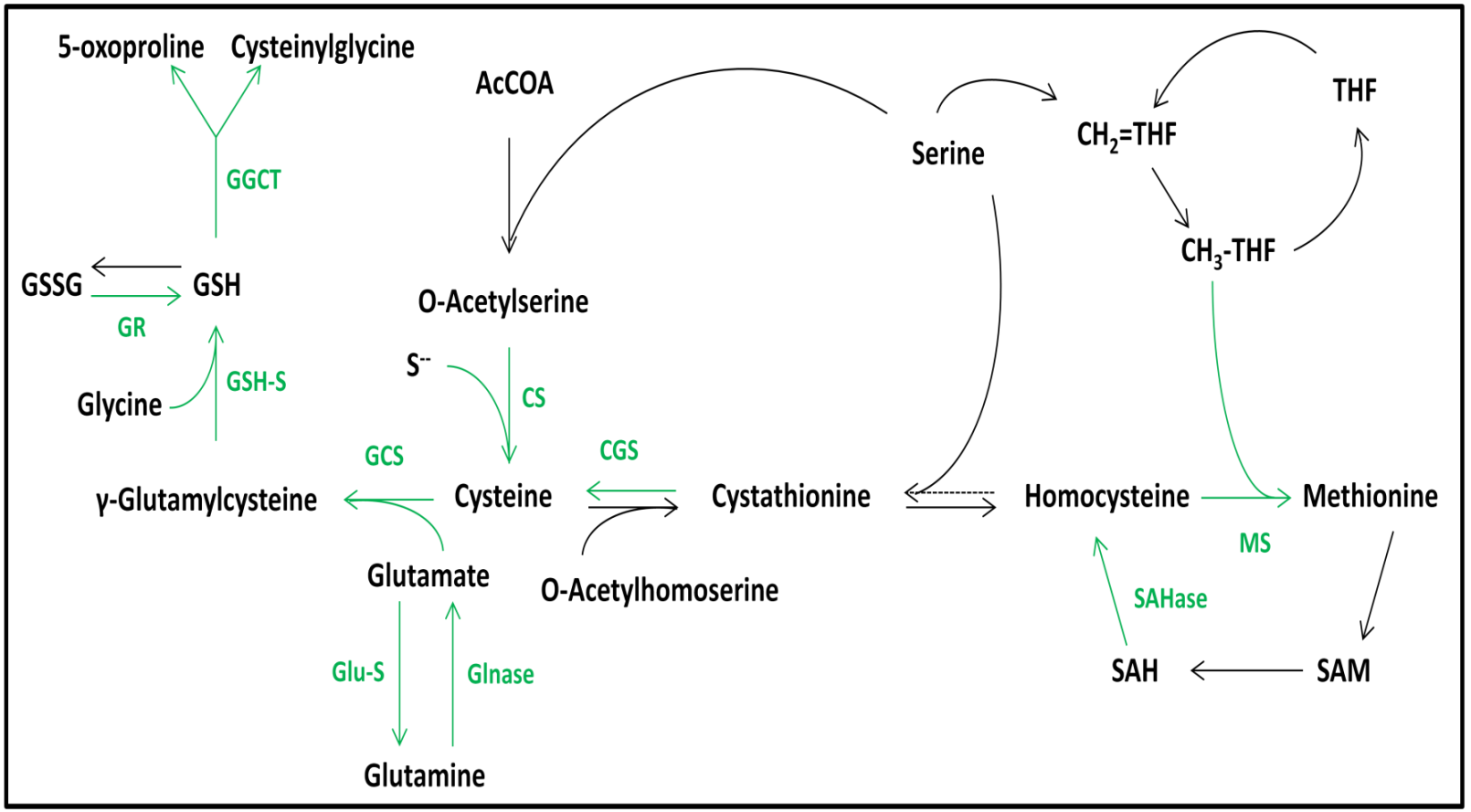

Figure 7.5. Proteins associated with glutathione and methionine metabolism which show decreased abundance in *A. fumigatus* Δ*vipC*^{26933} compared to ATCC26933. Proteins with decreased abundance are shown in green. Abbreviations: GCS, Gamma-Glutamylcysteine Synthetase Regulatory Subunit; MS Methionine Synthase; GGCT, Glutathione-Specific Gamma-Glutamylcyclotransferase; CS, Cysteine Synthase; SAHase, Adenosylhomocysteinase; Glu-S, Glutamine Synthetase; GR, Glutathione Oxidoreductase; GSH-S, glutathione Synthase; CGL, Cystathionine γ-Lyase; Glnase, Glutaminase.

7.7 The role of VipC in *A. fumigatus* Δ*egtA*^{26933}

Interestingly, the results of the phenotypic characterisation of Δ*vipC*^{26933} provided insight into the observed increase in VipC abundance in Δ*egtA*^{26933} compared to ATCC26933 under both basal and ROS conditions. Of particular interest was the analysis of total GSH via LC-MS/MS and supporting LFQ proteomic data which demonstrated that Δ*vipC*^{26933} had decreased levels of total GSH compared to ATCC26933. Thus, absence of VipC resulted in reduced levels of GSH. In Δ*egtA*^{26933}, levels of total GSH were demonstrated to be increased compared to ATCC26933. Thus, decreased levels of total GSH are associated with absence of VipC in Δ*vipC*^{26933} and increased levels of total GSH are associated with increased abundance of VipC in Δ*egtA*^{26933}. Levels of total GSH were therefore demonstrated to correlate with abundance of VipC in *A. fumigatus*, indicating that VipC possibly plays a role in regulating GSH biosynthesis.

Related to this, both Δ*vipC*^{26933} and Δ*egtA*^{26933} appear to have experienced a shift in redox state following the respective gene deletions. Δ*egtA*^{26933} demonstrated altered abundance of a variety of reductases, oxidases, stress response proteins and enzymes with oxidising products, while Δ*vipC*^{26933} showed a decrease in abundance of proteins with oxido-reductase activity. A key protein in the redox shift of both mutants was HapC, as discussed previously. HapC was absent in Δ*egtA*^{26933} compared to ATCC26933, while it was unique in Δ*vipC*^{26933} compared to ATCC26933.

VipC abundance therefore appears to correlate with absence of HapC, with increased abundance of HapC observed in in Δ*vipC*^{26933} and decreased abundance of HapC observed in Δ*egtA*^{26933}, which has increased abundance of VipC. As HapC functions to detect changes in the redox state of the cell (Thon et al., 2010), this correlation suggests that VipC abundance is associated with increased levels of ROS, perhaps related to regulation of metabolic processes as discussed previously. It was noted that HapC was present in ATCC26933 in the Δ*egtA*^{26933} LFQ proteomic analysis and absent in ATCC26933 in the Δ*vipC*^{26933}LFQ proteomic analysis. This was attributed to differences in the culture media, as the Δ*egtA*^{26933} study was performed using rich media (Sabaouraud Dextrose Broth) while the Δ*vipC*^{26933} study was performed in minimal media (AMM).

Another metabolic pathway altered by deletion of *vipC* was that of the methionine cycle (Owens et al., 2015). Methionine sythase and adenosylhomocysteinase both underwent decreased abundance in Δ*vipC*^{26933} compared to ATCC26933, which was speculated to disrupt SAM/SAH levels in Δ*vipC*^{26933} (Figure 7.5). Related to this, Δ*egtA*^{26933} under ROS conditions had increased abundance of CBL, which would increase levels of homocysteine (Ravanel, 1997) and was speculated to be part of a shift towards SAM production in order to attempt EGT biosynthesis (Figure 7.4). Thus we see decreased activity in the methionine cycle associated with absence of VipC and increased activity in the methionine cycle associated with increased abundance of VipC in Δ*egtA*^{26933}. This represents another metabolic pathway potentially influenced by VipC in Δ*egtA*^{26933}.

The "cystathionine switch" was previously discussed in relation to prioritising the biosynthesis of either GSH or SAM in Δ*egtA*^{26933} (Figure 7.4). VipC has been demonstrated to influence both of these biosynthetic pathways (Figure 7.5), and thus may regulate the "cystathionine switch" observed in Δ*egtA*^{26933}. In support of this, cystathionine γ-lyase (CGL; AFUA_8G04340) had a $\log_2$ -2.03 fold decrease in Δ*vipC*^{26933} compared to ATCC26933. CGL catalyses the conversion of cystathionine into cysteine, α-ketobutyrate, and ammonia (Ravanel, 1997). This is the opposite reaction to CGS, which is absent in Δ*egtA*^{26933} compared to ATCC26933 under basal conditions. Thus, VipC appears to controls the direction of cystathionine metabolism via regulation of enzymes catalysing its biosynthesis and catabolism.

Δ*egtA*^{26933} demonstrated disruption to conidiation and cell wall biosynthesis, supported by LFQ proteomic data. While Δ*vipC*^{26933} did not display any alteration in conidiation, the increased growth phenotype observed would require a concurrent increase in cell wall biosynthesis. LFQ proteomic data for Δ*vipC*^{26933} suggests increased abundance of VipC in Δ*egtA*^{26933} may have influenced the alterations in conidiation and cell wall biosynthesis observed. Specifically, SomA, Rho1 and Rho3, which had increased abundance in Δ*vipC*^{26933}, have been demonstrated to regulate conidiation and/or cell wall biosynthesis. SomA is an important regulator of asexual development in *A. fumigatus*, regulating key developmental proteins such as *brlA*, *medA*, *stuA* and *flbA* (Lin et al., 2015). Rho1 participates in CWI signalling and conditional downregulation of *rho1* resulted in reduced conidiation (Dichtl et al., 2010, 2012). Rho3 is also predicted to be involved in CWI signalling (Dichtl et al., 2010). Additionally, conidial hydrophobin RodB,

absent in Δ*egtA*^{26933}, had a $\log_2$ -5.22 fold decrease in abundance. Thus, VipC may influence conidiation and cell wall biosynthesis, even though no phenotype for conidiation reported in Δ*vipC*^{26933}. It could be that absence of VipC does not result in a phenotype, but increased expression, as observed in Δ*egtA*^{26933} does. If this was the case, increase abundance of VipC in Δ*egtA*^{26933} may be linked to the conidiation and cell wall phenotypes observed. Proposed mechanisms for the role of VipC in regulation of cell wall biosynthesis and conidiation are outlined in Figures 7.6 and 7.7 respectively.

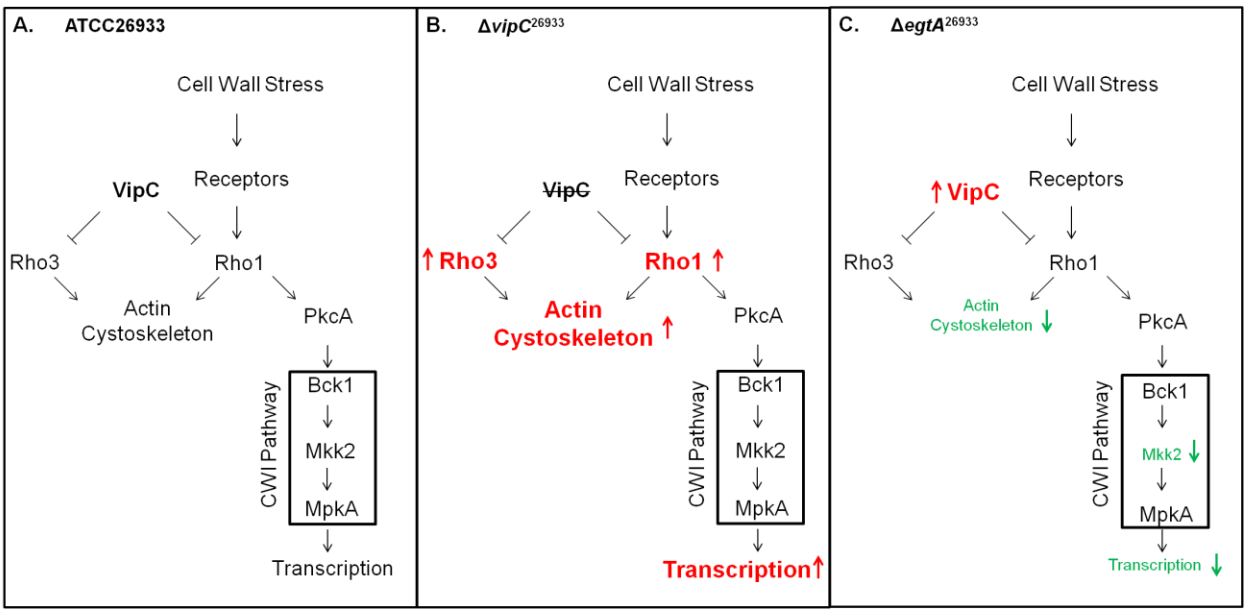

Figure 7.6. Proposed role for VipC in regulation of cell wall biosynthesis in *A. fumigatus*. Image modified from Ditchl et al. (2010). (A) In wild-type *A. fumigatus*, VipC negatively regulates Rho GTPases Rho1 and Rho3, which in turn regulate organisation of the actin cytoskeleton and CWI signalling. (B) In Δ*vipC*^{26933}, absence of VipC leads to increased abundance of Rho1 and Rho3, as observed in LFQ proteomic analysis. Increased abundance of Rho1 and Rho3 results in positive regulation of the actin cystoskeleton and CWI signalling, which facilitates increased growth levels as observed. (C) In Δ*egtA*^{26933}, VipC has increased abundance. This may lead to increased negative regulation of Rho1 and Rho3, resulting in disruption to the actin cytoskeleton and CWI signalling (Mkk2, a component of the CWI pathway, is absent in Δ*egtA*^{26933} compared to ATCC26933). This could explain the observed sensitivity to congo red and calcofluor white in Δ*egtA*^{26933}.

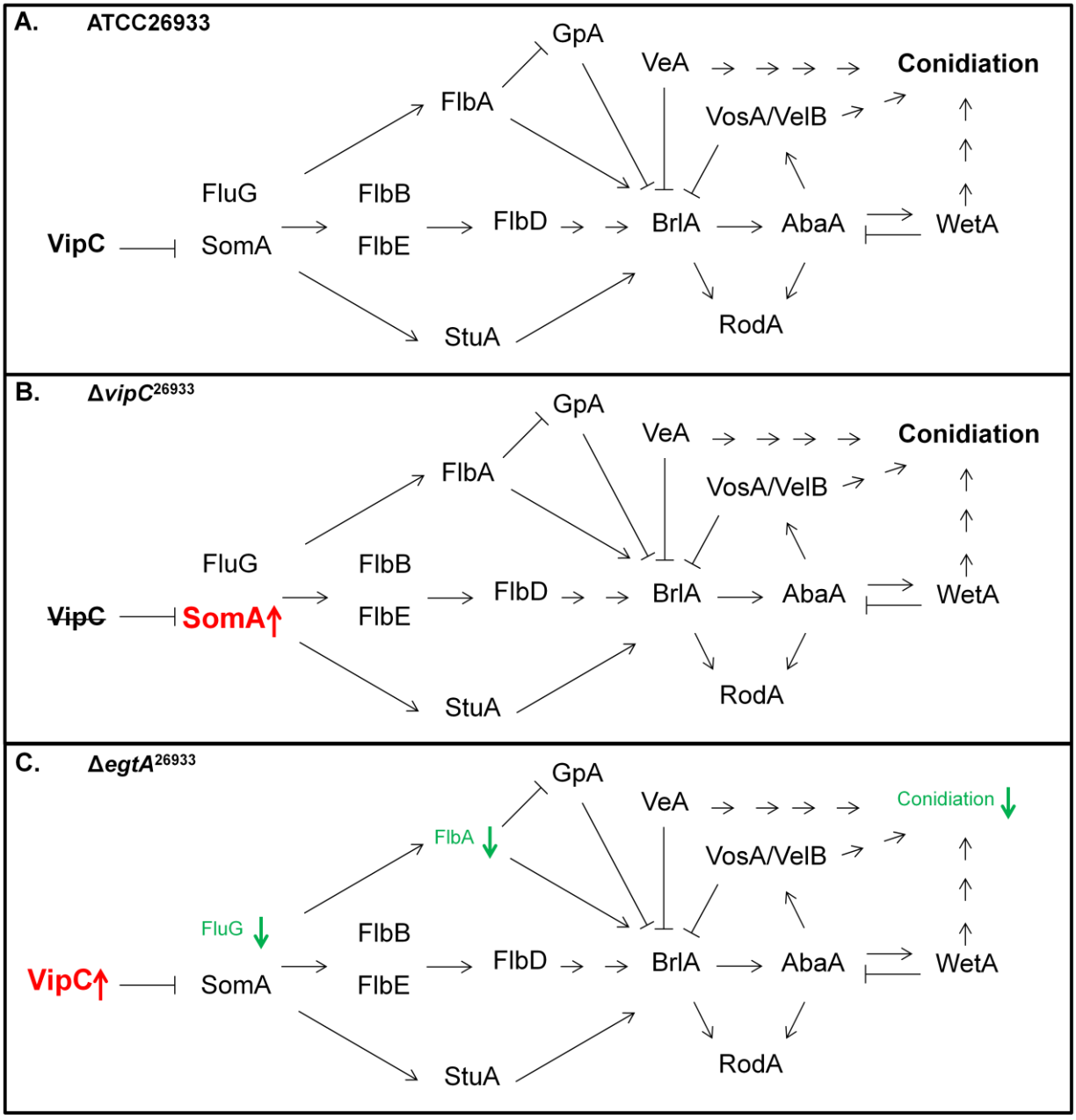

Figure 7.7. Proposed role for VipC in regulation of conidiation in *A. fumigatus*. Image modified from Mah and Yu (2005), Sheppard et al. (2005) and Alkhayyat et al. (2015). (A) In wild-type, VipC contributes to regulation of conidiation via repression of the upstream regulator SomA. (B) In Δ*vipC*^{26933}, absence of VipC results in increased abundance of SomA. However no discernible effect on conidiation was observed in Δ*vipC*^{26933}. (C) Increased abundance of VipC in Δ*egtA*^{26933} may result in increased repression of SomA. This would have impact downstream proteins, as observed by the absence of FluG and FlbA in Δ*egtA*^{26933} compared to ATCC26933. This results in reduced levels of conidiation, as observed.

Of interest, EgtB had a $\log_2$ -1.35 fold decrease in abundance in Δ*vipC* compared to ATCC26933. This would suggest at alterations to EGT biosynthesis in Δ*vipC*^{26933}, however no significant difference in the levels of EGT was detected in Δ*vipC*^{26933} compared to ATCC26933. As discussed previously, while EgtB contributes to EGT biosynthesis, it is not essential for EGT production. It could be that through regulating EgtB levels, VipC only "fine-tunes" EGT levels in *A. fumigatus* and loss of VipC, therefore, does not lead to a significant change. Relevantly, it was speculated that increased abundance of CBL in Δ*egtA*^{26933} may be part of a shift towards increased SAM production in order to attempt EGT biosynthesis. Increased abundance of VipC may control that metabolic shift via control of the "cystathionine switch" as discussed previously and also through regulation of EgtB.

This data indicates that increased abundance in VipC in Δ*egtA*^{26933}, under both basal and ROS conditions, is responsible for many of the differences noted in Δ*egtA*^{26933} compared to ATCC26933 on both a phenotypic and proteomic level. VipC may therefore regulate the *A. fumigatus* response in adapting to EGT absence by regulating metabolic changes to order to maintain redox homeostasis in Δ*egtA*^{26933}. This suggests that VipC function in *A. fumigatus* revolves around regulating metabolism in response to the changing environment of the cell. This is a completely novel role for VipC that has never been described before and was not reported in the study of *A. fumigatus* VipC by Elgabbar and Han (2015).

7.8 Conclusion

In summary, this thesis presents the first identification of an EGT biosynthetic pathway and the first characterisation of EGT function in *A. fumigatus*. EGT functions as an antioxidant in *A. fumigatus* and is important for detoxifying high levels of ROS. Deletion of *egtA* led to significant proteomic remodelling and caused a metabolic shift that resulted in increased levels of GSH and decreased levels of gliotoxin. EGT was thus demonstrated to play an important role in balancing GSH and gliotoxin biosynthesis. EGT absence also affected other systems, with conidiation and cell wall biosynthesis demonstrated to be altered in Δ*egtA*^{26933} compared to ATCC26933. It was hypothesised that through the management of ROS levels, EGT acts to regulate these processes. This thesis also presents the first functional characterisation of the methyltransferase VipC. VipC was demonstrated to influence growth, development and metabolism in *A. fumigatus* and appears to play a key role in regulating the metabolic response to EGT absence.

Chapter 8

Bibliography

Adams, D. J. (2004). Fungal cell wall chitinases and glucanases. *Microbiology, 150*(7), 2029-2035.

Adams, T. H., Boylan, M. T., & Timberlake, W. E. (1988). brlA is necessary and sufficient to direct conidiophore development in Aspergillus nidulans. *Cell, 54*(3), 353-362.

Adams, T. H., Wieser, J. K., & Yu, J. H. (1998). Asexual sporulation in Aspergillus nidulans. *Microbiology and Molecular Biology Reviews : MMBR, 62*(1), 35-54.

Alamgir, K. M., Masuda, S., Fujitani, Y., Fukuda, F., & Tani, A. (2015). Production of ergothioneine by methylobacterium species. *Frontiers in Microbiology, 6*

Albrecht, D., Guthke, R., Brakhage, A. A., & Kniemeyer, O. (2010). Integrative analysis of the heat shock response in Aspergillus fumigatus. *BMC Genomics, 11*(1), 1.

Alcazar-Fuoli, L., Cairns, T., Lopez, J. F., Zonja, B., Pérez, S., Barceló, D., et al. (2014). A modified recombineering protocol for the genetic manipulation of gene clusters in Aspergillus fumigatus. *PloS One, 9*(11), e111875.

Alfonso-Prieto, M., Biarnés, X., Vidossich, P., & Rovira, C. (2009). The molecular mechanism of the catalase reaction. *Journal of the American Chemical Society, 131*(33), 11751-11761.

Alkhayyat, F., Kim, S. C., & Yu, J. (2015). Genetic control of asexual development in Aspergillus fumigatus. *Advances in Applied Microbiology, 90*, 93-107.

Amich, J., Schafferer, L., Haas, H., & Krappmann, S. (2013). Regulation of sulphur assimilation is essential for virulence and affects iron homeostasis of the human-pathogenic mould Aspergillus fumigatus. *PLoS Pathog, 9*(8), e1003573.

Amich, J., Dumig, M., O'Keeffe, G., Binder, J., Doyle, S., Beilhack, A., et al. (2016). Exploration of sulfur assimilation of Aspergillus fumigatus reveals biosynthesis of sulfur-containing amino acids as a virulence determinant. *Infection and Immunity, 84*(4), 917-929.

Anderson, M., Trudell, J., Voehringer, D., Tjioe, I., & Herzenberg, L. (1999). An improved monobromobimane assay for glutathione utilizing tris-(2-carboxyethyl) phosphine as the reductant. *Analytical Biochemistry, 272*(1), 107-109.

Andrianopoulos, A., & Timberlake, W. E. (1994). The Aspergillus nidulans abaA gene encodes a transcriptional activator that acts as a genetic switch to control development. *Molecular and Cellular Biology, 14*(4), 2503-2515.

Aruoma, O. I., Spencer, J. P. E., & Mahmood, N. (1999). Protection against oxidative damage and cell death by the natural antioxidant ergothioneine. *Food and Chemical Toxicology, 37*(11), 1043-1053.

Balibar, C. J., & Walsh, C. T. (2006). GliP, a multimodular nonribosomal peptide synthetase in Aspergillus fumigatus, makes the diketopiperazine scaffold of gliotoxin. *Biochemistry, 45*(50), 15029-15038.

Bantscheff, M., Schirle, M., Sweetman, G., Rick, J., & Kuster, B. (2007). Quantitative mass spectrometry in proteomics: A critical review. *Analytical and Bioanalytical Chemistry, 389*(4), 1017-1031.

Barger, G., & Ewins, A. J. (1911). The constitution of ergothioneine: A betaine related to histidine. *Journal of the Chemical Society, Transactions, 99*, 2336-2341.

Bayram, O., & Braus, G. H. (2012). Coordination of secondary metabolism and development in fungi: The velvet family of regulatory proteins. *FEMS Microbiology Reviews, 36*(1), 1-24.

Beauvais, A., Schmidt, C., Guadagnini, S., Roux, P., Perret, E., Henry, C., et al. (2007). An extracellular matrix glues together the aerial-grown hyphae of Aspergillus fumigatus. *Cellular Microbiology, 9*(6), 1588-1600.

Bello, M. H., Mogannam, J. C., Morin, D., & Epstein, L. (2014). Endogenous ergothioneine is required for wild type levels of conidiogenesis and conidial survival but does not protect against 254nm UV-induced mutagenesis or kill. *Fungal Genetics and Biology, 73*, 120-127.

Bello, M. H., Barrera-Perez, V., Morin, D., & Epstein, L. (2012). The Neurospora crassa mutant NcΔEgt-1 identifies an ergothioneine biosynthetic gene and demonstrates that ergothioneine enhances conidial survival and protects against peroxide toxicity during conidial germination. *Fungal Genetics and Biology, 49*(2), 160-172.

Ben-Ami, R., Lewis, R. E., & Kontoyiannis, D. P. (2010). Enemy of the (immunosuppressed) state: An update on the pathogenesis of Aspergillus fumigatus infection. *British Journal of Haematology, 150*(4), 406-417.

Berlett, B. S., & Stadtman, E. R. (1997). Protein oxidation in aging, disease, and oxidative stress. *The Journal of Biological Chemistry, 272*(33), 20313-20316.

Bernard, M., & Latgé, J. (2001). Aspergillus fumigatus cell wall: Composition and biosynthesis. *Medical Mycology, 39*(1), 9-17.

Bernardo, P. H., Brasch, N., Chai, C. L., & Waring, P. (2003). A novel redox mechanism for the glutathione-dependent reversible uptake of a fungal toxin in cells. *The Journal of Biological Chemistry, 278*(47), 46549-46555.

Biswas, S., Chida, A. S., & Rahman, I. (2006). Redox modifications of protein–thiols: Emerging roles in cell signaling. *Biochemical Pharmacology, 71*(5), 551-564.

Bok, J. W., Balajee, S. A., Marr, K. A., Andes, D., Nielsen, K. F., Frisvad, J. C., et al. (2005). LaeA, a regulator of morphogenetic fungal virulence factors. *Eukaryotic Cell, 4*(9), 1574-1582.

Bok, J. W., Chung, D., Balajee, S. A., Marr, K. A., Andes, D., Nielsen, K. F., et al. (2006). GliZ, a transcriptional regulator of gliotoxin biosynthesis, contributes to Aspergillus fumigatus virulence. *Infection and Immunity, 74*(12), 6761-6768.

Bok, J. W., & Keller, N. P. (2004). LaeA, a regulator of secondary metabolism in Aspergillus spp. *Eukaryotic Cell, 3*(2), 527-535.

Bowman, S. M., & Free, S. J. (2006). The structure and synthesis of the fungal cell wall. *Bioessays, 28*(8), 799-808.

Bowman, J. C., Hicks, P. S., Kurtz, M. B., Rosen, H., Schmatz, D. M., Liberator, P. A., et al. (2002). The antifungal echinocandin caspofungin acetate kills growing cells of Aspergillus fumigatus in vitro. *Antimicrobial Agents and Chemotherapy, 46*(9), 3001-3012.

Brakhage, A. A., & Langfelder, K. (2002). Menacing mold: The molecular biology of Aspergillus fumigatus. *Annual Reviews in Microbiology, 56*(1), 433-455.

Breitenbach, M., Weber, M., Rinnerthaler, M., Karl, T., & Breitenbach-Koller, L. (2015). Oxidative stress in fungi: Its function in signal transduction, interaction with plant hosts, and lignocellulose degradation. *Biomolecules, 5*(2), 318-342.

Brigelius-Flohé, R., & Maiorino, M. (2013). Glutathione peroxidases. *Biochimica Et Biophysica Acta (BBA)-General Subjects, 1830*(5), 3289-3303.

Bruns, S., Kniemeyer, O., Hasenberg, M., Aimanianda, V., Nietzsche, S., Thywißen, A., et al. (2010). Production of extracellular traps against Aspergillus fumigatus in vitro and in infected lung tissue is dependent on invading neutrophils and influenced by hydrophobin RodA. *PLoS Pathog, 6*(4), e1000873.

Burns, C., Geraghty, R., Neville, C., Murphy, A., Kavanagh, K., & Doyle, S. (2005). Identification, cloning, and functional expression of three glutathione transferase genes from Aspergillus fumigatus. *Fungal Genetics and Biology, 42*(4), 319-327.

Cabib, E. (2009). Two novel techniques for determination of polysaccharide cross-links show that Crh1p and Crh2p attach chitin to both beta(1-6)- and beta(1-3)glucan in the Saccharomyces cerevisiae cell wall. *Eukaryotic Cell, 8*(11), 1626-1636.

Calera, J. A., Paris, S., Monod, M., Hamilton, A. J., Debeaupuis, J. P., Diaquin, M., et al. (1997). Cloning and disruption of the antigenic catalase gene of Aspergillus fumigatus. *Infection and Immunity, 65*(11), 4718-4724.

Camm, E., & Towers, G. (1969). Phenylalanine and tyrosine ammonia lyase activity in Sporobolomyces roseus. *Phytochemistry, 8*(8), 1407-1413.

Campbell, I. M., Gallo, M. A., Jones, C. A., LaSitis, P. R., & Rosato, L. M. (1987). Role of cinnamate in benzoate production in Penicillium brevicompactum. *Phytochemistry, 26*(5), 1413-1415.

Carberry, S., & Doyle, S. (2007). Proteomic studies in biomedically and industrially relevant fungi. *Cytotechnology, 53*(1-3), 95-100.

Caudill, M. A., Wang, J. C., Melnyk, S., Pogribny, I. P., Jernigan, S., Collins, M. D., et al. (2001). Intracellular S-adenosylhomocysteine concentrations predict global DNA hypomethylation in tissues of methyl-deficient cystathionine beta-synthase heterozygous mice. *The Journal of Nutrition, 131*(11), 2811-2818.

Chang, S., Chiang, Y., Yeh, H., Wu, T., & Wang, C. C. (2013). Reconstitution of the early steps of gliotoxin biosynthesis in Aspergillus nidulans reveals the role of the monooxygenase GliC. *Bioorganic & Medicinal Chemistry Letters, 23*(7), 2155-2157.

Cheah, I. K., & Halliwell, B. (2012). Ergothioneine; antioxidant potential, physiological function and role in disease. *Biochimica Et Biophysica Acta (BBA)-Molecular Basis of Disease, 1822*(5), 784-793.

Chelikani, P., Fita, I., & Loewen, P. C. (2004). Diversity of structures and properties among catalases. *Cellular and Molecular Life Sciences CMLS, 61*(2), 192-208.

Conesa, A., Punt, P. J., & van den Hondel, Cees AMJJ. (2002). Fungal peroxidases: Molecular aspects and applications. *Journal of Biotechnology, 93*(2), 143-158.

Cooke, M. S., Evans, M. D., Dizdaroglu, M., & Lunec, J. (2003). Oxidative DNA damage: Mechanisms, mutation, and disease. *FASEB Journal : Official Publication of the Federation of American Societies for Experimental Biology, 17*(10), 1195-1214.

Cox, J., & Mann, M. (2008). MaxQuant enables high peptide identification rates, individualized ppb-range mass accuracies and proteome-wide protein quantification. *Nature Biotechnology, 26*(12), 1367-1372.

Cullen, D., Leong, S., Wilson, L., & Henner, D. (1987). Transformation of Aspergillus nidulans with the hygromycin-resistance gene, hph. *Gene, 57*(1), 21-26.

Dagenais, T. R., & Keller, N. P. (2009). Pathogenesis of Aspergillus fumigatus in invasive aspergillosis. *Clinical Microbiology Reviews, 22*(3), 447-465.

Dahlgren, C., & Karlsson, A. (1999). Respiratory burst in human neutrophils. *Journal of Immunological Methods, 232*(1), 3-14.

Dalle-Donne, I., Rossi, R., Colombo, G., Giustarini, D., & Milzani, A. (2009). Protein S-glutathionylation: A regulatory device from bacteria to humans. *Trends in Biochemical Sciences, 34*(2), 85-96.

Davin, L. B., & Lewis, N. G. (1992). Phenylpropanoid metabolism: Biosynthesis of monolignols, lignans and neolignans, lignins and suberins. *Phenolic metabolism in plants* (pp. 325-375) Springer.

Davis, C., Carberry, S., Schrettl, M., Singh, I., Stephens, J. C., Barry, S. M., et al. (2011). The role of glutathione S-transferase GliG in gliotoxin biosynthesis in Aspergillus fumigatus. *Chemistry & Biology, 18*(4), 542-552.

De Carvalho, M.P., & Abraham, W. (2012). Antimicrobial and biofilm inhibiting diketopiperazines. *Current Medicinal Chemistry, 19*(21), 3564-3577.

Dedon, P. C. (2007). The chemical toxicology of 2-deoxyribose oxidation in DNA. *Chemical Research in Toxicology, 21*(1), 206-219.

Deiana, M., Rosa, A., Casu, V., Piga, R., Assunta Dessì, M., & Aruoma, O. I. (2004). L-ergothioneine modulates oxidative damage in the kidney and liver of rats in vivo: Studies upon the profile of polyunsaturated fatty acids. *Clinical Nutrition, 23*(2), 183-193.

Desikan, R., Reynolds, A., Hancock, J. T., & Neill, S. J. (1998). Harpin and hydrogen peroxide both initiate programmed cell death but have differential effects on defence gene expression in Arabidopsis suspension cultures. *The Biochemical Journal, 330*(1), 115-120.

Dhingra, S., Andes, D., & Calvo, A. M. (2012). VeA regulates conidiation, gliotoxin production, and protease activity in the opportunistic human pathogen Aspergillus fumigatus. *Eukaryotic Cell, 11*(12), 1531-1543.

Di Menna, M., Smith, B., & Miles, C. (2009). A history of facial eczema (pithomycotoxicosis) research. *New Zealand Journal of Agricultural Research, 52*(4), 345-376.

Dichtl, K., Ebel, F., Dirr, F., Routier, F. H., Heesemann, J., & Wagener, J. (2010). Farnesol misplaces tip-localized Rho proteins and inhibits cell wall integrity signalling in Aspergillus fumigatus. *Molecular Microbiology, 76*(5), 1191-1204.

Dichtl, K., Helmschrott, C., Dirr, F., & Wagener, J. (2012). Deciphering cell wall integrity signalling in Aspergillus fumigatus: Identification and functional characterization of cell wall stress sensors and relevant Rho GTPases. *Molecular Microbiology, 83*(3), 506-519.

Dietl, A., Amich, J., Leal, S., Beckmann, N., Binder, U., Beilhack, A., et al. (2016). Histidine biosynthesis plays a crucial role in metal homeostasis and virulence of Aspergillus fumigatus. *Virulence 7*(4), 465-476.

Dixon, R. A., & Paiva, N. L. (1995). Stress-induced phenylpropanoid metabolism. *The Plant Cell, 7*(7), 1085-1097.

Dolan, S. K., O'Keeffe, G., Jones, G. W., & Doyle, S. (2015). Resistance is not futile: Gliotoxin biosynthesis, functionality and utility. *Trends in Microbiology, 23*(7), 419-428.

Domingo, M. P., Colmenarejo, C., Martínez-Lostao, L., Müllbacher, A., Jarne, C., Revillo, M. J., et al. (2012). Bis (methyl) gliotoxin proves to be a more stable and reliable marker for invasive aspergillosis than gliotoxin and suitable for use in diagnosis. *Diagnostic Microbiology and Infectious Disease, 73*(1), 57-64.

Dupres, V., Alsteens, D., Wilk, S., Hansen, B., Heinisch, J. J., & Dufrêne, Y. F. (2009). The yeast Wsc1 cell surface sensor behaves like a nanospring in vivo. *Nature Chemical Biology, 5*(11), 857-862.

Eichner, R., Al Salami, M., Wood, P., & Müllbacher, A. (1986). The effect of gliotoxin upon macrophage function. *International Journal of Immunopharmacology, 8*(7), 789-797.

Eichner, R. D., Waring, P., Geue, A. M., Braithwaite, A. W., & Mullbacher, A. (1988). Gliotoxin causes oxidative damage to plasmid and cellular DNA. *The Journal of Biological Chemistry, 263*(8), 3772-3777.

Eisendle, M., Schrettl, M., Kragl, C., Muller, D., Illmer, P., & Haas, H. (2006). The intracellular siderophore ferricrocin is involved in iron storage, oxidative-stress resistance, germination, and sexual development in Aspergillus nidulans. *Eukaryotic Cell, 5*(10), 1596-1603.

Ejzykowicz, D. E., Cunha, M. M., Rozental, S., Solis, N. V., Gravelat, F. N., Sheppard, D. C., et al. (2009). The Aspergillus fumigatus transcription factor Ace2 governs pigment production, conidiation and virulence. *Molecular Microbiology, 72*(1), 155-169.

Ejzykowicz, D. E., Solis, N. V., Gravelat, F. N., Chabot, J., Li, X., Sheppard, D. C., et al. (2010). Role of Aspergillus fumigatus DvrA in host cell interactions and virulence. *Eukaryotic Cell, 9*(10), 1432-1440.

Elgabbar, M. A. A., & Han, K. (2015). Isolation and characterization of two methyltransferase genes, AfuvipB and AfuvipC in Aspergillus fumigatus. *The Korean Journal of Mycology, 43*(1), 33-39.

Etienne-Manneville, S., & Hall, A. (2002). Rho GTPases in cell biology. *Nature, 420*(6916), 629-635.

Ey, J., Schömig, E., & Taubert, D. (2007). Dietary sources and antioxidant effects of ergothioneine. *Journal of Agricultural and Food Chemistry, 55*(16), 6466-6474.

Fang, W., Ding, W., Wang, B., Zhou, H., Ouyang, H., Ming, J., et al. (2010). Reduced expression of the O-mannosyltransferase 2 (AfPmt2) leads to deficient cell wall and abnormal polarity in Aspergillus fumigatus. *Glycobiology, 20*(5), 542-552.

Fedorova, N. D., Khaldi, N., Joardar, V. S., Maiti, R., Amedeo, P., Anderson, M. J., et al. (2008). Genomic islands in the pathogenic filamentous fungus Aspergillus fumigatus. *PLoS Genet, 4*(4), e1000046.

Fillinger, S., Chaveroche, M., Van Dijck, P., de Vries, R., Ruijter, G., Thevelein, J., et al. (2001). Trehalose is required for the acquisition of tolerance to a variety of stresses in the filamentous fungus Aspergillus nidulans. *Microbiology, 147*(7), 1851-1862.

Flatmark, T., & Stevens, R. C. (1999). Structural insight into the aromatic amino acid hydroxylases and their disease-related mutant forms. *Chemical Reviews, 99*, 2137-2160.

Fontaine, T., Simenel, C., Dubreucq, G., Adam, O., Delepierre, M., Lemoine, J., et al. (2000). Molecular organization of the alkali-insoluble fraction of Aspergillus fumigatus cell wall. *The Journal of Biological Chemistry, 275*(36), 27594-27607.

Fritz, R. R., Hodgins, D. S., & Abell, C. W. (1976). Phenylalanine ammonia-lyase. induction and purification from yeast and clearance in mammals. *The Journal of Biological Chemistry, 251*(15), 4646-4650.

Fu, Y. H., Paietta, J. V., Mannix, D. G., & Marzluf, G. A. (1989). Cys-3, the positive-acting sulfur regulatory gene of Neurospora crassa, encodes a protein with a putative leucine zipper DNA-binding element. *Molecular and Cellular Biology, 9*(3), 1120-1127.

Fulneček, J., Matyášek, R., Votruba, I., Holý, A., Křížová, K., & Kovařík, A. (2011). Inhibition of SAH-hydrolase activity during seed germination leads to deregulation of flowering genes and altered flower morphology in tobacco. *Molecular Genetics and Genomics, 285*(3), 225-236.

Galano, A., & Alvarez-Idaboy, J. R. (2011). Glutathione: Mechanism and kinetics of its non-enzymatic defense action against free radicals. *Rsc Advances, 1*(9), 1763-1771.

Gallagher, L., Owens, R. A., Dolan, S. K., O'Keeffe, G., Schrettl, M., Kavanagh, K., et al. (2012). The Aspergillus fumigatus protein GliK protects against oxidative stress and is essential for gliotoxin biosynthesis. *Eukaryotic Cell, 11*(10), 1226-1238.

Gardiner, D. M., & Howlett, B. J. (2005). Bioinformatic and expression analysis of the putative gliotoxin biosynthetic gene cluster of Aspergillus fumigatus. *FEMS Microbiology Letters, 248*(2), 241-248.

Gardiner, D. M., Waring, P., & Howlett, B. J. (2005). The epipolythiodioxopiperazine (ETP) class of fungal toxins: Distribution, mode of action, functions and biosynthesis. *Microbiology (Reading, England), 151*(4), 1021-1032.

Gastebois, A., Clavaud, C., Aimanianda, V., & Latgé, J. (2009). Aspergillus fumigatus: Cell wall polysaccharides, their biosynthesis and organization. *Future Microbiology, 4*(5), 583-595.

Gastebois, A., Mouyna, I., Simenel, C., Clavaud, C., Coddeville, B., Delepierre, M., et al. (2010). Characterization of a new beta(1-3)-glucan branching activity of Aspergillus fumigatus. *The Journal of Biological Chemistry, 285*(4), 2386-2396.

Gehrke, A., Heinekamp, T., Jacobsen, I. D., & Brakhage, A. A. (2010). Heptahelical receptors GprC and GprD of Aspergillus fumigatus are essential regulators of colony growth, hyphal morphogenesis, and virulence. *Applied and Environmental Microbiology, 76*(12), 3989-3998.

Geissler, A., Haun, F., Frank, D., Wieland, K., Simon, M., Idzko, M., et al. (2013). Apoptosis induced by the fungal pathogen gliotoxin requires a triple phosphorylation of bim by JNK. *Cell Death & Differentiation, 20*(10), 1317-1329.

Goncharenko, K. V., Vit, A., Blankenfeldt, W., & Seebeck, F. P. (2015). Structure of the sulfoxide synthase EgtB from the ergothioneine biosynthetic pathway. *Angewandte Chemie International Edition, 54*(9), 2821-2824.

Graham, S., Chevallier, O., Kumar, P., Türko&gcaron, O., & Bahado-Singh, R. (2016). Metabolomic profiling of brain from infants who died from sudden infant death syndrome reveals novel predictive biomarkers. *Journal of Perinatology*, 1-7.

Gründemann, D. (2012). The ergothioneine transporter controls and indicates ergothioneine activity—a review. *Preventive Medicine, 54*, S71-S74.

Gründemann, D., Harlfinger, S., Golz, S., Geerts, A., Lazar, A., Berkels, R., et al. (2005). Discovery of the ergothioneine transporter. *Proceedings of the National Academy of Sciences of the United States of America, 102*(14), 5256-5261.

Grundmann, A., Kuznetsova, T., Afiyatullov, S. S., & Li, S. (2008). FtmPT2, an N-Prenyltransferase from Aspergillus fumigatus, catalyses the last step in the biosynthesis of fumitremorgin B. *ChemBioChem, 9*(13), 2059-2063.

Guo, Q., Lin, S., Wang, Y., Zhu, C., Xu, C., & Shi, J. (2016). Gastrolatathioneine, an unusual ergothioneine derivative from an aqueous extract of “tian ma”: A natural product co-produced by plant and symbiotic fungus. *Chinese Chemical Letters, 27*(10), 1577-1581.

Haas, H. (2012). Iron - A key nexus in the virulence of Aspergillus fumigatus. *Frontiers in Microbiology, 3*, 28.

Hacker, G. (2013). A bim-activating mould. *Cell Death and Differentiation, 20*(10), 1289-1290.

Halliwell, B., & Gutteridge, J. (2007). Cellular responses to oxidative stress: Adaptation, damage, repair, senescence and death. *Free radicals in biology and medicine* (4th ed., pp. 187-267). New York: Oxford University Press Oxford.

Hand, C. E., Taylor, N. J., & Honek, J. F. (2005). Ab initio studies of the properties of intracellular thiols ergothioneine and ovothiol. *Bioorganic & Medicinal Chemistry Letters, 15*(5), 1357-1360.

Hartman, P. E. (1990). Ergothioneine as antioxidant. *Methods in Enzymology, 186*, 310-318.

Hartmann, T., Dumig, M., Jaber, B. M., Szewczyk, E., Olbermann, P., Morschhauser, J., et al. (2010). Validation of a self-excising marker in the human pathogen Aspergillus fumigatus by employing the beta-rec/six site-specific recombination system. *Applied and Environmental Microbiology, 76*(18), 6313-6317.

Hatano, T., Saiki, S., Okuzumi, A., Mohney, R. P., & Hattori, N. (2016). Identification of novel biomarkers for parkinson's disease by metabolomic technologies. *Journal of Neurology, Neurosurgery, and Psychiatry, 87*(3), 295-301.

Hillmann, F., Bagramyan, K., Strassburger, M., Heinekamp, T., Hong, T. B., Bzymek, K. P., et al. (2016). The crystal structure of peroxiredoxin Asp f3 provides mechanistic insight into oxidative stress resistance and virulence of Aspergillus fumigatus. *Scientific Reports, 6*, 33396.

Hissen, A. H., Wan, A. N., Warwas, M. L., Pinto, L. J., & Moore, M. M. (2005). The Aspergillus fumigatus siderophore biosynthetic gene sidA, encoding L-ornithine N5-oxygenase, is required for virulence. *Infection and Immunity, 73*(9), 5493-5503.

Hohl, T. M., & Feldmesser, M. (2007). Aspergillus fumigatus: Principles of pathogenesis and host defense. *Eukaryotic Cell, 6*(11), 1953-1963.

Huang, Z., & van der Donk, Wilfred A. (2015). An unexpected role for ergothioneine. *National Science Review,2,* 382–384.

Hyun, M. W., Yun, Y. H., Kim, J. Y., & Kim, S. H. (2011). Fungal and plant phenylalanine ammonia-lyase. *Mycobiology, 39*(4), 257-265.

Imlay, J. A. (2003). Pathways of oxidative damage. *Annual Reviews in Microbiology, 57*(1), 395-418.

Ishikawa, Y., Israel, S. E., & Melville, D. B. (1974). Participation of an intermediate sulfoxide in the enzymatic thiolation of the imidazole ring of hercynine to form ergothioneine. *The Journal of Biological Chemistry, 249*(14), 4420-4427.

Jain, R., Valiante, V., Remme, N., Docimo, T., Heinekamp, T., Hertweck, C., et al. (2011). The MAP kinase MpkA controls cell wall integrity, oxidative stress response, gliotoxin production and iron adaptation in Aspergillus fumigatus. *Molecular Microbiology, 82*(1), 39-53.

Jones, D. H. (1984). Phenylalanine ammonia-lyase: Regulation of its induction, and its role in plant development. *Phytochemistry, 23*(7), 1349-1359.

Jones, G. W., Doyle, S., & Fitzpatrick, D. A. (2014). The evolutionary history of the genes involved in the biosynthesis of the antioxidant ergothioneine. *Gene, 549*(1), 161-170.

Kalghatgi, K., Nambudiri, A., Bhat, J., & Subba-Rao, P. (1974). Degradation of L-phenylalanine by Rhizoctonia solani. *Indian Journal of Biochemistry,*

Kärkönen, A., & Kuchitsu, K. (2015). Reactive oxygen species in cell wall metabolism and development in plants. *Phytochemistry, 112*, 22-32.

Kato, N., Suzuki, H., Takagi, H., Uramoto, M., Takahashi, S., & Osada, H. (2011). Gene disruption and biochemical characterization of verruculogen synthase of Aspergillus fumigatus. *ChemBioChem, 12*(5), 711-714.

Kayano, Y., Tanaka, A., Akano, F., Scott, B., & Takemoto, D. (2013). Differential roles of NADPH oxidases and associated regulators in polarized growth, conidiation and hyphal fusion in the symbiotic fungus Epichloë festucae. *Fungal Genetics and Biology, 56*, 87-97.

Keller, N. P., Turner, G., & Bennett, J. W. (2005). Fungal secondary metabolism—from biochemistry to genomics. *Nature Reviews Microbiology, 3*(12), 937-947.

Khaldi, N., Seifuddin, F. T., Turner, G., Haft, D., Nierman, W. C., Wolfe, K. H., et al. (2010). SMURF: Genomic mapping of fungal secondary metabolite clusters. *Fungal Genetics and Biology, 47*(9), 736-741.

Kim, D., Hayles, J., Kim, D., Wood, V., Park, H., Won, M., et al. (2010). Analysis of a genome-wide set of gene deletions in the fission yeast Schizosaccharomyces pombe. *Nature Biotechnology, 28*(6), 617-623.

Kim, S. H., Kronstad, J. W., & Ellis, B. E. (1996). Purification and characterization of phenylalanine ammonia-lyase from Ustilago maydis. *Phytochemistry, 43*(2), 351-357.

Kim, S. S., & Shin, K. S. (2013). The developmental regulators, FlbB and FlbE, are involved in the virulence of Aspergillus fumigatus. *Journal of Microbiology and Biotechnology, 23*(6), 766-770.

Kishishita, S., Shimizu, K., Murayama, K., Terada, T., Shirouzu, M., Yokoyama, S., et al. (2008). Structures of two archaeal diphthine synthases: Insights into the post-translational modification of elongation factor 2. *Acta Crystallographica Section D: Biological Crystallography, 64*(4), 397-406.

Kniemeyer, O., Lessing, F., & Brakhage, A. A. (2009). Proteome analysis for pathogenicity and new diagnostic markers for Aspergillus fumigatus. *Medical Mycology, 47*(sup1), S248-S254.

Korkina, L. (2007). Phenylpropanoids as naturally occurring antioxidants: From plant defense to human health. *Cell Mol Biol, 53*(1), 15-25.

Krappmann, S., Sasse, C., & Braus, G. H. (2006). Gene targeting in Aspergillus fumigatus by homologous recombination is facilitated in a nonhomologous end- joining-deficient genetic background. *Eukaryotic Cell, 5*(1), 212-215.

Kubodera, T., Yamashita, N., & Nishimura, A. (2000). Pyrithiamine resistance gene (ptrA) of Aspergillus oryzae: Cloning, characterization and application as a dominant selectable marker for transformation. *Bioscience, Biotechnology, and Biochemistry, 64*(7), 1416-1421.

Kupfahl, C., Heinekamp, T., Geginat, G., Ruppert, T., Härtl, A., Hof, H., et al. (2006). Deletion of the gliP gene of Aspergillus fumigatus results in loss of gliotoxin production but has no effect on virulence of the fungus in a low-dose mouse infection model. *Molecular Microbiology, 62*(1), 292-302.

Kwon, N., Shin, K., & Yu, J. (2010). Characterization of the developmental regulator FlbE in Aspergillus fumigatus and Aspergillus nidulans. *Fungal Genetics and Biology, 47*(12), 981-993.

Kwon-Chung, K. J., & Sugui, J. A. (2013). Aspergillus fumigatus—what makes the species a ubiquitous human fungal pathogen? *PLoS Pathog, 9*(12), e1003743.

Lambou, K., Lamarre, C., Beau, R., Dufour, N., & Latge, J. (2010). Functional analysis of the superoxide dismutase family in Aspergillus fumigatus. *Molecular Microbiology, 75*(4), 910-923.

Latge, J. P. (1999). Aspergillus fumigatus and aspergillosis. *Clinical Microbiology Reviews, 12*(2), 310-350.

Lee, I., Oh, J., Shwab, E. K., Dagenais, T. R., Andes, D., & Keller, N. P. (2009). HdaA, a class 2 histone deacetylase of Aspergillus fumigatus, affects germination and secondary metabolite production. *Fungal Genetics and Biology, 46*(10), 782-790.

Lessing, F., Kniemeyer, O., Wozniok, I., Loeffler, J., Kurzai, O., Haertl, A., et al. (2007). The Aspergillus fumigatus transcriptional regulator AfYap1 represents the major regulator for defense against reactive oxygen intermediates but is dispensable for pathogenicity in an intranasal mouse infection model. *Eukaryotic Cell, 6*(12), 2290-2302.

Levin, D. E. (2011). Regulation of cell wall biogenesis in Saccharomyces cerevisiae: The cell wall integrity signaling pathway. *Genetics, 189*(4), 1145-1175.

Li, J., Kogan, M., Knight, S. A., Pain, D., & Dancis, A. (1999). Yeast mitochondrial protein, Nfs1p, coordinately regulates iron-sulfur cluster proteins, cellular iron uptake, and iron distribution. *The Journal of Biological Chemistry, 274*(46), 33025-33034.

Liao, S., Li, R., Shi, L., Wang, J., Shang, J., Zhu, P., et al. (2012). Functional analysis of an S-adenosylhomocysteine hydrolase homolog of chestnut blight fungus. *FEMS Microbiology Letters, 336*(1), 64-72.

Lieber, C. S., & Packer, L. (2002). S-adenosylmethionine: Molecular, biological, and clinical aspects--an introduction. *The American Journal of Clinical Nutrition, 76*(5), 1148S-50S.

Lin, C., Sasse, C., Gerke, J., Valerius, O., Irmer, H., Frauendorf, H., et al. (2015). Transcription factor SomA is required for adhesion, development and virulence of the human pathogen Aspergillus fumigatus. *PLoS Pathog, 11*(11), e1005205.

Lin, H., Chooi, Y., Dhingra, S., Xu, W., Calvo, A. M., & Tang, Y. (2013). The fumagillin biosynthetic gene cluster in Aspergillus fumigatus encodes a cryptic terpene cyclase involved in the formation of β-trans-bergamotene. *Journal of the American Chemical Society, 135*(12), 4616-4619.

Liscombe, D. K., Louie, G. V., & Noel, J. P. (2012). Architectures, mechanisms and molecular evolution of natural product methyltransferases. *Natural Product Reports, 29*(10), 1238-1250.

Livak, K. J., & Schmittgen, T. D. (2001). Analysis of relative gene expression data using real-time quantitative PCR and the 2− ΔΔCT method. *Methods, 25*(4), 402-408.

López-Mirabal, H. R., & Winther, J. R. (2008). Redox characteristics of the eukaryotic cytosol. *Biochimica Et Biophysica Acta (BBA)-Molecular Cell Research, 1783*(4), 629-640.

Lu, S. C. (2009). Regulation of glutathione synthesis. *Molecular Aspects of Medicine, 30*(1), 42-59.

Lushchak, V. I. (2011). Adaptive response to oxidative stress: Bacteria, fungi, plants and animals. *Comparative Biochemistry and Physiology Part C: Toxicology & Pharmacology, 153*(2), 175-190.

Macheleidt, J., Mattern, D. J., Fischer, J., Netzker, T., Weber, J., Schroeckh, V., et al. (2016). Regulation and role of fungal secondary metabolites. *Annual Review of Genetics, 50*(1)

Mah, J. H., & Yu, J. H. (2006). Upstream and downstream regulation of asexual development in Aspergillus fumigatus. *Eukaryotic Cell, 5*(10), 1585-1595.

Maiya, S., Grundmann, A., Li, X., Li, S., & Turner, G. (2007). Identification of a hybrid PKS/NRPS required for pseurotin A biosynthesis in the human pathogen Aspergillus fumigatus. *Chembiochem, 8*(14), 1736-1743.

Mandaviya, P. R., Stolk, L., & Heil, S. G. (2014). Homocysteine and DNA methylation: A review of animal and human literature. *Molecular Genetics and Metabolism, 113*(4), 243-252.

Markova, N. G., Karaman-Jurukovska, N., Dong, K. K., Damaghi, N., Smiles, K. A., & Yarosh, D. B. (2009). Skin cells and tissue are capable of using L-ergothioneine as an integral component of their antioxidant defense system. *Free Radical Biology and Medicine, 46*(8), 1168-1176.

Marusich, W. C., Jensen, R. A., & Zamir, L. O. (1981). Induction of L-phenylalanine ammonia-lyase during utilization of phenylalanine as a carbon or nitrogen source in Rhodotorula glutinis. *Journal of Bacteriology, 146*(3), 1013-1019.

Marzluf, G. A. (1997). Molecular genetics of sulfur assimilation in filamentous fungi and yeast. *Annual Reviews in Microbiology, 51*(1), 73-96.

McCord, J. M., & Fridovich, I. (1969). Superoxide dismutase. an enzymic function for erythrocuprein (hemocuprein). *The Journal of Biological Chemistry, 244*(22), 6049-6055.

McCormick, A., Heesemann, L., Wagener, J., Marcos, V., Hartl, D., Loeffler, J., et al. (2010). NETs formed by human neutrophils inhibit growth of the pathogenic mold Aspergillus fumigatus. *Microbes and Infection, 12*(12), 928-936.

Medentsev, A., & Akimenko, V. (1998). Naphthoquinone metabolites of the fungi. *Phytochemistry, 47*(6), 935-959.

Miyayama, T., Ishizuka, Y., Iijima, T., Hiraoka, D., & Ogra, Y. (2011). Roles of copper chaperone for superoxide dismutase 1 and metallothionein in copper homeostasis. *Metallomics, 3*(7), 693-701.

Moloney, N. M., Owens, R. A., Meleady, P., Henry, M., Dolan, S. K., Mulvihill, E., et al. (2016). The iron-responsive microsomal proteome of Aspergillus fumigatus. *Journal of Proteomics, 136*, 99-111.

Moore, K., & Towers, G. (1967). Degradation of aromatic amino acids by fungi: I. Fate of L-phenylalanine in Schizophyllum commune. *Canadian Journal of Biochemistry, 45*(11), 1659-1665.

Mouyna, I., & Fontaine, T. (2009). Cell wall of Aspergillus fumigatus: A dynamic structure. *Aspergillus fumigatus and aspergillosis* (pp. 169-183) American Society of Microbiology.

Mouyna, I., Hartl, L., & Latgé, J. (2013). β-1, 3-glucan modifying enzymes in Aspergillus fumigatus. *Frontiers in Microbiology, 4*, 81.

Mouyna, I., Kniemeyer, O., Jank, T., Loussert, C., Mellado, E., Aimanianda, V., et al. (2010). Members of protein O-mannosyltransferase family in Aspergillus fumigatus differentially affect growth, morphogenesis and viability. *Molecular Microbiology, 76*(5), 1205-1221.

Mullbacher, A., & Eichner, R. D. (1984). Immunosuppression in vitro by a metabolite of a human pathogenic fungus. *Proceedings of the National Academy of Sciences of the United States of America, 81*(12), 3835-3837.

Mullins, J., Harvey, R., & Seaton, A. (1976). Sources and incidence of airborne Aspergillus fumigatus (fres). *Clinical & Experimental Allergy, 6*(3), 209-217.

Mullins, J., Hutcheson, P. S., & Slavin, R. (1984). Aspergillus fumigatus spore concentration in outside air: Cardiff and St. Louis compared. *Clinical & Experimental Allergy, 14*(4), 351-354.

Munday, R. (1982). Studies on the mechanism of toxicity of the mycotoxin, sporidesmin. I. Generation of superoxide radical by sporidesmin. *Chemico-Biological Interactions, 41*(3), 361-374.

Munday, R. (1984). Studies on the mechanism of toxicity of the mycotoxin sporidesmin. 2—Evidence for intracellular generation of superoxide radical from sporidesmin. *Journal of Applied Toxicology, 4*(4), 176-181.

Munday, R. (1987). Studies on the mechanism of toxicity of the mycotoxin, sporidesmin. V. Generation of hydroxyl radical by sporidesmin. *Journal of Applied Toxicology, 7*(1), 17-22.

Muramatsu, H., Matsuo, H., Okada, N., Ueda, M., Yamamoto, H., Kato, S., et al. (2013). Characterization of ergothionase from Burkholderia sp. HME13 and its application to enzymatic quantification of ergothioneine. *Applied Microbiology and Biotechnology, 97*(12), 5389-5400.

Nakajima, S., Satoh, Y., Yanashima, K., Matsui, T., & Dairi, T. (2015). Ergothioneine protects streptomyces coelicolor A3 (2) from oxidative stresses. *Journal of Bioscience and Bioengineering, 120*(3), 294-298.

Nambudiri, A., Rao, P. S., & Bhat, J. V. (1970). Metabolism of aromatic compounds by an Alternaria species. *Phytochemistry, 9*(4), 687-693.

Nanduri, J., & Tartakoff, A. M. (2001). The arrest of secretion response in yeast: Signaling from the secretory path to the nucleus via WSC proteins and Pkc1p. *Molecular Cell, 8*(2), 281-289.

Natorff, R., Balińska, M., & Paszewski, A. (1993). At least four regulatory genes control sulphur metabolite repression in Aspergillus nidulans. *Molecular and General Genetics MGG, 238*(1-2), 185-192.

Natorff, R., Sieńko, M., Brzywczy, J., & Paszewski, A. (2003). The Aspergillus nidulans metR gene encodes a bZIP protein which activates transcription of sulphur metabolism genes. *Molecular Microbiology, 49*(4), 1081-1094.

Ni, M., Gao, N., Kwon, N., Shin, K., & Yu, J. (2010). Regulation of Aspergillus conidiation. *Cellular and Molecular Biology of Filamentous Fungi, ,* 559-576.

Nielsen, M. L., Albertsen, L., Lettier, G., Nielsen, J. B., & Mortensen, U. H. (2006). Efficient PCR-based gene targeting with a recyclable marker for Aspergillus nidulans. *Fungal Genetics and Biology, 43*(1), 54-64.

Niide, O., Suzuki, Y., Yoshimaru, T., Inoue, T., Takayama, T., & Ra, C. (2006). Fungal metabolite gliotoxin blocks mast cell activation by a calcium-and superoxide-dependent mechanism: Implications for immunosuppressive activities. *Clinical Immunology, 118*(1), 108-116.

Niki, E. (2009). Lipid peroxidation: Physiological levels and dual biological effects. *Free Radical Biology and Medicine, 47*(5), 469-484.

O'Gorman, C. M. (2011). Airborne Aspergillus fumigatus conidia: A risk factor for aspergillosis. *Fungal Biology Reviews, 25*(3), 151-157.

O'Gorman, C. M., Fuller, H. T., & Dyer, P. S. (2009). Discovery of a sexual cycle in the opportunistic fungal pathogen Aspergillus fumigatus. *Nature, 457*(7228), 471-474.

Ogata, K., Uchiyama, K., Yamada, H., & Tochikura, T. (1967). Metabolism of aromatic amino acid in microorganisms: Part II. Properties of phenylalanine ammonia-lyase of Rhodotorula. *Agricultural and Biological Chemistry, 31*(5), 600-606.

O'Keeffe, G., Jöchl, C., Kavanagh, K., & Doyle, S. (2013). Extensive proteomic remodeling is induced by eukaryotic translation elongation factor 1Bγ deletion in Aspergillus fumigatus. *Protein Science, 22*(11), 1612-1622.

Ott, M., Gogvadze, V., Orrenius, S., & Zhivotovsky, B. (2007). Mitochondria, oxidative stress and cell death. *Apoptosis, 12*(5), 913-922.

Owens, R. A., Hammel, S., Sheridan, K. J., Jones, G. W., & Doyle, S. (2014). A proteomic approach to investigating gene cluster expression and secondary metabolite functionality in Aspergillus fumigatus. *PloS One, 9*(9), e106942.

Owens, R. A., O'Keeffe, G., Smith, E. B., Dolan, S. K., Hammel, S., Sheridan, K. J., et al. (2015). Interplay between gliotoxin resistance, secretion, and the Methyl/Methionine cycle in Aspergillus fumigatus. *Eukaryotic Cell, 14*(9), 941-957.

Palmer, J. M., Bok, J. W., Lee, S., Dagenais, T. R., Andes, D. R., Kontoyiannis, D. P., et al. (2013). Loss of CclA, required for histone 3 lysine 4 methylation, decreases growth but increases secondary metabolite production in Aspergillus fumigatus. *PeerJ, 1*, e4.

Papanikolaou, G., & Pantopoulos, K. (2005). Iron metabolism and toxicity. *Toxicology and Applied Pharmacology, 202*(2), 199-211.

Paris, S., Debeaupuis, J. P., Crameri, R., Carey, M., Charles, F., Prevost, M. C., et al. (2003a). Conidial hydrophobins of Aspergillus fumigatus. *Applied and Environmental Microbiology, 69*(3), 1581-1588.

Paris, S., Wysong, D., Debeaupuis, J. P., Shibuya, K., Philippe, B., Diamond, R. D., et al. (2003b). Catalases of Aspergillus fumigatus. *Infection and Immunity, 71*(6), 3551-3562.

Park, E., Lee, W. Y., Kim, S. T., Ahn, J. K., & Bae, E. K. (2010). Ergothioneine accumulation in a medicinal plant Gastrodia elata. *Journal of Medicinal Plants Research, 4*(12), 1141-1147.

Park, H., Bayram, Ö., Braus, G. H., Kim, S. C., & Yu, J. (2012a). Characterization of the velvet regulators in Aspergillus fumigatus. *Molecular Microbiology, 86*(4), 937-953.

Park, H., Ni, M., Jeong, K. C., Kim, Y. H., & Yu, J. (2012b). The role, interaction and regulation of the velvet regulator VelB in Aspergillus nidulans. *PloS One, 7*(9), e45935.

Park, H., & Yu, J. (2016). Developmental regulators in Aspergillus fumigatus. *Journal of Microbiology, 54*(3), 223-231.

Paszewski, A., Brzywczy, J., & Natorff, R. (1994). Sulphur metabolism. *Progress in Industrial Microbiology, 29*, 299-319.

Pathak, V., Rendon, I. S. H., & Ciubotaru, R. L. (2011). Invasive pulmonary aspergillosis in an immunocompetent patient. *Respiratory Medicine CME, 4*(3), 105-106.

Paul, B., & Snyder, S. (2010). The unusual amino acid L-ergothioneine is a physiologic cytoprotectant. *Cell Death & Differentiation, 17*(7), 1134-1140.

Pfeiffer, C., Bauer, T., Surek, B., Schömig, E., & Gründemann, D. (2011). Cyanobacteria produce high levels of ergothioneine. *Food Chemistry, 129*(4), 1766-1769.

Pluskal, T., Ueno, M., & Yanagida, M. (2014). Genetic and metabolomic dissection of the ergothioneine and selenoneine biosynthetic pathway in the fission yeast, S. pombe, and construction of an overproduction system.

Ponts, N., Pinson-Gadais, L., Verdal-Bonnin, M., Barreau, C., & Richard-Forget, F. (2006). Accumulation of deoxynivalenol and its 15-acetylated form is significantly modulated by oxidative stress in liquid cultures of Fusarium graminearum. *FEMS Microbiology Letters, 258*(1), 102-107.

Ponts, N., Pinson-Gadais, L., Barreau, C., Richard-Forget, F., & Ouellet, T. (2007). Exogenous H2O2 and catalase treatments interfere with tri genes expression in liquid cultures of Fusarium graminearum. *FEBS Letters, 581*(3), 443-447.

Power, D., Towers, G., & Neish, A. (1965). Biosynthesis of phenolic acids by certain wood-destroying Basidiomycetes. *Canadian Journal of Biochemistry, 43*(9), 1397-1407.

Pridham, J., & Woodhead, S. (1974). Multimolecular forms of phenylalanine-ammonia lyase in Alternaria. *Biochemical Society Transactions, 2*(5), 1070-1072.

Priebe, S., Kreisel, C., Horn, F., Guthke, R., & Linde, J. (2015). FungiFun2: A comprehensive online resource for systematic analysis of gene lists from fungal species. *Bioinformatics (Oxford, England), 31*(3), 445-446.

Puddu, P., Puddu, G. M., Cravero, E., Rosati, M., & Muscari, A. (2008). The molecular sources of reactive oxygen species in hypertension. *Blood Pressure, 17*(2), 70-77.

Pusztahelyi, T., Klement, É., Szajli, E., Klem, J., Miskei, M., Karányi, Z., et al. (2011). Comparison of transcriptional and translational changes caused by long-term menadione exposure in Aspergillus nidulans. *Fungal Genetics and Biology, 48*(2), 92-103.

Rahman, I., Kode, A., & Biswas, S. K. (2006). Assay for quantitative determination of glutathione and glutathione disulfide levels using enzymatic recycling method. *Nature Protocols, 1*(6), 3159-3165.

Ravanel, S. (1997). Methionine biosynthesis in higher plants: Biochemical and molecular characterization of the transsulfuration pathway enzymes. *Comptes Rendus De l'Académie Des Sciences - Series III - Sciences De La Vie, 320*(6), 497-504.

Reverberi, M., Fabbri, A., Zjalic, S., Ricelli, A., Punelli, F., & Fanelli, C. (2005). Antioxidant enzymes stimulation in Aspergillus parasiticus by Lentinula edodes inhibits aflatoxin production. *Applied Microbiology and Biotechnology, 69*(2), 207-215.

Reverberi, M., Zjalic, S., Ricelli, A., Punelli, F., Camera, E., Fabbri, C., et al. (2008). Modulation of antioxidant defense in Aspergillus parasiticus is involved in aflatoxin biosynthesis: A role for the ApyapA gene. *Eukaryotic Cell, 7*(6), 988-1000.

Rhodes, J. C., & Askew, D. S. (2010). Aspergillus fumigatus. *Cellular and Molecular Biology of Filamentous Fungi*, 697-716 .

Rieder, G., Merrick, M. J., Castorph, H., & Kleiner, D. (1994). Function of hisF and hisH gene products in histidine biosynthesis. *Journal of Biological Chemistry, 269*(20), 14386-14390.

Rispail, N., Soanes, D. M., Ant, C., Czajkowski, R., Grünler, A., Huguet, R., et al. (2009). Comparative genomics of MAP kinase and calcium–calcineurin signalling components in plant and human pathogenic fungi. *Fungal Genetics and Biology, 46*(4), 287-298.

Rokas, A. (2013). Aspergillus. *Current Biology, 23*(5), R187-R188.

Roncero, C., & Duran, A. (1985). Effect of calcofluor white and congo red on fungal cell wall morphogenesis: In vivo activation of chitin polymerization. *Journal of Bacteriology, 163*(3), 1180-1185.

Saini, V., Cumming, B. M., Guidry, L., Lamprecht, D. A., Adamson, J. H., Reddy, V. P., et al. (2016). Ergothioneine maintains redox and bioenergetic homeostasis essential for drug susceptibility and virulence of mycobacterium tuberculosis. *Cell Reports, 14*(3), 572-585.

Saint-Macary, M. E., Barbisan, C., Gagey, M. J., Frelin, O., Beffa, R., Lebrun, M. H., et al. (2015). Methionine biosynthesis is essential for infection in the rice blast fungus magnaporthe oryzae. *PloS One, 10*(4), e0111108.

Sao Emani, C., Williams, M. J., Wiid, I. J., Hiten, N. F., Viljoen, A. J., Pietersen, R. D., et al. (2013). Ergothioneine is a secreted antioxidant in Mycobacterium smegmatis. *Antimicrobial Agents and Chemotherapy, 57*(7), 3202-3207.

Sarikaya-Bayram, Ö., Bayram, Ö., Feussner, K., Kim, J., Kim, H., Kaever, A., et al. (2014). Membrane-bound methyltransferase complex VapA-VipC-VapB guides epigenetic control of fungal development. *Developmental Cell, 29*(4), 406-420.

Sauter, M., Moffatt, B., Saechao, M. C., Hell, R., & Wirtz, M. (2013). Methionine salvage and S-adenosylmethionine: Essential links between sulfur, ethylene and polyamine biosynthesis. *The Biochemical Journal, 451*(2), 145-154.

Scharf, D. H., Chankhamjon, P., Scherlach, K., Heinekamp, T., Roth, M., Brakhage, A. A., et al. (2012). Epidithiol formation by an unprecedented twin Carbon–Sulfur lyase in the gliotoxin pathway. *Angewandte Chemie, 124*(40), 10211-10215.

Scharf, D. H., Chankhamjon, P., Scherlach, K., Heinekamp, T., Willing, K., Brakhage, A. A., et al. (2013). Epidithiodiketopiperazine biosynthesis: A Four-Enzyme cascade converts glutathione conjugates into transannular disulfide bridges. *Angewandte Chemie International Edition, 52*(42), 11092-11095.

Scharf, D. H., Remme, N., Habel, A., Chankhamjon, P., Scherlach, K., Heinekamp, T., et al. (2011). A dedicated glutathione S-transferase mediates carbon–sulfur bond formation in gliotoxin biosynthesis. *Journal of the American Chemical Society, 133*(32), 12322-12325.

Scheltema, R. A., Hauschild, J. P., Lange, O., Hornburg, D., Denisov, E., Damoc, E., et al. (2014). The Q exactive HF, a benchtop mass spectrometer with a pre-filter, high-performance quadrupole and an ultra-high-field orbitrap analyzer. *Molecular & Cellular Proteomics : MCP, 13*(12), 3698-3708.

Schrettl, M., Bignell, E., Kragl, C., Sabiha, Y., Loss, O., Eisendle, M., et al. (2007). Distinct roles for intra-and extracellular siderophores during Aspergillus fumigatus infection. *PLoS Pathogens, 3*(9), e128.

Schrettl, M., Carberry, S., Kavanagh, K., Haas, H., Jones, G. W., O'Brien, J., et al. (2010). Self-protection against gliotoxin—a component of the gliotoxin biosynthetic cluster, GliT, completely protects Aspergillus fumigatus against exogenous gliotoxin. *PLoS Pathogens, 6*(6), e1000952.

Schrettl, M., Bignell, E., Kragl, C., Joechl, C., Rogers, T., Arst, H. N.,Jr, et al. (2004). Siderophore biosynthesis but not reductive iron assimilation is essential for Aspergillus fumigatus virulence. *The Journal of Experimental Medicine, 200*(9), 1213-1219.

Schubert, H. L., Blumenthal, R. M., & Cheng, X. (2003). Many paths to methyltransfer: A chronicle of convergence. *Trends in Biochemical Sciences, 28*(6), 329-335.

Schwede, T. F., Rétey, J., & Schulz, G. E. (1999). Crystal structure of histidine ammonia-lyase revealing a novel polypeptide modification as the catalytic electrophile. *Biochemistry, 38*(17), 5355-5361.

Seebeck, F. P. (2010). In vitro reconstitution of mycobacterial ergothioneine biosynthesis. *Journal of the American Chemical Society, 132*(19), 6632-6633.

Servillo, L., Castaldo, D., Casale, R., D'Onofrio, N., Giovane, A., Cautela, D., et al. (2015). An uncommon redox behavior sheds light on the cellular antioxidant properties of ergothioneine. *Free Radical Biology and Medicine, 79*, 228-236.

Sheng, Y., Abreu, I. A., Cabelli, D. E., Maroney, M. J., Miller, A., Teixeira, M., et al. (2014). Superoxide dismutases and superoxide reductases. *Chemical Reviews, 114*(7), 3854-3918.

Sheppard, D. C., Doedt, T., Chiang, L. Y., Kim, H. S., Chen, D., Nierman, W. C., et al. (2005). The Aspergillus fumigatus StuA protein governs the up-regulation of a discrete transcriptional program during the acquisition of developmental competence. *Molecular Biology of the Cell, 16*(12), 5866-5879.

Sheridan, K. J., Lechner, B. E., O' Keeffe, G., Keller, M. A., Werner, E. R., Lindner, H., et al. (2016). Ergothioneine biosynthesis and functionality in the opportunistic fungal pathogen, *Aspergillus fumigatus*. *Scientific Reports, 6*

Sheridan, K. J., Dolan, S. K., & Doyle, S. (2015). Endogenous cross-talk of fungal metabolites. *Frontiers in Microbiololgy, 5*(732), 1-11.

Shin, K., Kwon, N., & Yu, J. (2009). Gβγ-mediated growth and developmental control in Aspergillus fumigatus. *Current Genetics, 55*(6), 631-641.

Sieńko, M., Natorff, R., Owczarek, S., Olewiecki, I., & Paszewski, A. (2009). Aspergillus nidulans genes encoding reverse transsulfuration enzymes belong to homocysteine regulon. *Current Genetics, 55*(5), 561-570.

Singh, A. R., Strankman, A., Orkusyan, R., Purwantini, E., & Rawat, M. (2016). Lack of mycothiol and ergothioneine induces different protective mechanisms in mycobacterium smegmatis. *Biochemistry and Biophysics Reports, 8*, 100-106.

Sohn, M. J., Yoo, S. J., Oh, D., Kwon, O., Lee, S. Y., Sibirny, A. A., et al. (2014). Novel cysteine-centered sulfur metabolic pathway in the thermotolerant methylotrophic yeast Hansenula polymorpha. *PloS One, 9*(6), e100725.

Song, H., Her, A. S., Raso, F., Zhen, Z., Huo, Y., & Liu, P. (2014). Cysteine oxidation reactions catalyzed by a mononuclear non-heme iron enzyme (OvoA) in ovothiol biosynthesis. *Organic Letters, 16*(8), 2122-2125.

Song, H., Hu, W., Naowarojna, N., Her, A. S., Wang, S., Desai, R., et al. (2015). Mechanistic studies of a novel CS lyase in ergothioneine biosynthesis: The involvement of a sulfenic acid intermediate. *Scientific Reports, 5*

Song, T., Chen, C., Liao, J., Ou, H., & Tsai, M. (2010). Ergothioneine protects against neuronal injury induced by cisplatin both in vitro and in vivo. *Food and Chemical Toxicology, 48*(12), 3492-3499.

Sotgia, S., Pisanu, E., Pintus, G., Erre, G. L., Pinna, G. A., Deiana, L., et al. (2013). Plasma L-ergothioneine measurement by high-performance liquid chromatography and capillary electrophoresis after a pre-column derivatization with 5-iodoacetamidofluorescein (5-IAF) and fluorescence detection. *PloS one, 8*(7), e70374.

Sotgia, S., Zinellu, A., Mangoni, A. A., Pintus, G., Attia, J., Carru, C., et al. (2014). Clinical and biochemical correlates of serum L-ergothioneine concentrations in community-dwelling middle-aged and older adults. *PloS One, 9*(1), e84918.

Spicer, S. S., Wooley, J. G., & Kessler, V. (1951). Ergothioneine depletion in rabbit erythrocytes and its effect on methemoglobin formation and reversion. *Experimental Biology and Medicine, 77*(3), 418-420.

Starkov, A. A. (2008). The role of mitochondria in reactive oxygen species metabolism and signaling. *Annals of the New York Academy of Sciences, 1147*(1), 37-52.

Struck, A., Thompson, M. L., Wong, L. S., & Micklefield, J. (2012). S-Adenosyl-Methionine-Dependent methyltransferases: Highly versatile enzymes in biocatalysis, biosynthesis and other biotechnological applications. *ChemBioChem, 13*(18), 2642-2655.

Sugui, J. A., Pardo, J., Chang, Y. C., Zarember, K. A., Nardone, G., Galvez, E. M., et al. (2007). Gliotoxin is a virulence factor of Aspergillus fumigatus: GliP deletion attenuates virulence in mice immunosuppressed with hydrocortisone. *Eukaryotic Cell, 6*(9), 1562-1569.

Svab, Z., & Maliga, P. (1993). High-frequency plastid transformation in tobacco by selection for a chimeric aadA gene. *Proceedings of the National Academy of Sciences of the United States of America, 90*(3), 913-917.

Swimburne, T., & Brown, A. E. (1975). The biosynthesis of benzoic acid in bramley's seedling apples infected by nectria galligena bres. *Physiological Plant Pathology, 6*(3), 259-264.

Ta, P., Buchmeier, N., Newton, G. L., Rawat, M., & Fahey, R. C. (2011). Organic hydroperoxide resistance protein and ergothioneine compensate for loss of mycothiol in mycobacterium smegmatis mutants. *Journal of Bacteriology, 193*(8), 1981-1990.

Takemoto, D., Tanaka, A., & Scott, B. (2007). NADPH oxidases in fungi: Diverse roles of reactive oxygen species in fungal cellular differentiation. *Fungal Genetics and Biology, 44*(11), 1065-1076.

Tao, L., & Yu, J. (2011). AbaA and WetA govern distinct stages of Aspergillus fumigatus development. *Microbiology, 157*(2), 313-326.

Thon, M., Al Abdallah, Q., Hortschansky, P., Scharf, D. H., Eisendle, M., Haas, H., et al. (2010). The CCAAT-binding complex coordinates the oxidative stress response in eukaryotes. *Nucleic Acids Research, 38*(4), 1098-1113.

Thornalley, P. J. (1990). The glyoxalase system: New developments towards functional characterization of a metabolic pathway fundamental to biological life. *The Biochemical Journal, 269*(1), 1-11.

Tonnessen, B. W., Manosalva, P., Lang, J. M., Baraoidan, M., Bordeos, A., Mauleon, R., et al. (2015). Rice phenylalanine ammonia-lyase gene OsPAL4 is associated with broad spectrum disease resistance. *Plant Molecular Biology, 87*(3), 273-286.

Turrens, J. F. (2003). Mitochondrial formation of reactive oxygen species. *The Journal of Physiology, 552*(2), 335-344.

Twumasi-Boateng, K., Yu, Y., Chen, D., Gravelat, F. N., Nierman, W. C., & Sheppard, D. C. (2009). Transcriptional profiling identifies a role for BrlA in the response to nitrogen depletion and for StuA in the regulation of secondary metabolite clusters in Aspergillus fumigatus. *Eukaryotic Cell, 8*(1), 104-115.

Valiante, V., Jain, R., Heinekamp, T., & Brakhage, A. A. (2009). The MpkA MAP kinase module regulates cell wall integrity signaling and pyomelanin formation in Aspergillus fumigatus. *Fungal Genetics and Biology, 46*(12), 909-918.

Valiante, V., Macheleidt, J., Föge, M., & Brakhage, A. A. (2015). The Aspergillus fumigatus cell wall integrity signaling pathway: Drug target, compensatory pathways, and virulence. *Frontiers in Microbiology, 6*, 325.

Verwer, P. E., van Duijn, M. L., Tavakol, M., Bakker-Woudenberg, I. A., & van de Sande, W. W. (2012). Reshuffling of Aspergillus fumigatus cell wall components chitin and beta-glucan under the influence of caspofungin or nikkomycin Z alone or in combination. *Antimicrobial Agents and Chemotherapy, 56*(3), 1595-1598.

Vit, A., Mashabela, G. T., Blankenfeldt, W., & Seebeck, F. P. (2015). Structure of the Ergothioneine-Biosynthesis amidohydrolase EgtC. *ChemBioChem, 16*(10), 1490-1496.

Vit, A., Misson, L., Blankenfeldt, W., & Seebeck, F. P. (2014). Crystallization and preliminary X-ray analysis of the ergothioneine-biosynthetic methyltransferase EgtD. *Acta Crystallographica Section F: Structural Biology Communications, 70*(5), 676-680.

Vödisch, M., Scherlach, K., Winkler, R., Hertweck, C., Braun, H., Roth, M., et al. (2011). Analysis of the Aspergillus fumigatus proteome reveals metabolic changes and the activation of the pseurotin A biosynthesis gene cluster in response to hypoxia. *Journal of Proteome Research, 10*(5), 2508-2524.

Wang, D. N., Toyotome, T., Muraosa, Y., Watanabe, A., Wuren, T., Bunsupa, S., et al. (2014). GliA in Aspergillus fumigatus is required for its tolerance to gliotoxin and affects the amount of extracellular and intracellular gliotoxin. *Medical Mycology, 52*(5), 506-518.

Wang, M., You, J., Bemis, K. G., Tegeler, T. J., & Brown, D. P. (2008). Label-free mass spectrometry-based protein quantification technologies in proteomic analysis. *Briefings in Functional Genomics & Proteomics*, *7*(5), 329-339.

Ward, O., Qin, W., Dhanjoon, J., Ye, J., & Singh, A. (2005). Physiology and biotechnology of Aspergillus. *Advances in Applied Microbiology, 58*, 1-75.

Waring, P., Sjaarda, A., & Lin, Q. H. (1995). Gliotoxin inactivates alcohol dehydrogenase by either covalent modification or free radical damage mediated by redox cycling. *Biochemical Pharmacology*, *49*(9), 1195-1201.

Webb, K. J., Lipson, R. S., Al-Hadid, Q., Whitelegge, J. P., & Clarke, S. G. (2010). Identification of protein N-terminal methyltransferases in yeast and humans. *Biochemistry, 49*(25), 5225-5235.

Weidner, G., d'Enfert, C., Koch, A., Mol, P. C., & Brakhage, A. A. (1998). Development of a homologous transformation system for the human pathogenic fungus Aspergillus fumigatus based on the pyrG gene encoding orotidine 5′-monophosphate decarboxylase. *Current Genetics, 33*(5), 378-385.

Weisshaar, B., & Jenkins, G. I. (1998). Phenylpropanoid biosynthesis and its regulation. *Current Opinion in Plant Biology*, *1*(3), 251-257.

Wheeler, G. L., & Grant, C. M. (2004). Regulation of redox homeostasis in the yeast Saccharomyces cerevisiae. *Physiologia Plantarum, 120*(1), 12-20.

Wiemann, P., & Keller, N. P. (2014). Strategies for mining fungal natural products. *Journal of Industrial Microbiology & Biotechnology*, *41*(2), 301-313.

Wösten, H. A., Asgeirsdottir, S. A., Krook, J. H., Drenth, J. H., & Wessels, J. G. (1994). The fungal hydrophobin Sc3p self-assembles at the surface of aerial hyphae as a protein membrane constituting the hydrophobic rodlet layer. *European journal of cell biology*, *63*(1), 122-129.

Xiang, L., & Moore, B. S. (2005). Biochemical characterization of a prokaryotic phenylalanine ammonia lyase. *Journal of Bacteriology, 187*(12), 4286-4289.

Xiao, P., Shin, K. S., Wang, T., & Yu, J. H. (2010). Aspergillus fumigatus flbB encodes two basic leucine zipper domain (bZIP) proteins required for proper asexual development and gliotoxin production. *Eukaryotic Cell, 9*(11), 1711-1723.

Xie, Z. P., Staehelin, C., Vierheilig, H., Wiemken, A., Jabbouri, S., Broughton, W. J., et al. (1995). Rhizobial nodulation factors stimulate mycorrhizal colonization of nodulating and nonnodulating soybeans. *Plant Physiology, 108*(4), 1519-1525.

Yamada, A., Kataoka, T., & Nagai, K. (2000). The fungal metabolite gliotoxin: Immunosuppressive activity on CTL-mediated cytotoxicity. *Immunology Letters, 71*(1), 27-32.

Yoshida, L. S., Abe, S., & Tsunawaki, S. (2000). Fungal gliotoxin targets the onset of superoxide-generating NADPH oxidase of human neutrophils. *Biochemical and Biophysical Research Communications, 268*(3), 716-723.

Yu, J., & Keller, N. (2005). Regulation of secondary metabolism in filamentous fungi. *Annu.Rev.Phytopathol., 43,* 437-458.

Yu, J. H., Wieser, J., & Adams, T. H. (1996). The Aspergillus FlbA RGS domain protein antagonizes G protein signaling to block proliferation and allow development. *The EMBO Journal, 15*(19), 5184-5190.

Zhang, X., & Liu, C. (2015). Multifaceted regulations of gateway enzyme phenylalanine ammonia-lyase in the biosynthesis of phenylpropanoids. *Molecular Plant, 8*(1), 17-27.

Zhu, W., Smith, J. W., & Huang, C. M. (2010). Mass spectrometry-based label-free quantitative proteomics. *Journal of Biomedicine & Biotechnology, 2010*, 840518.

Chapter 9

Appendices

9.1 Appendix 1

Table 9.1: Proteins with significant log_2 fold change or unique/absent in *A. fumigatus* Δ*egtA*^{26933} compared to ATCC26933 under basal conditions. Data sorted by fold change, in descending order.

Protein Description	Present/log_2 (Fold Change)	p value	Peptides	Sequence coverage [%]	Protein IDs
Uncharacterized protein	Unique	n/a	2	2.9	AFUA_1G16010
HAD superfamily hydrolase, putative	Unique	n/a	5	15.5	AFUA_2G02580
Bax Inhibitor family protein	Unique	n/a	2	8.5	AFUA_5G09310
CaaX farnesyltransferase beta subunit Ram1	Unique	n/a	4	12.9	AFUA_4G10330
phenylalanine ammonia-lyase	2.70643	0.000689	26	52.8	AFUA_2G09110
tRNA dihydrouridine synthase	1.53089	0.014702	10	22.6	AFUA_1G14770
Endo alpha-1,4 polygalactosaminidase, putative	1.48557	0.030844	4	23	AFUA_3G07890
2-dehydropantoate 2-reductase	1.48361	0.018129	5	16.7	AFUA_4G13960
WD repeat-containing protein jip5	1.42535	0.049898	7	26.9	AFUA_6G07080
Uncharacterized protein	1.33556	0.00468	11	42.2	AFUA_3G09110
Polyadenylation factor subunit CstF64, putative	1.30692	0.02093	5	21.3	AFUA_2G09100
Methyltransferase SirN-like, putative	1.28453	0.020655	19	76	AFUA_8G00550
Methyltransferase LaeA-like, putative (VipC)	1.22923	0.015225	6	13.8	AFUA_8G01930
Sulfhydryl oxidase	1.22122	0.008832	7	37.3	AFUA_3G08850
GDSL Lipase/Acylhydrolase family protein	1.21561	0.026784	5	32.3	AFUA_2G08920
Uncharacterized protein	1.20463	0.005663	2	9.1	AFUA_1G11480
1,3-beta-glucanosyltransferase	1.17592	0.006731	4	8.8	AFUA_8G02130
Lysine decarboxylase-like protein	1.11025	0.000385	7	29.2	AFUA_6G04800
Oxidoreductase, 2OG-Fe(II) oxygenase family	1.10977	0.018011	16	58.7	AFUA_1G01000
60S ribosomal protein L44	1.10977	0.006855	4	12	AFUA_2G08130
YjgH family protein	1.10359	0.024331	7	56.3	AFUA_3G02253
Zinc-binding alcohol dehydrogenase, putative	1.05598	0.000562	20	75.6	AFUA_8G02430
Uncharacterized protein	1.05039	0.004103	3	50.6	AFUA_3G14660
Profilin	1.04314	0.003378	8	71.3	AFUA_4G03050
40S ribosomal protein S25, putative	1.03637	0.016534	5	32.3	AFUA_1G16523
Glutathione S-transferase, putative	1.02663	0.015653	12	53.2	AFUA_2G00590
Small nuclear ribonucleoprotein SmB, putative	-1.00329	0.004928	6	25.2	AFUA_4G07740
Oxidoreductase, short chain dehydrogenase/reductase family	-1.0044	0.00741	13	86.4	AFUA_5G14000
Cytochrome P450 monooxygenase, putative	-1.01068	0.030958	15	34.7	AFUA_6G02210
Uncharacterized protein	-1.03003	0.009562	11	30.5	AFUA_3G02430
Putative uncharacterized protein	-1.05502	0.011856	4	31.3	AFUA_1G07430
Alpha-1,4 glucan phosphorylase	-1.05664	0.037906	14	23.2	AFUA_1G12920
5-oxo-L-prolinase, putative	-1.08559	0.000788	65	63.9	AFUA_6G14330
Isoflavone reductase family protein (Oxidoreductase activty)	-1.09131	0.021158	13	57	AFUA_1G12510

Mitochondrial protein, putative	-1.13605	0.000355	8	55.9	AFUA_6G08630
Tripeptidyl-peptidase sed2	-1.15094	0.003075	14	34.6	AFUA_4G03490
ATP dependent RNA helicase (Dob1), putative	-1.20061	0.016778	14	19.1	AFUA_4G07160
50S ribosomal protein L30, putative	-1.20395	0.000141	5	52.1	AFUA_4G10480
Mitochondrial enoyl reductase, putative	-1.23179	0.001484	17	61.8	AFUA_3G03330
Pyruvate decarboxylase, putative	-1.23973	0.003236	12	37.2	AFUA_6G00750
Protein arginine N-methyltransferase	-1.26534	0.005959	14	24.1	AFUA_5G11610
Glutathione S-transferase, putative	-1.32809	0.006247	13	59.8	AFUA_4G14380
Isochorismatase family hydrolase, putative	-1.35348	0.000708	8	44.5	AFUB_024850
Cyanamide hydratase, putative	-1.5086	0.000348	10	59.8	AFUA_7G06270
RWD domain protein (Gir2), putative	-1.5132	0.027459	5	24.2	AFUA_4G12100
Ribonuclease T2-like	-1.52431	0.018544	2	5.1	AFUA_3G11220
Threonine aldolase, putative	-1.60586	0.010153	7	28.9	AFUA_7G06540
Ribosome biogenesis protein (Rrs1), putative	-1.62255	0.011722	4	30	AFUA_7G04430
DNA-directed RNA polymerases i, ii, and iii 145 kDa polypeptide	-1.73969	0.017096	2	26.9	AFUA_5G11120
HypA-like protein, putative	-1.902	0.022665	7	14.4	AFUA_5G03330
Oxidoreductase, zinc-binding dehydrogenase family	-2.01615	0.02697	12	61	AFUA_1G15610
Elongation of fatty acids protein	-2.05175	0.013248	4	14	AFUA_5G02760
Coatomer subunit epsilon, putative	-2.15529	0.012902	6	58	AFUA_1G13260
Importin beta-5 subunit, putative	-2.26175	0.006274	16	24.6	AFUA_2G15870
High expression lethality protein Hel10, putative	-3.18792	0.001458	4	39.1	AFUA_1G06580
GTP:AMP phosphotransferase, mitochondrial	Absent	n/a	4	25.1	AFUA_1G03420
CCAAT-binding factor complex subunit HapC	Absent	n/a	3	23.8	AFUA_1G03840
Tartrate dehydrogenase, putative	Absent	n/a	6	22.3	AFUA_1G04150
Protein vts1	Absent	n/a	5	11.1	AFUA_1G04990
MAP kinase kinase (Mkk2), putative	Absent	n/a	2	5.8	AFUA_1G05800
Golgi phosphoprotein 3 (GPP34) domain containing protein	Absent	n/a	7	35.1	AFUA_1G06630
Protein O-mannosyl transferase (PMT2)	Absent	n/a	3	4.1	AFUA_1G07690
Ankyrin repeat protein	Absent	n/a	4	30.1	AFUA_1G09700
Uncharacterized protein	Absent	n/a	12	14.3	AFUA_1G10400
Mitochondrial dynamin GTPase (Msp1), putative	Absent	n/a	8	11.3	AFUA_1G11970
Protein translocation complex componenet (Npl1), putative	Absent	n/a	8	15.8	AFUA_1G14940
Uncharacterized protein	Absent	n/a	6	16.4	AFUA_1G15830
Aminotransferase, class III	Absent	n/a	8	30.7	AFUA_1G16810
Conidial hydrophobin RodB	Absent	n/a	5	67.9	AFUA_1G17250
1-aminocyclopropane-1-carboxylate deaminase, putative	Absent	n/a	8	33.4	AFUA_2G01030
Prefoldin subunit 3, putative	Absent	n/a	5	35.2	AFUA_2G02230
Mitochondrial import inner membrane translocase subunit tim14	Absent	n/a	2	17.1	AFUA_2G02700
Histone deacetylase RpdA/Rpd3	Absent	n/a	5	9.3	AFUA_2G03390
Uridine kinase	Absent	n/a	7	18.5	AFUA_2G05430

NADH-ubiquinone oxidoreductase 64 kDa subunit, putative	Absent	n/a	6	11.4	AFUA_2G05450
Pre-mRNA-splicing factor cef1	Absent	n/a	9	15.2	AFUA_2G05540
Rho GTPase ModA, putative	Absent	n/a	3	15.1	AFUA_2G05740
Glutamate 5-kinase, putative	Absent	n/a	6	23	AFUA_2G07570
Folic acid synthesis protein	Absent	n/a	6	16.5	AFUA_2G09840
NOT2 family protein	Absent	n/a	6	13	AFUA_2G11130
Developmental regulator FlbA	Absent	n/a	9	17.8	AFUA_2G11180
Pre-rRNA processing protein Tsr1, putative	Absent	n/a	9	17.9	AFUA_2G12880
Chromosome segregation protein SudA, putative	Absent	n/a	10	10.5	AFUA_2G14080
Nuclear cohesin complex subunit (Psc3), putative	Absent	n/a	7	7.4	AFUA_2G16080
DNA-directed RNA polymerase III RPC4, putative	Absent	n/a	3	6.2	AFUA_2G16170
Amino acid transporter, putative	Absent	n/a	4	8.2	AFUA_2G17790
FAD-dependent oxygenase, putative	Absent	n/a	4	10.3	AFUA_3G00840
Chitin synthase activator (Chs3), putative	Absent	n/a	7	16.1	AFUA_3G05580
Exosome complex exonuclease Rrp4, putative	Absent	n/a	4	16.4	AFUA_3G05860
Pre-mRNA splicing factor, putative	Absent	n/a	6	14.7	AFUA_3G06440
NIPSNAP family protein	Absent	n/a	8	29.6	AFUA_3G06660
COP9 signalosome subunit 2 (CsnB), putative	Absent	n/a	6	15.7	AFUA_3G06700
Extracellular developmental signal biosynthesis protein FluG	Absent	n/a	8	15.8	AFUA_3G07140
Transcription elongation factor S-II	Absent	n/a	5	22	AFUA_3G07670
PX domain protein	Absent	n/a	7	7.6	AFUA_3G08020
Cell wall protein, putative	Absent	n/a	2	2.9	AFUA_3G08110
Uncharacterized protein	Absent	n/a	4	49.1	AFUA_3G08370
Glycine-rich RNA-binding protein, putative	Absent	n/a	3	45.8	AFUA_3G08580
Cell wall glucanase, putative	Absent	n/a	3	8	AFUA_3G09250
ADP-ribosylation factor 6, putative	Absent	n/a	6	53.8	AFUA_3G12080
Enoyl-CoA hydratase/isomerase family protein	Absent	n/a	4	15.1	AFUA_3G14520
Uncharacterized protein	Absent	n/a	4	16.8	AFUA_3G15010
Uncharacterized protein	Absent	n/a	2	6.8	AFUA_4G03890
Uncharacterized protein	Absent	n/a	4	12.6	AFUA_4G03990
Uncharacterized protein	Absent	n/a	2	15.1	AFUA_4G06220
Ribosome biogenesis protein ytm1	Absent	n/a	10	35.2	AFUA_4G07630
CaaX farnesyltransferase alpha subunit Ram2	Absent	n/a	4	15.9	AFUA_4G07800
Probable 4-hydroxyphenylpyruvate dioxygenase 2	Absent	n/a	6	24.1	AFUA_4G10620
DlpA domain protein	Absent	n/a	5	27	AFUA_4G10940
Proteasome activator subunit 4, putative	Absent	n/a	18	12.5	AFUA_4G11290
C6 finger domain protein, putative	Absent	n/a	7	15.5	AFUA_4G11850
Nitrilase, putitive	Absent	n/a	6	35	AFUA_4G12240
COP9 signalosome subunit 7 (CsnG), putative	Absent	n/a	5	28	AFUA_4G12630
Citrate lyase beta subunit, putative	Absent	n/a	6	24.2	AFUA_4G13030

ATP-dependent RNA helicase has1	Absent	n/a	8	14.8	AFUA_4G13330
Carboxypeptidase S1, putative	Absent	n/a	4	10.2	AFUA_5G01200
DUF455 domain protein	Absent	n/a	5	6.1	AFUA_5G01840
Glycogen synthase Gsy1, putative	Absent	n/a	6	9	AFUA_5G02480
Protein phosphatase regulatory subunit (Ssc1), putative	Absent	n/a	6	10.7	AFUA_5G02560
GTP cyclohydrolase I, putative	Absent	n/a	6	16.8	AFUA_5G03140
Translation initiation factor eIF4E3, putative	Absent	n/a	3	13.3	AFUA_5G03180
RNA polymerase II transcription elongation factor (Ctr9), putative	Absent	n/a	9	10.5	AFUA_5G05870
Uncharacterized protein	Absent	n/a	3	20.2	AFUA_5G08100
Cytochrome c oxidase assembly protein (Pet191), putative	Absent	n/a	2	26.5	AFUA_5G08965
Sec1 family superfamily	Absent	n/a	8	16.5	AFUA_5G10810
Uncharacterized protein	Absent	n/a	4	43.9	AFUA_5G12325
U6 small nuclear ribonucleoprotein (Lsm3), putative	Absent	n/a	3	74.7	AFUA_5G12570
Uncharacterized protein	Absent	n/a	5	17.2	AFUA_5G14865
Uncharacterized protein	Absent	n/a	2	15.3	AFUA_6G02800
FAD dependent oxidoreductase, putative	Absent	n/a	7	27.2	AFUA_6G04220
RNA polymerase II Elongator subunit, putative	Absent	n/a	8	14.4	AFUA_6G05090
Uncharacterized protein	Absent	n/a	6	49.4	AFUA_6G08070
Mitochondrial intermediate peptidase	Absent	n/a	7	9.6	AFUA_6G08640
Uncharacterized protein	Absent	n/a	3	15.2	AFUA_6G09030
Uncharacterized protein	Absent	n/a	4	16	AFUA_6G09090
Gliotoxin oxidoreductase GliT	Absent	n/a	9	43.4	AFUA_6G09740
Dynamin GTPase, putative	Absent	n/a	7	12.4	AFUA_6G11890
TPR repeat protein	Absent	n/a	6	22	AFUA_6G13600
Cystathionine gamma-synthase	Absent	n/a	7	30.6	AFUA_7G01590
Nuclear pore complex subunit Nup85, putative	Absent	n/a	8	10.7	AFUA_7G01940
Mitochondrial molecular chaperone (Atp12), putative	Absent	n/a	7	27.2	AFUA_7G02490
Guanyl-nucleotide exchange factor (Sec7), putative	Absent	n/a	18	12.6	AFUA_7G05700
Cytochrome P450 oxidoreductase OrdA-like, putative	Absent	n/a	5	11.9	AFUA_8G00510
Mannosyltransferase PMT4	Absent	n/a	3	5.4	AFUA_8G04500
Pirin, putative	Absent	n/a	6	33.4	AFUA_8G04510
COP9 signalosome subunit 1 (CsnA), putative	Absent	n/a	3	12.7	AFUA_8G04880
Integral membrane protein, putative	Absent	n/a	2	15.3	AFUA_8G07235

9.2 Appendix 2

Table 9.2. Proteins with significant log_2 fold change or unique/absent in *A. fumigatus* Δ*egtA*^{26933} compared to ATCC26933 under oxidative stress conditions. Data sorted by fold change, in descending order.

Protein Description	Present/log_2 (Fold Change)	p value	Peptides	Sequence coverage [%]	Protein IDs
GrpB domain protein	Unique	n/a	2	24.2	AFUA_1G01530
Ubiquitin carboxyl-terminal hydrolase	Unique	n/a	4	4.9	AFUA_1G07160
Pre-mRNA-processing ATP-dependent RNA helicase prp5	Unique	n/a	2	2.4	AFUA_1G10050
Transcriptional elongation factor Iws1, putative	Unique	n/a	4	13	AFUA_1G12260
37S ribosomal protein Rsm22	Unique	n/a	3	4.1	AFUA_2G02290
Chromosome segregation protein SudA, putative	Unique	n/a	7	7.9	AFUA_2G14080
Autophagy protein Atg20, putative	Unique	n/a	3	7.5	AFUA_2G14160
Epoxide hydrolase, putative	Unique	n/a	4	19	AFUA_2G16900
Uncharacterized protein	Unique	n/a	5	7.3	AFUA_2G17200
Septin	Unique	n/a	4	6.5	AFUA_3G07015
Uncharacterized protein	Unique	n/a	3	6.2	AFUA_3G08240
Protein kinase Yak1, putative	Unique	n/a	4	5.5	AFUA_4G03850
Chromatin modification-related protein eaf3	Unique	n/a	4	16.1	AFUA_4G10660
Splicing factor 3a subunit 3, putative	Unique	n/a	2	2.8	AFUA_5G02420
DnaJ chaperone (Caj1), putative	Unique	n/a	1	6.4	AFUA_6G06590
Actin binding protein, putative	Unique	n/a	2	9.6	AFUA_6G07150
Putative uncharacterized protein	Unique	n/a	3	4.7	AFUA_3G13465
Zinc-binding oxidoreductase CipB	Unique	n/a	6	28.8	AFUA_4G00700
HD superfamily hydrolase, putative	Unique	n/a	2	11.9	AFUA_1G03035
BAG domain protein	Unique	n/a	3	17	AFUA_1G06080
Golgi phosphoprotein 3 (GPP34) domain containing protein	Unique	n/a	5	25.8	AFUA_1G06630
Uncharacterized protein	Unique	n/a	2	2.9	AFUA_1G16010
Flavin containing amine oxidase, putative	Unique	n/a	3	9.3	AFUA_3G12150
Uncharacterized protein	Unique	n/a	3	10.4	AFUA_4G09260
ABC multidrug transporter, putative	Unique	n/a	1	0.5	AFUA_5G00790
Nuclear condensin complex subunit 3, putative	Unique	n/a	1	1.2	AFUA_5G02170
Pre-mRNA-splicing factor syf1	Unique	n/a	4	8.5	AFUA_5G11910
Putative uncharacterized protein	Unique	n/a	2	3.5	AFUA_1G16020
Nuclear export protein Noc3	Unique	n/a	2	3.2	AFUA_2G17050
RNA Polymerase II CTD phosphatase Fcp1, putative	Unique	n/a	1	1.8	AFUA_3G11410
Uncharacterized protein	Unique	n/a	2	2.6	AFUA_3G13300
Small nucleolar ribonucleoprotein complex subunit, putative	Unique	n/a	3	6.2	AFUA_4G07500
Cytochrome P450, putative	Unique	n/a	1	4	AFUA_5G01360
Alpha-1,2-mannosyltransferase (Alg2), putative	Unique	n/a	1	4.3	AFUA_5G13210

Mitochondrial intermediate peptidase	Unique	n/a	3	5.7	AFUA_6G08640
Noc1p protein, putative	Unique	n/a	2	4.6	AFUA_8G04660
IQ and HECT domain protein	Unique	n/a	4	5	AFUA_1G04210
TIM-barrel enzyme family protein	5.92033	0.000472	3	18.6	AFUA_1G10110
Uncharacterized protein	5.87209	0.032885	2	9.1	AFUA_4G06410
COP9 signalosome complex subunit 5	5.0354	0.001582	4	11.7	AFUA_2G16250
Steroid alpha reductase family protein	4.61499	0.00464	5	21.2	AFUA_4G10760
3-ketosteroid reductase	4.49051	0.003899	7	21.6	AFUA_4G11500
NADPH-dependent FMN reductase Lot6, putative	4.40163	0.00432	8	69.2	AFUA_7G06600
Small nuclear ribonucleoprotein SmD2, putative	4.21148	0.011957	3	40.2	AFUA_5G12910
WD repeat protein	4.09183	0.001544	8	12.7	AFUA_5G11870
Oligosaccharyl transferase subunit (Gamma), putative	4.00277	0.038989	4	22.5	AFUA_2G06280
Calcium homeostasis protein Regucalcin, putative	3.97213	0.001059	6	20.6	AFUA_4G08610
Asparaginyl-tRNA synthetase Slm5, putative	3.92433	0.003895	6	18.2	AFUA_3G09630
Glycogen branching enzyme GbeA, putative	3.86537	0.037875	5	11.2	AFUA_5G10540
tRNA (adenine(58)-N(1))-methyltransferase non-catalytic subunit trm6	3.77874	0.00946	6	17.7	AFUA_5G01850
Phenylalanine ammonia-lyase	3.72865	0.020255	26	55.8	AFUA_2G09110
BET3 family protein	3.71531	0.007944	3	12	AFUA_5G12880
Mitochondrial ATPase (Afg1), putative	3.67003	0.035905	6	16.2	AFUA_4G04130
WD repeat-containing protein jip5	3.66549	0.033602	5	18.8	AFUA_6G07080
Nucleoside-diphosphate-sugar epimerase family protein	3.62394	0.035036	5	24.1	AFUA_6G11740
Pyridoxal kinase, putative	3.61996	0.007665	7	34.6	AFUA_1G02900
Translation regulator GCD7	3.55368	0.00112	7	24.6	AFUA_1G09450
SNARE-dependent exocytosis protein (Sro7), putative	3.4968	0.034112	10	15.6	AFUA_3G11040
Thiamin pyrophosphokinase, putative	3.43252	0.026301	4	12.2	AFUA_1G01830
Rho GTPase activator (Rgd1), putative	3.40581	0.023563	6	15.7	AFUA_3G06280
Kynureninase 1	3.39219	0.004419	12	34	AFUA_2G10360
Exosome complex subunit Csl4, putative	3.35962	0.016873	4	26.9	AFUA_5G13530
NmrA-like family protein	3.19014	0.010049	8	44.7	AFUA_6G00280
Uncharacterized protein	3.17489	0.011677	8	11.1	AFUA_1G14500
Hexokinase family protein XprF, putative	3.15965	0.008759	7	13	AFUA_2G15700
Cystathionine beta-lyase MetG	3.09553	0.035534	8	32.5	AFUA_4G03950
C6 finger domain protein, putative	3.04109	0.039396	5	8.5	AFUA_6G07800
Uncharacterized protein	3.01403	0.001047	8	26.1	AFUA_4G11990
PAP2 domain protein	3.00705	0.000123	3	9.7	AFUA_4G08970
Pre-mRNA splicing factor, putative	2.95321	0.00563	3	7.1	AFUA_3G06440
RNA polymerase II transcription elongation factor (Ctr9), putative	2.91844	0.009561	10	12.6	AFUA_5G05870
GDSL Lipase/Acylhydrolase family protein	2.91671	0.020083	3	19.6	AFUA_2G08920
Hsp70 nucleotide exchange factor fes1	2.91037	0.015253	11	67.1	AFUA_6G04750
HMG box protein, putative	2.90121	0.004952	7	41.4	AFUA_1G04550

Uncharacterized protein	2.89507	0.007283	3	22.9	AFUA_1G00760
Oxidoreductase, 2OG-Fe(II) oxygenase family	2.88667	0.002938	18	60	AFUA_1G01000
Ankyrin repeat protein (Yar1), putative	2.8775	0.033214	5	35.7	AFUA_5G09560
Short chain dehydrogenase family protein	2.87187	0.011169	6	23	AFUA_1G16630
CsgA-like short chain dehydrogenase/reductase, putative	2.86184	0.046537	6	62.8	AFUB_075540
Heat shock protein Hsp30-like, putative	2.85856	0.043402	7	52.3	AFUA_6G06470
Small nuclear ribonucleoprotein SmE, putative	2.85356	0.04101	6	54.7	AFUA_7G05980
Isoleucyl-tRNA synthetase, putative	2.83275	0.023614	5	8.4	AFUA_7G01420
DSB repair complex subunit Ku70, putative	2.76057	0.014473	9	17.1	AFUA_5G07740
50S ribosomal subunit L7, putative	2.75017	0.016585	14	57.2	AFUA_5G06430
ATP-dependent RNA helicase fal1	2.73637	0.038245	19	40.2	AFUA_5G02410
Splicing factor 3B subunit 1, putative	2.73212	0.018136	11	14.3	AFUA_2G13780
Developmental regulator FlbA	2.72199	0.014741	12	21.5	AFUA_2G11180
uncharacterized protein	2.70833	0.015402	3	3.6	AFUA_2G08660
U-box domain protein, putative	2.69522	0.00639	9	46.1	AFUA_2G11040
WW domain protein	2.65057	0.024386	7	9.2	AFUA_6G06520
O-methyltransferase, putative	2.64354	0.005237	10	53.2	AFUA_6G01830
NifU-related protein	2.62307	0.048628	7	44.8	AFUA_1G04680
Aromatic-L-amino-acid decarboxylase, putative	2.60669	0.002154	19	36.3	AFUA_3G02240
Acid phosphatase, putative	2.60623	0.049938	5	25.3	AFUA_4G01070
RNA exonuclease Rex2, putative	2.59105	0.000845	5	30.4	AFUA_3G11820
Transcription initiation factor TFIID, 31kD subunit, putative	2.58688	0.016378	3	17.3	AFUA_1G14600
Flavin-binding monooxygenase-like protein	2.56424	0.027902	8	21.2	AFUA_6G01900
Dolichyl-diphosphooligosaccharide--protein glycosyltransferase subunit WBP1	2.53911	0.029135	13	32.9	AFUA_5G08970
Serine/threonine protein kinase, putative	2.53288	0.026905	9	20.2	AFUA_4G11890
BAR adaptor protein RVS161, putative	2.53092	0.004572	12	49.8	AFUA_5G05950
DUF567 domain protein	2.51696	0.036334	7	40.1	AFUA_8G05720
Ortholog(s) have cytochrome-c oxidase activity, role in aerobic respiration, mitochondrial electron transport, cytochrome c to oxygen and mitochondrial respiratory chain complex IV localization	2.50787	0.028945	5	21.3	AFUA_Mt00120
Methyltransferase LaeA-like, putative (VipC)	2.49862	0.000127	9	21.5	AFUA_8G01930
60S ribosomal protein L3	2.48244	0.01963	12	50.4	AFUA_1G12730
Zinc-binding alcohol dehydrogenase, putative	2.48156	0.001253	21	77.3	AFUA_8G02430
Uncharacterized protein	2.48149	0.046452	5	8.8	AFUA_5G08450
Acetyltransferase, GNAT family, putative	2.46315	0.020592	3	20.3	AFUA_4G02980
Short-chain dehydrogenase, putative	2.45341	0.019904	7	29.3	AFUA_8G00280
Alpha-amylase, putative	2.45109	0.009808	6	19.8	AFUA_3G00900
Transcription elongation factor S-II	2.44125	0.005319	3	13.2	AFUA_3G07670
Vacuolar targeting protein Atg24, putative	2.44043	0.027605	7	19.7	AFUA_4G12950

Mitochondrial DnaJ chaperone (Mdj1), putative	2.43118	0.013723	5	16.2	AFUA_2G11750
Calcineurin binding protein, putative	2.41938	0.010398	5	19.1	AFUA_2G13060
Nonsense-mediated mRNA decay protein 3	2.37081	0.000358	4	7.3	AFUA_2G16750
Myo-inositol-1(Or 4)-monophosphatase	2.36977	0.037423	6	29.1	AFUA_4G04200
O-methyltransferase, putative	2.36381	0.038931	13	66.7	AFUB_096510
Uncharacterized protein	2.35526	0.000228	7	7.9	AFUA_2G08640
Alpha-1,3-glucan synthase Ags1	2.32836	0.042328	4	2.6	AFUA_3G00910
Thioesterase family protein	2.32798	0.030021	5	23.5	AFUA_1G10800
Kinesin family protein	2.28591	0.031839	8	24.1	AFUA_1G01640
Golgi to endosome transport protein (Ent3), putative	2.28077	0.016134	10	32	AFUA_2G03650
Dynein light chain (Tctex1), putative	2.27221	0.014268	7	61.5	AFUA_1G09550
Uncharacterized protein	2.25293	0.039784	3	12.6	AFUA_4G07030
Uncharacterized protein	2.23964	0.033311	6	46.7	AFUA_3G07740
Sulfite reductase, putative	2.22575	0.003046	35	31.2	AFUA_2G15590
NADH-ubiquinone oxidoreductase subunit GRIM-19, putative	2.20179	0.038593	4	34.6	AFUA_3G08770
Translation initiation factor IF3, putative	2.17014	0.03893	4	11.2	AFUA_1G12160
Choline sulfatase, putative	2.16137	0.049261	15	39.4	AFUA_6G13440
uncharacterized protein	2.12057	0.037434	3	3.9	AFUA_6G03025
Stomatin family protein	2.07913	0.019136	14	49	AFUA_1G09780
KH domain RNA binding protein	2.07516	0.026911	16	53.7	AFUA_2G04940
Mitochondrial carrier protein, putative	2.0702	0.017636	5	31.9	AFUA_6G12550
Importin beta-3 subunit, putative	2.0596	0.002819	39	54.6	AFUA_1G06790
Class V chitinase, putative	2.04796	0.025086	14	56.8	AFUA_3G11280
Proteasome regulatory particle subunit (RpnE), putative	2.04714	0.004918	29	62.4	AFUA_3G06610
40S ribosomal protein S10a	2.04549	0.016185	7	50	AFUA_2G02150
Histone H2B	2.02733	0.014674	6	33.6	AFUA_3G05350
Aflatoxin B1-aldehyde reductase GliO-like, putative	2.01845	0.049263	13	48.3	AFUA_1G13370
Uridine nucleosidase Urh1, putative	1.97912	0.019106	5	22.9	AFUA_1G05530
Aspartic protease pep1	1.9734	0.034066	7	26.6	AFUA_5G13300
T-complex protein 1, zeta subunit, putative	1.94269	0.007998	30	74.1	AFUA_3G09590
AN1 zinc finger protein	1.91664	0.022847	3	11.2	AFUA_4G04280
DUF255 domain protein	1.88685	0.041084	12	20.8	AFUA_1G12370
40S ribosomal protein S13	1.87422	0.009102	5	26.6	AFUA_4G07640
Cytosine deaminase-uracil phosphoribosyltransferase fusion protein	1.86909	0.009581	11	49.6	AFUA_5G05460
TAM domain methyltransferase, putative	1.85912	0.018744	4	17.2	AFUA_2G15860
Polyketide synthase, putative	1.84371	0.002937	60	36.3	AFUA_1G01010
Glutaryl-CoA dehydrogenase, putative	1.83794	0.007301	10	41.1	AFUA_3G06040
COP9 signalosome subunit 1 (CsnA), putative	1.82649	0.032548	4	14.7	AFUA_8G04880
2-dehydropantoate 2-reductase	1.80192	0.041835	4	16.1	AFUA_3G00740
HAD superfamily hydrolase, putative	1.79199	0.02004	14	73.5	AFUA_6G10760

Heat shock protein Hsp98/Hsp104/ClpA, putative	1.77987	0.004247	54	53	AFUA_1G15270
Ubiquitin carboxyl-terminal hydrolase	1.76662	0.015637	15	85.2	AFUA_2G05590
Aspartyl aminopeptidase	1.75773	0.002988	20	56.7	AFUA_3G08290
General amidase, putative	1.74267	0.026522	9	23.1	AFUA_4G00370
COP9 signalosome subunit 8 (CsnH), putative	1.73581	0.037207	1	10.2	AFUA_8G04440
Kynurenine 3-monooxygenase	1.73399	0.029138	12	34.4	AFUA_6G07340
L-PSP endoribonuclease family protein, putative	1.71522	0.004075	3	22.7	AFUA_2G17470
Thioesterase family protein	1.68023	0.010773	5	32.2	AFUA_7G03960
NUDIX domain, putative	1.66635	0.008172	5	32.9	AFUA_5G13840
Alanine racemase family protein, putative	1.66134	0.020917	13	62.2	AFUA_4G04300
60S ribosomal protein L25, putative	1.65806	0.015796	7	47.7	AFUA_4G09000
Vacuolar ATP synthase catalytic subunit A, putative	1.65689	0.018725	40	63.8	AFUA_5G02370
Uncharacterized protein	1.6496	0.019697	2	7.2	AFUA_6G14120
Uncharacterized protein	1.64845	0.04011	5	34.4	AFUA_5G06960
Purple acid phosphatase	1.64701	0.040466	2	5.4	AFUA_5G01330
Pentafunctional AROM polypeptide	1.63777	9.59E-05	52	49.2	AFUA_1G13740
Glutamyl-tRNA synthetase	1.63324	0.000912	46	69.4	AFUA_5G03560
Cell wall integrity signaling protein Lsp1/Pil1, putative	1.63067	0.008446	10	41.5	AFUA_6G07520
40S ribosomal protein S5, putative	1.62899	0.024461	15	60.2	AFUA_1G15020
2-oxo acid dehydrogenases acyltransferase, putative	1.62889	0.037992	17	46.3	AFUA_4G12010
Mitochondrial import inner membrane translocase subunit TIM44	1.61088	0.024164	15	31.9	AFUA_1G09840
Uncharacterized protein	1.60551	0.022517	8	72.6	AFUA_8G00430
60S ribosomal protein L35Ae	1.59475	0.040963	6	42	AFUA_3G08460
Small oligopeptide transporter, OPT family	1.58771	0.02923	1	1.5	AFUA_2G15240
Phosphoinositide phospholipase C	1.57657	0.016158	8	17.9	AFUA_3G07940
uncharacterized protein	1.57177	0.041712	11	58	AFUA_2G02490
uncharacterized protein	1.5613	0.002834	4	43.9	AFUA_5G12325
Arginyl-tRNA synthetase	1.55487	0.000121	50	72.6	AFUA_2G14030
Hybrid NRPS/PKS enzyme, putative (PsoA)	1.54538	0.028801	45	16.2	AFUA_8G00540
Ubiquitin-protein ligase (Tom1), putative	1.54369	0.014006	54	17.3	AFUA_4G10780
Conserved lysine-rich protein, putative	1.5242	0.001805	33	66	AFUA_4G12450
Mitochondrial Hsp70 chaperone (Ssc70), putative	1.51405	0.024378	51	64.2	AFUA_2G09960
NADH-ubiquinone oxidoreductase 304 kDa subunit	1.50531	0.043681	16	52.1	AFUA_6G08810
Synaptobrevin-like protein Sybl1, putative	1.50039	0.021808	4	29.2	AFUA_6G11270
Calponin homology domain protein	1.49789	0.006881	6	10.6	AFUA_4G13250
G-protein complex gamma subunit GpgA	1.48694	0.049955	5	52.2	AFUA_1G05210
Methyltransferase SirN-like, putative	1.47973	0.022785	21	78.2	AFUA_8G00550
Sister chromatid separation protein (Src1), putative	1.45998	0.027908	5	9.3	AFUA_6G08530
AhpC/TSA family protein	1.44847	0.014711	11	54.1	AFUA_6G12500
Ribose phosphate diphosphokinase Prs1, putative	1.44778	0.038843	9	23.3	AFUA_7G05670

NADH-dependent flavin oxidoreductase, putative	1.43235	0.030737	33	76.1	AFUA_7G06420
Pyridoxal reductase (AKR8), putative	1.42837	0.01439	11	38.6	AFUA_1G10270
Tubulin subunit TubB	1.41187	0.026163	24	69.8	AFUA_2G14990
Aldehyde reductase (GliO), putative	1.40263	0.017969	28	84.1	AFUA_5G02020
WD repeat protein	1.40237	0.038759	8	12.5	AFUA_2G04360
ATP-dependent RNA helicase dbp2	1.39022	0.006535	20	43.5	AFUA_2G10750
Uncharacterized protein	1.38839	0.039818	2	11.2	AFUA_2G11650
Glycerol dehydrogenase (GldB), putative	1.37995	0.019009	30	85.5	AFUA_4G11730
Pre-mRNA-processing protein 45	1.35882	0.029083	2	5.2	AFUA_5G03050
Mitochondrial ribosomal protein S19, putative	1.35708	0.004164	6	61.7	AFUB_059030
OPA3 domain protein	1.35389	0.012597	2	5.8	AFUA_8G05670
Importin beta-1 subunit	1.35372	0.02131	29	53	AFUA_1G15720
37S ribosomal protein S25, mitochondrial	1.34439	0.02861	14	48.1	AFUA_4G07250
NRPS-like enzyme, putative	1.33723	0.041076	41	44.1	AFUA_5G10120
Amino acid transporter, putative	1.31178	0.039383	3	5.8	AFUA_4G07760
TPR domain protein	1.29981	0.017062	2	7.2	AFUA_4G12110
Arsenate reductase (Arc2), putative	1.27464	0.027714	9	63.3	AFUA_6G13400
Clathrin heavy chain	1.2721	0.013103	79	63.7	AFUA_4G07700
SnRNP assembly factor, putative	1.26941	0.013025	7	16.8	AFUA_4G07520
Amino-acid acetyltransferase, mitochondrial	1.2612	0.025429	3	4.7	AFUA_2G11490
Methionyl-tRNA synthetase	1.2505	0.017722	29	53.9	AFUA_1G09010
Ribulose-phosphate 3-epimerase	1.24989	0.043566	5	31.6	AFUA_2G15190
Metallopeptidase family M24, putative	1.2442	0.008232	6	17.3	AFUA_6G09190
Uncharacterized protein	1.24148	0.04921	4	9.5	AFUA_5G10850
2-methylcitrate dehydratase, putative	1.23478	0.009205	38	65.2	AFUA_6G03730
Uncharacterized protein	1.23095	0.038532	2	9.1	AFUA_4G09670
Glutathione S-transferase, putative	1.2279	0.045908	13	60.8	AFUA_2G00590
ATP-dependent RNA helicase mrh4, mitochondrial	1.22367	0.024149	3	5.5	AFUA_2G08480
DNA damage-inducible protein 1	1.21829	0.034152	24	73.8	AFUA_7G06050
Uncharacterized protein	1.21237	0.018308	2	17.6	AFUA_1G05350
Proteasome regulatory particle subunit Rpt5, putative	1.19989	0.031911	29	69	AFUA_1G06170
Uncharacterized protein	1.19715	0.031891	1	25	AFUA_1G12740
Short chain dehydrogenase/reductase family protein	1.17302	0.024341	13	80.5	AFUA_1G00990
Fructosamine-3-kinase, putative	1.16272	0.003539	13	47.4	AFUA_1G07040
DNA topoisomerase 2	1.15761	0.022823	4	3.5	AFUA_6G13690
Uncharacterized protein	1.15517	0.043732	9	53.3	AFUA_3G10390
General amidase, putative	1.14363	0.006564	9	23.5	AFUB_100900
Actin-related protein 2/3 complex subunit 1A, putative	1.14358	0.043581	18	60.1	AFUA_6G06500
Pyridoxamine phosphate oxidase, putative	1.13607	0.038128	17	52.4	AFUA_5G10650
GMC oxidoreductase, putative	1.12674	0.01303	28	56	AFUA_3G01580

Imidazole glycerol phosphate synthase subunit hisF	1.10807	0.024405	32	74.4	AFUA_2G06230
Lon protease homolog, mitochondrial	1.10384	0.039972	29	34.7	AFUA_2G11740
Alanine--tRNA ligase	1.09797	0.048228	56	66.8	AFUA_8G03880
Uncharacterized protein	1.09239	0.033914	2	34.8	AFUA_4G12220
YjgH family protein	1.08735	0.008854	8	59.6	AFUA_3G02253
Clustered mitochondria protein homolog	1.07508	0.009679	52	52.9	AFUA_3G10800
40S ribosomal protein S10b	1.06593	0.01039	7	47.1	AFUA_6G12660
Uncharacterized protein	1.04523	0.022485	14	51.2	AFUA_5G09500
UBX domain protein	1.03996	0.031287	3	7.2	AFUA_3G06360
Ribosome associated DnaJ chaperone Zuotin, putative	1.03867	0.040415	18	47.8	AFUA_4G03650
Uncharacterized protein	1.03697	0.046468	29	60	AFUA_3G12690
DUF636 domain protein	1.03567	0.025099	10	87.5	AFUA_2G15290
Nucleoporin SONB, putative	1.03057	0.029446	17	12.7	AFUA_4G11070
Actin cortical patch component, putative	1.02943	0.020218	26	62.6	AFUA_2G06040
Phosphatidylserine synthase	1.02661	0.007655	1	4.9	AFUA_4G13680
RNase III domain protein	1.01868	0.023784	6	23.2	AFUA_5G09670
Protein transport protein sec24	1.01468	0.001738	29	48.6	AFUA_6G12830
Ribose 5-phosphate isomerase A	1.00722	0.034898	12	47.8	AFUA_6G10610
37S ribosomal protein Mrp10, mitochondrial	1.00706	0.011891	2	16.8	AFUA_1G04400
Aldehyde dehydrogenase, putative	-1.07759	0.046538	24	53.7	AFUA_2G00720
Cytochrome B	-1.13698	0.017889	2	4.9	AFUA_Mt00001
Transcriptional elongation regulator Elc1/Elongin C, putative	-1.16689	0.012493	2	17.3	AFUA_6G10530
Trimethyllysine dioxygenase TmlH, putative	-1.27237	0.027847	6	25.2	AFUA_1G06180
Cyclin Ccl1, putative	-1.28282	0.029271	2	4.2	AFUA_5G07030
GDP-mannose pyrophosphorylase A	-1.41181	0.011752	17	49.4	AFUA_6G07620
uncharacterized protein	-1.4512	0.040524	3	13	AFUA_5G04380
uncharacterized protein	-1.59667	0.049842	5	28.6	AFUA_2G12100
tRNA splicing 2' phosphotransferase 1	-1.60176	0.03059	3	11	AFUA_2G02890
Peptide methionine sulfoxide reductase	-1.65017	0.028258	6	57.6	AFUA_2G03140
Kelch repeats protein, putative	-1.766	0.029777	3	5.5	AFUA_2G04970
Peptidyl-prolyl cis-trans isomerase	-1.82857	0.035488	12	66	AFUB_064740
Succinyl-CoA:3-ketoacid-coenzyme A transferase	-1.93972	0.00699	24	52.9	AFUA_6G12250
Glycerol kinase, putative	-1.99179	0.048473	7	20.7	AFUA_4G11540
Na/K ATPase alpha 1 subunit, putative	-1.9937	0.0284	18	23.4	AFUA_7G04570
CobW domain protein	-2.03634	0.039494	16	35.9	AFUA_8G02620
Nuclear pore protein (Nic96), putative	-2.07972	0.04427	10	16.2	AFUA_4G04720
DsDNA-binding protein PDCD5, putative	-2.12738	0.031351	4	32.5	AFUA_3G06420
BolA domain protein	-2.17693	0.004201	6	51.1	AFUA_7G01520
Vacuolar protein sorting-associated protein 27	-2.59406	0.000905	6	10.3	AFUA_2G04740
DnaJ domain protein	-2.66553	0.03948	4	25.6	AFUA_8G04610

rRNA biogenesis protein RRP5, putative	-2.81516	0.040028	12	10.4	AFUA_2G16040
Endoribonuclease ysh1	-3.13103	0.044313	5	8	AFUA_1G16800
C2H2 finger domain protein, putative	-4.06568	0.007799	3	5.3	AFUA_1G02010
Ribonuclease T2-like	-4.09965	0.004917	3	12.7	AFUA_3G11220
Extracellular serine-rich protein, putative	-4.26486	0.000262	5	9.1	AFUA_3G07870
Thiamine pyrophosphate enzyme, putative	-4.51397	0.002554	3	9.8	AFUA_6G11680
Uncharacterized protein	Absent	n/a	1	16.7	AFUA_2G05050
Uncharacterized protein	Absent	n/a	2	9.9	AFUA_4G08820
TRAPP complex component Bet3, putative	Absent	n/a	2	12.7	AFUA_7G02270
GABA permease (Uga4), putative	Absent	n/a	1	3.4	AFUA_4G03370
Ferrooxidoreductase Fet3, putative	Absent	n/a	2	5.6	AFUA_5G03790
Protein bfr2	Absent	n/a	3	6.2	AFUA_6G09820
Oxidoreductase CipA-like, putative	Absent	n/a	3	13.4	AFUA_1G12460
Acetyltransferase, GNAT family family	Absent	n/a	2	12	AFUA_3G01260
Splicing factor 3b, subunit 2, 145kD	Absent	n/a	3	8.3	AFUA_5G04420
TRAPP complex component Bet3, putative	Absent	n/a	2	5.4	AFUA_5G12350
Uncharacterized protein	Absent	n/a	2	21.9	AFUA_5G13100
Dynamin GTPase, putative	Absent	n/a	5	8.9	AFUA_6G11890
rRNA maturation protein (Nop14), putative	Absent	n/a	2	2	AFUA_8G04220

9.3 Appendix 3

Table 9.3. Proteins with significant $\log_2$ fold change or unique/absent in *A. fumigatus* Δ*egtA*^{26933} under oxidative stress conditions compared to Δ*egtA*^{26933} under basal conditions. Data sorted by fold change, in descending order.

Protein Description	Present/$\log_2$ (Fold Change)	p value	Peptides	Sequence coverage [%]	Protein IDs
Glycogen debranching enzyme Gdb1, putative	Unique	n/a	6	5	AFUA_1G02140
Uncharacterized protein	Unique	n/a	3	15.1	AFUA_1G04610
Protein vts1	Unique	n/a	5	11.4	AFUA_1G04990
Uncharacterized protein	Unique	n/a	2	17.6	AFUA_1G05350
Uridine nucleosidase Urh1, putative (EC 3.2.2.-)	Unique	n/a	5	22.9	AFUA_1G05530
GTP binding protein, putative	Unique	n/a	8	27.6	AFUA_1G05560
Ribosome biogenesis protein Ssf2, putative	Unique	n/a	2	5.6	AFUA_1G06230
Protein O-mannosyl transferase	Unique	n/a	4	5.8	AFUA_1G07690
50S ribosomal protein L17	Unique	n/a	5	34	AFUA_1G09410
37S ribosomal protein S11, putative	Unique	n/a	3	18.5	AFUA_1G09850
Casein kinase 2 beta' regulatory subunit Ckb2, putative (EC 2.7.1.-)	Unique	n/a	2	8.5	AFUA_1G09950
TIM-barrel enzyme family protein	Unique	n/a	3	18.6	AFUA_1G10110
Pre-mRNA-splicing factor prp46 (Pre-mRNA-processing protein 46)	Unique	n/a	5	14.3	AFUA_1G10710

Prolyl-tRNA synthetase (EC 6.1.1.15)	Unique	n/a	6	13.5	AFUA_1G10750
Myosin class II heavy chain (MHC), putative	Unique	n/a	7	4.4	AFUA_1G11450
Translation initiation factor IF3, putative	Unique	n/a	4	13.3	AFUA_1G12160
ATP-dependent RNA helicase drs1 (EC 3.6.4.13)	Unique	n/a	4	4.9	AFUA_1G14990
Uncharacterized protein	Unique	n/a	5	14.2	AFUA_1G15830
Probable mitochondrial transport protein (Fungal sideroflexin)	Unique	n/a	5	16.3	AFUA_1G16750
Pre-mRNA splicing factor (Prp24), putative	Unique	n/a	8	7	AFUA_2G01820
Ubiquinone biosynthesis protein Coq7, putative	Unique	n/a	4	24.9	AFUA_2G01890
Mitochondrial import inner membrane translocase subunit tim14 (Presequence translocated-associated motor subunit pam18)	Unique	n/a	2	17.1	AFUA_2G02700
Carboxyphosphonoenolpyruvate phosphonomutase, putative (EC 4.1.3.30)	Unique	n/a	3	11.1	AFUA_2G03820
Succinate dehydrogenase assembly factor 3, mitochondrial (SDH assembly factor 3) (SDHAF3)	Unique	n/a	5	38.6	AFUA_2G05090
NADH-ubiquinone oxidoreductase 64 kDa subunit, putative (EC 1.6.99.3)	Unique	n/a	4	6.9	AFUA_2G05450
Pre-mRNA-splicing factor cef1	Unique	n/a	7	12.9	AFUA_2G05540
mRNA decapping hydrolase, putative	Unique	n/a	8	30.5	AFUA_2G05580
Autophagy ubiquitin-activating enzyme ApgG, putative	Unique	n/a	6	9.1	AFUA_2G06250
Eukaryotic translation initiation factor 5, putative	Unique	n/a	3	6.2	AFUA_2G08990
Kynureninase 1 (EC 3.7.1.3) (Biosynthesis of nicotinic acid protein 5-1) (L-kynurenine hydrolase 1)	Unique	n/a	10	27.9	AFUA_2G10360
Nucleolar GTP-binding protein 1	Unique	n/a	7	13.7	AFUA_2G11510
Uncharacterized protein	Unique	n/a	2	11	AFUA_2G12540
Translocation protein Sec62, putative	Unique	n/a	4	12	AFUA_2G12580
Urease accessory protein UreG, putative	Unique	n/a	8	36.2	AFUA_2G12900
Uncharacterized protein	Unique	n/a	2	6.9	AFUA_2G14070
Ubiquitin carboxyl-terminal hydrolase (EC 3.4.19.12)	Unique	n/a	8	6.6	AFUA_2G14130
Nuclear cohesin complex subunit (Psc3), putative	Unique	n/a	8	7.6	AFUA_2G16080
Acyl-CoA dehydrogenase, putative	Unique	n/a	3	8.4	AFUA_3G01920
U2 auxiliary factor small subunit, putative	Unique	n/a	4	36.8	AFUA_3G02380
Spindle poison sensitivity protein Scp3, putative	Unique	n/a	3	7.3	AFUA_3G05570
Uncharacterized protein	Unique	n/a	2	11	AFUA_3G05980
Transcription elongation factor S-II	Unique	n/a	3	13.5	AFUA_3G07670
Probable dipeptidyl-aminopeptidase B (DPAP B) (EC 3.4.14.5)	Unique	n/a	6	9.6	AFUA_3G07850
PX domain protein	Unique	n/a	6	6.2	AFUA_3G08020
Uncharacterized protein	Unique	n/a	3	6.2	AFUA_3G08240
RNA binding protein, putative	Unique	n/a	3	5.6	AFUA_3G09620
Asparaginyl-tRNA synthetase Slm5, putative (EC 6.1.1.22)	Unique	n/a	2	4.9	AFUA_3G09630
ADP-ribosylation factor 6, putative	Unique	n/a	7	65.8	AFUA_3G12080
Queuine tRNA-ribosyltransferase (EC 2.4.2.29)	Unique	n/a	7	31.2	AFUA_4G04260
AN1 zinc finger protein	Unique	n/a	3	11.2	AFUA_4G04280

Uncharacterized protein	Unique	n/a	2	15.1	AFUA_4G06220
Ribosome biogenesis protein ytm1	Unique	n/a	10	30.3	AFUA_4G07630
40S ribosomal protein S13	Unique	n/a	5	26.6	AFUA_4G07640
CaaX farnesyltransferase alpha subunit Ram2 (EC 2.5.1.-)	Unique	n/a	4	15.9	AFUA_4G07800
Sphinganine-1-phosphate aldolase BST1, putative (EC 4.1.2.27)	Unique	n/a	3	9.6	AFUA_4G10470
DlpA domain protein	Unique	n/a	3	14.9	AFUA_4G10940
TPR domain protein	Unique	n/a	2	7.2	AFUA_4G12110
Calponin homology domain protein	Unique	n/a	6	10.6	AFUA_4G13250
DUF455 domain protein	Unique	n/a	3	5.1	AFUA_5G01840
Translation initiation factor eIF4E3, putative	Unique	n/a	3	13.3	AFUA_5G03180
Pyruvate dehydrogenase kinase, putative (EC 2.7.1.-)	Unique	n/a	6	14.3	AFUA_5G03240
Thymidylate kinase (EC 2.7.4.9)	Unique	n/a	7	36.2	AFUA_5G03460
Transcription elongation factor spt4 (Chromatin elongation factor spt4)	Unique	n/a	3	34	AFUA_5G06690
Uncharacterized protein	Unique	n/a	5	34.4	AFUA_5G06960
NADH-ubiquinone oxidoreductase B12 subunit, putative	Unique	n/a	2	23.2	AFUA_5G07380
Nuclear migration protein (ApsA), putative	Unique	n/a	5	3.2	AFUA_5G07710
MutT/nudix family protein	Unique	n/a	4	28.2	AFUA_5G08240
WD repeat protein	Unique	n/a	4	14.7	AFUA_5G08320
U1 small nuclear ribonucleoprotein 70 kDa	Unique	n/a	4	14.2	AFUA_5G13480
CCCH finger DNA binding protein, putative	Unique	n/a	5	16.1	AFUA_5G13930
3' exoribonuclease family protein (EC 3.1.-.-)	Unique	n/a	2	7.8	AFUA_6G02160
Aspartate aminotransferase (EC 2.6.1.1)	Unique	n/a	8	24.3	AFUA_6G02490
Uncharacterized protein AFUA_6G02800	Unique	n/a	3	18.2	AFUA_6G02800
Probable aspartic-type endopeptidase opsB (EC 3.4.23.-)	Unique	n/a	6	26.4	AFUA_6G05350
Endoplasmic reticulum DnaJ domain protein Erj5, putative	Unique	n/a	3	9.3	AFUA_6G06610
COPII vesicles protein Yip3, putative	Unique	n/a	4	27.6	AFUA_6G06620
WD repeat-containing protein jip5	Unique	n/a	5	18.8	AFUA_6G07080
mRNA splicing factor (Prp17), putative	Unique	n/a	2	3.8	AFUA_6G07300
Uncharacterized protein	Unique	n/a	3	22.5	AFUA_6G07550
DNA polymerase V, putative (EC 2.7.7.7)	Unique	n/a	11	13.9	AFUA_6G08170
Ubiquitin-protein ligase E3 component (UBR1), putative	Unique	n/a	8	4	AFUA_6G08420
Uncharacterized protein	Unique	n/a	3	12.1	AFUA_6G09090
ABC transporter, putative	Unique	n/a	8	17.6	AFUA_6G11360
TPR repeat protein	Unique	n/a	3	8.2	AFUA_6G13600
Mitochondrial molecular chaperone (Atp12), putative	Unique	n/a	6	20.3	AFUA_7G02490
Amine oxidase (EC 1.4.3.-)	Unique	n/a	5	10.8	AFUA_7G04180
Serine/threonine protein kinase, putative (EC 2.7.1.-)	Unique	n/a	4	11.1	AFUA_7G04550
Glyoxalase family protein	Unique	n/a	2	9.3	AFUA_7G05015
Small nuclear ribonucleoprotein SmE, putative	Unique	n/a	6	54.7	AFUA_7G05980
Threonine aldolase, putative (EC 4.1.2.-)	Unique	n/a	8	32.2	AFUA_7G06540

Uncharacterized protein	Unique	n/a	14	19.2	AFUA_8G00780
Thioredoxin, putative	Unique	n/a	2	14.7	AFUA_8G01090
DNA repair/transcription protein, putative	Unique	n/a	8	11	AFUA_8G05370
Dehydrogenase, putative	Unique	n/a	5	25	AFUA_8G05760
Alanyl-tRNA synthetase, putative (EC 6.1.1.7)	Unique	n/a	5	31.9	AFUA_8G07110
Hybrid PKS/NRPS enzyme EqiS-like, putative	Unique	n/a	2	0.4	AFUB_045790
Small nuclear ribonucleoprotein (LSM7), putative	2.53918	0.0447206	4	20.1	AFUA_1G14290
High expression lethality protein Hel10, putative	2.46315	0.0273076	5	39.6	AFUA_1G06580
Succinate dehydrogenase subunit CybS, putative	2.38886	0.0316124	4	29.4	AFUA_1G15590
Isochorismatase family hydrolase, putative	2.08009	0.0234628	6	68	AFUA_6G12220
Elongation of fatty acids protein (EC 2.3.1.199) (Very-long-chain 3-oxoacyl-CoA synthase)	2.02084	0.0287129	4	16	AFUA_5G02760
Small nuclear ribonucleoprotein SmB, putative	1.3701	0.000483799	6	25.2	AFUA_4G07740
Heat shock protein Hsp30-like, putative	1.33229	0.00951935	7	52.3	AFUA_6G06470
Translational activator, putative	1.30078	0.0252425	43	25.4	AFUA_2G07960
Alpha,alpha-trehalose-phosphate synthase (UDP-forming) (EC 2.4.1.15) (Trehalose-6-phosphate synthase)	1.29376	0.036481	13	35.1	AFUA_2G04010
Molybdopterin binding domain protein	1.13164	0.0124949	7	34.7	AFUA_5G11210
RNA processing protein Emg1, putative	1.11232	0.033944	9	40.9	AFUA_3G06010
RNase III domain protein	1.08371	0.017722	7	25.9	AFUA_5G09670
Cyclin dependent kinase inhibitor Pho81, putative	1.06558	0.00839668	15	22.5	AFUA_4G06020
Small nuclear ribonucleoprotein SmD3, putative	1.02921	0.00392039	5	37.9	AFUA_4G10240
Hsp70 nucleotide exchange factor fes1	1.0107	0.00151961	11	67.1	AFUA_6G04750
Uncharacterized protein	1.001	0.0368742	2	10.3	AFUA_3G05670
Phytanoyl-CoA dioxygenase family protein	-1.00669	0.0173754	4	18.4	AFUA_2G01850
SnRNP and snoRNP protein (Snu13), putative	-1.01382	0.0283058	3	52.4	AFUA_2G05950
Superoxide dismutase copper chaperone Lys7, putative	-1.11686	0.0497396	10	54.7	AFUA_2G09700
Uncharacterized protein	-1.13093	0.00676312	6	45.8	AFUA_1G09030
Uncharacterized protein	-1.32621	0.00978505	9	46.7	AFUA_2G04930
PH domain protein	-1.34678	0.000211844	11	27.1	AFUA_6G07910
MFS peptide transporter Ptr2, putative	-1.36993	0.00945255	3	6.9	AFUA_7G01490
Uncharacterized protein	-1.48516	0.0439162	8	72.6	AFUA_8G00430
Uncharacterized protein	-1.61708	0.0410222	7	66.9	AFUA_6G02830
Mannitol-1-phosphate 5-dehydrogenase (M1PDH) (MPD) (MPDH)	-1.63191	0.0147944	14	54.6	AFUA_2G10660
Uncharacterized protein	-3.13222	0.0487647	2	8.4	AFUA_3G03610
DNA-directed RNA polymerase I, II, and III subunit Rpb6 (EC 2.7.7.6)	Absent	n/a	2	13	AFUA_1G05160
General amidase, putative	Absent	n/a	5	10.2	AFUA_1G14530
Phosphoesterase superfamily protein (EC 3.1.4.-)	Absent	n/a	5	15.4	AFUA_1G17590
TOR signalling pathway protein TipA, putative	Absent	n/a	3	9.4	AFUA_2G07540
NAD(P)H-hydrate epimerase (EC 5.1.99.6) (NAD(P)HX epimerase)	Absent	n/a	3	28.7	AFUA_5G08360

ABC transporter, putative (EC 3.6.3.-)	Absent	n/a	12	11.2	AFUA_5G10510
Bis(5'-nucleosyl)-tetraphosphatase, putative	Absent	n/a	2	7.5	AFUA_8G05000
TAM domain methyltransferase, putative	Absent	n/a	3	13.5	AFUA_2G15860

9.4 Appendix 4

Table 9.4. Proteins with significant log_2 fold change or unique/absent in *A. fumigatus* ATCC26933 under oxidative stress conditions compared to ATCC26933 under basal conditions. Data sorted by fold change, in descending order.

Protein Description	Present/log_2 (Fold Change)	p value	Peptides	Sequence coverage [%]	Protein IDs
Probable dipeptidyl-aminopeptidase B (DPAP B) (EC 3.4.14.5)	Unique	n/a	3	6.6	AFUA_3G07850
N-acetyltransferase family protein, putative	Unique	n/a	5	16.1	AFUA_4G10930
Metallo-beta-lactamase family protein	Unique	n/a	5	28.9	AFUA_5G12770
Mitochondrial phosphate carrier protein (Ptp), putative	Unique	n/a	8	30.2	AFUA_1G02730
Inosine-5'-monophosphate dehydrogenase (IMP dehydrogenase) (IMPD) (IMPDH) (EC 1.1.1.205)	Unique	n/a	31	76.6	AFUA_2G03610
Vacuolar protein sorting-associated protein 27	Unique	n/a	8	16.2	AFUA_2G04740
Ribonucleoprotein, putative	Unique	n/a	4	20.1	AFUA_7G05810
Uncharacterized protein	Unique	n/a	3	7	AFUA_1G09570
Uncharacterized protein	Unique	n/a	2	27.5	AFUA_3G09870
Uncharacterized protein	Unique	n/a	7	22.2	AFUA_4G14050
Thymidylate kinase (EC 2.7.4.9)	Unique	n/a	3	22.2	AFUA_5G03460
HypA-like protein, putative	1.61045	0.00147373	11	27.4	AFUA_5G03330
Glycine-rich RNA-binding protein, putative	1.58587	0.0280039	3	45.8	AFUA_3G08580
CHCH domain protein	1.55624	0.0263444	3	12.7	AFUA_3G06370
Protein arginine methyltransferase RmtB	1.48822	0.0106819	5	11.8	AFUA_3G12490
GNAT family N-acetyltransferase, putative	1.42225	0.00392018	5	47.8	AFUA_3G00870
SET domain protein	1.37637	0.0198835	7	20.1	AFUA_6G04520
Uncharacterized protein	1.33313	0.00935387	4	8.7	AFUA_4G04190
Branchpoint-bridging protein	1.30618	0.0403665	5	12.9	AFUA_3G10840
Polyadenylation factor subunit CstF64, putative	1.29843	0.0305713	5	24.3	AFUA_2G09100
DSB repair complex subunit Ku70, putative	1.20911	0.00753736	5	10.1	AFUA_5G07740
tRNA-dihydrouridine(47) synthase [NAD(P)(+)] (EC 1.3.1.89) (tRNA-dihydrouridine synthase 3)	1.17689	0.0207612	9	19.3	AFUA_1G14770
Ankyrin repeat protein	1.11234	0.0262974	7	53.8	AFUA_1G06370
Uncharacterized protein	1.10887	0.00174686	4	39.6	AFUA_1G01950
Ribosome biogenesis GTPase Lsg1, putative	1.08539	0.0381372	8	13.9	AFUA_5G06510
Guanylate kinase (EC 2.7.4.8)	1.04394	0.00622572	13	64	AFUA_1G08840
Chromatin remodeling complex subunit (Arp8), putative	1.03054	0.00653048	10	18.1	AFUA_2G10990
Uncharacterized protein	1.01566	0.0363161	13	20.8	AFUA_1G10440

60S ribosomal protein L24a	-1.00594	0.0373174	5	23.8	AFUA_6G02440
Uncharacterized protein	-1.03263	0.00254852	10	64.1	AFUA_3G00960
Riboflavin kinase (EC 2.7.1.26) (Flavin mononucleotide kinase 1)	-1.04681	0.0470412	6	63.6	AFUA_2G05820
Isocitrate dehydrogenase LysB (EC 1.1.1.41)	-1.10504	0.00302761	17	50.8	AFUA_6G07390
Calcium/calmodulin-dependent protein kinase, putative (EC 2.7.11.17)	-1.12351	0.0266042	11	36.4	AFUA_2G13680
Isoflavone reductase family protein (EC 1.3.1.-)	-1.15597	0.0206647	12	51.9	AFUA_1G12510
Zinc-containing alcohol dehydrogenase, putative (EC 1.1.1.1)	-1.2389	0.00058003	15	63.5	AFUA_4G08240
Phosducin family protein	-1.27893	0.00735141	6	27.4	AFUA_2G02550
Electron transfer flavoprotein-ubiquinone oxidoreductase (EC 1.5.5.1)	-1.2864	0.0158434	8	20.6	AFUA_3G10110
CsgA-like short chain dehydrogenase/reductase, putative	-1.39785	0.00306685	4	52.1	AFUB_075540
ABC metal ion transporter, putative	-1.48928	0.0421382	10	9.1	AFUA_5G07970
mRNA decapping hydrolase, putative	-1.55983	0.0471714	9	37.2	AFUA_2G05580
Ribosome biogenesis protein Ria1, putative	-1.56757	0.0167107	12	14.9	AFUA_5G13520
DNA-directed RNA polymerase III RPC4, putative	-1.63323	0.0075939	3	6.2	AFUA_2G16170
Oxidoreductase, zinc-binding dehydrogenase family, putative (EC 1.3.1.-)	-1.65097	0.0348013	12	61	AFUA_1G15610
Transcription elongation factor S-II	-1.70446	0.0230974	4	18.4	AFUA_3G07670
Oxidoreductase, short chain dehydrogenase/reductase family (EC 1.1.1.159)	-2.03448	0.000278332	13	86.4	AFUA_5G14000
SnRNP and snoRNP protein (Snu13), putative	-2.60299	0.022395	3	52.4	AFUA_2G05950
Nucleoporin NUP49/NSP49, putative	-4.38796	2.46E-05	4	12.5	AFUA_6G10730
HD superfamily hydrolase, putative	Absent	n/a	4	31.3	AFUA_1G03035
Acetylserotonin methytransferase-like protein (ASMTL), putative	Absent	n/a	2	9.2	AFUA_1G15580
Citrate lyase beta subunit, putative (EC 4.1.3.6)	Absent	n/a	4	18	AFUA_4G13030
Vacuolar protein sorting/targeting protein 10 (Carboxypeptidase Y receptor) (CPY receptor) (Sortilin vps10)	Absent	n/a	6	5.3	AFUA_8G02780
CCAAT-binding factor complex subunit HapC	Absent	n/a	3	23.8	AFUA_1G03840
BCAS2 family protein	Absent	n/a	6	47.7	AFUA_1G06460
Golgi phosphoprotein 3 (GPP34) domain containing protein	Absent	n/a	7	35.1	AFUA_1G06630
Fatty acid hydroxylase, putative (EC 1.14.-.-)	Absent	n/a	5	14.8	AFUA_1G15820
Bax Inhibitor family protein	Absent	n/a	3	12.2	AFUA_2G03220
NOT2 family protein	Absent	n/a	4	8.1	AFUA_2G11130
Amino acid transporter, putative	Absent	n/a	4	8.2	AFUA_2G17790
C-4 methyl sterol oxidase Erg25, putative (EC 1.-.-.-)	Absent	n/a	4	16.9	AFUA_4G04820
Aldo-keto reductase (AKR), putative	Absent	n/a	7	28	AFUA_5G01910
Pheromone-processing carboxypeptidase kex1 (EC 3.4.16.6) (Carboxypeptidase D)	Absent	n/a	3	6.5	AFUA_1G08940
Pre-mRNA-splicing factor cef1	Absent	n/a	7	9.3	AFUA_2G05540
Deoxycytidylate deaminase, putative (EC 3.5.4.12)	Absent	n/a	5	22.2	AFUA_2G06240
Rho GTPase activator (Rgd1), putative	Absent	n/a	7	15.4	AFUA_3G06280
COP9 signalosome subunit 2 (CsnB), putative	Absent	n/a	5	13.7	AFUA_3G06700
Glutamate carboxypeptidase Tre2, putative	Absent	n/a	7	12.5	AFUA_3G10650

ATP-dependent RNA helicase has1 (EC 3.6.4.13)	Absent	n/a	8	13.8	AFUA_4G13330
RNA polymerase II transcription elongation factor (Ctr9), putative	Absent	n/a	6	5.7	AFUA_5G05870
Uncharacterized protein	Absent	n/a	4	14.4	AFUA_5G14865
Mitochondrial intermediate peptidase (MIP) (EC 3.4.24.59) (Octapeptidyl aminopeptidase)	Absent	n/a	4	6.4	AFUA_6G08640
Uncharacterized protein	Absent	n/a	6	13.3	AFUA_6G03460

9.5 Appendix 5

Table 9.5. Proteins with significant $\log_2$ fold change or unique/absent in *A. fumigatus* Δ*vipC*^{26933} compared to ATCC26933 under basal conditions. Data sorted by fold change, in descending order.

Protein Description	Present/$\log_2$ Fold Change	p-value	Peptides	Sequence coverage [%]	Protein IDs
CCAAT-binding factor complex subunit HapC	Unique	n/a	3	23.8	AFUA_1G03840
Endo-1,3-beta-glucanase Engl1 (EC 3.2.1.6)	Unique	n/a	6	7.6	AFUA_1G04260
G-protein complex gamma subunit GpgA	Unique	n/a	3	34.4	AFUA_1G05210
Cytochrome c oxidase assembly protein Cox19, putative	Unique	n/a	2	20.4	AFUA_1G09757
Ammonium transporter	Unique	n/a	2	5.2	AFUA_1G10930
Smr domain protein	Unique	n/a	2	20.1	AFUA_1G13150
Uncharacterized protein	Unique	n/a	4	5.9	AFUA_2G08560
Uncharacterized protein	Unique	n/a	5	17.6	AFUA_2G10290
Uncharacterized protein	Unique	n/a	3	9.5	AFUA_2G11470
Zinc/cadmium resistance protein	Unique	n/a	6	14.3	AFUA_2G14570
SIR2 family histone deacetylase, putative (EC 3.5.1.-)	Unique	n/a	4	15.4	AFUA_3G00520
N2,N2-dimethylguanosine tRNA methyltransferase	Unique	n/a	2	5.1	AFUA_3G04200
Rho GTPase Rho3	Unique	n/a	3	21.8	AFUA_3G06690
Structural maintenance of chromosomes protein	Unique	n/a	5	5.4	AFUA_3G08260
Endosomal cargo receptor (Erp5), putative	Unique	n/a	5	34.6	AFUA_4G07390
Sit4-associated protein (Sap185), putative	Unique	n/a	2	3.1	AFUA_4G11012
Arginine biosynthesis bifunctional protein ArgJ	Unique	n/a	5	15.7	AFUA_5G08120
U2 small nuclear ribonucleoprotein A' (U2 snRNP A')	Unique	n/a	4	30	AFUA_5G11000
Oxidoreductase, 2OG-Fe(II) oxygenase family	Unique	n/a	6	26.8	AFUA_5G12470
Synaptobrevin-like protein Sybl1, putative	Unique	n/a	4	21.3	AFUA_6G11270
Transcriptional activator soma	Unique	n/a	2	4.5	AFUA_7G02260
Protein OS-9 homolog	Unique	n/a	6	26.9	AFUA_8G04530
Putative DNA helicase ino80 (EC 3.6.4.12)	Unique	n/a	6	4.8	AFUA_5G06260
Amino acid transporter, putative	Unique	n/a	7	13.3	AFUA_8G00800
Glucoamylase (EC 3.2.1.3) (1,4-alpha-D-glucan glucohydrolase)	4.69436	0.0248347	17	53.1	AFUA_2G00690
Tropomyosin, putative	3.01673	0.0106091	30	91.6	AFUA_7G04210
Small oligopeptide transporter, OPT family	2.9185	0.0144799	10	18.1	AFUA_2G15240

Uncharacterized protein	2.84709	0.0142601	5	44.8	AFUA_7G02020
Uncharacterized protein	2.80325	0.0053967	4	18.2	AFUB_039390
LipA and NB-ARC domain protein	2.67597	0.0450569	19	45.3	AFUA_3G14650
H+/nucleoside cotransporter	2.6571	0.0480087	5	11.8	AFUA_6G13190
Allergen Asp f 4 (allergen Asp f 4)	2.61566	0.0078489	11	55	AFUA_2G03830
CipC-like antibiotic response protein, putative	2.43259	0.0101168	17	89.2	AFUA_5G09330
Uncharacterized protein	2.38161	0.0427608	16	25	AFUA_2G12410
MFS peptide transporter Ptr2, putative	2.17966	0.00657	7	14	AFUA_7G01490
MFS phospholipid transporter (Git1), putative	2.16428	0.0123344	5	17.6	AFUA_6G07750
NADH-ubiquinone oxidoreductase	1.94662	0.025202	11	83	AFUA_1G12290
Thiamine thiazole synthase (Thiazole biosynthetic enzyme)	1.94062	0.045295	10	53.3	AFUA_6G08360
Uncharacterized protein	1.93594	0.0070151	6	63	AFUA_8G05650
Thiamine biosynthesis protein (Nmt1), putative	1.92433	0.041293	22	77.5	AFUA_5G02470
Ribosomal S30/ubiquitin fusion	1.91968	0.0495854	3	19.4	AFUA_6G02450
NADH-ubiquinone oxidoreductase B18 subunit, putative	1.88806	0.0309145	2	26.9	AFUA_3G13910
Amino acid permease (Gap1), putative	1.88198	0.0129507	10	19	AFUA_7G04290
Methylthioribose-1-phosphate isomerase (M1Pi) (MTR-1-P isomerase)	1.77106	0.0415603	20	62.5	AFUA_4G05830
Aryl-alcohol dehydrogenase, putative (EC 1.1.-.-)	1.743	0.0004814	18	48.1	AFUA_4G00610
Uncharacterized protein	1.72276	0.0074674	6	31.1	AFUA_8G02800
Glycogen synthase Gsy1, putative (EC 2.4.1.11)	1.72097	0.0043134	15	30.3	AFUA_5G02480
Uncharacterized protein	1.70252	0.0241192	8	85.2	AFUA_1G09890
Uncharacterized protein	1.69953	0.0176889	2	12.1	AFUA_8G01690
Pathogenesis associated protein Cap20, putative	1.69411	0.0024607	13	79.1	AFUA_1G06350
Alcohol dehydrogenase, putative (EC 1.1.1.1)	1.66047	0.006741	17	62.9	AFUA_7G01010
6-phosphofructo-2-kinase 1	1.65222	0.0260854	15	27	AFUA_1G07220
WW domain protein	1.64097	0.0412963	12	58	AFUA_4G03322
Structural maintenance of chromosomes protein	1.57865	0.0087512	16	19.4	AFUA_2G14080
GPR/FUN34 family protein	1.55823	0.0412971	2	13.6	AFUA_2G04080
Uncharacterized protein	1.54829	0.005589	6	43.1	AFUA_3G00730
Uncharacterized protein	1.52439	0.0381581	9	85	AFUA_3G00550
Glycolipid transfer protein HET-C2, putative	1.52004	0.0168031	8	44.8	AFUA_3G13820
ABC transporter, putative	1.51771	0.0219184	50	45.2	AFUA_1G14330
SNF7 family protein	1.51372	0.0292409	7	36.1	AFUA_1G06420
Clathrin light chain	1.51159	0.0361573	10	33.9	AFUA_4G10020
Uncharacterized protein	1.50097	0.0367368	5	12	AFUA_2G01540
40S ribosomal protein S15, putative	1.4861	0.0114505	10	76.5	AFUA_2G10090
ATP synthase subunit E, putative (EC 3.6.3.14)	1.4361	0.0011168	10	47	AFUA_6G02090
Histone H4	1.43371	0.0417729	10	53.4	AFUA_1G13780
Phosphoserine phosphatase (EC 3.1.3.3)	1.42824	0.0216512	7	26.7	AFUA_3G06550
Urease (EC 3.5.1.5) (Urea amidohydrolase)	1.41819	0.039067	15	29.1	AFUA_1G04560

Cytochrome c subunit Vb, putative	1.40972	0.0465272	11	67	AFUA_2G03010
Adenylyl-sulfate kinase (EC 2.7.1.25)	1.40367	0.0296912	7	46.9	AFUA_1G10820
RNP domain protein	1.36409	0.0064053	3	25.6	AFUA_1G09490
Malate synthase (EC 2.3.3.9)	1.34951	0.0084706	11	25.8	AFUA_6G03540
Alpha-1,4 glucan phosphorylase (EC 2.4.1.1)	1.34691	0.0336936	31	45.7	AFUA_1G12920
NACHT and TPR domain protein	1.34662	0.0215508	11	10.3	AFUA_7G06670
Phosphoglycerate kinase (EC 2.7.2.3)	1.33227	0.0454454	39	85.9	AFUA_1G10350
Endosomal cargo receptor (Erp5), putative	1.32874	0.0419246	5	28.1	AFUB_064480
Calcium/calmodulin-dependent protein kinase, putative (EC 2.7.11.17)	1.2996	0.0283656	9	34.3	AFUA_2G13680
Uncharacterized protein	1.29389	0.0102144	5	20.2	AFUA_1G04760
Glycylpeptide N-tetradecanoyltransferase	1.28905	0.0304352	14	37.6	AFUA_4G08070
Xanthine-guanine phosphoribosyl transferase Xpt1, putative	1.28178	0.0214742	10	75.7	AFUA_4G04550
Glutamine-serine-proline rich protein, putative	1.28176	0.010393	6	26.4	AFUA_7G04870
Dynamin GTPase, putative (EC 3.6.5.5)	1.28098	0.0081304	10	17.6	AFUA_6G11890
Uncharacterized protein	1.2714	0.0093326	18	82.4	AFUA_5G14680
ATP synthase D chain, mitochondrial, putative (EC 3.6.3.14)	1.26418	0.0291395	9	42.7	AFUA_6G03810
UPF0136 domain protein	1.26412	0.049667	3	31.4	AFUA_1G03720
Eukaryotic translation initiation factor 3 subunit J (eIF3j)	1.26255	0.0389505	5	29.6	AFUA_6G06760
Protein phosphatase PP2A regulatory subunit B	1.24912	0.0080004	10	31.2	AFUA_8G05560
Uncharacterized protein	1.24551	0.0026272	7	23.6	AFUA_5G02850
Aminotransferase, putative	1.24488	0.0137447	5	23.5	AFUA_6G02030
Uncharacterized protein	1.23742	0.0124597	8	12.8	AFUA_2G08090
ATP synthase delta chain, mitochondrial, putative (EC 3.6.3.14)	1.23138	0.0022145	6	72.7	AFUA_1G03100
Proteasome regulatory particle subunit (RpnK), putative	1.21836	0.0411085	12	51.3	AFUA_2G03400
Aflatoxin B1-aldehyde reductase GliO-like, putative (EC 1.1.1.-)	1.2167	0.0011308	8	36.9	AFUA_1G13370
Glycerol-3-phosphate dehydrogenase [NAD(+)] (EC 1.1.1.8)	1.20969	0.0160771	18	57	AFUA_1G02150
Uncharacterized protein	1.20528	0.0421702	5	50	AFUA_6G02830
Proteasome regulatory particle subunit (RpnF), putative	1.20108	0.0483408	13	36.7	AFUA_1G06300
Extracellular cellulase CelA/allergen Asp F7-like, putative	1.19558	0.0318824	4	25.6	AFUA_5G08030
Glycerophosphoryl diester phosphodiesterase family protein (EC 3.1.4.46)	1.19555	0.0346109	5	23.2	AFUA_2G00990
Indoleamine 2,3-dioxygenase family protein (EC 1.13.11.-)	1.19518	0.0016299	10	36.1	AFUA_7G02010
Phosphopantothenate-cysteine ligase, putative	1.19441	0.0413487	8	33.9	AFUA_3G07230
Rho GTPase Rho1	1.19404	0.0317957	10	64	AFUA_6G06900
Translation initiation factor SUI1, putative	1.19097	0.0365835	7	68.4	AFUA_3G06260
Succinate-semialdehyde dehydrogenase Uga2, putative (EC 1.2.1.24)	1.18987	0.0316673	9	34.3	AFUA_4G08170
Mitochondrial tricarboxylate transporter (Ctp), putative	1.18326	0.0325544	6	29.4	AFUA_3G05420
HAD superfamily hydrolase, putative	1.18276	0.0493669	17	68	AFUA_5G08270
Small nuclear ribonucleoprotein SmF, putative	1.17408	0.0114853	5	54.5	AFUA_2G15500
Integral membrane protein 25D9-6	1.16213	0.0173895	4	20.6	AFUA_2G17080

60S ribosomal protein L22, putative	1.15504	0.017245	5	44.4	AFUA_3G12300
Nudix/MutT family protein	1.15135	0.009741	3	30.4	AFUA_2G13080
Sorting nexin mvp1	1.15114	0.0185654	14	31.8	AFUA_2G17180
Uncharacterized protein	1.15089	0.0032034	4	38.7	AFUA_1G02290
DnaJ domain protein	1.14136	0.0386229	20	50	AFUA_7G01230
T-complex protein 1, beta subunit, putative	1.14097	0.0219699	17	44.5	AFUA_1G01740
AdoMet-dependent tRNA methyltransferase (MTase) complex subunit Trm112, putative	1.13911	0.0087446	5	57.2	AFUA_6G06330
Ubiquitin C-terminal hydrolase, putative (EC 3.1.2.15)	1.1238	0.0416768	14	38.7	AFUA_6G02380
Vacuolar ATP synthase catalytic subunit A, putative (EC 3.6.3.14)	1.1222	0.0366562	35	60.3	AFUA_5G02370
Coproporphyrinogen III oxidase, putative (EC 1.3.3.3)	1.11856	0.0017532	12	40.9	AFUA_1G07480
Secreted beta-glucosidase sun1 (EC 3.2.1.-)	1.10681	0.0321931	14	53.9	AFUA_7G05450
Ribosome recycling factor, putative	1.1053	0.0014963	2	7.5	AFUA_8G03940
CCAAT-binding factor complex subunit HapE	1.09962	0.0205649	5	25.1	AFUA_6G05300
Vacuolar protein sorting-associated protein VpsB	1.09012	0.0392633	8	22.9	AFUA_6G04870
Pyruvate dehydrogenase complex component Pdx1, putative	1.07806	0.0246284	5	25.7	AFUA_3G08270
Nuclear segregation protein (Bfr1), putative	1.07437	0.0252053	17	41.4	AFUA_1G14120
Phosphoglycerate mutase, 2,3-bisphosphoglycerate-independent	1.07375	0.012372	36	80	AFUA_3G09290
Histone H2A.Z	1.06943	0.0399999	3	20.3	AFUA_5G01950
DNA binding protein SART-1, putative	1.06153	0.0446231	6	10.7	AFUA_4G10420
Uncharacterized protein	1.06148	0.0445837	3	24.7	AFUA_6G07550
Uncharacterized protein	1.05775	0.0203983	13	27.5	AFUA_5G09270
Mitogen-activated protein kinase (EC 2.7.11.24)	1.05492	0.0447993	12	35.4	AFUA_4G13720
Fatty acid activator Faa4, putative (EC 6.2.1.3)	1.04615	0.0414864	25	44.2	AFUA_2G09910
Sorting nexin-4 (Autophagy-related protein 24)	1.02087	0.0014391	8	27.2	AFUA_4G12950
Ribose-phosphate pyrophosphokinase (EC 2.7.6.1)	1.01487	0.000887	10	28.7	AFUA_3G13380
ADP-ribosylation factor 6, putative	1.00644	0.0415546	3	26.1	AFUA_3G12080
Diphosphomevalonate decarboxylase (EC 4.1.1.33)	-1.00043	0.0324085	22	80	AFUA_4G07130
Small nuclear ribonucleoprotein SmD1, putative	-1.00904	0.0378531	3	46.7	AFUA_2G05110
Uncharacterized protein	-1.01386	0.0381539	7	11.7	AFUA_1G13590
Glyoxylate reductase (EC 1.1.1.95)	-1.02229	0.0493176	16	69.8	AFUA_4G11840
cAMP-dependent protein kinase regulatory subunit	-1.0364	0.0081586	16	56.9	AFUA_3G10000
RNA binding protein, putative	-1.04433	0.0366886	11	20.2	AFUB_039550
Histone chaperone asf1 (Anti-silencing function protein 1)	-1.047	0.0101194	9	64.9	AFUA_3G11030
Ubiquitin fusion degradation protein Ufd1, putative	-1.04765	0.0035942	7	24.5	AFUA_1G02430
Short chain dehydrogenase/reductase family protein (EC 1.1.1.100)	-1.04842	0.0370941	8	56.4	AFUA_4G14010
Isocitrate dehydrogenase [NADP] (EC 1.1.1.42)	-1.05025	0.0075024	38	67.9	AFUA_3G08660
RNA binding protein (Rbm8A), putative	-1.0537	0.0463482	3	29.1	AFUA_2G03260
Pantetheine-phosphate adenylyltransferase family protein	-1.05671	0.0222362	10	44.8	AFUA_4G08550
Alanyl-tRNA synthetase, putative (EC 6.1.1.7)	-1.08222	0.035019	7	42.5	AFUA_8G07110

UV-damaged DNA binding protein, putative	-1.08722	0.005705	17	22	AFUA_6G10980
Glutaminyl-tRNA synthetase (EC 6.1.1.18)	-1.09192	0.0269592	28	58.7	AFUA_2G01920
Tripeptidyl-peptidase sed2 (EC 3.4.14.-) (Sedolisin-B)	-1.11798	0.042504	14	36.9	AFUA_4G03490
NmrA-like family protein (EC 1.3.1.-)	-1.12278	0.0374258	8	41.5	AFUA_6G00280
2-nitropropane dioxygenase family oxidoreductase, putative (EC 1.3.1.9)	-1.12943	0.0140751	9	37.6	AFUA_5G09600
Profilin	-1.13316	0.0499957	6	71.3	AFUA_4G03050
Peptidyl-prolyl cis-trans isomerase (PPIase) (EC 5.2.1.8)	-1.14477	0.0065496	9	49.3	AFUA_2G03720
Aspartate-semialdehyde dehydrogenase (EC 1.2.1.11)	-1.14656	0.0318739	13	48.2	AFUA_3G06830
Malate dehydrogenase (EC 1.1.1.37)	-1.14731	0.0009595	25	77.9	AFUA_7G05740
UDP-glucose 4-epimerase (EC 5.1.3.2)	-1.14891	0.0264306	25	84.6	AFUA_5G10780
Aminomethyltransferase (EC 2.1.2.10)	-1.1498	0.0365544	14	55.1	AFUA_1G10780
Threonyl-tRNA synthetase, putative (EC 6.1.1.3)	-1.15259	0.0054856	33	58.2	AFUA_4G13700
DUF866 domain protein	-1.1556	0.0120287	11	83.1	AFUA_2G15510
Fumarylacetoacetate hydrolase family protein	-1.16075	0.0145021	8	36.6	AFUA_3G08140
Gamma-cysteine synthetase regulatory subunit, putative	-1.16194	0.0294871	8	46.3	AFUA_3G14280
Methyltransferase SirN-like, putative	-1.17769	0.0140022	29	89.7	AFUA_8G00550
Branched-chain-amino-acid aminotransferase (EC 2.6.1.42)	-1.18114	0.0141411	14	54.2	AFUA_2G10420
Proline utilization protein PrnX, putative (EC 4.3.1.12)	-1.18227	0.0161236	16	61.5	AFUA_6G08780
Probable cytosolic iron-sulfur protein assembly protein 1	-1.18265	0.0034154	14	49.1	AFUA_1G08930
Transaldolase (EC 2.2.1.2)	-1.20285	0.024829	25	84.6	AFUA_5G09230
Pyruvate dehydrogenase E1 component subunit alpha (EC 1.2.4.1)	-1.20539	0.0006282	21	69.7	AFUA_1G06960
Nuclear pore complex subunit, putative	-1.21763	0.02056	10	41.7	AFUA_6G10620
Probable D-xylulose kinase A (Xylulokinase A) (EC 2.7.1.17)	-1.22422	0.002209	17	39.1	AFUA_5G09840
Peptidyl-prolyl cis-trans isomerase D (PPIase D) (EC 5.2.1.8) (Rotamase D)	-1.23241	0.007257	16	68.7	AFUA_2G02050
Hydroxymethylglutaryl-CoA lyase (EC 4.1.3.4)	-1.23855	0.019141	9	49.7	AFUA_2G12450
CECR1 family adenosine deaminase, putative	-1.24283	0.0011191	13	26.5	AFUA_6G13180
PHD finger domain protein, putative	-1.2476	0.0389946	3	6.4	AFUA_7G05250
Oxidoreductase, short-chain dehydrogenase/reductase family (EC 1.1.-.-)	-1.2485	0.014793	14	76.3	AFUA_5G02870
DUF636 domain protein	-1.25066	0.0170914	5	74.3	AFUA_2G15290
Cobalamin-independent methionine synthase MetH/D (EC 2.1.1.14)	-1.25468	0.0031553	67	73.8	AFUA_4G07360
Flavin containing amine oxidase, putative (EC 1.4.3.-)	-1.25696	0.0265187	12	34.9	AFUA_3G12150
1,3-beta-glucanosyltransferase (EC 2.4.1.-)	-1.26623	0.0025503	8	14	AFUA_8G02130
NAP family protein	-1.27085	0.0024644	14	43.2	AFUA_5G02910
Uncharacterized protein	-1.27124	0.0128833	23	55.1	AFUA_3G12690
Alanine racemase family protein, putative	-1.27143	0.0123628	11	48.3	AFUA_4G04300
Ran GTPase activating protein 1 (RNA1 protein)	-1.28004	0.0301051	14	50	AFUA_3G07680
Aromatic-L-amino-acid decarboxylase, putative (EC 4.1.1.28)	-1.29528	0.0435669	13	34.2	AFUA_3G02240

Dienelactone hydrolase family protein (EC 3.1.1.-)	-1.29822	0.0091578	12	58.8	AFUA_1G07130
Pyruvate decarboxylase, putative (EC 4.1.1.1)	-1.30638	0.0150329	14	41	AFUA_6G00750
Poly(A)+ RNA transport protein (UbaA), putative (EC 6.3.2.19)	-1.30854	0.0064411	50	75	AFUA_2G15760
Leukotriene A-4 hydrolase homolog (LTA-4 hydrolase) (EC 3.3.2.6) (Leukotriene A(4) hydrolase)	-1.30951	0.0199644	28	48.4	AFUA_2G07520
Alkaline phosphatase (EC 3.1.3.1)	-1.31342	0.0323733	15	42.5	AFUA_2G03110
Kynureninase 1 (EC 3.7.1.3) (Biosynthesis of nicotinic acid protein 5-1)	-1.3255	0.0133443	14	35.4	AFUA_2G10360
Fructosyl amino acid oxidase, putative (EC 1.5.3.-)	-1.32973	4.95E-06	12	42.4	AFUA_8G06440
Ornithine carbamoyltransferase (EC 2.1.3.3)	-1.33493	0.0201104	15	60.4	AFUA_4G07190
GNAT family N-acetyltransferase, putative	-1.33518	0.0263455	7	47.8	AFUA_3G00870
FAD dependent oxidoreductase superfamily	-1.33639	0.0103546	11	39.2	AFUA_8G05850
Copper resistance protein Crd2, putative	-1.34204	0.0159024	3	41.4	AFUA_4G04318
Delta-1-pyrroline-5-carboxylate dehydrogenase PrnC (EC 1.2.1.88)	-1.34282	0.0111921	19	48.6	AFUA_6G08750
Aminotransferase family protein (LolT), putative (EgtB)	-1.34821	0.0005891	21	74.6	AFUA_2G13295
Oxidoreductase, putative	-1.36883	0.0040351	11	32.9	AFUA_2G14810
Spermidine synthase (EC 2.5.1.16)	-1.37119	0.0276863	20	79.2	AFUA_1G13490
Dipeptidyl peptidase, putative (EC 3.4.14.4)	-1.38226	0.0086309	42	58.3	AFUA_4G06140
rRNA processing protein Pwp1, putative	-1.38229	0.0111472	7	21.4	AFUA_1G02630
NAD dependent epimerase/dehydratase family protein (EC 1.1.1.133)	-1.386	0.026218	11	47	AFUA_5G02240
Cytosine deaminase, putative (EC 3.5.4.1)	-1.39743	0.0311643	9	61.5	AFUA_1G05050
Saccharopine dehydrogenase Lys9, putative (EC 1.5.1.7)	-1.39879	0.0075875	30	80.4	AFUA_4G11340
Fumarylacetoacetate hydrolase FahA (EC 3.7.1.2)	-1.41687	0.0038182	17	59.2	AFUA_2G04230
Uncharacterized protein	-1.42622	0.0211742	8	46.2	AFUA_2G02490
Haloalkanoic acid dehalogenase, putative (EC 3.8.1.-)	-1.44701	0.0031527	12	67.5	AFUA_6G14460
ThiJ/PfpI family protein	-1.44971	0.022028	7	43.6	AFUA_5G01430
6,7-dimethyl-8-ribityllumazine synthase (DMRL synthase) (EC 2.5.1.78)	-1.4624	0.0217791	10	90.4	AFUA_6G06345
Uncharacterized protein	-1.46339	0.0019636	13	78.7	AFUA_2G04930
Maleylacetoacetate isomerase MaiA (EC 5.2.1.2)	-1.4671	0.0444102	10	56.7	AFUA_2G04240
Peroxisomal dehydratase, putative	-1.47188	0.0238904	7	42.5	AFUA_5G00640
3-hydroxyisobutyryl-CoA hydrolase, mitochondrial (EC 3.1.2.4) (3-hydroxyisobutyryl-coenzyme A hydrolase)	-1.47736	0.0088731	21	44.4	AFUA_5G12790
Toxin biosynthesis peroxidase, putative (EC 1.11.-.-)	-1.48623	0.0455488	6	31.2	AFUA_4G02780
Acid phosphatase, putative	-1.49047	0.0011107	17	57.7	AFUA_1G16480
Glutathione S-transferase, putative	-1.49575	0.0018108	14	63.3	AFUA_8G00580
Uncharacterized protein	-1.50415	0.0069789	7	31.1	AFUA_6G09090
Glutathione-specific gamma-glutamylcyclotransferase (EC 2.3.2.-)	-1.50449	0.0002845	8	40.3	AFUA_3G08560
Enoyl-CoA hydratase/isomerase family protein (EC 4.2.-.-)	-1.50682	0.0089032	7	42	AFUA_2G14850
Eukaryotic translation initiation factor 6 (eIF-6)	-1.50907	0.0400842	8	48.2	AFUA_5G06010

Extracellular phytase, putative (EC 3.1.3.8)	-1.5096	0.0455601	10	28.6	AFUA_3G00310
Pyruvate dehydrogenase E1 beta subunit PdbA, putative (EC 1.2.4.1)	-1.51062	0.0055343	15	54.6	AFUA_3G04170
Ribulose-phosphate 3-epimerase (EC 5.1.3.1)	-1.51065	0.0016886	7	36.7	AFUA_2G15190
Sucrase/ferredoxin-like family protein, putative	-1.52074	0.0322815	7	31.5	AFUA_4G11477
Mitochondrial enoyl reductase, putative	-1.52192	0.0064706	18	50.1	AFUA_3G04150
Adenosine kinase, putative (EC 2.7.1.20)	-1.54142	0.004053	22	79	AFUA_5G06390
Uncharacterized protein	-1.54816	0.0475248	26	27.4	AFUA_1G07090
Cysteine synthase (O-acetylserine (Thiol)-lyase) (Csase) (EC 2.5.1.47)	-1.54878	0.0020114	10	42	AFUA_5G02180
DUF833 domain protein	-1.55215	0.0076722	13	61.2	AFUA_2G09530
Mitochondrial presequence protease (EC 3.4.24.-)	-1.55271	0.0071377	32	43.8	AFUA_4G07910
Putative peroxiredoxin pmp20 (EC 1.11.1.15)	-1.55902	0.0012818	18	91.1	AFUA_6G02280
RNA binding protein Ligatin/Tma64, putative	-1.5596	0.0151092	10	28.1	AFUA_1G12570
Formyltetrahydrofolate deformylase, putative (EC 3.5.1.10)	-1.56986	0.0103306	10	55.1	AFUA_6G11620
THUMP domain protein	-1.57034	0.0430798	7	37.5	AFUA_3G11060
Uncharacterized protein	-1.57288	0.0279353	3	14.8	AFUA_7G02300
Galactose-1-phosphate uridylyltransferase (EC 2.7.7.12)	-1.57647	0.0137686	18	51.4	AFUA_2G11560
Acyl-CoA:6-aminopenicillanic-acid-acyltransferase, putative	-1.57662	0.0099089	15	68.8	AFUA_3G12620
Nuclear transport factor NTF-2, putative	-1.60027	0.0059374	4	40.3	AFUA_3G10460
Nucleoside-diphosphate-sugar epimerase family protein	-1.60144	0.0080693	14	57.5	AFUA_3G02640
Probable endopolygalacturonase B (EC 3.2.1.15) (Pectinase B) (Polygalacturonase B)	-1.60304	0.0217355	11	41.5	AFUA_8G01970
Alpha-1,3-glucan synthase Ags3 (EC 2.4.1.183)	-1.61135	0.0242588	34	21.3	AFUA_1G15440
Uncharacterized protein	-1.62161	0.0327148	3	12.8	AFUA_1G11480
PUA RNA binding domain protein, putative	-1.62536	0.0174703	8	59.3	AFUA_1G09810
Alkaline protease 2 (ALP2) (EC 3.4.21.63)	-1.63035	0.0098581	15	40.6	AFUA_5G09210
Uncharacterized protein	-1.63043	0.0143305	7	43.7	AFUA_3G03610
Aspartyl aminopeptidase	-1.63759	0.0148919	22	60.3	AFUA_3G08290
DUF967 domain protein	-1.65071	0.0027212	7	56.4	AFUA_2G04610
Cyanate hydratase (Cyanase) (EC 4.2.1.104) (Cyanate hydrolase)	-1.65396	0.0358129	11	85.1	AFUA_2G16530
Proline iminopeptidase (EC 3.4.11.5)	-1.65705	0.0116292	17	48.8	AFUA_2G05000
Nicotinate phosphoribosyltransferase (EC 6.3.4.21)	-1.66553	0.0033016	13	34.3	AFUA_7G01880
Ubiquitin carboxyl-terminal hydrolase (EC 3.4.19.12)	-1.674	0.0239616	10	53.2	AFUA_2G05590
Thioredoxin Trx1, putative	-1.67432	0.0064429	4	35.8	AFUA_3G14970
Phosphotransferase (EC 2.7.1.-)	-1.68779	0.0071848	37	75.5	AFUA_2G05910
Endo alpha-1,4 polygalactosaminidase, putative	-1.68873	0.0087238	5	27	AFUA_3G07890
Aldo-keto reductase, putative (EC 1.1.1.-)	-1.6893	0.0196378	21	71.7	AFUA_4G11260
Branched-chain-amino-acid aminotransferase (EC 2.6.1.42)	-1.69406	0.0093951	13	39.4	AFUA_4G06160
Iron/copper transporter Atx1, putative	-1.70582	0.0282784	4	75.9	AFUA_1G08880
Oxidoreductase CipA-like, putative (EC 1.3.1.-)	-1.71706	0.0153205	17	52.1	AFUA_1G01630
3-isopropylmalate dehydrogenase (EC 1.1.1.85)	-1.72294	0.0395933	16	55.5	AFUA_1G15780

Lysophospholipase 3 (EC 3.1.1.5) (Phospholipase B 3)	-1.75445	0.0146471	19	33.2	AFUA_3G14680
FAD/FMN-containing isoamyl alcohol oxidase MreA	-1.75912	0.004275	12	37.8	AFUA_6G03620
Myo-inositol-phosphate synthase, putative (EC 5.5.1.-)	-1.78755	0.0034845	25	71.3	AFUA_2G01010
Probable Xaa-Pro aminopeptidase AFUA_1G14920 (EC 3.4.11.9) (Aminoacylproline aminopeptidase) (Prolidase)	-1.7877	0.012214	21	48.7	AFUA_1G14920
Inorganic diphosphatase, putative (EC 3.6.1.1)	-1.78805	0.0035457	27	62.9	AFUA_3G08380
Adenosylhomocysteinase (EC 3.3.1.1)	-1.79604	0.0010387	36	74.2	AFUA_1G10130
Catalase B (EC 1.11.1.6) (Antigenic catalase) (Slow catalase)	-1.80239	0.0077993	18	38.6	AFUA_3G02270
Aconitate hydratase, mitochondrial	-1.80632	0.0018982	47	71.5	AFUA_6G12930
OTU-like cysteine protease, putative	-1.80964	0.0071167	6	25.7	AFUA_3G05550
Mitochondrial dihydroxy acid dehydratase, putative (EC 4.2.1.-)	-1.81586	0.0028484	21	70.7	AFUA_1G03550
CAIB/BAIF family enzyme	-1.81747	0.0016485	21	62.6	AFUA_3G09240
Glyceraldehyde-3-phosphate dehydrogenase	-1.83346	0.0157514	32	84.3	AFUB_049500
S-formylglutathione hydrolase (EC 3.1.2.12)	-1.83625	0.0032647	18	79.1	AFUA_5G09860
Quinone oxidoreductase, putative (EC 1.6.5.5)	-1.83926	0.0104127	10	41.6	AFUA_1G02090
Alcohol dehydrogenase, zinc-containing, putative (EC 1.1.1.1)	-1.85088	0.0098128	12	56.6	AFUA_2G00970
Dihydroxy acid dehydratase Ilv3, putative	-1.85153	0.002332	30	71	AFUA_2G14210
4-aminobutyrate transaminase GatA (EC 2.6.1.19)	-1.86949	0.0012947	31	83	AFUA_5G06680
HypA-like protein, putative	-1.87855	0.0223651	14	35.3	AFUA_5G03330
Aldo-keto reductase (AKR13), puatative (EC 1.1.1.-)	-1.8801	0.007858	24	77.1	AFUA_7G00700
Uncharacterized protein	-1.88657	0.0023501	16	72.7	AFUA_6G03100
Mannosyl-oligosaccharide glucosidase, putative	-1.88794	0.0198943	20	35.2	AFUA_6G04210
Probable Xaa-Pro aminopeptidase pepP (EC 3.4.11.9)	-1.89136	0.0022494	24	62.4	AFUA_2G07500
Nucleoside diphosphate kinase (NDK) (NDP kinase) (EC 2.7.4.6)	-1.89349	0.0037831	11	79.1	AFUA_5G03490
Glutaryl-CoA dehydrogenase, putative (EC 1.3.8.6)	-1.89408	0.0030634	13	52.7	AFUA_3G06040
Short chain oxidoreductase/dehydrogenase, putative	-1.89469	0.0379655	8	56.7	AFUA_1G01770
Aldo-keto reductase, putative (EC 1.1.1.-)	-1.89938	0.027854	21	59.6	AFUA_2G01410
Glutamine synthetase, putative (EC 6.3.1.2)	-1.90463	0.0165266	16	45.1	AFUA_6G03530
Phosphotransferase (EC 2.7.1.-)	-1.91136	0.0053303	39	85.6	AFUA_6G02230
Glutathione oxidoreductase Glr1, putative (EC 1.8.1.7)	-1.91151	0.0093008	25	67.4	AFUA_1G15960
Oxidoreductase family, NAD-binding Rossmann fold protein	-1.92097	0.0119471	13	40.9	AFUA_2G16380
DSB repair complex subunit Ku70, putative	-1.93321	0.0040587	28	51.4	AFUA_5G07740
Glutamate carboxypeptidase Tre2, putative	-1.93664	0.0338926	15	27.5	AFUA_3G10650
Uncharacterized protein	-1.94429	0.006011	19	55.4	AFUA_3G02430
Phosphoglucomutase (PGM) (EC 5.4.2.2) (Glucose phosphomutase)	-1.94759	0.0081111	46	90.5	AFUA_3G11830
O-acetyltransferase, putative (EC 2.3.1.-)	-1.95039	0.0203931	8	46.1	AFUA_3G11510
Ribose 5-phosphate isomerase A (EC 5.3.1.6)	-1.96193	0.0024206	14	48.5	AFUA_6G10610
Ribonuclease T2-like (RNase T2-like) (EC 3.1.27.1)	-1.96521	0.0049226	12	48.2	AFUA_3G11220
DUF636 domain protein	-1.96864	0.0044137	5	46.9	AFUA_1G03180
F-box domain protein	-1.97097	0.0019983	13	42.1	AFUA_4G00200

Lysine decarboxylase-like protein	-1.97138	0.0003705	4	20.6	AFUA_6G04800
Peptidyl-prolyl cis-trans isomerase (PPIase) (EC 5.2.1.8)	-1.97335	0.0031844	12	74.8	AFUA_3G07430
Nucleoside-diphosphate-sugar epimerase, putative	-1.97395	0.0382535	13	66.3	AFUA_5G07170
Glutathione synthetase (GSH-S) (EC 6.3.2.3)	-1.97585	0.0054128	21	63.8	AFUA_5G06610
Lactoylglutathione lyase (EC 4.4.1.5) (Glyoxalase I)	-1.98281	0.0095249	26	85.5	AFUA_6G07940
Probable 4-hydroxyphenylpyruvate dioxygenase 1 (4HPPD 1) (HPD 1) (HPPDase 1) (EC 1.13.11.27)	-1.98312	0.0118759	19	53.8	AFUA_2G04200
Uncharacterized protein	-2.00017	0.0122164	10	42.4	AFUA_4G12880
GDSL Lipase/Acylhydrolase family protein	-2.00165	0.0017301	8	47.7	AFUA_2G08920
Uncharacterized protein	-2.01486	0.0047392	13	57.1	AFUA_3G09110
Nitrilase family protein (Nit3), putative	-2.0271	0.0077196	16	72.3	AFUA_6G13230
Cystathionine gamma-lyase (EC 4.4.1.8)	-2.03402	0.0076254	12	56.8	AFUA_8G04340
Probable Xaa-Pro aminopeptidase P (AMPP) (Aminopeptidase P)	-2.03436	0.0058493	32	65.3	AFUA_5G08050
Carnitine acetyl transferase	-2.05208	0.001231	34	62	AFUA_2G12530
Uroporphyrinogen decarboxylase (EC 4.1.1.37)	-2.06859	0.0042713	15	49.7	AFUA_1G05060
Inositol monophosphatase, putative	-2.07563	0.0313603	7	36	AFUA_3G04250
Possible apospory-associated protein c	-2.07798	0.0053532	18	89	AFUA_4G08880
Thioredoxin reductase (EC 1.8.1.9)	-2.07939	0.0044825	17	64.5	AFUA_4G12990
Uncharacterized protein	-2.09036	0.0002383	15	58.2	AFUA_4G09240
Short-chain dehydrogenase, putative (EC 1.-.-.-)	-2.095	0.0113509	16	57.8	AFUA_8G00280
Uncharacterized protein	-2.11387	0.0077628	9	60.6	AFUA_3G00960
ThiJ/PfpI family protein	-2.1423	8.65E-05	7	34.3	AFUA_5G02670
NADH-dependent flavin oxidoreductase, putative (EC 1.-.-.-)	-2.16525	0.0384993	16	47.6	AFUA_7G06420
Porphyromonas-type peptidyl-arginine deiminase superfamily	-2.17562	0.0050247	19	69.2	AFUA_3G01850
Kynurenine aminotransferase, putative (EC 2.6.1.-)	-2.18252	0.0033473	18	59.8	AFUA_4G11190
Uncharacterized protein	-2.18469	0.0298192	2	4.4	AFUA_1G09590
Uncharacterized protein	-2.18873	0.0004677	3	14.3	AFUA_5G09380
Allantoicase Alc, putative (EC 3.5.3.4)	-2.20027	0.0039565	16	53.7	AFUA_3G12560
Dienelactone hydrolase family protein	-2.21715	0.004	19	63.4	AFUA_6G01940
Uncharacterized protein	-2.22389	0.03592	10	59.8	AFUA_8G02420
5-formyltetrahydrofolate cyclo-ligase, putative	-2.22677	0.0326988	6	37	AFUA_7G05990
Zinc-containing alcohol dehydrogenase, putative	-2.2391	0.0020093	13	54	AFUA_3G01950
Mannitol-1-phosphate 5-dehydrogenase (M1PDH) (MPD) (MPDH)	-2.25502	0.0030695	23	69.6	AFUA_2G10660
Ribokinase (EC 2.7.1.15)	-2.29361	0.0029809	8	44	AFUA_5G02530
Agmatinase, putative (EC 3.5.3.11)	-2.29452	0.0111136	14	57.3	AFUA_5G13180
Allergen, putative (EC 1.-.-.-)	-2.30127	0.0018717	11	71.3	AFUA_5G01440
Succinyl-CoA:3-ketoacid-coenzyme A transferase (EC 2.8.3.5)	-2.31709	0.0063545	18	51.9	AFUA_6G12250
Aldehyde reductase (AKR1), putative (EC 1.1.1.2)	-2.32385	0.0043191	22	82	AFUA_6G10260
Asp-hemolysin (Asp-HS)	-2.32658	0.0009185	10	71.9	AFUA_3G00590
Vacuolar carboxypeptidase Cps1, putative (EC 3.4.17.-)	-2.32932	0.0028206	10	27	AFUA_3G07040

Acyl-CoA dehydrogenase, putative (EC 1.3.99.-)	-2.33151	0.003498	20	60	AFUA_1G14850
Proliferating cell nuclear antigen	-2.33973	0.0024044	13	85.4	AFUA_1G04900
Formamidase FmdS (EC 3.5.1.49)	-2.36059	0.0085728	13	42.6	AFUA_2G02020
D-amino acid oxidase (EC 1.4.3.3)	-2.36282	0.0016141	23	71.2	AFUA_5G11290
Cell wall biogenesis protein/glutathione transferase (Gto1), putative	-2.40308	0.003675	20	52.5	AFUA_2G15770
S-methyl-5'-thioadenosine phosphorylase	-2.40348	0.004488	15	64.9	AFUA_6G08720
DUF636 domain protein	-2.4095	0.0015275	9	73.3	AFUA_3G01340
General amidase, putative	-2.41743	0.0074634	16	45.5	AFUB_100900
ATP-dependent (S)-NAD(P)H-hydrate dehydratase	-2.44414	0.0136577	19	78	AFUA_2G10120
Dienelactone hydrolase family protein (EC 3.1.1.-)	-2.44846	0.0064431	19	69.4	AFUA_6G12740
MutT/nudix family protein	-2.45264	0.002231	11	81.8	AFUA_5G08240
Zinc-binding oxidoreductase ToxD, putative	-2.45293	0.0091683	18	74.6	AFUA_6G10120
Kelch repeat protein	-2.46605	0.0066756	17	70.8	AFUA_5G12780
Oxidoreductase, short chain dehydrogenase/reductase family superfamily	-2.47309	0.0019731	10	65.9	AFUA_3G13450
Alpha-mannosidase (EC 3.2.1.-)	-2.48583	0.0021653	41	51.9	AFUA_3G08200
Oxidoreductase, short-chain dehydrogenase/reductase family, putative	-2.49185	0.0036323	10	49.2	AFUA_5G14340
Oxidoreductase, short chain dehydrogenase/reductase family	-2.49998	0.0127866	14	86.8	AFUA_8G05590
Epoxide hydrolase, putative	-2.50661	0.001963	14	44.1	AFUA_3G08960
Short chain dehydrogenase/reductase (EC 1.1.-.-)	-2.50854	0.0055688	14	45.7	AFUA_2G00830
Thiamine biosynthetic bifunctional enzyme, putative	-2.52849	0.0039941	14	40.7	AFUA_2G08970
Uncharacterized protein	-2.53396	0.0357952	9	71.7	AFUA_2G05720
Uncharacterized protein	-2.5503	0.0133262	3	15.4	AFUA_1G11120
Endothelin-converting enzyme (EC 3.4.24.-)	-2.55051	0.0036315	21	39.9	AFUA_3G12420
Aldose 1-epimerase, putative (EC 5.1.3.3)	-2.56226	0.0149956	9	33.5	AFUA_3G13240
Vacuolar aspartyl aminopeptidase Lap4, putative	-2.57091	0.0022238	18	50.2	AFUA_5G03990
Isovaleryl-CoA dehydrogenase IvdA, putative (EC 1.3.8.4)	-2.57329	0.006896	17	48.3	AFUA_5G08930
Uncharacterized protein	-2.63221	0.0018701	8	47.5	AFUA_5G10990
TIM-barrel enzyme family protein	-2.66703	0.0034144	8	52	AFUA_1G10110
Beta-hexosaminidase (EC 3.2.1.52)	-2.66741	0.0033775	22	57.5	AFUA_8G05020
Sorbitol/xylulose reductase Sou1-like, putative (EC 1.-.-.-)	-2.69917	0.0051158	15	74.1	AFUA_2G15430
Aminopeptidase (EC 3.4.11.7)	-2.71944	0.0029456	64	69.2	AFUA_4G09030
Glutaminase, putative	-2.74585	0.0295248	18	33.6	AFUA_3G10910
Superoxide dismutase [Cu-Zn] (EC 1.15.1.1)	-2.82331	0.0100683	13	82.9	AFUA_5G09240
Uncharacterized protein	-2.84812	0.0011028	13	59.9	AFUA_3G10390
Uncharacterized protein	-2.84887	0.0070039	8	84.4	AFUA_2G00790
Homogentisate 1,2-dioxygenase (HmgA), putative (EC 1.13.11.5)	-2.8556	0.0057077	25	86.9	AFUA_2G04220
Aldose 1-epimerase, putative (EC 5.1.3.3)	-2.85628	0.0027781	22	71	AFUA_3G05740
Beta-glucosidase, putative	-2.90574	0.0023249	27	66.5	AFUA_1G14710
Endonuclease/exonuclease/phosphatase family protein	-2.91538	0.0034253	10	43.3	AFUA_2G16830

NmrA-like family protein, putative	-2.92523	0.0016372	12	72.6	AFUA_4G02840
Integral ER membrane protein Scs2, putative	-2.94082	0.0074905	9	47	AFUA_4G06950
3,4-dihydroxy-2-butanone 4-phosphate synthase (DHBP synthase)	-2.94771	0.0146427	10	48.7	AFUA_6G13140
Ser/Thr protein phosphatase family	-2.94997	0.0025816	21	49.5	AFUA_3G04160
Cytidine deaminase, putative (EC 3.5.4.-)	-2.95075	0.0046452	7	74.8	AFUA_8G02770
Methylmalonate-semialdehyde dehydrogenase, putative (EC 1.2.1.27)	-2.9656	0.002058	31	57.6	AFUA_4G12870
Oxidoreductase, short chain dehydrogenase/reductase family	-2.973	0.0051071	13	54.2	AFUA_8G06840
Probable carboxypeptidase AFUA_6G06800 (EC 3.4.17.-)	-3.00512	0.0028738	9	32	AFUA_6G06800
Phosphatidylserine decarboxylase family protein (EC 4.1.1.-)	-3.03712	0.0247092	8	49.3	AFUA_6G00260
Uncharacterized protein	-3.08088	0.0122566	6	22.4	AFUA_6G02010
L-PSP endoribonuclease family protein Brt1, putative	-3.10319	0.0053939	4	65.6	AFUA_5G03780
Betaine aldehyde dehydrogenase, putative (EC 1.2.1.8)	-3.12066	0.0330817	19	68.7	AFUA_1G00470
ATP-dependent DNA helicase II subunit 2 (EC 3.6.4.12)	-3.12682	0.0056819	18	35.4	AFUA_2G02620
Acetyl-coA hydrolase Ach1, putative (EC 2.8.3.8)	-3.14153	0.0145817	23	72.4	AFUA_8G05580
Peptide hydrolase (EC 3.4.-.-)	-3.2636	0.0029561	16	57.3	AFUA_2G00220
Uncharacterized protein	-3.30253	0.0146039	14	64.4	AFUA_2G01840
Glycosyl hydrolase family 75 chitosanase	-3.35811	0.0024479	7	35.7	AFUA_4G01290
Extracelular serine carboxypeptidase, putative (EC 3.4.-.-)	-3.41205	0.0162056	11	33.4	AFUA_2G17330
IgE-binding protein, putative	-3.45793	0.0218676	3	39.9	AFUA_6G03560
Class II aldolase/adducin domain protein	-3.47715	0.0036019	9	64.5	AFUA_3G09800
Kynureninase 2 (EC 3.7.1.3) (Biosynthesis of nicotinic acid protein 5-2)	-3.60717	0.008983	24	83	AFUA_4G09840
Uncharacterized protein	-3.65234	0.0014706	12	27.8	AFUA_8G01360
D-arabinitol dehydrogenase ArbD, putative (EC 1.1.1.69)	-3.67014	0.0008151	10	40.8	AFUA_5G08900
Class II aldolase/adducin domain protein	-3.73134	0.0116476	14	54.3	AFUA_3G01330
Fe-containing alcohol dehydrogenase, putative (EC 1.1.1.-)	-3.90924	0.0020302	20	55.3	AFUA_2G04520
Fructosyl amino acid oxidase, putative	-4.66424	0.0246961	20	54.7	AFUA_6G03440
Probable dipeptidyl-aminopeptidase B (DPAP B) (EC 3.4.14.5)	-4.71065	0.0035162	17	32.2	AFUA_3G07850
Phosphatidylglycerol specific phospholipase, putative (EC 3.1.4.-)	-5.15335	0.0102591	10	37.6	AFUA_3G01530
Conidial hydrophobin RodB	-5.21637	0.001205	4	61.4	AFUA_1G17250
Thiamin pyrophosphokinase, putative (EC 2.7.6.-)	Absent	n/a	9	33.6	AFUA_1G01830
Cut9 interacting protein Scn1, putative	Absent	n/a	5	22.3	AFUA_1G03870
Uncharacterized protein	Absent	n/a	3	18.8	AFUA_1G05270
Mandelate racemase/muconate lactonizing enzyme family protein	Absent	n/a	3	14.1	AFUA_1G05520
Histone H2A.Z-specific chaperone chz1	Absent	n/a	4	51.2	AFUA_1G07430
DUF431 domain protein	Absent	n/a	4	38.5	AFUA_1G08950
DUF1000 domain protein	Absent	n/a	4	43.6	AFUA_1G09230
Probable alpha-L-arabinofuranosidase C (ABF C) (Arabinosidase C)	Absent	n/a	4	11.6	AFUA_1G09900
GPI anchored protein, putative	Absent	n/a	7	28.3	AFUA_1G10590
Rho GTPase activator Rga, putative	Absent	n/a	4	5.4	AFUA_1G12680

Small nuclear ribonucleoprotein (LSM7), putative	Absent	n/a	3	19.4	AFUA_1G14290
Uncharacterized protein	Absent	n/a	7	13.6	AFUA_1G16430
Short chain dehydrogenase family protein (EC 1.-.-.-)	Absent	n/a	9	37.9	AFUA_1G16630
Uncharacterized protein	Absent	n/a	2	9.4	AFUA_1G16650
GNAT family acetyltransferase, putative	Absent	n/a	3	15.8	AFUA_2G00570
GAF domain nucleotide-binding protein	Absent	n/a	3	20.1	AFUA_2G01360
Signal recognition particle 14kD protein, putative	Absent	n/a	2	23.7	AFUA_2G01990
Cell polarity protein (Tea1), putative	Absent	n/a	4	3.5	AFUA_2G02520
Aldehyde reductase, putative (EC 1.1.1.-)	Absent	n/a	7	37.3	AFUA_2G02950
Uncharacterized protein	Absent	n/a	2	22.6	AFUA_2G03155
Asparaginase, putative (EC 3.5.1.1)	Absent	n/a	3	8.9	AFUA_2G04280
Sugar hydrolase, putative	Absent	n/a	9	17	AFUA_2G05400
IdgA domain protein (EC 2.7.1.-)	Absent	n/a	8	14.8	AFUA_2G05800
GYF domain protein	Absent	n/a	3	2.2	AFUA_2G13290
Lactoylglutathione lyase (Glo1), putative (EC 4.4.1.5)	Absent	n/a	5	37.3	AFUA_2G13550
Thiamine pyrophosphate enzyme, putative (EC 4.1.-.-)	Absent	n/a	10	32	AFUA_2G13620
Probable endo-1,3(4)-beta-glucanase AFUA_2G14360 (EC 3.2.1.6) (Mixed-linked glucanase AFUA_2G14360)	Absent	n/a	2	6.6	AFUA_2G14360
L-PSP endoribonuclease family protein, putative	Absent	n/a	2	28	AFUA_2G17470
Uncharacterized protein	Absent	n/a	2	28.4	AFUA_3G07000
Uncharacterized protein	Absent	n/a	3	39.4	AFUA_3G07945
N,N-dimethylglycine oxidase (EC 1.5.8.3)	Absent	n/a	7	35.8	AFUA_4G01150
Protein kinase Scy1, putative	Absent	n/a	3	7.3	AFUA_4G06150
Calcium homeostasis protein Regucalcin, putative	Absent	n/a	9	48.8	AFUA_4G08610
Uncharacterized protein	Absent	n/a	2	11.3	AFUA_4G09890
CaaX farnesyltransferase beta subunit Ram1 (EC 2.5.1.58)	Absent	n/a	5	19.8	AFUA_4G10330
N-acetyltransferase family protein, putative	Absent	n/a	2	5.8	AFUA_4G10930
DlpA domain protein	Absent	n/a	5	22	AFUA_4G10940
Metallo-beta-lactamase domain protein, putative	Absent	n/a	2	12.2	AFUA_4G13310
Mannitol 2-dehydrogenase (M2DH) (MDH) (EC 1.1.1.67)	Absent	n/a	13	36.9	AFUA_4G14450
Glutathione S-transferase Ure2-like, putative	Absent	n/a	4	29.8	AFUA_4G14530
Ribokinase (RK) (EC 2.7.1.15)	Absent	n/a	6	27.4	AFUA_4G14650
Uncharacterized protein	Absent	n/a	3	21.6	AFUA_5G00870
NADH-dependent flavin oxidoreductase, putative (EC 1.-.-.-)	Absent	n/a	9	40	AFUA_5G01450
Amidohydrolase family protein	Absent	n/a	8	30.4	AFUA_5G01480
Isopenicillin N-CoA epimerase, putative	Absent	n/a	11	37.2	AFUA_5G03740
Oxidoreductase, short-chain dehydrogenase/reductase family	Absent	n/a	5	47	AFUA_5G09150
Beta-lactamase	Absent	n/a	6	29.2	AFUA_5G09790
Arsenic methyltransferase Cyt19, putative (EC 2.1.1.137)	Absent	n/a	11	51.2	AFUA_5G15020
Probable arabinan endo-1,5-alpha-L-arabinosidase C (EC 3.2.1.99)	Absent	n/a	3	14.9	AFUA_6G00770

Phenol 2-monooxygenase, putative	Absent	n/a	15	34.4	AFUA_6G03490
Sucrase/ferredoxin-like family protein Fmi1, putative	Absent	n/a	5	30.2	AFUA_6G04900
Glutaminase, putative	Absent	n/a	17	28.7	AFUA_6G09910
Thiamine pyrophosphate enzyme, putative (EC 4.1.-.-)	Absent	n/a	9	31.1	AFUA_6G11680
DNA damage-binding protein cmr1	Absent	n/a	6	30	AFUA_6G12330
Putative heme-binding peroxidase (EC 1.11.1.-)	Absent	n/a	7	35.4	AFUA_6G13570
Uncharacterized protein	Absent	n/a	11	38.3	AFUA_6G13900
Phosphatidylglycerol specific phospholipase C, putative (EC 3.1.4.3)	Absent	n/a	7	16.7	AFUA_7G04910
Glyoxalase family protein	Absent	n/a	5	34.6	AFUA_7G05015
Uncharacterized protein	Absent	n/a	2	38.1	AFUA_7G05730
Probable beta-glucosidase L (EC 3.2.1.21)	Absent	n/a	7	18.8	AFUA_7G06140
Cyanamide hydratase, putative (EC 4.2.1.69)	Absent	n/a	5	24.7	AFUA_7G06270
Fumitremorgin biosynthesis protein H	Absent	n/a	9	36.3	AFUA_8G00250
Dimethylallyl tryptophan synthase, putative (EC 2.5.1.-)	Absent	n/a	9	27.3	AFUA_8G00620
Arylsulfatase (AS) (EC 3.1.6.1) (Aryl-sulfate sulphohydrolase)	Absent	n/a	2	4	AFUA_8G02520
AraC-like ligand binding domain protein, putative	Absent	n/a	4	27.2	AFUA_6G14370
Fumarylacetoacetate hydrolase family protein	Absent	n/a	5	31.3	AFUA_1G02370
Thiamin pyrophosphokinase-related protein	Absent	n/a	6	33.2	AFUA_5G11110
Ureidoglycolate hydrolase, putative (EC 3.5.3.19)	Absent	n/a	10	65.5	AFUA_8G04760
Uncharacterized protein	Absent	n/a	4	34.3	AFUB_084960
Verruculogen synthase (Fumitremorgin biosynthesis protein F)	Absent	n/a	6	26.5	AFUA_8G00230
Uncharacterized protein	Absent	n/a	4	31.2	AFUB_086760